RADIOLOGY AND ONCOLOGY

vol.59 no.4
december 2025

RADIOLOGY AND ONCOLOGY

December 2025
Vol. 59 No. 4
Pages 467-634
ISSN 1318-2099
UDC 616-006
CODEN: RONCEM
eISSN: 1581-3207

Publisher
Association of Radiology and Oncology

Aims and Scope
Radiology and Oncology (ISSN 1318-2099) is a multidisciplinary journal devoted to the publishing original and high-quality scientific papers and review articles, pertinent to oncologic imaging, interventional radiology, nuclear medicine, radiotherapy, clinical and experimental oncology, radiobiology, medical physics, and radiation protection. Papers on more general aspects of interest to the radiologists and oncologists are also published (no case reports).

Editorial office

Radiology and Oncology
Zaloška cesta 2
P. O. Box 2217
SI-1000 Ljubljana
Slovenia
Phone: +386 1 5879 369
Phone/Fax: +386 1 5879 434
E-mail: gsersa@onko-i.si

Reader for English
Vida Kološa

Secretary
Mira Klemenčič, Zvezdana Vukmirović, Vijoleta Kaluža, Uroš Kuhar

Design
Monika Fink-Serša, Samo Rovan, Ivana Ljubanović

Layout
Matjaž Lužar

Printed by
Tiskarna Ozimek, Slovenia

Published quarterly in 300 copies

Beneficiary name: DRUŠTVO RADIOLOGIJE IN ONKOLOGIJE
Zaloška cesta 2
1000 Ljubljana
Slovenia

Beneficiary bank account number: SI56 02010-0090006751
IBAN: SI56 0201 0009 0006 751
Our bank name: Nova Ljubljanska banka, d.d.,
Ljubljana, Trg republike 2,
1520 Ljubljana; Slovenia

SWIFT: LJBASI2X

Subscription fee for institutions EUR 100, individuals EUR 50

The publication of this journal is subsidized by the Slovenian Research Agency.

Indexed and abstracted by:

- *Baidu Scholar*
- *Case*
- *Chemical Abstracts Service (CAS) - CAplus*
- *Chemical Abstracts Service (CAS) - SciFinder*
- *CNKI Scholar (China National Knowledge Infrastructure)*
- *CNPIEC - cnpLINKer*
- *Dimensions*
- *DOAJ (Directory of Open Access Journals)*
- *EBSCO (relevant databases)*
- *EBSCO Discovery Service*
- *Embase*
- *Genamics JournalSeek*
- *Google Scholar*
- *Japan Science and Technology Agency (JST)*
- *J-Gate*
- *Journal Citation Reports/Science Edition*
- *JournalGuide*
- *JournalTOCs*
- *KESLI-NDSL (Korean National Discovery for Science Leaders)*
- *Medline*
- *Meta*
- *Microsoft Academic*
- *Naviga (Softweco)*
- *Primo Central (ExLibris)*
- *ProQuest (relevant databases)*
- *Publons*
- *PubMed*
- *PubMed Central*
- *PubsHub*
- *QOAM (Quality Open Access Market)*
- *ReadCube*
- *Reaxys*
- *SCImago (SJR)*
- *SCOPUS*
- *Sherpa/RoMEO*
- *Summon (Serials Solutions/ProQuest)*
- *TDNet*
- *Ulrich's Periodicals Directory/ulrichsweb*
- *WanFang Data*
- *Web of Science - Current Contents/Clinical Medicine*
- *Web of Science - Science Citation Index Expanded*
- *WorldCat (OCLC)*

This journal is printed on acid- free paper

On the web: ISSN 1581-3207
https://reference-global.com/journal/RAON
http://www.radioloncol.com

contents

clinical oncology

review

Between defence and delivery: the DNA sensing response to gene electrotransfer

Tanja Jesenko[1,2], Masa Omerzel[1,2,3], Loree C Heller[4], Maja Cemazar[1,2,5]

[1] Department of Experimental Oncology, Institute of Oncology Ljubljana, Ljubljana, Slovenia
[2] Faculty of Medicine, University of Ljubljana, Ljubljana, Slovenia
[3] Faculty of Health Sciences, University of Ljubljana, Ljubljana, Slovenia
[4] Department of Medical Engineering, University of South Florida, Tampa, Florida, USA
[5] Faculty of Health Sciences, University of Primorska, Izola, Slovenia

Radiol Oncol 2025; 59(4): 467-476.

Received 10 November 2025
Accepted 17 November 2025

Correspondence to: Prof. Maja Cemazar, Ph.D., Institute of Oncology Ljubljana, Zaloška 2, SI-1000 Ljubljana, Slovenia.
E-mail: mcemazar@onko-i.si

Disclosure: No potential conflicts of interest were disclosed.

Background. Gene therapy has emerged as a transformative biomedical approach, offering new therapeutic possibilities from many so far uncurable diseases through the introduction of recombinant nucleic acids into target cells. Among non-viral delivery techniques, gene electrotransfer (GET) has become one of the frequently applied methods in clinical trials. It is based on the application of short, high-intensity electric pulses that transiently permeabilize cell membranes and enable the efficient transfer of plasmid DNA or other types of recombinant nucleic acids into various cell types. Beyond its role in gene delivery, GET can trigger complex cellular responses, as the introduced DNA interacts with intracellular DNA sensing pathways involved in innate immunity and inflammation. These responses can influence the therapeutic outcome – either by enhancing antitumour and vaccine-related immune activation or by reducing transfection efficiency when excessive inflammation or cell death occur. Our experimental findings in tumour, muscle, and skin models have shown that even non-coding plasmid DNA delivered by GET can induce local immune stimulation and tissue-specific inflammatory signaling, suggesting that the delivered DNA itself contributes to therapeutic efficacy.

Conclusions. The dual nature of cellular responses following plasmid DNA GET represents both an opportunity and a challenge. Controlled activation of innate immunity can be harnessed to amplify antitumour or vaccine efficacy, while excessive responses may hinder applications requiring cell survival and sustained expression. Understanding these mechanisms enables the rational optimization of GET parameters and plasmid vector design to fully exploit the adjuvant effect or reduce the off-target effect of DNA sensing after GET, based on the desired application.

Key words: gene electrotransfer; DNA sensors; gene therapy; immune response; plasmid DNA

Introduction

Gene therapy offers groundbreaking new opportunities for the treatment of various diseases. Several gene therapy medicines were approved in the last few years. Per the American Society for Gene and Cell Therapy (ASGTC) Q2 2025 Quarterly Data Report, 4,469 therapies are in development, ranging from preclinical through pre-registration, with oncology and rare diseases being the most targeted gene therapy areas. This report identifies 143 gene, cell and RNA therapies currently approved globally for clinical use.[1,2] In oncology, gene therapy holds great promise in the treatment of cancer and can also be used for specific anti-tumour vaccination purposes.[3,4]

In general, a recombinant gene is a stretch of DNA that is created in the laboratory, bringing together DNA from different sources. Different methods can be used for the delivery of the recombinant genes. *In vivo* gene delivery methods are broadly divided into viral and non-viral categories. Each delivery type has applications in gene therapy, and each has associated problems. Viral delivery is effective; however, there are still some concerns, including the potential for insertional mutagenesis or induction of specific immune responses.[5,6] However, due to the gained knowledge and evolvement of this technology, viral vectors are now generally considered as a safe delivery method.[7,8] On the other hand, non-viral gene delivery is associated with low transfection efficiency, so chemical or physical assistance is often used, including lipid or polymer conjugation, particle-mediated delivery, hydrodynamic delivery, ultrasound or electroporation.[9-11]

Gene electrotransfer (GET), one of the most established non-viral methods for gene delivery, is based on the application of short electric pulses, which transiently permeabilize the cell membrane.[12] This enables the efficient uptake of recombinant nucleic acids, including plasmid DNA, mRNA, and small interfering RNAs, into a wide range of cell types. GET has been widely applied in cancer gene therapy, partially for antiangiogenic therapy, but primarily for delivering plasmids encoding cytokines, such as interleukin-12 (IL-12), to stimulate strong antitumour immune responses, with several clinical trials demonstrating effectiveness of such approach.[13-15] GET is also used in DNA vaccination, where it significantly enhances antigen expression and immune activation against infectious diseases. It also plays a role in the development of chimeric antigen receptor- T cell therapies (CAR-T), where electroporation is used *ex vivo* to insert genetic material, such as a construct or genome-editing tools into T cells as a non-viral alternative to viral vectors.[16]

Upon the delivery of the transgene product into the cells using viral or non-viral delivery methods, we can expect the on-target action of the delivered transgene as well as off-target cell-specific responses. These cellular responses evolved to maintain organismal homeostasis in response to the microbial infection. The innate immune system utilizes numerous germ-line encoded receptors termed pattern-recognition receptors (PRRs) to detect various pathogen-associated molecular patterns (PAMPs) and damage-associated molecular patterns (DAMPs).[17,18] Nucleic acids can act as PAMP or DAMP, depending on its composition, origin or localization.[19,20] When PRRs sense DNA, they are also called DNA sensors. The activation of these pathways results in innate antiviral immune responses in the form of proinflammatory cytokines and type I interferons and can also lead to cell death (Figure 1).[21,22] On one hand, this activation can significantly impair the efficacy of gene therapy. On the other hand, the activation of the innate immune response can also be beneficial when the gene therapy is delivered to boost the anti-tumour immune response.[23]

In this review, we present the clinical applications of GET, outline the mechanisms underlying DNA delivery into cells, and discuss how the delivered DNA is recognized by cellular DNA-sensing pathways. Building on these insights, we further explore how such DNA sensing influences the current challenges and future perspectives of GET-based gene therapy.

Clinical applications of GET

In the last decade, non-clinical research of GET has progressed into early human clinical trials, especially in the field of cancer vaccines and immunotherapy, but also for the vaccination against infectious disease. Numerous clinical trials, Phase 1–Phase 3, have been registered at ClinicalTrials database (ClinicalTrials.gov) and numerous reports already published in medical journals.

In cancer immunotherapy, intratumoral GET of plasmid encoding IL-12[14,24,25] in patients with melanoma is most studied gene therapy (NCT01502293, NCT01502293, NCT05077033). IL-12 GET was safe, with no grade 3–4 toxicities and showed tumour necrosis, lymphocytic infiltration, and tumour regression even in non-injected lesions, implying a systemic immune stimulation and abscopal effect. IL-12 GET have also been combined with anti-PD-1 inhibitors (NCT03132675, NCT02493361) and studies suggested that adding intratumoral IL-12 GET may sensitize tumours to checkpoint inhibition by modifying the tumour microenvironment to become more immunogenic.[26,27] The safety and effectiveness of combination treatment of IL-12 GET and pembrolizumab has also been proven in triple negative breast cancer (NCT03567720)[28], however the treatment demonstrated ineffective in metastatic head and neck squamous cell carcinoma, leading to trial termination (NCT03823131). IL-12 GET demonstrated favourable safety profile and feasibility of therapeutic administration also in basal cell carcinoma.[13]

Anti-angiogenic therapy using GET for cancer treatment has been tested in clinical studies (NCT 01664273, NCT 01764009) with Antiangiogenic MEtargidin Peptide plasmid (AMEP)[15,29], encoding an integrin-binding protein that inhibits tumour angiogenesis and proliferation. GET of plasmid AMEP was demonstrated feasible, safe (in a small cohort), and achieved local transfection of the plasmid. However, the trials were terminated due to insufficient patient enrolment following EMA approval of ipilimumab, as the inclusion criteria assumes exhaustion of all available treatment options.

Recent clinical studies explored a range of GET-delivered DNA-based cancer vaccines designed to induce targeted immune responses against tumour-associated antigens. For instance, the ElporCEA vaccine (NCT01064375) targets colorectal cancer using a plasmid DNA encoding carcinoembryonic antigen (CEA) fused with a tetanus toxoid helper epitope, while GX-188E (NCT01634503) and VGX-3100 (NCT03185013, NCT01304524) target HPV-16 and HPV-18 in cervical neoplasia.[30,31] Similarly, INVAC-1 (NCT02301754)[32] encodes the human telomerase reverse transcriptase (hTERT), over-expressed in most cancers, and INO-5150 (NCT02514213) combines prostate-specific antigen (PSA) and prostate-specific membrane antigen (PSMA) sequences to elicit prostate cancer immunity. Collectively, these trials demonstrate the versatility of DNA vaccines delivered via GET in oncology, showing favourable safety, tolerability, and immune activation across multiple tumour types.

GET is a promising method also for the delivery of DNA-based vaccines for infectious diseases. Several clinical studies have demonstrated the safety and tolerability of GET-delivered plasmids, encoding antigens, across infectious diseases, including HIV (PENNVAX™-B; NCT01082692, NCT02431767), influenza (VGX-3400X and H1/H5 formulations (NCT01142362, NCT03721978, NCT01405885), Ebola (INO-4201/4212, NCT02464670)[33], and COVID-19 (INO-4800; NCT04447781, NCT04336410).[34] GET promoted efficient antigen expression and robust immune responses, including both antibody and T-cell activation.

Mechanisms of DNA delivery into cells via GET

The entry of DNA into mammalian cells during GET is a complex, multistep process involving the coordinated traversal of several biological barriers, the plasma membrane, cytoskeleton-rich cytoplasm, and nuclear envelope. The phenomenon underlying GET which induced the permeabilization of the first biological barrier, the plasma membrane, was first observed in the early 1970s, when short, high-intensity electric pulses were found to transiently increase the permeability of vesicular membranes.[35] The extent and duration of this permeabilization depend on the pulse amplitude, duration, and frequency, allowing controlled delivery of nucleic acids into the cells.[36,37] The first successful demonstration of gene transfer by pulsed electric fields was reported by Neumann *et al*. in 1982, who introduced the herpes simplex thymidine kinase gene into mouse lyoma cells.[38] Since then, GET has been widely used in both *in vitro* and *in vivo* applications for the transfer of various nucleic acids.[37]

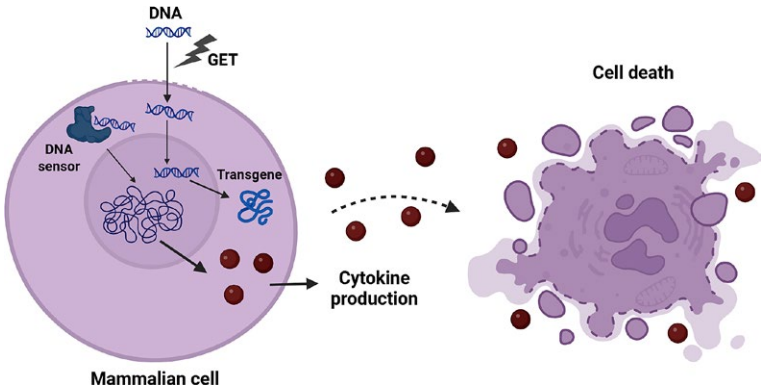

FIGURE 1. Delivery of DNA into the cells induces transgene expression as well as the activation of DNA sensing pathways, resulting in cytokine expression and cell death. Created in BioRender. Cemazar, M. (2025) https://BioRender.com/jazpf7t

The GET process proceeds through several key stages: (1) plasma membrane electroporation, (2) DNA–membrane interaction, (3) DNA translocation across the membrane, (4) intracellular migration toward the nucleus, and (5) gene expression.[39] Efficient transfection requires that each of these steps be successfully completed. Despite decades of research, the precise mechanisms of DNA uptake remain debated, particularly concerning the mode of transmembrane DNA transport. Two majors, not mutually exclusive, models have been proposed: the pore theory and the endocytosis theory. The pore theory posits that the applied electric field induces transient, nanometre-scale hydrophilic pores within the lipid bilayer, allowing charged macromolecules such as nucleic acids to pass into the cytosol.[40] Although direct visualization of such pores has not yet been achieved,

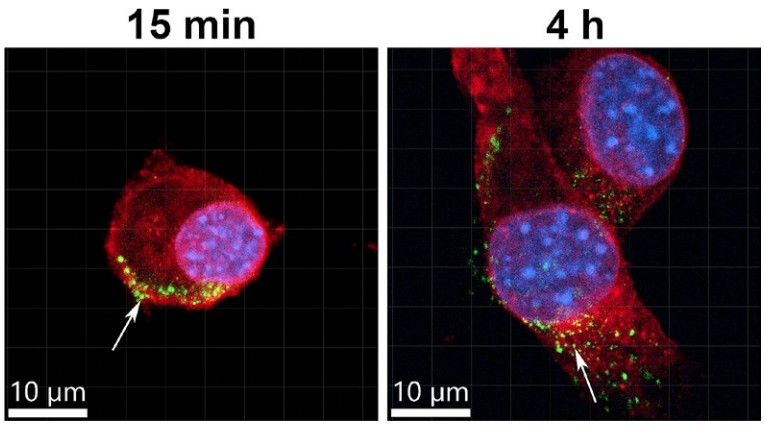

FIGURE 2. Localization of plasmid DNA after gene electrotransfer (GET) into C2C12 cell line, demonstrating DNA-membrane complexes after 15 min and internalization and presence in the cytoplasm and nucleus after 4 h. Plasma membrane is marked in red, nuclei in blue and plasmid DNA in green. Arrows represent plasmid DNA foci.

their existence is supported by mathematical modelling and the observed entry of otherwise impermeable fluorescent markers.[41,42] Theoretical estimates suggest that pore diameters reach from 22.8 to 419 nm, and their lifetime is exceedingly short (on the order of 10 milliseconds) far shorter than the minutes-long timescale of plasmid DNA internalization.[41,43] This discrepancy suggests that DNA uptake cannot occur solely through passive diffusion across transient pores. In contrast, the endocytosis theory is now supported by multiple experimental lines of evidence and proposes that DNA uptake occurs primarily via endocytic pathways. After application of electric pulses, plasmid DNA molecules are electrophoretically driven toward the plasma membrane, where they form stable DNA-membrane complexes that subsequently undergo internalization (Figure 2).[42,43] Pharmacological inhibition and RNA interference studies have demonstrated that clathrin-mediated and caveolin/raft-mediated endocytosis are major contributors to plasmid DNA uptake, together accounting for approximately 75% of internalized DNA.[44] This theory was also demonstrated in vivo in the mouse muscle tissue using an endocytosis inhibitor, showing that endocytosis is the main mechanism of entrance of DNA after GET, which leads to the production of the transgene.[45]

Following internalization, DNA must traverse the cytoplasm to reach the nucleus (Figure 2) a journey hindered by the dense cytoskeletal network. DNA aggregates were demonstrated to be actively transported by the actin and the microtubule networks.[46,47] An *in vitro* study has indicated that DNA delivered via GET uses the classical endosomal trafficking pathways as plasmid DNA trajectories were co-localized with the biomarkers for endosomes.[48]

The last and the most challenging barrier is the nuclear membrane. The exact mechanism by which plasmid DNA crosses the nuclear barrier remains incompletely understood. The plasmid DNA must first escape the endosomes to be release into the cytosol to be able to enter the nucleus and be transcribed. Typically, macromolecules traverse the nuclear envelope through nuclear pore complexes (NPCs), which allow passive diffusion of small molecules (<9 nm or ~40 kDa) and active transport of larger molecules up to 39 nm when equipped with nuclear localization signals (NLSs).[49] However, plasmid DNA, with a radius of gyration of approximately 100 nm, is far too large for passive diffusion through NPCs and the presence of NLSs is not ensured in all DNA constructs. Therefore, the most straightforward mechanism is reached in dividing cells. During mitosis, the nuclear envelope breaks down and facilitates passive nuclear entry of plasmid DNA during the formation of nuclear envelope in anaphase of mitosis, which can be enhanced by synchronizing cells at the G2–M phase before electroporation or transfection.[50]

Taken together, these findings indicate that at every stage of the GET process, plasmid DNA can transiently reside within the cytoplasmic compartment, where it may be detected by cellular DNA sensors. Although the majority of DNA internalization (~75%) proceeds via endocytic and endosomal pathways that deliver the cargo close to the perinuclear region, a significant proportion – approximately 25% – likely enters the cytosol through alternative routes.[47] Furthermore, even DNA internalized by endocytosis can become cytosol-accessible following endosomal escape, a critical step for efficient transgene expression. This transient cytosolic presence of exogenous DNA provides the molecular basis for its recognition by intracellular DNA-sensing pathways.

Intracellular DNA sensors

The immune-stimulatory role of nucleic acids is well established. Its immunogenicity was first described in immune cells. The most well-characterized DNA sensor is Toll-like receptor 9 (TLR9), which is found predominantly in the endosomes of immune cells and detects mainly CpG motif DNA and RNA-DNA hybrids.[51,52] In contrast, other

intracellular DNA sensors are nuclear or cytosolic, are ubiquitous and present in virtually any mammalian cell, including tumour cells, and detect various DNA motifs.[17,53]

The DNA sensors are germline-encoded and function in the detection of intracellular pathogens, including viruses. Although viral proteins may trigger specific PRRs, the predominant viral components activating them are nucleic acids.[54] Viruses, including viral vectors commonly used for gene therapy applications, trigger these pathways. For example, adenoviruses activate multiple pattern recognition pathways[55-57], while adeno-associated viruses show significant, but reduced production type I interferon mRNA when compared to adenovirus[58], although the innate immune responses can influence the outcome of these gene therapies.[59] HIV1, upon which lentiviral gene therapy vectors are based, inhibit the host's type I interferon response at several levels.[60] These host-directed viral activities reduce, but do not completely reverse the production of inflammatory molecules.

There are multiple DNA sensing pathways identified, and the list of newly recognized DNA sensors grows every year.[22,53,61,62] Their ligands and signalling cascades are incompletely characterized; however, cytosolic DNA sensor binding is known to control the production of pro-inflammatory cytokines and interferons.[17,62] Their activation can also lead to the induction of cell death that elicits inflammation.[22] DNA-dependent activator of interferon regulator factor (ZBP1), was the first intracellular DNA sensor described.[63] The observation that ZBP1 deficient mice responded similarly to DNA vaccination as wild type mice suggested that redundant DNA sensors might exist. Subsequently, several groups reported that DNA binding to absent in melanoma 2 (AIM2) induces caspase-1 activation, leading to the secretion of interleukin-1 beta (IL-1β) and interleukin 18 (IL-18).[64,65] DNA binding and activation of the AIM2-like protein gamma-interferon-inducible protein Ifi-16 (IFI16; mouse orthologue ifi204) mediates interferon beta (IFNβ) production, particularly in myeloid cells.[66] Several members of the DexD/H-box helicases (DDX) family bind DNA ligands and induce pro-inflammatory cytokine production. DDX60 binds both RNA and DNA[67] and is required for RIG-1/DDX58 upregulation of Type I interferon gene expression.[68] RIG-I can be activated indirectly by cytosolic DNA when RNA polymerase III transcribes DNA into its activator, dsRNA containing a 5' triphosphate.[69] Additional DNA binding proteins putatively mediating inflammatory have been described. Binding of DNA to Ku70, a component of DNA protein kinase induces the production of Type III, not Type I interferon.[70] IFNβ is produced after DNA binding by cyclic GMP-AMP synthase (cGAS).[71] The synthesized cGAMP acts as a second messenger required for STING (stimulator of IFN genes)-dependent IFNβ production. Recent literature highlights STING as the central regulator of cytosolic DNA sensing and downstream innate immune signalling, orchestrating the induction of type I interferons and proinflammatory cytokines.[72,73] The readers can find more extensive knowledge on DNA sensors in other reviews.[20,22,62]

Activation of DNA sensing after plasmid DNA GET

Non-viral gene therapies induce cells to produce inflammatory molecules, and this effect was extensively studied by our research group after plasmid DNA GET.[74-79] In our experiments, we found that after GET of non-coding plasmid DNA, some mouse melanoma [75,77,80] and sarcoma tumours[81] completely regressed. Similar observations were also made by other groups investigating *in vivo* GET.[82-87] Tumour regression required the presence of both electric pulses and DNA, although inclusion of a therapeutic gene was not essential. The extent of regression correlated with the plasmid DNA concentration and the specific electric pulse parameters applied. Elevated levels of inflammatory proteins were associated with this regression, indicating that inflammation may play a contributory role.[88]

Because GET introduces DNA into both the cytosol and endosomes of the cell, we wondered whether the observed inflammation results from activation of the well-established endosomal PRR TLR9 or from the more recently identified cytosolic DNA sensors in tumour cells. Because DNA sensors are expressed across various cell types, the profile of downstream regulated proteins likely depends on the cellular composition of the target tissue. We have demonstrated that, while TLR9 mRNA levels were unchanged after DNA GET, mRNA levels of specific DNA sensors (ZBP1, ddx60 and ifi204) and IFNβ1 were upregulated in tumour cells, which could be the mechanism behind the observed anti-tumour effects of DNA GET.[76-78] We have demonstrated this observation in WEHI164 fibrosarcoma cells, TS/A mammary adenocarcinoma cells[76] and in B16F10 melanoma

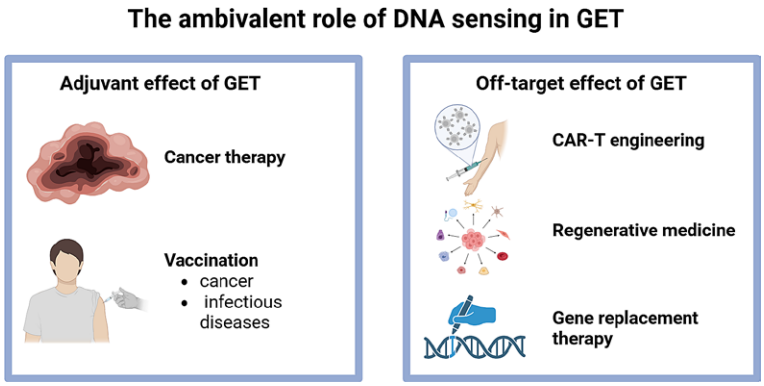

FIGURE 3. Ambivalent role of DNA sensing in plasmid DNA gene electrotransfer (GET), acting as a positive or negative ally. Created in BioRender. Cemazar, M. (2025) https://BioRender.com/zqbdsxi

cells[78], spheroids[89] and tumours.[75,77,80,88] B16F10 tumours respond to plasmid DNA GET with the production of several pro-inflammatory cytokines and chemokines and ifi204 mRNA upregulation.[77]

When comparing GET with an empty plasmid to that with a plasmid encoding IL-12 in B16F10 and CT26 tumour cells, we observed that both plasmids induced an increase in mRNA levels of several DNA sensors, many of which are associated with cell death, most prominent among them DDX60 and ZBP1.[79] However, cytokine profiling showed that some cytokines were expressed only after GET with the therapeutic IL-12 plasmid.[79] This indicates that the cellular response to plasmid GET is multilayered, involving activation of multiple signalling cascades. Importantly, IL-12 GET led to the induction of two inducible damage-associated molecular patterns (iDAMPs), IL-6 and TNF-α. The presence of these iDAMPs suggests that therapeutic GET provides a dual advantage: not only are constitutive DAMPs released from dying cells, but tumour-resident antigen-presenting cells such as dendritic cells and macrophages can also be activated by iDAMPs, thereby promoting efficient $CD8^+$ T-cell cross-priming within the tumour microenvironment.[90,91]

Further, we were also interested in the applications of DNA GET in muscle or in the skin for applications of DNA vaccination. C2C12 myoblasts reacted robustly to backbone plasmid DNA GET and the effect was more pronounced as in tumour cells. IFNβ mRNA was upregulated four hours after GET and protein levels mirror this upregulation, suggesting DNA sensor activation.[74] This correlated with significant increases in the mRNAs of DNA sensors ZBP1, DDX60 and ifi204. Other DNA sensors, specifically DDX41, DHX9, DHX36, Ku70, MRE11, PQBP1 and cGAS, were detected in these cells but not upregulated, while RIG-I and TLR9 were not detected. This mRNA upregulation was also reflected in protein levels. An increase in IFNβ mRNA also occurred after delivery using another method of non-viral delivery, a non-liposomal formulation comprised of a lipid and a protein/polyamine mixture. This upregulation was paralleled by the upregulation of a similar repertoire of DNA sensors mRNAs, supporting the concept that this effect is not limited to GET and is universal after gene delivery.[74] In myoblasts we also demonstrated that upregulation of mRNAs and proteins do not necessarily predict DNA detection and binding. We revealed early events upon plasmid DNA entrance into the cell and identified ZBP1, ifi204, and DHX9 as early plasmid DNA binding proteins.[74]

Since myoblasts in culture respond strongly to plasmid DNA GET with the DNA sensor-dependent production of pro-inflammatory proteins, it is possible that this pathway is responsible for the inflammation observed after intramuscular delivery *in vivo*. Inflammation associated with DNA GET was demonstrated to increase vaccine therapeutic efficacy and this effect was initially described nearly 20 years ago.[92-94] The activation of the innate immune response can therefore influence the vaccination efficiency and should be considered when developing gene therapy drug products for vaccination purposes. This response is not limited to DNA delivery by GET but is rather ubiquitous to all types of viral and non-viral delivery methods that deliver nucleic acids into the cell cytosol.

Building on these findings, we extended our investigation of DNA sensing to the skin as an organ for DNA vaccination. The skin is the body's largest and one of its most immunologically active organs, serving not only as a physical barrier but also as an interface rich in innate and adaptive immune elements. Its complex cellular architecture comprising keratinocytes, fibroblasts, and immune cells makes it a particularly suitable site for GET, where the delivery of plasmid DNA can trigger diverse intracellular signalling pathways depending on cell type. Our studies demonstrated that noncoding plasmid DNA GET activates cytosolic DNA sensing mechanisms in skin cells, similar to those previously observed in muscle and tumour models. Specifically, qPCR analysis revealed the upregulation of DDX60, AIM2, ZBP1, ifi202, and ifi204 mRNAs in keratinocytes, and of DDX60, ZBP1, and ifi204 in fibroblasts.[95] These transcriptional changes were accompanied by increased production of

cytokines and chemokines, confirming a strong innate immune activation following DNA GET. In vivo experiments in mouse skin further supported these results, showing elevated expression of DNA sensor mRNA and pro-inflammatory cytokines IFN-β1, TNFα and Il-1β. IFN-β1 and TNFα were immunohistologically detected in fibroblasts, keratinocytes and macrophages in skin which correlated with our observed gene and protein expression *in vitro* and *in vivo*. In contrast, Il-1β was detected in keratinocytes and macrophages but not in fibroblasts, which also correlated with *in vitro* results. Thus, immunofluorescent staining identified keratinocytes, fibroblasts, and macrophages as principal contributors to the local immune response to plasmid DNA GET.

The ambivalent role of DNA sensing in plasmid DNA GET

The widespread presence of DNA sensors across mammalian cell types underscores the complex and context-dependent nature of the innate immune response to plasmid DNA GET. Tumour, muscle, and skin cells each exhibit distinct transcriptional and cytokine response profiles following DNA delivery, reflecting tissue-specific engagement of cytosolic DNA sensing pathways. This cellular diversity presents both an opportunity and a challenge on one hand, it allows for the exploitation of tissue-specific immunogenicity to enhance therapeutic outcomes, while on the other, it complicates the prediction of the *in vivo* responses. Collectively, current evidence indicates that the antitumour and immunostimulatory effects of plasmid DNA GET are not entirely dependent on the encoded therapeutic gene but can arise intrinsically from the introduction of nucleic acid itself. This intrinsic immunogenicity, mediated through activation of DNA sensors and subsequent cytokine production, can be regarded as an adjuvant effect that potentiates immune activation, leading to more potent antitumour or vaccination effects (Figure 3).

However, this activation not only triggers a strong innate immune response but also leads to various forms of cell death, depending on the cell type and intensity of stimulation. While cell death is highly advantageous in the context of antitumour therapy, where the release DAMPs and cytokines enhance immune activation and tumour clearance, it poses a significant limitation in applications where cell survival and functionality are required, such as engineering of CAR-T cells, regenerative medicine or gene replacement therapy (Figure 3).[96-98] A notable example is CAR-T cell therapy, in which efficient gene delivery must be achieved without compromising T-cell viability, proliferation, and effector function. In this setting, excessive activation of DNA sensing pathways or strong GET parameters can impair cell viability and reduce therapeutic potency. Therefore, careful optimization of both the vector design to minimize immunostimulatory motifs and improve expression efficiency and the electric parameters to balance membrane permeability and cell survival is essential to ensure successful transfection while preserving cell viability.

Conclusions

In summary, DNA sensing pathway activation represents both an opportunity and a challenge in GET-based applications. When harnessed appropriately, the resulting inflammation and cell death can act as an intrinsic adjuvant effect, amplifying the therapeutic outcome in cancer treatment and DNA vaccination. Conversely, when gene delivery aims to produce functional proteins in viable cells, as in CAR-T cell engineering, gene replacement therapy or regenerative medicine, such immune activation and cytotoxicity may become detrimental. It is therefore critical to tailor gene delivery strategies to the intended biological goal leveraging the adjuvant properties of DNA sensing in immunogenic applications, while minimizing off-target effects and preserving cell viability in cases requiring sustained cellular function.

Acknowledgements

The authors acknowledge the financial support from the Slovenian Research and Innovation Agency (program No. P3-0003, project number J3-50111).

References

1. Bulaklak K, Gersbach CA. The once and future gene therapy. *Nat Commun* 2020; **11:** 5820. doi: 10.1038/s41467-020-19505-2
2. ASGCT. Gene, Cell and RNA Therapy Landscape Report, Q2 2025 Quarterly Data Report. *American Society of Gene & Cell Therapy.* [internet]. [cited 2025 Oct 15]. Available at: https://asgct.org/publications/landscape-report
3. Lopes A, Vandermeulen G, Préat V. Cancer DNA vaccines: current preclinical and clinical developments and future perspectives. *J Exp Clin Cancer Res* 2019; **38:** 146. doi: 10.1186/s13046-019-1154-7

4. Belete TM. The current status of gene therapy for the treatment of cancer. *Biologics* 2021; **15:** 67-77. doi: 10.2147/BTT.S302095

5. Romano G, Marino IR, Pentimalli F, Adamo V, Giordano A. Insertional mutagenesis and development of malignancies induced by integrating gene delivery systems: implications for the design of safer gene-based interventions in patients. *Drug News Perspect* 2009; **22:** 185-96. doi: 10.1358/dnp.2009.22.4.1367704

6. Shirley JL, de Jong YP, Terhorst C, Herzog RW. Immune responses to viral gene therapy vectors. *Mol Ther* 2020; **28:** 709-22. doi: 10.1016/j.ymthe.2020.01.001

7. Maurya S, Sarangi P, Jayandharan GR. Safety of Adeno-associated virus-based vector-mediated gene therapy-impact of vector dose. *Cancer Gene Ther* 2022; **29:** 1305-6. doi: 10.1038/S41417-021-00413-6.

8. Bulcha JT, Wang Y, Ma H, Tai PWL, Gao G. Viral vector platforms within the gene therapy landscape. *Signal Transduct Target Ther* 2021; **6:** 53. doi: 10.1038/s41392-021-00487-6

9. Mohammadinejad R, Dehshahri A, Sagar Madamsetty V, Zahmatkeshan M, Tavakol S, Makvandi P, et al. In vivo gene delivery mediated by non-viral vectors for cancer therapy. *J Control Release* 2020; **325:** 249-75. doi: 10.1016/j.jconrel.2020.06.038

10. Durymanov M, Reineke J. Non-viral delivery of nucleic acids: insight into mechanisms of overcoming intracellular barriers. *Front Pharmacol* 2018; **21:** 971. doi: 10.3389/fphar.2018.00971

11. Sachdev S, Potočnik T, Rems L, Miklavčič D. Revisiting the role of pulsed electric fields in overcoming the barriers to in vivo gene electrotransfer. *Bioelectrochemistry* 2022; **144:** 107994. doi: 10.1016/j.bioelechem.2021.107994

12. Rakoczy K, Kisielewska M, Sędzik M, Jonderko L, Celińska J, Sauer N, et al. Electroporation in clinical applications – the potential of gene electrotransfer and electrochemotherapy. *Appl Sci* 2022*;* **12:** 10821. doi: 10.3390/app122110821

13. Strojan P, Jesenko T, Omerzel M, Jamsek C, Groselj A, Lampreht Tratar U, et al. Phase I trial of phIL12 plasmid intratumoral gene electrotransfer in patients with basal cell carcinoma in head and neck region. *Eur J Surg Oncol* 2025; **51:** 109574. doi: 10.1016/j.ejso.2025.109574

14. Daud AI, DeConti RC, Andrews S, Urbas A, Riker AI, Sondak VK, et al. Phase I trial of interleukin-12 plasmid electroporation in patients with metastatic melanoma. *J Clin Oncol* 2008; **26:** 5896-903. doi: 10.1200/JCO.2007.15.6794

15. Spanggaard I, Snoj M, Cavalcanti A, Bouquet C, Sersa G, Robert C, *et al.* Gene electrotransfer of plasmid antiangiogenic metargidin peptide (AMEP) in disseminated melanoma: safety and efficacy results of a phase I first-in-man study. *Hum Gene Ther Clin Dev* 2013; **24:** 99-107. doi: 10.1089/humc.2012.240

16. Yu G, Ye Z, Yuan Y, Wang X, Li T, Wang Y, et al. Recent advancements in biomaterials for chimeric antigen receptor T cell immunotherapy. *Biomater Res* 2024; **15:** 0045. doi: 10.34133/bmr.0045

17. Vanpouille-Box C, Demaria S, Formenti SC, Galluzzi L. Cytosolic DNA sensing in organismal tumor control. *Cancer Cell* 2018; **34**: 361-78. doi: 10.1016/j.ccell.2018.05.013

18. Zindel J, Kubes P. DAMPs, PAMPs, and LAMPs in immunity and sterile inflammation. *Annu Rev Pathol* 2020; **15**: 493-518. doi: 10.1146/annurev-pathmechdis-012419-032847

19. Pisetsky DS. The origin and properties of extracellular DNA: from PAMP to DAMP. *Clin Immunol* 2012; **144:** 32-40. doi: 10.1016/j.clim.2012.04.006

20. Yu L, Liu P. Cytosolic DNA sensing by cGAS: regulation, function, and human diseases. *Signal Transduct Target Ther* 2021; **6:** 170. doi: 10.1038/s41392-021-00554-y

21. Elkon KB. Review: Cell death, nucleic acids, and immunity: inflammation beyond the grave. *Arthritis Rheumatol* 2018; **70:** 805-16. doi: 10.1002/art.40452

22. Maelfait J, Liverpool L, Rehwinkel J. Nucleic acid sensors and programmed cell death. *J Mol Biol* 2020; **432:** 552-68. doi: 10.1016/j.jmb.2019.11.016

23. Galluzzi L, Buqué A, Kepp O, Zitvogel L, Kroemer G. Immunogenic cell death in cancer and infectious disease. *Nat Rev Immunol* 2017; **17:** 97-111. doi: 10.1038/nri.2016.107

24. Algazi A, Bhatia S, Agarwala S, Molina M, Lewis K, Faries M, et al. Intratumoral delivery of tavokinogene telseplasmid yields systemic immune responses in metastatic melanoma patients. *Ann Oncol* 2020; **31:** 532-40. doi: 10.1016/j.annonc.2019.12.008

25. Canton DA, Shirley S, Wright, Connolly R, Burkart C, Mukhopadhyay A, et al. Melanoma treatment with intratumoral electroporation of tavokinogene telseplasmid (pIL-12, tavokinogene telseplasmid). *Immunotherapy* 2017; **9:** 1309-21. doi: 10.2217/imt-2017-0096

26. Dollin Y, Rubin J, Carvajal RD, Rached H, Nitzkorsk JR. Pembrolizumab and tavokinogene telseplasmid electroporation in metastatic melanoma. *Int J Surg Case Rep* 2020; **77:** 591-4. doi: 10.1016/j.ijscr.2020.11.063

27. Tarhini AA, Eroglu Z, Eljilany I, Zager JS, Gonzales RJ, Sarnaik AA, et al. Neoadjuvant intratumoral plasmid IL-12 electro-gene-transfer and nivolumab in patients with operable, locoregionally advanced melanoma. *Clin Cancer Res* 2024; **30:** 5333-41. doi: 10.1158/1078-0432.CCR-24-2768

28. Telli ML, Nagata H, Wapnir I, Acharya CR, Zablotsky K, Fox BA, et al. Intratumoral plasmid IL12 expands CD8 + T cells and induces a CXCR3 gene signature in triple-negative breast tumors that sensitizes patients to Anti-PD-1 therapy. *Clin Cancer Res* 2021; **27**, 2481-93. doi: 10.1158/1078-0432.CCR-20-3944

29. Spanggaard I, Dahlstroem K, Laessoee L, Hansen RH, Johannesen HH, Hendel HW, et al. Gene therapy for patients with advanced solid tumors: a phase I study using gene electrotransfer to muscle with the integrin inhibitor plasmid AMEP. *Acta Oncol* 2017; **56:** 909-16. doi: 10.1080/0284186X.2017.1315171

30. Kim TJ, Jin H, Hur S, Yang HG, Seo YB, Hong SR, *et al.* Clearance of persistent HPV infection and cervical lesion by therapeutic DNA vaccine in CIN3 patients. *Nat Commun* 2014; **5:** 5317. doi: 10.1038/ncomms6317

31. Bhuyan PK, Dallas M, Kraynyak K, Herring T, Morrow M, Boyer J, et al. Durability of response to VGX-3100 treatment of HPV16/18 positive cervical HSIL. *Hum Vaccin Immunother* 2021; **17:** 1288-93. doi: 10.1080/21645515.2020.1823778

32. Teixeira L, Medioni J, Garibal J, Adotevi O, Doucet L, Dragon Durey M, et al. A first-in-human phase I study of INVAC-1, an optimized human telomerase DNA vaccine in patients with advanced solid tumors. *Clin Cancer Res* 2020; **26:** 588-97. doi: 10.1158/1078-0432.CCR-19-1614

33. Tebas P, Kraynyak KA, Patel A, Maslow JN, Morrow MP, Sylvester AJ, et al. Intradermal SynCon® ebola GP DNA vaccine is temperature stable and safely demonstrates cellular and humoral immunogenicity advantages in healthy volunteers. *J Infect Dis* 2019; **220:** 400-10. doi: 10.1093/infdis/jiz132

34. Kraynyak KA, Blackwood E, Agnes J, Tebas P, Giffear M, Amante D, et al. SARS-CoV-2 DNA vaccine INO-4800 induces durable immune responses capable of being boosted in a phase 1 open-label trial. *J Infect Dis* 2022; **225:** 1923-32. doi: 10.1093/infdis/jiac016

35. Neumann E, Rosenheck K. Permeability changes induced by electric impulses in vesicular membranes. *J Membr Biol* 1972; **10:** 279-90. doi: 10.1007/BF01867861

36. Wolf H, Rols M, Boldt E, Neumann E, Teissié J. Control by pulse parameters of electric field-mediated gene transfer in mammalian cells. *Biophys J* 1994; **66:** 524-31. doi: 10.1016/s0006-3495(94)80805-7

37. Potočnik T, Maček Lebar A, Kos Š, Reberšek M, Pirc E, Serša G, et al. Effect of experimental electrical and biological parameters on gene transfer by electroporation: a systematic review and meta-analysis. *Pharmaceutics* 2022; **14:** 2700. doi: 10.3390/pharmaceutics14122700.

38. Neumann E, Schaefer-Ridder M, Wang Y, Hofschneider PH. Gene transfer into mouse lyoma cells by electroporation in high electric fields. *EMBO J* 1982; **1:** 841-5. doi: 10.1002/j.1460-2075.1982.tb01257.x

39. Batista Napotnik T, Miklavčič D. In vitro electroporation detection methods. An overview. *Bioelectrochemistry* 2018; **120:** 166-82. doi: 10.1016/j.bioelechem.2017.12.005

40. Kotnik T, Rems L, Tarek M, Miklavcic D. Membrane electroporation and electropermeabilization: Mechanisms and models. *Annu Rev Biophys* 2019; **48:** 63-91. doi: 10.1146/annurev-biophys-052118-115451

41. Krassowska W, Filev PD. Modeling electroporation in a single cell. *Biophys J* 2007; **92:** 404-17. doi: 10.1529/biophysj.106.094235

42. Paganin-Gioanni A, Bellard E, Escoffre JM, Rols M, Teissié J, Golzio M. Direct visualization at the single-cell level of siRNA electrotransfer into cancer cells. *Proc Natl Acad Sci U S A* 2011; **108:** 10443-7. doi: 10.1073/pnas.1103519108

43. Wu M, Yuan F. Membrane binding of plasmid DNA and endocytic pathways are involved in electrotransfection of mammalian cells. *PLoS One* 2011; **6:** e20923. doi: 10.1371/journal.pone.0020923

44. Rosazza C, Phez E, Escoffre J, Cézanne L, Zumbusch A, Rols M. Cholesterol implications in plasmid DNA electrotransfer: evidence for the involvement of endocytotic pathways. *Int J Pharm* 2012; **423:** 134-43. doi: 10.1016/j.ijpharm.2011.05.024

45. Markelc B, Skvarca E, Dolinsek T, Prevodnik Kloboves V, Coer A, Sersa G, et al. Inhibitor of endocytosis impairs gene electrotransfer to mouse muscle in vivo. *Bioelectrochemistry* 2015; **103:** 111-9. doi: 10.1016/j.bioelechem.2014.08.020

46. Rosazza C, Buntz A, Rieß T, Wöll D, Zumbusch A, Rols M. Intracellular tracking of single-plasmid DNA particles after delivery by electroporation. *Molecular Therapy* 2013; **21:** 2217-26. doi: 10.1038/mt.2013.182

47. Rosazza C, Escoffre JM, Zumbusch A, Rols M. The actin cytoskeleton has an active role in the electrotransfer of plasmid DNA in mammalian cells. *Molecular Therapy* 2011; **19:** 913-21. doi: 10.1038/mt.2010.303

48. Rosazza C, Deschout H, Buntz A, Braeckmans K, Rols M, Zumbusch A. Endocytosis and endosomal trafficking of DNA after gene electrotransfer in vitro. *Mol Ther Nucleic Acids* 2016; **5:** e286. doi: 10.1038/mtna.2015.59

49. Pérez-Martínez FC, Guerra J, Posadas I, Ceña V. Barriers to non-viral vector-mediated gene delivery in the nervous system. *Pharm Res* 2011; **28:** 1843-58. doi: 10.1007/s11095-010-0364-7

50. Cervia LD, Chang CC, Wang L, Mao M, Yuan F. Enhancing electrotransfection efficiency through improvement in nuclear entry of plasmid DNA. *Mol Ther Nucleic Acids* 2018; **11:** 263-71. doi: 10.1016/j.omtn.2018.02.009

51. Rigby RE, Webb LM, Mackenzie KJ, Li Y, Leitch A, Reijns MAM, et al. RNA:DNA hybrids are a novel molecular pattern sensed by TLR9. *EMBO J* 2014; **33:** 542-58. doi: 10.1002/embj.201386117

52. Hemmi H, Takeuchi O, Kawai T, Kaisho T, Sato S, Sanjo H, et al. A Toll-like receptor recognizes bacterial DNA. *Nature* 2000; **408:** 740-5. doi: 10.1038/35047123

53. Fukuda K. Immune regulation by cytosolic DNA sensors in the tumor microenvironment. *Cancers (Basel)* 2023; **15:** 2114. doi: 10.3390/cancers15072114

54. Thompson MR, Kaminski JJ, Kurt-Jones EA, Fitzgerald KA. Pattern recognition receptors and the innate immune response to viral infection. *Viruses* 2011; **3:** 920-40. doi: 10.3390/v3060920

55. Minamitani T, Iwakiri D, Takada K. Adenovirus virus-associated RNAs induce type I interferon expression through a RIG-I-mediated pathway. *J Virol* 2011; **85:** 4035-40. doi: 10.1128/JVI.02160-10

56. Yu X, Wang H, Li X, Guo C, Yuan F, Fisher PB, et al. Activation of the MDA-5-IPS-1 viral sensing pathway induces cancer cell death and type I IFN-dependent antitumor immunity. *Cancer Res* 2016; **76:** 2166-76. doi: 10.1158/0008-5472.CAN-15-2142

57. Eichholz K, Bru T, Phuong Tran TT, Fernandes P, Welles H, Mennechet FJD, et al. Immune-complexed adenovirus induce AIM2-mediated pyroptosis in human dendritic cells. *PLoS Pathog* 2016; **12:** e1005871. doi: 10.1371/journal.ppat.1005871

58. Suzuki M, Bertin TK, Rogers GL, Cela RC, Zolotukhin I, Palmer DJ, et al. Differential type I interferon-dependent transgene silencing of helper-dependent adenoviral vs. adeno-associated viral vectors in vivo. *Mol Ther* 2013; **21:** 796-805. doi: 10.1038/mt.2012.277

59. Colella P, Ronzitti G, Mingozzi F. Emerging issues in AAV-mediated in vivo gene therapy. *Mol Ther Methods Clin Dev* 2017; **8**: 87-104. doi: 10.1016/j.omtm.2017.11.007

60. Sandstrom TS, Ranganath N, Angel JB. Impairment of the type I interferon response by HIV-1: Potential targets for HIV eradication. *Cytokine Growth Factor Rev* 2017, **37:** 1-16. doi: 10.1016/j.cytogfr.2017.04.004

61. Roers A, Hiller B, Hornung V. Recognition of endogenous nucleic acids by the innate immune system. *Immunity* 2016; **44:** 739-54. doi: 10.1016/j.immuni.2016.04.002

62. Okude H, Ori D, Kawai T. Signaling through nucleic acid sensors and their roles in inflammatory diseases. *Front Immunol* 2021; **11:** 625833. doi: 10.3389/fimmu.2020.625833

63. Takaoka A, Wang Z, Choi MK, Yanai H, Negishi H, Ban T, et al. DAI (DLM-1/ZBP1) is a cytosolic DNA sensor and an activator of innate immune response. *Nature* 2007; **448:** 501-5. doi: 10.1038/nature06013

64. Hornung V, Ablasser A, Charrel-Dennis M, Bauernfeind F, Horvath G, Caffrey DR, et al. AIM2 recognizes cytosolic dsDNA and forms a caspase-1-activating inflammasome with ASC. *Nature* 2009; **458**: 514-8. doi: 10.1038/nature07725

65. Fernandes-Alnemri T, Yu JW, Datta P, Wu J, Alnemri ES. AIM2 activates the inflammasome and cell death in response to cytoplasmic DNA. *Nature* 2009; **458:** 509-13. doi: 10.1038/nature07710

66. Unterholzner L, Keating SE, Baran M, Horan KA, Jensen SB, Sharma S, et al. IFI16 is an innate immune sensor for intracellular DNA. *Nat Immunol* 2010; **11:** 997-1004. doi: 10.1038/ni.1932

67. Miyashita M, Oshiumi H, Matsumoto M, Seya T. DDX60, a DEXD/H box helicase, is a novel antiviral factor promoting RIG-I-like receptor-mediated signaling. *Mol Cell Biol* 2011; **31:** 3802-19. doi: 10.1128/MCB.01368-10

68. Choi MK, Wang Z, Ban T, Yanai H, Lu Y, Koshiba R, et al. A selective contribution of the RIG-I-like receptor pathway to type I interferon responses activated by cytosolic DNA. *Proc Natl Acad Sci U S A* 2009; **106:** 17870-5. doi: 10.1073/pnas.0909545106

69. Ablasser A, Bauernfeind F, Hartmann G, Latz E, Fitzgerald KA, Hornung V. RIG-I-dependent sensing of poly(dA:dT) through the induction of an RNA polymerase III-transcribed RNA intermediate. *Nat Immunol* 2009; **10**: 1065-72. doi: 10.1038/ni.1779

70. Zhang X, Brann TW, Zhou M, Yang J, Oguariri RM, Lidie KB, et al. Cutting edge: Ku70 is a novel cytosolic DNA sensor that induces type III rather than type I IFN. *J Immunol* 2011; **186:** 4541-5. doi: 10.4049/jimmunol.1003389

71. Sun L, Wu J, Du F, Chen X, Chen ZJ. Cyclic GMP-AMP synthase is a cytosolic DNA sensor that activates the type I interferon pathway. *Science* 2013; **339:** 786-91. doi: 10.1126/science.1232458

72. Motwani M, Pesiridis S, Fitzgerald KA. DNA sensing by the cGAS-STING pathway in health and disease. *Nat Rev Genet* 2019; **20:** 657-74. doi: 10.1038/s41576-019-0151-1

73. Dvorkin S, Cambier S, Volkman HE, Stetson DB. New frontiers in the cGAS-STING intracellular DNA-sensing pathway. *Immunity* 2024; **57:** 718-30. doi: 10.1016/j.immuni.2024.02.019

74. Semenova N, Bosnjak M, Markelc B, Znidar K, Cemazar M, Heller L. Multiple cytosolic DNA sensors bind plasmid DNA after transfection. *Nucleic Acids Res* 2019; **47:** 10235-46. doi: 10.1093/nar/gkz768

75. Heller L, Todorovic V, Cemazar M. Electrotransfer of single-stranded or double-stranded DNA induces complete regression of palpable B16.F10 mouse melanomas. *Cancer Gene Ther* 2013; **20:** 695-700. doi: 10.1038/cgt.2013.71

76. Znidar K, Bosnjak M, Semenova N, Pakhomova O, Heller L, Cemazar M. Tumor cell death after electrotransfer of plasmid DNA is associated with cytosolic DNA sensor upregulation. *Oncotarget* 2018; **9:** 18665–18681. doi: 10.18632/oncotarget.24816

77. Bosnjak M, Jesenko T, Kamensek U, Sersa G, Lavrencak J, Heller L, et al. Electrotransfer of different control plasmids elicits different antitumor effectiveness in B16.F10 melanoma. *Cancers (Basel)* 2018; **10:** 37. doi: 10.3390/cancers10020037

78. Znidar K, Bosnjak M, Cemazar M, Heller LC. Cytosolic DNA sensor upregulation accompanies DNA electrotransfer in B16.F10 melanoma cells. *Mol Ther Nucleic Acids* 2016; **5:** e322. doi: 10.1038/mtna.2016.34

79. Medved A, Omerzel M, Jesenko T, Bucek S, Sersa G, Cemazar M. Expression of inducible damage-associated molecular patterns after interleukin-12 gene electrotransfer in mouse melanoma and colorectal cell lines. *Biomed Pharmacother* 2025; **190:** 118414. doi: 10.1016/j.biopha.2025.118414

80. Heller L, Coppola D. Electrically mediated delivery of vector plasmid DNA elicits an antitumor effect. *Gene Ther* 2002; **9:** 1321-5. doi: 10.1038/sj.gt.3301802

81. Grosel A, Sersa G, Kranjc S, Cemazar M. Electrogene therapy with p53 of murine sarcomas alone or combined with electrochemotherapy using cisplatin. *DNA Cell Biol* 2006; **25**: 674-83. doi: 10.1089/dna.2006.25.674

82. Marrero B, Shirley S, Heller R. Delivery of interleukin-15 to B16 melanoma by electroporation leads to tumor regression and long-term survival. *Technol Cancer Res Treat* 2014; **13:** 551-60. doi: 10.7785/tcrtexpress.2013.600252

83. Ugen KE, Kutzler MA, Marrero B, Westover J, Coppola D, Weiner DB*, et al.* Regression of subcutaneous B16 melanoma tumors after intratumoral delivery of an IL-15-expressing plasmid followed by in vivo electroporation. *Cancer Gene Ther* 2006; **13:** 969-74. doi: 10.1038/sj.cgt.7700973

84. McCray AN, Ugen KE, Muthumani K, Kim JJ, Weiner DB, Heller R. Complete regression of established subcutaneous B16 murine melanoma tumors after delivery of an HIV-1 Vpr-expressing plasmid by in vivo electroporation. *Mol Ther* 2006; **14:** 647-55. doi: 10.1016/j.ymthe.2006.06.010.

85. Radkevich-Brown O, Piechocki MP, Back JB, Weise AM, Pilon-Thomas S, Wei W. Intratumoral DNA electroporation induces anti-tumor immunity and tumor regression. *Cancer Immunol Immunother* 2010; **59:** 409-17. doi: 10.1007/s00262-009-0760-1

86. Forde PF, Hall LJ, de Kruijf M, Bourke MG, Doddy T, Sadadcharm M, et al. Non-viral immune electrogene therapy induces potent antitumour responses and has a curative effect in murine colon adenocarcinoma and melanoma cancer models. *Gene Ther* 2015; **22:** 29-39. doi: 10.1038/gt.2014.95

87. Forde PF, Sadadcharam M, Hall LJ, O' Donovan TR, de Kruijf M, Byrne WL, et al. Enhancement of electroporation facilitated immunogene therapy via T-reg depletion. *Cancer Gene Ther* 2014; **21:** 349-54. doi: 10.1038/cgt.2014.35

88. Heller LC, Cruz YL, Ferraro B, Yang H, Heller R. Plasmid injection and application of electric pulses alter endogenous mRNA and protein expression in B16.F10 mouse melanomas. *Cancer Gene Ther* 2010; **17:** 864-71. doi: 10.1038/cgt.2010.43

89. Znidar K, Bosnjak M, Jesenko T, Heller LC, Cemazar M. Upregulation of DNA sensors in B16.F10 melanoma spheroid cells after electrotransfer of pDNA. *Technol Cancer Res Treat* 2018; **17:** 1533033818780088. doi: 10.1177/1533033818780088

90. Melero I, Quetglas JI, Reboredo M, Dubrot J, Rodriguez-Madoz JR, Mancheño U, et al. Strict requirement for vector-induced type I interferon in efficacious antitumor responses to virally encoded IL12. *Cancer Res* 2015; **75:** 497-507. doi: 10.1158/0008-5472.CAN-13-3356

91. Meier P, Legrand AJ, Adam D, Silke J. Immunogenic cell death in cancer: targeting necroptosis to induce antitumour immunity. *Nat Rev Cancer* 2024; **24**, 299-315. doi: 10.1038/s41568-024-00674-x

92. Babiuk S, Baca-Estrada ME, Foldvari M, Storms M, Rabussay D, Widera G, et al. Electroporation improves the efficacy of DNA vaccines in large animals. *Vaccine* 2002; **20:** 3399-408. doi: 10.1016/s0264-410x(02)00269-4

93. Babiuk LA, Pontarollo R, Babiuk S, Loehr B, van Drunen Littel-van den Hurk S. Induction of immune responses by DNA vaccines in large animals. *Vaccine* 2003; **21:** 649-58. doi: 10.1016/s0264-410x(02)00574-1

94. Lefesvre P, Attema J, van Bekkum DA. comparison of efficacy and toxicity between electroporation and adenoviral gene transfer. *BMC Mol Biol* 2002; **3:** 12. doi: 10.1186/1471-2199-3-12

95. Bosnjak M, Znidar K, Sales Conniff AS, Jesenko T, Markelc B, Semenova N, et al. In vitro and in vivo correlation of skin and cellular responses to nucleic acid delivery. *Biomed Pharmacother* 2022; **150:** 113088. doi: 10.1016/j.biopha.2022.113088

96. Hosseinkhani H, Domb AJ, Sharifzadeh G, Nahum V. Gene therapy for regenerative medicine. *Pharmaceutics* 2023; **15**: 856. doi: 10.3390/pharmaceutics15030856

97. Abdo L, Batista-Silva LR, Bonamino MH. Cost-effective strategies for CAR-T cell therapy manufacturing. *Mol Ther Oncol* 2025; **33:** 200980. doi: 10.1016/j.omton.2025.200980

98. Gibson J, Dhungana A, Pokhrel M, Arthur B, Suresh P, Adebayo O, et al. Validation of clinical-grade electroporation systems for CRISPR-Cas9-mediated gene therapy in primary hepatocytes for the correction of inherited metabolic liver disease. *Cells* 2025; **14:** 711. doi: 10.3390/cells14100711

review

Breaking the pain barrier: implantable intrathecal pump therapy as a game-changer in cancer pain management

Iztok Potocnik[1,2], Branka Strazisar[1,2], Helena Lenasi[3], Teodora Zupanc[1,2]

[1] Department of Anesthesiology, Intensive Care and Pain Therapy, Institute of Oncology Ljubljana, Ljubljana, Slovenia
[2] Department of Anesthesiology and Reanimatology, Faculty of Medicine, University of Ljubljana, Ljubljana, Slovenia
[3] Institute of Physiology, Faculty of Medicine, University of Ljubljana, Ljubljana, Slovenia

Radiol Oncol 2025; 59(4): 477-487.

Received 09 May 2025
Accepted 06 September 2025

Correspondence to: Asst. Prof. Iztok Potočnik, M.D., Ph.D., Department of Anesthesiology, Intensive Care and Pain Therapy, Institute of Oncology Ljubljana, Zaloška 2, SI-1000 Ljubljana, Slovenia. Email: ipotocnik@onko-i.si

Iztok Potocnik and Branka Strazisar contributed equally and share first authorship.

Disclosure: No potential conflicts of interest were disclosed.

Background. Chronic cancer pain, especially in advanced stages, remains a significant clinical challenge, often necessitating complex multimodal strategies. Although systemic opioids are standard therapy, many patients experience inadequate relief or adverse effects. Implantable intrathecal drug delivery systems (IDDS) have emerged as a promising alternative, enabling targeted analgesia with reduced opioid burden and improved quality of life. This narrative review summarizes current evidence on the clinical application, efficacy, safety, and cost-effectiveness of IDDS in cancer pain management. Literature sources include clinical trials, observational studies, health-economic evaluations, and international guidelines published between 2002 and 2023. A Slovenian case report is included, detailing the first national experience with IDDS implantation for refractory cancer pain. Clinical outcomes were assessed using the Visual Analogue Scale (VAS), European Organization for the Research and Treatment of Cancer Quality of Life Questionnaire (EORTC QLQ-C30), and the revised Edmonton Symptom Assessment System (r-ESAS).

Conclusions. Findings from the literature confirm that intrathecal pumps provide substantial and sustained pain relief, often with a significant reduction in systemic opioid doses and associated side effects. Compared to conventional pharmacotherapy, intrathecal delivery is associated with improved patient-reported outcomes, fewer hospitalizations, and lower long-term healthcare costs. In the Slovenian case, VAS scores decreased from > 8 to 3 shortly after implantation, with parallel improvements in quality-of-life indices. IDDS represent a clinically effective and economically sustainable option for selected patients with complex cancer pain, particularly when systemic therapy proves insufficient. Their integration into multidisciplinary palliative care pathways supports personalized, safe, and compassionate treatment approaches. By combining an evidence-based overview with real-world national experience, this review underscores the therapeutic value of intrathecal drug delivery and calls for broader clinical awareness and future research.

Key words: cancer pain; intrathecal drug delivery; implantable pumps; palliative care; opioid-sparing therapy

Introduction

The increased survival rate among cancer patients over recent decades has significantly transformed the clinical approach to cancer-related pain, shifting the primary objective from short-term symptom control to long-term management of chronic pain conditions.[1,2] As cancer increasingly becomes

a chronic illness for many, the burden of persistent pain affects a substantial proportion of patients, with direct implications for physical functioning, psychological well-being, and overall quality of life. This clinical evolution necessitates treatment modalities that not only ensure sustained analgesia but also carry a minimal side-effect profile and support the patient's autonomy and daily functioning.[3]

In this context, considerable attention has been directed toward optimizing drug delivery systems to achieve more effective and tolerable pain control. Alternative routes of administration have been widely explored to enhance the therapeutic ratio of analgesics, aiming to maintain efficacy while reducing systemic toxicity and improving patient comfort.[4,5] These strategies are especially critical in advanced or refractory cases where conventional oral or transdermal analgesics fail to provide sufficient relief or are associated with intolerable side effects.

For patients with intractable or complex pain syndromes, medications have traditionally been administered via subcutaneous infusion or directly into the central nervous system, either into the subarachnoid or epidural space. These approaches involve the use of specialized catheters and external infusion pumps designed to deliver analgesics continuously or intermittently.[6] However, despite their analgesic effectiveness, external pump systems often pose logistical challenges: frequent replacement of drug mixtures is typically required due to high infusion volumes, necessitating repeated visits to the pharmacy and healthcare providers – on average every 5 to 7 days – which can impose significant burdens on patients and caregivers alike.[7,8]

In response to these limitations, implantable intrathecal pump systems have been introduced in many developed countries, including the United States, Canada, and nations in Western Europe.[9] These systems involve the surgical implantation of a programmable pump connected to a catheter that delivers medication directly into the intrathecal space. The delivery rate can be precisely adjusted using a physician-controlled programmer, allowing individualized treatment regimens.[10] Evidence supports the use of intrathecal analgesia via implantable pumps as a safe and effective modality for managing chronic cancer pain, particularly in patients with high opioid requirements or intolerance to systemic routes.[11]

The advantages of this method over systemic and epidural analgesia are considerable. These include improved pain control with lower total drug dosages, a reduction in systemic and neurotoxic side effects, fewer complications related to catheter management, lower infection rates, and decreased need for maintenance procedures.[12] Importantly, intrathecal delivery also reduces systemic opioid exposure, which may help mitigate the risk of opioid-induced tumour progression, a phenomenon that has been associated with activation of μ-opioid receptors present on certain tumour cells.[13,14]

Cancer pain

Pain remains one of the most prevalent and distressing symptoms experienced by individuals with cancer and is a leading cause of suffering in this population. Its incidence and intensity tend to increase as the disease advances, affecting an estimated 60% to 90% of patients in the later stages of illness.[1,2] This high prevalence reflects the complex and multifactorial nature of cancer pain, which often results from a combination of direct tumour-related effects, treatment-induced injuries, and systemic consequences of malignancy. Effective management of cancer pain is not only essential for alleviating physical discomfort but is also a cornerstone of preserving patient dignity, emotional well-being, and overall quality of life.[1,2]

Cancer pain is pathophysiologically heterogeneous, encompassing a broad spectrum of mechanisms that frequently coexist in the same patient. Nociceptive pain, one of the primary components, arises from activation of pain receptors due to direct tissue injury. This may result from tumor infiltration into bones, soft tissues, visceral organs or tissue damage, caused by surgery or radiation.[1,2] In contrast, neuropathic pain stems from damage or dysfunction of the peripheral or central nervous system, often due to tumour compression of neural structures, neurotoxic effects of chemotherapy, or post-radiation nerve injury. Notably, many cancer patients experience mixed pain – a complex combination of nociceptive and neuropathic components – which complicates both diagnostic clarity and therapeutic planning.

Beyond these direct mechanisms, several additional factors modulate the perception and intensity of cancer pain. Psychological distress – including anxiety, depression, existential suffering, and anticipatory fear – has a well-documented capacity to amplify pain perception and reduce patients' coping ability. Furthermore, chronic inflammation, paraneoplastic syndromes, metabolic derangements, and immunological changes asso-

ciated with malignancy may further sensitize pain pathways or lower the threshold for nociception.[1,2]

The inherently dynamic and evolving nature of cancer pain necessitates a personalized, multidisciplinary approach to assessment and treatment. Comprehensive pain management must integrate not only pharmacological interventions tailored to the underlying pathophysiology but also address psychosocial and spiritual dimensions of the patient's experience. Early recognition and proactive treatment are therefore critical to prevent pain chronification, maintain functional capacity, and enhance the overall trajectory of care in oncology patients.[1,2]

Recommendations on cancer pain treatment

Managing chronic refractory cancer pain remains one of the most persistent and complex challenges in oncology and palliative care. Unlike many other clinical symptoms, the severity of cancer-related pain often does not exhibit a straightforward correlation with tumour burden or anatomical progression, making both assessment and treatment highly individualized and unpredictable. When left inadequately controlled, cancer pain not only impairs functional capacity and emotional resilience, but also negatively affects adherence to anticancer treatments, potentially compromising therapeutic outcomes and overall prognosis.

The World Health Organization (WHO) established a foundational framework for cancer pain management with its three-step analgesic ladder, which proposes a progressive escalation of pharmacological therapy based on pain severity: beginning with non-opioid analgesics, advancing to weak opioids for moderate pain, and strong opioids for severe pain.[1,15] More recently, this model has been conceptually expanded with the addition of a fourth step, encompassing interventional regional techniques such as peripheral nerve blocks, neuraxial analgesia, and implanted catheters (Figure 1). These interventions are intended to supplement each level of pharmacological treatment, particularly in cases where conventional therapies fail or are poorly tolerated.

However, despite the availability of this structured framework and its broad endorsement across international guidelines, a substantial proportion of cancer patients experience insufficient pain control when treated solely according to the WHO ladder.[3] Multimodal and individualized pain management strategies – integrating pharmacological, interventional, and psychosocial modalities are increasingly recognized as the gold standard, as reflected in most European and global recommendations.[2,3] Indeed, clinical studies have revealed that after four weeks of opioid-based treatment, only about 25% of cancer patients report satisfactory pain relief (VAS < 4).[4] Moreover, systemic administration of opioids is frequently accompanied by debilitating adverse effects, including nausea, vomiting, constipation, confusion, and excessive sedation, all of which can limit both adherence and tolerability.[5]

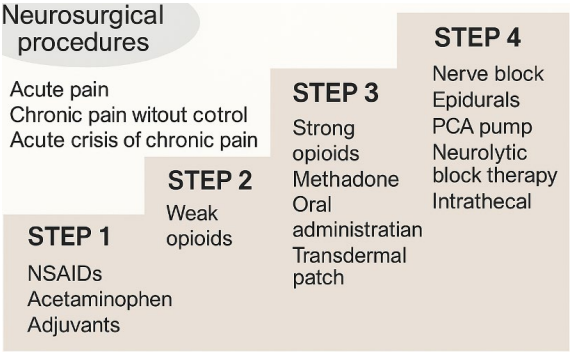

FIGURE 1. Updated WHO analgesic ladder. Stepwise model of cancer pain management, progressing from NSAIDs to intrathecal and neurosurgical interventions.

IDDS = intrathecal drug delivery system; NRS = Numerical Rating Scale; NSAIDs = nonsteroidal anti-inflammatory drugs; PCA = patient-controlled analgesia; VAS = Visual Analogue Scale; WHO = World Health Organization

A comprehensive and personalized assessment of pain is essential for effective management. This includes characterizing the intensity, location, temporal pattern, and underlying mechanisms of pain whether nociceptive, neuropathic, or mixed. Standardized assessment tools such as the VAS or the Numerical Rating Scale (NRS) allow quantifiable tracking of symptom severity over time. For mild pain, first-line agents typically include non-opioid analgesics such as acetaminophen or nonsteroidal anti-inflammatory drugs (NSAIDs). For moderate to severe pain, strong opioids – such as morphine, oxycodone, or transdermal fentanyl – are indicated, in accordance with the WHO ladder (Table 1). In cases involving neuropathic components or inflammatory pain, adjuvant agents such as antidepressants (e.g., duloxetine), anticonvulsants (e.g., gabapentin), or corticosteroids are commonly employed to enhance analgesic efficacy.

For patients with refractory or complex pain syndromes, interventional strategies become necessary. These may include neuraxial techniques

TABLE 1. Pharmacological treatment according to the WHO analgesic ladder

Mild pain	Moderate pain	Severe pain
NSAID Paracetamol Metamizole	Tramadol Codeine	Morphine Fentanyl Methadone Oxycodone Hydromorphone Buprenorphine Tapentadol

NSAIDs = nonsteroidal anti-inflammatory drugs; WHO = World Health Organization

such as epidural or intrathecal administration of analgesics, peripheral nerve blocks, or neuromodulatory interventions like spinal cord stimulation. In parallel, the integration of psychological support, structured palliative care involvement, and family-based interventions is vital to address the multifaceted emotional and existential dimensions of cancer pain.

According to the European Society for Medical Oncology (ESMO), the presence of persistent and often disabling pain – particularly in advanced disease – demands a systematic, patient-centered management approach. As survival rates improve due to advances in oncological therapies, an increasing number of patients are living with chronic pain resulting from the disease itself, its treatments, or both. Despite access to clinical guidelines and pharmacological resources, undertreatment remains widespread, due to factors including underreporting of symptoms, inadequate assessment, opioid hesitancy among clinicians, and systemic barriers to care.[16,15]

ESMO guidelines therefore strongly advocate early and proactive involvement of palliative care teams, even during the active phase of cancer treatment. This interdisciplinary model promotes regular reassessment of pain control, titration of analgesics, and aggressive management of side effects such as opioid-induced constipation and sedation – measures that significantly enhance both compliance and therapeutic outcomes. Furthermore, the guidelines highlight the critical importance of ongoing education and training for healthcare professionals to overcome clinical inertia and misconceptions surrounding opioid prescribing.[16]

Ultimately, the goal of cancer pain management extends beyond mere symptom suppression. It encompasses restoration of dignity, autonomy, and engagement in life, regardless of prognosis. Tailoring analgesic strategies to individual needs – while addressing the physical, emotional, and psychosocial domains of suffering – is fundamental to high-quality oncological and palliative care.[1,2,16]

Breakthrough pain

Managing breakthrough pain (BTP) in cancer patients presents a distinct and complex therapeutic challenge. Despite increasing clinical recognition over the past decades, persistent inconsistencies in the definition and classification of BTP continue to hinder timely diagnosis and appropriate intervention.[16] As a result, many patients endure frequent and intense pain exacerbations, often for prolonged periods and with inadequate symptom relief, even after initial identification of the condition.[16]

Breakthrough pain, first formally characterized in the 1990s, refers to transient episodes of severe pain that occur despite otherwise controlled baseline pain achieved through around-the-clock opioid therapy.[17] These episodes typically represent acute exacerbations superimposed on a stable analgesic regimen and are frequently unpredictable in onset. Epidemiological studies report that approximately 60% of patients with advanced cancer experience severe breakthrough pain (VAS > 7), and a further 30% report episodes of moderate intensity (VAS > 5).[6,7] The high prevalence and severity of BTP underscore its significant impact on patient well-being, daily functioning, and overall quality of life.

According to Rudowska's 2012 definition, breakthrough pain is characterized by sudden-onset, high-intensity pain episodes – often described as "flares" – which generally last around 30 minutes and occur in the same anatomical region as the patient's background pain.[19,18] These episodes are typically rated between 7 and 10 on the VAS, indicating severe intensity. Importantly, BTP is not merely a transient discomfort but a profound clinical event that significantly exacerbates physical suffering and psychological distress. Delays in treatment initiation or insufficient rescue medication not only prolong pain duration but also impair functional status, reduce treatment adherence, and negatively influence the overall cancer care experience.[7,8,9]

Despite effective control of background pain, breakthrough pain remains common, with up to 60% of patients in advanced stages of cancer reporting such episodes.[10,11] The episodic and often unpredictable nature of BTP necessitates rapid-onset, short-acting analgesics, tailored to the individual characteristics of each pain episode. Prompt recog-

nition and intervention are therefore paramount. In clinical practice, rescue medications – usually fast-acting opioids – are administered at the onset of a breakthrough episode to restore adequate analgesia. The choice of agent and route of administration depends on the anticipated onset, intensity, and duration of pain. Sublingual, buccal, or intranasal fentanyl preparations are commonly preferred for their rapid absorption and onset of action, making them suitable for short-lived, severe pain episodes that demand immediate relief.[12,15,16,17] For episodes with a slower onset or prolonged duration, oral morphine may be considered, although it is generally less effective for managing the sudden peaks in pain characteristic of BTP. Regardless of the pharmacological agent used, the timing of administration is critical; delays can substantially reduce efficacy and compound the patient's suffering.

Overall, the management of breakthrough pain requires not only appropriate pharmacological strategies but also ongoing patient education, routine monitoring, and anticipatory guidance. Patients and caregivers should be equipped to recognize early signs of BTP and initiate treatment promptly, ideally within minutes of onset. Integrating breakthrough pain protocols into comprehensive cancer pain management plans enhances therapeutic outcomes and aligns with the overarching goals of maintaining dignity, autonomy, and comfort throughout the cancer trajectory.[6–12,15–17]

Multimodal approach to cancer pain management

The management of chronic refractory cancer pain remains one of the most intricate and demanding aspects of oncological and palliative care. A central challenge lies in the fact that pain severity in cancer patients often does not correlate linearly with objective indicators such as tumour size or anatomical progression. This discordance complicates clinical assessment and underscores the need for individualized and dynamic treatment strategies. Inadequate control of cancer pain – whether persistent or episodic – not only compromises physical functioning and quality of life but also contributes to psychological morbidity, reduced adherence to anticancer therapies, and, ultimately, poorer clinical outcomes.[1,2]

Contemporary evidence and international guidelines strongly support the use of multimodal approaches for the management of both persistent and breakthrough cancer pain.[1,2,3] These strategies aim to address the complex and multifactorial nature of cancer-related pain by combining various therapeutic modalities, each targeting different components of the pain pathway. Effective multimodal pain management is not a one-size-fits-all approach; rather, it requires tailoring interventions to the patient's individual clinical profile, taking into account the underlying pathophysiology, psychosocial context, and treatment goals.[16]

Central to the multimodal paradigm is the integration of neuromodulatory techniques – particularly the intrathecal or epidural administration of analgesics – which enable targeted drug delivery directly into the central nervous system.[4,5] These methods offer potent analgesia with substantially reduced systemic opioid exposure and are especially valuable in patients with refractory pain who have not responded adequately to non-invasive or systemic therapies. The use of implantable pump systems for continuous intrathecal delivery has demonstrated sustained efficacy in pain relief, reduced side effects, and improved patient autonomy and quality of life.[6,9,18]

In parallel, less invasive and complementary approaches such as acupuncture, physical therapy, psychological support, and cognitive-behavioural interventions play a crucial role in enhancing analgesic outcomes and supporting the emotional and functional resilience of patients. The synergistic effect of combining pharmacological, interventional, and supportive therapies allows for improved symptom control while minimizing reliance on any single modality.[3]

The selection of an appropriate neuromodulatory technique must be guided by a comprehensive assessment of the patient's clinical condition, including pain characteristics, comorbidities, functional status, psychosocial context, and patient preferences.[18] Factors such as age, cancer type and stage, history of response to previous pain treatments, and anticipated prognosis all inform the therapeutic plan. Importantly, a thorough evaluation should extend beyond somatic symptoms to include emotional, cognitive, and spiritual domains, recognizing the total pain experience as defined in palliative medicine.

The multimodal approach places strong emphasis on personalized care, ongoing reassessment, and interdisciplinary collaboration. Pain management is most effective when delivered within a coordinated framework involving oncologists, palliative care specialists, anesthesiologists, psychologists, physiotherapists, and nursing staff. This

integrative model ensures that treatment remains aligned with evolving disease status and patient priorities. Regular review of therapeutic efficacy, tolerability, and emerging needs allows for timely adjustments and optimal resource allocation.[2,7]

Ultimately, the goal of multimodal cancer pain management is not merely to reduce pain intensity but to enhance the overall well-being, dignity, and quality of life of patients at every stage of the disease trajectory. When tailored to the unique and dynamic needs of the individual, multimodal strategies can transform the experience of pain from a source of suffering to a domain of compassionate and effective clinical care.[1,3]

Invasive techniques for cancer pain treatment

Invasive techniques constitute a vital component of cancer pain management, particularly for patients who are unable to tolerate oral medications due to side effects such as persistent nausea, vomiting, or dysphagia, as well as for those suffering from neuropathic pain unresponsive to systemic therapies. These methods provide a targeted, often more effective approach to analgesia when conventional pharmacological strategies prove inadequate. Among these, intrathecal drug administration is widely recognized for its superior efficacy and safety profile, offering several advantages over other invasive modalities, including the use of significantly lower analgesic doses, reduced systemic toxicity, fewer side effects, lower risk of infection, and improved overall pain control.[5,6,18] Additionally, minimizing systemic opioid use through intrathecal delivery may help attenuate opioid-related adverse effects and mitigate concerns about potential cancer progression driven by opioid receptor activation.

Beyond intrathecal therapy, a range of interventional pain management techniques plays a crucial role in addressing refractory cancer pain. These include nerve blocks, spinal cord stimulation (SCS), and neurolytic procedures, each offering distinct benefits based on pain type and anatomical location. Nerve blocks, administered using local anesthetics or neurolytic agents such as alcohol or phenol, can provide profound and lasting relief for well-localized cancer pain, such as that associated with pancreatic or pelvic malignancies. For instance, celiac plexus blocks are commonly employed in upper abdominal cancers, while superior hypogastric plexus blocks are indicated for pelvic tumours.[5,6,18]

Spinal cord stimulation, involving the implantation of an electrode system to deliver electrical impulses to the dorsal columns of the spinal cord, is an effective treatment for selected cases of chronic, refractory neuropathic pain, particularly when pharmacological options have been exhausted or poorly tolerated. It modulates pain signal transmission without the systemic burdens of opioid therapy and can significantly improve quality of life in patients with intractable pain syndromes.

Neurolytic procedures, aimed at ablating specific nerve pathways, are typically used for visceral pain in advanced cancer stages. Techniques such as celiac plexus or hypogastric nerve ablation are particularly effective for deep-seated abdominal or pelvic pain, offering sustained relief that may last weeks to months, thereby reducing analgesic burden and improving patient comfort.[5,6,18]

The decision to implement invasive techniques must be based on a comprehensive, multidisciplinary evaluation, considering factors such as the nature and mechanism of pain, expected prognosis, existing comorbidities, patient preferences, and overall functional and psychological status. Pre-procedural assessments, including imaging, functional testing, and temporary diagnostic blocks, are essential to predict treatment response and mitigate risks. The primary aim is not merely analgesia but the preservation of functionality, enhancement of quality of life, and support for the patient's emotional and existential well-being.[18]

Recent technological advances, including image-guided interventions and programmable intrathecal pump systems, have further refined the precision and efficacy of invasive pain control. These innovations allow for tailored targeting of pain generators and permit dynamic modulation of analgesic delivery in response to clinical changes. Integration of invasive procedures into a broader multimodal pain management framework ensures a holistic, patient-centered approach that concurrently addresses the physical, psychological, and spiritual dimensions of suffering.[5,6,18,19]

While invasive techniques are generally reserved for patients with complex, refractory, or advanced-stage pain, they have emerged as cornerstones of modern cancer pain therapy. Their success exemplifies the value of individualized, evidence-based intervention, as well as the indispensable role of ongoing research, innovation, and interdisciplinary collaboration in optimizing outcomes for cancer patients confronting intractable pain.[5,6,18,19]

Implantable intrathecal pumps

Implantable intrathecal pump systems represent a pivotal advancement in the field of cancer pain management, offering targeted, sustained analgesia for patients with refractory or complex pain syndromes. First introduced in Western Europe in 1984, these devices have progressively gained acceptance as an integral component of neuromodulatory pain therapy. In Slovenia, their use was initially established in 2001 for the treatment of spasticity and was expanded to include cancer-related analgesia in January 2024 at the Institute of Oncology, Ljubljana.[20] These systems are now recognized as a safe and effective modality for delivering analgesics directly into the intrathecal space, enabling significant reductions in drug dosage compared to systemic or parenteral administration, with a corresponding decrease in adverse effects.[20]

The implantation procedure involves the surgical insertion of a catheter into the intrathecal space, typically under general anesthesia, and the subcutaneous placement of the pump reservoir. The procedure is generally well tolerated and is performed by specialized neurosurgeons or anesthesiologists with expertise in interventional pain management. Once implanted, the system allows precise control over drug delivery, with programmable infusion parameters that can be tailored to the patient's evolving clinical needs. Moreover, many devices offer patient-controlled bolus functionality, which enables the patient to self-administer additional doses in the event of breakthrough pain, thus enhancing autonomy and responsiveness of care.

A major clinical advantage of intrathecal pump therapy is the significant reduction in systemic opioid-related side effects, particularly gastrointestinal toxicity. For example, constipation rates in patients treated with intrathecal opioids are markedly lower (7%) compared to those receiving systemic opioids (43%).[21] The reduced incidence of sedation, nausea, and cognitive impairment further supports the preference for intrathecal delivery in appropriate candidates. Additionally, due to the high concentration and low volume of medication required, the frequency of pump refills is substantially reduced, decreasing the burden on patients and caregivers and improving overall quality of life.[21]

The efficacy of intrathecal analgesia in cancer pain has been supported by clinical research. Studies conducted by Dupoiron *et al*. have demonstrated the capacity of these systems to maintain stable and long-lasting pain control while minimizing systemic opioid use and associated toxicities, thereby reinforcing their role in individualized pain management protocols.[22] Likewise, Likar *et al*. have shown that incorporating intrathecal pumps into palliative care pathways significantly improves patient outcomes in advanced cancer, where conventional pharmacotherapy frequently fails to provide adequate relief.[23]

Technological advancements have further enhanced the utility of intrathecal pump systems. Programmable pumps now allow real-time adjustment of infusion rates and regimens, offering flexibility to respond to fluctuating pain intensities in patients with complex or rapidly changing pain profiles. In addition, multidrug infusions – such as combinations of opioids with local anesthetics or adjuvants like clonidine – provide synergistic analgesic effects, allowing for more comprehensive pain modulation while minimizing single-agent toxicity.[24]

Long-term management of intrathecal systems requires ongoing interdisciplinary collaboration among oncologists, anesthesiologists, palliative care teams, and nursing staff. Regular monitoring, periodic refills, and prompt troubleshooting are essential for maintaining safety and efficacy. Despite the need for consistent follow-up, patients typically report substantial improvements in quality of life, increased mobility, and reduced emotional distress – benefits that justify the procedural and maintenance demands associated with this modality.

In conclusion, implantable intrathecal pumps are a cornerstone intervention within the multimodal framework of cancer pain management. Their effectiveness, adaptability, and patient-centered nature make them an indispensable tool, particularly in advanced-stage disease. As emphasized by Dupoiron[22] and Likar.[23], continued clinical research is essential for refining the indications, optimizing protocols, and expanding the accessibility of these devices to broader patient populations.

Cost-effectiveness of intrathecal implantable pumps

Intrathecal implantable pumps represent a sophisticated and clinically effective solution for delivering targeted analgesia in patients with severe, refractory cancer pain, particularly within palliative care and oncology settings. Although the initial

costs associated with surgical implantation and device acquisition are relatively high, a growing body of evidence suggests that intrathecal therapy is cost-effective over the long term, primarily due to its ability to reduce medication requirements, limit treatment-related complications, and decrease healthcare resource utilization.

Intrathecal drug delivery permits the direct administration of opioids and adjuvants into the cerebrospinal fluid, bypassing the systemic circulation and enabling the use of substantially lower drug doses compared to oral or parenteral routes.[24] This pharmacokinetic advantage results in lower cumulative costs for analgesics, especially in patients requiring high-dose opioid therapy over extended periods. Importantly, by reducing systemic exposure, intrathecal administration also significantly decreases the incidence and severity of opioid-related side effects such as constipation, nausea, sedation, and cognitive dysfunction, which are common drivers of additional healthcare interventions, hospital admissions, and patient distress.

Patients receiving intrathecal therapy demonstrate improved symptom control, which translates into fewer emergency department visits, unplanned hospitalizations, and reduced need for supportive care associated with uncontrolled pain.[25] These factors not only alleviate the burden on healthcare systems but also contribute to a higher quality of life and functional preservation for patients in advanced stages of disease. The capacity of intrathecal pumps to stabilize complex pain syndromes with minimal systemic burden makes them particularly valuable in resource-sensitive environments focused on optimizing both clinical outcomes and economic sustainability.

While the upfront investment in intrathecal pump therapy – including surgical placement, pump programming, and ongoing maintenance – may appear cost-prohibitive at first glance, multiple health economic evaluations have demonstrated long-term financial advantages. A landmark study by Rauck *et al*. showed that patients treated with intrathecal therapy incurred lower cumulative healthcare costs after the first year of treatment when compared with those managed with systemic opioids. These savings were attributed to reduced drug expenditures, fewer side-effect-related interventions, and a marked decrease in hospital resource consumption.[26,27]

In addition to economic benefits, the clinical efficiency of intrathecal systems justifies their integration into multimodal pain management frameworks, particularly for patients with high analgesic requirements, complex pharmacological profiles, or contraindications to systemic therapy. The long-term sustainability of these systems is further supported by advances in pump technology, which allow for programmable dose modulation, extended refill intervals, and combination drug infusions – all of which improve therapeutic precision and patient satisfaction.[24]

In summary, although intrathecal implantable pumps require initial capital investment, their ability to reduce ongoing treatment costs, improve patient outcomes, and decrease healthcare utilization supports their use as a cost-effective solution in the comprehensive management of cancer pain. As healthcare systems increasingly prioritize value-based care, intrathecal therapy stands out as a compelling option for addressing the dual imperatives of clinical efficacy and economic efficiency in advanced oncologic pain management.[24–27]

Decrease in opioid consumption with intrathecal administration

A fundamental advantage of intrathecal opioid administration lies in its ability to achieve potent analgesia with a drastically lower total opioid dose compared to systemic delivery – 100-fold or even 300-fold lower compared with oral administration.[24,26,27] This approach takes advantage of direct access to the opioid receptors located in the dorsal horn of the spinal cord, allowing for highly localized receptor activation. By bypassing first-pass hepatic metabolism and systemic distribution, intrathecal administration ensures maximal pharmacodynamic efficiency at the site of action while minimizing peripheral drug exposure. This substantial reduction in required opioid quantity translates into a marked decline in the incidence of opioid-related side effects, such as sedation, nausea, vomiting, constipation, urinary retention, and cognitive impairment, which are often dose-dependent and can severely limit the tolerability of systemic analgesic regimens.[28]

In addition to improving tolerability, lower opioid exposure also reduces the likelihood of developing opioid tolerance, which necessitates escalating doses over time and contributes to a vicious cycle of increasing toxicity and diminishing efficacy. Intrathecal therapy helps interrupt this cycle by stabilizing analgesic requirements and delaying or preventing opioid-induced hyperalgesia – a paradoxical condition in which opioids worsen rather than relieve pain. Furthermore, by minimizing systemic opioid load, intrathecal administration

may lower the risk of physical dependence and iatrogenic addiction, especially in patients requiring long-term therapy for chronic cancer pain or palliative indications.[29]

The reduction in opioid dose made possible through intrathecal administration not only enhances clinical safety and effectiveness but also contributes to cost savings by decreasing the need for adjunctive medications used to manage side effects and by reducing hospitalization rates related to opioid toxicity. The ability to deliver precisely titrated, low-dose opioid regimens tailored to patient needs makes intrathecal therapy a particularly attractive modality in complex or refractory pain syndromes.

In conclusion, intrathecal opioid delivery provides a targeted, efficient, and safer alternative to systemic opioid therapy. Its capacity to drastically reduce opioid requirements while maintaining effective analgesia supports its expanding role in the long-term management of severe cancer pain, particularly in patients for whom systemic therapy is no longer viable or tolerable.[24,26–29]

Our experiences with implantable intrathecal pumps

In Slovenia, three implantable intrathecal pumps have been successfully utilized to date. Here, we present our first case experience.

The patient was a 71-year-old female diagnosed with metastatic ocular malignant melanoma and inoperable urothelial carcinoma. She suffered from severe refractory nociceptive and neuropathic pain, significant side effects from high-dose opioid therapy, and a markedly reduced quality of life. Her pain was attributed to osteolytic metastases in the spine, radiating to the abdomen, lower extremities, and neurogenic bladder. Despite a multimodal pain management approach – including high-dose opioids, non-opioid analgesics, neuropathic agents, and adjuvants administered via various routes such as subcutaneous injections – the pain remained intractable. Palliative radiotherapy to metastatic sites was also provided.

Numerous modifications to her analgesic regimen yielded no significant relief, and her suffering became unbearable. Prior to intrathecal pump implantation, the patient's regimen included a buprenorphine transdermal patch at 105 μg/hour, oral morphine 40 mg up to four times daily for breakthrough pain, paracetamol 1000 mg every 8 hours, and mirtazapine 30 mg. Despite this, her pain intensity remained severe (VAS > 8), predominantly localized to the lower abdomen and pelvic region, with mild radiation to both lower limbs. The pain was mixed in nature – somatic, visceral, and neuropathic. She also reported burning sensations during urination and frequent urinary urgency with minimal urine output.

TABLE 2. Improvement in patients symptoms shown by EORTC QLQ-C30 questionnaire

Category	Parameter	Before (0-100)	After 3 months (0-100)
Symptoms	Pain	83.3	50
	Insomnia	100	33.3
	Appetite Loss	66.7	0
	Constipation	100	66.7
	Nausea and Vomiting	50	0
Functioning	Physical	73.3	80
	Role	66.7	100
	Emotional	0	75
	Cognitive	50	100
	Social	**50**	**100**

EORTC QLQ-C30 = European Organization for the Research and Treatment of Cancer Quality of Life Questionnarire

The implantable intrathecal pump was inserted under general anesthesia by skilled neurosurgeons at Celje General Hospital. Initially, the pump was programmed to deliver 1 mg/day of morphine and 6 mg/day of bupivacaine intrathecally. Within three days, the patient experienced substantial pain reduction, with her VAS score decreasing to 3. For breakthrough pain, sublingual fentanyl was administered alongside continued peripheral analgesics. As the disease progressed, intrathecal doses were gradually increased; clonidine (65 μg/day) was added, and morphine and bupivacaine doses were titrated to 2.6 mg/day and 19.5 mg/day, respectively.

Pain and quality of life were assessed using the VAS score, the EORTC QLQ-C30, and the revised Edmonton Symptom Assessment System.[30,31,32]

- **EORTC QLrQ-C30** is a validated multidimensional questionnaire designed to assess quality of life in cancer patients. It evaluates functional domains (physical, role, emotional, cognitive, social), symptoms (fatigue, nausea/vomiting, pain, insomnia, appetite loss, constipation), and global health status/quality of life. Higher functional scores indicate better functioning; higher symptom scores indicate greater symptom bur-

TABLE 3. Improvement in patients symptoms shown by r-ESAS questionnaire. Each symptom is rated on a scale from 0 to 10, with a higher value indicating a more severe symptom

Parameter	Before (0-10)	After 3 months (0-10)
VAS (Pain)	5	0
Fatigue	3	0
Dizziness	3	0
Nausea	2	0
Inappetence	1	0
Dyspnoea	1	0
Depression	4	0
Anxiety	4	2
Overall Well-Being	4	2

r-ESAS = revised Edmonton Symptom Assessment System

den. Higher global health status scores represent better overall quality of life and health.[31]

- **r-ESAS** is a widely used tool in palliative care for monitoring nine core symptoms on a numerical scale from 0 (none) to 10 (worst possible), plus an optional patient-defined symptom. It assesses pain, tiredness, nausea, depression, anxiety, drowsiness, appetite loss, well-being, and shortness of breath, enabling symptom tracking over time and assessment of treatment efficacy.[32]

Before pump implantation, the patient experienced opioid-related adverse effects such as constipation and dizziness due to high systemic opioid doses. Transitioning to intrathecal delivery allowed for a substantial opioid dose reduction and a corresponding decrease in side effects.

Three months post-implantation, significant improvements in quality of life were observed, reflected in both questionnaires (Tables 2 and 3). The EORTC QLQ-C30 showed improved symptom burden and functional domains. As expected, the global health status score did not improve due to disease progression and the patient's subsequent death. Nevertheless, the primary goal – enhancing quality of life – was achieved. The r-ESAS results also indicated symptom improvement.

The patient's condition gradually deteriorated with disease progression, and she passed away six months after pump implantation.

Discussion

Implantable intrathecal pumps represent a major advancement in the field of cancer pain management, offering precise, individualized, and long-term analgesia with a significantly improved side-effect profile compared to conventional systemic therapies. By delivering medication directly into the cerebrospinal fluid, these systems enable the use of substantially lower opioid doses, thus minimizing systemic exposure and associated toxicities such as sedation, nausea, and constipation. Furthermore, their programmable features and capacity for combination therapy allow for flexible, patient-centered pain control, even in cases involving complex or mixed pain mechanisms.

Globally, the adoption of implantable intrathecal pump therapy is reshaping standards in palliative oncology, offering a more effective and humane solution for both chronic baseline pain and breakthrough pain in patients with advanced disease. Our clinical experience – presented here in the form of a case report – demonstrates that intrathecal therapy can provide rapid, durable, and meaningful symptom relief, significantly enhancing quality of life in a patient suffering from refractory cancer pain. In this case, the introduction of intrathecal analgesia not only controlled previously intractable symptoms but also reduced opioid-related side effects and enabled improved functional capacity in the final months of life.

Beyond individual patient benefit, intrathecal pumps also offer systemic advantages for healthcare systems. Improved pain control reduces emergency department visits, hospital admissions, and the need for complex symptom management interventions, thereby lowering the burden on healthcare providers. Multiple cost-effectiveness studies have confirmed that, despite higher initial expenses for implantation and equipment, long-term use of intrathecal pumps results in reduced cumulative healthcare costs, particularly after the first year of therapy, owing to decreased drug use and resource utilization.

The successful implementation of the first intrathecal analgesia case in Slovenia marks a critical milestone in the integration of advanced pain management strategies within standard palliative care. This experience has laid the groundwork for broader clinical application and has prompted the development of a larger-scale study to systematically evaluate the clinical outcomes, safety, and economic impact of intrathecal pump therapy in cancer patients.

In conclusion, intrathecal therapy using implantable pumps should be regarded not only as an advanced technological intervention, but as a compassionate and evidence-based tool in the ser-

vice of alleviating suffering. As our healthcare systems evolve to meet the growing demands of aging and oncologic populations, the integration of such therapies into routine care pathways is both a clinical imperative and an ethical responsibility.

References

1. Zhang H. Cancer pain management-new therapies. *Curr Oncol Rep* 2022; **24:** 223-6. doi: 10.1007/s11912-021-01166-z
2. Bandara S, Bicket MC, McGinty EE. Trends in opioid and non-opioid treatment for chronic non-cancer pain and cancer pain among privately insured adults in the United States, 2012-2019. *PLoS ONE* 2022; **17**: e0272142. doi: 10.1371/journal.pone.0272142
3. Daud ML, Simone GG. Management of pain in cancer patients - an update. *Ecancermedicalscience* 2024; **18**: 1821. doi: 10.3332/ecancer.2024.1821
4. Bhatia G, Lau ME, Koury KM, Gulur P. Intrathecal Drug Delivery (ITDD) systems for cancer pain. *F1000Res* 2013; **2**: 96. doi: 10.12688/f1000research.2-96.v4
5. Gilmer-Hill HS, Boggan JE, Smith KA, Wagner FC Jr. Intrathecal morphine delivered via subcutaneous pump for intractable cancer pain: a review of the literature. *Surg Neurol* 1999; **51**: 12-5. doi: 10.1016/s0090-3019(98)00080-9
6. Dupoiron D, Duarte R, Carvajal G, Aubrun F, Eldabe S. Rationale and recent advances in targeted drug delivery for cancer pain: Is it time to change the paradigm? *Pain Physician* 2022; **25**: E414-E425
7. Goel V, Kaizer A, Darrow D, Rosielle D, Owens B, Blaes A. Cancer patients quality of life after intrathecal drug delivery for advanced pain management: a patient-reported outcome analysis. *Pain Med* 2025; **26**: 261-8. doi: 10.1093/pm/pnaf012
8. Green P, Schneider A, Lange J. Navigating large-volume subcutaneous injections of biopharmaceuticals: a systematic review of clinical pipelines and approved products. *MAbs* 2024; **16**: 2402713. doi: 10.1080/19420862.2024.2402713
9. Abd-Sayed A, Fiala K, Weisbein J, Chopra P, Lam C, Kalia H, et al. Intrathecal drug delivery systems survey: Trends in utilization in pain practice. *J Pain Res* 2022; **15**: 1305-14. doi: 10.2147/JPR.S344409
10. Wilkes D. Programmable intrathecal pumps for the management of chronic pain: recommendations for improved efficiency. *J Pain Res* 2014; **7:** 571-7. doi: 10.2147/JPR.S46929
11. Chalil A, Staudt MD, Harland TA, Leimer EM, Bhullar R, Argoff CE. A safety review of approved intrathecal analgesics for chronic pain management. *Expert Opin Drug Saf* 2021; **20**: 439-51. doi: 10.1080/14740338.2021.1889513
12. Perruchoud C, Dupoiron D, Papi B, Calabrese A, Brogan SE. Management of cancer-related pain with intrathecal drug delivery: A systematic review and meta-analysis of clinical studies. *Neuromodulation* 2023; **26**: 1142-52. doi: 10.1016/j.neurom.2021.12.004
13. Grandhi RK, White RS, Chen KY, Nair S, Hall C, Shaparin N. Does opioid use cause angiogenesis and metastasis? *Pain Med* 2017; **18:** 140-6. doi: 10.1093/pm/pnw161
14. Wang R, Li S, Wang B, Zheng H, Wang G. Impact of opioids and mu-opioid receptors on oncologic metastasis. *Am J Cancer Res* 2024; **14**: 4236-47. doi: 10.62347/SCLS3277
15. World Health Organization. Cancer pain relief: With a guide to opioid availability. 2nd ed. Geneva: WHO; 1996. Available from: https://apps.who.int/iris/handle/10665/37896
16. Ripamonti CI, Santini D, Maranzano E, Berti M, Roila F. Management of cancer pain: ESMO Clinical Practice Guidelines. *Ann Oncol* 2012; **23**: 139-54. doi: 10.1093/annonc/mds233
17. Sessler DI, Riedel B. Anesthesia and cancer recurrence: Context and perspective. *Anesthesiology* 2019; **130**: 3-5. doi: 10.1097/ALN.0000000000002506
18. Smith TJ, Staats PS, Deer T, Stearns LJ, Rauck RL, Boortz-Marx RL, et al. Randomized clinical trial of an implantable drug delivery system compared with comprehensive medical management for refractory cancer pain: impact on pain, drug-related toxicity, and survival. *J Clin Oncol* 2002; **20**: 4040-9. doi: 10.1200/JCO.2002.02.118
19. Novy DM, Aigner CJ. The biopsychosocial model in cancer pain. *Curr Opin Support Palliat Care* 2014; **8**: 117-23. doi: 10.1097/SPC.0000000000000046
20. Benrath J, Hatzenbühler M, Fresenius M, Heck M. Repetitorium Schmerztherapie: Zur Vorbereitung auf die Prüfung "Spezielle Schmerztherapie". 4. Aufl. Heidelberg: Springer; 2015. doi: 10.1007/978-3-662-47865-3
21. Dupoiron D. Cancer pain management: A European perspective. *Cancer Treat Res* 2021; **182**: 39-55. doi: 10.1007/978-3-030-81526-4_4
22. Dupoiron D. Intrathecal therapy for pain in cancer patients. *Curr Opin Support Palliat Care*. 2019; **13**: 75-80. doi: 10.1097/SPC.0000000000000427
23. Warner LL, Moeschler SS, Pittelkow TP, Strand JJ. Attitudes of hospice providers regarding intrathecal targeted drug delivery for patients with cancer. *Am J Hosp Palliat Care* 2019; **36**: 955-8. doi: 10.1177/1049909119852928
24. Wang W, Shi Q, Cao Y, Fan B, Yang Y. Intrathecal drug delivery systems for cancer pain: A retrospective analysis at a single tertiary medical center in China. *Heliyon* 2024; **10:** e34522. doi: 10.1016/j.heliyon.2024.e34522. PMID: 39114043; PMCID: PMC11305181.
25. Hamza M, Doleys DM, Wells M, Weisbein J, Hoff J, Martin M, et al. Prospective study of 3-year follow-up of low-dose intrathecal opioids in the management of chronic nonmalignant pain. *Pain Med* 2012; **13**: 1304-13. doi: 10.1111/j.1526-4637.2012.01451.x
26. Rauck RL, Cherry D, Boyer MF, Kosek P, Dunn J, Alo K. Long-term intrathecal opioid therapy with a patient-activated, implanted delivery system for the treatment of refractory cancer pain. *J Pain*. 2003; **4**: 441-7. doi: 10.1067/s1526-5900(03)00730-2
27. Bolash R, Udeh B, Saweris Y, Guirguis M, Dalton JE, Makarova N, et al. Longevity and cost of implantable intrathecal drug delivery systems for chronic pain management: a retrospective analysis of 365 patients. *Neuromodulation* 2015; **18**: 150-5; discussion 155-6. doi: 10.1111/ner.12235
28. De Andrés J, Rubio-Haro R, De Andres-Serrano C, Asensio-Samper JM, Fabregat-Cid G. Intrathecal drug delivery. *Methods Mol Biol* 2020; **2059**: 75-108. doi: 10.1007/978-1-4939-9798-5_3
29. De Andres J, Hayek S, Perruchoud C, Lawrence MM, Reina MA, De Andres-Serrano C, et al. Intrathecal drug delivery: Advances and applications in the management of chronic pain patient. *Front Pain Res (Lausanne)* 2022; **3**: 900566. doi: 10.3389/fpain.2022.900566
30. Price DD, McGrath PA, Rafii A, Buckingham B. The validation of visual analogue scales as ratio scale measures for chronic and experimental pain. *Pain* 1983; **17**: 45-56. doi: 10.1016/0304-3959(83)90126-4
31. European Organisation for Research and Treatment of Cancer (EORTC). EORTC QLQ-C30: Quality of Life Questionnaire - Core 30, English Version. Brussels: EORTC; 2018 [cited 2024 June 17]. Available from: https://www.eortc.org/app/uploads/sites/2/2018/08/Specimen-QLQ-C30-English.pdf.
32. Alberta Health Services. Edmonton Symptom Assessment System Revised (ESAS-r) Form [Internet]. Alberta Health Services; 2015 [cited 2024 Dec 17]. Available from: https://www.albertahealthservices.ca/frm-07903.pdf

research article

The utility of ^{18}F-FDG PET/CT in assessing bone marrow involvement and prognosis in newly diagnosed diffuse large B-cell lymphoma

Chunyan Yang[1], Hong Liu[2], Furui Duan[1], Ximei Wang[1], Ping Li[1], Dalong Wang[1]

[1] Department of PET/CT, The Second Affiliated Hospital of Harbin Medical University, Harbin, China
[2] Department of Nuclear Medicine and Radiation Oncology, Zibo Central Hospital, Shandong Province, China

Radiol Oncol 2025; 59(4): 488-497.

Received 23 February 2025
Accepted 26 August 2025

Correspondence to: Dalong Wang, M.D., Department of PET/CT, The Second Affiliated Hospital of Harbin Medical University, 246 Xuefu Road, Harbin 150001, Heilongjiang, China Harbin, China. E-mail: wangdalongbao@163.com

Chunyan Yang and Hong Liu contributed equally and share first authorship

Disclosure: No potential conflicts of interest were disclosed.

Background. The presence of bone marrow involvement (BMI) in patients with diffuse large B-cell lymphoma (DLBCL) has a significant impact on treatment plans and prognosis, but clinical diagnosis is difficult. The purpose of this study was to evaluate the utility of PET/CT in the assessment of BMI and prognosis in newly diagnosed DLBCL.

Patients and methods. This retrospective study included 57 eligible DLBCL patients who underwent bone marrow biopsy (BMB) and PET/CT prior to any treatment initiation. Increased FDG uptake in the bone marrow on PET/CT scans was indicative of BMI positivity, with such instances not attributable to benign findings. If BMB yielded positive results, or if the marrow uptake resolved concurrently with other lymphoma lesions during PET/CT monitoring, the diagnosis of BMI was established. The evaluation of bone marrow status via PET/CT involved both visual analysis and a quantitative index, specifically the ratio of maximum standardized uptake values of bone marrow to liver (BLR). Factors associated with 2-year progression-free survival (PFS) was analyzed utilizing the Cox proportional hazards regression model.

Results. 34 patients were diagnosed with BMI. PET/CT demonstrated superior accuracy (93.0% *vs.* 75.4%) and sensitivity (94.1% *vs.* 58.8%) compared to BMB. During the follow-up period, 15 patients experienced disease progression. Survival analysis identified Eastern Cooperative Oncology Group performance status (ECOG PS), BLR, and PET/CT bone marrow status as the sole independent predictors of PFS ($p = 0.010$, 0.002, and 0.015, respectively).

Conclusions. PET/CT played an important role in evaluating BMI and predicting PFS in newly diagnosed DLBCL.

Key words: PET/CT; DLBCL; bone marrow biopsy; bone marrow involvement

Introduction

Diffuse large B-cell lymphoma (DLBCL) represents a prevalent and aggressive form of lymphoma, constituting approximately 30% of all non-Hodgkin lymphoma cases.[1] Bone marrow involvement (BMI) serves as a critical prognostic indicator for lymphoma patients, significantly impacting disease staging and prognosis. Accurate determination of BMI is therefore paramount. Traditionally, bone marrow biopsy (BMB) has been regarded as the gold standard for assessing BMI in DLBCL due to its ability to evaluate the bone marrow (BM) status of lymphoma patients. However, the advent and advancement of nuclear imaging technology have posed a challenge to its longstanding position in clinical practice. In previous literature reports, its conventional performance has been controversial. BMB, as an invasive procedure, carries the potential for patient anxiety and the risk of bleeding. Moreover, it is prone to yield false negative outcomes, particularly in

cases where the true lesion is missed due to biopsy site limitations, notably with respect to distant BM lesions from the iliac spine.[2,3] Furthermore, certain studies propose that routine BMB may lack therapeutic relevance.[4]

^{18}F-FDG positron emission tomography (PET)/computed tomography (CT) is capable of accurately depicting the glucose metabolism status of tissues or lesions through the utilization of its glucose analogues, offering vital physiological and pathological insights for clinical utility. The heightened metabolic activity of malignant tumor cells results in significant FDG uptake, rendering PET/CT particularly advantageous for diagnostic purposes, disease staging, treatment response assessment, and surveillance of lymphoma recurrence. Whole-body PET/CT imaging enables comprehensive visualization of tumor location, morphology, size, and extent, aligning with recommendations from the European Society for Medical Oncology guidelines as the preferred modality for evaluating systemic disease dissemination in DLBCL patients.[5] Highlights that, in comparison to BMB, PET/CT imaging allows for the assessment of BM status throughout the entire body rather than at a single anatomical site. In a recent study by Doma *et al.* found that the sensitivity and accuracy of PET/CT in diagnosing BMI were significantly higher than BMB, at 88.4% *vs.* 41.9% and 96.5% *vs.* 61.5%, respectively.[6] They advocated for PET/CT as a viable alternative to BMB for evaluating BMI in patients with DLBCL. Nonetheless, the precise role of BM FDG uptake in DLBCL patients remains a topic of ongoing discussion.

In this study, we aim to assess the correlation and prognostic significance of PET/CT and BMB in BMI among newly diagnosed DLBCL patients, providing clinical practitioners with diagnostic insights and therapeutic considerations to aid in treatment decision-making processes.

Patients and methods

Patients

A retrospective analysis was conducted on DLBCL patients who underwent PET/CT scans between 2017 and 2024. These patients had not undergone radiotherapy, chemotherapy, hematopoietic factor therapy, or had a previous history of other malignancies prior to the PET/CT scans. Patient confidentiality was maintained in compliance with national regulations. The study was approved by the Ethics Committee of the Second Affiliated Hospital of Harbin Medical University (Approval No. YJSKY2023-327, 2023-09-04).

Clinical data was sourced from institutional information systems. A review was conducted on the following clinical parameters: age, sex, Eastern Cooperative Oncology Group performance status (ECOG PS), B-symptoms, clinical manifestations (pain, nosebleeds, loss of appetite, bloating, among others), and extranodal involvement. The baseline laboratory findings obtained within a 2-week window before and after PET/CT imaging encompassed serum lactate dehydrogenase (LDH), lymphocyte-to-monocyte ratio (LMR > 3), neutrophil-to-lymphocyte ratio (NLR > 2.5)[7], leukopenia (< 4×10^9/L), anemia (hemoglobin < 120g/L), and thrombocytopenia (platelet counts < 100×10^9/L). The International Prognostic Index (IPI) score was based on these data. Following PET/CT scans, all patients underwent first-line therapy. The study cohort was derived according to the process detailed in Supplementary Figure 1.

Acquisition of PET/CT images

Imaging was performed using a PET/CT system (Biograph64 mCT, Siemens Healthcare, Berlin, Germany) with a full-ring PET scanner. Patients fasted for 6 hours and maintained blood glucose levels below 11 mmol/L before the procedure. After FDG injection (0.11 mCi/kg), patients rested supine for 60 minutes. CT was performed with a 120 kV tube voltage and modulated tube current (CARE Dose). PET acquisition was conducted at 1.6 mm/s, and images were reconstructed with the TrueD algorithm for attenuation correction using CT data. The PET matrix was 200×200 (voxel size: 4.07×4.07×3 mm), and the CT matrix was 512×512 (voxel size: 0.78×0.78×1 mm), with PET images reconstructed using the TrueX + TOF method.

Evaluation of PET/CT images and analysis of FDG uptake

Image interpretation was conducted through visual and semi-quantitative analysis, utilizing glucose activity in the normal liver as a reference to assess the presence of BMI. In cases where BM lesions were identified, they were classified as focal lesions (demonstrating elevated FDG uptake in one or more localized regions) or diffuse lesions (exhibiting a uniform increase in FDG uptake across the entire marrow space). These lesions, with or without associated bone destruction, were distinguished from benign findings based on standard

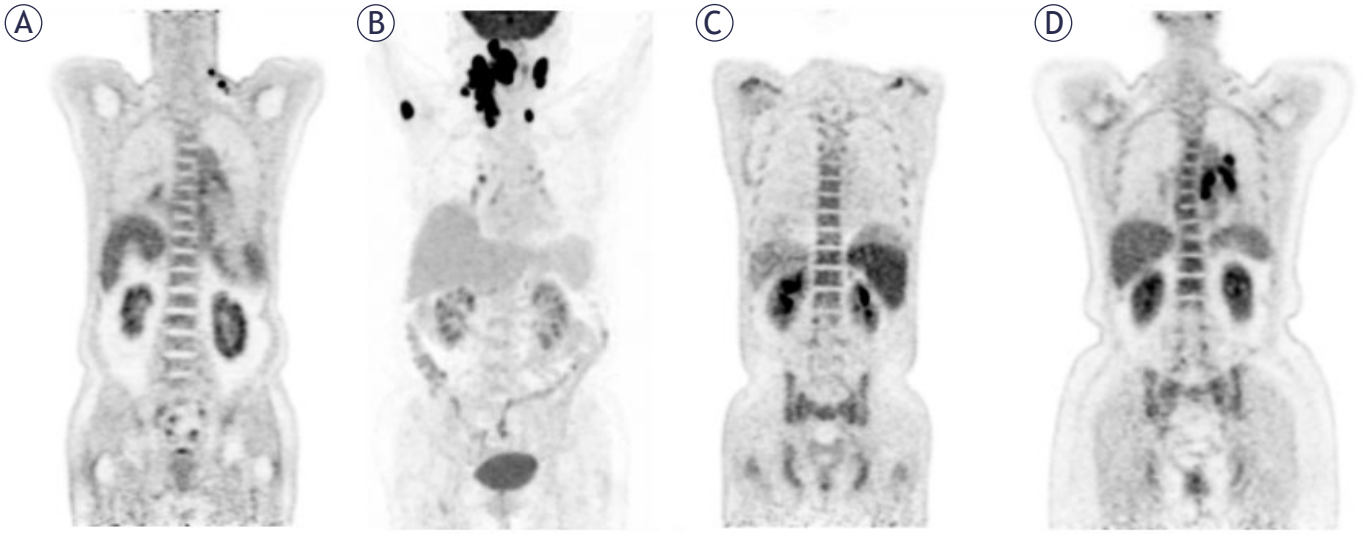

FIGURE 1. The initial PET maximum-intensity projection images, and lymph nodes pathology confirmed DLBCL with normal **(A)**, focal increased in the right humerus **(B)**, diffuse increased **(C, D)**.

CT images or medical history (*e.g.,* fractures). In such cases, BM positivity on PET/CT was ascertained. The maximum standardized uptake value (SUVmax) of the liver was measured in a 2-cm region of interest in the right lobe, while the highest SUVmax for BM was assessed at lumbar vertebrae 1-5 in cases of diffuse uptake. The BM-to-liver SUVmax ratio (BLR) was calculated to investigate survival outcomes. Two experienced nuclear medicine specialists, each possessing more than 5 years of professional experience, independently interpreted the images, with discrepancies resolved by consensus (Figure 1).

Bone marrow biopsy (BMB) and pathological analysis

All patients underwent unilateral iliac BM core needle biopsy and aspiration without imaging guidance. BMB samples were collected within one month before or after the PET/CT imaging and evaluated by a senior hematologist.

Definition of the final diagnosis of bone marrow involvement (BMI)

If BM uptake paralleled the uptake activity of other lymphoma lesions during follow-up with PET/CT or was confirmed by BMB, the diagnosis of BMI was confirmed.[8,9]

Statistical analysis

Receiver operating characteristic (ROC) curve analysis was employed to establish the optimal BLR threshold for survival analysis. Progression-free survival (PFS) was defined as the duration from the definitive diagnosis to the first occurrence of disease progression or relapse, all-cause mortality, or the most recent follow-up. The Shapiro-Wilk test was utilized for assessing the distribution of continuous variables in the baseline data. Continuous variables were expressed as median and interquartile range. Categorical data were presented as patient counts and percentages. Disparities in variables between the two groups were assessed using logistic regression analysis and the chi-square test. Comparison of SUVmax and BLR was conducted using the Kruskal-Wallis test and Dunn's post-hoc test. Cox proportional hazards regression models were utilized to analyze the impact of factors such as IPI and related components, BLR, and BM status on survival outcomes. Survival analysis was performed using Kaplan-Meier curves and log-rank tests. Statistically significant variables ($p < 0.05$) from the univariate analysis were entered into the multivariate Cox regression. The resulting independent prognostic factors were incorporated to construct a prognostic nomogram. The model was validated internally using bootstrap resampling with 1,000 iterations. The discriminative ability of

TABLE 1. Baseline characteristics at diagnosis

Characteristic	PET/CT		p -value	BMB		p-value
	(-) (n = 23)	(+) (n = 34)		(-) (n = 37)	(+) (n = 20)	
Male, no. (%)	11 (47.83)	16 (47.06)	0.955	17 (45.95)	10 (50.00)	0.770
Leukopenia, no. (%)	2 (8.70)	6 (17.65)	0.571	2 (5.41)	6 (30.00)	0.031
Anaemia, no. (%)	4 (17.39)	15 (44.12)	0.036	7 (18.92)	12 (60.00)	0.002
Thrombocytopenia, no. (%)	2 (8.70)	8 (23.53)	0.276	3 (8.11)	7 (35.00)	0.029
LMR > 3, no. (%)	15 (65.22)	20 (58.82)	0.627	26 (70.27)	9 (45.00)	0.061
NLR > 2.5, no. (%)	10 (43.5)	21 (61.8)	0.174	19 (51.40)	12 (60.00)	0.532
Age > 60 years, no. (%)	10 (43.48)	20 (58.82)	0.255	19 (51.35)	11 (55.00)	0.792
Stage III/IV, no. (%)	19 (82.61)	29 (85.29)	1	28 (75.68)	20 (100)	0.043
ECOG PS ≥ 2, no. (%)	8 (34.78)	14 (41.18)	0.627	11 (29.73)	11 (55.00)	0.061
Clinical systemic symptoms, no. (%)	21 (91.30)	25 (73.53)	0.185	31 (83.78)	15 (75.00)	0.652
Biological systemic symptoms, no. (%)	11 (47.83)	20 (58.82)	0.413	18 (48.65)	13 (65.00)	0.237
LDH (+), no. (%)	8 (34.78)	18 (52.94)	0.177	15 (40.54)	11 (55.00)	0.296
IPI score > 2, no. (%)	8 (34.78)	18 (52.94)	0.177	12 (32.43)	14 (70.00)	0.007
Extranodal sites ≥ 2	6 (26.09)	13 (38.24)	0.340	8 (21.62)	11 (55.00)	0.011
BMB (+), no. (%)	2 (8.70)	18 (52.94)	< 0.001	-	-	-
PET (+), no. (%)	-	-	-	16 (43.24)	18 (90.00)	< 0.001
High level of BLR, no. (%)	0	27 (79.41)	< 0.001	10 (27.03)	17 (85.00)	< 0.001
BM SUVmax, median (P25, P75)	2.48 (2.12,3.02)	4.74 (3.42,9.43)	0.002	2.78 (2.28,3.55)	6.39 (4.47,11.73)	0.003

BLR = the ratio of the maximum standardized uptake values of bone marrow-to-liver; BMB = bone marrow biopsy; BM SUVmax = maximum standardized uptake value of bone marrow; ECOG PS = Eastern Cooperative Oncology Group physical status score; IPI = international prognostic index; LDH = lactate dehydrogenase; LMR = lymphocyte-to-monocyte ratio; NLR = neutrophil-to-lymphocyte ratio

the nomogram was quantified by the concordance index (C-index), and its accuracy was visually assessed with a calibration curve comparing predicted probabilities against observed frequencies. Statistical analyses were performed using IBM SPSS 27 and R 4.3.3 software.

Results

Clinical characteristics

In this study, a total of 57 DLBCL cases were analyzed in Table 1. The cohort showed 27 males (47.4%) and 30 females (52.6%), with a median age of 61 years old (range: 28–81). Among 57 patients, 30 (52.6%) were aged 60 years or older.

The baseline characteristics of the patients defined by the two diagnostic methods – (1) the PET/CT-based cohort and (2) the BMB-based cohort – were compared. There were no significant differences between the two groups in terms of sex, age, LMR > 3, NLR > 2.5, clinical symptoms, B-symptoms, LDH (+), ECOG PS ≥ 2, extranodal sites ≥ 2, or IPI score > 2. However, there were statistical differences in the anemia, BM SUVmax, and BLR levels (all $p < 0.05$).

PET/CT and BMB diagnostic performance

Out of the 34 patients detected as BMI positive by PET/CT, 32 were confirmed as true positive cases (20 confirmed via BMB, 12 through follow-up). Among the 23 patients identified as BMI negative by PET/CT, 2 were verified as false negative by BMB, while the remaining 21 were confirmed as negative by BMB or follow-up assessments (Table 2).

We identified 34 patients (59.6%) with BMI and 23 (40.4%) without BMI. Using the final clinical diagnosis as the reference standard, PET/CT correctly identified 32 (56.1%) true positive cases, while BMB correctly identified 20 (35.1%) true positive cases. The diagnostic results from PET/CT and BMB were consistent in 39 cases. Specifically, 18 (31.6%) demonstrated concordant positive findings on both BMB and PET/CT tests, while 21 (36.8%) displayed negative outcomes for BMB and PET/CT. However, there were 18 (31.6%) cases where the

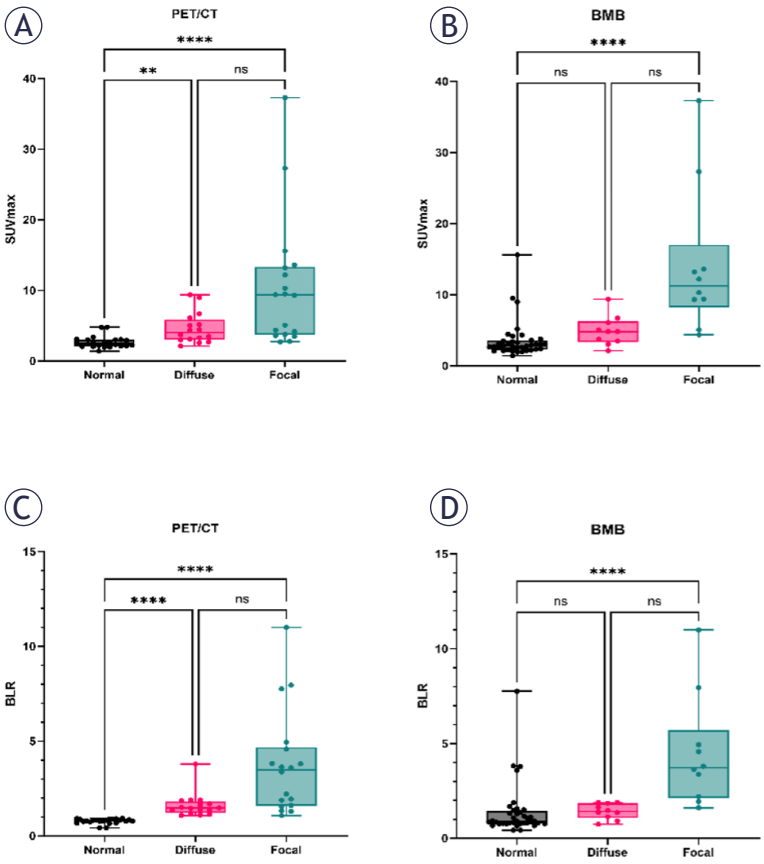

FIGURE 2. Distribution of uptake according to bone marrow biopsy (BMB) and PET/CT.

**, p = 0.006;
****, p < 0.0001; BLR = the ratio of the maximum standardized uptake values of bone marrow-to-liver; ns = statistically nonsignificant; SUVmax = maximum standardized uptake value of bone marrow

diagnostic results between PET/CT and BMB were inconsistent, including 16 (28.1%) that tested positive for PET/CT yet negative for BMB, and 2 (3.5%) that tested negative for PET/CT but positive for BMB (Table 3).

Table 4 compares the diagnostic performance of PET/CT and BMB against the pre-defined BMI. PET/CT demonstrated superior diagnostic efficacy, with an accuracy of 93.0% and a sensitivity of 94.1%. Its specificity, positive predictive value

TABLE 2. Comparison of bone marrow biopsy (BMB) and PET/CT results with bone marrow involvement (BMI)

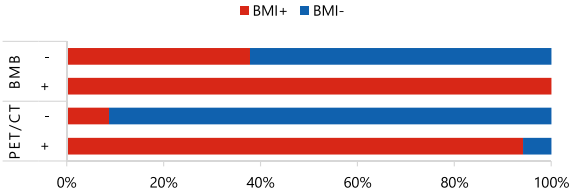

	PET/CT		BMB	
	+	-	+	-
BMI+	32	2	20	14
BMI-	2	21	0	23

TABLE 3. Diagnostic performance in all diffuse large B-cell lymphoma (DLBCL) patients

		PET/CT		Total
		(+)	(-)	
BMB	(+)	18	2	20
	(-)	16	21	37
Total		34	23	57

BMB = bone marrow biopsy

(PPV), and negative predictive value (NPV) were 91.3%, 94.1%, and 91.3%, respectively. The high Youden index (0.854) and excellent agreement with the reference standard (kappa = 0.854) further confirm its robustness.

PET/CT characteristics

Utilizing the optimal cut-off value of BLR = 1.340 (AUC = 0.755, p = 0.004), patients were stratified into high- and low-BLR groups. All 27 patients (100%) in the high-BLR group were interpreted as positive by visual PET/CT assessment. In contrast, only 7 of the 30 patients (23.3%) in the low-BLR group were PET/CT-positive. The agreement between the quantitative (BLR-based) and visual PET/CT assessments was excellent (p < 0.001, kappa = 0.757).

Among all patients, the median SUVmax of 23 patients with normal BM uptake was 2.48 (2.12,

TABLE 4. Comparison of bone marrow biopsy (BMB) and PET/CT to detect bone marrow involvement (BMI)

	Accuracy (%)	Sensitivity (%)	Specificity (%)	PPV (%)	NPV (%)	YI	kappa	AUC
PET/CT (BMB as standard)	68.4 (95 CI,76.9–100)	56.8 (95 CI, 40.8–72.7)	52.9 (95 CI, 36.2–69.7)	52.9 (95 CI, 36.2–69.7)	91.3 (95 CI, 79.8–100)	0.468	0.403	0.734
PET/CT (BMI as standard)	93.0 (95 CI, 92.8–93.2)	94.1 (95 CI, 86.2–100)	91.3 (95 CI, 79.8–100)	94.1 (95 CI, 86.2–100)	91.3 (95 CI, 79.8–100)	0.854	0.854	0.927
BMB (BMI as standard)	75.4 (95 CI, 74.8–76.1)	58.8 (95 CI,42.3–75.4)	100 (95 CI,100–100)	100 (95 CI,100–100)	62.2 (95 CI,46.5–77.8)	0.588	0.536	0.794

AUC = area under ROC curve; CI = confidence interval; NPV = negative predictive value; PPV = positive predictive value; YI = Youden index

3.02), and the BLR was 0.80 (0.75, 0.87). In contrast, the median SUVmax of 18 patients with focal BM uptake was 9.36 (3.73, 13.30; $p < 0.001$), BLR was 3.49 (1.60, 4.67; $p < 0.001$), and the median SUVmax of 16 patients with diffuse BM uptake was 4.04 (3.04, 5.86; $p = 0.006$), BLR was 1.48 (1.23, 1.81; $p < 0.001$). The difference in SUVmax and BLR between focal and diffuse uptake groups was not statistically significant (Figure 2A and C). The median SUVmax and BLR of 34 patients with increased BM uptake were 1.77 (1.37, 3.68) and 4.74 (3.42, 9.43), respectively, with statistical differences (both $p < 0.001$). Using BMB as the standard for analysis, the median SUVmax and BLR of 37 cases of BMB (-) were 2.78 (2.28, 3.55) and 0.79 (0.89, 1.44), while 20 cases of BMB (+) had higher median SUVmax and BLR, which were 6.39 (4.47, 11.73; $p < 0.001$) and 1.89 (1.40, 3.78; $p < 0.001$), respectively. The median SUVmax of focal and diffuse BM uptake were 11.25 (8.25, 17.03) and 4.80 (3.35, 6.24), respectively, and the median BLR were 3.72 (2.15, 5.70) and 1.42 (1.09, 1.86), respectively (Figure 2B and D). The 18 patients who were positive on both PET/CT and BMB exhibited significantly elevated median SUVmax and BLR compared to the rest of the cohort: SUVmax 8.00 (4.20–12.45) *vs.* 2.92 (2.32–3.78), and BLR 1.92 (1.57–4.00) *vs.* 0.89 (0.78–1.39); all comparisons were statistically significant ($p < 0.001$).

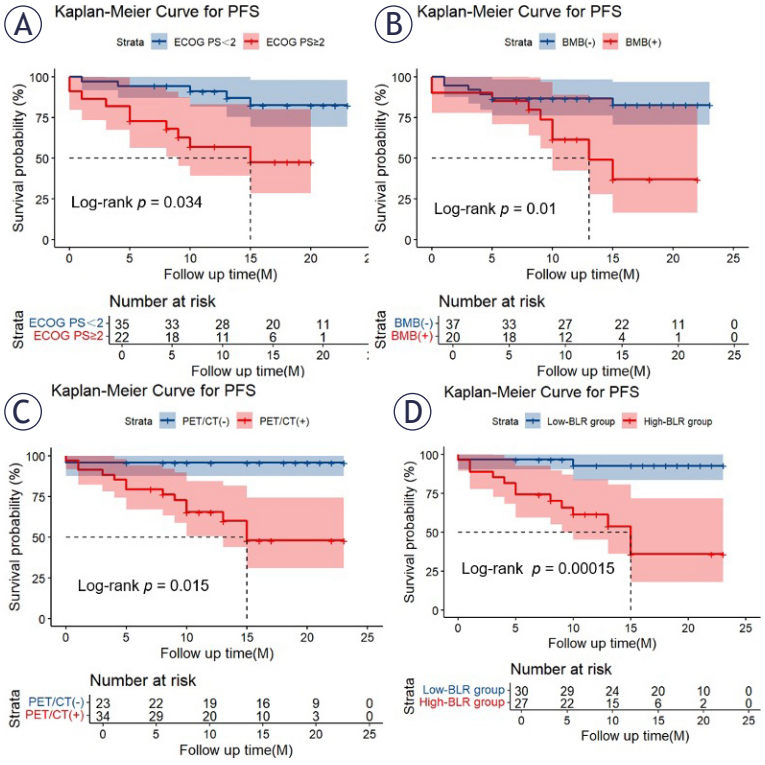

FIGURE 3. Kaplan-Meier curves for progression-free survival (PFS) in total study patients according to Eastern Cooperative Oncology Group performance status (ECOG PS) **(A)**, bone marrow biopsy (BMB) **(B)**, PET/CT **(C)** and the ratio of the maximum standardized uptake values of bone marrow-to-liver (BLR) groups **(D)**.

PET/CT and BMB findings on staging

According to the Ann Arbor stage, PET/CT and BMB were independently assessed. PET/CT classified 46 patients (80.7%) as stage IV, while BMB classified 44 patients (77.2%) as stage IV. The final clinical diagnosis, which integrated all available data, led to the downstaging of two patients: one from stage to I stage IV, and another from stage III to stage IV. This demonstrates that PET/CT plays a crucial role in preventing understaging, thereby ensuring more accurate disease staging.

Survival analysis

All 57 patients were included in the survival analysis. The median survival time was not reached at the time of analysis, with 15 patients experiencing disease progression or death. 34 patients were BMI (+), with a median PFS of 15 months and the 2-year PFS rate 47.9% ± 10.7%. In visual analysis, both a positive BMB ($p = 0.016$, Figure 3A) and a positive PET/CT finding ($p = 0.012$, Figure 3B) were significantly associated with shorter PFS; In quantitative analysis, high BLR levels (cut-off value, 1.340) were correlated with shorter PFS ($p < 0.001$, Figure 3C). The 2-year PFS rates were 92.6% ± 5.0% for the low-BLR group and 35.8% ± 12.7% for the high-BLR group.

Variables found to be significant in the univariate Cox analysis for PFS are listed in Table 5. Multivariate analysis confirmed that high BLR levels and an ECOG PS ≥ 2 were independent risk factors for shorter PFS (Table 5). Kaplan-Meier survival plots visually corroborated the poor prognosis associated with a high BLR and an ECOG PS ≥ 2 (Figure 3A and D).

Based on the results of the multivariate analysis, we constructed a nomogram for predicting PFS (Supplementary Figure 2). The nomogram demonstrated good predictive accuracy for PFS, with a C-index of 0.812. The calibration curve for PFS survival probabilities showed strong agreement between the actual observed probabilities and those predicted by the nomogram (Supplementary Figure 3).

TABLE 5. Univariate and multivariate Cox analysis of risk factors for progression-free survival (PFS) in 57 patients with diffuse large B-cell lymphoma (DLBCL)

Characteristics	Univariable		Multivariable	
	HR (95%CI)	*p*-value	HR (95%CI)	*p*-value
Male	0.619 (0.220–1.747)	0.365		
Leukopenia	0.370 (0.049–2.821)	0.338		
Anaemia	1.880 (0.680–5.199)	0.224		
Thrombocytopenia	0.772 (0.174–3.429)	0.734		
LMR > 3	0.251 (0.085–0.737)	0.012		
NLR > 2.5	2.763 (0.877–8.708)	0.083		
Age<60 years	1.270 (0.458–3.521)	0.646		
Clinical systemic symptoms	1.500 (0.338–6.656)	0.594		
Biological systemic symptoms	0.636 (0.217–1.866)	0.410		
Stage III or IV	1.268 (0.286–5.624)	0.755		
ECOG PS ≥ 2	4.368 (1.479–12.896)	0.008	4.286 (1.422–12.919)	0.010
LDH (+)	3.856 (1.227–12.122)	0.021		
Extranodal sites ≥ 2	3.638 (1.292–10.245)	0.014		
IPI score<2	3.110 (1.055–9.163)	0.040		
BMB (+)	3.663 (1.267–10.415)	0.016		
PET (+)	12.850 (1.678–98.407)	0.014		
High level of BLR	10.527 (2.340–47.364)	0.002	10.518 (2.305–47.986)	0.002
BM SUVmax	1.021 (0.954–1.093)	0.543		

BMB = bone marrow biopsy; BLR = the ratio of the maximum standardized uptake values of bone marrow-to-liver; ECOG PS = Eastern Cooperative Oncology Group performance status; CI = confidence interval; ECOG PS = Eastern Cooperative Oncology Group physical status score; IPI = international prognostic index; LDH = lactate dehydrogenase; LMR = lymphocyte-to-monocyte ratio; NLR = neutrophil-to-lymphocyte ratio

Discussion

In our retrospective study, we observed that PET/CT scans exhibited superior diagnostic accuracy compared to BMB, which was consistent with findings from various other studies reporting the heightened sensitivity of PET/CT over BMB.[6,8-12] Reviews and meta-analyses conducted further supported these observations, highlighting the superior performance of PET/CT in assessing BMI in DLBCL patients, detecting additional marrow infiltration missed by BMB, and affirming the higher diagnostic value of FDG PET/CT results over BMB.[13-15]

Numerous studies and reviews have highlighted the notable sensitivity of PET/CT in evaluating BM status in DLBCL patients.[6,8-11,16,17] For newly diagnosed DLBCL patients, the detection of negative BM uptake on PET/CT imaging may obviate the need for BMB, unless there are apprehensions regarding potential oversight of low-grade lymphoma involvement by PET/CT. Nevertheless, it has yet to be established that PET/CT can serve as a definitive substitute for BMB in clinical practice. In our study, a total of 34 patients were assessed as BMI through combined PET/CT monitoring and follow-up, a proportion higher than that reported in previous studies (11–50%).[8,9,18,19] This higher detection rate may be attributed to the predominance of advanced-stage patients (91.2%) in our cohort, wherein PET/CT imaging and follow-up monitoring could more effectively detect early metastatic lymphoma infiltration in the BM. Furthermore, following the detection of BMI via PET/CT, 2 patients (3.5%) in our cohort were reclassified with advanced stage, aligning with findings from previous research. Berthet *et al.* and Pelosi *et al.* reported upstaging rates of 10% and 21%, respectively, through PET/CT evaluations.[12,20] PET/CT demonstrates enhanced accuracy in staging and BMI detection. Assessing infiltration in cases with partially diffuse BM uptake can be challenging, as it may result from inflammatory or proliferative conditions. In our study, 8 out of 10 cases displaying diffusely increased BM uptake were confirmed as DLBCL via BMB, mirroring the heightened BMI

incidence in the diffuse BM uptake pattern investigated through many studies.[11,12,19,21,22] There were 2 cases of diffuse FDG metabolic increase with BMB (-), which may be caused by various factors, such as active marrow hyperplasia, inflammation, or infection, rather than malignant infiltration.[23,24] In this study, the median SUVmax of BM in patients with diffuse BM FDG uptake was higher than normal (4.04 *vs.* 2.48, p = 0.006). A study conducted by Lim *et al.* reported a notable disparity (p < 0.001) in the visual evaluation of BM uptake between 64 patients diagnosed with DLBCL and the remaining 448 patients showing no elevation in BM uptake.[24] Xiao-Xue *et al.* also reached a similar conclusion, and their study showed that the median values of SUVmax in the patients detected to have BMB (+) were significantly higher than patients with BMB (-) among subgroups of aggressive B-cell lymphoma, marginal zone lymphoma, T cell non-Hodgkin's lymphoma (p < 0.05).[25] Based on previous researches, we believe that the observed BM uptake pattern should be considered an indicator or high-risk factor for DLBCL BM infiltration, given the relatively low rate of false positives in cases of diffuse BM uptake on PET/CT. In this study, two patients with negative PET/CT results were later confirmed to have bone lesions upon histological biopsy. However, due to the diverse morphologies of tumor cells, the specific type of lymphoma could not be definitively identified. This ambiguity may be attributed to either a low tumor burden or small-cell (discordant) BMI, which could potentially exhibit limited FDG avidity, leading to potential oversight by PET/CT imaging.[26,27] We recommend multidisciplinary review or next-generation sequencing (NGS) to resolve PET/CT-BMB discordance.

In our study, univariate analysis identified LMR > 3, ECOG PS ≥ 2, LDH (+), extranodal sites ≥ 2, IPI > 2, BMB (+), PET/CT (+), and high-BLR group as factors associated with 2-year PFS, while multivariate analysis found high-BLR group and ECOG PS ≥ 2 to be independent predictors. In the study by Lim *et al.*, elevated BM FDG uptake was linked to patient prognosis in cases with positive biopsy results (HR = 2.79; p = 0.008), a correlation that aligns with the outcomes of our research.[24] El Karak *et al.* similarly documented, in a study involving 54 patients with DLBCL prior to treatment, that PET held prognostic significance in BMI, which was closely associated with PFS (HR = 3.81, p = 0.013) and overall survival (OS) (HR = 4.12; p = 0.03), while BMB did not.[16] Similar finding was reported by Berthet *et al.*, who conducted a study comparing PFS and OS at the 2-year mark in 133 patients based on BMI as determined by BMB and PET/CT.[12] Their research indicated that BM disease detected on PET was an independent prognostic indicator for both PFS and OS, a result consistent with the prognostic value observed for BMI determined by BMB. Interestingly, other researchers reported differing results, noting that BMI identified on PET did not hold prognostic significance, with only BMI identified by BMB serving as an independent predictive factor.[9,21,22,28] Chen-Liang *et al.* noticed in their study that BMB (-) BMI (+) was independently associated with shorter PFS (HR = 3.6; p = 0.001), rather than PET/CT (-) BMI (+), which contradicts our results.[19] In addition, as a quantitative indicator of BM uptake, we found that BLR levels were independently associated with PFS in lymphoma patients. Chen *et al.* found PET (+) to be of great significance for predicting PFS and OS.[29] Interestingly, BLR (cut-off value, 1.50) was significant for PFS and OS (p < 0.001 and p = 0.002), resonating well with our findings. It is noteworthy to highlight that El Azony *et al.*, in a study encompassing 135 patients with newly diagnosed DLBCL, concluded that the BLR served as a prognostic factor for recurrence free survival (RFS) and OS in patients with DLBCL (HR = 2.83, p = 0.030 and HR = 2.38, p = 0.041).[30] Only a small number of studies addressed and supported the idea that BLR was associated with the prognosis of PFS and OS in lymphoma patients, and was even an independent predictor.[13,29,31]

The variations observed in PFS outcomes across studies may be attributed to differences in patient demographics and the duration of follow-up. Distinguishing our study from prior research, we specifically assessed BMI in patients with DLBCL. Currently, there is limited literature on the prognostic value of BLR in B-cell lymphoma, especially in the context of DLBCL. Our research findings provide valuable references for future studies. In addition, different methods between studies may lead to differences in the determination of BM status, as some rely solely on BMB, which may result in false negative results.

We recognize the limitations inherent in our research design. Our study is retrospective and conducted at a single institution with a relatively small cohort, potentially introducing selection and information bias into the data. Additionally, one of the criteria for diagnosing BMI involves the reduction or disappearance of intense focal uptake, a condition that could lead to false positive results. Prospective large-scale studies are needed to further verify these results.

Conclusions

In summary, our research findings indicate that PET/CT and BMB are complementary in evaluating BMI and predicting prognosis in patients with DLBCL. Additionally, high BLR levels are an independent factor affecting PFS in patients.

Acknowledgments

The authors declare that we have no known competing financial interests or personal relationships that could have appeared to influence the work reported in this paper.

References

1. Alaggio R, Amador C, Anagnostopoulos I, Attygalle AD, Araujo IBdO, Berti E, et al. The 5th edition of the World Health Organization classification of haematolymphoid tumours: lymphoid neoplasms. *Leukemia* 2022; **36:** 1720-48. doi: 10.1038/s41375-022-01620-2

2. Teagle AR, Barton H, Charles-Edwards E, Dizdarevic S, Chevassut T. Use of FDG PET/CT in identification of bone marrow involvement in diffuse large B cell lymphoma and follicular lymphoma: comparison with iliac crest bone marrow biopsy. *Acta Radiologica* 2017; **58:** 1476-84. doi: 10.1177/0284185117701305

3. Hopkins E, Devenish G, Evans G, Leopold G, Rees J and Parry-Jones N. Subcutaneous seeding of 'double hit' diffuse large B-cell lymphoma from staging bone marrow biopsy. *Br J Haematol* 2014; **166:** 635-5. doi: 10.1111/bjh.12979

4. Adams HJA, de Klerk JMH, Fijnheer R, Heggelman BGF, Dubois SV, Nievelstein RAJ, et al. Bone marrow biopsy in diffuse large B-cell lymphoma: useful or redundant test? *Acta Oncol* 2014; **54:** 67-72. doi: 10.3109/0284186x.2014.958531

5. Tilly H, Gomes da Silva M, Vitolo U, Jack A, Meignan M, Lopez-Guillermo A, et al. Diffuse large B-cell lymphoma (DLBCL): ESMO Clinical Practice Guidelines for diagnosis, treatment and follow-up. *Ann Oncol* 2015; **26:** v116-25. doi: 10.1093/annonc/mdv304

6. Doma A, Zevnik K, Studen A, Prevodnik VK, Gasljevic G, Novakovic BJ. Detection performance and prognostic value of initial bone marrow involvement in diffuse large B-cell lymphoma: a single centre 18F-FDG PET/CT and bone marrow biopsy evaluation study. *Radiol Oncol* 2024; **58:** 15-22. doi: 10.2478/raon-2024-0004

7. Chen Y, Xu J, Meng J, Ding M, Guo Y, Fu D, et al. Establishment and evaluation of a nomogram for predicting the survival outcomes of patients with diffuse large B-cell lymphoma based on International Prognostic Index scores and clinical indicators. *Ann Transl Med* 2023; **11:** 71. doi: 10.21037/atm-22-6023

8. Kaddu-Mulindwa D, Altmann B, Held G, Angel S, Stilgenbauer S, Thurner L, et al. FDG PET/CT to detect bone marrow involvement in the initial staging of patients with aggressive non-Hodgkin lymphoma: results from the prospective, multicenter PETAL and OPTIMAL>60 trials. *Eur J Nucl Med Mol Imaging* 2021; **48:** 3550-9. doi: 10.1007/s00259-021-05348-6

9. Khan AB, Barrington SF, Mikhaeel NG, Hunt AA, Cameron L, Morris T, et al. PET-CT staging of DLBCL accurately identifies and provides new insight into the clinical significance of bone marrow involvement. *Blood* 2013; **122:** 61-7. doi: 10.1182/blood-2012-12-473389

10. Elamir Y, Elazab M, Owis AS, Elsayed HF. PET/CT and bone marrow biopsy (BMB) in evaluating bone marrow in lymphoma. *Egypt J Radiol Nucl Med* 2020; **51:** doi: 10.1186/s43055-020-00318-8

11. Büyükşimşek M, Kolsuz İ, Yetişir AE, Tohumcuoğlu M, Oğul A, Mirili C, et al. Performance of positron emission tomography-computed tomography and bone marrow biopsy in detecting bone marrow infiltration in lymphoma cases. *Turk J Haematol* 2020; **37:** 220-5. doi: 10.4274/tjh.galenos.2020.2019.0361

12. Berthet L, Cochet A, Kanoun S, Berriolo-Riedinger A, Humbert O, Toubeau M, et al. In newly diagnosed diffuse large B-cell lymphoma, determination of bone marrow involvement with 18F-FDG PET/CT provides better diagnostic performance and prognostic stratification than does biopsy. *J Nucl Med* 2013; **54:** 1244-50. doi: 10.2967/jnumed.112.114710

13. Pakos EE, Fotopoulos AD, Ioannidis JP. 18F-FDG PET for evaluation of bone marrow infltration in staging of lymphoma: a meta-analysis. *J Nucl Med* 2005; **46:** 958-63. PMID: 15937306

14. Li Z, Li C, Chen B, Shi L, Gao F, Wang P, et al. FDG-PET/CT versus bone marrow biopsy in bone marrow involvement in newly diagnosed paediatric lymphoma: a systematic review and meta-analysis. *J Orthop Surg Res* 2021; **16:** 485. doi: 10.1186/s13018-021-02521-3

15. Adams HJA, Kwee TC, de Keizer B, Fijnheer R, de Klerk JMH, Nievelstein RAJ. FDG PET/CT for the detection of bone marrow involvement in diffuse large B-cell lymphoma: systematic review and meta-analysis. *Eur J Nucl Med Mol Imaging* 2013; **41:** 565-74. doi: 10.1007/s00259-013-2623-4

16. El Karak F, Bou-Orm IR, Ghosn M, Kattan J, Farhat F, Ibrahim T, et al. PET/CT scanner and bone marrow biopsy in detection of bone marrow involvement in diffuse large B-cell lymphoma. *PLoS One* 2017; **12:** e0170299. doi: 10.1371/journal.pone.0170299

17. Al-Sabbagh A, Ibrahim F, Szabados L, Soliman DS, Taha RY, Fernyhough LJ. The role of integrated positron emission tomography/computed tomography (PET/CT) and bone marrow examination in staging large B-cell lymphoma. *Clin Med Insights Oncol* 2020; **14:** 1179554920953091. doi: 10.1177/1179554920953091

18. Mittal BR, Manohar K, Malhotra P, Das R, Kashyap R, Bhattacharya A, et al. Can fluorodeoxyglucose positron emission tomography/computed tomography avoid negative iliac crest biopsies in evaluation of marrow involvement by lymphoma at time of initial staging? *Leuk Lymphoma* 2011; **52:** 2111-6. doi: 10.3109/10428194.2011.593273

19. Chen-Liang TH, Martín-Santos T, Jerez A, Rodríguez-García G, Senent L, Martínez-Millán C, et al. Bone marrow biopsy superiority over PET/CT in predicting progression-free survival in a homogeneously-treated cohort of diffuse large B-cell lymphoma. *Cancer Med* 2017; **6:** 2507-14. doi: 10.1002/cam4.1205

20. Pelosi E, Penna D, Douroukas A, Bellò M, Amati A, Arena V, et al. Bone marrow disease detection with FDG-PET/CT and bone marrow biopsy during the staging of malignant lymphoma: results from a large multicentre study. *Q J Nucl Med Mol Imaging* 2011; **55:** 469-75. PMID: 21150862

21. Hong J, Lee Y, Park Y, Kim SG, Hwang KH, Park SH, et al. Role of FDG-PET/CT in detecting lymphomatous bone marrow involvement in patients with newly diagnosed diffuse large B-cell lymphoma. *Ann Hematol* 2011; **91:** 687-95. doi: 10.1007/s00277-011-1353-6

22. Adams HJA, Kwee TC, Fijnheer R, Dubois SV, Nievelstein RAJ, de Klerk JMH. Bone marrow 18F-fluoro-2-deoxy-d-glucose positron emission tomography/computed tomography cannot replace bone marrow biopsy in diffuse large B-cell lymphoma. *Am J Hematol* 2014; **89:** 726-31. doi: 10.1002/ajh.23730

23. Zhou M, Chen Y, Liu J, Huang G. A predicting model of bone marrow malignant infiltration in ^{18}F-FDG PET/CT images with increased diffuse bone marrow FDG uptake. *J Cancer* 2018; **9:** 1737-44. doi: 10.7150/jca.24836

24. Lim CH, Hyun SH, Cho YS, Choi JY, Lee KH. Prognostic significance of bone marrow 2-[^{18}F]-fluoro-2-deoxy-d-glucose uptake in diffuse large B-cell lymphoma: relation to iliac crest biopsy results. *Clin Radiol* 2021; **76:** 550.e19-550.e28. doi: 10.1016/j.crad.2021.02.023

25. Xiao-Xue W, Xinyue H, Lijun Z. Whole body FDG-PET/CT for the assessment of bone marrow infiltration in patients with newly diagnosed lymphoma. *Med Clin (Barc)* 2020; **154:** 61-5. doi: 10.1016/j.medcli.2019.07.022

26. Paone G, Itti E, Haioun C, Gaulard P, Dupuis J, Lin C, et al. Bone marrow involvement in diffuse large B-cell lymphoma: correlation between FDG-PET uptake and type of cellular infiltrate. *Eur J Nucl Med Mol Imaging* 2008; **36:** 745-50. doi: 10.1007/s00259-008-1021-9

27. Alzahrani M, El-Galaly TC, Hutchings M, Hansen JW, Loft A, Johnsen HE, et al. The value of routine bone marrow biopsy in patients with diffuse large B-cell lymphoma staged with PET/CT: a Danish-Canadian study. *Ann Oncol* 2016; **27:** 1095-9. doi: 10.1093/annonc/mdw137

28. Vishnu P, Wingerson A, Lee M, Mandelson MT, Aboulafia DM. Utility of bone marrow biopsy and aspirate for staging of diffuse large B cell lymphoma in the era of positron emission tomography with 2-deoxy-2-[Fluorine-18]fluoro-deoxyglucose integrated with computed tomography. *Clin Lymphoma Myeloma Leuk* 2017; **17:** 631-6. doi: 10.1016/j.clml.2017.06.010

29. Chen J, Zhao Y. Pre-treatment [^{18}F]FDG PET/CT for assessing bone marrow involvement and prognosis in patients with newly diagnosed peripheral T-cell lymphoma. *Hematology* 2024; **29:** doi: 10.1080/16078454.2024.2325317

30. El-Azony A, Basha MAA, Almalki YE, Abdelmaksoud B, Hefzi N, Alnagar AA, et al. The prognostic value of bone marrow retention index and bone marrow-to-liver ratio of baseline 18F-FDG PET/CT in diffuse large B-cell lymphoma. *Eur Radiol* 2023; **34:** 2500-11. doi: 10.1007/s00330-023-10150-z

31. Koh Y, Lee JM, Woo GU, Paeng JC, Youk J, Yoon SS, et al. FDG PET for evaluation of bone marrow status in T-cell lymphoma. *Clin Nucl Med* 2019; **44:** 4-10. doi: 10.1097/rlu.0000000000002320

research article

A comparison of transcatheter aortic valve prosthesis platforms: Myval, Sapien, and Evolut in severe symptomatic aortic stenosis and low-moderate risk patients

Matjaz Bunc[1,2], Klemen Steblovnik[1], Simon Terseglav[1], Jana Ambrozic[1], Mojca Bervar[1], Ljupka Dimitrovska[1], Miha Cercek[1], Ana Kovac[1], Patricija Pleskovic[1], Polonca Kogoj[1], Zlatko Fras[1,3], Miha Sustersic[1], Bojan Vrtovec[1]

[1] Clinical Department for Cardiology, University Clinical Centre Ljubljana, Ljubljana, Slovenia
[2] Institute for Pathophysiology, Faculty of Medicine Ljubljana, Ljubljana, Slovenia
[3] Faculty of Medicine Ljubljana, Ljubljana, Slovenia

Radiol Oncol 2025; 59(4): 498-509.

Received 21 March 2025
Accepted 24 June 2025

Correspondence to: Prof. Matjaž Bunc, M.D., Ph.D., Clinical Department for Cardiology, UKC Ljubljana, Zaloška cesta 7, Ljubljana, Slovenia. E-mail: mbuncek@yahoo.com

Disclosure: No potential conflicts of interest were disclosed.

Background. This article compares the real-world performance and safety of the three transcatheter aortic valve implantation (TAVI) platforms: Myval, Sapien, and Evolut in patients with severe symptomatic aortic stenosis and low to moderate surgical risk.

Patients and methods. Between September 2019 and September 2023, 1053 TAVI procedures were performed in the University Medical Centre Ljubljana, Slovenia. We used propensity-score match analysis to compare the Myval, Sapien, and Evolut platforms. 180 patients were enrolled in the propensity-score matching study, 60 for each platform. The study endpoints included haemodynamic outcomes compared to baseline, in-hospital clinical safety outcomes, and all-cause mortality at 30 days and one year.

Results. Changes in peak aortic valve velocity, mean aortic gradient, effective orifice area, and left ventricular ejection fraction were comparable between the platforms. After propensity score matching (tri-match), the rates of stroke (3.4% *vs.* 3.4% *vs.* 0.0%, p = 0.548), life-threatening bleeding (1.7% *vs.* 1.7% *vs.* 1.7 %), periprocedural myocardial infarction (3.3% *vs.* 0.0% *vs.* 0.0%, p = 0.330), postprocedural permanent pacemaker implantation rate (11.9% *vs.* 10.2% *vs.* 15.0%, p = 0.719), all-cause mortality at 30 days (3.3% *vs.* 5.0% *vs.* 3.3%; p = 1.000) and at 1 year (8.3% *vs.* 8.3% *vs.* 10.0%, p = 0.934) were comparable between the Myval, Sapien, and Evolut series, respectively. 2 cases of moderate paravalvular regurgitation were reported, one in Myval, and one in Sapien series.

Conclusions. The tri-match analysis of the real-world aortic stenosis patients with low to moderate surgical risk treated with the Myval, Sapien, and Evolut series showed comparable performance, safety, efficacy, and survival.

Key words: transcatheter aortic valve implantation; aortic stenosis; real-world comparison

Introduction

Transcatheter aortic valve implantation (TAVI) has become the preferred treatment option for older patients with severe aortic stenosis (AS) in all risk categories, with the expansion of therapeutic indications being supported by real-world data.[1-4] In the elderly population, a longer life expectancy alters how outcomes are evaluated. Once-acceptable rates of paravalvular regurgitation (PVR) or permanent pacemaker implantation (PPI) may need improvement.[5]

The growing range of transcatheter heart valves (THVs) aims to limit the risks associated with TAVI and thus improve clinical outcomes. The newly developed TAVI devices limit the risks associated with previous-generation devices, such as needing a new permanent pacemaker or significant residual aortic regurgitation after TAVI.[6] However, as we consider more and more variables and patient characteristics, it is becoming clearer that real-life direct comparisons are essential for the personalised decision-making process.

Balloon-expandable valves (BEVs) and self-expanding valves (SEVs) are widely used THVs in clinical practice. Supra-annular SEVs have larger effective orifice areas (EOA) and lower gradients. SEVs can also be repositioned during implantation to gain the best outcome. BEVs have a lower risk of requiring permanent pacemaker implantation (PPI) and paravalvular leaks comparable to SEVs. The Myval THV (Meril Life Sciences, India) is a novel BEV that enables precise anatomy-sizing of the device with 1.5 mm diameter increments and 9 different valve sizes. The Sapien 3 THV (Edwards Lifesciences, California, USA) has a cobalt-chromium frame with bovine pericardial tissue leaflets and an outer skirt. It is known for its low-profile delivery system and has been accepted for AS patients in all risk categories. Evolut THV series (Medtronic, Minneapolis, USA) are SEVs with nitinol frames and are approved for severe AS patients in all risk groups. Sapien and Evolut series have consistently shown good clinical outcomes and are a well-known treatment option for severe symptomatic aortic stenosis.[7,8] They have 10-year performance that is comparable to SAVR.[9] The Myval series has been shown to be safe and effective in clinical trials and real-life data. It provides another option for people with aortic stenosis who are at high or intermediate risk for traditional severe AS surgery, but long-term durability still must be proven.[10-13] The Landmark trial showed that the Myval THV series was non-inferior to the Evolut and Sapien series for the primary composite endpoint at 30 days.[14] Although there are some direct and indirect comparisons of Myval, Sapien, and Evolut series valves in different combinations, the amount of comparative data for all three platforms is still limited.

In this study, we investigated haemodynamic performance (maximal aortic blood velocity, residual gradient, EOA, and PVR), safety according to the Valve Academic Research Consortium-3 (VARC-3) criteria[15], and 30-day and 1-year all-cause mortality of the Myval, Sapien, and Evolut series in severe AS patients with low to moderate surgical risk.

Patients and methods

Study design and population

Consecutive patients with severe AS on native aortic valve, a previous TAVI prosthesis, or a surgically implanted aortic valve (SAVR) were included in this study. They were at low to intermediate risk and received one of three TAVI devices (Myval, Sapien, or Evolut series) at the University Medical Centre Ljubljana, Slovenia. The clinical data of all patients who underwent TAVI between September 2019 and September 2023 were prospectively collected in a registry database. All three devices were available to the institution's heart team, and operators were free to choose which specific THVs to use according to computer tomography angiography (CTA) measurements and other patients' characteristics.

The study was conducted in accordance with the principles of Good Clinical Practice and tenets of the Declaration of Helsinki and was approved by the National Medical Ethics Committee of the Republic of Slovenia (No.: 0120-315/2024-2711-3).

Study devices

From the Sapien platform only Sapien 3 devices were used in this study. The device is a BEV. The valve consists of a cobalt-chromium frame, three bovine pericardium leaflets, and a polyethylene terephthalate (PET) skirt to minimise PVR. The valve is available in 20 mm, 23 mm, and 26 mm sizes and is compatible with a 14Fr expandable sheath, while the 29 mm size is compatible with a 16Fr expandable sheath.[16] The beneficial performance of Sapien-3 has also been demonstrated in the PARTNER clinical trials in intermediate and low-risk patients.[2,3]

The Evolut is a series of SEVs with nitinol frames. The design incorporates porcine pericardial supra-annular leaflets and a porcine pericardium fabric skirt. The available sizes include 23 mm, 26 mm, 29 mm, and the extra-large size 34 mm. The 23–29 mm sizes are implanted through a 14Fr-compatible delivery system or an 18Fr sheath; the larger 34 mm prosthesis is implanted through a 16Fr-compatible delivery system or a 20Fr sheath. In our study, some patients in the Evolut group received Evolut Pro and Evolut Pro+ valves, which feature an updated design aimed at reducing PVR

TABLE 1. Summary of differences between Myval series, Sapien series, and Evolut series

Device	Myval series	Sapien series	Evolut series
Images	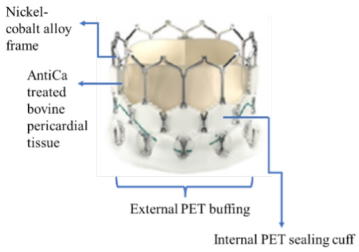	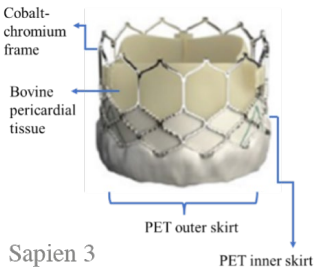	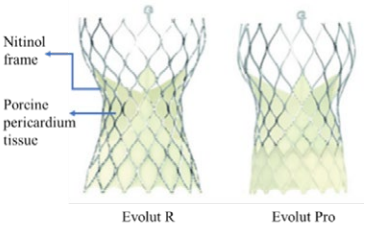
Support structure	Nickel-cobalt alloy	Cobalt-chromium alloy	Nitinol (nickel-titanium) frame
Valve structure	53% open cells on the upper half and 47% closed cells on the lower half form the hexagonal frame for the hybrid honeycomb cell design concept	Heterogeneous frame design that incorporates hexagons and diamonds. Overall, the frame consists of 5 rungs and 12 open cells, where the upper cells are larger and the lower cells are smaller	A radiopaque self-expanding nitinol support frame with a diamond cell configuration
Conventional sizes	20, 23, 26, 29 mm	20, 23, 26, 29 mm	23, 26, 29 mm
Intermediate sizes	21.5, 24.5, 27.5 mm	Not available	Not available
Extra-large sizes	30.5, 32 mm	Not available	34 mm
Valve annulus size range	18.5-32.7 mm (area derived diameter)	18.6-29.5 mm (area derived diameter)	17/18–30 mm (CT-derived diameters)
Introducer sheath	14F Python introducer sheath for all diameters (20-32 mm) Full retrievability of the undeployed Myval THV Series system	14F eSheath for 20-26mm 16F eSheath for 29mm The Sapien THV system cannot be retrieved once inside the patient	Evolut R & Evolut Pro: A 14F delivery system or an 18F sheath for 23–29 mm; a 16F delivery system or a 20F sheath for 34 mm. Evolut Pro+: 14F InLine sheath for 23-29 mm and 18 Fr InLine sheath for 34 mm Can be retrieved before full deployment
Deployment technique	The design generates a specific "zebra crossing" like pattern under fluoroscopy. This is used for position and deployment.	The design does not generate any specific pattern. Positioning is at 50% using balloon radiopaque marker.	The design does not generate any specific pattern. Positioning is controlled by radiopaque markers.

TAVI = transcatheter aortic valve implantation; THV = transcatheter heart valve

(with the help of external tissue wrap on the frame and other features). Evolut Pro is available in 23 mm, 26 mm, and 29 mm sizes.

The Myval series is a next-generation BEV approved by Conformité Européene. The frame (nickel-cobalt) is made of continuous hexagons arranged in a hybrid honeycomb fashion. Bovine pericardium tissue with the anti-calcification treatment (AntiCa) forms a tri-leaflet valve. The lower frame cells are covered internally and externally with PET, minimising the potential for PVR. The Myval series is manufactured in conventional sizes (20 mm, 23 mm, 26 mm, and 29 mm), intermediate sizes (21.5 mm, 24.5 mm, and 27.5 mm), and extra-large sizes (30.5 mm and 32 mm). All diameters are compatible with a 14-Fr Python introducer sheath (Meril Life Sciences, India).[10] The safety and efficacy of the Myval series in intermediate- to high-risk patients have been demonstrated in several studies.[10-13] However, the present study focuses on low- to intermediate-surgical-risk patients.

A summary of the main differences between these THVs is shown in Table 1.

Procedure

Procedures were performed in the hybrid operating room or in the catheterisation laboratory under shallow sedation in the majority of cases with local anaesthetic given at the puncture site or in general anaesthesia. Unfractionated heparin was given after all the vascular access sites were punc-

TABLE 2. Baseline characteristics and medical history of unmatched and matched cohorts with severe aortic stenosis who underwent TAVI with different THVs. Data availability is provided in the first row for each variable, n (%)

BASELINE CHARACTERISTICS	Overall Cohort (n = 1053)	Unmatched cohorts				Matched cohorts			
		Myval series (n = 97)	Sapien series (n = 400)	Evolut series (n = 556)	p-value* (Overall)	Myval series (n = 60)	Sapien series (n = 60)	Evolut series (n = 60)	p-value* (Overall)
Age (Years), mean ± SD	n = 1053 (100) 81.3 ± 6.4	n = 97 (100) 81.0 ± 6.5	n = 400 (100) 80.7 ± 6.4	n = 556 (100) 81.5 ± 6.7	0.682	n = 60 (100) 81.3 ± 6.7	n = 60 (100) 80.5 ± 6.6	n = 60 (100) 81.5 ± 7.1	0.729
Sex, n (%)	n = 1053 (100)	n = 97 (100)	n = 400 (100)	n = 556 (100)		n = 60 (100)	n = 60 (100)	n = 60 (100)	
Male, n (%)	542 (51.5)	52 (53.6)	209 (46.2)	311 (55.9)	0.009	29 (48.3)	24 (40.0)	31 (51.7)	0.419
Female, n (%)	511 (48.5)	45 (46.4)	243 (53.8)	245 (44.1)		31 (51.7)	36 (60.0)	29 (48.3)	
BMI (kg/m2), mean ± SD	n = 1001 (95) 27.59 ± 4.87	n = 97 (100) 28.56 ± 5.31	n = 377 (94) 27.99 ± 5.18	n = 527 (95) 27.12 ± 4.49	0.003	n=60 (100) 28.06 ± 5.12	n = 60 (100) 27.62 ± 5.14	n = 60 (100) 27.83 ± 4.66	0.885
Body surface area (m2), mean ± SD	n = 1001 (95) 1.83 ± 0.21	n = 97 (100) 1.87 ± 0.22	n = 377 (94) 1.81 ± 0.21	n = 527 (95) 1.83 ± 0.2	0.041	n = 60 (100) 1.85 ± 0.22	n = 60 (100) 1.78 ± 0.18	n = 60 (100) 1.82 ± 0.21	0.134
Indication, n (%)	n = 1051 (100)	n = 97 (100)	n = 398 (100)	n = 556 (100)		n = 60 (100)	n = 60 (100)	n = 60 (100)	
Stenosis	1038 (98.8)	96 (99.0)	391 (98.2)	551 (99.1)	0.445	60 (100.0)	59 (98.3)	60 (100.0)	1.000
Regurgitation	13 (1.2)	1 (1.0)	7 (1.8)	5 (0.9)		0 (0.0)	1 (1.7)	0 (0.0)	
Etiology, n (%)	n = 1050 (100)	n = 97 (100)	n = 399 (100)	n = 554 (100)		n = 60 (100)	n = 60 (100)	n = 60 (100)	
Degenerative	980 (93.3)	91 (93.8)	366 (91.7)	523 (94.4)	0.414	55 (91.7)	53 (88.3)	55 (91.7)	0.024
Rheumatic	3 (0.3)	0 (0.0)	1 (0.3)	2 (0.4)		0 (0.0)	0 (0.0)	1 (1.7)	
ViV, n (%)	67 (6.4)	6 (6.2)	32 (8.0)	29 (5.2)		5 (8.3)	5 (8.3)	0 (0.0)	
Creatinine (µmol/L), mean ± SD	n = 995 (95) 111.95 ± 74.74	n = 97 (100) 102.32 ± 68.56	n = 368 (92) 105.00 ± 64.36	n = 530 (95) 118.55 ± 81.70	0.011	n = 60 (100) 94.58 ± 36.27	n = 60 (100) 100.97 ± 54.30	n = 60 (100) 111.13 ± 82.84	0.326
DVI, mean ± SD	n = 704 (67) 0.20 ± 0.06	n = 68 (70) 0.20 ± 0.04	n = 263 (66) 0.20 ± 0.08	n = 373 (67) 0.20 ± 0.05	0.985	n = 48 (80) 0.20 ± 0.03	n = 50 (83) 0.19 ± 0.05	n = 51 (85) 0.19 ± 0.04	0.706
Systolic pulmonary artery pressure (mm Hg), mean ± SD	n = 675 (64) 42.9 ± 13.3	n = 60 (62) 40.6 ± 14.3	n = 247 (62) 42.3 ± 13.3	n = 368 (66) 43.7 ± 13.1	0.158	n = 42 (70) 38.8 ± 12.8	n = 51 (85) 41.8 ± 12.38	n = 53 (88) 42.4 ± 13.3	0.355
Euroscore 2, mean ± SD	n = 920 (87) 6.17 ± 6.74	n = 96 (99) 5.41 ± 5.30	n = 321 (80) 6.05 ± 6.51	n = 503 (91) 6.40 ± 7.11	0.384	n = 60 (100) 4.74 ± 3.82	n = 60 (100) 6.40 ± 8.23	n = 60 (100) 5.7 ± 4.72	0.307
STS score, mean ± SD	n = 830 (79) 4.43 ± 4.03	n = 97 (100) 3.78 ± 3.09	n = 284 (71) 4.28 ± 3.97	n = 449 (81) 4.67 ± 4.24	0.219	n = 60 (100) 3.90 ± 3.65	n = 60 (100) 4.64 ± 5.51	n = 60 (100) 5.07 ± 4.18	0.359
Annular perimeter (mm), mean ± SD	n = 949 (90) 80.2 ± 35.5	n = 91 (94) 79.5 ± 7.2	n = 359 (90) 79.6 ± 31.3	n = 499 (90) 80.8 ± 41.0	0.871	n = 56 (93) 79.1 ± 6.8	n = 59 (98) 77.3 ± 10.2	n = 60 (100) 79.0 ± 7.2	0.407
Annular area (mm^2), mean ± SD	n = 968 (92) 464.5 ± 97.6	n = 92 (95) 476.7 ± 94.7	n = 368 (92) 459.6 ± 88.1	n = 508 (91) 465.9 ± 104.3	0.293	n = 57 (95) 473.6 ± 92.3	n = 59 (98) 461.5 ± 95.3	n = 60 (100) 468.7 ± 85.8	0.774

BASELINE CHARACTERISTICS	Overall Cohort (n = 1053)	Unmatched cohorts				Matched cohorts			
		Myval series (n = 97)	Sapien series (n = 400)	Evolut series (n = 556)	p-value* (Overall)	Myval series (n = 60)	Sapien series (n = 60)	Evolut series (n = 60)	p-value* (Overall)
NYHA class before, n (%)	n = 994 (94)	n = 97 (100)	n = 367 (92)	n = 530 (95)		n = 60 (100)	n = 60 (100)	n = 60 (100)	
1	22 (2.2)	4 (4.1)	9 (2.5)	9 (1.7)	0.471	3 (5.0)	2 (3.3)	1 (1.7)	
2	205 (20.6)	17 (17.5)	75 (20.4)	113 (21.3)		12 (20.0)	15 (25.0)	14 (23.3)	0.963
3	653 (65.7)	68 (70.1)	245 (66.8)	340 (64.2)		40 (66.7)	38 (63.3)	41 (68.3)	
4	114 (11.5)	8 (8.2)	38 (10.4)	68 (12.8)		5 (8.3)	5 (8.3)	4 (6.7)	
Aortic regurgitation before, n (%)	n = 918 (87)	n = 84 (87)	n = 333 (83)	n = 501 (90)		n = 53 (88)	n = 60 (100)	n = 59 (98)	
None/trace	284 (30.9)	31 (36.9)	101 (30.3)	152 (30.3)	0.300	21 (39.6)	11 (18.3)	12 (20.3)	
Mild	522 (56.9)	40 (47.6)	194 (58.3)	288 (57.5)		25 (47.2)	43 (71.7)	43 (72.9)	0.032
Moderate	90 (9.8)	12 (14.3)	27 (8.1)	51 (10.2)		7 (13.2)	5 (8.3)	4 (6.8)	
Severe	22 (2.4)	1 (1.2)	11 (3.3)	10 (2.0)		0 (0.0)	1 (1.7)	0 (0.0)	
Mitral regurgitation before, n (%)	n = 882 (84)	n = 82 (85)	n = 327 (82)	n = 473 (85)		n = 52 (87)	n = 59 (98)	n = 58 (97)	
None/trace	111 (1.2)	17 (20.7)	35 (10.7)	59 (12.5)	0.090	12 (23.1)	4 (6.8)	2 (3.4)	
Mild	697 (75.9)	64 (78.1)	261 (79.8)	372 (78.6)		40 (76.9)	50 (84.7)	50 (86.2)	0.002
Moderate	69 (7.5)	1 (1.2)	29 (8.9)	39 (8.2)		0 (0.0)	5 (8.5)	6 (10.3)	
Severe	5 (0.5)	0 (0.0)	2 (0.6)	3 (0.6)		0 (0.0)	0 (0.0)	0 (0.0)	
Medical history, n (%)									
Arterial hypertension	878 (83.4)	88 (90.7)	327 (81.8)	463 (83.3)	-	56 (93.3)	56 (93.3)	54 (90.0)	-
Diabetes - oral antidiabetics	179 (17.0)	12 (12.4)	63 (15.8)	104 (18.7)	-	5 (8.3)	8 (13.3)	10 (16.7)	-
Diabetes – insulin dependent	72 (6.8)	7 (7.2)	22 (5.5)	43 (7.7)	-	6 (10.0)	6 (10.0)	5 (8.3)	-
Pulmonary disease	139 (13.2)	17 (17.5)	43 (10.8)	79 (14.2)	-	9 (15.0)	9 (15.0)	11 (18.3)	-
CKD (eGF < 60 mL/min/1.73 m²)	278 (26.4)	28 (28.9)	94 (23.5)	156 (28.1)	-	18 (30.0)	17 (28.3)	13 (21.7)	-
CKD - dialysis	24 (2.3)	1 (1.0)	5 (1.3)	18 (3.2)	-	0 (0.0)	1 (1.7)	1 (1.7)	-
Hyperlipidemia	300 (28.5)	31 (32.0)	107 (26.8)	162 (29.1)	-	18 (30.0)	23 (38.3)	19 (31.7)	-
Cardiac history, n (%)									
IHD (any type of revascularization, proximal significant coronary stenosis)	254 (24.1)	26 (26.8)	79 (19.8)	149 (26.8)	-	17 (28.3)	11 (18.3)	18 (30.0)	-
AV block I	94 (8.9)	8 (8.2)	23 (5.8)	63 (11.3)	-	3 (5.0)	4 (6.7)	9 (15.0)	-
AV block II	8 (0.8)	0 (0.0)	0 (0.0)	8 (1.4)	-	0 (0.0)	0 (0.0)	1 (1.7)	-
RBBB	72 (6.8)	8 (8.2)	26 (6.5)	38 (6.8)	-	7 (11.7)	3 (5.0)	4 (6.7)	-
LBBB	89 (8.5)	10 (10.3)	33 (8.3)	46 (8.3)	-	5 (8.3)	9 (15.0)	5 (8.3)	-
Atrial fibrillation	15 (1.4)	1 (1.03)	4 (1.00)	10 (1.8)	-	1 (1.67)	2 (3.3)	4 (6.7)	-
Atrial fibrillation - slow ventricular response	242 (23.0)	22 (22.7)	91 (22.8)	129 (23.2)	-	12 (20)	14 (23.3)	9 (15.0)	-
Electrosystolic rhythm	66 (6.3)	3 (3.1)	32 (8.0)	31 (5.6)	-	1 (1.67)	4 (6.7)	4 (6.7)	-

AV = atrioventricular; BMI = body mass index; CKD = Chronic kidney disease; DVI = Doppler velocity index; eGFR = estimated glomerular filtration rate; IHD = Ischemic heart disease; LBBB = Left bundle branch block; NYHA = New York Heart Association; RBBB = right bundle branch block; SD = standard deviation; STS = Society of Thoracic Surgeons; THV = transcatheter heart valve; TAVI = transcatheter valve implantation; ViV = valve-in-valve.

tured. A transfemoral approach (TF) was used in all cases. THV implantation was done according to the manufacturer's guidelines. Femoral closure devices included ProGlide/ProStyle (Abbott Vascular Devices, California, USA) and AngioSeal (St. Jude Medical, Minnesota, USA) in various ratios according to the operator's discretion.

Ultrasound analysis

Transthoracic echocardiograms (TTE) were obtained at baseline and at 30 days of follow-up, and the measured parameters followed the recommendations of the European and American guidelines.[17,18] The performance of each THV was assessed by its maximum aortic blood velocity (Vmax), mean aortic gradient, effective orifice area (EOA), and left ventricular ejection fraction (LVEF). TTE was done before hospital discharge and after 30 days after hospital discharge.

Outcomes

We looked at the following in-hospital cardiac complications: cardiac tamponade, annular rupture, valve embolisation, pericardial effusion, incorrect valve position, switching to open-heart surgery, periprocedural myocardial infarction (MI), and spontaneous myocardial infarction (MI). Other complications included access site complications, bleeding complications, and other components of post-procedure safety assessment. All the complications were assessed according to VARC-3 criteria.[15] The analysis also included haemodynamic performance at 30 days as assessed by TTE (Vmax, mean aortic gradient, EOA, and LVEF). We compared the 30-day and 1-year all-cause mortality between the matched groups.

Statistical analysis

Baseline characteristics were presented with descriptive statistics. Continuous variables were shown as mean and standard deviation, while nominal variables were presented as frequencies and percentages. The between-group comparisons were performed using an independent sample t-test and ANOVA in the case of quantitative variables, as appropriate. A paired t-test was used for the post-hoc analysis to evaluate the significant differences between pre-procedure and post-procedure data within each group. The Chi-square/Fisher's exact test was used for qualitative variables, as appropriate. Propensity score matching analysis was performed using the nearest neighbour matching method to balance the study groups based on key baseline characteristics. Patients were matched based on their age, gender, Society of Thoracic Surgeons (STS), LVEF, body mass index (BMI), body surface area (BSA), New York Heart Association (NYHA) functional class, pre-procedural serum creatinine level, baseline conduction abnormalities (Right Bundle Branch Block, RBBB), and baseline atrial fibrillation at the inclusion in the study. A P-value < 0.05 was considered statistically significant. Statistical analysis was performed using R software.

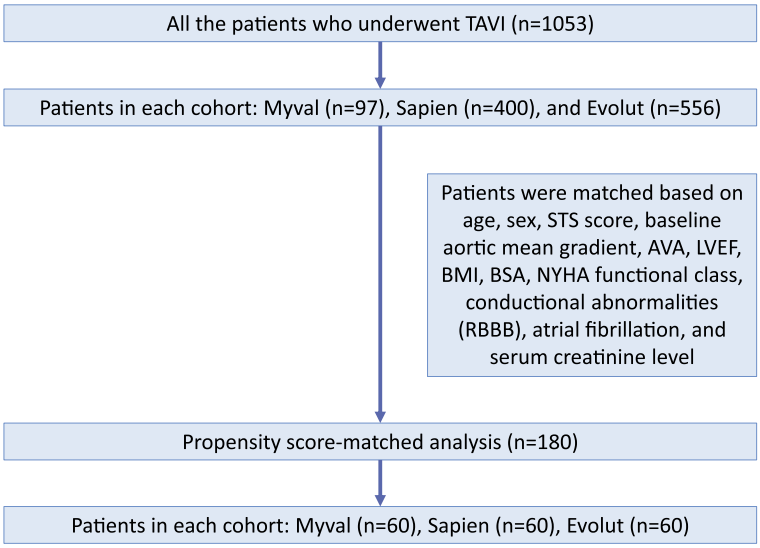

FIGURE 1. Flowchart of patient selection and propensity score matching in transcatheter aortic valve implantation (TAVI) cohorts.

AVA = aortic valve area; BMI = body mass index; BSA = body surface area; LVEF = left ventricular ejection fraction; NYHA = New York Heart Association; RBBB = Right Bundle Branch Block; STS = Society of Thoracic Surgeons

Results

A total of 1053 patients who underwent TAVI were included in the analysis. Out of 1053 TAVI patients, 97 patients received the Myval series, 400 patients received the Sapien series, and 556 patients received the Evolut series (Table 2, Figure 1). The mean age of the cohort was 81.3 ± 6.4 years, and 51.5% of the patients were male. 878 (83.4%) of the patients had arterial hypertension. The other common comorbidities included diabetes (23.8%), pulmonary disease (13.2%), chronic kidney disease (CKD) (28.7%), ischaemic heart disease (24.1%), hyperlipidaemia (28.5%), and atrial fibrillation (24.4%) (Table 2). In terms of the surgical risk in the cohort,

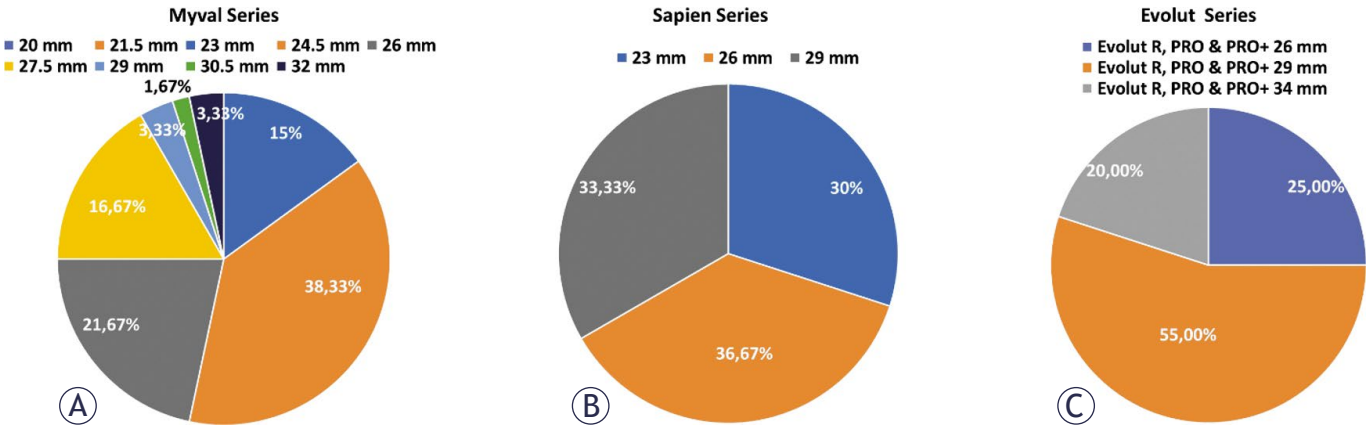

FIGURE 2. Sizes of implanted transcatheter heart valves – **(A)** Myval series, **(B)** Sapien series, **(C)** Evolut series.

the mean EuroScore II score was 6.17 ± 6.74% (n = 920) and the mean STS score was 4.43 ± 4.03% (n = 830). (Table 2).

A total of 180 patients from the large cohort were included in the propensity-score matching analysis. The most important baseline parameters of this subpopulation were aligned with the overall patient population. Three groups (60 for each device) were formed using propensity score matching to ensure equivalence by the essential baseline characteristics and clinical assessments. The baseline characteristics and confirmation of the absence of significant differences between the groups can be found in Table 2.

The study compared the three THV series in a low- to intermediate-risk population of patients with severe symptomatic AS. The mean STS score was 3.90 ± 3.65% in the Myval series, 4.64 ± 5.51% in the Sapien series, and 5.07 ± 4.18% in the Evolut series (p = 0.359). The mean EuroScore II was 4.74 ± 3.82 in the Myval series, 6.40 ± 8.23 in the Sapien series, and 5.70 ± 4.72 in the Evolut series (p = 0.307). The groups did not differ significantly by NYHA functional class before TAVI. Most patients were in Class III (66.7% *vs.* 63.3% *vs.* 68.3%) or Class II (20.0% *vs.* 25.0% *vs.* 23.3%) in the Myval, Sapien, and Evolut series, respectively. Previous surgical valve replacement was reported in five patients (8.3%) in the Myval series, five patients (8.3%) in the Sapien series, and none of the patients from the Evolut series.

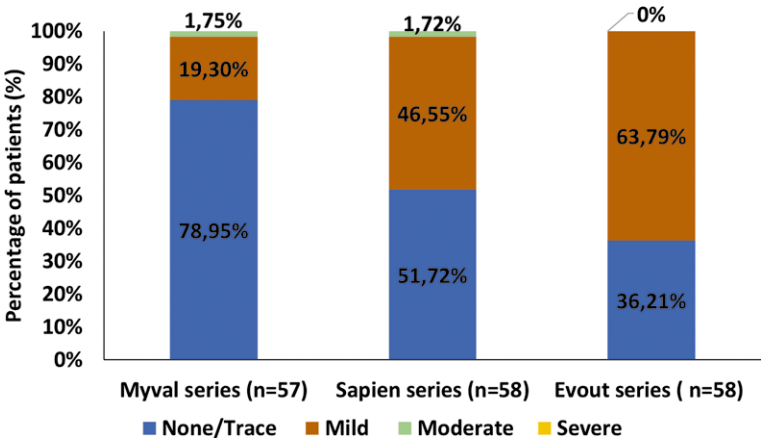

FIGURE 3. Paravalvular regurgitation after transcatheter implantation of Myval, Sapien, and Evolut series.

The study evaluated clinical outcomes in terms of safety and performance of the device. Few patients required conversion from percutaneous to surgical closure of access site: 3 (5.0%) in the Myval series, 1 (1.7%) in the Sapien series, and 3 (5.0%) in the Evolut series. The only series in which no patient received general anaesthesia was the Myval series. Sizes of the implanted valves are illustrated in Figure 2.

Pre-dilation was performed more frequently in the Evolut series and Sapien series than in the Myval series (39 [65.0%] *vs.* 58 [37.9%] *vs.* 2 [3.3%]). Post-dilatation was more frequent in the Evolut series (29.3%) than in the Myval series (5.0%) and Sapien series (0.0%), respectively.

The groups did not vary significantly in terms of cardiac complications such as periprocedural myocardial infarction (MI) (less than 72 hours), spontaneous MI (more than 72 hours), tamponade, annular rupture, valve embolisation, improper valve position, and new pericardial effusion. The details are listed in Table 3. Regarding PVR after TAVI, most patients in all groups fell into the none/trace and mild categories (Figure 3). The new PPI

TABLE 3. In-hospital cardiac complications in the propensity-score matched cohort. Data availability is provided in the first row for each variable, n (%)

In-hospital outcomes, n (%)	Myval series (n = 60)	Sapien series (n = 60)	Evolut series (n = 60)	p-value overall	p-value Myval series vs Evolut series	p-value Myval series vs. Sapien series	p-value Evolut series vs. Sapien series
Cardiac complications	n = 59 (98) 3 (5.1)	n = 60 (100) 6 (10.0)	n = 59 (98) 2 (3.4)	0.390	1.000	0.491	0.272
New pericardial effusion	0 (0.0)	1 (1.7)	1 (1.7)	1.000	1.000	1.000	1.000
Tamponade	0 (0.0)	4 (6.7)	1 (1.7)	0.129	1.000	0.119	0.364
Annular rupture	1 (1.7)	1 (1.7)	0 (0.0)	1.000	1.000	1.000	1.000
Valve embolization	0 (0.0)	0 (0.0)	0 (0.0)	1.000	1.000	1.000	1.000
Improper valve position	0 (0.0)	1 (1.7)	0 (0.0)	1.000	1.000	1.000	1.000
Conversion to heart surgery	0 (0.0)	0 (0.0)	0 (0.0)	1.000	1.000	1.000	1.000
Periprocedural myocardial infarction (< 72h)	2 (3.3)	0 (0.0)	0 (0.0)	0.330	0.496	0.496	1.000
Spontaneous myocardial infarction (> 72h)	0 (0.0)	0 (0.0)	0 (0.0)	1.000	1.000	1.000	1.000
Neurological complications	n = 58 (97) 3 (5.2)	n = 58 (97) 2 (3.4)	n = 59 (98) 1 (1.7)	0.534	0.364	1.000	0.619
Transient ischemic attack	1 (1.7)	0 (0.0)	1 (1.7)	1.000	1.000	1.000	1.000
Ischemic cerebrovascular insult	2 (3.4)	2 (3.4)	0 (0.0)	0.548	0.496	1.000	0.496
Hemorrhagic cerebrovascular insult	0 (0.0)	0 (0.0)	0 (0.0)	1.000	1.000	1.000	1.000
Bleeding	n = 59 (98) 4 (6.8)	n = 59 (98) 6 (10.2)	n = 60 (100) 6 (10.0)	0.768	0.743	0.741	1.000
Bleeding - minor	3 (5.0)	1 (1.7)	2 (3.3)	0.872	1.000	0.619	1.000
Bleeding - major	0 (0.0)	4 (6.7)	3 (5.0)	0.164	0.246	0.119	1.000
Bleeding - life-threatening	1 (1.7)	1 (1.7)	1 (1.7)	1.000	1.000	1.000	1.000
Other complications							
Acute kidney injury	n = 60 (100) 1 (1.7)	n = 60 (100) 5 (8.3)	n = 60 (100) 4 (6.7)	0.350	0.364	0.207	1.000
New left bundle branch block	n = 60 (100) 5 (8.3)	n = 60 (100) 2 (3.3)	n = 60 (100) 5 (8.3)	0.495	1.000	0.439	0.439
New atrial fibrillation	n = 60 (100) 2 (3.3)	n = 60 (100) 2 (3.3)	n = 60 (100) 1 (1.7)	1.000	1.000	1.000	1.000
Permanent pacemaker implantation after TAVI	n = 60 (100) 7 (11.9)	n = 60 (100) 6 (10.0)	n = 60 (100) 9 (15.0)	0.719	0.816	1.000	0.605
30-day mortality	n = 60 (100) 2 (3.3)	n = 60 (100) 3 (5.0)	n = 60 (100) 2 (3.3)	1.000	1.000	1.000	1.000
1-year mortality	n = 60 (100) 5 (8.3)	n = 60 (100) 5 (8.3)	n = 60 (100) 6 (10.0)	0.934	1.000	1.000	1.000

MI = myocardial infarction; TAVI = transcatheter aortic valve implantation

rate was numerically lower in the Myval (11.9%) and Sapien (10.2%) series compared to the Evolut series (15.0%), but the difference was not statistically significant (Table 3). Significant improvement (between pre- and post-TAVI) in Vmax and EOA was observed in all three groups. It is worth noting that the proportion of valve-in-valve procedures was 8.3% in both the Myval and Sapien series, while no ViV procedures were performed in the Evolut group. Given that ViV procedures are known to be associated with higher post-procedural transvalvular gradients, this difference may have contributed to the slightly higher gradients observed in the Myval and Sapien groups. Significant improvement of LVEF was seen only in the Sapien series (p = 0.023), while in the Myval (p =

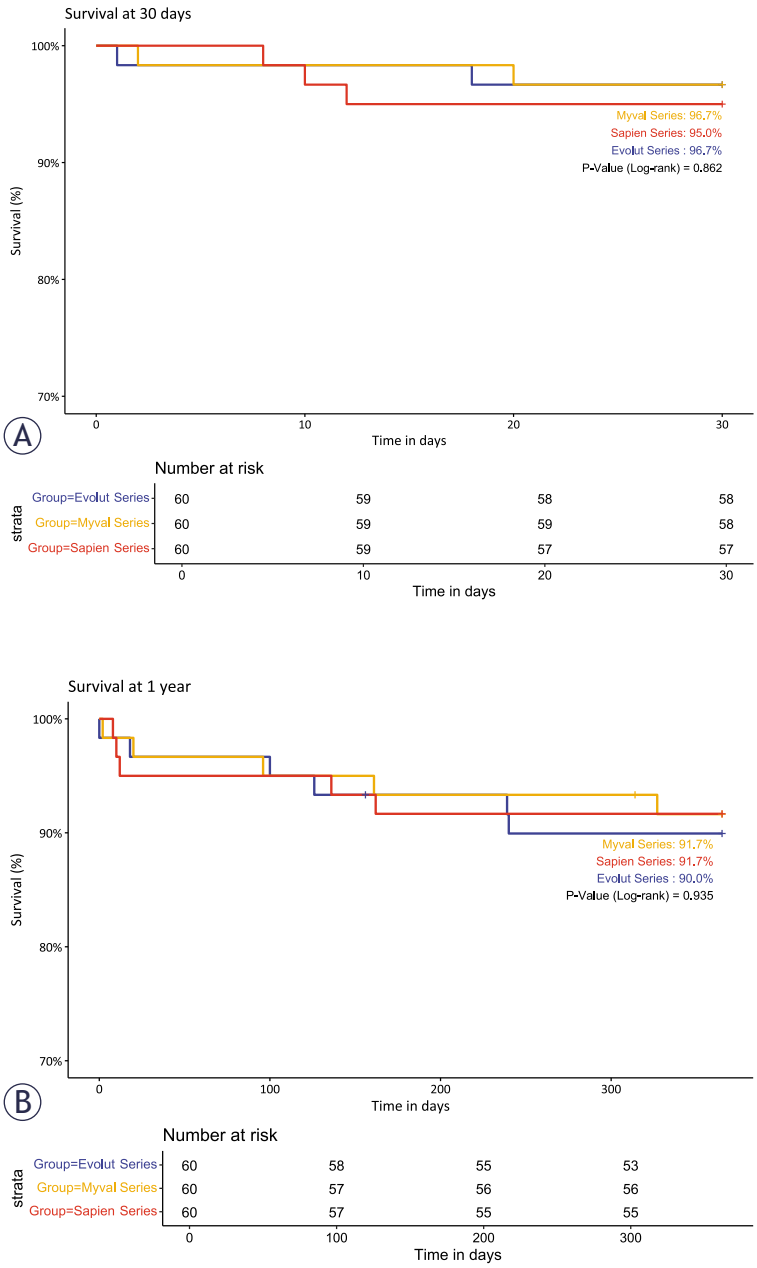

FIGURE 4. Kaplan-Meier survival curves of matched cohorts for 30 days **(A)** and 1 year **(B)** after transcatheter implantation of Myval, Sapien, and Evolut series in patients with severe symptomatic aortic stenosis.

0.061) and Evolut series (p = 0.057) did not reach the level of significance. See Table 4 for further details.

In the matched cohort, there were two in-hospital deaths (both cardiac deaths) in the Myval series (heart failure and severe retroperitoneal bleeding after vascular complications); three in-hospital deaths (one cardiac and two non-cardiac) in the Sapien 3 series group; and two in-hospital deaths (one cardiac and one non-cardiac) in the Evolut series. Figures 4A and 4B display the Kaplan-Meier survival curves for propensity-matched cohorts at 30 days and 1 year.

Discussion

This study was conducted to compare the real-world performance and safety of the Myval series with contemporary TAVI devices, including the Sapien and Evolut platforms. All three Evolut R, Evolut Pro, and Evolut Pro+ devices were used in this study. A previous comparison of the Myval series and the Sapien series has shown that the Myval series was favourable in terms of safety, haemodynamics, and PVR. The latter were evaluated in blinded echocardiographic assessments.[19]

Our study also showed negligible or mild PVR in the majority of cases and the absence of severe PVR in all cases. Precise sizing may also play a role in PVR reduction. The traditional diameters of TAVI prostheses were 20, 23, 26, and 29 mm. This limited-size matrix means that the nominal volume of the balloon needs to be changed so that the prosthesis fits correctly around the patient's area-derived annulus diameter and the aortic root complex is not damaged. The Myval series' size matrix with intermediate sizes might help to address this important issue.

Several previous studies have compared the Myval and Evolut series in patients with symptomatic severe AS. The early clinical performance and safety of Myval and the Evolut R were compared in a single-centre retrospective cohort study. 108 patients received the Evolut R THV, and 58 patients were treated with the Myval THV. The Myval series provided comparable performance to the Evolut series, and it was associated with lower rates of PPI and ≥ moderate PVR within 30 days and 6 months after the procedure.[12] A new study using propensity score matching discovered that the two valves were comparable in terms of safety and effectiveness, with the Evolut series having a higher PPI rate. Up to 1-year of follow-up, clinical outcomes showed acceptable rates of stroke and cardiac death for both valves.[7] In the EVAL registry, 2-year clinical and echocardiographic outcomes of TAVI were compared between the Myval and Evolut series. Both THVs showed similar 2-year clinical outcomes. Benefits from the Myval series included decreased PVR incidence and increased clinical effectiveness.[13]

TABLE 4. Comparison of haemodynamic parameters in a matched cohort. Data availability is provided in the first row for each variable, n (%)

Hemodynamic Outcomes in Matched Cohort				P value
Parameters	**Cohort**	**Before procedure**	**After procedure**	
Aortic Vmax (m/s), mean ± SD	Myval series	n = 56 (93) 4.3 ± 0.5	n = 58 (97) 2.1 ± 0.5	< 0.001
	Evolut series	n = 59 (98) 4.3 ± 0.6	n = 54 (90) 1.8 ± 0.4	< 0.001
	Sapien series	n = 58 (97) 4.3 ± 0.6	n = 55 (92) 2.2 ± 0.4	< 0.001
	p-value (Myval vs. Evolut)	0.780	< 0.001	
	p-value (Myval vs. Sapien)	0.908	0.355	
Aortic mean gradient (mm Hg), mean ± SD	Myval series	n = 60 (100) 47.2 ± 13.1	n = 58 (97) 11.1 ±5.4	< 0.001
	Evolut series	n = 60 (100) 46.6 ± 15.3	n = 54 (90) 6.7 ± 2.61	< 0.001
	Sapien series	n = 60 (100) 47.3 ± 14.8	n = 54 (90) 10.8 ± 3.9	< 0.001
	p-value (Myval vs. Evolut)	0.808	< 0.001	
	p-value (Myval vs. Sapien)	0.958	0.684	
AVA and EOA (cm2), mean ± SD	Myval series	n = 60 (100) 0.7 ±0.1	n = 57 (95) 1.9 ± 0.5	< 0.001
	Evolut series	n = 60 (100) 0.7 ± 0.1	n = 51 (85) 1.8 ± 0.5	< 0.001
	Sapien series	n = 60 (100) 0.6 ± 0.2	n = 56 (93) 1.7 ± 0.5	< 0.001
	p-value (Myval vs. Evolut)	0.121	0.807	
	p-value (Myval vs. Sapien)	0.068	0.026	
LVEF (%), mean ± SD	Myval series	n = 59 (98) 59.2 ± 11.1	n = 52 (87) 61.6 ± 9.9	0.061
	Evolut series	n = 60 (100) 54.8 ± 14.7	n = 52 (87) 58.5 ± 12.4	0.057
	Sapien series	n = 60 (100) 56.1 ± 15.8	n = 53 (88) 58.3 ± 14.9	0.023
	p-value (Myval vs. Evolut)	0.063	0.170	
	p-value (Myval vs. Sapien)	0.211	0.180	

AVA = aortic valve area; EOA = effective orifice area; LVEF = left ventricular ejection fraction. All in-group differences were significant ($p < 0.05$ for all within-group comparisons). Mean ± SD = Mean values and standard deviation.

In examining the outcomes associated with the Myval series, it is important to note that the SAPIEN 3 Ultra (S3U) valve has demonstrated comparable rates of death and other clinical outcomes up to 30 days post-TAVI, with both devices exhibiting remarkably low rates that align with findings from larger series involving the SAPIEN 3 (S3) valve.[3,20,21] Notably, the S3U valve was associated with a significantly lower rate of mild PVR compared to its predecessor, with rates of 43.0% for the S3 versus 18.7% for the S3U. Interestingly, there was no significant difference in the rates of moderate or severe PVR, reported at 1.3% for the S3 and 2.7% for the S3U.[22] These findings underscore the potential benefits of the S3U valve in achieving improved outcomes related to mild PVR, which is a critical consideration for future studies comparing it to the Myval. Discussing these comparisons may help inform best practices in valve selection and management of PVR in TAVI procedures. In another study, Stinis *et al*. compared outcomes of the SAPIEN 3 Ultra Resilia valve (S3UR) with its predecessors, the S3/S3U. After propensity matching, 10312 patients were included in each cohort. This fifth-generation BEV demonstrated significantly better haemodynamic performance compared to S3/S3U at discharge and 30 days.[23]

Frangieh *et al*. (2017) described a standardised minimalist approach for TF-TAVI using SAPIEN 3 devices through extensive operator experience at a high-volume center. The approach consists of 10 structured steps executed under fluoroscopic guidance, underscoring the importance of a collaborative heart-team strategy to optimise patient outcomes. The key findings highlight a significant reduction in intubation rates and intervention times, alongside a marked decrease in PPI from 18% to 5.6% due to optimised valve positioning. This structured framework is particularly advantageous for operators, enhancing safety and efficacy in TAVI procedures.[24] In our study, the PPI rate for Sapien 3 was comparably lower than this study (10.17%). However, these rates can further be reduced by utilising this technique.

Four different SEVs (Evolut, Acurate [Boston Scientific, USA], Portico [Abbott, USA], and Allegra [NVT, Germany]) and one BEV (Sapien 3) were compared in an Academic European registry of 1131 consecutive patients with severe AS against Myval. The comparison was based on conduction disturbances. The results showed that Myval had similar procedural and in-hospital outcomes to the Sapien-3. It also had much lower early PPI rates than SEVs like Evolut, Portico, and Allegra. A few early conduction disruptions were associated with the Myval THVs, while some SEV choices resulted in significant variations in the PR and QRS wavelengths.[25] These findings are consistent with our findings from the current study. The size range of the Myval THV is wider than that of the Evolut series and the Sapien 3 series. In our matched groups, almost half of the patients used the intermediate sizes of Myval THVs. Intermediate sizes of the Evolut and Sapien series may also improve conduction disturbances and PVR.

The LANDMARK trial was a prospective, randomised, multinational, open-label non-inferiority trial that demonstrated non-inferiority of the Myval over Sapien and Evolut series for the primary combined safety and effectiveness endpoint (25% *vs*. 27%; risk difference: 2.3%, p-non-inferiority < 0.0001) at 30 days in severe AS patients.[14] In a recent subset analysis, the LANDMARK trial has demonstrated the non-inferiority of the Myval over the Sapien and Evolut series individually.[26] Myval series had a significantly better EOA than Sapien and a comparable EOA with Evolut series for similar THV sizes. In small aortic annuli patients, the Myval series had a comparable rate of primary composite endpoint compared to the Sapien and Evolut series.[26]

Our study has several limitations. First, the data were collected at a single centre as part of routine clinical practice. Because of this observational study design and the collection of data from real-world practice, some echocardiographic examinations and outcome assessments were not available for some of the patients, and 1-year echocardiographic data is not available. Echocardiography was performed locally as per standard practice at the study centre and not in a core echocardiographic laboratory. Second, all-cause mortality was the only outcome assessed at 1-year follow-up. While mortality is a critical outcome, the absence of longer-term follow-up data restricts a comprehensive evaluation of other important patient outcomes and the sustainability of treatment effects. Data would have been better with an echocardiographic assessment and an assessment of clinical outcomes at 1 year. Another limitation is the relatively small sample size of 180 patients, divided into three groups of 60 patients each in the propensity score-matched group, which may limit the statistical power and generalisability of the findings. Since this is a tri-match propensity score study, the results would have been more robust if the sample had been larger.

Acknowledgements

We thank nurses, laboratory technicians and physicians who assisted in this study.

References

1. Bhogal S, Rogers T, Aladin A, Ben-Dor I, Cohen JE, Shults CC, et al. TAVR in 2023: Who should not get it? *Am J Cardiol* 2023; **193:** 1-18. doi: 10.1016/j.amjcard.2023.01.040

2. Leon MB, Smith CR, Mack MJ, Makkar RR, Svensson LG, Kodali SK, et al. Transcatheter or surgical aortic-valve replacement in intermediate-risk patients. *N Engl J Med* 2016; **374:** 1609-20. doi: 10.1056/NEJMoa1514616

3. Mack MJ, Leon MB, Thourani VH, Makkar R, Kodali SK, Russo M, et al. Transcatheter aortic-valve replacement with a balloon-expandable valve in low-risk patients. *N Engl J Med* 2019; **380:** 1695-705. doi: 10.1056/NEJMoa1814052

4. Deeb GM, Reardon MJ, Chetcuti S, Patel HJ, Grossman PM, Yakubov SJ, et al. 3-year outcomes in high-risk patients who underwent surgical or transcatheter aortic valve replacement. *J Am Coll Cardiol* 2016; **67:** 2565-74. doi: 10.1016/j.jacc.2016.03.506

5. Webb JG, Blanke P, Meier D, Sathananthan J, Lauck S, Chatfield AG, et al. TAVI in 2022: remaining issues and future direction. *Arch Cardiovasc Dis* 2022; **115:** 235-42. doi: 10.1016/J.ACVD.2022.04.001

6. Zaid S, Atkins MD, Kleiman NS, Reardon MJ, Tang GHL. What's new with TAVR? An update on device technology. *Methodist Debakey Cardiovasc J* 2023; **19:** 4-14. doi:10.14797/mdcvj.1230

7. Halim J, Rooijakkers M, den Heijer P, El Haddad M, van den Branden B, Vos J, et al. Assessing the novel Myval balloon-expandable valve with the evolut valve: A propensity-matched study. *J Clin Med* 2023; **12:** 4213. doi: 10.3390/jcm12134213

8. Kalogeras K, Ruparelia N, Kabir T, Jabbour R, Naganuma T, Vavuranakis M, et al. Comparison of the self-expanding Evolut-PRO transcatheter aortic valve to its predecessor Evolut-R in the real world multicenter ATLAS registry. *Int J Cardiol* 2020; **310:** 120-5. doi: 10.1016/j.ijcard.2020.02.070

9. Thyregod HGH, Jørgensen TH, Ihlemann N, Steinbrüchel DA, Nissen H, Kjeldsen BJ, et al. Transcatheter or surgical aortic valve implantation: 10-year outcomes of the NOTION trial. *Eur Heart J* 2024; **45:** 1116-24. doi: 10.1093/eurheartj/ehae043

10. Sharma SK, Rao RS, Chandra P, Goel PK, Bharadwaj P, Joseph G, et al. First-in-human evaluation of a novel balloon-expandable transcatheter heart valve in patients with severe symptomatic native aortic stenosis: the MyVal-1 study. *EuroIntervention* 2020; **16:** 421-9. doi: 10.4244/EIJ-D-19-00413

11. Sharma SK, Rao RS, Chopra M, Sonawane A, Jose J, Sengottuvelu G. Myval transcatheter heart valve system in the treatment of severe symptomatic aortic stenosis. *Future Cardiol* 2021; **17:** 73-80. doi: 10.2217/fca-2020-0020

12. Barki M, Ielasi A, Buono A, Maliandi G, Pellicano M, Bande M, et al. Clinical comparison of a novel balloon-expandable versus a self-expanding transcatheter heart valve for the treatment of patients with severe aortic valve stenosis: The EVAL Registry. *J Clin Med* 2022; **11:** 959. doi: 10.3390/jcm11040959

13. Moscarella E, Ielasi A, Montonati C, Pellegrini D, Pellicano M, Briguglia D, et al. Comparing two-year outcomes of balloon-expandable Myval and self-expanding Evolut R in severe aortic valve stenosis. *Int J Cardiol* 2024; **400:** 131701. doi: 10.1016/j.ijcard.2023.131701

14. Baumbach A, van Royen N, Amat-Santos IJ, Hudec M, Bunc M, Ijsselmuiden A, et al. LANDMARK comparison of early outcomes of newer-generation Myval transcatheter heart valve series with contemporary valves (Sapien and Evolut) in real-world individuals with severe symptomatic native aortic stenosis: a randomised non-inferiority trial. *Lancet* 2024; **403:** 2695-708. doi: 10.1016/S0140-6736(24)00821-3

15. Généreux P, Piazza N, Alu MC, Nazif T, Hahn RT, Pibarot P, et al. Valve academic research consortium 3: Updated endpoint definitions for aortic valve clinical research. *J Am Coll Cardiol* 2021; **77:** 2717-46. doi: 10.1016/J.JACC.2021.02.038

16. Rheude T, Blumenstein J, Möllmann H, Husser O. Spotlight on the SAPIEN 3 transcatheter heart valve. *Med Devices Evid Res* 2018; **11:** 353-60. doi: 10.2147/MDER.S143897

17. Galderisi M, Cosyns B, Edvardsen T, Cardim N, Delgado V, Di Salvo G, et al. Standardization of adult transthoracic echocardiography reporting in agreement with recent chamber quantification, diastolic function, and heart valve disease recommendations: An expert consensus document of the European Association of Cardiovascular Imaging. *Eur Heart J Cardiovasc Imaging* 2017; **18:** 1301-10. doi: 10.1093/ehjci/jex244

18. Mitchell C, Rahko PS, Blauwet LA, Canaday B, Finstuen JA, Foster MC, et al. Guidelines for performing a comprehensive transthoracic echocardiographic examination in adults: Recommendations from the American Society of Echocardiography. *J Am Soc Echocardiogr* 2019; **32:** 1-64. doi: 10.1016/j.echo.2018.06.004

19. Delgado-Arana JR, Gordillo-Monge MX, Halim J, De Marco F, Trani C, Martin P, et al. Early clinical and haemodynamic matched comparison of balloon-expandable valves. *Heart* 2022; **108:** 725-32. doi: 10.1136/heartjnl-2021-319349

20. Wendler O, Schymik G, Treede H, Baumgartner H, Dumonteil N, Neumann FJ, et al. SOURCE 3: 1-year outcomes post-transcatheter aortic valve implantation using the latest generation of the balloon-expandable transcatheter heart valve. *Eur Heart J* 2017; **38:** 2717-26 doi: 10.1093/eurheartj/ehx294

21. Kodali S, Thourani VH, White J, Malaisrie SC, Lim S, Greason KL, et al. Early clinical and echocardiographic outcomes after SAPIEN 3 transcatheter aortic valve replacement in inoperable, high-risk and intermediate-risk patients with aortic stenosis. *Eur Heart J* 2016; **37:** 2252-62. doi: 10.1093/eurheartj/ehw112

22. Rheude T, Pellegrini C, Lutz J, Alvarez-Covarrubias HA, Lahmann AL, Mayr NP, et al. Transcatheter aortic valve replacement with balloon-expandable valves: Comparison of SAPIEN 3 Ultra versus SAPIEN 3. *JACC Cardiovasc Interv* 2020; **13:** 2631-8. doi: 10.1016/j.jcin.2020.07.013

23. Stinis CT, Abbas AE, Teirstein P, Makkar RR, Chung CJ, Iyer V, et al. Real-world outcomes for the fifth-generation balloon expandable transcatheter heart valve in the United States. *JACC Cardiovasc Interv* 2024; **17:** 1032-44. doi: 10.1016/j.jcin.2024.02.015

24. Frangieh AH, Ott I, Michel J, Shivaraju A, Joner M, Mayr NP, et al. Standardized minimalistic transfemoral transcatheter aortic valve replacement (TAVR) using the SAPIEN 3 device: Stepwise description, feasibility, and safety from a large consecutive single-center single-operator cohort. *Struct Hear* 2017; **1:** 1-10. doi: 10.1080/24748706.2017.1358832

25. Santos-Martinez S, Halim J, Castro-Mejía A, De Marco F, Trani C, Martin P, et al. Myval versus alternative balloon- and self-expandable transcatheter heart valves: A central core lab analysis of conduction disturbances. *Int J Cardiol* 2022; **351:** 25-31. doi: 10.1016/j.ijcard.2021.12.049

26. van Royen N, Amat-Santos IJ, Hudec M, Bunc M, Ijsselmuiden A, Laanmets P, et al. Early outcomes of the novel Myval THV series compared to SAPIEN THV series and Evolut THV series in individuals with severe aortic stenosis. *EuroIntervention* 2025; **21:** e105-18. doi: 10.4244/EIJ-D-24-00951

research article

Cardiotoxicity in low-to-moderate cardiovascular risk patients undergoing anti-HER2 therapy: a prospective cardiac magnetic resonance study

Sainan Cheng[1], Mei Deng[1], Linlin Qi[1], Fenglan Li[1], Jiaqi Chen[1], Shulei Cui[1], Yawen Wang[1], Jianing Liu[1], Yang Fan[2], Lizhi Xie[2], Jianwei Wang[1]

[1] Department of Diagnostic Radiology, National Cancer Center/National Clinical Research Center for Cancer/Cancer Hospital, Chinese Academy of Medical Sciences and Peking Union Medical College, Beijing, China

[2] MR Research China, GE Healthcare, Beijing Economic-Technological Development Area, Beijing, China

Radiol Oncol 2025; 59(4): 510-521.

Received 16 March 2025
Accepted 23 May 2025

Correspondence to: Prof. Jianwei Wang, Ph.D., Department of Diagnostic Radiology, National Cancer Center/National Clinical Research Center for Cancer/Cancer Hospital, Chinese Academy of Medical Sciences and Peking Union Medical College, China. E-mail: dr_jianweiwang@163.com

Disclosure: No potential conflicts of interest were disclosed.

Background. The study aimed to investigate cardiotoxicity among individuals undergoing anti- human epidermal growth factor receptor 2 (HER2) therapy with a low-to-moderate risk of cardiovascular complications. Cardiac magnetic resonance (CMR) imaging was employed in the investigation.

Patients and methods. HER2-positive breast cancer patients who underwent CMR examinations both before and during therapy (first follow-up: 3−5 months; second follow-up: 6−12 months) between January 2021 and December 2022 were prospectively included. Each patient was evaluated for the risk of cardiovascular toxicity.

Results. Thirty-five HER2-positive breast cancer patients were included (48.86 ± 10.34 years). Eighty-nine percent of patients had low cardiovascular toxicity risk, and 11% had moderate cardiovascular toxicity risk. At follow-up CMR, nine (25.71%) patients developed cardiac dysfunction. At follow-up 1, there was a notable decrease in left ventricular ejection fraction, stroke volume index, cardiac output index, and absolute strain values, accompanied by higher T1 and T2 values as well as end-systolic volume index compared to baseline ($p \leq 0.002$). At follow-up 2, the T1 and T2 values recovered to near baseline. The cardiac output index exhibited a continuous decline ($p = 0.022$), while other variables were similar ($p > 0.05$). Furthermore, at follow-up 1, the T1 value displayed a marked increase in patients with 1−3 points in cardiovascular toxicity risk factors compared to those with no risk factors ($p \leq 0.043$).

Conclusions. It is common for patients with low-to-moderate cardiovascular risk to experience early cardiotoxicity during anti-HER2 therapy. T1 mapping was a valuable approach for quantifying the specific extent of subtle tissue damage.

Key words: breast cancer; cardiotoxicity; cardiac magnetic resonance imaging; HER2; T1 mapping

Introduction

Advancements in breast cancer therapy, especially with targeted treatments, have yielded promising results for individuals diagnosed with human epidermal growth factor receptor 2 (HER2)-positive breast cancer. While displaying remarkable anticancer effects, the frequent incidence of cardiotoxicity resulting from cancer treatments hampers their clinical application and could compromise the quality of life for cancer survivors.[1] The European Society of Cardiology Guidelines

on cardio-oncology recommend a comprehensive evaluation of cardiovascular toxicity risk prior to initiating anticancer therapy, along with diligent cardiovascular monitoring throughout the cancer treatment journey.[2] Early detection of changes in myocardial structure and function plays a pivotal role in preventing treatment disruptions and maintaining cardiac function.[2-4] However, in clinical practice, cardiac surveillance during anticancer therapies is often overlooked among breast cancer patients without high cardiovascular toxicity risk and among those who have received non-anthracycline-based HER2-targeted therapy. Hence, clarifying cardiac functional alterations in patients with low-to-moderate cardiovascular toxicity risk undergoing anti-HER2 therapy is crucial. This clarification can assist in devising more practical and cost-effective screening strategies.

Cardiac magnetic resonance (CMR) imaging plays a crucial role in monitoring cancer therapy-related cardiotoxicity in this scenario, as it enables non-invasive identification of myocardial pathologies such as diffuse fibrosis, oedema, and inflammation using tissue characterization techniques.[5] While CMR studies have highlighted cardiac systolic function changes during anti-HER2 therapy, they have not assessed the cardiovascular toxicity risk of HER2-positive breast cancer patients.[6-9] Data on CMR changes after anticancer therapy among HER2-positive patients with low-to-moderate cardiovascular toxicity risk are limited. Therefore, this study aims to explore alterations in myocardial structure and function among HER2-positive breast cancer patients presenting a low-to-moderate cardiovascular toxicity risk profile employing CMR.

Patients and methods

Study participants

During the period spanning from January 2021 to December 2022, we conducted prospective enrolment of patients diagnosed with HER2-positive breast cancer, all of whom were slated to undergo anti-HER2 therapy. The oncologist exercised discretion in managing anticancer therapy. The anti-HER2 therapy regimen comprises two categories: single-targeted therapy (trastuzumab) and dual-targeted therapy (trastuzumab plus pertuzumab). Within the dual-targeted therapy, there are further subdivisions: one includes anthracycline-based drugs (anthracycline chemotherapy followed by taxane plus dual-targeted therapy), and the other does not involve anthracycline-based drugs (taxane plus carboplatin plus dual-targeted therapy). The treatment lasts for a cycle of 21 days. The exclusion criteria comprised a history of prior anticancer therapy, pre-existing symptomatic cardiac conditions, contraindications to undergo CMR, and refusal to take part in the study.

Based on recent clinical study findings, most instances of cancer therapy-related cardiac dysfunction (CTRCD) manifest within the initial 6 months' treatment. Therefore, our study was included three CMR examinations, conducted before therapy (baseline), in the early stages after therapy initiation (at 3~5 months for follow-up 1), and in the mid-to-late stages (at 6~12 months for follow-up 2). Those who underwent at least one follow-up CMR examination were eligible for inclusion in the study. The study obtained approval from the hospital's research ethics committee (Approval No. NCC2020C-508) and all participants furnished written consent with full understanding.

According to the HFA-ICOS (Heart Failure Association–International Cardio-Oncology Society) cardiovascular toxicity risk stratification, a low-risk level is characterized by the absence of risk factors or the presence of one moderate risk factor, each of which is assigned 1 point, while a moderate-risk level is defined as having moderate risk factors totalling 2~4 points.[2] The baseline 1-point cardiovascular toxicity risk factor including elevated baseline cardiac biomarkers with anthracycline chemotherapy, hypertension, chronic kidney disease, diabetes mellitus, anthracycline before HER2-targeted therapy, previous exposure to non-anthracycline chemotherapy, current smoker or significant smoking history, obesity (BMI > 30 kg/m^2). The baseline 2-point cardiovascular toxicity risk factors including previous arrhythmia with HER2-targeted therapies, left ventricular ejection fraction (LVEF) 50–54%, elevated baseline cardiac biomarkers with HER2-targeted therapies, age 65–79 years, previous exposure to anthracycline, previous exposure to radiotherapy to left chest or mediastinum.

Symptomatic CTRCD indicates heart failure, a clinical syndrome characterized by primary symptoms like breathlessness, ankle swelling, and fatigue. Asymptomatic CTRCD is categorized into three levels: (1) mild, indicated by a LVEF of 50% or higher, alongside a notable decrease in global longitudinal strain (GLS) exceeding 15%; (2) moderate, indicated by a new decrease in LVEF of at least 10 percentage points resulting in an LVEF ranging from 40–49%, or a decrease in LVEF of less than

10 percentage points resulting in an LVEF ranging from 40–49%, accompanied by a new decline in GLS exceeding 15%; (3) severe, characterized by a new reduction in LVEF to below 40%.[2,10]

CMR protocols and image analysis

Scanning was conducted utilizing a 3.0 T scanner (SIGNA Architect, GE Healthcare, Waukesha, WI, USA). We acquired images by employing breath-holding techniques. Cine images were acquired in LV 2-chamber, 4-chamber, LV outflow tract and multisection stacks of short-axis views to perform LV function and volumes. Oedema evaluation was conducted using T2-weighted dual inversion-recovery imaging in the mid-LV short-axis orientation. For T1 mapping, a modified look-locker inversion-recovery sequence was employed, capturing images in a 3(3)3(3)5 heartbeat pattern. To conduct T2 mapping, a multi-echo fast spine echo sequence utilizing double inversion-recovery was utilized, featuring four distinct echo times: 10.8 ms, 32.4 ms, 54.0 ms, and 75.5 ms. Both T1 and T2 mapping sequences were acquired in the mid-LV short-axis orientation.

CMR parameters were calculated with the CVI42 software, developed by Circle Cardiovascular Imaging Inc. in Calgary, Canada, by a radiologist with eight years of expertise in CMR. The radiologist was blinded to patients' clinical data during the analysis process. LV volumes parameters including LVEF, end-diastolic and end-systolic volumes, cardiac output, stroke volume and myocardial mass. Variables were adjusted for body surface area and expressed as indexes. Parameters (except for ejection fraction) were calibrated based on body surface area and presented as indices. We measured the T1 and T2 values at the mid-LV septum in the short-axis plane. GLS was mainly derived from LV 2-chamber and 4-chamber view. Global radial strain (GRS) and global circumferential strain (GCS) were calculated using short-axis imaging. For intraobserver reproducibility test, the same radiologist re-examined measurements in 12 randomly sampled patients after a one-month interval. For interobserver reproducibility test, a second observer, unaware of the patients' clinical data, independently analysed scans from 12 randomly chosen patients.

Statistical analysis

Continuous variables are displayed as means ± standard deviation. Categorical variables are displayed as frequencies and percentages. The analysis encompassed comparing measurements at two different time points, utilizing a paired test for continuous variables demonstrating normal distribution and employing the Wilcoxon signed-rank test for variables without a normal distribution. Comparison between groups (patients with and without risk factors and patients treated with anthracycline-based and non-anthracycline-based anti-HER2 therapies) were assessed using either the unpaired t-test or the Mann–Whitney U test. Statistical significance was established for p-values less than 0.05. Statistical analyses were conducted using SPSS Statistics version 26 (IBM) and Prism version 9.3.0 (GraphPad Software).

Results

Patient characteristics and cancer therapy-related cardiac dysfunction (CTRCD)

35 female patients diagnosed with HER2-positive breast cancer were ultimately included (mean age ± standard deviation, 48.86 years ± 10.34). Of the 35 patients, 17 (48%) received taxane plus carboplatin plus trastuzumab plus pertuzumab (TCbHP), 8 (23%) received taxane plus carboplatin plus trastuzumab (TCbH) and 10 (29%) received anthracycline chemotherapy followed by a taxane plus trastuzumab plus pertuzumab (AC/EC-THP) treatment (Figure 1). Five (14%) patients had hypertension, four were obese and two were above the age of 65 at baseline. All patients underwent an electrocardiogram examination before treatment, but for young patients with no prior medical history, cardiac biomarker tests were not performed. There were no apparent abnormalities in the patient's baseline electrocardiogram. All patients were non-smokers with no significant smoking history, and none had chronic kidney disease. 89% of the patients exhibited a low-risk level for cardiovascular toxicity, while 11% presented a moderate-risk level. Table 1 presents the foundational traits at the study's outset.

Thirty-two patients underwent cardiac MR scans at follow-up 1, with a mean time interval of 102.22 ± 20.58 days. Sixteen patients underwent cardiac MR scans at follow-up 2, with a mean time interval of 242.81 ± 68.29 days. Thirteen patients completed cardiac MR scans at both follow-up 1 and follow-up 2. For patients receiving both targeted therapy and anthracycline drugs, targeted therapy was administered sequentially after the

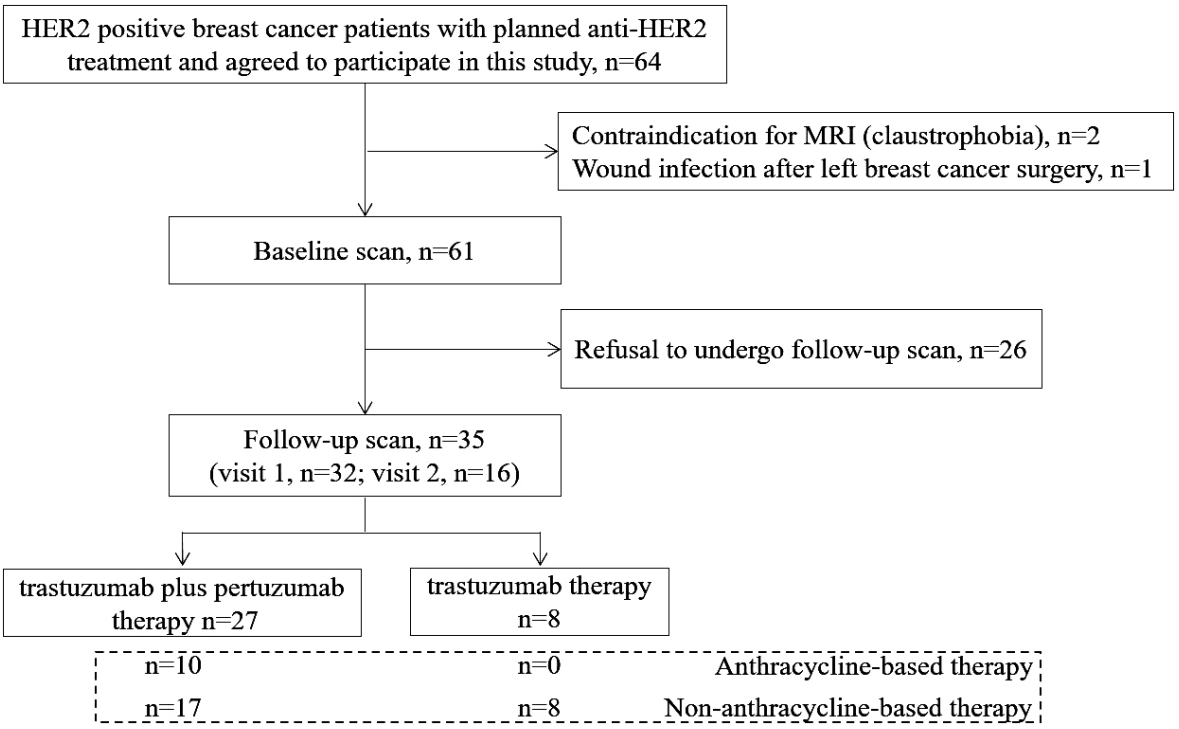

FIGURE 1. Study flow diagram.

HER2 = human epidermal growth factor receptor 2

completion of anthracycline treatment, with no instances of simultaneous usage.

We observed a significant increase in heart rate at follow-up 1 compared to baseline. However, no significant changes were detected in other vital signs, such as blood pressure or respiratory rate, during the same period.

A total of nine (25.71%) patients had experienced CTRCD during the follow-up CMR scans. Five of these patients showed no cardiovascular toxicity risk factors, while four of them showed 1–3 points risk factors.

One patient developed symptomatic CTRCD at follow-up 1, classified as New York Heart Association functional class III, with fatigue and dyspnoea as the primary symptoms. This was accompanied by a decrease in LVEF from 56% to 35%, a reduction in GLS from -11.18 to -9.48, a decrease in GRS from 18.65 to 15.78, a decrease in GCS from -12.76 to -11.42, an increased in native T1 value from 1239 msec to 1271 msec, and an increased in T2 value from 47.90 msec to 48.57 msec. The patient sought treatment at a hospital outside the local area, where she was treated with the traditional Chinese medicine for heart failure and also received antihypertensive therapy. Subsequently, the patient discontinued breast cancer treatment and did not return to our hospital for further follow-up.

Seven out of the nine patients exhibited mild asymptomatic CTRCD (six at follow-up 1 and one at follow-up 2), while one patient demonstrated moderate asymptomatic CTRCD at follow-up 2. Among the nine patients with CTRCD, three received anthracycline-based chemotherapy followed by taxane and dual-targeted therapy. Four received taxane in combination with carboplatin and dual-targeted therapy, while two were treated with taxane, carboplatin and trastuzumab. One patient with mild asymptomatic CTRCD had a history of hypertension for over 20 years and had been on long-term telmisartan therapy. None of the other patients received specific guideline-directed medical therapy for heart failure, such as ACE inhibitors, beta-blockers, or mineralocorticoid receptor antagonists, as recommended in the 2022 ESC cardio-oncology guidelines. Two representative clinical cases are shown in Figures 2 and 3.

TABLE 1. Clinical characteristics and treatment of the study participants

Variable	Value
No. of participants	35
Age, years*	48.86 ± 10.34
Height (cm)*	160.97 ± 4.20
Weight (kg)*	62.61 ± 8.36
Body surface area (m^2)*	1.63 ± 0.12
Hypertension†	5 (14%)
Chronic kidney disease	0
Current smoker or significant smoking history	0
Obesity (BMI > 30 kg/m^2) †	4 (11%)
Age 65–79 years†	2 (6%)
Diabetes	0
Hyperlipidaemia	0
Prior cardiovascular disease	0
HFA-ICOS baseline cardiovascular toxicity risk stratification†	
Moderate risk (moderate risk factors with a total of 2–3 points)	4 (11%)
Low risk	31 (89%)
No risk factor	18 (52%)
One moderate risk factor with a total of 1 point	13 (37%)
Therapies†	
HER2-targeted therapies without anthracycline	25 (71%)
Trastuzumab	8 (23%)
Trastuzumab and pertuzumab	17 (48%)
Anthracycline chemotherapy followed by a taxane plus trastuzumab plus pertuzumab	10 (29%)

* Data are given as means ± standard deviations. †Data in parentheses are percentages.

BMI = body mass index; HFA-ICOS = Heart Failure Association-International Cardio-Oncology Society; HER2 = human epidermal growth factor receptor 2

Differences in cardiac magnetic resonance (CMR) results before treatment and during the early stage after treatment

At follow-up 1, the LV systolic function showed a significant decrease compared to the baseline measurement, including reductions in LVEF (64.03% ± 4.16 *vs.* 57.34% ± 5.32; $p < 0.001$), stroke volume index (43.36 mL/m^2 ± 8.12 *vs.* 37.10 mL/m^2 ± 6.43; $p < 0.001$) and cardiac output index (3.23 $L/min \times m^2$ ± 0.58 *vs.* 2.91 $L/min \times m^2$ ± 0.49; $p = 0.002$). The decline in LV systolic function is primarily attributed to the increase in LV end-systolic volume (24.53 mL/m^2 ± 6.17 *vs.* 28.26 mL/m^2 ± 9.15; $p = 0.001$), with no significant changes observed in end-diastolic volume ($p = 0.057$). The LV mass index showed no significant statistical difference ($p = 0.369$).

We observed significantly decreases in absolute myocardial strain values: 33.59% ± 7.31 *vs.* 28.81% ± 6.37 for GRS, -18.86% ± 2.41 *vs.* -17.38% ± 2.31 for GCS, and -16.12% ± 1.55 *vs.* -15.09% ± 1.85 for GLS; all with a p-value of ≤ 0.001).

T2-weighted short-tau inversion-recovery imaging did not reveal apparent myocardial oedema. However, we noted significant increases in both T1 (1231.16 msec ± 46.49 *vs.* 1255.81 msec ± 45.23; $p = 0.001$) and T2 values (47.86 msec ± 2.17 *vs.* 49.43 msec ± 2.71; $p = 0.001$) (Table 2).

Differences in cardiac magnetic resonance (CMR) results before treatment and during the mid-to-late stage after treatment

Similarly to the aforementioned findings, there were significant decreases observed in LVEF, stroke volume index, cardiac output index, and absolute strain parameter values from baseline to follow-up 2 ($p < 0.05$). Conversely, the LV end-systolic volume index showed a notable increase ($p = 0.002$). Noteworthy, no substantial changes were detected in T1 and T2 values ($p > 0.05$) (Table 2, Figure 4).

Differences in cardiac magnetic resonance (CMR) results between two subsequent follow-up scans

The average time span between the two subsequent follow-up CMR scans was 136.92 ± 67.70 days. A notable decrease in cardiac output index was observed (3.01 $L/min \times m^2$ ± 0.47 *vs.* 2.60 $L/min \times m^2$ ± 0.54; $p = 0.022$). No statistically notable differences were detected in the remaining variables ($p > 0.05$) (Table 3).

Differences in cardiac magnetic resonance (CMR) results between patients with and without risk factors at the early stage after treatment

Thirty-two patients completed cardiac MR scans at follow-up 1, 16 of whom had no cardiovascular toxicity risk factors and 16 of whom had 1-3 risk factors. Patients presenting with 1-3 risk factors exhibited significantly higher LV mass index

TABLE 2. Cardiac magnetic resonance (CMR) parameter results at baseline and follow-up

Variable	Follow-up 1 (n = 32)			Follow-up 2 (n = 16)		
	Baseline 1	Follow-up 1	P Value	Baseline 2	Follow-up 2	P Value
LV ejection fraction (%)	64.03 ± 4.16	57.34 ± 5.32	< 0.001	66.23 ± 4.19	57.45 ± 5.54	< 0.001
LV end-diastolic volume index (mL/m²)	68.23 ± 12.41	65.63 ± 12.97	> 0.057	68.20 ± 11.56	64.94 ± 14.01	0.275
LV end-systolic volume index (mL/m²)	24.53 ± 6.17	28.26 ± 9.15	0.001	22.91 ± 5.02	27.70 ± 7.60	0.002
LV mass index (g/m²)	37.17 (33.96, 43.69)	38.24 (34.40, 41.45)	0.369	39.23 ± 6.31	40.03 ± 6.78	0.261
Stroke volume index (mL/m²)	43.36 ± 8.12	37.10 ± 6.43	< 0.001	44.84 ± 8.12	39.46 (30.13, 42.17)	0.002
Cardiac output index (L/min×m²)	3.23 ± 0.58	2.91 ± 0.49	0.002	3.19 ± 0.38	2.65 ± 0.51	0.001
Global radial strain	33.59 ± 7.31	28.81 ± 6.37	0.001	37.16 ± 8.99	30.07 ± 6.18	< 0.001
Global circumferential strain	-18.86 ± 2.41	-17.38 ± 2.31	< 0.001	-19.93 ± 2.81	-17.23 ± 2.34	< 0.001
Global longitudinal strain	-16.12 ± 1.55	-15.09 ±1.85	0.001	-16.67 ± 1.28	-14.88 ± 1.60	0.004
T1 value (msec)	1231.16 46.49	1255.81 ± 45.23	0.001	1222.00 ± 40.89	1237.13 ± 35.19	0.051
T2 value (msec)	47.86 ± 2.17	49.43 ± 2.71	0.001	48.13 ± 2.15	48.84 ± 1.75	0.306
Heart rate during MR scan (bpm)	74.50 ± 11.11	79.47 ± 13.40	0.048	72.50 ± 9.68	72.69 ± 12.28	0.928

Data are given as means ± standard deviations or medians with interquartile ranges in parentheses. Baseline 1 and 2 were calculated separately for patients who underwent follow-up exams 1 and 2.

bpm = beats per minute; LV = left ventricular

(37.07 g/m² ± 6.68 *vs.* 43.03 g/m² ± 8.86, p = 0.040) and T1 value (1235.06 ± 36.77 *vs.* 1276.56 msec ± 44.25, p = 0.007) (Figure 5). However, no statistically significant disparity in LV mass index or T1 value was observed between these two groups at baseline. The two groups also had similar LV ejection fraction, volume index, cardiac output index, strain parameters and T2 values (p > 0.05) (Table 4).

Differences in cardiac magnetic resonance (CMR) results between patients with and without anthracycline therapy at the early stage after treatment

Ten patients were taking anthracycline-based therapy and 22 patients were taking non-anthracycline-based therapy at follow-up 1. The group treated with anthracycline showed a notably elevated T1 value (1280.90 msec ± 43.10 *vs.* 1244.41 msec ± 42.29, p = 0.032). At baseline, the T1 value did not show any significant variance between the two groups. The two groups were similar in all other variables (p > 0.05) (Table 5).

Discussion

In this research, our aim was to explore cardiotoxicity among individuals undergoing anti-HER2 therapy with a low-to-moderate risk of cardiovascular complications. The main findings are as follows: (1) Subclinical CTRCD was frequently observed in low-to-moderate cardiovascular toxicity risk patients with anti-HER2 therapy. (2) CTRCD was detected as early as the third month of anticancer therapy and persisted for at least approximately eight months. (3) After anticancer therapy, patients with 1–3 cardiovascular toxicity risk points, including those who underwent anthracycline-based therapy, exhibited higher T1 values compared to those without such risk factors, while showing no notable differences in LVEF or myocardial strain values.

Breast cancer patients categorized with low-to-moderate cardiovascular toxicity risk demonstrate an extended life expectancy relative to those with high cardiovascular toxicity risk, potentially allowing for the consideration of more aggressive targeted therapy and chemotherapy interventions.[10] In our study, 89% of breast cancer patients were at low

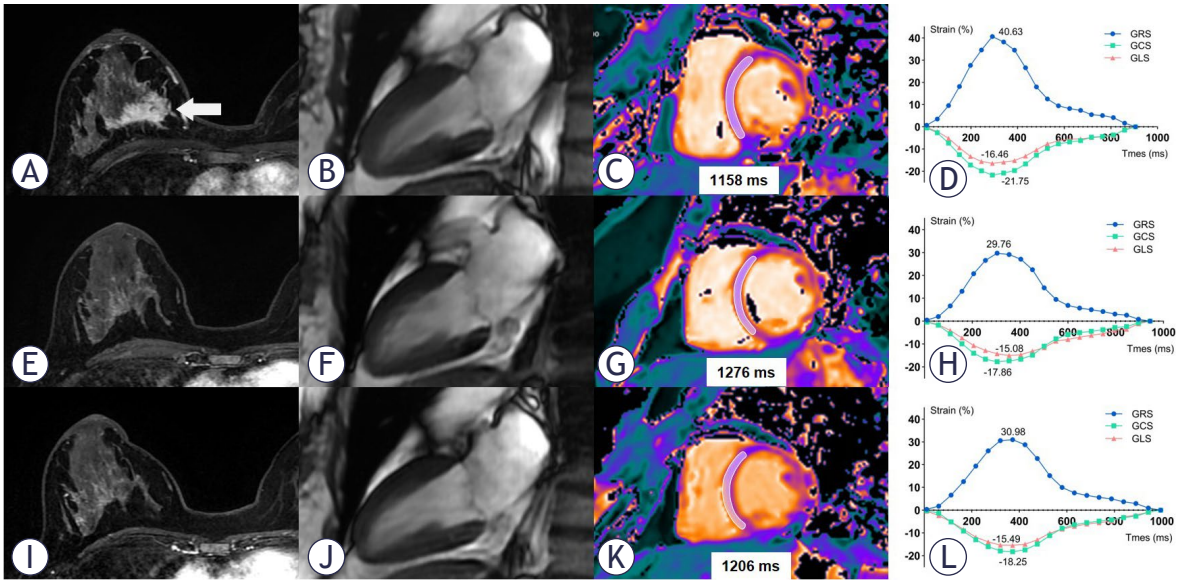

FIGURE 2. CMR imaging in a 44-year-old woman with human epidermal growth factor receptor 2 (HER2)-positive right-side breast cancer. The top row images **(A, B, C, D)** represent the baseline. The middle row images **(E, F, G, H)** correspond to the condition after 4 cycles of the TCbHP regimen (104 days after the baseline scan). The bottom row images **(I, J, K, L)** show the status after 9 cycles of the TCbHP regimen (203 days after the baseline scan). In the axial breast enhancement scan images **(A, E, I)**, a decrease in the tumour size of the right breast is observed (arrow). The diastolic phase images of left ventricular two-chamber plane **(B, F, J)** demonstrate a slight increase in left ventricular systolic volume. T1 mapping images **(C, G, I)** reveal an increase in T1 value in the septum of the mid short-axis slice during follow-up 1, followed by a decrease during follow-up 2. The global radial, circumferential and longitudinal strain (GRS, GCS and GLS) curves before and after TCbHP treatment are presented **(D, H, L)**.

CMR = cardiac magnetic resonance; GCS = global circumferential strain; GLS = global longitudinal strain; GRS = global radial strain; HER2 = human epidermal growth factor receptor 2; TCbHP = taxane plus carboplatin plus trastuzumab plus pertuzumab

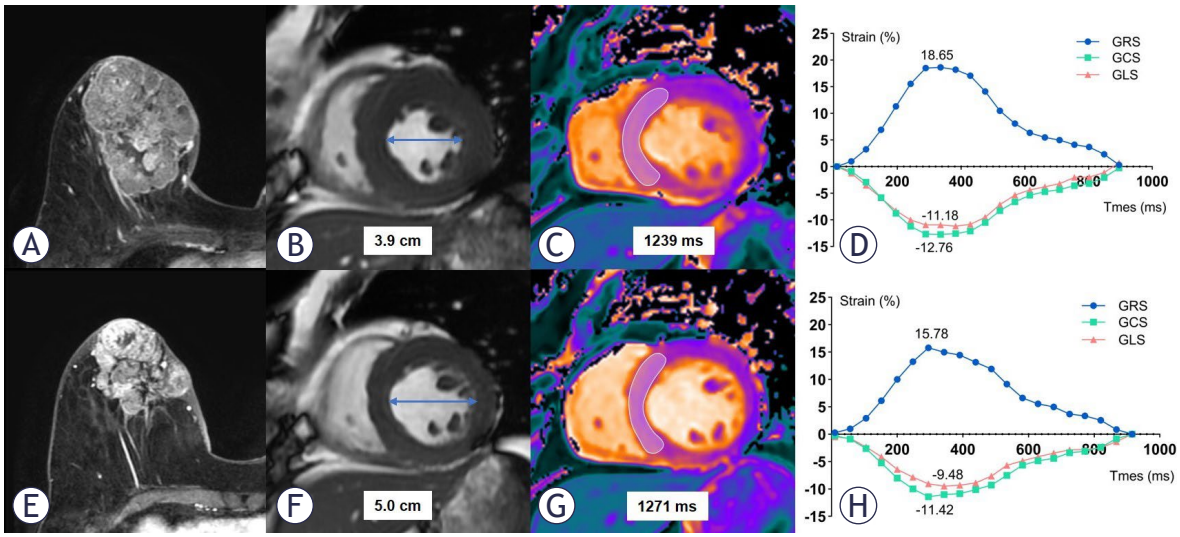

FIGURE 3. CMR imaging in a 68-year-old woman with HER2-positive right-side breast cancer. The upper images **(A, B, C, D)** depict the baseline condition. The lower images **(E, F, G, H)** represent the status after 4 cycles of the TCbHP regimen (106 days following the baseline scan). Axial breast enhancement scan images **(A, E)** exhibit a reduction in the tumour size of the right breast. Short-axis cine images reveal an enlargement in the left ventricular diastolic diameter **(B, F)**. T1 mapping images **(C, G)** reveal an increase in T1 value in the septum of the mid short-axis slice during the follow-up. Strain curves demonstrate a reduction in the absolute values of global radial, circumferential and longitudinal strain (GRS, GCS and GLS) before and after treatment **(D, H)**.

CMR = cardiac magnetic resonance; GCS = global circumferential strain; GLS = global longitudinal strain; GRS = global radial strain; HER2 = human epidermal growth factor receptor 2; TCbHP = taxane plus carboplatin plus trastuzumab plus pertuzumab

TABLE 3. Cardiac magnetic resonance (CMR) parameter results between follow-up 1 and follow-up 2 (n = 13)

Variable	Follow-up 1	Follow-up 2	P Value
LV ejection fraction (%)	58.45 ± 4.44	57.76 ± 5.53	0.545
LV end-diastolic volume index (mL/m²)	66.33 ± 11.13	62.32 ± 14.02	0.055
LV end-systolic volume index (mL/m²)	27.59 ± 6.20	26.35 ± 7.46	0.294
LV mass index (g/m²)	38.07 (36.22, 44.09)	39.13 (35.77, 43.31)	0.650
Stroke volume index (mL/m²)	39.37 (35.27, 43.55)	39.44 (27.44, 40.83)	0.101
Cardiac output index (L/min×m²)	3.01 ± 0.47	2.60 ± 0.54	0.022
Global radial strain	28.69 ± 8.12	29.70 ± 6.48	0.670
Global circumferential strain	-17.70 ± 2.52	-17.12 ± 2.30	0.172
Global longitudinal strain	-15.01 ± 1.46	-14.74 ±1.70	0.647
T1 value (msec)	1245.31 ± 22.46	1236.77 ± 40.36	0.486
T2 value (msec)	49.67 ± 2.19	49.11 ± 2.12	0.465
Heart rate during MR scan (bpm)	78.38 ± 14.67	73.92 ± 13.09	0.189

Data are given as means ± standard deviations or medians with interquartile ranges in parentheses.

bpm = beats per minute; CMR = cardiac magnetic resonance; LV = left ventricular

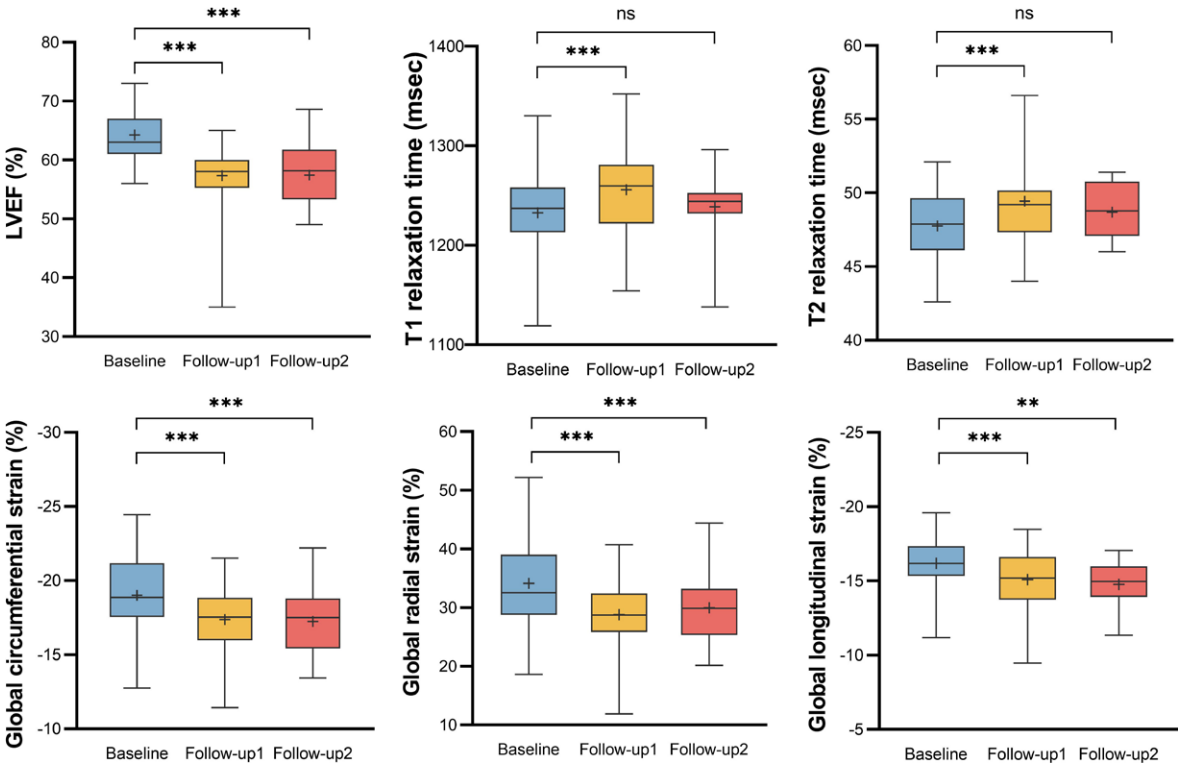

FIGURE 4. Box plot show changes in cardiac magnetic resonance (CMR) variables between the baseline and follow-up CMR examinations. The results of CMR variables at baseline (n = 35), follow-up 1 (n = 32) and follow-up 2 (n = 16) were shown in blue, yellow and red box plot. Left ventricular ejection fraction (LVEF) decreased significantly at follow-up 1 and follow-up 2. T1 and T2 value increased significantly at follow-up 1, but recovered to a level not significantly different from the baseline. Global longitudinal strain (GLS), global radial strain (GRS) and global circumferential strain (GCS) decreased significantly at follow-up 1 and follow-up 2.

TABLE 4. Differences in CMR parameters at follow-up 1 between patients with and without baseline risk factors

Variable	Patients with no risk factor (n = 16)	Patients with 1-3 risk factors (n = 16)	P Value
LV ejection fraction (%)	57.92 ± 3.43	56.75 ± 6.79	0.543
LV end-diastolic volume index (mL/m^2)	63.88 ± 10.89	67.39 ± 14.92	0.454
LV end-systolic volume index (mL/m^2)	26.89 ± 5.66	29.63 ± 11.70	0.406
LV mass index (g/m^2)	37.07 ± 6.68	43.03 ± 8.86	0.040
Stroke volume index (mL/m^2)	36.60 ± 6.67	37.61 ± 6.36	0.665
Cardiac output index (L/min×m^2)	2.84 ± 0.48	2.99 ± 0.49	0.387
Global radial strain	30.56 ± 5.40	27.07 ± 6.94	0.123
Global circumferential strain	-17.94 ± 2.16	-16.82 ± 2.37	0.174
Global longitudinal strain	-15.11 ± 1.85	-15.06 ± 1.90	0.938
T1 value (msec)	1235.06 ± 36.77	1276.56 ± 44.25	0.007
T2 value (msec)	48.95 ± 2.28	49.94 ± 3.07	0.318
Heart rate during MR scan (bpm)	77.56 ± 11.28	81.38 ± 15.37	0.430

Data are given as means ± standard deviations or medians with interquartile ranges in parentheses.

CMR = cardiac magnetic resonance; LV = left ventricular

TABLE 5. CMR parameter results between patients treated with anthracycline-based and non-anthracycline-based anti-human epidermal growth factor receptor 2 (HER2) therapies at follow-up 1

Variable	Anthracycline-based therapy (n = 10)	Non-anthracycline-based therapy (n = 22)	P Value
LV ejection fraction (%)	57.01 ± 3.68	57.49 ± 5.99	0.816
LV end-diastolic volume index (mL/m^2)	67.51 ± 12.83	64.78 ± 13.24	0.590
LV end-systolic volume index (mL/m^2)	28.88 ± 6.01	27.98 ± 10.38	0.800
LV mass index (g/m^2)	41.76 ± 7.91	39.28 ± 8.53	0.442
Stroke volume index (mL/m^2)	38.58 ± 7.78	36.43 ± 5.80	0.389
Cardiac output index (L/min×m^2)	3.13 ± 0.49	2.82 ± 0.46	0.094
Global radial strain	26.73 ± 6.62	29.76 ± 6.16	0.218
Global circumferential strain	-17.09 ± 1.92	-17.52 ± 2.49	0.637
Global longitudinal strain	-15.36 (-16.56, -13.74)	-15.07 ± 2.05	1.000
T1 value (msec)	1280.90 ± 43.10	1244.41 ± 42.29	0.032
T2 value (msec)	49.65 (47.06, 53.10)	49.04 ± 2.23	0.231
Heart rate during MR scan (bpm)	84.20 ± 18.44	77.32 ± 10.20	0.182

Data are given as means ± standard deviations or medians with interquartile ranges in parentheses.

CMR = cardiac magnetic resonance; LV = left ventricular

cardiovascular toxicity risk, and 52% had no risk factors. As demonstrated in Table 4, the presence of risk factors did not appear to significantly influence CMR parameters at follow-up 1. Patients with 1–3 risk factors exhibited higher LV mass index and native T1 values, whereas other parameters, such as LV ejection fraction, volume index, cardiac output index, strain parameters and T2 values, remained comparable between groups. These findings suggest that monitoring cardiac function during anticancer therapy is equally important even in patients with low cardiovascular toxicity risk.

In our study, 25.71% of patients developed CTRCD during treatment, as monitored through

CMR examinations. Among the CTRCD patients, more than half had no risk factors before anticancer treatment. Despite the relatively low-to-moderate risk profile of our study population, the determined rate of CTRCD aligned with the ranges in earlier studies[11,12] and was similar to a recent result.[13] Thus, this is a critical group to monitor for cardiac toxicity during anticancer therapy. Regular evaluation of LV function, utilizing measurements of LVEF and GLS, is advised before starting HER2-targeted therapy and should continue every three months during the treatment monitoring period.[2,14] In the case of asymptomatic mild CTRCD within this patient cohort, the guidelines propose the consideration of cardioprotective therapy (angiotensin-converting enzyme inhibitors, angiotensin receptor blockers and beta-adrenergic blockers). Additionally, it's recommended to continue HER2-targeted treatment.[2,14-16] However, cardiac surveillance is not always strictly performed in real-world clinical practice. In a clinical study encompassing 4,325 patients, it was observed that just 46.2% of breast cancer patients receiving trastuzumab underwent the suggested cardiac surveillance.[17] Among low cardiovascular toxicity risk patients, the frequency of cardiac surveillance might be even less frequent in actual practice. For low cardiovascular toxicity risk patients, monitoring cardiac function during anticancer therapy remains equally important, but perhaps the monitoring frequency could be appropriately reduced.

In our study, cardiac dysfunction was observed at the third month of anticancer therapy, and this significant decline persisted into the eighth month. Cardiac motion function did not change significantly between the third and eighth months.

Notably, there was a substantial rise in T1 and T2 values noted at the early stage after treatment, but by the mid-to-late stage after treatment, these values had reverted to a level that did not show significant variance compared to the baseline. In essence, cardiotoxicity manifested as early as the third month of anticancer therapy, but for the majority of patients, its progression did not continue beyond approximately the eighth month. Our study aligns with findings from prior research. Houbois *et al.*'s findings suggest a decrease in both LVEF and strain values over the follow-up duration, with the lowest point reached at three months into trastuzumab therapy.[7] At both 6 and 12 months, Gong *et al.* observed noteworthy declines in systolic function; however, these disparities ceased to be significant by the 18-month mark.[9] Recent analyses on real-world data demonstrated

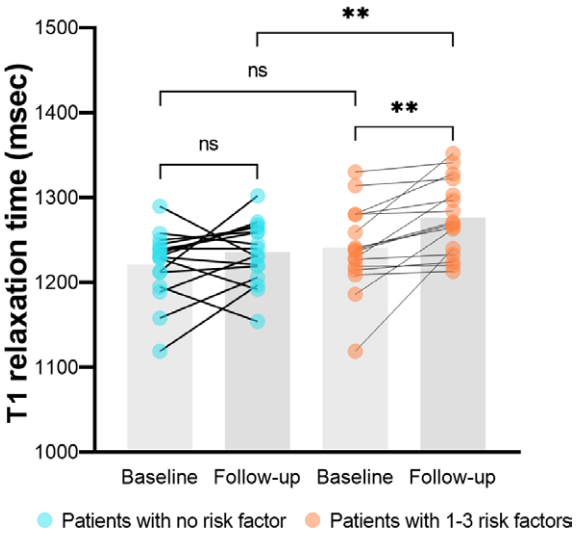

FIGURE 5. The comparison of T1 value between the baseline and follow-up cardiac magnetic resonance (CMR) examinations. Bars represent median T1 value. Blue dots represent human epidermal growth factor receptor 2 (HER2)-positive breast cancer patients with no cardiovascular toxicity risk factor and orange dots represent patients with 1–3 risk factors.

that the time of onset of HER2 inhibitor-related cardiotoxicity was 80.50~103.00 days.[18,19] This finding holds significance, indicating that among individuals diagnosed with HER2-positive breast cancer and presenting mild-to-moderate cardiovascular toxicity risk factors, conducting early and less frequent cardiotoxicity screenings could potentially improve cost-effectiveness.

Another significant observation from this study was that HER2-positive breast cancer patients with 1–3 cardiovascular toxicity risk factors displayed a minor yet statistically significant elevation in native T1 value following anticancer therapy, in comparison to those without any risk factors. However, there were no notable variations found in terms of statistical significance concerning LV ejection fraction or myocardial strain values. Typically, a rise in native T1 values correlates with myocardial conditions such as oedema, inflammation, and fibrosis[20], which is able to reflect subtle myocardial histological changes. A previous clinical study has demonstrated that early cardiac changes, there was a progressive increase in native T1 and T2 values. Subsequently, as treatment progressed, there was a normalization of T2 time, while non-contrast T1 values remained persistently elevated, indicating the presence of myocardial fibrosis.21 The detection rate of cardiac abnormalities after cancer therapy was 87% based on T1 and T2 map-

ping. In comparison, abnormalities based on GLS and LVEF were found in 71% and 66% of patients respectively.[21] Therefore, in identifying myocardial alterations among HER2-positive breast cancer patients following anticancer therapy, T1 mapping is a favoured method for precisely measuring the particular degree of tissue damage. This specific damage might not be easily identified through traditional cine sequences or strain analysis.

During the follow-up period, we noticed a notable increase in native T1 values among patients who underwent anthracycline-based therapy compared to those who underwent non-anthracycline-based therapy. This difference may be attributed to the potential of anthracycline chemotherapy to induce acute, subacute, and chronic myocellular injuries. Our findings align with a previous study, demonstrating increased T1 value in individuals with prior anthracycline chemotherapy exposure.[22]

There were several limitations acknowledged in this study. Firstly, the sample size was comparatively limited. This prospective study aimed to compare CMR parameters before and after anticancer treatment, illustrating the temporal changes in these parameters over time. Consequently, only patients with at least two CMR scans were included, underscoring the necessity for a study with a larger sample size. Secondly, the follow-up duration for CMR monitoring was short, which hindered the assessment of the enduring cardiac repercussions of anti-HER2 therapy. This area requires further investigation in future research. Thirdly, cardiac biomarkers included in patients' haematological tests were not used for cardiovascular toxicity risk stratification prior to treatment, which may have introduced some bias. However, most patients in our cohort did not receive anthracycline-based chemotherapy and were relatively young, without a history or symptoms of cardiovascular disease, making abnormal biomarker levels unlikely. Therefore, the impact of this limitation was expected to be minimal, although it would be addressed more thoroughly in future studies.

In conclusion, asymptomatic cardiac dysfunction was common among HER2-positive breast cancer patients with low-moderate cardiovascular toxicity risk after cancer therapy. This subgroup of patients can potentially benefit from early post-anticancer therapy monitoring at longer intervals, thus enhancing cost-effectiveness. T1 mapping is a valuable approach for quantifying the specific extent of tissue damage, particularly in the presence of subtle tissue changes. There's a need for studies that encompass larger cohorts and extended follow-up durations.

Acknowledgments

This study has received funding by National Natural Science Foundation of China (Grant No. 82402230, 81971616), Beijing Natural Science Foundation (Grant No.7222148), Medical and Health Science and Technology Innovation Project of Chinese Academy of Medical Sciences (Grant No. 2021-I2M-C&T-B-065), Beijing Hope Run Special Fund of Cancer Foundation of China (Grant No.LC2020B19) and National High Level Hospital Clinical Research Funding and Cooperation Fund of CHCAMS and SZCH Fund (CFA202202016).

References

1. Herrmann J. Adverse cardiac effects of cancer therapies: cardiotoxicity and arrhythmia. *Nat Rev Cardiol* 2020; **17:** 474-502. doi: 10.1038/s41569-020-0348-1
2. Lyon AR, Lopez-Fernandez T, Couch LS, Asteggiano R, Aznar MC, Bergler-Klein J, et al. 2022 ESC Guidelines on cardio-oncology developed in collaboration with the European Hematology Association (EHA), the European Society for Therapeutic Radiology and Oncology (ESTRO) and the International Cardio-Oncology Society (IC-OS). *Eur Heart J Cardiovasc Imaging* 2022; **23:** e333-e465. doi: 10.1093/ehjci/jeac106
3. Thavendiranathan P, Negishi T, Somerset E, Negishi K, Penicka M, Lemieux J, et al. Strain-guided management of potentially cardiotoxic cancer therapy. *J Am Col Cardiol* 2021; **77:** 392-401. doi: 10.1016/j.jacc.2020.11.020
4. Goulas K, Farmakis D, Constantinidou A, Kadoglou NPE. Cardioprotective agents for the primary prevention of trastuzumab-associated cardiotoxicity: a systematic review and meta-analysis. *Pharmaceuticals* 2023; **16:** 983. doi: 10.3390/ph16070983
5. Taylor AJ, Salerno M, Dharmakumar R, Jerosch-Herold M. T1 mapping: basic techniques and clinical applications. *JACC: Cardiovas Imag* 2016; **9**: 67-81. doi: 10.1016/j.jcmg.2015.11.005
6. Cheng S, Wang J, Wang Y, Qi L, Li F, Liu J, et al. Longitudinal assessment of cardiac parameters through MRI in breast cancer patients treated with anti-HER2 therapy. *Eur Radiol Exper* 2023; **7:** 1-9. doi: 10.1186/s41747-023-00338-9
7. Houbois CP, Nolan M, Somerset E, Shalmon T, Esmaeilzadeh M, Lamacie MM, et al. Serial cardiovascular magnetic resonance strain measurements to identify cardiotoxicity in breast cancer: comparison with echocardiography. *JACC Cardiovasc Imaging* 2021; **14:** 962-74. doi: 10.1016/j.jcmg.2020.09.039
8. Gong IY, Ong G, Brezden-Masley C, Dhir V, Deva DP, Chan KKW, et al. Early diastolic strain rate measurements by cardiac MRI in breast cancer patients treated with trastuzumab: a longitudinal study. *Int J Cardiovasc Imaging* 2019; **35:** 653-62. doi: 10.1007/s10554-018-1482-2
9. Song L, Brezden-Masley C, Ramanan V, Ghugre N, Barfett JJ, Chan KK, et al. Serial measurements of left ventricular systolic and diastolic function by cardiac magnetic resonance imaging in patients with early stage breast cancer on trastuzumab. *Am J Cardiol* 2019; **123***:* 1173-9. doi: 10.1016/j.amjcard.2018.12.046
10. Thavendiranathan P, Abdel-Qadir H, Fischer HD, Camacho X, Amir E, Austin PC, et al. Breast cancer therapy-related cardiac dysfunction in adult women treated in routine clinical practice: a population-based cohort study. *J Clin Oncol* 2016; **34:** 2239-46. doi: 10.1200/jco.2015.65.1505

11. Bouwer NI, Liesting C, Kofflard MJM, Brugts JJ, Kock MCJ, Kitzen J, et al. 2D-echocardiography vs cardiac MRI strain: a prospective cohort study in patients with HER2-positive breast cancer undergoing trastuzumab. *Cardiovasc Ultrasound* 2021; **19:** 35. doi: 10.1186/s12947-021-00266-x

12. Tarantini L, Cioffi G, Gori S, Tuccia F, Boccardi L, Bovelli D, et al. Trastuzumab adjuvant chemotherapy and cardiotoxicity in real-world women with breast cancer. *J Card Fail* 2012; **18:** 113-9. doi: 10.1016/j.cardfail.2011.10.015

13. Esmaeilzadeh M, Urzua Fresno CM, Somerset E, Shalmon T, Amir E, Fan CS, et al. A combined echocardiography approach for the diagnosis of cancer therapy-related cardiac dysfunction in women with early-stage breast cancer. *JAMA Cardiol* 2022; **7:** 330-40. doi: 10.1001/jamacardio.2021.5881

14. Curigliano G, Lenihan D, Fradley M, Ganatra S, Barac A, Blaes A, et al. Management of cardiac disease in cancer patients throughout oncological treatment: ESMO consensus recommendations. *Ann Oncol* 2020; **31**: 171-90. doi: 10.1016/j.annonc2019.10.023

15. Leong DP, Cosman T, Alhussein MM, Kumar Tyagi N, Karampatos S, Barron CC, et al. Safety of continuing trastuzumab despite mild cardiotoxicity: a phase I trial. *Cardio Oncology* 2019; **1**: 1-10. doi: 10.1016/j.jaccao.2019.06.004

16. Omland T, Heck SL, Gulati G. The role of cardioprotection in cancer therapy cardiotoxicity: JACC: CardioOncology state-of-the-art review. *Cardio Oncology* 2022; **4:** 19-37. doi: 10.1016/j.jaccao.2022.01.101

17. Henry ML, Niu J, Zhang N, Giordano SH, Chavez-MacGregor M. Cardiotoxicity and cardiac monitoring among chemotherapy-treated breast cancer patients. *JACC Cardiovasc Imaging* 2018; **11:** 1084-93. doi: 10.1016/j.jcmg.2018.06.005

18. Zhao M, Chen C, Zhang C, Xu X, Tian F, Wu B, et al. Cardiotoxicity with human epidermal growth factor receptor-2 inhibitors in breast cancer: disproportionality analysis of the FDA adverse event reporting system. *Int J Cardiol* 2023; **375:** 87-93. doi: 10.1016/j.ijcard.2022.12.043

19. Barbieri MA, Sorbara EE, Cicala G, Santoro V, Cutroneo PM, Franchina T, et al. Adverse drug reactions with HER2-positive breast cancer treatment: an analysis from the Italian Ph8-z.armacovigilance Database. *Drugs Real World Outcomes* 2021; **9:** 91-107. doi: 10.1007/s40801-021-0027

20. Messroghli DR, Moon JC, Ferreira VM, Grosse-Wortmann L, He T, Kellman P, et al. Clinical recommendations for cardiovascular magnetic resonance mapping of T1, T2, T2* and extracellular volume: a consensus statement by the Society for Cardiovascular Magnetic Resonance (SCMR) endorsed by the European Association for Cardiovascular Imaging (EACVI). *J Cardiovasc Magn Reson* 2017; **19:** 1-24. doi: 10.1186/s12968-017-0389-8

21. Haslbauer JD, Lindner S, Valbuena-Lopez S, Zainal H, Zhou H, D'Angelo T, et al. CMR imaging biosignature of cardiac involvement due to cancer-related treatment by T1 and T2 mapping. *Int J Cardiol* 2019; **275:** 179-86. doi: 10.1016/j.ijcard.2018.10.023

22. Jordan JH, D'Agostino RB, Jr., Hamilton CA, Vasu S, Hall ME, Kitzman DW, et al. Longitudinal assessment of concurrent changes in left ventricular ejection fraction and left ventricular myocardial tissue characteristics after administration of cardiotoxic chemotherapies using T1-weighted and T2-weighted cardiovascular magnetic resonance. *Circ Cardiovasc Imaging* 2014; **7:** 872-9. doi: 10.1161/CIRCIMAGING.114.002217

research article

The influence of catheter type, the number of sutures and patients' age on percutaneous nephrostomy displacement

Dimitrij Kuhelj[1,2,3], Ana Sustersic[1], Urban Zdesar[4]

[1] Clinical Radiology Institute, University Medical Centre Ljubljana, Ljubljana, Slovenia
[2] Faculty of Medicine, University of Ljubljana, Ljubljana, Slovenia
[3] Faculty of Health Sciences, University of Novo mesto, Novo mesto, Slovenia
[4] Institute of Occupational Safety, Ljubljana, Slovenia

Radiol Oncol 2025; 59(4): 522-525.

Received 15 January 2025
Accepted 24 April 2025

Correspondence to: Assoc. Prof. Dimitrij Kuhelj, M.D., Ph.D., Clinical Radiology Institute, University Medical Centre Ljubljana, Zaloška 7, SI-1000 Ljubljana, Slovenia. E-mail: dimitrij.kuhelj@guest.arnes.si

Disclosure: No potential conflicts of interest were disclosed.

Background. Percutaneous nephrostomy displacement results in procedure failure, reducing quality of life in patients with hydronephrosis. Scarce data about factors influencing displacement led to evaluation of our data in order to give better insight into this topic.

Patients and methods. Patients admitted for percutaneous nephrostomy (PCN) exchange between March 3rd and October 3rd 2023 were included in our prospective observational study aiming to determine possible factors influencing PCN displacement. Catheter type, number of sutures and patients' age over 70 years were analyzed. Descriptive statistics and Pearson's chi-square test were used; value less than 0.05 was determined as statistically significant.

Results. We included 57 patients (35 males; mean age 71.4 years) in the study. Loop catheters with strings were implanted 58 times and without strings 17 times. Fixation was achieved by 55 single and by 20 double sutures. 17 PCN (22.7%) were displaced in designated period. The mean time from PCN implantation to exchange was 4.16 months. Neither catheter type, number of sutures or patients' age significantly influenced PCN displacement (chi-square 0.57, 0.34 and 0.61, respectively).

Conclusions. No significant difference in PCN displacement between two types of catheters and the number of fixing sutures was detected. Elderly patients had similar rates of PCN displacements as younger ones. The most important causes of PCN displacement remained probably patients' activity and a care for PCN during months after the implantation. Proper patients' education and care of the PCN are possibly the keys for long-term success.

Key words: percutaneous nephrostomy; displacement; catheter type; suture number; age

Introduction

Percutaneous nephrostomy (PCN) has been an effective, minimally invasive method of renal collecting system drainage for more than a half of century.[1] PCN can be temporary or permanent, guided by ultrasound (US), computed tomography (CT), fluoroscopy or combination of methods. Alternatively, catheters may be inserted during renal operations.[2] Catheter-based drainage is used in malignant or benign obstructions as well as in non-obstructed collective system in case of urinary trauma with high success rates with minimal or even without irradiation of patients.[3]

In patients with prolonged PCN, displacement of catheter is described between 5.5% and 26.3%.[2,4-6] Catheter displacement leads to obstructive uropathy, infections, electrolytic disbalance and addi-

tional hospitalizations, influencing patients' well-being and increasing healthcare costs.

Scarce literature available for the factors influencing PCN displacement, as stated also in recent meta-analysis[7], as well as a lack of our own data were decisive to review our series of patients. The use of catheter type and the number of sutures, fixing the PCN, is based on the decision of the operator. The aim of our observational study was to determine possible impact of catheter type, the number of sutures fixing PCN to the skin as well as patients' age on displacement of the PCN at the time of its exchange.

Patients and methods

Our prospective observational study included consecutive patients, admitted for PCN exchange during 7-month period (March 3rd to October 3rd 2023) in our Institute. Primary procedures were performed by interventional radiologists using US guidance. 18G needle was used for puncture and after fluoroscopic confirmation of pyelocaliceal system with iodine contrast media, 0.035 inches' guidewire was introduced into renal collective system. Dilator was used to facilitate catheter insertion and PCN catheter was inserted into pyelon through renal parenchyma. Two types of PCN catheters were used, 8 Fr pigtail without locking strings (Optimed Medical Instruments GMBH, Ettlingen, Germany) or 8.5 Fr pigtail with locking strings (Cook Medical, Bloomington, USA). After the PCN catheter insertion it was fixed to skin by single or by two sutures, based on operators' choice. Patients age above 70 years was also evaluated as a potential factor, influencing PCN displacement.

PCN exchange was performed under fluoroscopic guidance, confirming the PCN position with contrast media. The 0.035 inches' guidewire was placed through PCN into renal pyelon, the PCN was extracted and exchanged with a new one. In case of displacement, guidewire and/or dilator were inserted through the existing canal if possible, otherwise new, US guided puncture was performed and the procedure was repeated.

PCN exchange was planned in 6 months after the initial procedure, however due to complications in certain patients' (displacement, obstruction, bleeding etc.) in some patients PCN had to be exchanged earlier.

Descriptive statistics was used to determine percentages and ranges; Pearson's chi-square test was used to check independence of variables. Value less than 0.05 was determined as statistically significant.

All the patients signed informed consent for a procedure. All procedures performed in present study were in accordance with the ethical standards and with the 1964 Helsinki declaration and its later amendments or comparable ethical standards.

Results

Between March 3rd to October 3rd 2023; 75 PCN were exchanged 62 times in 57 patients. Majority of patients were male (35 males; 22 female) with the mean age 71.4 years (range 43–94). 52 patients were admitted for PNS exchange once, three patients were admitted twice and one was admitted three times, latter always due to PNS displacement. Majority of exchanged PCN catheters were loop catheters with strings (58 PCN; 77.3%), while the remaining 17 were loop catheters without strings. 55 catheters (73.3%) were primarily stabilized by a single suture, while the remaining 20 were stabilized by a double suture. At exchange, sutures were not functional in 24 cases out of 95 sutures made (25.6%) (Figures 1, 2, 3). The mean time from PCN implantation to its exchange was 4.16 months and in 17 pts (24.7%), 17 PCN (22.7%) were displaced at the time of admission.

Out of 58 PCN with strings, 14 (24%) were displaced at the time of admission, while 3 (17.7%) out of 17 without strings were displaced at designated period. The difference between different types of PCN catheters was not statistically significant (chi-square 0.57).

Also, double suturing did not prevent PCN displacement, since in 55 PCN, fixed by a single suture, 14 were displaced (25.4%) and out of 20, fixed by double suture, 3 PCN (15%) were displaced at the time of admission, chi-square 0.34.

Patient age above 70 years did not prove to be significant for PCN displacement, since out of 27 PCN in patients with age less than 70 years, 7 (25.9%) were displaced and in 48 PCN in patients older than 70 years, 10 PCN catheters (20.8%) were displaced (chi-square 0.61).

Discussion

Catheter displacement is one of the most common complications in long-term derivation of urine

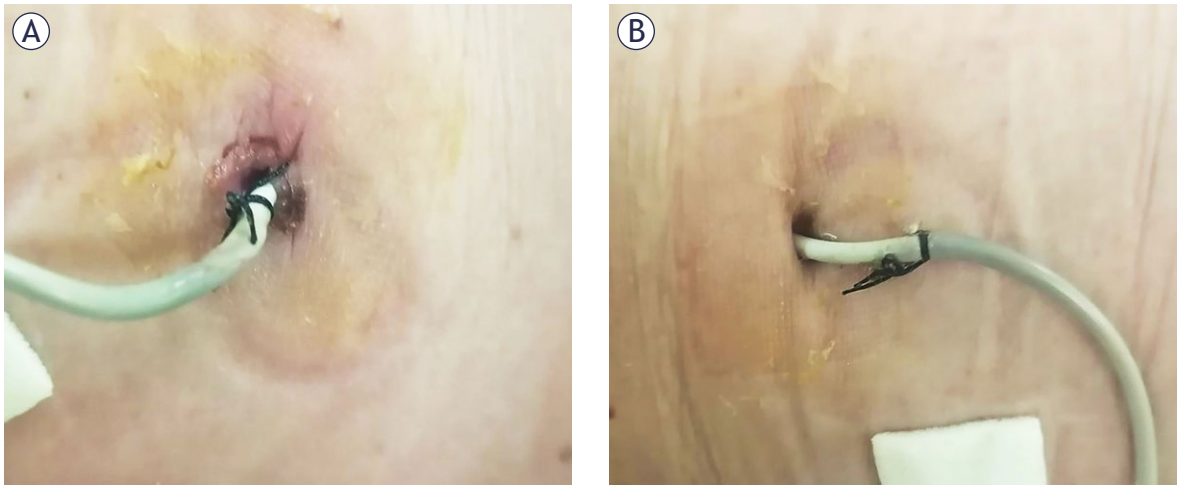

FIGURE 1. Loop percutaneous nephrostomy (PCN) catheters with strings 6 months after implantation. **(A)** Single suture on the left image is intact, while single suture on the other side **(B)** is not fixed to the skin anymore.

by PCN and in the literature it can be as high as 26.3%.[2] Different types of catheters and skin sutures are used to overcome this problem. The aim of our study was to determine PCN displacement rate by the catheter type (with or without locking strings) and by a number of sutures fixing PCN (one or two sutures).

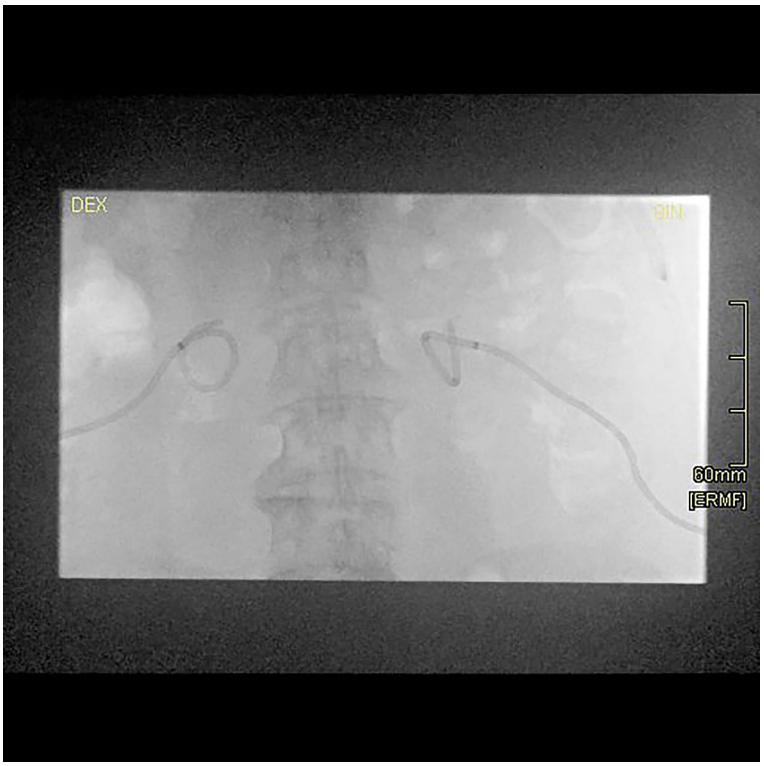

FIGURE 2. Fluoroscopic image of the same patient. Catheter position is correct, despite non-fixing suture on the right side.

Perioperatively inserted catheters are often larger and have different shape than minimally invasive percutaneously implanted under imaging guidance, as in our series. Based on that, the procedure itself might result in different ranges of displacement. The frequency of PCN displacement in postoperative and completely percutaneous implantation ranges from 5.5% to 26%.[2,4-6] However, comparing the rates of catheter displacement in patients with intraoperatively implanted PCN, when large catheters are used (up to 30 Fr) and between PCN catheters, implanted by minimally invasive, image guided procedure, when 8–9 Fr catheters are implanted, might not be objective.

The rate of PCN displacement in our series (22.7%) is higher as in a study by Carrafiello *et al.*[4], reporting 14.4% of PCN displacement in patients with malignant disease. This study included younger and malignant patients (mean age 65.7 years *vs.* 71.4 years in our series). Anyhow, our data showed that the rate of PCN displacement is not influenced by age (chi-square 0.61). One of the reasons of higher displacement rates in our patients might be the fact that our study included also non-malignant patients, that are more active and as such more prone to inadvertent PCN displacement. More similar rates of PCN displacement to our data were presented by Saad *et al.*[5], reporting 26% PCN displacement in 6-months period in patients with malignant and benign obstruction.

Two types of catheters are used for PCN in our Institute. Although catheter design with string-

locking pig-tail would suggest less displacement, the PCN catheter design showed no statistical difference between both catheter types used in our series (chi-square 0.57). Similar to our data, Chuang *et al*.[8] find no difference in displacement of catheters with or without strings.

To our knowledge, the number of sutures fixing PCN was not in the focus in any of the studies. Fixing PCN with two sutures is expected to be more durable, however this was not confirmed by our results. Additionally, there was a report of custom-made solution in enhancing PCN fixation to the skin that could reduce PCN displacement.[9] However, to our knowledge, no data about methods' success was published since.

We also want to emphasis drawbacks of our study. The main is a relatively low number of patients included as well as observational type of the study. Larger series and randomized data should confirm our results, as stated also by last years' meta-analysis.[7] There are also other factors influencing PCN displacement, such as patients' awareness of the importance of PCN as well as post procedural care of the catheter, that were not taken in consideration in a present study. One of our patients, admitted three times in 7 months for PCN exchange due to its displacement, points towards the importance for post-procedural care of the catheter itself.

PCN displacement is a common complication limiting successful long-term drainage of pyelocaliceal collecting system by PCN inserted during urological operation or by interventional radiologists. It influences patients' quality of life and increases the costs of the treatment. Our study showed that no kind of catheter is resistant to displacement and that double suturing is no guarantee of solid PCN fixation. Also, in contrast to common belief, elderly patients had similar rates of PCN displacements as younger ones.

The most important causes of PCN displacement remains probably patients' activity and a care for PCN during days and months after the implantation. Proper patients' education and explanation about the importance of careful catheter handling during daily activity as well as proper education of nursing staff about the importance of meticulous catheter care after the implantation are probably the keys for long- term effective PCN function. Standard discharge instructions should be a part of discharge protocol for each patient and regular training about catheter care and handling should be provided to nursing staff, including family and other persons, involved in patients' care.

References

1. Goodwin WE, Casey WC, Woolf W. Percutaneous trocar (needle) nephrostomy in hydronephrosis. *J Am Med Assoc* 1955; **157:** 891-4. doi: 10.1001/jama.1955.02950280015005
2. Panach-Navarrete J, Tonazzi-Zorrilla R, Martínez-Jabaloyas JM. Dislodgement in long-term patients with nephrostomy tube: risk factors and comparative analysis between two catheter designs. *J Endourol* 2020; **34:** 227-32. doi: 10.1089/end.2019.0655
3. Degirmenci T, Gunlusoy B, Kozacioglu Z, Arslan M, Ceylan Y, Ors B, et al. Utilization of a modified Clavien Classification System in reporting complications after ultrasound-guided percutaneous nephrostomy tube placement: comparison to standard Society of Interventional Radiology practice guidelines. *Urology* 2013; **81:** 1161-7. doi: 10.1016/j.urology.2013.02.038
4. Carrafiello G, Laganà D, Mangini M, Lumia D, Recaldini C, Bacuzzi A, et al. Complications of percutaneous nephrostomy in the treatment of malignant ureteral obstructions: single-centre review. *Radiol Med* 2006; **111:** 562-71. English, Italian. doi: 10.1007/s11547-006-0051-2
5. Saad WE, Virdee S, Davies MG, Patel NC, Sahler LG, Lee DE, et al. Inadvertent discontinuation of percutaneous nephrostomy catheters in adult native kidneys: incidence and percutaneous management. *J Vasc Interv Radiol* 2006; **17:** 1457-64. doi: 10.1097/01-RVI.0000235703.68819.8C
6. Bayne D, Taylor ER, Hampson L, Chi T, Stoller ML. Determinants of nephrostomy tube dislodgment after percutaneous nephrolithotomy. *J Endourol* 2015; **29:** 289-92. doi: 10.1089/end.2014.0387
7. Iyer D, Konstantinidis M, Li H, Bercu Z, Moon J. Impact of drainage catheter material, size, and anti-dislodgement mechanism on percutaneous nephrostomy exchange intervals: a systematic review protocol. *F1000Res* 2023; **12:** 1417. doi: 10.12688/f1000research.135431.1
8. Chuang MT, Lu CH, Tsai YS, Tsai HM, Kuo TN, Liu YS. Comparative study of percutaneous nephrostomy using catheters with and without locking strings. *Clin Nephrol* 2011; **76:** 226-32. doi: 10.5414/cn106946
9. Zhou T, Gao X, Yang C, Peng Y, Xiao L, Xu C, et al. Reinforcement for percutaneous nephrostomy tubes with a new technique. *J Endourol* 2011; **25:** 41-4. doi: 10.1089/end.2010.0209

research article

Efficacy and safety of percutaneous microwave ablation for liver tumors using an antenna with anti-phase technology offering ultraspherical ablation

Erbil Arik[1], Onur Taydas[2], Tunahan Dertli[2], Omer Faruk Sevinc[3], Ahmet Burak Kara[4], Omer Faruk Topaloglu[2], Mustafa Ozdemir[2], Adem Senturk[5], Alp Omer Canturk[5], Ilhan Hacibekiroglu[6], Mehmet Halil Ozturk[2]

[1] Marmara University, Faculty of Medicine, Department of Radiology, İstanbul, Turkey
[2] Sakarya University, Faculty of Medicine, Department of Radiology, Sakarya, Turkey
[3] Kocaeli City Hospital, Department of Radiology, Kocaeli, Turkey
[4] Gaziantep City Hospital, Department of Radiology, Gaziantep, Turkey
[5] Sakarya University, Faculty of Medicine, Department of General Surgery, Sakarya, Turkey
[6] Sakarya University, Faculty of Medicine, Department of Medical Oncology, Sakarya, Turkey

Radiol Oncol 2025; 59(4): 526-534.

Received 24 April 2025
Accepted 1 November 2025

Correspondence to: Assoc. Prof. Onur Taydas, M.D., Sakarya University, Faculty of Medicine, Department of Radiology, Sakarya, Turkey.
E-mail: taydasonur@gmail.com

Disclosure: No potential conflicts of interest were disclosed.

Background. Anti-phase technology, a novel advancement in microwave antennas for percutaneous liver ablations, forms more spherical ablation zones. This study aimed to evaluate the efficacy and safety of microwave ablation (MWA) treatment for liver tumors using a microwave antenna equipped with anti-phase technology.

Patients and methods. The study included 92 patients (133 lesions) treated with MWA for hepatocellular carcinoma (HCC) or liver metastases. Of these, nine patients had HCC, and 83 had metastases (46 colorectal and 37 non-colorectal metastases). Retrospective analysis was conducted on patients' age, sex, pre- and post-procedural laboratory values (white blood cell count, neutrophil-to-lymphocyte ratio), tumor and ablation zone dimensions (pre-procedure and post-procedure day 1 and months 1, 3, and 6), details of the single-shot MWA procedure (duration, power output), procedure-related complications, and local progression/recurrence during follow-up.

Results. The technical success rate of MWA was 100%. Ablations were performed at a median power output of 80 watts (range: 50–100), and the mean ablation duration was 5.2 ± 2.1 minutes. Follow-up imaging revealed an ablation zone diameter-to-tumor diameter ratio of 1.63 ± 0.3. Major complications occurred in three patients (3.2%) and included liver abscess (n = 1/92), hemorrhage (n = 1/92), and pleural effusion (n = 1/92). Minor complications were observed in 29 patients (31.5%). The median follow-up time of the patients was 33 (range 10–36) months. The median disease-free survival time was 25 months (95% confidence interval: 21–27). During the 24-month follow-up, local tumor progression occurred in 39 patients (42.4%). Tumor size was identified as an independent risk factor for local progression (p = 0.012).

Conclusions. This study represents the longest follow-up duration and the largest patient cohort for the MWA treatment of liver tumors using anti-phase technology. The results demonstrated high technical success and acceptable local control and complication rates.

Key words: hepatocellular carcinoma; liver metastasis; thermal ablation; microwave ablation; ultraspherical ablation

Introduction

Hepatocellular carcinoma (HCC) accounts for 85% of primary liver malignancies and is the third leading cause of cancer-related organ-specific mortality globally. If left untreated, the five-year survival rate is approximately 5–9%. The liver is also a common site for distant metastases, particularly from the gastrointestinal system.[1,2] Surgical resection is the standard treatment for early- and very early-stage HCC or liver metastases. However, only 10–20% of patients qualify for resection or transplantation due to factors such as advanced cirrhosis, insufficient liver function, multifocal or advanced disease, tumor location, portal venous invasion, and comorbidities. Surgical treatment is associated with a 2–5% mortality rate and a 20% morbidity rate.[1,3] For patients with HCC or metastatic liver tumors who are unsuitable for surgery, interventional treatments such as transarterial therapies and thermal ablation (TA) methods are available. Transarterial therapies involve selective delivery of chemotherapeutic agents (transarterial chemoperfusion, chemoembolization, and embolization) or radioactive materials (radioembolization) to the liver. TA methods include radiofrequency ablation (RFA), microwave ablation (MWA), laser-induced interstitial thermotherapy, and cryoablation.[2] These methods can be used as standalone treatments or as bridging therapies before liver transplantation.[1]

RFA and MWA are the most commonly used TA techniques. Both aim to deliver heat to malignant tissues, raising the temperature above 60°C to induce coagulation necrosis. Like surgical margins, complete ablation targets the tumor and a surrounding 5–10 mm margin of healthy tissue.[4,5]

RFA, which has been in use longer, generates frictional heating by ionic agitation using alternating current. However, RFA has two significant limitations. The first is the boiling and charring that occur in tissue at temperatures of 100°C and above. The gas or charred tissue formed can obstruct heat conduction, creating unwanted insulation. The second limitation is the "heat-sink" effect, in which vascular structures near the ablation zone dissipate the heat from this area. These factors may prevent the tissue from reaching the necessary temperature, leading to incomplete ablation.[3] MWA, on the other hand, is a newer method that relies on heating water molecules through an electromagnetic field oscillating at frequencies of 900 or 2,450 MHz. This frictional heating increases the temperature in all the tissue around the antenna to a different degree. Compared to RFA, MWA offers several theoretical advantages due to using electromagnetic fields instead of electrical energy. Due to its physical principle, microwave ablation (MWA) is less affected by the heat-sink effect and tissue charring and, therefore, less influenced by heat insulation caused by these factors.[6] As a result, it can achieve higher intratumoral temperatures, leading to larger and more homogeneous ablation zones in a shorter time.[3,7] Furthermore, multiple antennas can be used to create larger ablation zones.[8] However, MWA presents specific challenges, including difficulties achieving safe and effective power distribution, larger antenna diameters, and an increased risk of overheating at the antenna tip and connecting cable.[9] Since its coming into use, various innovations in technique and device technology have been developed to enhance the efficacy of MWA.

A microwave antenna consists of a coaxial cable, which includes an inner conductor, dielectric material, and an outer conductor. In microwave antennas, leaking currents can result in backward heating, which causes the ablation zone, ideally shaped as ellipsoidal or spherical, to become comet-shaped. The tail of this comet shape represents the ablation of normal tissue located behind the active tip of the antenna. Technological developments have addressed this issue by incorporating slots, chokes, or sleeves in the antenna, installing cooling systems, optimizing the outer conductor structure, or adjusting the electromagnetic energy frequency.[10] The recently introduced anti-phase technology integrates these advancements by incorporating a mechanism within the antenna to create opposing-phase microwave radiation. It suppresses backward currents at the edge of the ablation zone, preventing backward heating and enabling more spherical (ultraspherical) ablation. This microwave antenna technology has been addressed in limited ex-vivo, in-vivo preclinical, and in-vivo clinical current studies.[11-14] To the best of our knowledge, our study has the largest number of patients and lesions among in-vivo clinical studies. This study aimed to investigate liver tumor ablation's success, efficacy, and safety using microwave antennas equipped with anti-phase technology.

Patients and methods

This retrospective, cross-sectional, single-center study was conducted in compliance with the prin-

TABLE 1. Inclusion and exclusion criteria of the study

Included	Excluded
Lesions not amenable to surgical treatment	Presence of extrahepatic metastases
Insufficient functional liver capacity after surgery	Suspected pregnancy
Patients unable to undergo general anesthesia due to comorbidities	Uncorrectable coagulopathy
Cases with the use of the particular antenna technology	Any other transarterial or percutaneous treatment

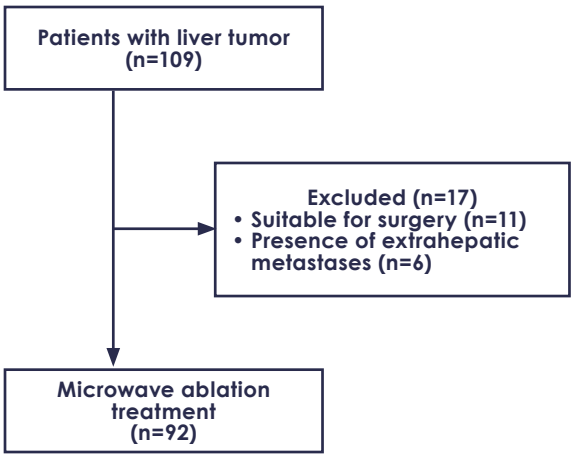

FIGURE 1. Flowchart of the patients.

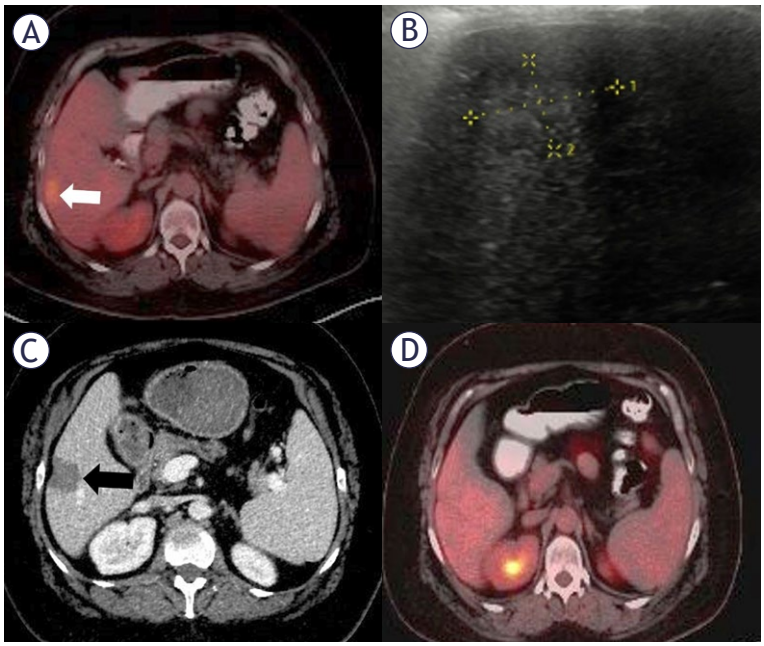

FIGURE 2. (A-D) Radiological findings in a 48-year-old woman with ductal breast carcinoma. PET-CT revealed a hypermetabolic metastasis in segment 6, **(A)** (white arrow). Ultrasound showed a subcapsular hypoechoic lesion **(B),** which was treated with percutaneous microwave ablation under ultrasound guidance. Follow-up CT one day after ablation demonstrated a lesion/ablation area ratio of 1.6 without contrast enhancement, **(C)** (black arrow). PET-CT at 36 months showed no pathological FDG uptake in the liver **(D)**.

ciples of the Declaration of Helsinki after receiving ethical approval (number: E-71522473-050.04-349246-63/26.03.2024). Patients who underwent thermal liver ablation at our clinic between January 2019 and March 2024 were included (Figure 1). A multidisciplinary tumor board made all decisions regarding MWA treatment. The inclusion and exclusion criteria are summarized in Table 1.

Retrospective analysis was conducted on patients' age, sex, pre- and post-procedure laboratory values (white blood cell count, neutrophil-to-lymphocyte ratio), tumor dimensions (pre-procedure and post-procedure day 1 and months 1, 3, and 6), details of the MWA procedure (duration, power output), complications, and local progression or recurrence during follow-up.

Procedures

An interventional radiologist with 12 years of experience in interventional oncology performed all procedures. Prophylactic antibiotics were administered to all patients before the procedure. MWA was performed under deep sedation and analgesia under the supervision of an anesthesiologist. Local anesthesia with 10 cc of prilocaine (Priloc 2%, Vem Pharmaceuticals, Turkey) was applied to the subcutaneous region and liver capsule under sterile conditions.

Lesions were accessed under ultrasound guidance using a convex probe (V8, Samsung, Republic of Korea). For MWA, a 15-gauge Dophi™ M150E antenna (Surgnova, China) was utilized, operating at a frequency of 2.45 GHz with a power output of 50–100 watts. This shaft-cooled antenna with continuous energy transfer was equipped with anti-phase technology (Figure 2A-D). Ablation parameters, including power and duration, were adjusted based on the manufacturer's ablation chart according to the lesion size. For 16 patients (17.4%), additional hydrodissection with 5% dextrose solution was performed for lesions within 5 mm of bowel loops, the diaphragm, or major vessels.

For all patients, the ratio of the post-procedure ablation zone diameter to the pre-procedure tumor diameter was calculated based on contrast-enhanced CT images obtained the day after the procedure (64-slice multidetector CT, Aquilion 64; Toshiba Medical Systems, USA). All measurements were made manually based on the diameter of the longest axes before the procedure and after a single ablation session. Follow-up imaging was performed every three months during the first year and biannually thereafter, using CT, MRI, or positron emission tomography-CT (PET-CT) scans. Imaging findings were assessed using the modified Response Evaluation Criteria in Solid Tumors to determine the response. During follow-up, local tumor progression (LTP) was defined as detecting nodular enhancement adjacent to the ablation zone.

TABLE 2. Clinical and demographic characteristics of the patients

	n
Sex (female/male)	49 (53.3%)/43 (46.7%)
Age	59.8 ± 12.3
Age group (≤ 65 / > 65 years)	60 (65.2%)/32 (34.8%)
White blood cell count	6.5 ± 2.4 ×10³/L
White blood cell count group (≤ 8 ×10³/L / > 8 ×10³/L)	70 (76.1%)/22 (23.9%)
Neutrophil-to-lymphocyte ratio	2.6 (range: 1–10.4)
Neutrophil-to-lymphocyte ratio group (≤ 2 / > 2)	23 (25%)/69 (75%)
Tumor location (favorable/unfavorable)	109 (81.9%)/24 (18.1%)
Tumor size	26.1 ± 13.4 mm
Tumor size group (≤ 3 cm / >3 cm)	93 (69.9%)/40 (30.1%)

Definitions

The target ablation zone was defined as the ablation of the tumor with a 10-mm safety margin while preserving normal parenchyma and non-target tissues. Technical success was defined as complete ablation of the target lesion as confirmed by contrast-enhanced CT one day after the procedure. Complications were classified as minor or major according to the Society of Interventional Radiology reporting standards.[15] Minor complications required only observation without treatment or hospitalization, while major complications necessitated prolonged hospitalization, an unplanned increase in patient care level, or resulted in squeal or death.

Statistical analysis

MedCalc (version 12, Ostend, Belgium) was used for statistical analyses. Descriptive statistics were presented as median (minimum-maximum) and mean ± standard deviation values. Categorical variables were expressed as frequencies and percentages. Fisher, Pearson's chi-squared, and Yates' corrected version of Pearson's chi-squared tests were used to compare categorical variables. The independent-sample t-test was used for the comparison of continuous variables with a normal distribution, and the Mann-Whitney U test was for the data that did not conform to the normal distribution according to the Kolmogorov-Smirnov test. Univariate and multivariate Cox proportional hazards models were utilized to identify risk factors for LTP. The Kaplan-Meier analysis was used to evaluate disease-free survival analysis. A p-value of < 0.05 was accepted as statistically significant.

Results

A total of 92 patients who underwent MWA treatment for HCC or liver metastases were included in the study. The procedure was performed on a total of 133 lesions. The mean age of the patients was 59.8 ± 12.3 years; 49 were female (53.3%), while 43 were male (46.7%). The mean white blood cell count was 6.5 ± 2.4 ×10³/μL, and the median neutrophil-to-lymphocyte ratio was 2.6 (range: 1–10.4). The mean tumor size was 26.1 ± 13.4 mm. The clinical and demographic characteristics of the patients are summarized in Table 2.

Of the 92 patients, nine (9.8%) were diagnosed with HCC, and 83 (90.2%) had metastases. Among patients with metastases, 46 (55.4%) had colorectal metastases, and 37 (44.6%) had non-colorectal metastases (Table 3).

MWA achieved the targeted ablation zone in all patients, resulting in a technical success rate of 100%. A median power of 80 watts (50–100 range) was applied to the lesions, and the mean ablation duration was 5.2 ± 2.1 minutes. The mean ratio of the ablation zone area to the tumor area was 1.63 ± 0.3.

Minor complications occurred in 29 patients (31.5%), including post-procedural pain (n = 15), subfebrile fever (n = 8), and fatigue (n = 6). All minor complications were resolved within 48 hours.

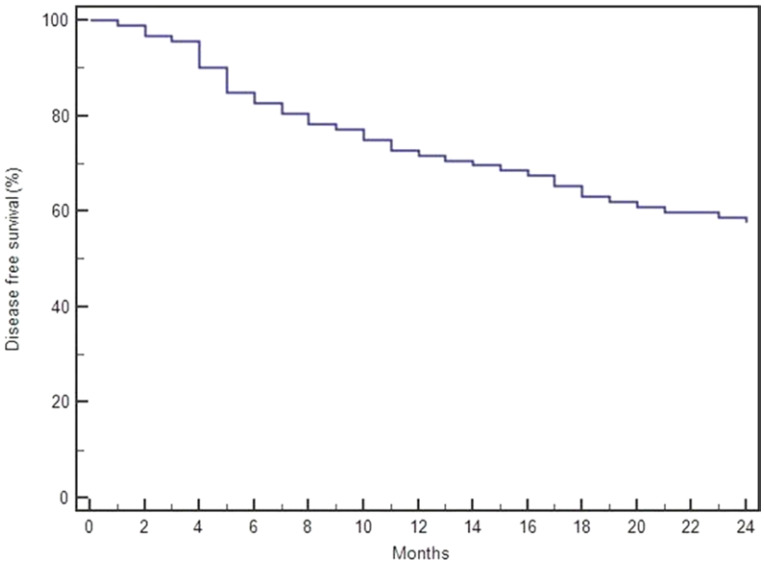

FIGURE 3. Analysis of disease-free survival (DFS) in patients who underwent microwave ablation (MWA).

Major complications were observed in 3 patients (3.2%). They included a liver abscess requiring drainage (n = 1), hemorrhage necessitating embolization eight hours after the procedure (n = 1), and pleural effusion requiring drainage two hours after the procedure (n = 1).

The median follow-up time of the patients was 33 (range 10–36) months. According to the Kaplan-Meier analysis, the third-, sixth-, 12th-, and 24th-month disease-free survival (DFS) rates were 95.6%, 82.6%, 72.8%, and 57.6%, respectively. The median DFS time was 25 months (95% confidence interval: 21–27) (Figure 3).

TABLE 4. Univariate analysis of factors associated with local tumor progression in MWA-treated patients

Variables	p
Sex (male vs. female)	0.372
Age (≤ 65 vs. > 65 years)	0.415
White blood cell count (≤8 ×10³/L vs. > 8 ×10³/L)	0.554
Neutrophil-to-lymphocyte ratio (≤2 vs. > 2)	0.297
Primary tumor (HCC vs. metastasis)	0.624
Metastasis type (colorectal vs. non-colorectal)	0.198
Tumor location (favorable vs. unfavorable)	0.339
Tumor size (≤3 cm vs. > 3 cm)	0.012

HCC = hepatocellular carcinoma; MWA = microwave ablation

TABLE 3. Primary tumors of patients who underwent ablation due to liver metastasis

	n	%
Colorectal		
Colon	32	38.5
Rectum	14	16.9
Non-colorectal		
Breast	14	16.9
Gastric	8	9.6
Pancreas	5	6
Ovarian	5	6
Lung	3	3.6
Endometrium	2	2.5

During the 24-month follow-up, local tumor progression was observed in 39 patients (42.4%). Univariate analysis identified tumor size as the only independent risk factor for LTP (p = 0.012) (Table 4). In a multivariate analysis, tumor size was categorized as ≤3 cm, 3–5 cm, and ≥5 cm. It was determined to be an independent risk factor for local tumor progression (LTP), with a hazard ratio of 1.733 (95% CI: 1.541–2.873) and a p-value of 0.037.

Discussion

The most notable feature of our study is its focus on the use of an MWA antenna with anti-phase technology offering ultraspherical ablation, making it, to our knowledge, the second study in vivo on humans and the largest to date, with the longest follow-up period. In addition, unlike the previous clinical study involving the same antenna, the lesions treated in our research predominantly included metastatic lesions, with a significant proportion originating from colorectal cancer.

The principle underlying MWA involves the application of an electromagnetic field at frequencies ranging from 900 to 2,500 MHz to achieve lethal temperatures within tissues, resulting in tissue destruction. Microwave energy is delivered to tissues via an antenna, with heating concentrated around the antenna's periphery. Microwave energy can propagate in environments with low thermal-electrical conductivity or high impedance, such as lung tissue, bone, and charred or desiccated tissues. This characteristic allows microwave ablation (MWA) to overcome the limitations of RFA,

which has reduced efficacy in such tissue types.[9] Furthermore, the simultaneous use of multiple MWA antennas enables synergistic thermal effects within the same lesion when placed proximally or simultaneous ablation of separate lesions when positioned distally.[9]

The MWA system comprises three components: the generator, the power delivery system, and antennas. Unlike RFA, the power output from the generator in MWA is unaffected mainly by tissue type. In MWA, there is no significant reduction in power output when operating in high-impedance tissues. The energy generated in the MWA generator is transmitted to the antenna via coaxial cables. However, while flexible and thin-caliber cables are designed to enhance usability, they also introduce disadvantages, such as heating and power loss.[9] Antennas represent the final component of the system, transferring microwave energy to the tissue. Structurally, antennas consist of an inner conductor, dielectric material, and an outer conductor. The most basic antenna designs include dipole, monopole, and slot antennas. The dipole antenna differs from the monopole design by incorporating a metal block at the distal end of the coaxial cable, leaving a gap for electromagnetic energy emission. The inner and outer conductors are soldered together in slot antennas at the coaxial cable's end. However, a gap is left near the soldered junction, allowing electromagnetic waves to pass into the tissue. A common challenge in all three antenna designs is generating leaking currents from the antenna back toward the generator.[10] These currents can cause unintended heating of tissues behind the target area, leading to a comet-tail ablation zone instead of the desired spherical or ellipsoidal shape. Technological advancements have aimed to address this issue.[10]

Compared to RFA, MWA offers distinct advantages due to its underlying physical principles, including achieving larger, more homogeneous ablation zones in a shorter time. However, MWA also has disadvantages, such as less predictable ablation zones, cable heating, the larger calibration of probes, and the creation of elongated and narrow ablation zones.[16] The indications for MWA are similar to those for other TA techniques and include curative, debulking, or palliative treatments. For colorectal metastases, MWA is recommended for oligometastatic lesions (≤ 4 lesions) smaller than 3 cm.[17] For HCC, it is indicated for very early-stage (stage 0) and, in selected cases, early-stage (stage A) disease based on the Barcelona Clinic Liver Cancer staging system.[18]

In a review including 11 studies (four randomized and seven observational) and involving 2,169 patients, Spiliotis *et al*. compared the outcomes of MWA and RFA. They reported no significant difference between the two methods in terms of LTP. However, a subgroup analysis of randomized trials in patients with HCC demonstrated lower LTP rates with MWA. No differences were observed between the two techniques regarding complete ablation rates, distant recurrence (DR), or complication rates. The authors emphasized that LTP was the most critical criterion for evaluating the efficacy of ablation techniques.[19]

MWA has been shown to produce more spherical ablation zones, which correspond to larger treatment volumes.[20] A more spherical ablation zone is expected to ensure complete coverage of the target lesion margin within the ablation area.[21] Advances in MWA probe design have aimed to achieve this ideal shape. A study by Cazzato *et al*. demonstrated that using multiple MWA antennas (e.g., two antennas for tumors between 2–3 cm, three antennas for tumors > 3 cm) facilitates the creation of ablation zones closer to a spherical shape.[22]

In all ablation methods, including MWA, clinical outcomes are evaluated using parameters such as technical success, the efficacy of the ablation (complete ablation or LTP/local recurrence [LR] in the case of incomplete ablation), complications, and survival (DFS and overall survival [OS]).[19,23] In a retrospective study by Xu *et al*. involving 142 patients and 294 tumors, technical success was 95.2%, with LTP and DR rates of 15% and 68.3%, respectively. The DFS rates at the first, third, and fifth years were 76%, 33.1%, and 19.5%, respectively, while the OS rates at the same time points were 97.2%, 75.4%, and 50.6%, respectively.[23] Compared to our study, our three-month DFS rate (95.6%) was significantly better despite our higher LTP rate. Furthermore, tumor sizes were larger in the study by Xu *et al*. (31 ± 13 *vs*. 26.1 ± 13.4 mm).

Pathak *et al*. systematically reviewed 13 studies with 406 patients with colorectal metastases. The OS rates in the first, third, and fifth 5 years were 73%, 30%, and 16%, respectively, while LR rates ranged from 2% to 14%. The minor and major complication rates were 6.7–90.5% and 0–19%, respectively. The authors emphasized that survival rates were higher in patients treated with MWA compared to those receiving palliative chemotherapy alone.[24] Compared with this review, our patients exhibited a higher recurrence rate (LTP), while the minor and major complication rates were within the range identified.

Leung *et al*. retrospectively analyzed 176 patients and 416 tumors, primarily colorectal metastases (81%), and reported LTP and DR rates of 7.9% and 38%, respectively. The study also demonstrated a significant relationship between tumor size and perivascular location with LR, with the LR rate reaching 33% in tumors larger than 3 cm. In addition, it was emphasized that the LR rate was higher for biliary carcinoma and non-colorectal metastases. The four-year OS rate during the follow-up was reported to be 58% for colorectal metastases and 79% for other pathologies, but no statistically significant differences were observed.[8] In our study, tumor size was also identified as an independent risk factor for LTP, although a similar relationship between tumor pathology and LTP was not demonstrated. While the cohort in the study by Leung *et al*., mostly consisting of patients with colorectal metastasis, shares similarities with our study, the median tumor size was smaller than ours (10 mm *vs*. 26.1 mm).

To our knowledge, the first clinical study utilizing the MWA antenna with anti-phase technology for ultraspherical ablation was conducted by Blain *et al*.[12] The authors performed ablation on 87 tumors in 68 patients using the same MWA antenna (Dophi™ M150E, Surgnova, China) as in our study. The lesions had a mean diameter of 17.8 ± 7.9 mm, and the ablation zone measured a maximum axis of 35.6 ± 11 mm. The mean follow-up duration was 10 months, during which local tumor control was observed in 84.7% of the patients who underwent ablation. In contrast, our study demonstrated a DFS rate of 72.8% at 12 months, with a lower tumor control rate than the previous study. Moreover, complications were reported in only two patients in that study (one case of stress ulcer and one of subcapsular hematoma). However, there are several key differences between the two studies, including the median follow-up period (10 months *vs*. 33 months), pre-procedure tumor sizes (median 17.8 cm *vs*. 26.1 cm), MWA procedural parameters (ablation time of 8 ± 4.5 minutes *vs*. 5.2 ± 2.1 minutes), and tumor types (more non-colorectal metastases and an equal number of colorectal metastases and HCC cases in the previous study).

In the prospective study of Zhang *et al*. covering 50 patients and 77 tumors, the majority of tumors were primary lesions [primary: 52, metastatic: 25 (colorectal: 19, non-colorectal: 6) lesions].[11] Technical success (defined as primary technical efficiency) was shown as 97.4%. Unlike our study, the short and long axes of the ablation zone were measured, and the ablation volume and sphericity index (SI = short axis/long axis) were calculated. When the ablation zone diameters were compared with the manufacturer's ablation chart and the ex-vivo study of Namakshenas *et al*., it was determined that the long diameters were parallel. In contrast, the short diameters were measured smaller.[14] It was thought that this situation may be due to the complexity and variable nature of in-vivo conditions. The parallelism of the ablation zone volumes with the in-vivo study of Blain *et al*. indicated that the antenna provided a predictable ablation zone. The SI value was shown as a mean of 0.77 ± 0.11, and SI was greater than 0.66 in the majority of lesions (86%). This result was interpreted as the ablation zone being "relatively well-rounded, though not perfectly spherical." In the study of Blain *et al*., where the same formulation was used, the mean SI was 0.78 ± 0.14, and the rate of SI > 0.66 was 82%, showing parallelism.12 No relationship was shown between SI and power and duration. As in our study, attention was paid to lesion locations; factors such as subcapsular location, proximity to the diaphragm and heart, and proximity to major blood vessels or other organs were considered. The clinical follow-up period was short, and multiphasic MRI was performed at 6 weeks, and CT was used in patients with contraindications. The complication rate was stated as 10%, 4% of which were major (liver abscess in 1 patient and liver hemorrhage in 1 patient). The major complication rate is similar to that of our study.

Namakshenas *et al*. investigated the performance of the MWA system used in our study in ex-vivo liver, lung, and kidney ablations.[14] When the ablation axis measurements were compared with the values in the manufacturer's chart, the values were generally consistent, especially in low-power settings and single antenna use. Mean SI was 0.95, 0.79, and 0.9 for liver, lung, and kidney, respectively, in single antenna use. It was observed that the SI value approached 1 for 75 W power settings and 10 minutes of ablation in dual antenna use. It was concluded that the ablation axes were predictable except for the highest energy level ablations performed in the lung. It was stated that an almost spherical ablation zone was reached in a single antenna used for the liver and kidney. It was stated that more homogeneous heat distribution was achieved in the tissue in dual antenna use compared to a single antenna. Habert *et al*. performed MWAs on pig liver (50 pieces) and lung (48 pieces) models under CT guidance with the antenna we used in our study and evaluated the ablation dimensions.[13] In the study, they performed 3, 5, 8, 10 and 15-minute ablations

with 50, 75 and 100 W power values. The ablation zone was evaluated 3-dimensionally with contrast-enhanced CT. SI values were determined to be between 0.50-0.80 for the liver and 0.40-0.69 for the lung. Although sphericity was defined as equal to 1, the long and short axes were squared in the SI calculation in this study, and the SI measurements differed from the other studies we mentioned. As a result of the study, it was determined that a shorter ablation time provided better energy efficiency [ablation zone volume (cm^3)/applied energy (W)], and the ablation zone was more predictable at a 10-minute ablation time.

Our study has certain limitations. Firstly, it was retrospective in design. Secondly, the patient cohort was relatively small and heterogeneous. Due to this heterogeneity, OS data for the patients were not included in the study. Thirdly, there is a notable difference between the HCC group (n = 9) and the metastatic group (n = 83), which could impact statistical analyses when examining subgroups. Lastly, all patients were treated using the same anti-phase technology antenna. While the literature has discussed the potential advantages of this technology over conventional MWA systems, this study did not include any direct comparisons. Further large-scale, comparative, and prospective studies could address these limitations.

The application of anti-phase technology in microwave ablation allows for the formation of more spherical and predictable ablation zones, potentially improving local tumor control and procedural safety in clinical practice.

In conclusion, MWA is a current treatment method for HCC and liver metastases, and technological advancements based on its physical principles are being explored to enhance ablation efficacy. Our study, including the longest follow-up duration and the largest patient population examining the antenna technology for ultraspherical ablation with anti-phase technology, demonstrated that this treatment had a high technical success rate and acceptable local control and complication rates.

References

1. Meloni MF, Chiang J, Laeseke PF, Dietrich CF, Sannino A, Solbiati M, et al. Microwave ablation in primary and secondary liver tumours: technical and clinical approaches. *Int J Hyperthermia* 2017; **33:** 15-24. doi: 10.1080/02656736.2016.1209694
2. Vogl TJ, Nour-Eldin N-EA, Hammerstingl RM, Panahi B, Naguib NNN. Microwave ablation (MWA): basics, technique and results in primary and metastatic liver neoplasms – review article. *Rofo* 2017; **189:** 1055-66. doi: 10.1055/s-0043-117410
3. Canwell CP, Gervais DA. Image-guided ablation of liver tumors. In: Kaufmn JA, Lee MJ, editors. *Vascular and interventional radiology: the requisites*. 2nd edition. Elsevier Health Sciences; 2013. p. 572-79.
4. Ahmed M, Solbiati L, Brace CL, Breen DJ, Callstrom MR, Charboneau JW, et al. Image-guided tumor ablation: standardization of terminology and reporting criteria – a 10-year update. *Radiology* 2014; **273:** 241-60. doi: 10.1148/radiol.14132958
5. Puijk RS, Ahmed M, Adam A, Arai Y, Arellano R, de Baère T, et al. Consensus guidelines for the definition of time-to-event end points in image-guided tumor ablation: results of the SIO and DATECAN initiative. *Radiology* 2021; **301:** 533-40. doi: 10.1148/radiol.2021203715
6. De Vita E, Lo Presti D, Massaroni C, Iadicicco A, Schena E, Campopiano S. A review on radiofrequency, laser, and microwave ablations and their thermal monitoring through fiber Bragg gratings. *iScience* 2023; **26:** 108260. doi: 10.1016/j.isci.2023.108260
7. Danışan G, Küpeli A, Taydaş O. Is microwave ablation therapy as effective as colorectal liver metastases in noncolorectal liver metastases? *Turk J Med Sci* 2022; **52:** 1336-43. doi: 10.55730/1300-0144.5440
8. Leung U, Kuk D, D'Angelica MI, Kingham TP, Allen PJ, DeMatteo RP, et al. Long-term outcomes following microwave ablation for liver malignancies. *Br J Surg* 2015; **102:** 85-91. doi: 10.1002/bjs.9649
9. Lubner MG, Brace CL, Hinshaw JL, Lee FT Jr. Microwave tumor ablation: mechanism of action, clinical results, and devices. *J Vasc Interv Radiol* 2010; **21:** S192-203. doi: 10.1016/j.jvir.2010.04.007.
10. Huang H, Zhang L, Moser MAJ, Zhang W, Zhang B. A review of antenna designs for percutaneous microwave ablation. *Physica Medica* 2021; **84:** 254-64. doi: 10.1016/j.ejmp.2021.03.010
11. Zhang L, Luerken L, Mayr V, Goetz A, Schlitt A, Stroszczynski C, et al. The efficacy and safety of a microwave ablation system with a dipole antenna design featuring floating sleeves and anti-phase technology in stereotactic percutaneous liver tumor ablation: results from a prospective study. *Cancers* 2024; **16:** 4211. doi: 10.3390/cancers16244211.
12. Blain M, Narayanan G, Ricoeur A, Kobe A, Mahendra AM, Jacks B, et al. Safety and efficacy of percutaneous liver microwave ablation using a fully water-cooled choke ring antenna: first multicenter clinical report. *Cardiovasc Intervent Radiol* 2023; **46:** 1086-91. doi: 10.1007/s00270-023-03481-3.
13. Habert P, Di Bisceglie M, Hak J-F, Brige P, Chopinet S, Mancini J, et al. Percutaneous lung and liver CT-guided ablation on swine model using microwave ablation to determine ablation size for clinical practice. *Int J Hyperthermia* 2021; **38:** 1140-8. doi: 10.1080/02656736.2021.1961883
14. Namakshenas P, Arcaini T, Cesare B, Dorato A, Durante E, Ricci M, et al. Performance of an anti-phase technology-powered microwave ablation system on ex vivo liver, lung and kidney: analysis of temperature trend, ablation size and sphericity. *Cardiovasc Intervent Radiol* 2024; **47:** 1392-401. doi: 10.1007/s00270-024-03811-z
15. Khalilzadeh O, Baerlocher MO, Shyn PB, Connolly BL, Devane AM, Morris CS, et al. Proposal of a new adverse event classification by the Society of Interventional Radiology Standards of Practice Committee. *J Vasc Interv Radiol* 2017; **28:** 1432-7.e3. doi: 10.1016/j.jvir.2017.06.019
16. Radosevic A, Quesada R, Serlavos C, Sánchez J, Zugazaga A, Sierra A, et al. Microwave versus radiofrequency ablation for the treatment of liver malignancies: a randomized controlled phase 2 trial. *Sci Rep* 2022; **12:** 316. doi: 10.1038/s41598-021-03802-x
17. Filoni E, Musci V, Di Rito A, Inchingolo R, Memeo R, Mannavola F. Multimodal management of colorectal liver metastases: state of the art. *Oncol Rev* 2023; **17:** 11799. doi: 10.3389/or.2023.11799
18. Tsilimigras DI, Aziz H, Pawlik TM. Critical analysis of the Updated Barcelona Clinic Liver Cancer (BCLC) group guidelines. *Ann Surg Oncol* 2022; **29:** 7231-4. doi: 10.1245/s10434-022-12242-4
19. Spiliotis AE, Gäbelein G, Holländer S, Scherber P-R, Glanemann M, Patel B. Microwave ablation compared with radiofrequency ablation for the treatment of liver cancer: a systematic review and meta-analysis. *Radiol Oncol* 2021; **55:** 247-58. doi: 10.2478/raon-2021-0030
20. Vogl TJ, Basten LM, Nour-Eldin N-EA, Kaltenbach B, Bodelle B, Wichmann JL, et al. Evaluation of microwave ablation of liver malignancy with enabled constant spatial energy control to achieve a predictable spherical ablation zone. *Int J Hyperthermia* 2018; **34:** 492-500. doi: 10.1080/02656736.2017.1358408.

21. Imajo K, Tomeno W, Kanezaki M, Honda Y, Kessoku T, Ogawa Y, et al. New microwave ablation system for unresectable liver tumors that forms large, spherical ablation zones. *J Gastroenterol Hepatol* 2018; **33:** 2007-14. doi: 10.1111/jgh.14294

22. Cazzato RL, De Marini P, Leclerc L, Dalili D, Koch G, Rao P, et al. Large nearly spherical ablation zones are achieved with simultaneous multi-antenna microwave ablation applied to treat liver tumours. *Eur Radiol* 2020; **30:** 971-5. doi: 10.1007/s00330-019-06431-1

23. Xu Y, Shen Q, Liu P, Xu Z, Wu P, Lu Z, et al. Microwave ablation for the treatment of hepatocellular carcinoma that met up-to-seven criteria: feasibility, local efficacy and long-term outcomes. *Eur Radiol* 2017; **27:** 3877-87. doi: 10.1007/s00330-017-4740-0

24. Pathak S, Jones R, Tang JMF, Parmar C, Fenwick S, Malik H, et al. Ablative therapies for colorectal liver metastases: a systematic review. *Colorectal Dis* 2011; **13:** e252-65. doi: 10.1111/j.1463-1318.2011.02695.x

research article

Invasive properties of patient-derived glioblastoma cells after reversible electroporation *in vitro*

Anja Blazic[1], Bernarda Majc[2], Metka Novak[2,3], Barbara Breznik[2,4], Lea Rems[1]

[1] Faculty of Electrical Engineering, University of Ljubljana, Ljubljana, Slovenia
[2] Department of Genetic Toxicology and Cancer Biology, National Institute of Biology, Ljubljana, Slovenia
[3] Biotechnical Faculty, University of Ljubljana, Ljubljana, Slovenia
[4] Faculty of Chemistry and Chemical Engineering, University of Ljubljana, Ljubljana, Slovenia

Radiol Oncol 2025; 59(4): 535-550.

Received 11 August 2025
Accepted 29 September 2025

Correspondence to: Assist. Prof. Lea Rems, Ph.D., Faculty of Electrical Engineering, University of Ljubljana, Tržaška cesta 25, SI-1000 Ljubljana, Slovenia. E-mail: lea.rems@fe.uni-lj.si

Disclosure: No potential conflicts of interest were disclosed.

Background. Electroporation-based therapies are being explored in glioblastoma (GB) treatment, as means of enhancing drug delivery or achieving nonthermal ablation. Yet, little is known about how sublethal exposure affects the invasive behaviour of GB tumour cells.

Materials and methods. Five patient-derived GB cell lines were initially screened for intrinsic invasive potential, and two most invasive (NIB140 CORE and NIB216 CORE) were selected for further experiments with electroporation treatment. Cells in suspension were exposed to bursts of high-frequency biphasic electric pulses resulting in electric field strength of 1 kV/cm, which corresponded to conditions of reversible electroporation. Changes in cell invasion and gene regulation were assessed 24 hours after electroporation using transwell assay and RNA transcriptome analysis, respectively.

Results. Reversible electroporation at 1.0 kV/cm enhanced invasion in a cell line-dependent manner. NIB140 CORE showed a consistent and pronounced increase, with a median of 3.74-fold (274%) higher number of invading cells compared to sham control. In contrast, NIB216 CORE exhibited only a modest increase in invasion (1.30-fold; 30%). Transcriptomic profiling identified modulation of genes linked to extracellular matrix organization and ion channel activity in NIB140 CORE, and cytoskeletal remodelling in NIB216 CORE, indicating the activation of invasion-related pathways.

Conclusions. These findings highlight a potential risk of pro-invasive responses in GB cells. In tumour ablation with irreversible electroporation, this concern relates to cells in the peripheral zone that may experience only sublethal electric fields, while in electrochemotherapy, a similar risk may arise if permeabilized cells are not effectively eliminated due to insufficient local drug delivery. Nevertheless, the two tested cell lines responded differently, underscoring patient-specific heterogeneity and the need for validation in more physiologically relevant models.

Key words: electroporation; high-frequency electric pulses; glioblastoma; patient-derived cells; invasion

Introduction

Electroporation is achieved by brief exposure of cells to high-intensity pulsed electric fields, creating nanoscale defects (i.e., pores) in the cell membrane. Depending on the extent of membrane disruption, cells may either restore homeostasis and survive (reversible electroporation) or fail to recover, leading to cell death (irreversible electroporation, IRE).[1] Clinically, electroporation has gained

recognition as a versatile tool in oncology. IRE can be used as a stand-alone, minimally invasive, non-thermal ablation technique[2,3], whereas reversible electroporation can be used to enhance the uptake and cytotoxicity of chemotherapeutic drugs while allowing for reduced drug dosages (electrochemotherapy; ECT).[4,5] Unlike thermal ablation, electroporation spares major blood vessels and the extracellular matrix, making it especially well-suited for tumours situated near vital or functionally critical structures.[2] Moreover, by enhancing drug delivery and promoting anti-tumour immune activation, electroporation has become recognized as a key component of multimodal cancer therapy.[2]

Glioblastoma (GB), a WHO grade IV astrocytoma, is the most lethal and treatment-resistant primary brain tumour, with a median patient survival of around 15 months and a five-year survival rate below 10%.[6-8] It is characterized by pronounced cellular and molecular heterogeneity, aggressive infiltration into surrounding brain tissue, and the development of a highly immunosuppressive microenvironment. Together, these biological features present significant challenges to developing effective treatments. The blood-brain barrier further limits drug delivery, while therapy-resistant GB stem cells and extensive genomic instability drive inevitable recurrence.[9] Despite the fact that surgery, radiotherapy, and chemotherapy remain the standard treatments for GB, emerging evidence indicates that tumour cells surviving these treatments may acquire an even more invasive phenotype, further complicating disease management.[10] This emphasizes the urgent need for novel, multimodal strategies capable of addressing complex tumour biology and preventing treatment-induced adaptation.

Given these challenges, there is growing interest in exploring alternative strategies for GB treatment. Several animal studies have demonstrated clinical potential of electroporation-based treatments for brain tumours. In canine models, research has primarily focused on IRE as a non-thermal ablation method. First-generation IRE protocols consisted of ninety 50-μs-long monophasic pulses at 4 Hz, producing well-controlled ablation volumes with sharp submillimeter transition zones between treated and healthy tissue.[11-13] A notable prospective study using the NanoKnife system in seven dogs with spontaneous gliomas demonstrated safety and feasibility of IRE for brain tumour treatment.[14] Individualized treatment plans were developed based on magnetic resonance image segmentation and computational optimization to ensure adequate electric field coverage of tumour by a sufficiently high electric field. Procedures involved craniotomy and stereotactic pulse delivery under general anaesthesia. Most adverse effects were mild to moderate and resolved with minimal intervention; however, two dogs experienced severe toxicity – one unrelated to IRE, and the other linked to the highest energy dose. Objective response was observed in four of five dogs with measurable lesions, with one dog remaining tumour-free for over five years.[15] To address limitations such as muscle contractions and neuromuscular stimulation, second-generation high-frequency IRE (H-FIRE) protocols have been developed to minimize these undesired effects.[16] A pilot study in three dogs with spontaneous meningiomas confirmed effective tumour ablation near critical vasculature with no major IRE-related side effects.[17] In addition, the potential of ECT for GB treatment was demonstrated in rodent studies. In rats with induced gliomas, ECT with intravenous bleomycin improved their survival[18], while intratumoral bleomycin combined with a newly designed electrode achieved complete tumour elimination in 69% of treated animals.[19] Another study combining IRE and ECT with intravenous cisplatin via monopolar electrode showed delayed tumour growth and improved survival in glioma-bearing rats.[20] These results led to a phase I clinical trial (NCT01322100) investigating ECT for brain metastases, which was however discontinued due to low patient enrolment.[21]

Despite these encouraging findings, electroporation has not yet been clinically established for brain tumours. Treatment responses in preclinical studies were variable, and complete tumour control was not achieved in all animals. The underlying causes of this heterogeneity remain unclear. One contributing factor may be the inhomogeneous electric field distribution during treatment, which creates a central region of IRE surrounded by a narrow peripheral zone of reversibly electroporated cells.[22-24] In highly infiltrative tumours like GB, some tumour cells are likely to be exposed only to sublethal electric field strengths, i.e. reversible electroporation, and survive the treatment. If electroporation alters the behaviour of surviving tumour cells, making them more invasive or aggressive, this might pose a potential risk for recurrence. A similar concern may arise in ECT, if insufficient drug delivery allows electroporated cells to survive the treatment. Thus, there is need for a deeper understanding of how reversible electroporation affects GB cells behaviour. Additionally,

further preclinical studies are warranted, as even the most relevant animal models, such as spontaneous canine gliomas, still show important discrepancies compared to human GB. While animal gliomas can mimic human GB tumour heterogeneity and histological features, they include a lower number of mutated genes and a different immune cell response.[25-27] Moreover, investigating the invasive behaviour of cells within sublethal regions is ethically and experimentally challenging *in vivo*, which further highlights the importance of clinically relevant *in vitro* models before progressing towards clinical application.

To investigate electroporation-induced changes in GB cell behaviour under clinically relevant conditions, we employed patient-derived primary cultures that more accurately reflect the genetic background, heterogeneity and invasive properties of human tumours compared to commercially available cell lines.[28] This study was motivated by increasing evidence that sublethal therapies may promote a more aggressive phenotype in surviving tumour cells.[10,29] Furthermore, our previous study[30] revealed that reversible electroporation activates Ca^{2+}-activated potassium channels in U-87 MG GB cell line, which are known to play a key role in regulating GB invasion.[31,32] Therefore, we focused specifically on evaluating how electroporation affects the invasion of GB cells. We began by characterizing the invasive potential of five patient-derived GB cell lines and selected two cultures with the highest invasive capacities for further investigation. We then evaluated changes in tumour cell invasion induced by reversible electroporation. To ensure that we specifically examined the response of reversibly electroporated cells only, we employed a suspension-based approach, which provides a controlled system without the confounding effects of mixed reversible and irreversible populations. To gain deeper insight into how electroporation affects gene expression in surviving tumour cells, we additionally performed RNA sequencing in treated and non-treated samples. The findings presented here provide important insights that may contribute to the development of effective electroporation-based strategies for GB therapy.

Materials and methods

Cells

Experiments were performed using five different cell lines obtained from Slovenian GlioBank managed by the National Institute of Biology (NIB).[33] Patients or their authorized representatives signed an informed consent in accordance with the Declaration of Helsinki. Collection and processing of tumour tissue material was approved by the National Medical Ethics Committee of the Republic of Slovenia (numbers 92/06/12, 0120-190/2018-4, 0120-190/2018-26, 0120-190/2018-32, and 0120-190/2018-35). Cell lines established from tumours were labelled with internal code numbers: NIB140 CORE, NIB216 CORE, NIB220 RIM, NIB237 CORE and NIB261 REC. CORE and RIM indicate the anatomical tumour regions from which the tumour cells were derived (the tumour core and infiltrative rim, respectively), while REC refers to cells isolated from a recurrent GB lesion. All cell lines were grown in Dulbecco's Modified Eagle Medium (DMEM; Gibco, #41965039), supplemented with 10% foetal bovine serum (Gibco, #10500064) and antibiotics Penicillin-Streptomycin (Sigma-Aldrich, Germany, #P0781), hereafter referred to as DMEM10.

Cells were routinely passaged every 3 to 4 days and were maintained in a humidified environment at 37°C with 5% CO_2. For determining the cell doubling time, $2x10^5$ cells were seeded per well of a 6-well plate (TPP, Switzerland), incubated at 37°C, 5% CO_2, and then trypsinized and counted at selected times 20–100 hours after seeding. For electroporation, cells were trypsinized, counted, and centrifuged at 300 × g for 3 minutes. The resulting pellet was resuspended in DMEM10 with 10 mM HEPES, Sigma-Aldrich, #H0887 (hereafter referred to as DMEM10+) to achieve a final cell density of 1×10^6 cells/ml.

Electric pulse exposure

Cells were exposed to H-FIRE pulses, which were previously used in GB investigations *in vitro*,[34] as well as *in vivo* for the treatment of spontaneous canine meningiomas[17] and in a study examining blood-brain barrier disruption mechanisms.[35] Specifically, we applied 100 bursts of biphasic pulses, with 2 μs negative and 2 μs positive phase, 5 μs interphase and 5 μs interpulse delay, 25 pulses/burst, at 1 Hz burst repetition frequency (Supplementary Figure S1). The pulse amplitude was varied between 100–400 V, corresponding to 0.5–2 kV/cm. Pulses were delivered by a high-frequency pulse generator L-POR (mPOR, Slovenia), through 2 mm electroporation cuvettes (VWR, #732-1136). The current and voltage were routinely monitored on an oscilloscope Wavesurfer

422, 200 MHz, using high-voltage differential probe ADP305 and current probe CP030 (all from Teledyne LeCroy, USA). The electric field to which the cells were exposed was estimated as the ratio between the applied voltage and the interelectrode distance.

We aimed to perform experiments at close-to-physiological temperature, which is relevant to *in vivo* tumour treatment. Thus, each cuvette was first preheated in an incubator at 33°C for at least 15 minutes. Subsequently, the cell suspension was added to the preheated cuvette, and placed back into the incubator at 33°C. Following an additional 10-minute incubation period, electric pulses were delivered to the cuvette inside the incubator. The temperature of 33°C was chosen based on our previous findings in U-87 MG GB cells, where electroporation at this temperature, but not at room temperature (~25°C), triggered activation of Ca^{2+}-activated potassium channels that are associated with membrane hyperpolarization and increased invasive potential.[30] In addition, responses at 33°C are expected to more closely approximate those at physiological temperature (37°C) than at room temperature, while maintaining a margin of safety against heating, as the sample temperature increased by > 8°C when the strongest electric pulses were delivered.

Joule heating of the sample due to pulse delivery was measured using a fibre optic sensor MPK-5 (OpSens Solutions, Canada). The sample temperature increased by 1.3°C ± 0.3°C at 200 V (1 kV/cm) and 8.3°C ± 0.7°C at 400 V (2 kV/cm), recordings shown in Supplementary Figure S2. This temperature increase was measured at room temperature (24–26°C); the increase during pulse delivery at 33°C is expected to be somewhat higher due to lower heat dissipation in warmer atmosphere.

Permeabilization assay

Cell suspension (150 µl, 1 × 10^6 cells/ml) prepared in DMEM10+ was mixed with propidium iodide (PI, Molecular probes, #P1304MP) in a final concentration of 100 µg/ml. PI is a nucleic acid stain that selectively penetrates cells with compromised membranes, where it binds to DNA and emits fluorescence. When added to cell suspension before pulse delivery, it enables identification of electroporated cells.[36] 3 minutes after pulse application, 350 µl of electroporation solution was added to the cell suspension and the sample was removed from the electroporation cuvette. The percentage of PI-stained cells was quantified by flow cytometer (Attune NxT, Carlsbad, CA, USA) using blue laser excitation at 488 nm and detecting the emitted fluorescence through a 574/26 nm band-pass filter. 10,000 events representing individual cells were obtained, and data were analysed using the Attune Nxt software. Cells with fluorescence intensity above a certain gate value, defined based on fluorescence intensity histogram, were considered electroporated. Gating was set according to sham control (0 V). Measurements for each data point were repeated at least three times on three different days.

PI-based viability assay

Cell suspension (150 µL, 1 × 10^6 cells/mL) was prepared in DMEM10+ and transferred to an electroporation cuvette. After pulse application and additional 10-minute incubation at 33 °C, 850 µL of DMEM10+ was added to the cuvette. Afterwards, 100 µL of the treated cell suspension was plated into 24-well plate (TPP, Switzerland) containing 1 mL of DMEM10, and the plate was incubated at 37°C in a humidified atmosphere with 5% CO_2 for 24 hours. PI was used to assess cell viability 24 hours after the electric pulse exposure. First, cells were harvested (attached and unattached) and centrifuged at 300 × g for 3 minutes. The cell pellet was then resuspended in 150 µL of growth medium together with PI in a final concentration of 100 µg/ml, and cells were incubated at room temperature for 5 minutes. The number of all cells (N_{total}) and the number of PI-stained cells (N_{PI+}) in a fixed sample volume was quantified by flow cytometer (Attune NxT; Life Technologies, USA), using a 488 nm blue laser and 574/26 nm band-pass filter. The percentage of viable cells was determined from $(N_{total}–N_{PI+})/N_{total,ctrl}$, as described in our previously published protocol[37], where $N_{total,ctrl}$ represents the total number of cells in sham control.

MTS-based viability assay

Cells were prepared and exposed to electric pulses in the same way as for the PI–based viability assay. 50 µL of the treated cell suspension was then plated into 96-well plate (TPP) containing 50 µL of DMEM10 and the plate was incubated at 37°C and 5% CO_2. MTS metabolic assay (CellTiter 96 AQueous One Solution Cell Proliferation Assay, Promega, USA) was used to assess cell viability 24 hours after pulse exposure. Viable cells reduce the MTS tetrazolium compound into a soluble formazan product, the concentration of which cor-

relates with the number of metabolically active cells and is determined by absorbance measurement. According to the manufacturer's instructions, 20 μL of MTS tetrazolium compound was added to the samples, and the 96-well plate was returned to the incubator for 2 hours. The absorbance of formazan was measured with a plate reader (Tecan Infinite M200, Tecan, Austria) at 490 nm. The percentage of viable cells was calculated by subtracting the background (absorbance in wells with medium only) and normalizing the sample absorbance to the absorbance of the sham control.

Transwell invasion assay

Transwell invasion assay was performed following a previously published protocol[38], as shown in Figure 1. Transwell inserts containing membranes with 8.0-μm pores (Corning Life Sciences, #353097), pre-coated with Matrigel (Corning, #354234), were used to assess the invasive potential of the cell lines. A total of 25 μL of Matrigel solution, diluted 1:3 in DMEM supplemented with 2% FBS, was added to each insert and incubated at 37°C for 30 minutes to allow gelling. The lower chambers of 24-well plates were filled with 500 μL of DMEM10. To prevent premature polymerization, Matrigel was handled on ice using pre-cooled pipette tips throughout the procedure. For each insert, 80 000 cells (pre-treated with pulse exposure or not) were suspended in 100 μL of DMEM with 2% FBS and mixed with 50 μL of Matrigel diluted in DMEM to achieve a final Matrigel concentration of 0.5 mg/mL. After a 10-minute incubation at 37°C in a humidified 5% CO_2 atmosphere, an additional 50 μL of DMEM with 2% FBS was added to each insert, resulting in a final volume of 200 μL. The inserts were then incubated for 24 hours.

Following incubation, non-invading cells and remaining Matrigel were removed from the upper surface of the membrane using a cotton swab. The inserts were transferred to fresh wells containing 500 μL of DPBS (Gibco, #14190) and washed twice. Cells on the underside of the membrane were fixed with 4% paraformaldehyde (Sigma-Aldrich, # 158127) for 15 minutes at room temperature, followed by two DPBS washes. Membranes were then incubated in DPBS containing 1% bovine serum albumin (BSA; Sigma-Aldrich, #A2153 or Fisher BioReagents, #BP9702) and 0.1% Triton X-100 (Sigma-Aldrich, #T8787) for 30 minutes at room temperature to block non-specific binding. For proliferation assessment, Ki-67 FITC-conjugated antibody (Miltenyi Biotec, #130-117-691) was added at a 1:50 dilution in DPBS, and membranes were incubated for 1 hour at room temperature. After one PBS wash, cell nuclei were counterstained with Hoechst 33342 (Thermo Fisher Scientific, #62249) diluted 1:1000 in PBS and incubated for at least 5 minutes.

Transwell invasion and proliferation assays were performed in five GB cell lines (NIB 140 CORE, NIB216 CORE, NIB220 RIM, NIB237 CORE and NIB261 REC) and selected electroporated samples (NIB 140 CORE and NIB216 CORE) to evaluate treatment-induced changes in GB cell behaviour. Tile-scan imaging of the entire membrane undersurface with invading cells was carried out using two fluorescence microscopy systems. For characterizing baseline invasion in all five GB cell lines, cells were imaged using the EVOS FL Auto 7000 system (Thermo Fisher Scientific, USA), which employed both brightfield and fluorescence channels to visualize nuclei stained with Hoechst and proliferating cells labelled with Ki-67 under 10× objective magnification. Imaging was performed using excitation wavelengths of 395 nm for Hoechst and 475 nm for Ki-67. For characterizing invasion in electroporated cells and corresponding sham control groups, the same fluorescence channels were used to image the samples on the Leica Thunder Imaging System with DMi8 inverted epifluorescence microscope and LED8 illumination source controlled by Las X software (all from Leica Microsystems, Germany) under 10× objective magnification.

Image analysis was performed using ImageJ Fiji.[39] Nuclei were first segmented based on Hoechst staining (as presented in Figure 1), and the resulting regions of interest (ROIs) were applied to the Ki-67 channel to extract signal intensity and determine proliferation status. Quantification of invading and proliferating cells was performed across at least three independent experiments.

Statistical analysis

All results are presented as mean ± standard deviation (SD), based on a least of three independent experiments performed on separate days. Statistical analyses were conducted using SigmaPlot version 11.0 (Systat Software Inc., San Jose, CA, USA), with analyses performed separately for each cell line. Normality was assessed using the Shapiro–Wilk test, and homogeneity of variance was evaluated using Levene's test. For datasets meeting assumptions of normality and equal variance, one-way ANOVA was applied, followed by Holm–Sidak's

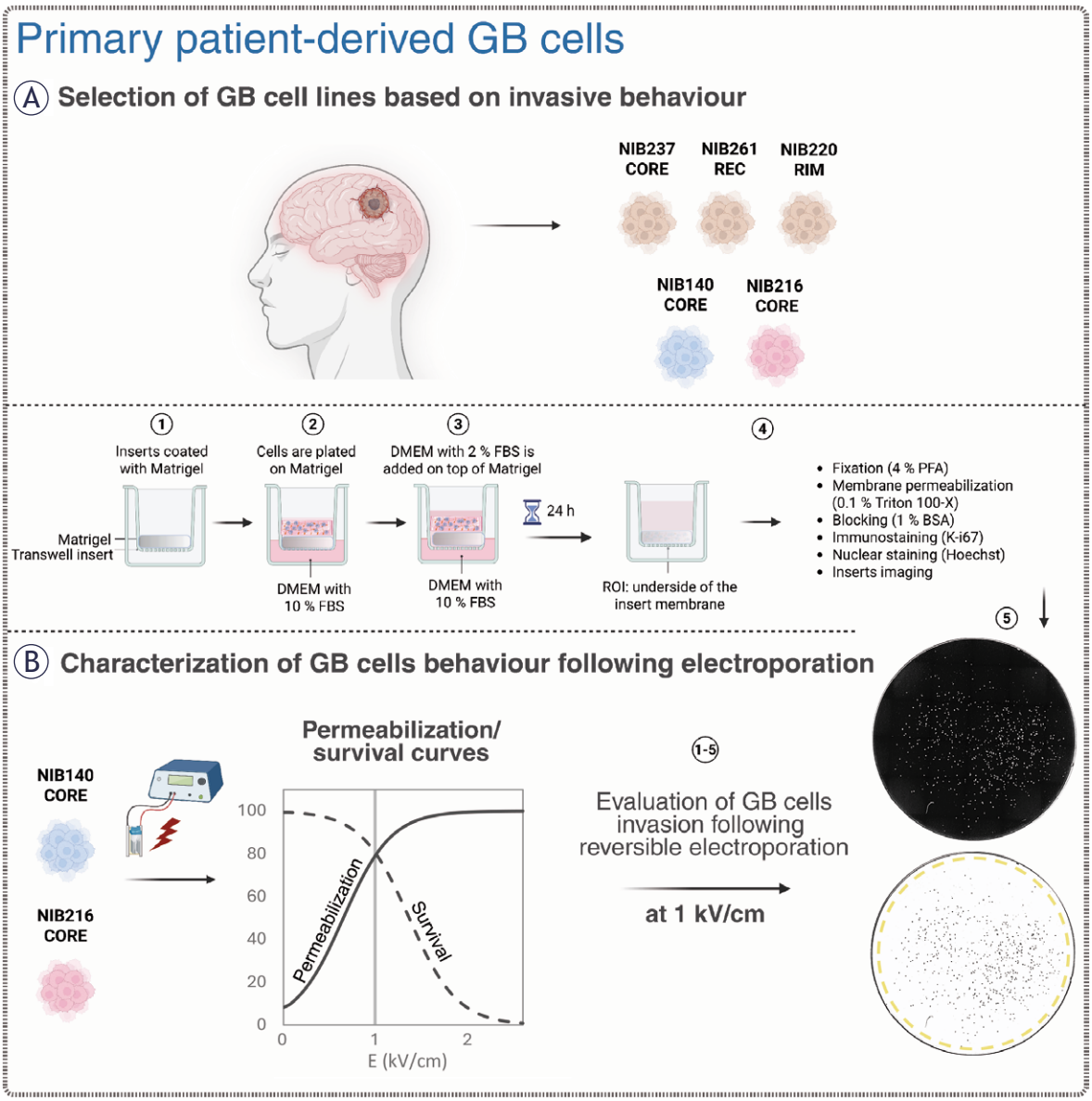

FIGURE 1. Overview of the experimental workflow for evaluating patient-derived glioblastoma (GB) cell behaviour before and after electroporation. Created with BioRender.com. **(A)** Five patient-derived glioblastoma cell lines, including cells from the tumour core (CORE), infiltrative rim (RIM), and a recurrent lesion (REC), were initially screened using a transwell invasion assay. Cells were plated on Matrigel-coated inserts and incubated for 24 hours. Invading cells migrating to the lower surface of the insert membrane were fixed, permeabilized, and stained with Hoechst (nuclei) and then immunostained for Ki-67 (a proliferation marker). The cells were subsequently imaged to quantify the number of invading and proliferating cells. **(B)** NIB140 CORE and NIB216 CORE were selected for further experiments with electroporation based on their invasive behaviour. Electric pulses of increasing electric field strength were applied to cells in electroporation cuvettes and the resulting membrane permeabilization and survival were quantified to generate characteristic response curves. Additionally, we assessed the metabolic activity of cells using MTS. Post-treatment invasion assay and fluorescence imaging was used to assess changes in invasive potential, with image analysis performed in ImageJ Fiji to quantify total and proliferating cell numbers based on nuclear segmentation and Ki-67 expression.

post hoc test for multiple comparisons. When assumptions were not met, nonparametric ANOVA on ranks was used, followed by Dunn's post hoc test. For comparisons involving two groups only, a Student's t-test was used when normality and variance assumptions were satisfied; otherwise, a Mann–Whitney U test was applied. A p-value < 0.05 was considered statistically significant.

RNA transcriptome analysis

Total RNA was extracted from GB cells (NIB140 CORE and NIB216 CORE) using the E.Z.N.A.® Total RNA Kit I (Omega Bio-Tek, Norcross, GA, USA; Cat. No. R6834). To replicate the conditions used in the Transwell invasion assay, cells were first exposed to an external electric field as described in the section above. Ten minutes following pulse exposure, 850 µL of DMEM10+ was added directly to the electroporation cuvette. The full volume was then transferred to a single well in 6-well plate, and an additional 2 mL of DMEM10 was added, bringing the total volume per well to 3 mL. Sham-treated control cells were handled identically but were not subjected to pulse exposure. The total RNA was extracted 24 hours after the pulse exposure.

Transcriptome analysis was performed by NovoGene (Munich, Germany). Total RNA was extracted from electroporated and sham control samples and subjected to quality control using the RNA Nano 6000 Assay Kit of the Bioanalyzer 2100 system (Agilent Technologies, CA, USA). mRNA was purified from total RNA using poly-T oligo-attached magnetic beads, fragmented, and reverse transcribed into cDNA. After second-strand synthesis and adaptor ligation, libraries containing 370–420 bp fragments were purified using the AMPure XP system and subsequently amplified by PCR. Following amplification, PCR products were purified again. Library quality was assessed using the Agilent Bioanalyzer 2100, and clustering was performed on a cBot Cluster Generation System using the TruSeq PE Cluster Kit v3-cBot-HS (CA, USA). The libraries were then sequenced on an Illumina NovaSeq platform, generating 150 bp paired-end reads. Raw reads were processed using fastp for adapter trimming and quality filtering. Clean reads were aligned to the reference genome using HISAT2 (v2.0.5), and transcript assembly was performed with StringTie (v1.3.3b). Gene-level read counts were generated with featureCounts (v1.5.0-p3), and gene expression was quantified as fragments per kilobase of transcript per million mapped reads (FPKM), which accounts for both transcript length and sequencing depth.

Differential gene expression analysis was performed in NovoMagic (https://eu-magic.novogene.com/) using DESeq2 (v1.20.0), based on a negative binomial model. Gene ontology (GO) enrichment analysis was conducted using the clusterProfiler R package, correcting for gene length bias. GO terms with adjusted $p < 0.05$ were considered significantly enriched. For visualization, unadjusted p-values ($p \leq 0.05$) were used in volcano plots to highlight global transcriptional changes, whereas adjusted p-values (Benjamini-Hochberg correction) were used in GO enrichment plots to account for multiple testing and reduce false discovery.

The raw RNA-seq data are publicly available in the Gene Expression Omnibus (GEO) repository under accession number GSE305017.

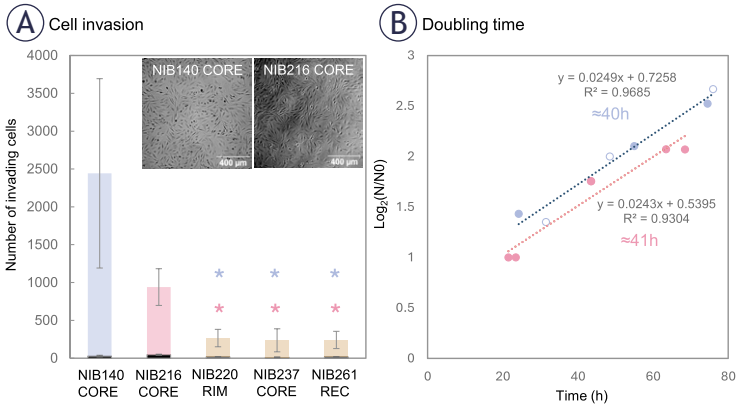

FIGURE 2. Patient-derived glioblastoma (GB) cell lines display variable intrinsic invasive potential. **(A)** Transwell invasion assay was performed with non-treated cell lines to assess the intrinsic invasive potential of five GB cell lines derived from different tumour regions. NIB140 CORE showed the highest number of invading cells, followed by NIB216 CORE, whereas NIB220 RIM, NIB237 CORE, and NIB261 REC displayed significantly lower invasion. Statistical analysis was performed using ANOVA on ranks. Significant differences are indicated with asterisks (*); $p < 0.05$. The number of Ki-67 positive (proliferating) cells, shown in black at the base of each bar, was low in all tested cell lines (< 10 %). Data are presented as mean ± SD from at least 4-5 independent experiments. **(B)** Doubling times were determined based on cell growth curves plotted as $\log_2(N/N_0)$ versus time, where N_0 is the number of seeded cells at time 0 h, and N is the number of cells at selected time points (hours). Linear regression was applied to each cell line (R^2 values shown), and doubling time was calculated from the slope of the fitted line. NIB140 CORE and NIB216 CORE showed similar doubling time (40–41 h).

Results

Selection of patient-derived GB cell lines based on their invasive properties

To characterize heterogeneity in invasive behaviour among patient-derived GB cell lines, we performed a standardized transwell invasion assay (Figure 1) using five lines representing distinct tumour regions. As shown in Figure 2, invasive potential varied markedly across the cell lines. NIB140 CORE and NIB216 CORE exhibited the highest levels of invasion, while NIB220 RIM, NIB237 CORE, and NIB261 REC displayed significantly lower invasive activity compared to NIB140 CORE and NIB216 CORE (ANOVA on ranks, $p <$

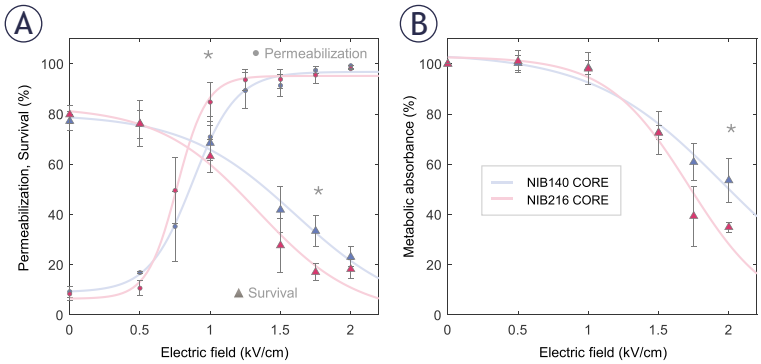

FIGURE 3. Permeabilization and survival of NIB140 CORE and NIB216 CORE glioblastoma (GB) cell lines in response to H-FIRE pulses resulting in different electric field strengths. **(A)** The percentage of permeabilized cells was assessed by propidium iodide (PI) uptake 3 minutes after pulse delivery (presented as •). The percentage of viable cells was assessed by PI assay 24 hours after pulse delivery (presented as ▲). **(B)** Cell survival was assessed by metabolic MTS assay 24 hours after pulse delivery. Data are presented as mean ± SD from at least three independent experiments. Solid lines are least-square fits to sigmoid curves. Statistically significant differences ($p < 0.05$) between cell lines at specific electric field strengths were tested using Student's t-test and are indicated by asterisks (*). Data for NIB140 CORE and NIB216 CORE are shown in blue and pink, respectively.

0.05). Based on their invasion profiles, NIB140 CORE and NIB216 CORE were selected for subsequent experiments to investigate electroporation responses across the two GB subtypes representing the highest levels of invasion. After 24 hours, the expression of the proliferation marker Ki-67 was low in all tested cell lines (< 10%), confirming that the observed invasion was not driven by cell proliferation, as shown in Figure 2A. The number of proliferating cells is represented at the base of each bar, illustrating that proliferation does not account for the observed invasive behaviour.

To further confirm that the observed invasion was not driven by proliferation, we measured the doubling time of each cell line. NIB140 CORE and NIB216 CORE displayed doubling times of ~40 and ~41 hours, respectively. Representative growth curves used for this estimation are shown in Figure 2B, illustrating that the 24-hour post-treatment time point falls well before either population is expected to divide. This supports the interpretation that the observed behaviour reflects actual invasion properties rather than proliferative expansion.

Permeabilization and survival at different electric field strengths

We next investigated how the selected NIB140 CORE and NIB216 CORE cell lines respond to pulses of increasing electric field intensities. Membrane permeabilization was assessed 3 minutes after electroporation using propidium iodide (PI) staining, while cell survival was evaluated 24 hours post-treatment using both PI staining and the metabolic MTS assay. Both NIB140 CORE and NIB216 CORE exhibited a characteristic sigmoidal increase in the percentage of permeabilized cells with increasing electric field strength, reaching maximal values above 1.25 kV/cm (Figure 3A). Survival determined by PI assay declined above 1 kV/cm (Figure 3A). These results align with previous H-FIRE studies demonstrating that glioma cells can recover metabolic activity and proliferative capacity when exposed to sublethal electric fields, whereas higher intensities induce irreversible membrane damage.[34]

NIB216 CORE displayed somewhat greater permeabilization at intermediate electric field strength and a more pronounced decrease in viability at higher field strengths compared to NIB140 CORE, indicating greater sensitivity to electroporation-induced stress. This was further supported by MTS assay results (Figure 3B), which showed a greater reduction in metabolic activity in NIB216 CORE. Statistically significant differences (Student's t-test) between the two cell lines were observed at 1 kV/cm for membrane permeabilization ($p=0.037$), 1.75 kV/cm for survival ($p=0.001$), and 2 kV/cm for metabolic activity ($p=0.024$), with significant differences indicated by asterisks (Figure 3). Nevertheless, the differences between the tested cell lines were relatively small, suggesting that similar electric field strengths can be used to treat different GB cell lines.

Reversible electroporation enhances invasion of GB cells in a cell type-dependent manner

Based on permeabilization and survival curves (Figure 3), we chose an electric field strength of 1.0 kV/cm to further assess whether sublethal electroporation alters GB cell invasion. At this electric field strength, both NIB140 CORE and NIB216 CORE cell lines reached > 80% permeabilization while maintaining viability above 80% relative to sham-treated control (0 kV/cm). The chosen electric field strength mimics the conditions in reversibly electroporated border zone surrounding the ablated area, when using IRE for tumour treatment. Also, these conditions of reversible electroporation are in line with clinically relevant protocols used for ECT.[40]

Electroporation enhanced the invasion potential of GB cells in a cell type-dependent manner, as quantified 24 hours following exposure to 1.0 kV/cm. Since the number of invading cells varied from day to day, already in control samples, we present results for each of the three biological replicates separately, with 2–3 technical replicates (transwell inserts) per one biological replicate. In NIB140 CORE, the number of invading cells was consistently and significantly higher in electroporated samples compared to sham-treated controls across all three biological replicates (Figure 4A; Student's t-test, $p < 0.05$; 2–3 technical replicates per one biological replicate). In contrast, NIB216 CORE showed a more variable response, with significance reached in one biological replicate only (Figure 4B), indicating a modest and less consistent effect. We then averaged the technical replicates and normalized this averaged number of invading cells in electroporated samples to the corresponding number in sham-treated controls for each biological replicate. The obtained fold-increase in invading cells across biological replicates is presented in the box plot in Figure 4C. This analysis confirmed a consistent increase in invasion in NIB140 CORE and only modest trend in NIB216 CORE. Notably, NIB140 CORE exhibited a significantly greater 3.74-fold increase compared to just 1.30-fold in NIB216 CORE (Student's t-test, $p < 0.05$), potentially reflecting intrinsic differences in these cell lines.

Enhanced cell invasion following sublethal electroporation was further supported by analysis of the proliferation marker Ki-67. The proportion of Ki-67–positive cells remained below 10% across all conditions (Figure 4D), with no significant differences between electroporated and sham-treated controls (Student's t-test). These findings reinforce the conclusion that proliferation did not contribute considerably to the increased number of invading cells following electroporation. An example of this electroporation-induced increase in invasion potential in NIB140 CORE cell line is illustrated in Figure 4E, where representative images demonstrate a higher number of invading cells after electroporation at 1 kV/cm.

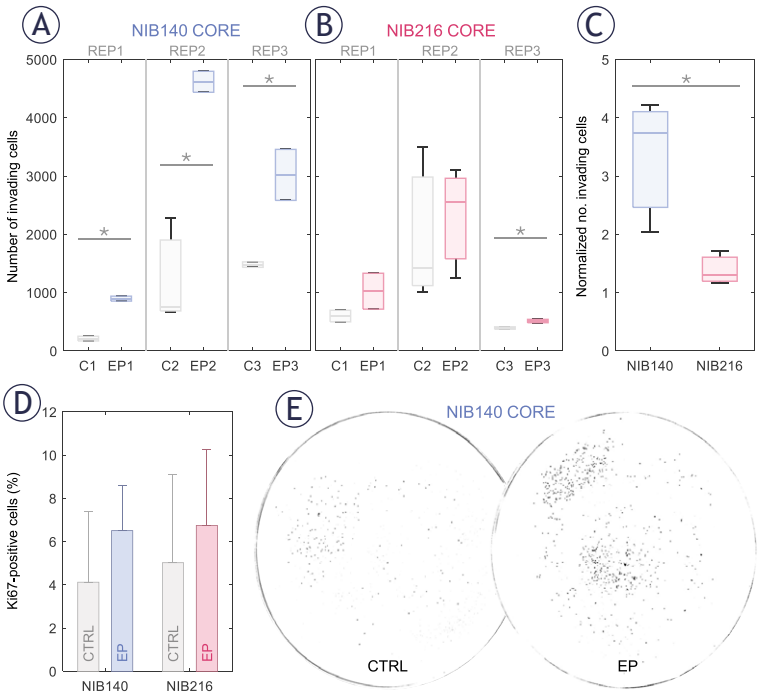

FIGURE 4. Electroporation enhances the invasion potential of patient-derived glioblastoma (GB) cell lines in a cell type-dependent manner. Invasion was assessed 24 hours after electroporation using H-FIRE pulses resulting in electric field strength of 1 kV/cm. **(A-B)** Box-and-whisker plots showing the number of invading cells in NIB140 CORE **(A)** and NIB216 CORE **(B)** in sham-treated (grey) and electroporated samples (blue or pink). Each group represents a separate biological replicate (REP1–REP3), with 2–3 technical replicates per biological replicate. The horizontal line within each box represents the median, and whiskers indicate the full range of values. **(C)** Relative increase in the number of invading cells in electroporated samples compared to sham controls. Data are presented as mean ± SD from three biological replicates. **(D)** Percentage of Ki-67–positive (proliferating) cells in sham-treated and electroporated samples. Values remained below 10 % across all conditions, demonstrating that the observed increase in invasion was not due to increased proliferation. **(E)** Representative masks obtained after thresholding images of Hoechst-stained NIB140 CORE invading cells, showing increased invasion following electroporation.

RNA transcriptome analysis corroborates enhanced invasion of reversibly electroporated GB cells

To gain insight into the molecular changes associated with electroporation, we performed RNA sequencing on NIB140 CORE and NIB216 CORE cells harvested 24 hours after exposure to 1.0 kV/cm. Gene expression level analysis in electroporated (EP) and sham-treated (CTRL) samples, presented through co-expression Venn diagrams (Figure 5A), revealed 222 and 239 genes that were uniquely expressed in the electroporated NIB140 CORE and NIB216 CORE samples, respectively. Differential gene expression analysis, presented through volcano plots (Figure 5B) further confirmed electroporation-induced transcriptomic changes in the two cell lines, with both significantly downregulated and upregulated genes.

Additionally, comparison between the sham-treated NIB140 CORE and NIB216 CORE revealed that these cell lines considerably differ in their baseline transcriptomic profiles. Co-expression

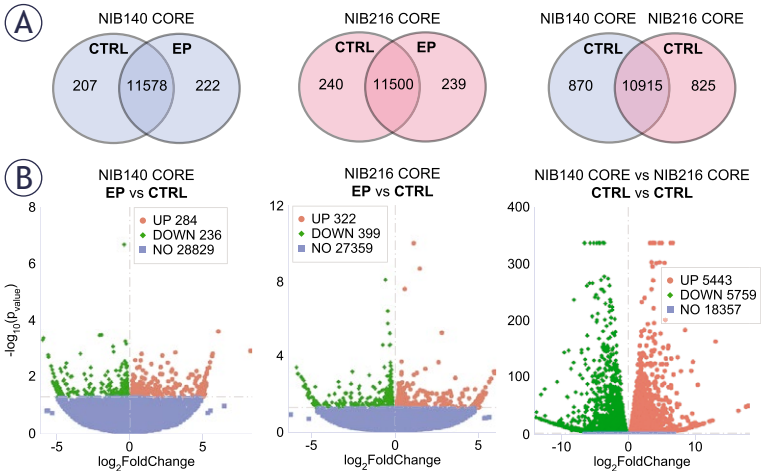

FIGURE 5. Transcriptomic differences between electroporated and sham-treated NIB140 CORE and NIB216 CORE cell lines. RNA transcriptome analysis was performed in cells harvested 24 hours after electroporation. **(A)** The gene expression levels analysis is presented through co-expression Venn diagrams showing the overlap in expressed genes between sham-treated (CTRL, 0 V) and electroporated (EP, 1 kV/cm) samples of each cell line, and between sham-treated NIB140 CORE and NIB216 CORE. **(B)** The differential gene expression analysis is presented through volcano plots. Red and green points represent significantly upregulated and downregulated genes, respectively ($p < 0.05$), while blue points indicate non-significant changes. Genes were classified as differentially expressed, if they met the threshold of $|\log_2 FoldChange| > 0.0$.

Venn diagram (Figure 5A) showed 10,915 genes co-expressed in both cell lines, with 870 and 825 genes uniquely expressed in NIB140 CORE and NIB216 CORE, respectively. Volcano plot (Figure 5B) further confirmed the large transcriptomic divergence between the two cell lines. This divergence indicates that the intrinsic transcriptomic differences between NIB140 CORE and NIB216 CORE exceed the shifts induced by electroporation, which may explain the different extents to which electroporation changed the invasion of these two cells lines (Figure 4).

To better understand the biological relevance of the observed transcriptomic changes, we performed gene ontology (GO) enrichment analysis on significantly upregulated and downregulated genes in NIB140 CORE and NIB216 CORE cells following electroporation (Figure 6). In NIB140 CORE, differentially expressed genes were enriched in invasion-associated pathways, including channel activity and extracellular matrix organization (Figure 6A), which aligned with the observed increase in invasion (Figures 4A, C). In contrast, the transcriptional response in NIB216 CORE lacked strong enrichment of motility-related pathways, consistent with the modest increase in invasion (Figures 4B, C). However, several downregulated categories in NIB216 CORE—including actin filament binding, actin cytoskeleton, extracellular matrix, and focal adhesion—suggest cytoskeletal remodelling and/or disruption. In addition, genes associated with leading-edge membrane, cell projection membrane, and synaptic membrane were upregulated. These differences underscore the intertumoral variability in molecular responses to electroporation and support a potential mechanistic link between transcriptomic changes and the significantly enhanced invasion observed in the NIB140 CORE cell line, which would, however, need to be further supported at the functional level.

Discussion

Our study investigated how sublethal exposure to electroporation pulses affects the invasion of GB tumour cells. After initial screening of five patient-derived GB cells lines for their intrinsic invasive potential, we selected the two most invasive cell lines (NIB140 CORE and NIB216 CORE) for further electroporation experiments. We characterized cell permeabilization and survival after exposure to H-FIRE pulses resulting in different electric field strengths and found that 1 kV/cm corresponds to conditions of reversible electroporation in both cell lines. At 1 kV/cm, the majority of cells became permeabilized due to electroporation while still retaining their viability 24 hours later. We then assessed changes in their invasion behaviour 24 hours after electroporation. Electroporation enhanced invasion in a cell line–dependent manner: NIB140 CORE consistently showed a pronounced response with a median 3.74-fold higher number of invading cells compared to sham-treated controls. While the number of invading cells was consistently higher in electroporated samples, we observed a rather high variability across biological replicates. This variability can be explained by the use of patient-derived cells, which are expected to respond more heterogeneously than established cell lines that often fail to replicate key tumour characteristics.[28,33,41] Unlike in NIB140 CORE, electroporation induced only a modest increase in the number of invading cells in NIB216 CORE (1.30-fold). Moreover, NGS-based profiling included in the clinical pathology report identified the *EGFRvIII* variant in NIB140 CORE cell line (but not in NIB216 CORE), a mutation known to enhance invasion and contribute to treatment resistance in GB.[42]

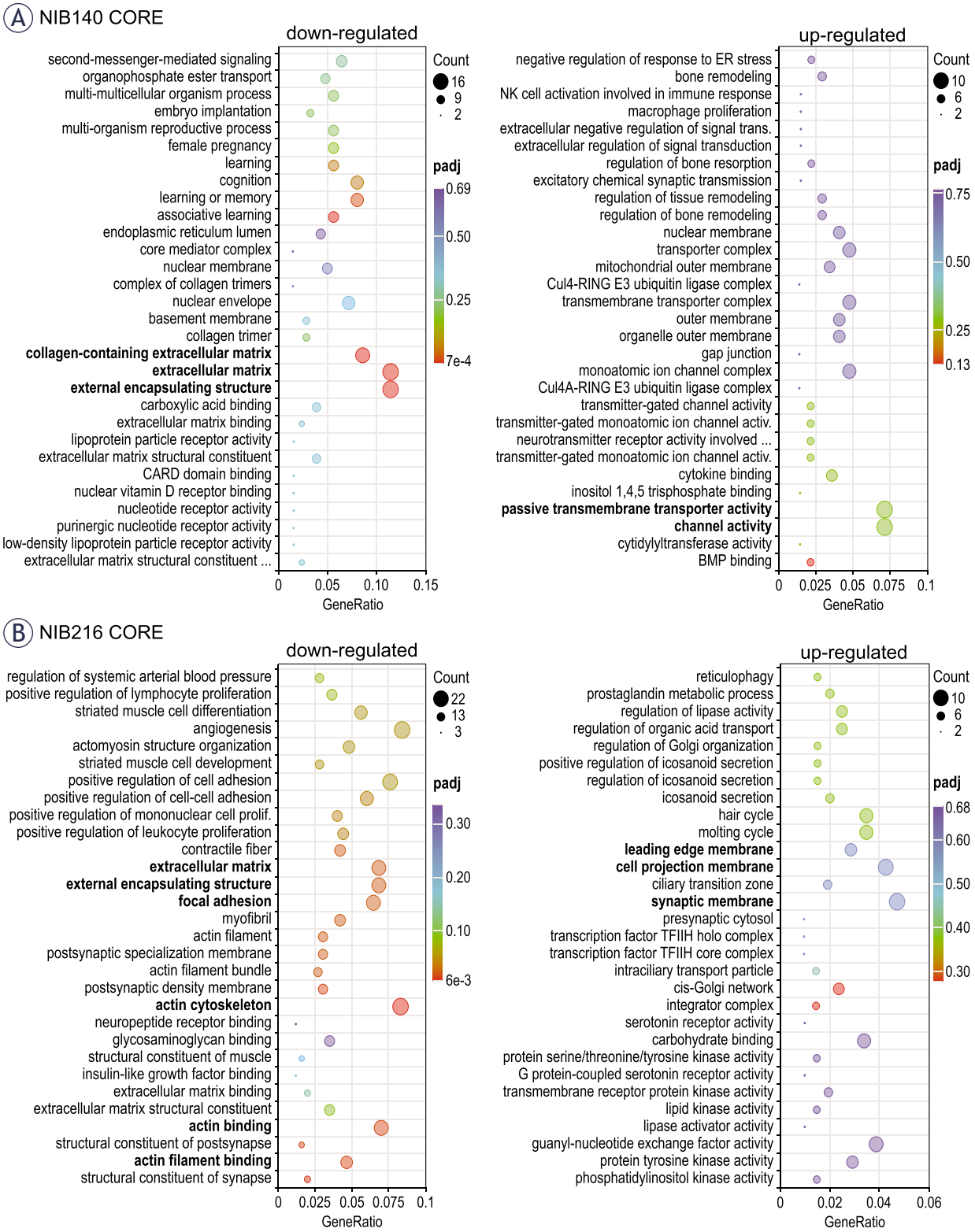

FIGURE 6. Functional enrichment analysis of differentially expressed genes following electroporation. **(A)** Gene ontology (GO) enrichment analysis of significantly upregulated (right) and downregulated (left) genes in NIB140 CORE cells 24 hours after electroporation. **(B)** GO enrichment analysis for NIB216 CORE. Dot size reflects the number of genes contributing to each GO term, while colour intensity indicates statistical significance (adjusted p-value, padj). The GeneRatio represents the proportion of differentially expressed genes associated with each GO term relative to the total number of input genes. Selected invasion-relevant categories are highlighted in bold. GO terms include biological processes, molecular functions, and cellular components.

To better understand the molecular basis of increased invasion after electroporation and the associated differences between the two tested cell lines, we performed transcriptomic analysis. In NIB140 CORE cells, we observed upregulation of genes associated with the channel activity and passive transmembrane transport activity – *CHRNE*, *KCNMA1*, *KCNAB1*, *TRPC4*, *GJC3*, *GPR89A*, *TTYH2*, *GRIN2A*, *RHCE*, and *GLRA3*.[43] Notably, ion channel–related genes such as *KCNMA1* and *KCNAB1*, i.e. the alpha and beta subunits of the big potassium K_{Ca} channel, were detected, supporting their potential role in enhanced invasive behaviour in GB observed in previous studies.[29,32] Genes related to extracellular matrix (ECM) organization (collagen containing ECM, ECM and external encapsulating structure) were downregulated (*COL14A1*, *EFEMP1*, *ITGB4*, *COL8A1*, *P3H2*, *THBS2*, *INHBE*, *MATN4*, *PTPRZ1*, *MMP9*, *ANGPTL5* and *COL5A2)* indicating ECM remodelling.[44,45] In this context, it is notable that MMP9, a metalloproteinase classically associated with invasion, was downregulated in NIB140 CORE. This may appear counterintuitive given the observed increase in invasion, but it is consistent with reports that GB cells can compensate protease activity by other protease families or proteases of the same family, adopt protease-independent, ion channel- and adhesion-driven or even adhesion-independent migration strategies.[46] Thus, while MMP9 itself was not upregulated, ECM- and ion channel–related pathways were altered, supporting the idea that alternative mechanisms may drive invasion in this context.[46] In contrast, NIB216 CORE showed downregulation of genes involved in cytoskeleton remodelling and focal adhesion (*COL11A1*, *CNN1*, *ALPL*, *HAPLN1*, *TGFB1I1*, *F3*, *IGFBP7*, *ADAM19*, *COL4A1*, *POSTN*, *LOXL4*, *MXRA7*, *CCN2*, *LGALS1*, *COL4A2*, *GPC4*, *TFPI2*, *CD248*, *VASP*, *TAGLN*, *TPM2*, *PDLIM7*, *PPP1R18*, *ARPC4*, *CORO1A*, *ACTN1*, *FHDC1*, *PICK1*, *SPTBN2*, *ADSS1*, *MYOZ1*, *TMEM201*, *MARCKSL1* and *MYH9*) suggesting cytoskeletal disruption.[47] Meanwhile, upregulated response was linked to membrane dynamics – leading edge membrane, cell projection membrane and synaptic membrane (*ANK1*, *DPP4*, *LAMP5*, *EGFR*, *C2CD5* and *PSD3*) indicating changes in membrane plasticity and intracellular communication.[48] It should be noted that, based on our data, we cannot determine whether the observed effects arise directly from pulse-induced biophysical changes or indirectly through stress-mediated signalling. Furthermore, this data should be interpreted with caution, as validation at the protein level (e.g., Western blot or ELISA) will be required to confirm whether the observed gene expression changes translate into functional effects.

A recent study by Wang *et al*.[49] reported that electroporation suppresses invasion of U-87 MG GB cells. Similar to our study, cells in suspension were electroporated and changes in invasion were assessed 24 hours later using a transwell invasion assay. The pulse parameters used for electroporation was somewhat different from ours and consisted of 4–8 bursts of 50 biphasic 2 μs pulses with 0.2 μs interphase and 100 μs interpulse delay, 15 Hz burst repetition frequency, and 4 kV/cm electric field strength. With 6 and 8 bursts, cell survival dropped to ~73% and 42%, respectively, and this decrease in the number of viable cells was expectedly reflected in lower number of invading cells. Nevertheless, the number of invading cells decreased to ~56% of control also with 4 bursts, where ~90% cells survived the treatment. Decreased invasion was associated with downregulation of *SIRT1* gene and *SIRT2* genes and impaired mitochondrial function. In contrast, we observed increased invasion and no significant changes in any of *SIRT1–7* genes (p=0.1; Benjamini-Hochberg correction) in our study. Furthermore, we observed a trend of increased invasion even at higher electric field strength of 2 kV/cm, after compensating for the reduced number of surviving cells, although this increase in invasion was not statistically significantly different from control, results presented in Supplementary Figure S3. The different results obtained by us compared to Wang *et al*.[49] could stem from multiple reasons. Aside from differences in pulse parameters and sample temperature during electroporation, we used patient-derived GB cells lines. As shown by our transcriptomic analysis, different GB cells lines have considerably different gene expression profiles, which affects their response to electroporation. This highlights the value of patient-derived models in capturing clinically relevant transcriptional responses and treatment dynamics compared to immortalized cell lines. The importance of using patient-derived cells to better capture the biological complexity and treatment responses of GB is further illustrated by comparing our results to the study by Casciati *et al*.[50] In this study, adherent U-87 MG cells were exposed to five electric pulses, each lasting 40 μs at 1 Hz and 30 kV/cm (0.3 MV/m). While they also cultured neurospheres under serum-free conditions to enrich for GB stem-like cells, these were still derived from the U-87 MG line, which lacks key features of primary tumours,

including heterogeneity and true invasive behaviour.[51] Notably, Casciati *et al*. reported that pulse exposure substantially influenced the fate of GB neurospheres by differentially regulating genes involved in hypoxia, inflammation, and p53/cell cycle checkpoints, ultimately reducing their capacity for neurosphere formation and transmigration *in vitro*. Furthermore, pulse exposure also reduced the ability to form new neurospheres and inhibited invasion. Importantly, exclusively in U-87 neurospheres, pulse exposure altered the expression of stemness- and differentiation-related genes. While these findings are promising, the observed inconsistency with our results—despite differences in pulse parameters—might reflect cell model-specific differences in electroporation responses. This highlights the need to validate such effects in more physiologically relevant models. Given the aggressive, therapy-resistant nature of GB stem-like cells and their contribution to tumour progression and recurrence[52,53], future electroporation studies should consider the use of patient-derived stem-like populations to more accurately reflect clinically relevant outcomes.

While most preclinical studies of electroporation-based brain tumour therapy have focused on IRE as a non-thermal ablation method, particularly in canine glioma models[11,12,14,17,54], our findings highlight the less-explored effects on tumour cells located in the periphery of IRE-treated zones. This raises an important consideration regarding unintended effects in tumour margins that remain viable after treatment—regions likely exposed to sublethal electric fields due to the highly infiltrative nature of GB. Our results demonstrate that tumour cells surviving electroporation may acquire enhanced invasive potential, a concern that arises specifically when no cytotoxic agents are present. However, a similar concern applies to ECT if insufficient local drug concentrations are achieved, since permeabilized cells might survive the treatment. When adequate concentrations are ensured, ECT directly addresses this risk by eliminating reversibly permeabilized cells through enhanced intracellular accumulation of cytotoxic agents, such as bleomycin and cisplatin.[18,19] Bleomycin induces DNA strand breaks, while cisplatin causes DNA crosslinking and apoptosis—mechanisms that require cytosolic access and are otherwise ineffective across intact membranes.[55–56] Since the primary effect of electroporation is to increase membrane permeability, it provides a unique opportunity to deliver these otherwise impermeable drugs efficiently. In addition, electroporation has been shown in *in vivo* models to transiently disrupt the blood–brain barrier, further highlighting its potential for enhancing drug delivery to tumour tissue within the central nervous system.[35,57,58] Moreover, studies in melanoma cells showed that ECT does not affect the cells' metastatic potential.[59,60] Taken together, our findings suggest that ECT, by combining reversible electroporation with sufficient concentrations of cytotoxic agents, may offer a more effective and safer therapeutic strategy for glioblastoma than IRE as a standalone treatment. Furthermore, this approach may help overcome some limitations of current chemotherapy regimens, such as temozolomide, which has been shown to expand the GB stem cell population through conversion of differentiated tumour cells both *in vitro* and *in vivo*.[61]

While our results offer new insights into GB cell responses to electroporation, this study has several limitations. First, the use of suspension cultures does not fully recapitulate the structural complexity, cell–cell interactions, and diffusion gradients present *in vivo*. These factors may influence electroporation-induced processes such as membrane repair, intracellular signalling, and invasion. Although patient-derived GB cells were used, future studies should also examine cells from spatially distinct tumour regions (e.g., core vs. rim), which may exhibit different responses due to intratumoral heterogeneity. In addition, GB stem-like cells, known for their high invasion potential and therapy resistance[52,63], were not specifically addressed here and represent a critical subpopulation for further investigation. To better approximate the tumour microenvironment, future experiments should employ advanced *in vitro* models such as multicellular spheroids or organoids, which incorporate three-dimensional architecture and preserve key features of GB biology, including heterogeneity, invasion, and treatment resistance. Arroyo *et al*.[63] have recently advanced this field by developing a multicellular spheroid–hydrogel platform, demonstrating that higher electric field strengths and longer pulse widths constrained migration and proliferation over several days, underscoring the importance of 3D models for validating electroporation responses. Finally, this study focused on short-term transcriptional and behavioural changes, with analysis limited to the 24-hours timepoint following electroporation. Long-term effects were not addressed here and remain to be explored, particularly in the context of combination therapies. Experiments were performed at 33°C to build on prior findings of ion

channel activation in GB cells[30], while also minimizing the risk of thermal damage. Future studies could further examine temperature dependence alongside 3D models to better approximate physiological conditions. Moreover, future work should investigate how electroporation interacts with established treatments, including radiation and chemotherapeutic agents such as temozolomide, cisplatin, or bleomycin, to better understand the impact on cell viability and invasion.

Overall, our findings suggest that sublethal electroporation can enhance GB cell invasion potential in a cell line-dependent manner. A more pronounced and consistent effect was observed in NIB140 CORE cells (3.74-fold increase), while NIB216 CORE showed only a modest increase (1.30-fold) in the number of invading cells following reversible electroporation. While our findings suggest that combining reversible electroporation with sufficient concentrations of cytotoxic agents (ECT) may offer advantages over IRE alone, this requires further validation in more physiologically relevant models.

Acknowledgments

This research was supported by Slovenian Research and Innovation Agency (ARIS) through research programmes P2-0249 and P1-0245, infrastructure programme I0-0022, and funding for Young Researchers. This work was supported by the Slovenian Research and Innovation Agency through research projects J3-4504, N3-0394 and NC-25002 and NIB Development pillar funds RSF projects 842/2024 and 946/2025. The research was also supported by the European Union and ARIS through NextGenerationEU and NOO funding within project MN-0023 and European Union's Horizon project Twinning for excellence to strategically advance research in carcinogenesis and cancer (CutCancer; 101079113).

Use of AI-assisted technologies in the writing process

During the preparation of this paper, the authors used Claude (Anthropic, CA, USA) and ChatGPT (OpenAI, CA, USA) to improve the style and readability in some parts of the text. After using this tool/service, the authors have reviewed and edited the content as required and take full responsibility for the content of the publication.

References

1. Kotnik T, Rems L, Tarek M, Miklavčič D. Membrane electroporation and electropermeabilization: mechanisms and models. *Annu Rev Biophys* 2019; **48:** 63-91. doi: 10.1146/annurev-biophys-052118-115451
2. Aycock KN, Davalos RV. Irreversible electroporation: background, theory, and review of recent developments in clinical oncology. *Bioelectr* 2019; **1:** 214-234. doi: 10.1089/bioe.2019.0029
3. Jacobs EJ, Rubinsky B, Davalos RV. Pulsed field ablation in medicine: irreversible electroporation and electropermeabilization theory and applications. *Radiol Oncol* 2025; 59(4): 535-550.; **59:** 1-22. doi: 10.2478/raon-2025-0011
4. Mir LM, Gehl J, Serša G, Collins CG, Garbay JR, Billard V, et al. Standard operating procedures of the electrochemotherapy: instructions for the use of bleomycin or cisplatin administered either systemically or locally and electric pulses delivered by the CliniporatorTM by means of invasive or non-invasive electrodes. *EJC Suppl* 2006; **4:** 14-25. doi: 10.1016/j.ejcsup.2006.08.003
5. Miklavčič D, Mali B, Kos B, Heller R, Serša G. Electrochemotherapy: from the drawing board into medical practice. *BioMed Eng Online* 2014; **13:** 29. doi: 10.1186/1475-925X-13-29
6. Grochans S, Cybulska AM, Siminska D, Korbecki J, Kojder K, Chlubek D, et al. Epidemiology of glioblastoma multiforme-literature review. *Cancers* 2022; **14:** 2412. doi: 10.3390/cancers14102412
7. Ostrom QT, Price M, Neff C, Cioffi G, Waite KA, Kruchko C, et al. CBTRUS statistical report: primary brain and other central nervous system tumors diagnosed in the United States in 2015-2019. *Neuro Oncol* 2022; **24(Suppl 5):** v1-95. doi: 10.1093/neuonc/noac202
8. Obrador E, Moreno-Murciano P, Oriol-Caballo M, Lopez-Blanch R, Pineda B, Gutierrez-Arroyo JL, et al. Glioblastoma therapy: past, present and future. *Int J Mol Sci* 2024; **25:** 2529. doi: 10.3390/ijms25052529
9. Liu Y, Zhou F, Ali H, Lathia JD, Chen P. Immunotherapy for glioblastoma: current state, challenges, and future perspectives. *Cell Mol Immunol* 2024; **21:** 1354-75. doi: 10.1038/s41423-024-01226-x
10. Pichol-Thievend C, Anezo O, Pettiwala AM, Bourmeau G, Montagne R, Lyne AM, et al. VC-resist glioblastoma cell state: vessel co-option as a key driver of chemoradiation resistance. *Nat Commun* 2024; **15:** 3602. doi: 10.1038/s41467-024-47985-z
11. Garcia P, Rossmeisl JH, Neal R, Ellis TL, Olson JD, Henao-Guerrero N, et al. Intracranial nonthermal irreversible electroporation: in vivo analysis. *J Membr Biol* 2010; **236:** 127-36. doi: 10.1007/s00232-010-9284-z
12. Ellis TL, Garcia PA, Rossmeisl JH, Henao-Guerrero N, Robertson J, Davalos RV. Nonthermal irreversible electroporation for intracranial surgical applications. *J Neurosurg* 2011; **114:** 681-8. doi: 10.3171/2010.5.JNS091448
13. Rossmeisl JH, Garcia PA, Roberston JL, Ellis TL, Davalos RV. Pathology of nonthermal irreversible electroporation (N-TIRE)-induced ablation of the canine brain. *J Vet Sci* 2013; **14:** 433-40. doi: 10.4142/jvs.2013.14.4.433
14. Rossmeisl JH, Garcia PA, Pancotto TE, et al. Safety and feasibility of the NanoKnife system for irreversible electroporation ablative treatment of canine spontaneous intracranial gliomas. *J Neurosurg* 2015; **123:** 1008-25. doi: 10.3171/2014.12.JNS141768
15. Garcia PA, Kos B, Rossmeisl JH, Pavliha D, Miklavčič D, Davalos RV. Predictive therapeutic planning for irreversible electroporation treatment of spontaneous malignant glioma. *Med Phys* 2017; **44:** 4968-80. doi: 10.1002/mp.12401
16. Arena CB, Sano MB, Rossmeisl JH, Caldwell JL, Garcia PA, Rylander MN, et al. High-frequency irreversible electroporation (H-FIRE) for non-thermal ablation without muscle contraction. *Biomed Eng Online* 2011; **10:** 102. doi: 10.1186/1475-925X-10-102
17. Latouche EL, Arena CB, Ivey JW, Garcia PA, Pancotto TE, Pavlisko N, et al. High-frequency irreversible electroporation for intracranial meningioma: a feasibility study in a spontaneous canine tumor model. *Technol Cancer Res Treat* 2018; **17:** 1533033818785285. doi: 10.1177/1533033818785285
18. Salford LG, Persson BR, Brun A, Ceberg CP, Kongstad PC, Mir LM. A new brain tumour therapy combining bleomycin with in vivo electropermeabilization. *Biochem Biophys Res Commun* 1993; **194:** 938-43. doi: 10.1006/bbrc.1993.1911

19. Agerholm-Larsen B, Iversen HK, Ibsen P, Moller JM, Mahmood F, Jensen KS, et al. Preclinical validation of electrochemotherapy as an effective treatment for brain tumors. *Cancer Res* 2011; **71:** 3753-62. doi: 10.1158/0008-5472.CAN-11-0451

20. Sharabi S, Guez D, Daniels D, Cooper I, Atrakchi D, Liraz-Zaltsman S, et al. The application of point source electroporation and chemotherapy for the treatment of glioma: a randomized controlled rat study. *Sci Rep* 2020; **10:** 2178. doi: 10.1038/s41598-020-59152-7

21. Linnert M, Iversen HK, Gehl J. Multiple brain metastases – current management and perspectives for treatment with electrochemotherapy. *Radiol Oncol* 2012; **46:** 271-8. doi: 10.2478/v10019-012-0042-y

22. Jacobs Iv EJ, Campelo SN, Charlton A, Altreuter S, Davalos RV. Characterizing reversible, irreversible, and calcium electroporation to generate a burst-dependent dynamic conductivity curve. *Bioelectrochemistry* 2024; **155:** 108580. doi: 10.1016/j.bioelechem.2023.108580

23. Nakagawa H, Farshchi-Heydari S, Maffre J, Sharma T, Govari A, Beeckler C, et al. Evaluation of ablation parameters to predict irreversible lesion size during pulsed field ablation. *Circ Arrhythm Electrophysiol* 2024; **17:** e012814. doi: 10.1161/CIRCEP.124.012814

24. Miklavčič D, Šemrov D, Mekid H, Mir LM. A validated model of in vivo electric field distribution in tissues for electrochemotherapy and for DNA electrotransfer for gene therapy. *Biochim Biophys Acta Gen Subj* 2000; **1523:** 73-83. doi: 10.1016/S0304-4165(00)00101-X

25. Amin SB, Anderson KJ, Boudreau CE, Martinez-Ledesma E, Kocakavuk E, Johnson KC, et al. Comparative molecular life history of spontaneous canine and human gliomas. *Cancer Cell* 2020; **37:** 243-57.e7. doi: 10.1016/j.ccell.2020.01.004

26. Sahu U, Barth RF, Otani Y, McCormack R, Kaur B. Rat and mouse brain tumor models for experimental neuro-oncology research. *J Neuropathol Exp Neurol* 2022; **81:** 312-29. doi: 10.1093/jnen/nlac021

27. Chow L, Wheat W, Ramirez D, Impastato R, Dow S. Direct comparison of canine and human immune responses using transcriptomic and functional analyses. *Sci Rep* 2024; **14:** 2207. doi: 10.1038/s41598-023-50340-9

28. Xie Y, Bergström T, Jiang Y, Johnson P, Marinescu VD, Lindberg N, et al. The human glioblastoma cell culture resource: validated cell models representing all molecular subtypes. *EBioMedicine* 2015; **2:** 1351-1363 doi: 10.1016/j.ebiom.2015.08.026

29. Steinle M, Palme D, Misovic M, Rudner J, Dittmann K, Lukowski R, et al. Ionizing radiation induces migration of glioblastoma cells by activating BK K(+) channels. *Radiother Oncol* 2011; **101**: 122-126. doi: 10.1016/j.radonc.2011.05.069

30. Blažič A, Guinard M, Leskovar T, O'Connor RP, Rems L. Long-term changes in transmembrane voltage after electroporation are governed by the interplay between nonselective leak current and ion channel activation. *Bioelectrochemistry* 2025; **161:** 108802. doi: 10.1016/j.bioelechem.2024.108802

31. Younes S, Mourad N, Salla M, Rahal M, Hammoudi Halat D. Potassium ion channels in glioma: from basic knowledge into therapeutic applications. *Membranes* 2023; **13:** 434. doi: 10.3390/membranes13040434

32. D'Alessandro G, Monaco L, Catacuzzeno L, Antonangeli F, Santoro A, Esposito V, et al. Radiation increases functional KCa3.1 expression and invasiveness in glioblastoma. *Cancers* 2019; **11:** 279. doi: 10.3390/cancers11030279

33. Novak M, Majc B, Malavolta M, Porčnik A, Mlakar J, Hren M, et al. The Slovenian translational platform GlioBank for brain tumor research: identification of molecular signatures of glioblastoma progression. *Neurooncol Adv* 2025; **7:** vdaf015. doi: 10.1093/noajnl/vdaf015

34. Murphy KR, Aycock KN, Hay AN, Rossmeisl JH, Davalos RV, Dervisis NG. High-frequency irreversible electroporation brain tumor ablation: exploring the dynamics of cell death and recovery. *Bioelectrochemistry* 2022; **144:** 108001. doi: 10.1016/j.bioelechem.2021.108001

35. Partridge BR, Kani Y, Lorenzo MF, Campelo SN, Allen IC, Hinckley J, et al. High-frequency irreversible electroporation (H-FIRE) induced blood-brain barrier disruption is mediated by cytoskeletal remodeling and changes in tight junction protein regulation. *Biomedicines* 2022; **10:** 1384. doi: 10.3390/biomedicines10061384

36. Batista Napotnik T, Miklavčič D. In vitro electroporation detection methods – An overview. *Bioelectrochemistry* 2018; **120:** 166-182. doi: 10.1016/j.bioelechem.2017.12.005

37. Blažič A, Šmerc R, Polajžer T, Miklavčič D, Rems L. Reassessing lidocaine as an electroporation sensitizer in vitro. *Sci Rep* 2025; **15:** 25593. doi: 10.1038/s41598-025-11695-3

38. Hira VV, Breznik B, Van Noorden CJ, Lah T, Molenaar RJ. 2D and 3D in vitro assays to quantify the invasive behavior of glioblastoma stem cells in response to SDF-1α. *Biotechniques* 2020; **69:** 339-46. doi: 10.2144/btn-2020-0046

39. Schindelin J, Arganda-Carreras I, Frise E, Kaynig V, Longair M, Pietzsch T, et al. Fiji: an open-source platform for biological-image analysis. *Nat Methods* 2012; **9:** 676-82. doi: 10.1038/nmeth.2019

40. Morozas A, Malyško-Ptašinskė V, Kulbacka J, Ivaška J, Ivaškienė T, Novickij V. Electrochemotherapy for head and neck cancers: possibilities and limitations. *Front Oncol* 2024; **14:** 1353800. doi: 10.3389/fonc.2024.1353800

41. Li A, Walling J, Kotliarov Y, Center A, Steed MA, Ahn SJ, et al. Genomic changes and gene expression profiles reveal that established glioma cell lines are poorly representative of primary human gliomas. *Mol Cancer Res* 2008; **6:** 21-30. doi: 10.1158/1541-7786.MCR-07-0280

42. Keller S, Schmidt MHH. EGFR and EGFRvIII promote angiogenesis and cell invasion in glioblastoma: combination therapies for an effective treatment. *Int J Mol Sci* 2017; **18:** 1295. doi: 10.3390/ijms18061295

43. Abed T, Ganser K, Eckert F, Stransky N, Huber SM. Ion channels as molecular targets of glioblastoma electrotherapy. *Front Cell Neurosci* 2023; **17:** 1133984. doi: 10.3389/fncel.2023.1133984

44. Wei R, Zhou J, Bui B, Liu X. Glioma actively orchestrate a self-advantageous extracellular matrix to promote recurrence and progression. *BMC Cancer* 2024; **24:** 974. doi: 10.1186/s12885-024-12751-3

45. Aitchison EE, Dimesa AM, Shoari A. Matrix metalloproteinases in glioma: drivers of invasion and therapeutic targets. *BioTech* 2025; **14:** 28. doi: 10.3390/biotech14020028

46. Lehmann S, Boekhorst VT, Odenthal J, Bianchi R, Helvert S, Ikenberg K, et al. Hypoxia induces a HIF-1-dependent transition from collective-to-amoeboid dissemination in epithelial cancer cells. *Curr Biol* 2017; **27:** 392-400. doi: 10.1016/j.cub.2016.11.057

47. Graybill PM, Davalos RV. Cytoskeletal disruption after electroporation and its significance to pulsed electric field therapies. *Cancers* 2020; **12:** 1132. doi: 10.3390/cancers12051132

48. Azuaje F, Tiemann K, Niclou SP. Therapeutic control and resistance of the EGFR-driven signaling network in glioblastoma. *Cell Commun Signal* 2015; **13:** 23. doi: 10.1186/s12964-015-0098-6

49. Wang X, Hong T, Liu G, Rao J, Shi F, Wang H, et al. High-frequency irreversible electroporation suppresses invasion and metastasis by targeting SIRT1/2 in highly invasive tumor cells: an in vitro study. *Bioelectrochemistry* 2025; **166:** 109036. doi: 10.1016/j.bioelechem.2025.109036

50. Casciati A, Tanori M, Gianlorenzi I, Rampazzo E, Persano L, Viola G, et al. Effects of ultra-short pulsed electric field exposure on glioblastoma cells. *Int J Mol Sci* 2022; **23:** 3001. doi: 10.3390/ijms23063001

51. Allen M, Bjerke M, Edlund H, Nelander S, Westermark B. Origin of the U87MG glioma cell line: good news and bad news. *Sci Transl Med* 2016; **8:** 354re3. doi: 10.1126/scitranslmed.aaf6853

52. Cheng L, Wu Q, Guryanova OA, Huang Q, Rich JN, Bao S, et al. Elevated invasive potential of glioblastoma stem cells. *Biochem Biophys Res Commun* 2011; **406:** 643-8. doi: 10.1016/j.bbrc.2011.02.123

53. Prager BC, Bhargava S, Mahadev V, Hubert CG, Rich JN. Glioblastoma stem cells: driving resilience through chaos. *Trends Cancer* 2020; **6:** 223-235. doi: 10.1016/j.trecan.2020.01.009

54. Garcia PA, Pancotto T, Rossmeisl JH, Henao-Guerrero N, Gustafson NR, Daniel GB, et al. Non-thermal irreversible electroporation (N-TIRE) and adjuvant fractionated radiotherapeutic multimodal therapy for intracranial malignant glioma in a canine patient. *Technol Cancer Res Treat* 2011; **10:** 73-83. doi: 10.7785/tcrt.2012.500181

55. Dasari S, Bernard Tchounwou P. Cisplatin in cancer therapy: molecular mechanisms of action. *Eur J Pharmacol* 2014; **740:** 364-378. doi: 10.1016/j.ejphar.2014.07.025

56. Serša G, Čemažar M, Miklavčič D, Rudolf Z. Electrochemotherapy of tumours. *Radiol Oncol* 2006; **40:** 163-74. [internet]. [cited 2025 Jul 15]. Available at https://www.radioloncol.com/index.php/ro/article/view/1258

57. Lorenzo MF, Thomas SC, Kani Y, Hinckley J, Lee M, Adler J, et al. Temporal characterization of blood–brain barrier disruption with high-frequency electroporation. *Cancers* 2019; **11:** 1850. doi: 10.3390/cancers11121850

58. Sharabi S, Bresler Y, Ravid O, Shemesh C, Atrakchi D, Schnaider-Beeri M, et al. Transient blood-brain barrier disruption is induced by low pulsed electrical fields in vitro: an analysis of permeability and trans-endothelial electric resistivity. *Drug Deliv* 2019; **26:** 459-69. doi: 10.1080/10717544.2019.1571123

59. Todorovic V, Sersa G, Mlakar V, Glavac D, Flisar K, Cemazar M. Metastatic potential of melanoma cells is not affected by electrochemotherapy. *Melanoma Res* 2011; **21:** 196-205. doi: 10.1097/CMR.0b013e328337abd7

60. Todorovic V, Sersa G, Mlakar V, Glavac D, Cemazar M. Assessment of the tumourigenic and metastatic properties of SK-MEL28 melanoma cells surviving electrochemotherapy with bleomycin. *Radiol Oncol* 2012; **46:** 32-45. doi: 10.2478/v10019-012-0010-6

61. Auffinger B, Tobias AL, Han Y, Lee G, Guo D, Dey M, et al. Conversion of differentiated cancer cells into cancer stem-like cells in a glioblastoma model after primary chemotherapy. *Cell Death Differ* 2014; **21:** 1119-1131. doi: 10.1038/cdd.2014.31

62. Wang Z, Zhang H, Xu S, Liu Z, Cheng Q. The adaptive transition of glioblastoma stem cells and its implications on treatments. *Sig Transduct Target Ther* 2021; **6:** 1-13. doi: 10.1038/s41392-021-00491-w

63. Arroyo JP, Jacobs EJ, Ahmad RN, Amin AJ, Verbridge SS, Davalos RV. Characterization of glioma spheroid viability and metastatic potential following monophasic and biphasic pulsed electric fields. *Bioelectrochemistry* 2025; **165:** 109005. doi: 10.1016/j.bioelechem.2025.109005

research article

Heterogenous mitochondrial ultrastructure and metabolism of human glioblastoma cells: differences between stem-like and differentiated cancer cells in response to chemotherapy

Urban Bogataj[1], Metka Novak[2,3], Simona Katrin Galun[2,4], Klementina Fon Tacer[5,6], Milos Vittori[1,5,6], Cornelis JF Van Noorden[2], Barbara Breznik[2,5,6,7]

[1] University of Ljubljana, Biotechnical Faculty, Department of Biology, Ljubljana, Slovenia
[2] National Institute of Biology, Department of Genetic Toxicology and Cancer Biology, Ljubljana, Slovenia
[3] University of Ljubljana, Biotechnical Faculty, Ljubljana, Slovenia
[4] Jožef Stefan International Postgraduate School, Nanosciences and Nanotechnologies, Ljubljana, Slovenia
[5] Texas Tech University School of Veterinary Medicine, Amarillo, Texas, USA
[6] Texas Center for Comparative Cancer Research (TC3R), Texas Tech University, Amarillo, Texas, USA
[7] University of Ljubljana, Faculty of Chemistry and Chemical Engineering, Ljubljana, Slovenia

Radiol Oncol 2025; 59(4): 551-565.

Received 11 June 2025
Accepted 13 August 2025

Correspondence to: Assist. Prof. Barbara Breznik, Ph.D., Slovenia. E-mail: barbara.breznik@nib.si and Cornelis J.F. Van Noorden, Ph.D., Netherlands. E-mail: c.j.vannoorden@amsterdamumc.nl

Disclosure: No potential conflicts of interest were disclosed.

Background. Glioblastoma stem-like cells (GSCs) contribute to the resistance of glioblastoma (GBM) tumors to standard therapies. The background of the resistance of GSCs to the chemotherapeutic agent temozolomide is not yet fully understood in the context of cellular metabolism and the role of mitochondria. The aim of this study was to perform a detailed ultrastructural characterization of the mitochondria of GSCs prior and post temozolomide exposure and to compare it to differentiated GBM cells.

Materials and methods. Patient-derived and established GBM cell lines were used for the study. The ultrastructure of the mitochondria of the examined cell lines was assessed by transmission electron microscopy. The microscopic analysis was complemented and compared by an analysis of cell metabolism using Seahorse extracellular flux analysis.

Results. We found that the metabolic profile of GSCs is quiescent and aerobic. Their elongated mitochondria with highly organized cristae are indicating increased biogenesis and mitochondrial fusion and corresponds to a more oxidative phosphorylation (OXPHOS)-dependent metabolism. The metabolism of GSCs is dependent on OXPHOS and there are no changes in defective mitochondria fraction after the treatment with temozolomide. In contrast, differentiated GBM cells with fragmented mitochondria, which have less organized cristae, are more energetic and glycolytic. Temozolomide treatment induced ultrastructural mitochondrial damage in differentiated GBM cells.

Conclusions. We demonstrated differences in mitochondrial ultrastructure and cellular metabolism between GSCs and differentiated GBM cells in response to temozolomide, suggesting that mitochondria play an important role in the resistance of GSCs to temozolomide. This study provides a basis for further studies addressing GSC chemotherapy resistance in the context of mitochondrial structure and function.

Key words: glioblastoma; mitochondria ultrastructure; metabolism; chemotherapy resistance; stem cells

Introduction

Glioblastoma (GBM), the most common primary brain tumor in adults, remains one of the most aggressive malignancies with median survival of 16 months after diagnosis[1] and so far, incurable. Standard treatment includes maximal safe surgical removal of tumor tissue, radiotherapy and chemotherapy using the alkylating drug temozolomide (TMZ).[2] However, due to GBM heterogeneity, its invasive nature, and its resistance to chemotherapy and radiotherapy, the GBM almost always reoccurs in a more aggressive form.[1]

An important general characteristic of GBM is that it involves numerous heterogenous cell types including the glioma stem-like cells (GSCs)[3,4] that exhibit diverse metabolic profiles.[5,6] A consequence is enormous plasticity and adaptability to therapeutic interventions resulting in recurrence and resistance to therapy. GSCs play a crucial role in therapy resistance.[6] GSCs reside within specific niches within tumors that are primarily hypoxic.[4,7-9] The hypoxic tumor microenvironment is important for the maintenance of GSCs[10,11] but requires specific metabolic adaptations, with mitochondria playing a crucial role in the maintenance of GSCs.[12]

One of the common characteristics of cancer cell metabolism is the Warburg effect, which designates that cancer cells often rely primarily on glycolysis to produce adenosine triphosphate (ATP) even in the presence of oxygen. Dysfunctional mitochondria in cancer cells were suggested as one of the major culprits[13-15], however, recent data suggest that cancer cells and, in particularly cancer stem cells[16], including GSCs[5,17], often rather rely on oxidative phosphorylation (OXPHOS) to produce ATP.[18-20] The mitochondria are thus crucial in cancer cell biology through their direct involvement in OXPHOS, besides other roles they play in cell signalling, synthesis of macromolecules, oxidative stress and apoptosis.[21-23] Mitochondrial fusion and elongated mitochondria support efficient OXPHOS especially during nutrient withdrawal, whereas fragmented mitochondria are often associated with impaired OXPHOS and nutrient excess.[24] Cancer cells generally exhibit fragmented mitochondria, associated with low OXPHOS activity and increased glycolysis.[25-27] Cancer stem cells, however, exhibit increased biogenesis of mitochondria, consistent with increased OXPHOS[28,29], however, their role in therapy response and resistance is not well understood.

The ultrastructure of mitochondria in GBM cells is very variable, but a consistent observation is the presence of abundant swollen and electron-lucent mitochondria that display reduced and disorganized cristae.[18,19,30,31] So far, most ultrastructural analyses of GBM cells have been performed in tumor biopsies[32,33] and tissue explants obtained from patients during tumor excision.[34] These studies predominately focus on the cells that form the bulk of tumor mass and do not specifically address GSC properties and their response to chemotherapy.

Given the importance of GSC in therapy resistance, the aim of our study was to provide a detailed ultrastructural characterization of untreated cultured GSCs and the effects of exposure to the chemotherapeutic TMZ and compare it to differentiated GBM cells. The microscopic analysis was complemented and compared with cellular metabolism analysis using cell viability assay and extracellular flux analysis. A commonly used method for measuring cellular metabolism is extracellular flux (XF; also known as Seahorse) analysis. XF analysis measures extracellular acidification (ECAR) and oxygen consumption (OCR) rates as markers of glycolysis and mitochondrial OXPHOS, respectively[35,36], and was applied to evaluate cellular metabolism in GSCs and differentiated GBM cells.

We provide novel insights into structural and metabolic responses of GBM and GSC cells to chemotherapy and lay foundation for further studies addressing GSC therapeutic resistance and the effects of different treatment regimens on the mitochondrial structure and function of GSCs.

Materials and methods

All methods were performed in accordance with the relevant guidelines and regulations.

Cell cultures

Approval by the National Medical Ethics Committee of the Republic of Slovenia was obtained (number 0120-190/2018-2711-38) for collecting and processing tumor tissue material and performing research on patient's material. Patients or their authorized representatives signed the informed consent form in accordance with the Declaration of Helsinki.

In this study, two GSC lines (NCH644 and NCH421k) and two differentiated GBM cell cultures (U87 and NIB140) were included. Commercially available GSCs NCH421k and NCH644 were purchased from the Cell Lines Service (CLS) GmbH, Eppelheim, Germany. Cells were grown in serum

free conditions in Neurobasal Medium as described before.[37] Cell line U87 MG was obtained from the American Type Culture Collection (ATCC, Manassas, VA, USA) and was cultured in low glucose DMEM supplemented with 10% fetal bovine serum (FBS; Gibco, Thermo Fisher Scientific, Waltham, MA, USA), 2 mM L-glutamine and 1% penicillin/streptomycin (both: Sigma Aldrich, St. Louis, MO, USA). NIB140 are patient-derived cell cultures from fresh GBM tissues and were established as described before.[38-40] NIB140 cells were grown in Dulbecco's modified Eagle's medium (DMEM) (Hyclone, GE Healthcare, Chicago, IL, USA) supplemented with 10% FBS (Gibco), 2 mM L-glutamine, and 1× penicillin/streptomycin (both: Sigma Aldrich). Growing cells were detached with a 0.25% trypsin EDTA solution (Gibco). NIB140 cells express GBM cell markers.[39,41] All cells were cultured at 37°C, in the presence of 5% CO_2 and 95% humidity and checked for Mycoplasma using MycoAlert Mycoplasma Detection Kit (Lonza, Basel, Switzerland). Authentication of cells was performed by DNA fingerprinting using AmpFlSTR Profiler Plus PCR Amplification Kit, as described previously.[42]

Real-time quantitative polymerase chain reaction (RT-qPCR)

Total RNA was isolated using an AllPrep DNA/RNA/Protein Mini Kit (Qiagen, Germantown, MD, USA) according to the manufacturer's instructions. RT-qPCR was performed to determine the mRNA levels of genes in our samples using fluorescent dye -minor groove binder (FAM-MGB) probes listed in Table 1, Fluidigm BioMark HD System RT-PCR (Fluidigm Corporation, San Francisco, CA, USA) and the 48.48 Dynamic Arrays IFC. Visualization and analysis of RT-qPCR results were performed using Biomark Data Collection software, Fluidigm RT-qPCR analysis software (both: Fluidigm Corporation), and quantGenius software as described previously.[41] Relative copy numbers of cDNA were normalized to housekeeping genes *HPRT1* and *GAPDH*.

Cell viability assay

Viability of cells was determined after 48 h of treatment with TMZ (Sigma-Aldrich) using the 3-(4,5-dimethylthiazol- 2-yl)-2,5-diphenyltetrazolium-bromide; Sigma-Aldrich (MTT) reagent for U87 and NIB140 cells and MTS (3-(4,5-dimethylthiazol-2-yl)-5-(3-carboxymethoxyphenyl)-2-(4-sulfophenyl)-2H-tetrazolium; Promega, Madison, WI, USA) (MTS) reagent for NCH cells. Assays were performed according to the manufacturer's instructions. Briefly, cells were seeded into 96-well plates (8000 cells/well) and grown overnight. Cells were treated with different concentrations of TMZ (25–400 μM). Stock solutions of TMZ were prepared in dimethyl sulfoxide (DMSO, Sigma-Aldrich). Control incubation media contained the same amount of vehicle DMSO (0.9%, v/v). After 48 h, MTT or MTS was added and 3 h after incubation at, absorbance was measured as the change in optical density (ΔOD 570/690 nm) using a microplate reader (Synergy™ HT, Bio Tek Instruments Inc., Winooski, VT, USA). Cell viability data were analyzed using GraphPad Prism software (GraphPad Software, San Diego, CA, USA) and presented as % of vehicle control.

TABLE 1. List of TaqMan gene expression assays fluorescent dye -minor groove binder (FAM-MGB)

Gene name	Source	Identifier	Protein name
PROM1	Thermo Fisher Scientific	Hs01009259_m1	Prominin -1; CD133 antigen
OLIG2	Thermo Fisher Scientific	Hs00377820_m1	Oligodendrocyte transcription factor 2
NOTCH1	Thermo Fisher Scientific	Hs01062014_m1	Neurogenic locus notch homolog protein 1
SOX10	Thermo Fisher Scientific	Hs00366918_m1	SRY - Box transcription factor 10
SOX2	Thermo Fisher Scientific	Hs01053049_m1	SRY - Box transcription factor 2
TUBB3	Thermo Fisher Scientific	Hs00801390_s1	Tubulin beta 3 class III
HPRT1	Thermo Fisher Scientific	Hs02800695_m1	Hypoxanthine phosphoribosyltransferase 1
GAPDH	Thermo Fisher Scientific	Hs00909233_m1	Glial fibrillary acidic protein

Extracellular flux analysis

Extracellular flux (XF) analysis was performed using Seahorse XFe24 Flux Analyzer (Agilent Technologies, Santa Clara, CA, USA) to measure the oxygen consumption rate (OCR) and extracellular acidification rate (ECAR) of live cells in a 24-well plate format. GBM cells were grown in T25 flask as controls (0.5% DMSO) or treated with 100 μM of TMZ for 48 h. Before the XF experiment, cells were harvested, 80,000 cells/well were seeded in poly-d-Lysine (Poly-D-lysine hydrobromide, Sigma)-coated XF24 cell culture microplates in Seahorse XF DMEM medium (pH = 7.4 with 10 mM XF glucose, 1

mM XF pyruvate and 2 mM XF glutamine) in duplicates and centrifuged to allow the cells to attach to the bottom of the plates. The cells were transferred to a CO_2-free incubator at 37°C for 20 min. During this time, assays were prepared, and cartridges loaded. XF Real-time ATP Rate Assay Kit (#103592; Agilent), XF Glycolytic Rate Assay Kit (#103344; Agilent) and XF Cell Mito Stress Test Kit (#103015; Agilent) were applied according to manufacturer's instructions. Immediately after the run, the cells were fixed with 4% paraformaldehyde (PFA; Sigma) and incubated with Hoechst 33442 (Sigma) to count the number of cells in each well for normalization of the XF results. Hoechst signal was measured using Cytation 5 Cell Imaging multi-mode reader (Bio Tek) and cell counts were analyzed using Gen 5 software (Bio Tek). Flux rates were normalized to cell counts in each well. Data were analyzed using Wave software version 2.6.1 and an online software version at the Agilent cloud (https://seahorseanalytics.agilent.com/). Statistically significant differences in metabolic rates and parameters between different cells and between control and TMZ-treated samples were analyzed using GraphPad Prism software (GraphPad Software).

Transmission electron microscopy

Two series of experiments were conducted with transmission electron microscopy. In the first series of experiments, a detailed ultrastructural characterization of mitochondria in untreated GBM cells was performed and ultrastructural differences between mitochondria in GSCs and differentiated GBM cells were determined. Samples of cells from 5 biological replicates were analyzed in this set of experiments. In the second series of experiments the effect of TMZ treatment on the mitochondrial ultrastructure in GSCs and differentiated GBM cells was investigated. TMZ treated cells and control, untreated cells from 2 biological replicates were analyzed in this set of experiments.

Sample preparation

Cells used to investigate the effects of TMZ treatment on mitochondrial ultrastructure were exposed either to 100 μM TMZ (Sigma-Aldrich) or 0.9%, v/v DMSO (Sigma-Aldrich) (vehicle) for 48 h prior to fixation. The cells were fixed using 2.5% glutaraldehyde (SPI, West Chester, PA, USA) and 2% PFA (Sigma-Aldrich) in phosphate-buffered saline (PBS) (Gibco). Following fixation, the cells were rinsed in PBS and postfixed in 1% OsO_4 (SPI) in PBS (Gibco). Then, the cells were washed in PBS (Gibco) and embedded in 2% low melting point agarose (Sigma-Aldrich). The blocks of agarose with embedded cells were solidified on ice and cut into small pieces (<1 mm in smallest dimension). The pieces of agarose with cells were then dehydrated in graded series of ethanol (Honeywell, Seelze, Germany) and acetone (Merck, Darmstadt, Germany). Finally, the samples were embedded in epoxy resin Agar 100 (Agar Scientific, Rotherham, UK). The resin was polymerized for 24 h at 60°C in embedding molds. Semithin and ultrathin sections were prepared with a Reichert Ultracut S (Leica, Wetzlar, Germany) ultramicrotome, using glass and diamond knives. The semithin sections were stained with Azure II (Merck) – methylene blue (Sigma-Aldrich) and examined with a light microscope. The ultrathin sections were contrasted with uranyl acetate (SPI) and lead citrate (SPI).

Imaging

Contrasted ultrathin sections were imaged with a CM100 transmission electron microscope (Philips, Eindhoven, The Netherlands). The electron micrographs were acquired with an Orius 200 camera (Gatan, Pleasanton, CA, USA) and Digital Micrograph software (Gatan). Five cells were imaged for each biological replicate per cell line. Numerous partly overlapping images were acquired per cell at 3 different magnifications. The acquired images were stitched together with FIJI[43] open-source software and TrakEM2[44] plugin to obtain images with large field of view and high resolution. Stitched images at lowest magnification covered whole cells at sufficient resolution to obtain a general overview of cell ultrastructure and to perform stereological quantification of mitochondrial and nuclear volume densities. Stitched images at medium magnification covered large areas of cytoplasm with sufficient resolution to obtain overall ultrastructural features of individual cellular organelles and to perform measurements of mitochondrial length and width. Stitched images at highest magnification covered small areas of cytoplasm with sufficient resolution to distinguish fine ultrastructural features of mitochondria, such as the morphology of cristae.

Image analysis

We counted the number of mitochondrial cross-sections on stitched images covering whole cells using FIJI software with Cell counter plugin. For

the stereological quantification of mitochondrial and nuclear volume density, an overlay of multipurpose grid of test points was made on stitched images covering whole analyzed cells. We used the multipurpose grid that is available as a macro for ImageJ/FIJI at: https://imagej.nih.gov/ij/macros/Multipurpose_grid.txt. In the test grid parameters, we set the density of test points to 1 point per 0.5 μm². We counted the number of test points inside mitochondria, cell nuclei and other areas of cytoplasm with aid of the Cell counter plugin. From the obtained counts, we calculated the estimates for the volume density (volume fraction) of mitochondria and the volume density of cell nuclei according to the equation:

$$V(o) = \frac{P(o)}{P(t)},$$

where the *V(o)* is the volume density of organelle in question, *P(o)* is the count of test points inside the organelles in question and the *P(t)* is the total count of points inside cells. To describe the general morphology of the mitochondrial network analyzed in GBM cell lines, we measured the average length and width of mitochondrial cross-sections in stitched images at medium magnification. Then, we calculated the length:width ratio of mitochondrial cross-sections. If this ratio was close to 1, it indicated that the mitochondrial network consisted primarily of round mitochondria and was likely more fragmented. If this ratio was much greater than 1, it indicated that the mitochondrial network consisted of elongated mitochondria in a more interconnected mitochondrial network.

To investigate the effect of TMZ treatment on mitochondrial ultrastructure, features of mitochondria in 5 cells per biological replicate were evaluated. Based on their ultrastructural features, we classified the mitochondria into two following types: normal and defective. Normal mitochondria are defined as mitochondria with electron-dense matrix with narrow cristae (a) and mitochondria with electron-dense matrix with dilated cristae (b). Defective mitochondria are defined as mitochondria with electron-lucent matrix and cristae reduced in size and numbers (c) and mitochondria with abnormal ultrastructural alterations (swollen and containing membrane swirls) (d). The percentages/fractions of mitochondrial types in each cell were calculated from the total fraction of mitochondria with clearly visible ultrastructure at a 3400x magnification.

The TEM scoring was performed independently by two experienced TEM analysts to avoid bias observations.

MitoTracker staining

U87 and NIB140 cells were cultured on poly-L-lysine-coated coverslips in 24-well plates (Corning, NY, USA) and NCH421k cells were dissociated before stained using MitoTracker® Orange CMTMRos (Invitrogen, Thermo Fisher Scientific) according to the manufacturer's instructions. Stained cells were fixed in 4% PFA in PBS. Following fixation, the cells were rinsed in PBS and stained with Hoechst 33442 (Sigma) to visualize cell nuclei. Imaging was performed with an AxioImager Z.1 microscope equipped with an AxioCam MRm camera using Axiovision software (all from Zeiss, Oberkochen, Germany).

Statistical analysis

To compare morphometric parameters between the analyzed GBM cell lines (untreated cells), quantitative measurements in 5 biological replicates (n = 5) of each cell line were performed. For each biological replicate we analyzed 5 cells. The following morphometric parameters were investigated: the number of mitochondrial cross-sections, mitochondrial volume density, nuclear volume density and length/width ratio of mitochondria. The statistical analyses were performed in the R statistical software environment. To test for statistically significant differences between cell lines, the analysis of variance (ANOVA) followed by Tukey's test for pairwise comparisons was performed. Before the ANOVA analysis, we prepared Q-Q plots of residuals and performed a Shapiro-Wilk test to check the normality of data. We also performed Levene's test to check the equality of variances.

To compare fractions of different mitochondrial types and volume density of mitochondria between TMZ-treated and non-treated cells, the experiments were performed in two independent repeats (n = 2).

To compare metabolic profiles of GBM cells and GSCs, Seahorse analysis experiments were performed in 3 independent repeats (n = 3) and the statistical analyses were performed in GraphPad Prism software. Statistics were performed using Tukey's multiple comparisons test. Differences in ATP production rates between TMZ-treated and non-treated samples within each cell line were statistically evaluated using an unpaired t-test. Tukey's multiple comparisons test was used to compare all conditions after treatment with TMZ.

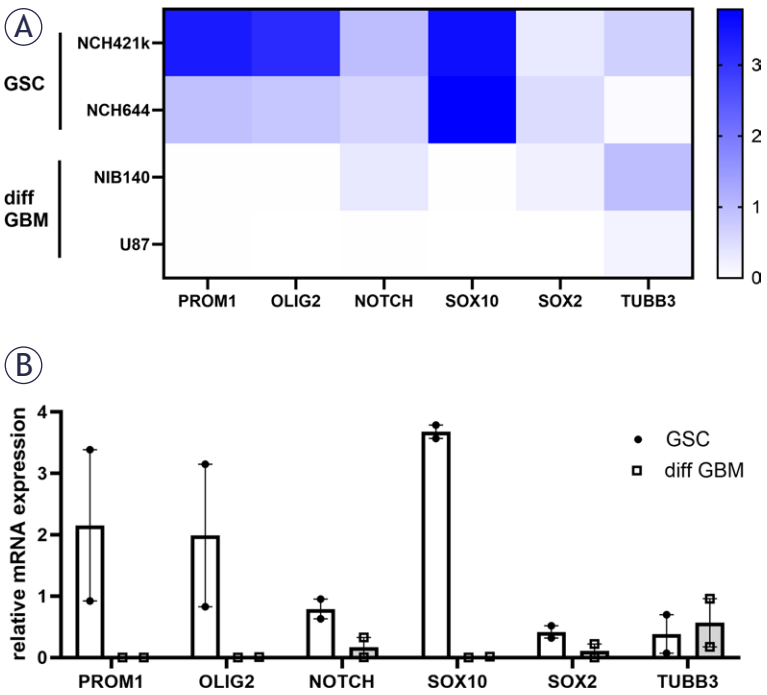

FIGURE 1. Relative mRNA expression of GSC (*PROM1, OLIG2, NOTCH, SOX10, SOX2*) and differentiation (*TUBB3*) markers in GSCs and differentiated GBM cells based on RT-qPCR analysis. **(A)** A heatmap of relative mRNA expression is shown for each cell lines. **(B)** Combined data are shown with mean values of relative mRNA expression ± SEM.

diff GBM = differentiated glioblastoma cell; GSC = glioblastoma stem-like cell; RT-qPCR = real-time quantitative polymerase chain reaction; SEM = standard error of the mean

Results

GSCs express high levels of cancer stem-like markers

Both types of GSCs, NCH421k and NCH644, expressed high gene expression levels of *PROM1, OLIG2, NOTCH, SOX10* and *SOX2* that are established GSC markers.[4,37,45] Differentiation marker tubulin beta-III (*TUBB3*) was expressed in the highest levels in differentiated GBM cells NIB140 (Figure 1).

Overall cellular ultrastructure

Both types of GSCs, NCH421k and NCH644, consisted of small cells of relatively homogeneous size and shape that aggregated in culture in small clusters. Both types of differentiated GBM cells, NIB140 and U87, were highly heterogeneous in terms of size and shape. Our stereological quantification of cell nuclear volume density indicated that the cell nuclei in GSCs occupied a significantly larger portion of cell volume than nuclei in differentiated GBM cells (Figure 2A). GSCs had oval cell nuclei with abundant heterochromatin and a single nucleolus (Supplementary Figures S1A, B). In differentiated GBM cells the cell nuclei contained hardly any heterochromatin and usually multiple nucleoli (Supplementary Figures S1C, D). We observed that the cisternae of the endoplasmic reticulum and Golgi stacks were considerably more abundant in differentiated GBM cells than in GSCs. The differentiated GBM cells also contained abundant multivesicular bodies and secondary lysosomes, which were scarce in GSCs (Supplementary Figure S2).

Mitochondrial ultrastructure differs between GBM cells

Quantification of mitochondrial cross-sections indicated a significant difference in mitochondrial numbers per cell between GSCs NCH421k and differentiated GBM cells U87 (Figure 2B), with mitochondria being more numerous in the U87 cells than in the NCH421k GSCs. Stereological quantification of mitochondrial volume density showed that the mitochondria in the differentiated GBM cells NIB140 occupied a significantly smaller proportion of cell cytoplasm than in both GSC lines (Figure 2C). Mitochondria in the differentiated GBM cells U87 occupied a significantly smaller proportion of cell cytoplasm than in the GSCs NCH421k. The quantification of ratio between mitochondrial length and width showed that the mitochondria in GSCs were more elongated than in differentiated GBM cells (Figure 2D).

The GSCs contained in general a higher number of large mitochondria and fewer smaller mitochondria, whereas differentiated GBM cells contained larger numbers of smaller mitochondria. In GSCs NCH644 and NCH421k, the most prevalent morphological type of mitochondria was represented by elongated, electron-dense mitochondria with narrow cristae which were oriented along the longitudinal axis of mitochondria (Figures 3A, C). Occasionally we observed dilated cristae (Figure 3B). In both types of GSCs, mitochondria occasionally displayed deformed cristae with swirled shape (Figure 3D).

In differentiated GBM cells U87 and NIB140, the mitochondria were rounder than in GSC lines and cristae were not organized, but rather oriented in variable directions (Figure 4). The two most prevalent morphological types of mitochondria in differentiated GBM cells were electron-lucent swollen mitochondria with reduced numbers of narrow

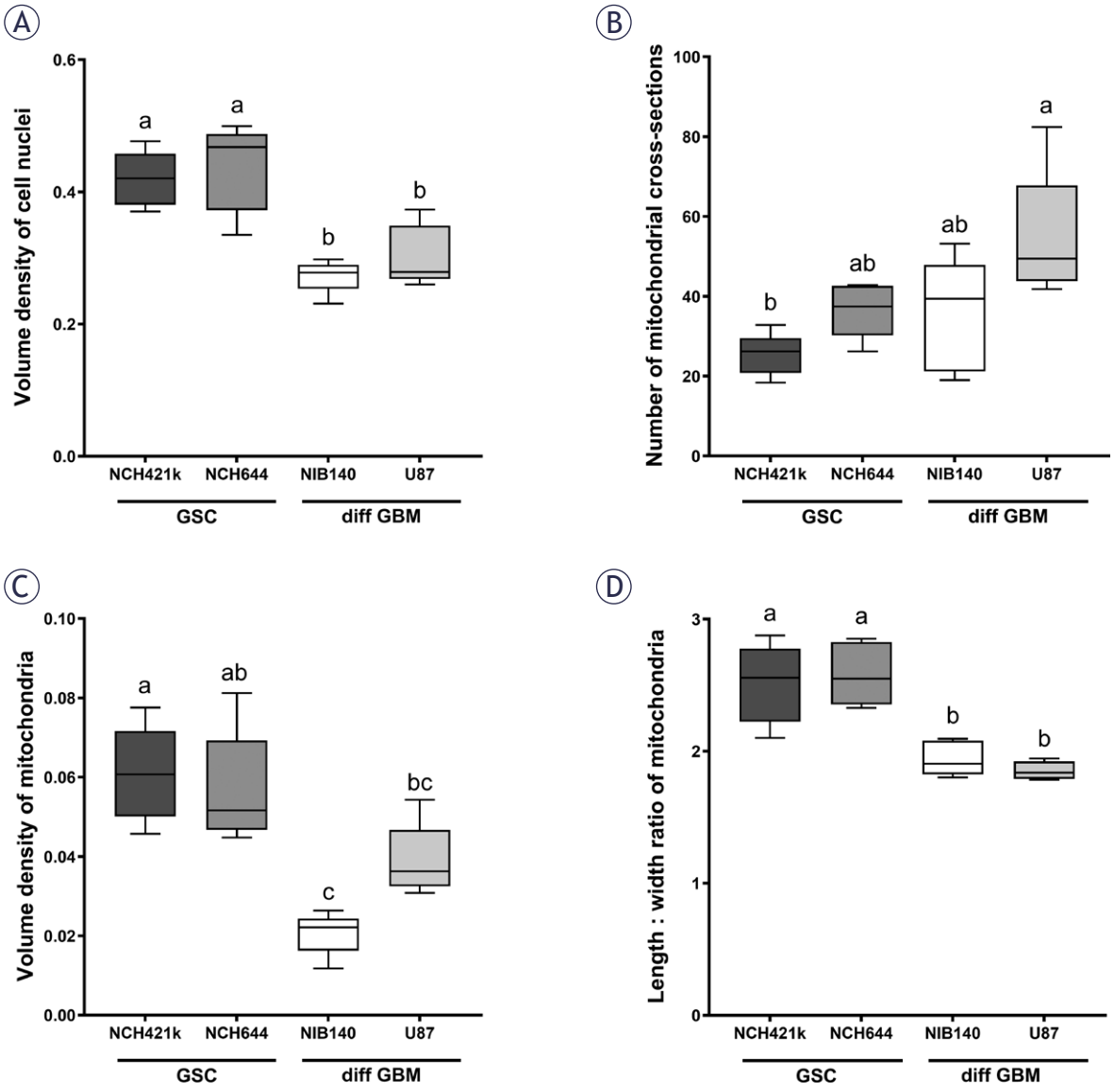

FIGURE 2. Quantification of **(A)** volume density of cell nuclei, **(B)** number of mitochondrial cross-sections per cell, **(C)** volume density of mitochondria and **(D)** length/width ratio of mitochondrial cross-sections. Data are represented by mean values ± SEM. Statistically significant differences are displayed with compact letters display (a, b, c). Cell lines that do not share any common letter have statistically significantly different means of a dependent variable ($p < 0.05$). Cell lines that share a common letter do not have statistically significant different means of a dependent variable ($p \geq 0.05$).

diff GBM = differentiated glioblastoma cell; GSC = glioblastoma stem-like cell; SEM = standard error of the mean

cristae (Figures 4A, C) and electron-dense mitochondria with numerous dilated cristae (Figures 4B, D). Quantification of these Figures are provided in Figure 2. In U87 cells, we frequently observed electron-dense mitochondria with narrow cristae. MitoTracker staining confirmed dense active mitochondria in the cells (Supplementary Figure S3).

Temozolomide treatment affected the mitochondrial ultrastructure but not the quantity of mitochondria in differentiated GBM cells

After exposure of GBM cells to 48 h treatment with 100 μM TMZ[46], the ultrastructure of mitochondria

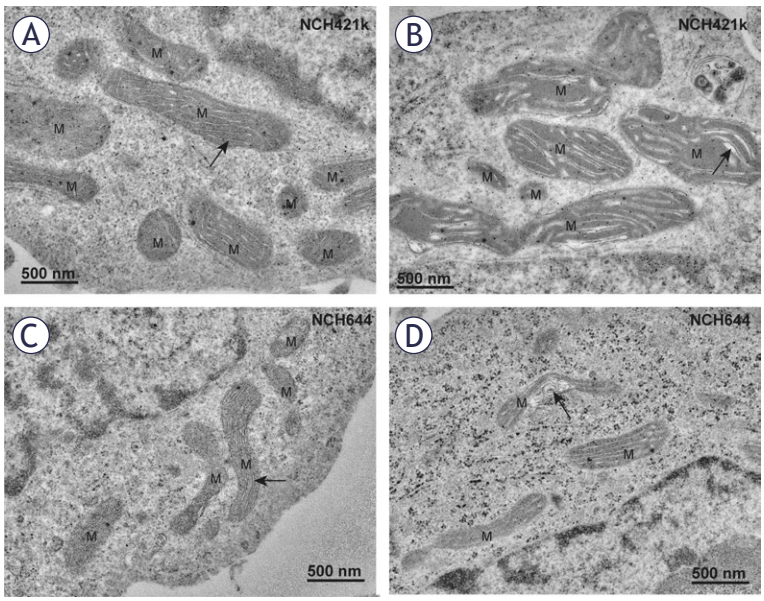

FIGURE 3. Mitochondria in GSCs have elongated mitochondria. **(A)** Electron-dense mitochondria (M) with narrow cristae (arrow) oriented along the longitudinal axis of mitochondria in the NCH421k glioblastoma stem-like cells (GSCs). **(B)** Electron-dense mitochondria (M) with dilated cristae (arrow) in the NCH421k GSCs. **(C)** Typical electron-dense mitochondria (M) with narrow cristae (arrow) oriented along the longitudinal axis of mitochondria in the NCH644 GSCs. **(D)** Deformed cristae with swirled shape (arrow) in a mitochondrion of a NCH644 cells.

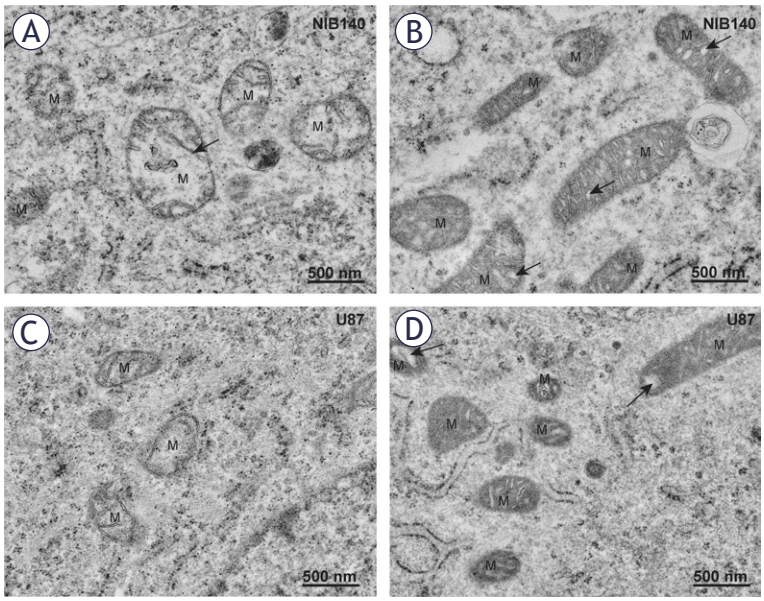

FIGURE 4. Mitochondria in differentiated GBM cells are smaller and fragmented. **(A)** Electron-lucent swollen mitochondria (M) with reduced cristae (arrow) in NIB140 cells. **(B)** Condensed electron-dense mitochondria (M) with dilated cristae (arrows) in NIB140 cells. **(C)** Electron-lucent swollen mitochondria (M) with reduced cristae in U87 cells. **(D)** Condensed electron-dense mitochondria (M) with dilated cristae (arrows) in U87 cells.

was evaluated and quantified. Based on their ultrastructural features, we classified the mitochondria into two following types: normal and defective (Figure 5A). TMZ treatment induced changes in the fractions of mitochondrial types only in differentiated GBM cells (Figures 5A, B). In both types of differentiated GBM cells an increased fraction of defective mitochondria was observed. In contrast, there were no changes in fraction of defective mitochondria in TMZ-treated GSCs. Despite the effect of TMZ treatment on mitochondrial ultrastructure of differentiated GBM cells, no effect on the volume density of mitochondria was observed after TMZ treatment in any of cell lines (Supplementary Figure S4). Structures indicative of autophagy, such as autophagic vacuoles and autophagosomes, were observed both in GSCs and differentiated GBM cells exposed to TMZ (Supplementary Figure S5).

GSCs are metabolically quiescent and rely more on OXPHOS than differentiated GBM cells

XF analysis was performed to evaluate mitochondrial OXPHOS and glycolysis rates in GSCs NCH421k and NCH644 in comparison to differentiated GBM cells U87 and NIB140 (Figures 6A, B). Based on ATP production measurements, the metabolic profile of GSCs was quiescent, as they produced less ATP than differentiated GBM cells (Figures 6C, E). GSCs rely more on OXPHOS than glycolysis for ATP production as the ratio between mitochondrial and glycolytic ATP production rate was higher in GSCs than in differentiated GBM cells (Figures 6D-E). Glycolysis rates were the highest in differentiated GBM cells U87 and NIB140 and patient-derived cells NIB140 displayed the highest energy production (Figure 6C).

GSC metabolism relies on OXPHOS after treatment with temozolomide

Cells were treated with 100 μM TMZ for 48 h and after that cellular metabolism was examined. Cell viability and total ATP production were not altered after TMZ treatment, except for the 50% decrease in NCH644 cell viability when treated with the highest concentration of TMZ (Supplementary Figure S6). Furthermore, the glycolytic and mitochondrial ATP production was not altered in cells after treatment with TMZ (Figure 7A). We observed that GSCs rely on OXPHOS after TMZ treatment since the ratio between mitochondrial and glyco-

lytic ATP production was above 2 which was much higher than in differentiated GBM cells (Figure 7B). After treatment with TMZ the Glycolytic Rate Assay Kit and Cell Mito Stress Test Kit were performed in cells to evaluate glycolytic rate and mitochondrial function, respectively. Differentiated GBM cells retained high glycolytic ATP production after TMZ treatment. NIB140 cells increased the ECAR rate and compensatory glycolysis after TMZ treatment. There was no change in glycolysis rates in U87, NCH644 and NCH421k cells after TMZ treatment (Supplementary Figure S7). There were also no changes in the monitored parameters of mitochondrial function in cells after treatment with TMZ, except increased maximal respiration in U87 cells after TMZ treatment. NIB140 cells showed the highest proton leak among the cell cultures used (Supplementary Figure S8).

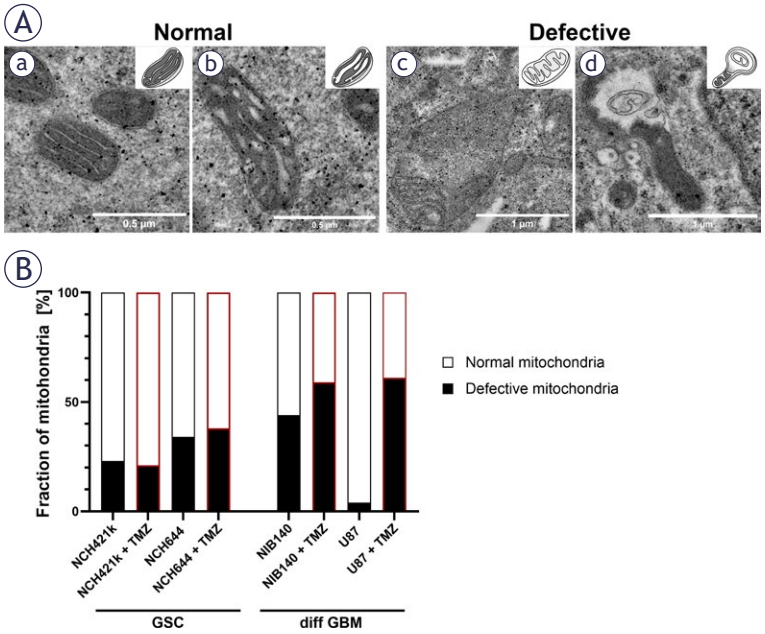

FIGURE 5. Mitochondrial ultrastructure and its quantification after exposure of cells to 100 µM TMZ. **(A)** Mitochondria were classified into two following types: normal and defective. Normal mitochondria are defined as mitochondria with electron-dense matrix with narrow cristae indicating metabolism with a high OXPHOS rate **(a)** and mitochondria with electron-dense matrix with dilated cristae indicating metabolism with a lower OXPHOS rate **(b)**. Defective mitochondria are defined as mitochondria with electron-lucent matrix and cristae reduced in size and numbers indicating metabolism without OXPHOS **(c)** and mitochondria with abnormal ultrastructural alterations (swollen with membrane swirls) indicating damage and stress in mitochondria **(d)**. **(B)** Quantification of the 2 categories of mitochondrial ultrastructure as fraction of all mitochondria. Experiments were performed in two independent repeats.

diff GBM = differentiated glioblastoma cell; GSC = glioblastoma stem-like cell; OXPHOS = oxidative phosphorylation; TMZ = temozolomide

Discussion

Results of our current study revealed that GSCs have a more quiescent and aerobic metabolic profile than differentiated GBM cells. This is supported both by the microscopic observations of mitochondrial morphology and ultrastructure and by the direct measurements of cellular metabolism by XF analysis.

General ultrastructure showed that GSCs contain less abundant rough endoplasmic reticulum and less Golgi apparatus and that their cell nuclei occupy a relatively large fraction of cytoplasm and contain more heterochromatin in comparison to the differentiated GBM cells. These observations are in agreement with the dedifferentiated status of GSCs and their metabolic quiescence which is one of important factors in their resistance to therapy.[6,19,47] The differentiated GBM cells contain extensive rough endoplasmic reticulum and more Golgi apparatus and nuclei with more euchromatin. This probably supports increased protein synthesis necessary for the excessive growth and proliferation of differentiated GBM cells. The results of the XF analysis support this, showing that GSCs are more metabolically quiescent with a lower ATP production rate, while differentiated GBM cells are more energetic, exhibiting a higher ATP production rate. Similar results were reported by Spehalski *et al.*[48] in their study of GSCs and differentiated GBM cells using XF analysis.

Despite their metabolically quiescent phenotype, we observed that the GSCs contained large, elongated mitochondria that occupied a large fraction of the cytoplasm. In contrast, the differentiated GBM cells had small round mitochondria that occupied a smaller portion of the cytoplasm. This indicates enhanced biogenesis and fusion of mitochondria in GSCs and a more fragmented mitochondrial network in differentiated GBM cells. Our XF analysis has shown that the ratio between mitochondrial and glycolytic ATP production is higher in GSCs than in the differentiated GBM cells. Taken together, this shows on cellular and molecular level that the GSCs have a more OXPHOS reliant metabolism, whereas the differentiated GBM cells are more glycolytic. Generally, highly fused mitochondrial networks of elongated mitochondria are associated with high OXPHOS activity particularly in conditions of nutrient withdrawal and mild stress, whereas the fragmented mitochondria indicate impaired OXPHOS and increased glycolysis particularly in conditions of nutrient excess or

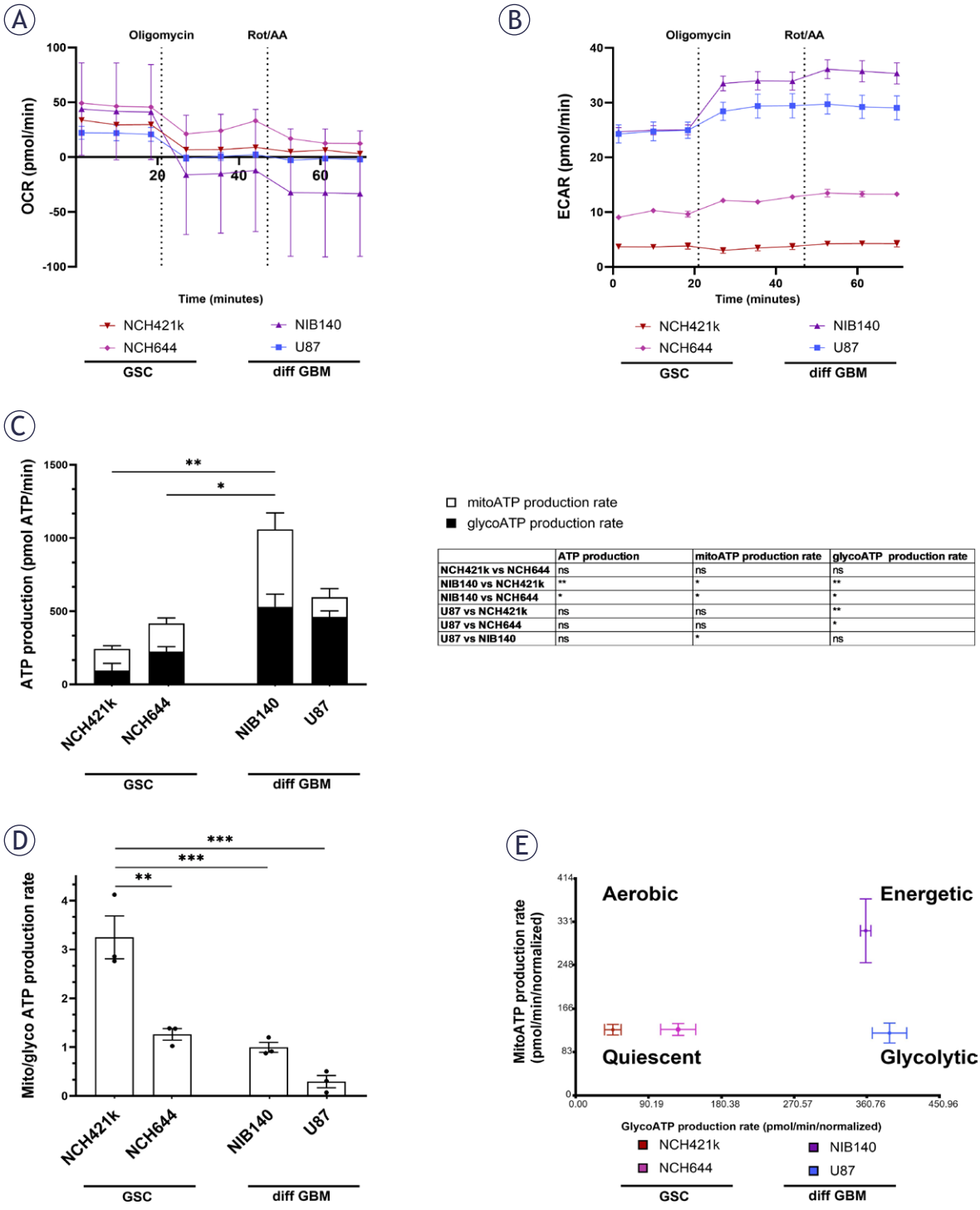

	ATP production	mitoATP production rate	glycoATP production rate
NCH421k vs NCH644	ns	ns	ns
NIB140 vs NCH421k	**	*	**
NIB140 vs NCH644	*	*	*
U87 vs NCH421k	ns	ns	**
U87 vs NCH644	ns	ns	*
U87 vs NIB140	ns	*	ns

FIGURE 6. Metabolic profiles of GSCs and differentiated GBM cells as determined by extracellular flux analysis and XF Real-time ATP Rate Assay Kit (Seahorse, Agilent). **(A, B)** Representative kinetic graphs of oxygen consumption rate (OCR) and extracellular acidification rate (ECAR) in response to oligomycin and rotenone/antimycin A (Rot/AA) are shown. **(C)** Mitochondrial (mito) and glycolytic (glyco) ATP production rate in cells with respective statistics are shown in the table. Statistically significant differences in ATP production are marked directly on the graph. **(D)** Ratio between mito ATP and glyco ATP production rates in cells. **(E)** Metabolic profiles of cells that can be aerobic, energetic, quiescent and glycolytic. Values are shown as means ± SD **(A, B)** or SEM **(C-E)**. Experiments were performed in 3 independent repeats (n = 3). Statistics were performed using Tukey's multiple comparisons test.

ATP = adenosine triphosphate; diff GBM = differentiated glioblastoma cell; GSC = glioblastoma stem-like cell; SEM = standard error of the mean; XF = extracellular flux; * $p < 0.05$; ** $p < 0.01$; *** $p < 0.001$

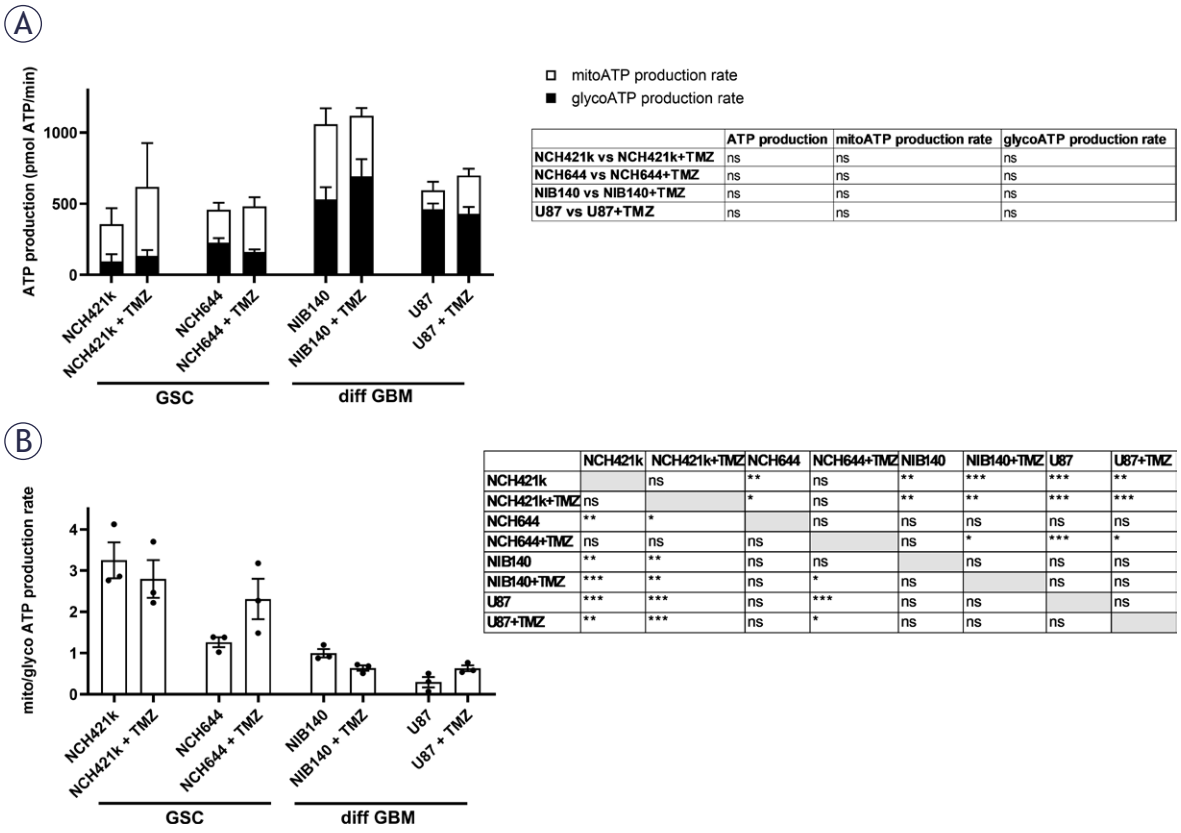

	ATP production	mitoATP production rate	glycoATP production rate
NCH421k vs NCH421k+TMZ	ns	ns	ns
NCH644 vs NCH644+TMZ	ns	ns	ns
NIB140 vs NIB140+TMZ	ns	ns	ns
U87 vs U87+TMZ	ns	ns	ns

	NCH421k	NCH421k+TMZ	NCH644	NCH644+TMZ	NIB140	NIB140+TMZ	U87	U87+TMZ
NCH421k		ns	**	ns	**	***	***	**
NCH421k+TMZ	ns		*	ns	**	**	***	***
NCH644	**	*		ns	ns	ns	ns	ns
NCH644+TMZ	ns	ns	ns		ns	*	***	*
NIB140	**	**	ns	ns		ns	ns	ns
NIB140+TMZ	***	**	ns	*	ns		ns	ns
U87	***	***	ns	***	ns	ns		ns
U87+TMZ	**	***	ns	*	ns	ns	ns	

FIGURE 7. Metabolic profiles and their differences after treatment with 100 μM TMZ in GSCs and differentiated GBM cells and determined by extracellular flux analysis and XF Real-time ATP Rate Assay Kit (Seahorse, Agilent). **(A)** Changes in ATP production, glycolytic (glyco) ATP and mitochondrial (mito) ATP production rate after treatment with TMZ were not detected. **(B)** Differences in ratio between mito and glyco ATP production rates after treatment with TMZ. Values are shown as means ± SEM. Experiments were performed in 3 independent repeats (n = 3). Unpaired t-test was performed to compare statistical difference between control and treated samples within each cell line **(A)**. Tukey's multiple comparisons test was used to compare all conditions after treatment with TMZ **(B)**.

ATP = adenosine triphosphate; SEM = standard error of the mean; TMZ = temozolomide; XF = extracellular flux; * $p < 0.05$, ** $p < 0.01$, *** $p < 0.001$

severe stress that induce apoptosis.[24,49,50] Similar to our findings on mitochondria networks in GSCs, it has been shown that mitochondria in GBM cells are connected via inter-mitochondrial junctions for intracellular (or intermitochondrial) communication. Microtubule-dependent mitochondrial nanotunnel-like bridges has been observed in GBM cells and not in non-tumorous astrocytes.[51] These different morphologies of mitochondrial networks in cancer stem cells reflect the differences in tumor microenvironment in which they reside, and the different energetic states related to their differentiation with more metabolically quiescent cells favoring fused mitochondria and OXPHOS.[16,26,52] In GBM, the heterogeneity of cell types is reflected in the heterogeneity of their metabolic profiles.[53] The results of our current study are in line with previous reports.[5,20]

Observed differences in metabolic profiles between GSCs and differentiated GBM cells were also evident in the ultrastructure of mitochondria, particularly in the morphology of cristae. GSCs contained structurally intact mitochondria. Most of GSCs contained electron-dense mitochondria with narrow cristae corresponding with high OXPHOS activity. In a smaller subset of GSCs, the mitochondria were electron-dense with dilated cristae corresponding with reduced OXPHOS activity. In contrast, the differentiated GBM cells contained mitochondria with varying ultrastructural features, with the two most common types being electron-dense mitochondria with dilated cristae,

which corresponded with reduced OXPHOS activity and the electron-lucent swollen mitochondria with reduced cristae, which associated with impaired OXPHOS activity. Previous reports on brain tumor cell ultrastructure, including GBM cells, also describe electron-dense mitochondria with dilated cristae and electron-lucent swollen mitochondria.[30,31,54] The electron-lucent swollen mitochondria with reduced cristae generally associate with the mitochondrial damage due to Ca^{2+} overload and excessive ROS production[55-57] and have impaired OXPHOS activity.[15,58]

Two important factors that affect the functionality and structural organization of mitochondria are mitochondrial DNA (mtDNA) mutations[59] and the mitochondrial epigenetic regulation.[60] Some mtDNA mutations appear to be important driver mutations in cancer.[61] The mutations in mtDNA are known to be reflected in ultrastructural changes and damage in mitochondria, often in the form of electron lucent swollen mitochondria with reduced and onion-shaped cristae.[62] The epigenetic regulation of mitochondria is primarily mediated by changes in the expression levels of nuclear-encoded mitochondrial genes due to methylation of nuclear DNA and post-translational modifications of histones, and certain mitochondrial metabolites serve as substrates in these processes. The epigenetic regulation of mitochondria is known to play important roles in certain types of cancer.[63] The effects of epigenetics on mitochondrial ultrastructure are not well understood. It has been shown that during the differentiation of neuroprogenitor cells, the acetylation in promoter regions of numerous nuclear DNA-encoded genes, including those involved in metabolic processes and mitochondrial homeostasis, promotes biogenesis of mitochondria and ultrastructural changes, including the elongation of mitochondria and cristae remodeling toward tightly stacked and narrow cristae.[64] The mtDNA mutations and the epigenetic regulation of mitochondria in cells of glioblastoma are two research fields that require further investigations and may provide important insights into the GBM therapeutic resistance and the effects of different treatment regimens on the mitochondrial structure and function of GSCs.

Another interesting observation in our investigation is the presence of cristae that are oriented along the longitudinal axis of the mitochondria. This was particularly prominent in GSCs, where nearly all mitochondria exhibited this orientation of cristae. The important regulators of cristae shape are the mitochondrial contact sites and cristae-organizing system (MICOS) complex, ATP synthase complex, optic atrophy 1 (OPA1) protein and lipid composition of the inner mitochondrial membrane.[50,65] In yeast, mutations in genes that encode certain subunits of ATP synthase and components of the MICOS complex result in mitochondrial cristae oriented along the long axis of mitochondria.[66-68] Thus, reduced or even absent amounts of longitudinal oriented cristae in differentiated GBM cell mitochondria may well indicate that the GBM cells exhibit defects in their ATP synthase or MICOS complex.

The observed high mitochondrial content, intact ultrastructural integrity of mitochondria and high ratio between mitochondrial and glycolytic ATP production in GSCs are in agreement with the findings of previous studies, which employed various metabolic assays and have shown that the GSC are less glycolytic than the differentiated GBM cells.[5,17,19] The GSCs are probably capable of surviving in hypoxic microenvironment due to their relatively quiescent state[6,16,19], which requires a relatively low production of ATP. Dilated cristae observed in mitochondria of differentiated GBM cells are associated with increased ROS production due to the less effective electron transport chain.[69] The increased production of ROS is known to induce certain signalling pathways that increase proliferation and survival of cancer cells[14,17,21,70] and are thus crucial in tumorigenesis. The relatively low mitochondrial content, the fragmented shape of the mitochondrial network and the presence of swollen mitochondria indicate that the differentiated GBM are heavily dependent on glycolysis. It is known that numerous cancer cells rely on glycolysis even in the presence of oxygen due to defective mitochondria.[13-15] The glycolysis provides highly proliferative cancer cells with high ATP production under low oxygen conditions. Besides this, it supplies the precursors for anabolic pathways and abundant NADPH for reductive biosynthetic reactions and antioxidant defenses.[6,21,22,71]

Our results indicate that treatment with chemotherapeutic TMZ that is used in standard treatment procedures for GBM patients induces ultrastructural mitochondrial damage in the differentiated GBM cells but has less effect on the ultrastructure of mitochondria in GSCs. However, the observed ultrastructural mitochondrial damage in the differentiated GBM cells after TMZ treatment is not reflected in the metabolic profile or cell viability. TMZ is a DNA alkylating agent. The DNA damage caused by the TMZ has been shown to induce increased ROS production in mitochon-

dria which contributes to the apoptosis of susceptible GBM cells.[72,73] Apoptosis is in a large part mediated by mitochondria, including the increased ROS generation in mitochondria, increased mitochondrial membrane permeability and finally the structural damage of mitochondria.[74,75] The mitochondria thus have a critical role in GBM resistance to TMZ treatment.[76] It has been shown that the TMZ-resistant GBM cells reorganize the electron transport chain in their mitochondria towards more efficient mitochondrial coupling and decreased ROS production.[77,78] This may well explain the decreased ultrastructural mitochondrial damage in GSCs in comparison to the differentiated GBM cells observed in our study after TMZ treatment.

Limitations of the present study are related to the limited number of GBM cell lines since GBM is a heterogeneous tumor on the genetic and cellular levels. We are aware that the U87 cell line was misidentified in the past and does not fully recapitulate GBM biology.[79] Therefore, further experiments will focus on a large cohort of primary GBM cell cultures from tumor biopsies that will be monitored for mitochondria structure and function. To gain mechanistically insights into the role of mitochondria in TMZ treatment resistance, TMZ treatment experiments in complex models with heterotypic cellular interactions, such as co-cultures and organoids, where mitochondria transfer occurs, will be designed. Screening of mitochondria-associated genes and proteins involved in mitochondrial-driven TMZ resistance will be performed using gene loss or gain of function experiments and blockers of signalling pathways in cell cultures.

Conclusions

Taken together, we showed differences in mitochondria ultrastructure and cellular metabolism between stem-like GSCs and differentiated GBM cells in normal conditions and upon chemotherapy. TMZ treatment induced ultrastructural mitochondrial damage in differentiated GBM cells and had less effect on mitochondria in GSCs, indicating that the mitochondria play an important role in GSC resistance to TMZ treatment. Although further studies are required to fully understand GBM therapeutic resistance and the effects of different treatment regimens on the mitochondrial structure and function of GSCs, this study establishes a foundation for a deeper understanding of the metabolic heterogeneity of glioblastoma cells, including both stem and differentiated cells, and their roles in therapy response and resistance.

Availability of data and materials

All data generated or analysed during this study are included in this published paper and its Supplementary File. The datasets generated and analysed during the current study are also available from the corresponding author upon reasonable request.

Authors' contributions

Conceptualization: UB, MN, MV, CJFVN and BB; Data curation: UB, MN, KFT, MV and BB; Formal analysis: UB, MN, KFT, MV and BB; Funding acquisition: MN, KFT, MV, CJFVN and BB; Investigation and Methodology: UB, MN, SKG, KFT, MV, CJFVN and BB; Project administration: MN, KFT, CJFVN and BB; Resources: UB, MN, KFT, MV, CJFVN and BB; Supervision: UB, MN, KFT, MV, CJFVN and BB; Visualization: UB, SKG, MV, CJFVN and BB; Writing – original draft: UB, MN, MV, CJFVN and BB; Writing – review and editing: UB, MN, SKG, KFT, MV, CJFVN and BB.

Acknowledgments and funding

We would like to thank Dhaval Patel from the Health Science Center at the Texas Tech University, Amarillo, USA, for technical assistance with Seahorse experiments.

This work was supported by the Slovenian Research and Innovation Agency (ARIS) grants (P1-0245 (B.B., M.N.), J3-4504 (M.N.), BI-US/22-24-007 (B.B), J3-2526 (C.J.F.V.N.), BI-US/24-26-022 (M.N.), N3-0394 (B.B.), NC-25002 (B.B.), Young Researcher grant (S.K.G.; 59639), University Infrastructural Centre "Microscopy of Biological Samples" at the Biotechnical Faculty, University of Ljubljana (M.V.), Texas Tech University start-up (to K.F.T.), Cancer Prevention and Research Institute of Texas Scholar Award RR200059 (to K.F.T.), the Foundation for Prader–Willi Syndrome Research Grant 22-0321 and 23-0447 (to K.F.T.), Fulbright Fellowship Scholar (B.B.) and European Union's Horizon project Twinning for excellence to strategically advance research in carcinogenesis and cancer (CutCancer; 101079113) (B.B. and M.N.) and European Union's

Horizon project Cancer Mission SPatial Analysis of Cancer Evolution in the Tumour Immune MicroEnvironment (SPACETIME; 101136552) (B.B. and M.N.).

References

1. van Solinge TS, Nieland L, Chiocca EA, Broekman MLD. Advances in local therapy for glioblastoma - taking the fight to the tumour. *Nat Rev Neurol* 2022; **18:** 221-36. doi:10.1038/S41582-022-00621-0
2. Stupp R, Hegi ME, Mason WP, van den Bent MJ, Taphoorn MJ, Janzer RC, et al. Effects of radiotherapy with concomitant and adjuvant temozolomide versus radiotherapy alone on survival in glioblastoma in a randomised phase III study: 5-year analysis of the EORTC-NCIC trial. *Lancet Oncol* 2009; **10:** 459-66. doi: 10.1016/S1470-2045(09)70025-7
3. Neftel C, Laffy J, Filbin MG, Hara T, Shore ME, Rahme GJ, et al. An integrative model of cellular states, plasticity, and genetics for glioblastoma. *Cell* 2019; **178:** 835-49.e21. doi: 10.1016/J.CELL.2019.06.024
4. Prager BC, Bhargava S, Mahadev V, Hubert CG, Rich JN. Glioblastoma stem cells: driving resilience through chaos. *Trends Cancer* 2020; **6:** 223-35. doi: 10.1016/j.trecan.2020.01.009
5. Vlashi E, Lagadec C, Vergnes L, Matsutani T, Masui K, Poulou M, et al. Metabolic state of glioma stem cells and nontumorigenic cells. *Proc Natl Acad Sci U S A* 2011; **108:** 16062-7. doi: 10.1073/PNAS.1106704108
6. Badr CE, Silver DJ, Siebzehnrubl FA, Deleyrolle LP. Metabolic heterogeneity and adaptability in brain tumors. *Cell Mol Life Sci* 2020; **77:** 5101-19. doi: 10.1007/S00018-020-03569-W
7. Hira VVV, Breznik B, Vittori M, Loncq de Jong A, Mlakar J, Oostra RJ, et al. Similarities between stem cell niches in glioblastoma and bone marrow: rays of hope for novel treatment strategies. *J Histochem Cytochem* 2020; **68:** 33-57. doi: 10.1369/0022155419878416
8. Hira VVV, Aderetti DA, van Noorden CJF. Glioma stem cell niches in human glioblastoma are periarteriolar. *J Histochem Cytochem* 2018; **66:** 349-58. doi: 10.1369/0022155417752676
9. Schiffer D, Annovazzi L, Casalone C, Corona C, Mellai M. Glioblastoma: microenvironment and niche concept. *Cancers (Basel)* 2019; **11:** 5. doi: 10.3390/cancers11010005
10. Li P, Zhou C, Xu L, Xiao H. Hypoxia enhances stemness of cancer stem cells in glioblastoma: an in vitro study. *Int J Med Sci* 2013; **10:** 399-407. doi: 10.7150/IJMS.5407
11. Heddleston JM, Li Z, McLendon RE, Hjelmeland AB, Rich JN. The hypoxic microenvironment maintains glioblastoma stem cells and promotes reprogramming towards a cancer stem cell phenotype. *Cell Cycle* 2009; **8:** 3274-84. doi: 10.4161/CC.8.20.9701
12. Iranmanesh Y, Jiang B, Favour OC, Dou Z, Wu J, Li J, et al. Mitochondria's role in the maintenance of cancer stem cells in glioblastoma. *Front Oncol* 2021; **11:** 582694. doi: 10.3389/FONC.2021.582694
13. Carew JS, Huang P. Mitochondrial defects in cancer. *Mol Cancer* 2002; **1:** 9. doi: 10.1186/1476-4598-1-9
14. Wallace DC. Mitochondria and cancer: Warburg addressed. *Cold Spring Harb Symp Quant Biol* 2005;**70:** 363-74. doi: 10.1101/SQB.2005.70.035
15. Seyfried TN, Flores RE, Poff AM, D'Agostino DP. Cancer as a metabolic disease: implications for novel therapeutics. *Carcinogenesis* 2014; **35:** 515-27. doi: 10.1093/CARCIN/BGT480
16. Peiris-Pagès M, Martinez-Outschoorn UE, Pestell RG, Sotgia F, Lisanti MP. Cancer stem cell metabolism. *Breast Cancer Res* 2016; **18: 55.** doi: 10.1186/S13058-016-0712-6
17. Strickland M, Stoll EA. Metabolic reprogramming in glioma. *Front Cell Dev Biol* 2017; **5:** 43. doi: 10.3389/FCELL.2017.00043
18. van Noorden CJF, Yetkin-Arik B, Serrano Martinez P, Bakker N, van Breest Smallenburg ME, Schlingemann RO, et al. New insights in ATP synthesis as therapeutic target in cancer and angiogenic ocular diseases. *J Histochem Cytochem* 2024; **72:** 329-52. doi: 10.1369/00221554241249515
19. van Noorden CJF, Breznik B, Novak M, van Dijck AJ, Tanan S, Vittori M, et al. Cell biology meets cell metabolism: energy production is similar in stem cells and in cancer stem cells in brain and bone marrow. *J Histochem Cytochem* 2022; **70:** 29-51. doi: 10.1369/00221554211054585
20. van Noorden CJF, Hira VVV, van Dijck AJ, Novak M, Breznik B, Molenaar RJ. Energy metabolism in IDH1 wild-type and IDH1-mutated glioblastoma stem cells: a novel target for therapy? *Cells* 2021; **10:** 1-16. doi: 10.3390/CELLS10030705
21. Wallace DC. Mitochondria and cancer. *Nat Rev Cancer* 2012; **12:** 685-98. doi: 10.1038/NRC3365
22. Vyas S, Zaganjor E, Haigis MC. Mitochondria and cancer. *Cell* 2016; **166:** 555-66. doi: 10.1016/J.CELL.2016.07.002
23. Ordys BB, Launay S, Deighton RF, McCulloch J, Whittle IR. The role of mitochondria in glioma pathophysiology. *Mol Neurobiol* 2010; **42:** 64-75. doi: 10.1007/S12035-010-8133-5
24. Wai T, Langer T. Mitochondrial dynamics and metabolic regulation. *Trends Endocrinol Metab* 2016; **27:** 105-17. doi: 10.1016/J.TEM.2015.12.001
25. Senft D, Ronai ZA. Regulators of mitochondrial dynamics in cancer. *Curr Opin Cell Biol* 2016; **39:** 43-52. doi: 10.1016/J.CEB.2016.02.001
26. Trotta AP, Chipuk JE. Mitochondrial dynamics as regulators of cancer biology. *Cell Mol Life Sci* 2017; **74:** 1999-2017. doi: 10.1007/S00018-016-2451-3
27. Maycotte P, Marín-Hernández A, Goyri-Aguirre M, Anaya-Ruiz M, Reyes-Leyva J, Cortés-Hernández P. Mitochondrial dynamics and cancer. *Tumour Biol* 2017; **39:** 1010428317698391. doi: 10.1177/1010428317698391
28. García-Heredia JM, Carnero A. Role of mitochondria in cancer stem cell resistance. *Cells* 2020; **9:** 1693. doi: 10.3390/CELLS9071693
29. De Luca A, Fiorillo M, Peiris-Pagès M, Ozsvari B, Smith DL, Sanchez-Alvarez R, et al. Mitochondrial biogenesis is required for the anchorage-independent survival and propagation of stem-like cancer cells. *Oncotarget* 2015; **6:** 14777-95. doi: 10.18632/ONCOTARGET.4401
30. Arismendi-Morillo GJ, Castellano-Ramirez A V. Ultrastructural mitochondrial pathology in human astrocytic tumors: potentials implications pro-therapeutics strategies. *J Electron Microsc* 2008; **57:** 33-9. doi: 10.1093/JMICRO/DFM038
31. Arismendi-Morillo G. Electron microscopy morphology of the mitochondrial network in gliomas and their vascular microenvironment. *Biochim Biophys Acta* 2011; **1807:** 602-8. doi: 10.1016/J.BBABIO.2010.11.001
32. Scheithauer BW, Bruner JM. The ultrastructural spectrum of astrocytic neoplasms. *Ultrastruct Pathol* 1987; **11:** 535-81. doi: 10.3109/01913128709048447
33. Liberski PP, Kordek R. Ultrastructural pathology of glial brain tumors revisited: a review. *Ultrastruct Pathol* 1997; **21:** 1-31. doi: 10.3109/01913129709023244
34. Sipe, JC, Herman, MM RL. Electron microscopic observations on human glioblastomas and astrocytomas maintained in organ culture systems. *Am J Pathol* 1973; **73:** 589-606.
35. Khurshed M, Aarnoudse N, Hulsbos R, Hira VVV, Van Laarhoven HWM, Wilmink JW, et al. IDH1-mutant cancer cells are sensitive to cisplatin and an IDH1-mutant inhibitor counteracts this sensitivity. *FASEB J* 2018; **32:** 6344-52. doi: 10.1096/FJ.201800547R
36. Verberk SGS, de Goede KE, Gorki FS, van Dierendonck XAMH, Argüello RJ, Van den Bossche J. An integrated toolbox to profile macrophage immunometabolism. *Cell Rep Methods* 2022; **2:** 100192. doi: 10.1016/J.CRMETH.2022.100192
37. Breznik B, Ko MW, Tse C, Chen PC, Senjor E, Majc B, et al. Infiltrating natural killer cells bind, lyse and increase chemotherapy efficacy in glioblastoma stem-like tumorospheres. *Commun Biol* 2022; **5:** 436. doi: 10.1038/S42003-022-03402-Z
38. Porčnik A, Novak M, Breznik B, Majc B, Hrastar B, Šamec N, et al. TRIM28 selective nanobody reduces glioblastoma stem cell invasion. *Molecules* 2021; **26:** 5141. doi: 10.3390/MOLECULES26175141
39. Majc B, Habič A, Novak M, Rotter A, Porčnik A, Mlakar J, et al. Upregulation of cathepsin X in glioblastoma: Interplay with γ-enolase and the effects of selective cathepsin X inhibitors. *Int J Mol Sci* 2022; **23:** 1784. doi: 10.3390/IJMS23031784

40. Novak M, Majc B, Malavolta M, Porčnik A, Mlakar J, Hren M, et al. The Slovenian translational platform GlioBank for brain tumour research: identification of molecular signatures of glioblastoma progression. *Neurooncol Adv* 2025; **7:** vdaf015. doi: 10.1093/NOAJNL/VDAF015

41. Majc B, Habič A, Malavolta M, Vittori M, Porčnik A, Bošnjak R, et al. Patient-derived tumor organoids mimic treatment-induced DNA damage response in glioblastoma. *iScience* 2024; **27:** 110604. doi: 10.1016/j.isci.2024.110604

42. Breznik B, Motaln H, Vittori M, Rotter A, Turnšek TL. Mesenchymal stem cells differentially affect the invasion of distinct glioblastoma cell lines. *Oncotarget* 2017; **8:** 25482-99. doi: 10.18632/oncotarget.16041

43. Schindelin J, Arganda-Carreras I, Frise E, Kaynig V, Longair M, Pietzsch T, et al. Fiji: an open-source platform for biological-image analysis. *Nat Methods* 2012; **9:** 676-82. doi: 10.1038/NMETH.2019

44. Cardona A, Saalfeld S, Schindelin J, Arganda-Carreras I, Preibisch S, Longair M, et al. TrakEM2 software for neural circuit reconstruction. *PLoS One* 2012; **7:** e38011. doi: 10.1371/JOURNAL.PONE.0038011

45. Mao P, Joshi K, Li J, Kim SH, Li P, Santana-Santos L, et al. Mesenchymal glioma stem cells are maintained by activated glycolytic metabolism involving aldehyde dehydrogenase 1A3. *Proc Natl Acad Sci U S A* 2013; **110:** 8644-9. doi: 10.1073/PNAS.1221478110

46. Ntafoulis I, Kleijn A, Ju J, Jimenez-Cowell K, Fabro F, Klein M, et al. Ex vivo drug sensitivity screening predicts response to temozolomide in glioblastoma patients and identifies candidate biomarkers. *Br J Cancer* 2023; **129:** 1327-38. doi: 10.1038/S41416-023-02402-Y,

47. Lah TT, Novak M, Breznik B. Brain malignancies: glioblastoma and brain metastases. *Semin Cancer Biol* 2020; **60:** 262-73. doi: 10.1016/J.SEMCANCER.2019.10.010

48. Spehalski EI, Lee JA, Peters C, Tofilon P, Camphausen K. The quiescent metabolic phenotype of glioma stem cells. *J Proteomics Bioinform* 2019; **12:** 96-103. doi: 10.35248/0974-276X.19.12.502

49. Galloway CA, Lee H, Yoon Y. Mitochondrial morphology-emerging role in bioenergetics. *Free Radic Biol Med* 2012; **53:** 2218-28. doi: 10.1016/J.FREERADBIOMED.2012.09.035

50. Glancy B, Kim Y, Katti P, Willingham TB. The functional impact of mitochondrial structure across subcellular scales. *Front Physiol* 2020; **11:** 541040. doi: 10.3389/FPHYS.2020.541040

51. Wang R, Lei H, Wang H, Qi L, Liu Y, Liu Y, et al. Dysregulated inter-mitochondrial crosstalk in glioblastoma cells revealed by in situ cryo-electron tomography. *Proc Natl Acad Sci U S A* 2024; **121:** e2311160121. doi: 10.1073/PNAS.2311160121

52. Peixoto J, Lima J. Metabolic traits of cancer stem cells. *Dis Model Mech* 2018; **11:** dmm033464. doi: 10.1242/DMM.033464

53. Duraj T, García-romero N, Carrión-navarro J, Madurga R, de Mendivil AO, Prat-acin R, et al. Beyond the Warburg effect: oxidative and glycolytic phenotypes coexist within the metabolic heterogeneity of glioblastoma. *Cells* 2021; **10:** 1-23. doi: 10.3390/CELLS10020202

54. Arismendi-Morillo G, Castellano-Ramírez A, Seyfried TN. Ultrastructural characterization of the mitochondria-associated membranes abnormalities in human astrocytomas: functional and therapeutics implications. *Ultrastruct Pathol* 2017; **41:** 234-44. doi: 10.1080/01913123.2017.1300618

55. Galindo MF, Jordán J, González-García C, Ceña V. Reactive oxygen species induce swelling and cytochrome c release but not transmembrane depolarization in isolated rat brain mitochondria. *Br J Pharmacol* 2003; **139:** 797-804. doi: 10.1038/SJ.BJP.0705309

56. Peng TI, Jou MJ. Mitochondrial swelling and generation of reactive oxygen species induced by photoirradiation are heterogeneously distributed. *Ann N Y Acad Sci* 2004; **1011:** 112-22. doi: 10.1007/978-3-662-41088-2_12

57. Kaasik A, Safiulina D, Zharkovsky A, Veksler V. Regulation of mitochondrial matrix volume. *Am J Physiol Cell Physiol* 2007; **292:** C157-63. doi: 10.1152/AJPCELL.00272.2006

58. Moscheni C, Malucelli E, Castiglioni S, Procopio A, De Palma C, Sorrentino A, et al. 3D quantitative and ultrastructural analysis of mitochondria in a model of doxorubicin sensitive and resistant human colon carcinoma cells. *Cancers* 2019; **11:** 1254. doi: 10.3390/CANCERS11091254

59. Szczepanowska J, Malinska D, Wieckowski MR, Duszynski J. Effect of mtDNA point mutations on cellular bioenergetics. *Biochim Biophys Acta* 2012; **1817:** 1740-6. doi: 10.1016/j.bbabio.2012.02.028

60. Zhang C, Meng Y, Han J. Emerging roles of mitochondrial functions and epigenetic changes in the modulation of stem cell fate. *Cell Mol Life Sci* 2024; **81:** 26. doi: 10.1007/S00018-023-05070-6

61. Smith ALM, Whitehall JC, Greaves LC. Mitochondrial DNA mutations in ageing and cancer. *Mol Oncol* 2022; **16:** 3276-94. doi: 10.1002/1878-0261.13291

62. Fu Y, Sacco O, DeBitetto E, Kanshin E, Ueberheide B, Sfeir A. Mitochondrial DNA breaks activate an integrated stress response to reestablish homeostasis. *Mol Cell* 2023; **83:** 3740-53.e9. doi: 10.1016/j.molcel.2023.09.026

63. Chatterjee D, Das P, Chakrabarti O. Mitochondrial epigenetics regulating inflammation in cancer and aging. *Front Cell Dev Biol* 2022; **10:** 929708. doi: 10.3389/FCELL.2022.929708

64. Uittenbogaard M, Brantner CA, Chiaramello A. Epigenetic modifiers promote mitochondrial biogenesis and oxidative metabolism leading to enhanced differentiation of neuroprogenitor cells. *Cell Death Dis* 2018; **9:** 360. doi: 10.1038/S41419-018-0396-1

65. Kondadi AK, Anand R, Reichert AS. Cristae membrane dynamics - a paradigm change. *Trends Cell Biol* 2020; **30:** 923-36. doi: 10.1016/J.TCB.2020.08.008

66. Paumard P, Vaillier J, Coulary B, Schaeffer J, Soubannier V, Mueller DM, et al. The ATP synthase is involved in generating mitochondrial cristae morphology. *EMBO J* 2002; **21:** 221-30. doi: 10.1093/EMBOJ/21.3.221

67. Stephan T, Brüser C, Deckers M, Steyer AM, Balzarotti F, Barbot M, et al. MICOS assembly controls mitochondrial inner membrane remodeling and crista junction redistribution to mediate cristae formation. *EMBO J* 2020; **39:** e104105. doi: 10.15252/EMBJ.2019104105

68. Klecker T, Westermann B. Pathways shaping the mitochondrial inner membrane. *Open Biol* 2021; **11:** 210238. doi: 10.1098/RSOB.210238

69. Plecitá-Hlavatá L, Ježek P. Integration of superoxide formation and cristae morphology for mitochondrial redox signaling. *Int J Biochem Cell Biol* 2016; **80:** 31-50. doi: 10.1016/J.BIOCEL.2016.09.010

70. Zick M, Rabl R, Reichert AS. Cristae formation-linking ultrastructure and function of mitochondria. *Biochim Biophys Acta* 2009; **1793:** 5-19. doi: 10.1016/J.BBAMCR.2008.06.013

71. Vaupel P, Multhoff G. Revisiting the Warburg effect: historical dogma versus current understanding. *J Physiol* 2021; **599:** 1745-57. doi: 10.1113/JP278810

72. Campos-Sandoval JA, Gómez-García MC, Santos-Jiménez J de los, Matés JM, Alonso FJ, Márquez J. Antioxidant responses related to temozolomide resistance in glioblastoma. *Neurochem Int* 2021; **149:** 105136. doi: 10.1016/J.NEUINT.2021.105136

73. Zhang W Bin, Wang Z, Shu F, Jin YH, Liu HY, Wang QJ, et al. Activation of AMP-activated protein kinase by temozolomide contributes to apoptosis in glioblastoma cells via p53 activation and mTORC1 inhibition. *J Biol Chem* 2010; **285:** 40461-71. doi: 10.1074/JBC.M110.164046

74. Gaiaschi L, Favaron C, Casali C, Gola F, De Luca F, Ravera M, et al. Study on the activation of cell death mechanisms: in search of new therapeutic targets in glioblastoma multiforme. *Apoptosis* 2023; **28:** 1241-57. doi: 10.1007/S10495-023-01857-X

75. Fleury C, Mignotte B, Vayssière JL. Mitochondrial reactive oxygen species in cell death signaling. *Biochimie* 2002; **84:** 131-41. doi: 10.1016/S0300-9084(02)01369-X

76. Li HY, Feng YH, Lin CL, Hsu TI. Mitochondrial mechanisms in temozolomide resistance: unraveling the complex interplay and therapeutic strategies in glioblastoma. *Mitochondrion* 2024; **75:** 101836. doi: 10.1016/J.MITO.2023.101836

77. Oliva CR, Nozell SE, Diers A, McClugage SG, Sarkaria JN, Markert JM, et al. Acquisition of temozolomide chemoresistance in gliomas leads to remodeling of mitochondrial electron transport chain. *J Biol Chem* 2010; **285:** 39759-67. doi: 10.1074/JBC.M110.147504

78. Oliva CR, Moellering DR, Gillespie GY, Griguer CE. Acquisition of chemoresistance in gliomas is associated with increased mitochondrial coupling and decreased ROS production. *PLoS One* 2011; **6:** e24665. doi: 10.1371/JOURNAL.PONE.0024665

79. Dolgin E. Venerable brain-cancer cell line faces identity crisis. *Nature* 2016; **537:** 149-50. doi: 10.1038/NATURE.2016.20515,

80 Sterne JA, Hernan MA, Reeves BC, Savovic J, Berkman ND, Viswanathan M, et al. ROBINS-I: a tool for assessing risk of bias in non-randomised studies of interventions. *BMJ* 2016; **355:** i4919. doi: 10.1136/bmj.i4919

research article

Human papillomavirus-related oropharyngeal squamous cell carcinoma exhibits enhanced radiosensitivity despite limited activation of cytosolic DNA sensing pathways and innate immune responses

Kristina Levpuscek[1,2], Tanja Jesenko[1,2], Tilen Komel[1,3], Simona Kranjc Brezar[1,2], Gregor Sersa[1,4], Maja Cemazar[1,5], Primoz Strojan[2,6]

[1] Department of Experimental Oncology, Institute of Oncology Ljubljana, Ljubljana, Slovenia
[2] Faculty of Medicine, University of Ljubljana, Ljubljana, Slovenia
[3] Faculty of Mathematics, Natural Sciences and Information Technologies, University of Primorska, Koper, Slovenia
[4] Faculty of Health Sciences, University of Ljubljana, Ljubljana, Slovenia
[5] Faculty of Health Sciences, University of Primorska, Koper, Slovenia
[6] Department of Radiation Oncology, Institute of Oncology, Ljubljana, Slovenia

Radiol Oncol 2025; 59(4): 566-578.

Received 27 August 2025
Accepted 5 September 2025

Correspondence to: Prof Primož Strojan, M.D., Ph.D., Department of Radiation Oncology, Institute of Oncology, Zaloška 2, Si-1000 Ljubljana, Slovenia. E-mail: pstrojan@onko-i.si

Disclosure: No potential conflicts of interest were disclosed.

Background. Pharyngeal squamous cell carcinoma (PSCC) is a significant health concern, with human papillomavirus 16 (HPV16) playing a key role in the etiology of oropharyngeal squamous cell carcinoma (OPSCC). HPV16-related OPSCC exhibits enhanced radiosensitivity compared to HPV16-unrelated PSCC, yet the underlying mechanisms remain poorly understood. As HPV16 oncoproteins E6 and E7 are known to interfere with innate immune signaling, we investigated how modulation of cytosolic DNA sensing pathways and innate immune responses changes after irradiation (IR) and whether this contributes to enhanced radiosensitivity in HPV16-related OPSCC.

Materials and methods. Using HPV16-related and -unrelated PSCC models, we examined baseline expression levels of DNA sensors and cytokines and assessed the effects of IR on double-stranded DNA (dsDNA) accumulation, activation of cytosolic DNA sensors, cytokines, and immune cell infiltration both *in vitro* and *in vivo*. Analyses were performed using real-time quantitative polymerase chain reaction (RT-qPCR) and immunofluorescent staining.

Results. HPV16-related OPSCC exhibited a distinct baseline expression profile of DNA sensors and cytokines, consistent with suppression of the stimulator of interferon genes (STING) pathway. While IR-induced activation of DNA sensors was dose- and time-dependent across models, HPV16-related OPSCC showed selective activation of cyclic GMP-AMP synthase (cGAS) and STING without significant cytokine upregulation or immune activation. In contrast, HPV16-related and unrelated PSCCs displayed activation of multiple DNA sensors, increased cytokine expression, and enhanced immune cell infiltration following IR.

Conclusions. The key finding was that the involvement of cytosolic DNA sensing pathways and innate immune system do not increase radiosensitivity of HPV16-related OPSCC. In PSCC models, DNA sensor and cytokine expression varied depending on IR dose and fractionation.

Key words: cytosolic DNA sensing pathways; innate immune response; human papillomavirus type 16; pharyngeal squamous cell carcinoma; radiation response

Introduction

Head and neck squamous cell carcinomas (HNSCCs) arise from the mucosal epithelium of the upper aerodigestive tract and represent the seventh most common cancer worldwide, with an estimated 800,000 new cases and 400,000 deaths in 2022.[1] HNSCCs are typically associated with excessive alcohol and tobacco use, while oropharyngeal squamous cell carcinoma (OPSCC) is increasingly linked to infection with human papillomavirus type 16 (HPV16).[2,3] HPV16 belongs to the Papillomaviridae family and is classified as a high-risk oncogenic type.[4] Epidemiological studies have shown a decline in the incidence of HPV16-unrelated HNSCC, whereas HPV16-related OPSCC is on the rise.[5,6] Standard treatments for HNSCCs include surgery, radiotherapy (RT), and chemotherapy. The survival rate has seen modest improvements over the last three decades. Previous studies have shown higher response rates to RT and chemotherapy and consequently improved survival for patients with HPV16-related OPSCC compared to those with HPV16-unrelated tumors.[7-9] However, the molecular and immunological mechanisms underlying this enhanced radiosensitivity remain poorly understood.

The innate immune response to ionizing radiation (IR) is emerging as a critical factor influencing tumor radiosensitivity. IR-induced DNA damage can lead to cytosolic accumulation of double-stranded DNA (dsDNA), which activates the cytosolic DNA sensing pathways such as cyclic GMP-AMP synthase (cGAS). cGAS detects dsDNA and produces cyclic GMP-AMP (cGAMP), a second messenger that binds to and activates the stimulator of interferon genes (STING). This leads to activation of downstream signaling pathways and ultimately the production of type I interferons (IFN-I) and other pro-inflammatory cytokines that drive the innate immune response against damaged or malignant cells. These pathways are also part of the fundamental mechanism of host defense.[10-13]

There is increasing evidence that HPV16 oncoproteins E6 and E7 disrupt host innate immune signaling to facilitate immune evasion and promote carcinogenesis. Studies have shown that these oncoproteins suppress several DNA sensors, including retinoic acid-inducible gene I (RIG-I) and Toll-like receptors (TLRs), and to directly inhibit the cGAS-STING axis in HPV16-related OPSCC.[14,15] This suppression impairs the production of IFN-I, which may enable infected cells to escape immune surveillance. The host immune response is a critical component of antitumor immunity. Therefore, immune dysregulation by HPV16 may significantly influence the efficacy of RT.[16]

In this study, we investigated how the HPV16 oncoproteins E6 and E7 modulate the activation of cytosolic DNA sensing pathways and innate immune response following IR in pharyngeal squamous cell carcinomas (PSCCs) models, and whether this modulation contributes to the enhanced radiosensitivity observed in HPV16-related OPSCC. Specifically, we assessed baseline expression and IR-induced activation of cytosolic DNA sensors, cytokine production, and innate immune cell infiltration in both tumor cells and the tumor microenvironment (TME), to better understand the immune landscape underlying the differential radiosensitivity of HPV16-related OPSCC.

Materials and methods

Cell lines

The *in vitro* experiments were performed with four human PSCC cell lines: HPV16-related OPSCC UPCI:SCC090 (RRID:CVCL_1899; ATCC® CRL-3239™, Manassas, VA, USA), HPV16-unrelated OPSCC UM-SCC-6 (RRID:CVCL_7773; Merck-Millipore, Burlington, MA, USA), HPV16-related hypopharyngeal squamous cell carcinoma (HPSCC) 2A3 (RRID:CVCL_0D71; ATCC® CRL-3212™, ATCC), and HPV16-unrelated HPSCC FaDu (RRID:CVCL_1218; ATCC® HTB-43™, ATCC). All cell lines were cultured at 37°C in a humidified atmosphere containing 5% CO_2 and were used within ten passages. UPCI:SCC090 and UM-SCC-6 cells were maintained in Advanced Dulbecco's Modified Eagle's Medium (ADMEM, Gibco, Thermo Fisher Scientific, Waltham, MA, USA). FaDu cells were cultured in Advanced Minimum Essential Medium (AMEM, Gibco), and 2A3 cells in ADMEM supplemented with 0.2 mg/ml G418 disulfate salt solution (Sigma-Aldrich LLC, St. Louis, MO, USA). All media were supplemented with 5% fetal bovine serum (FBS; Thermo Fisher Scientific), 1% GlutaMAX (Thermo Fisher Scientific), and 1% Penicillin-Streptomycin (Merck). Cells were routinely tested with MycoAlert™ PLUS Mycoplasma Detection Kit (Lonza, Basel, Switzerland). All experiments were performed with mycoplasma-free cells.

Experimental animals and tumor induction

In vivo experiments were performed on 8-week-old female Athymic Nude mice (Charles River, Lecco,

Italy), housed in sterile cages under a 12-hour light/dark cycle with controlled temperature and humidity, and provided water and food ad libitum. All procedures were approved by the Ministry of Agriculture, Forestry and Food of the Republic of Slovenia (permission No. U34401-33/2019/9 and U34401-35/2020/8) in accordance with EU directive 2010/63/EU. Subcutaneous tumors were established by injecting 100 μL of 0.9% NaCl containing 5×10^6 viable UPCI:SCC090 cells, 10×10^6 UM-SCC-6 cells, or 2×10^6 FaDu or 2A3 cells into the dorsal flank of mice. UM-SCC-6 tumor induction was unsuccessful despite attempts with various cell concentrations ($1x10^6$, $3x10^6$ or $10x10^6$) and co-injection with basement membrane matrix (Corning® Matrigel® Matrix, Corning, New York, USA). Once tumors reached a volume of approximately 45-50 mm^3, mice were distributed into different treatment groups.

Irradiation

IR was performed using a Gulmay CP225 X-Ray Generator (Gulmay Medical Ltd., Byfleet, UK) at 200 kV and 9.2 mA, with a dose rate of 1.96 Gy/min. For *in vitro* experiments, cells were IR with 4 Gy, 8 Gy, or a fractionated dose of 3×8 Gy. For *in vivo* studies, tumor-bearing mice were immobilized in custom-designed lead holders with apertures allowing localized tumor IR. Mice received either a single dose of 8 Gy or a fractionated regimen of 3×8 Gy.

Cell viability assay

Post-IR cell viability was evaluated using a resazurin-based assay (PrestoBlue™, Thermo Fisher Scientific). Cells were seeded in 96-well plates (VWR, Radnor, Pennsylvania, US) and allowed to adhere overnight prior to IR. Viability was assessed after four population doublings, accounting for doubling times of 24 h (FaDu, 2A3, UM-SCC-6) and four days (UPCI:SCC090). 10 μl PrestoBlue reagent was added per well, followed by a 1-hour incubation at 37°C in a humidified 5% CO_2 atmosphere. Fluorescence intensity was measured using a microplate reader (GEN-ios, Tecan, Männedorf, Switzerland).

Tumor growth measurement

Mice were distributed in experimental groups of 6 animals: control group, group irradiated with 8 Gy, or 3×8 Gy. Tumors were measured three times per week using a Vernier caliper, and volumes were calculated as $V = a \times b \times c \times \pi/6$ (a, b, c representing tumor diameters). Mice were humanely euthanized when their tumor volumes reached 500 mm^3, a threshold established as a humane endpoint for the Kaplan-Meier survival analysis. Complete response was defined as the absence of detectable tumors for 100 days

Tumor collection

Mice were euthanized 72 hours post-IR alongside their respective control groups. Tumors were excised. One-half of the tumor was fixed in 4% paraformaldehyde for 12 hours, then immersed in 30% sucrose for 24 hours, embedded in Optimal Cutting Temperature (OCT; VWR) compound, and flash-frozen in liquid nitrogen for immunofluorescence analysis. The other half was flash-frozen, pulverized, and stored at −80°C for subsequent RNA extraction.

Real-time quantitative polymerase chain reaction (RT-qPCR)

For the *in vitro* study, cells were seeded in T25 flasks (Corning), allowed to adhere, and then irradiated with 4, 8, or 3×8 Gy, except for the control group, which was also used to determine baseline expression of DNA sensing pathway genes. RNA was extracted at 48- or 72-hours post-IR using the peqGOLD Total RNA Kit (VWR, West Chester, PA, USA), following the manufacturer's instructions. For tumor samples, TRIzol Reagent (Thermo Fischer Scientific) was used for homogenization and extraction, followed by isolation of RNA. SuperScript VILO cDNA Synthesis Kit (Invitrogen, Thermo Fisher Scientific) was used for reverse transcription. RT-qPCR was performed on a QuantStudio 3 Real-Time PCR System (Thermo Fisher Scientific). The samples were prepared using PowerUp SYBR Green Master Mix (Thermo Fisher Scientific) and predesigned primers specific for human or mouse DNA sensors and cytokines (IDT, IA, USA). Mouse-specific primers enabled discrimination of TME components. Relative expression was calculated using the ΔCq method: Cq (gene of interest)- Cq (mean of housekeeping genes). Fold changes were determined using the $2^{-\Delta\Delta Ct}$ method.[17] Non-determined (N.D.) values were defined as Cq > 40. Detailed protocols and primer sequences are listed in Supplementary materials and Supplementary Table S1.

Accumulation of cytosolic dsDNA

Cells were seeded overnight in 12-well chamber slides (Ibidi, Gräfelfing, Germany) and IR with 4, 8, or 3×8 Gy. Controls remained unirradiated. After 48 or 72 hours, cells were stained with antibodies. Immunofluorescence microscopy was performed using an LSM 800 confocal microscope (Carl Zeiss, Oberkochen, Germany), and images were analyzed using Imaris software (Bitplane, Zurich, Switzerland). Antibody details and protocols are provided in Supplementary materials and Supplementary Table S2.

Tumor immunofluorescence staining

Tumor sections were prepared using a Leica CM1850 cryostat (Leica Biosystems, Wetzlar, Germany), mounted on Superfrost Plus glass slides (ThermoFisher Scientific), and stained with antibodies (Supplementary Table S3). Imaging was performed using an LSM 800 confocal microscope (Carl Zeiss), and image analysis was carried out using Imaris (Bitplane) and CellProfiler software (Broad Institute, Cambridge, MA, USA). Antibodies and staining protocols are listed in Supplementary materials and Supplementary Table S3.

Statistical analysis

Statistical analyses and data visualization were performed using GraphPad Prism version 9 (GraphPad Software, San Diego, CA, USA). All *in vitro* experiments were repeated three times unless otherwise stated. *In vivo* experiments were carried out once following the principles of the 3Rs. Data normality was assessed by the Shapiro-Wilk test. A two-tailed Student's t-test and One-way analysis of variance (ANOVA) were used to evaluate the statistical significance between different groups, followed by post hoc test or non-parametric data, the Kruskal-Wallis test with post hoc analysis was used. Kaplan-Meier survival curves were analyzed using a Log-rank test. Statistical significance was defined as $p < 0.05$.

Results

HPV16-related OPSCC exhibits enhanced radiosensitivity

We evaluated the effect of IR on the survival of various cell lines and mice bearing PSCC tumors. Our *in vitro* findings showed that the HPV16-related OPSCC cell line UPCI:SCC090 had a better response to IR than the HPV16-unrelated OPSCC cell line UM-SCC-6 and both HPSCC cell lines. No notable differences in radiosensitivity were detected among the other PSCC lines (Figure 1A). We also examined the effect of IR on survival in mice bearing different PSCC tumors. Mice with UPCI:SCC090 tumors showed significantly better survival after a single dose of 8 Gy compared to the other two models. Notably, this group exhibited one complete response, a phenomenon not observed in the other models. In contrast, no differences in survival were observed following irradiation with 3×8 Gy, as all groups showed high rate

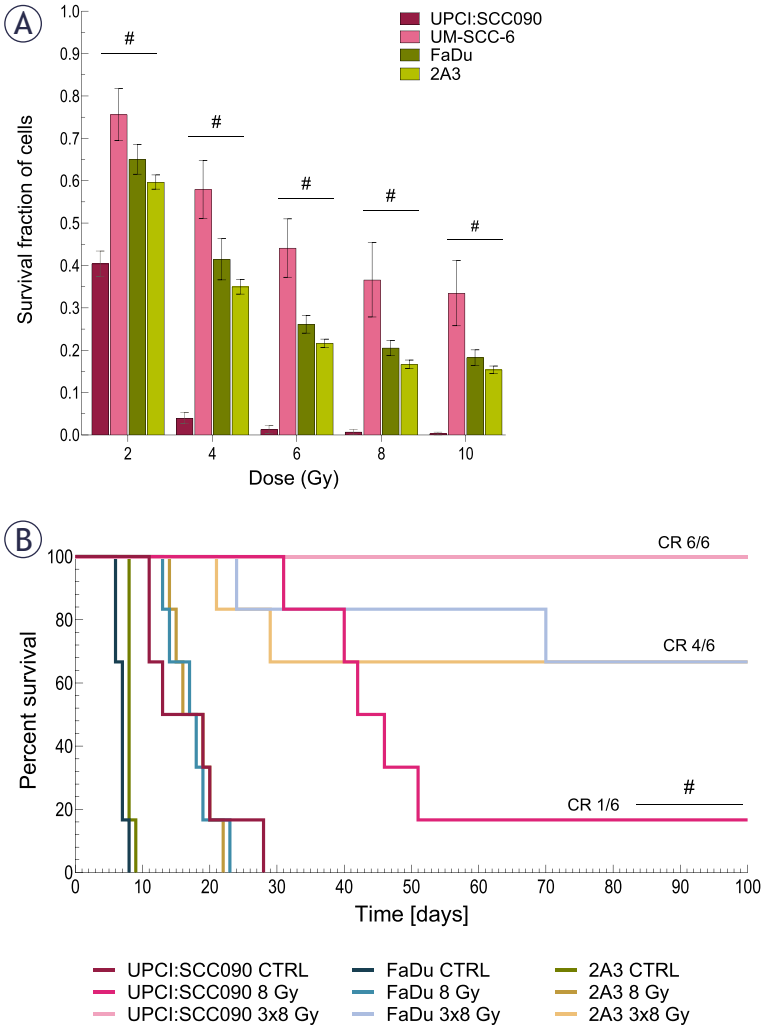

FIGURE 1. The effect of irradiation (IR) on cell survival and tumor growth. **(A)** Survival of cells after *in vitro* IR with 2, 4, 6, 8, and 10 Gy (n = 3). **(B)** Kaplan-Meier survival curve for mice bearing pharyngeal squamous cell carcinoma (PSCC) tumors treated with either a single dose of 8 Gy or 3x8 Gy, complete response (CR) (n = 6).

Data are presented as mean ± standard error of the mean (SEM); # = indicates $p < 0.05$ for comparisons between UPCI:SCC090 and other cell lines or tumor models; * = indicates $p < 0.05$ for comparisons between IR doses within the same cell line or tumor model.

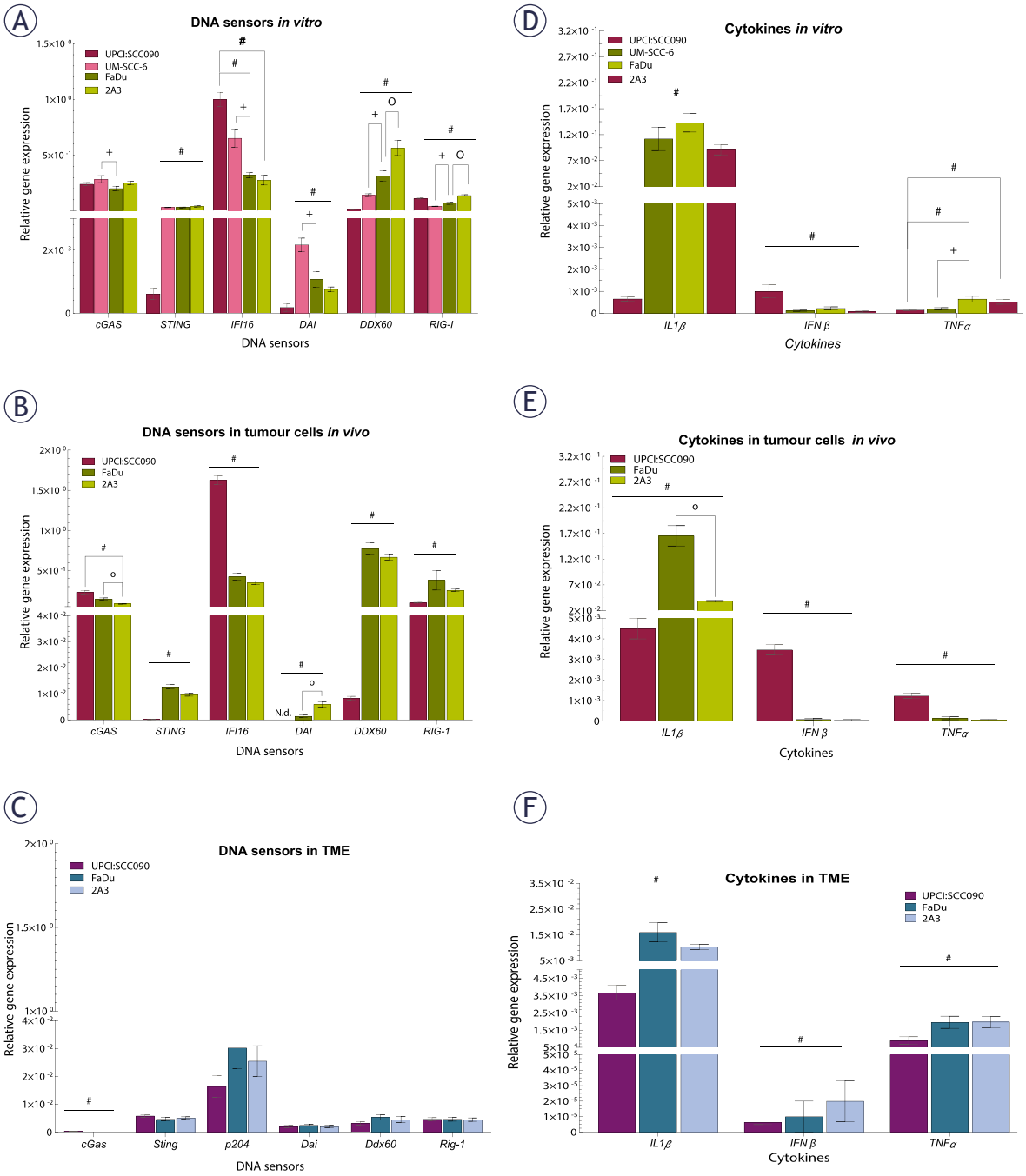

FIGURE 2. Baseline expression of cytosolic DNA sensors and cytokines in tumor cells and tumor microenvironment (TME) of pharyngeal squamous cell carcinomas (PSCCs). **(A)** Relative gene expression of cytosolic DNA sensors in cells *in vitro*, normalized to housekeeping genes (GUSB and B2M) (n = 3). **(B)** Relative gene expression of cytosolic DNA sensors in tumor cells *in vivo*, normalized to housekeeping genes (GUSB and B2M) (n = 5). **(C)** Relative gene expression of cytosolic DNA sensors in TME, normalized to housekeeping genes (BA and GADP) (n = 5). **(D)** Relative gene expression of cytokines in cells *in vitro*, normalized to housekeeping genes (GUSB and B2M) (n = 3). **(E)** Relative gene expression of cytokines in tumor cells *in vivo*, normalized to housekeeping genes (GUSB and B2M) (n = 5). **(F)** Relative gene expression of cytokines in TME, normalized to housekeeping genes (BA and GADP) (n = 5). Data is represented as mean ± standard error of the mean (SEM).

= indicates $p < 0.05$ for comparisons between UPCI:SCC090 and other cell lines or tumor models; * = indicates $p < 0.05$ for comparisons between irradiation (IR) doses within the same cell line or tumor model; o = indicates $p < 0.05$ for comparisons between FaDu and 2A3 models; + = indicates $p < 0.05$ for comparisons between UM-SCC-6 and FaDu

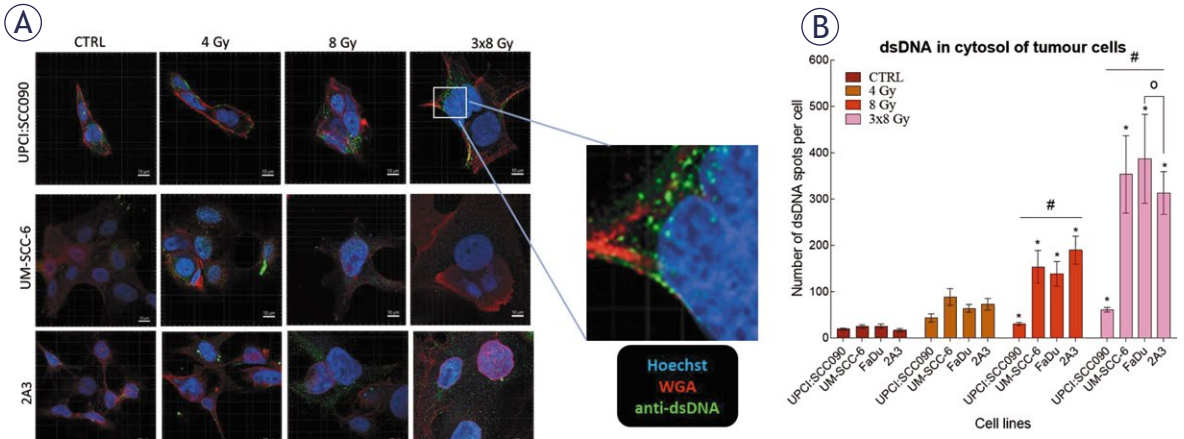

FIGURE 3. Irradiation (IR)-induced accumulation of dsDNA in the cytosol of pharyngeal squamous cell carcinoma (PSCC) cells. **(A)** Accumulation of dsDNA in the cytosol of cells 72 hours after IR. Green: dsDNA (anti-dsDNA), red: plasma membrane (WGA), blue: nucleus (Hoechst 33342), Scale bar = 10 μm. **(B)** Number of dsDNA spots per cell in cytosol 72 hours after IR with 4, 8, or 3x8 Gy (n = 8). Data is represented as mean ± standard error of the mean (SEM).

= indicates $p < 0.05$ for comparisons between UPCI:SCC090 and other cell lines or tumor models; * = indicates $p < 0.05$ for comparisons between IR doses within the same cell line or tumor model; o = indicates $p < 0.05$ for comparisons between FaDu and 2A3 models; + = indicates $p < 0.05$ for comparisons between UM-SCC-6 and FaDu

of tumor cures. All UPCI:SCC090-bearing mice were cured, while in the FaDu and 2A3 models, four out of six mice achieved complete response (Figure 1B).

Distinct baseline expression patterns of cytosolic DNA sensors and cytokines in HPV16-related OPSCC

Our next step was to investigate the baseline expression of cytosolic DNA sensing pathways in PSCC tumor cells, both *in vitro* and *in vivo*, as well as in the TME. Baseline expression of cytosolic DNA sensors STING, DAI and DDX60 in UPCI:SCC090 cells was significantly lower compared to other PSCC cell lines, both *in vitro* and *in vivo* (Figures 2A–B). In contrast, IFI16 expression was elevated in UPCI:SCC090. When comparing the HPSCC cell lines FaDu and 2A3 *in vitro*, differences were observed in the expression levels of DDX60 and RIG-I (Figure 2A), while *in vivo* models differed in cGAS and DAI expression in tumor cells (Figure 2B). For the HPV16-unrelated cell lines UM-SCC-6 and FaDu, significant differences were detected in the expression of cGAS, IFI16, DAI, DDX60, and RIG-I, except for STING (Figure 2A). In the TME, baseline expression of cytosolic DNA sensors did not differ significantly between tumor models regardless of HPV16 status, except for cGas (Figure 2C). Furthermore, the expression levels of cytosolic DNA sensors in the TME were generally lower than those in the tumor cells (Figure 2A–C). Regarding cytokines, IL1β expression level was significantly lower in UPCI:SCC090 both *in vitro* and *in vivo* when compared to other PSCC models (Figure 2D–E). In contrast, IFNβ expression in tumor cells was significantly higher in UPCI:SCC090. The expression level of tumor necrosis factor (TNF)α in UPCI:SCC090 differed in *in vitro* compared to *in vivo* experiments (Figure 2D–E). In the TME of UPCI:SCC090, all cytokine levels were significantly lower compared to HPSCC tumor models (Figure 2F). No significant cytokine expression differences were observed between the two HPSCC models in the TME (Figure 2F).

Limited activation of cytosolic DNA sensors following irradiation in HPV16-related OPSCC

We investigated how different PSCC cell lines respond to IR in terms of cytosolic accumulation of dsDNA. Our findings showed that dsDNA accumulation was both time- and dose-dependent, with the highest number of dsDNA spots observed 72 hours after IR with a dose of 3x8 Gy in all tested cell lines. The UPCI:SCC090 cell line exhibited fewer dsDNA spots than the other cell lines (Figure 3A–B, Supplementary Figure S1). Based on this observation, we explored the effect of cy-

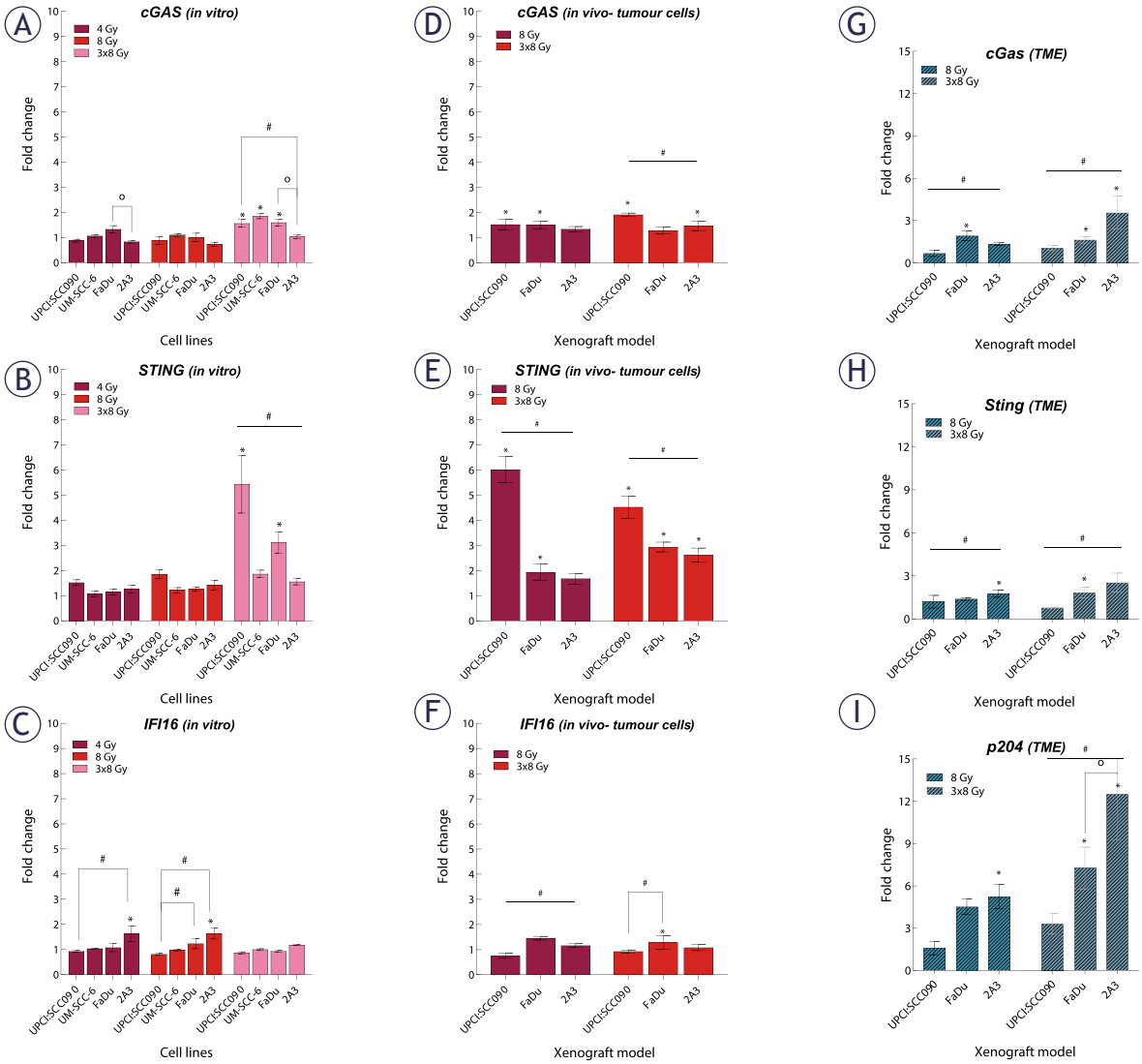

FIGURE 4. Effect of irradiation (IR) on cytosolic DNA sensors gene expression in tumor cells and and tumor microenvironment (TME) of pharyngeal squamous cell carcinoma (PSCC). **(A–C)** Fold change in expression of cyclic GMP-AMP synthase (cGAS) **(A)**, stimulator of interferon genes (STING) **(B)**, and IFI16 **(C)** *in vitro* 72 hours after IR with 4, 8, or 3x8 Gy, normalized to housekeeping genes (GUSB and B2M) and respective controls (n = 3). **(D–F)** Fold change in expression of cGAS **(D)**, STING **(E)**, and IFI16 **(F)** in tumor cells *in vivo* 72 hours after IR with 8 or 3x8 Gy, normalized to housekeeping genes (GUSB and B2M) and respective controls (n = 5). **(G–I)** Fold change in expression of cG ing **(H)**, and p204 **(I)** in tumor cells *in vivo* 72 hours after IR with 8 or 3x8 Gy, normalized to housekeeping genes (BA and GAPDH) and respective controls (n = 5). Data is represented as mean ± standard error of the mean (SEM).

= indicates $p < 0.05$ for comparisons between UPCI:SCC090 and other cell lines or tumor models; * = indicates $p < 0.05$ for comparisons between IR doses within the same cell line or tumor model; o = indicates $p < 0.05$ for comparisons between FaDu and 2A3 models; + = indicates $p < 0.05$ for comparisons between UM-SCC-6 and FaDu

tosolic dsDNA accumulation on the activation of DNA sensors. *In vitro*, we found that the upregulation of cytosolic DNA sensors in response to IR is also dose- and time-dependent, following the pattern of accumulation of dsDNA in the cytosol of cells with the most significant alterations occurred 72 hours post-IR at a dose of 3x8 Gy (Figure 4, Supplementary Figure S2–S3). In UPCI:SCC090 cells, an upregulation was noted solely in the cGAS and STING following exposure to IR at 3x8 Gy. In the other PSCC cell lines, we observed a trend toward increased expression of cGAS, STING, and DDX60 after IR. More substantial fold changes were seen in DAI and RIG-I, which showed moderate upregulation across PSCC lines. Furthermore, FaDu and UM-SCC-6 cells lines differed in their

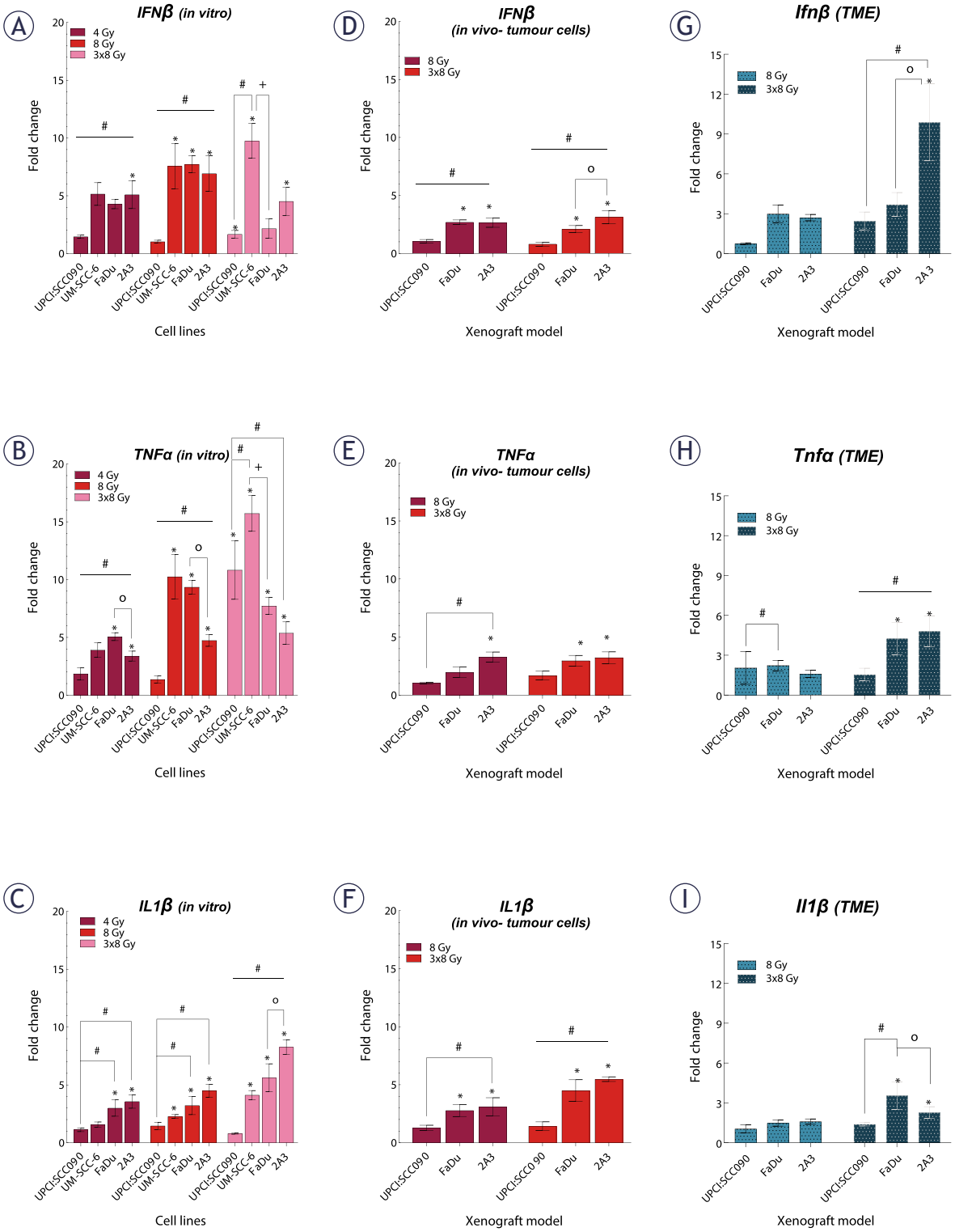

FIGURE 5. Effect of irradiation (IR) on cytokine gene expression in tumor cells and tumor microenvironment (TME) of pharyngeal squamous cell carcinoma (PSCC). **(A–C)** Fold change in expression of IFNβ **(A)**, tumor necrosis factor (TNF)a **(B)**, and IL1β **(C)** *in vitro* 72 hours after IR with 4, 8, or 3x8 Gy, normalized to housekeeping genes (GUSB and B2M) and respective controls (n = 3). **(D–F)** Fold change in expression of IFNβ **(D)**, TNFa **(E)**, and IL1β **(F)** in tumor cells *in vivo* 72 hours after IR with 8 or 3x8 Gy, normalized to housekeeping genes (GUSB and B2M) and control (n = 5). **(G–I)** Fold change in expression of Ifnβ **(G)**, TNFa **(H)**, and Il1β **(I)** in the TME *in vivo* 72 hours after IR with 8 or 3x8 Gy, normalized to housekeeping genes (BA and GADPH) and control (n = 5). Data is represented as mean ± standard error of the mean (SEM).

= indicates $p < 0.05$ for comparisons between UPCI:SCC090 and other cell lines or tumor models; * = indicates $p < 0.05$ for comparisons between IR doses within the same cell line or tumor model; o = indicates $p < 0.05$ for comparisons between FaDu and 2A3 models; + = indicates $p < 0.05$ for comparisons between UM-SCC-6 and FaDu

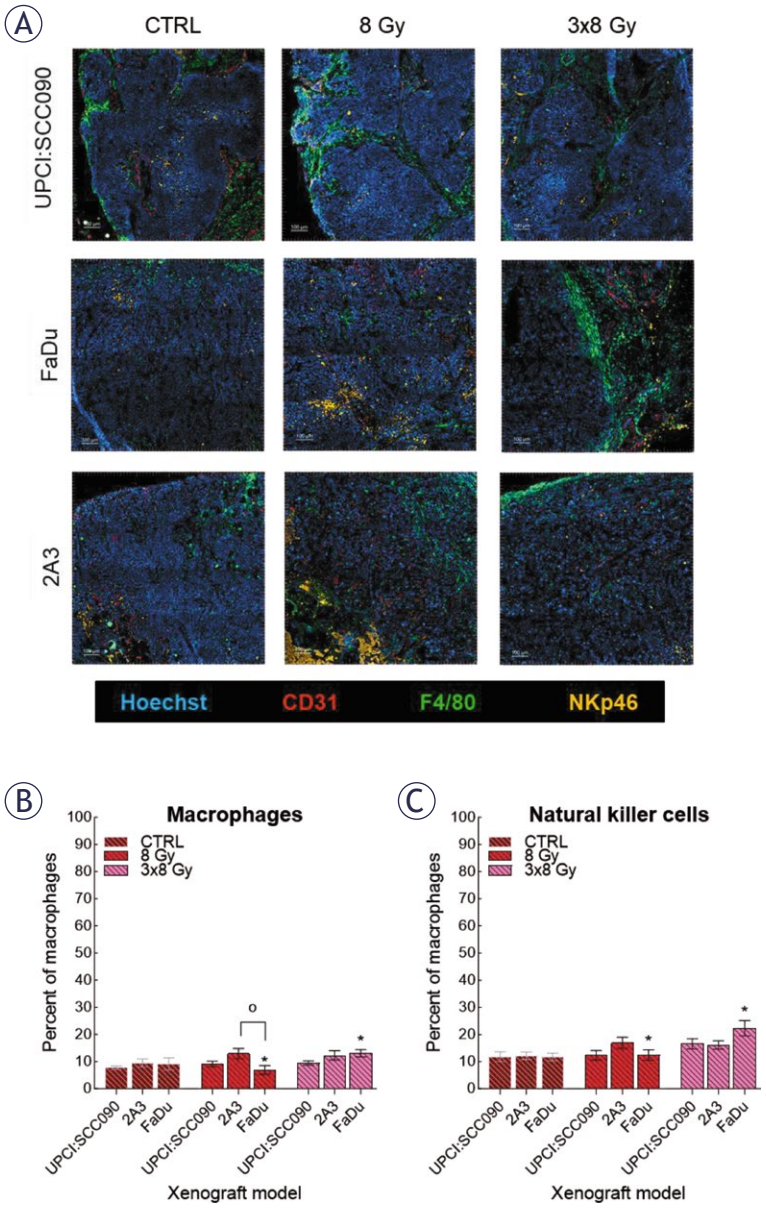

FIGURE 6. Response of the cellular innate immune system to irradiation (IR). **(A)** Frozen tumor sections were stained with anti-CD31 (red, Alexa 647), anti-F4/80 (green, Alexa 488), anti-natural killer cells (NK)p46 (orange, Cyanine 3), and Hoechst 33342 (blue). Scale bar: 100 μm. **(B)** Percentage of macrophages in tumor models before and after IR was determined by anti-F4/80 (calculated as the number of macrophages divided by the number of tumor cells). **(C)** Percentage NK cells in tumor models before and after IR was determined by anti-NKp46 (calculated as the number of NK divided by the number of tumor cells). Data are presented as mean ± standard error of the mean (SEM).

= indicates $p < 0.05$ for comparisons between UPCI:SCC090 and other cell lines or tumor models; * = indicates $p < 0.05$ for comparisons between IR doses within the same cell line or tumor model; o = indicates $p < 0.05$ for comparisons between FaDu and 2A3 models

activation of DAI and DDX60 (Figure 4A–C, Supplementary Figure S3). We extended our analysis to *in vivo* studies, examining the activation of cytosolic DNA sensors 72 hours after IR with doses of 8 or 3x8 Gy in both tumor cells and TME. Statistically significant differences were observed in the activation of cytosolic DNA sensors within tumor cells between the UPCI:SCC090 and HPSCC tumor models. In UPCI:SCC090 tumor cells, cGAS and STING were upregulated post-IR, consistent with *in vitro* data, and their levels were significantly higher than in HPSCC models (Figure 4D–E). Conversely, such activation of Sting and cGas was absent in the TME of UPCI:SCC090 (Figure 4G–H). In HPSCC tumor cells, overall upregulation of DNA sensors following IR was minimal, with no significant differences observed between the 2A3 and FaDu models (Figure 4D–F; Supplementary Figure S3). However, in the TME, we observed differential expression of p204, DAI, and DDX60 between FaDu and 2A3 tumors (Figure 4G–I; Supplementary Figure S3). Although the observed fold changes were relatively small, this may be partly due to high Ct values in the qPCR analysis, which indicate low baseline expression of these sensors in the tumor tissue.

Cytokine upregulation after irradiation is absent in HPV16-positive OPSCC tumors despite cGAS-STING activation

Following the observation that IR induces dsDNA release in cytosol and activates DNA sensing pathways, we examined the expression of downstream cytokines. We found that cytokine upregulation after IR *in vitro* was dose- and time-dependent, just like the upregulation of cytosolic DNA sensors. Changes were predominantly observed 72 hours after a 3x8 Gy regimen (Figure 5A–C, Supplementary Figure S4). The UPCI:SCC090 cell line showed no upregulation in IL1β or IFNβ gene expression, regardless of the IR dose or time, compared to other cell lines. Conversely, a significant upregulation of the TNFα was observed 72 hours post-IR with 3x8 Gy in this cell line (Figure 5B).

Next, we investigated cytokine gene expression 72 hours after IR with 8 or 3x8 Gy in both tumor cells and the TME of PSCC tumors on mRNA level (Figure 5D–I). Our findings indicated that in UPCI:SCC090, there was no upregulation of any cytokines in tumor cells after IR with 8 or 3x8 Gy. However, HPSCC tumor models 2A3 and FaDu showed significant upregulation of all three cytokines in tumor cells. These models differed only in IFNβ response (Figure 5F). No upregulation of cytokine mRNA after IR was observed in the TME of the UPCI:SCC090 tumor model. Similar to tumor cells, statistically significant upregula-

tion of all three cytokine mRNAs after IR was observed for 2A3 and FaDu in the TME (Figure 5G–I). Finally, we assessed cytokine production at the protein level by immunofluorescent staining of frozen tumor sections for IL1β, IFNβ, and TNFα. A statistically significant difference in IL1β levels was observed between UPCI:SCC090 and HPSCC tumors in control samples but not following IR with 3×8 Gy. HPSCC tumor models showed differences in TNFα levels across all experimental groups (Supplementary Figure S5).

Innate immune infiltration occurs only in HPV16-unrelated tumors after fractionated irradiation

Lastly, we investigated the cellular innate immune system's response to IR in different tumor models. Frozen tumor sections collected 72 hours after IR with either 8 or 3x8 Gy were used for analysis. Samples were immunofluorescently stained for macrophages (F4/80 expression) and natural killer cells (NK; NKp46 expression) (Figure 6A). Our analysis demonstrated no statistically significant differences in macrophages and NK cell infiltration among the tumor models, regardless of whether they were control or IR-treated. However, we observed increased infiltration of both macrophages and NK cells in the FaDu model following the fractionated IR regime of 3x8 Gy (Figure 6B and C).

Discussion

This study explored why HPV16-related OPSCC exhibits enhanced radiosensitivity, focusing on cytosolic DNA sensing pathways across HPV16-related and unrelated PSCC tumor models. Although we initially hypothesized that modulation of cytosolic DNA sensing pathways and innate immune responses by HPV16 oncoproteins E6 and E7 could explain the enhanced radiosensitivity of HPV16-related OPSCC, our findings suggest otherwise. We observed distinct baseline expressions of cytosolic DNA sensors and cytokines in HPV16-related OPSCC compared to other PSCCs, with HPV16-related OPSCC model exhibiting characteristics indicative of a suppressed STING pathway. After IR, expression of cytosolic DNA sensors and cytokines remained relatively unchanged in HPV16-related OPSCC, except for cGAS and STING sensors, whereas other PSCC models showed a time- and dose-dependent increase. The innate immune response to IR did not differ significantly across tumor models. Thus, our findings suggest cytosolic DNA sensing pathways and the innate immune response do not enhance radiosensitivity in HPV16-related OPSCC.

The response of cytosolic DNA sensing pathways to HPV16 infection is complex. We observed lower baseline STING expression in HPV16-related OPSCC tumor cells compared to other models, yet its activator, cGAS, showed no such difference. Previous studies demonstrated that HPV16 oncoproteins E6 and E7 suppress the cGAS-STING sensing pathway, aiding immune evasion.[18-20] Despite this suppression, we observed higher baseline expression levels of cytokines IFNβ and TNFα in tumor cells, indicating pathway activation. Previous research demonstrated that even when IFN-inducing pathways, including cGAS-STING, are inhibited, TNFα can independently activate cGAS via mitochondrial DNA release.[21,22] This explains why, despite the inhibition of E6 and E7 oncoproteins, the baseline expression of cGAS is not decreased in the HPV16-related OPSCC tumor model. TNFα and IFNβ are also released upon activation of IFI16, which was elevated in the HPV16-related OPSCC tumor model compared to other models. Similarly, IFI16, like cGAS-STING, detects viral DNA and triggers IFNβ induction and TNFα release from macrophages.[23,24] Our data indicate TNFα expression is lower *in vitro*, but higher *in vivo*, as macrophages are present there. Interestingly, down regulation of IFI16 resulted in an increased release of IL1β, crucial for innate immune defenses and tumor radiation responses.[25,26] Baseline IL1β expression was notably lower in both tumor cells and TME of HPV16-related OPSCC compared to other models, likely due to the activation of IFI16 by HPV16. Notable baseline differences in DNA sensors and cytokines between HPV16-related OPSCC and HPV16-related HPSCC, despite both containing HPV16 E6 and E7, are intriguing. This variance might stem from differences in the immune cell composition between oropharyngeal and hypopharyngeal tissues. However, the exact mechanisms underlying the tissue-specific response to HPV16 viral DNA in the pharynx are still unclear and require further investigation. Our data show differences in baseline expression of cytosolic DNA sensors and cytokines between HPV16-related OPSCC and other tumor models.

Cytosolic DNA sensing pathways play a key role in pathogen defense and responses to cellular damage. IR has been shown to activate these pathways by promoting the release of DNA into

the cytosol. Vanpouille-Box *et al*. demonstrated that fractionated doses of 3×8 Gy optimally activate these pathways, while a single high dose (20 Gy) induces TREX1-mediated degradation of cytosolic dsDNA, suppressing immunogenic signaling.[27] In our previous study, we found that 8 Gy induced the highest upregulation of DNA sensors *in vitro*.[28] Based on these findings, we selected 8 Gy and 3×8 Gy to investigate DNA sensor activation in PSCC models. Our results indicated IR-induced upregulation of cytosolic DNA sensors and cytokines was time- and dose-dependent. In HPV16-related OPSCC, upregulation of sensors cGAS and STING occurred only 72 hours after IR with 3x8 Gy, whereas expression of other DNA sensors remained unchanged. As previously mentioned, the STING sensor was initially suppressed by HPV16 E6 and E7 oncoproteins.[19,29] As demonstrated, this inhibition was later disrupted by fractionated IR doses. Previous studies showed IR causes an increased expression of HPV16 E6 and E7 oncoproteins, which in our case would mean that the STING sensor would continue to be suppressed, which is not the case.[30-33] We hypothesize fractionated IR disrupts HPV16 DNA rapid repair, resulting in suppressed expression of E6 and E7, leading to STING sensor activation. Despite activating the cGAS-STING pathway, cytokines IFNβ and TNFα mRNA levels remained unchanged *in vivo*, possibly due to the inactive IFI16 sensor. Expression of the cytokine IL1β remained low in HPV16-related OPSCC tumor cells. Previous studies have linked overexpression of IL1β to radioresistance. In HPV16-related OPSCC IL1β was downregulated, which could be one reason for better radiosensitivity of mentioned model.[26,34-36] In HPV16-related OPSCC model, we did not observe a significant upregulation of DNA sensors or cytokines within the TME, suggesting that the enhanced radiosensitivity of this model is not mediated by TME-related factors. Conversely, other tumor models exhibited increased DNA sensor and cytokine expression in tumor cells and TME, irrespective of HPV16 status.

A notable difference between HPV16-related OPSCC and other tumor models was the significantly lower cytosolic dsDNA release after IR in HPV16-related OPSCC model. This might result from upregulation of the three prime repair exonuclease (TREX1). Elevated TREX1 expression has been observed in HPV-associated cervical cancer, facilitating tumor proliferation and progression by impeding p53 functionality.[37] Furthermore, TREX1 also acts as a safeguard mechanism; under high IR doses, it is activated to degrade cytosolic DNA and thereby preventing activation of cytosolic DNA sensing pathway and subsequent immune response.[28,38] We hypothesize that activation of cytosolic DNA sensors in HPV16-related OPSCC is influenced by both HPV16 oncoproteins E6 and E7 as well as TREX1. While the former pair initially suppress immune recognition, TREX1, whose expression might also be elevated in HPV16-related OPSCC, can be triggered even at lower IR doses. These activation dynamics may contribute to the muted response of cytosolic sensors in this tumor model, consequently resulting in the absence of cytokine release.

Activation of cytosolic DNA sensors usually induces cytokine release, stimulating immune responses to IR.[39-41] Previous studies reported differences in macrophage and NK cell levels between HPV16-related OPSCC and HPV16-unrelated PSCC, which we did not observe in our mouse xenograft model.[42,43] Following 3x8 Gy IR, increased infiltration of both macrophages and NK cells occurred only in the HPV16-unrelated HPSCC model. Activation of the innate immune system partially occurred only in this model, where we had also observed activation of both cytosolic DNA sensors and cytokines. In contrast, no similar effect occurred in HPV16-related HPSCC tumor model, despite evident activation of cytosolic DNA sensing molecular pathways. This may be due to HPV16 oncoproteins E6 and E7, which still suppress immune system but not in the same way as in HPV16-related OPSCC. Previous studies have shown better IR response in HPV16-related OPSCC than HPV16-unnrelated PSCC, which partially aligned with our findings.[44,45] *In vitro*, the HPV16-related OPSCC cell line was the most radiosensitive, while no significant differences were observed among other PSCC cell lines. The HPV16-related OPSCC tumor group also showed improved survival following a single 8 Gy IR dose compared to the HPSCC group subjected to the same IR regimen. However, no survival differences were noted among groups that received a fractionated 3x8 Gy dose, possibly due to excessive overall dose toxicity inducing tumor cures. Our findings suggest that the absence of activation of cytosolic DNA sensing pathways in HPV16-related OPSCC leads to diminished innate immunity and therefore does not play a role in its enhanced radiosensitivity.

Despite an attempt to illuminate the role of cytosolic DNA sensing pathways in response to IR in PSCC tumor models, as comprehensively as possible, we must address potential limitations

of the present research. One limitation is the unsuccessful engraftment of the UM-SCC-6 tumor line, despite multiple attempts. Second, although the 2A3 cell line is HPV16-related, it lacks the complete viral genome and may not fully represent HPV16-associated biology. It was developed by transfecting FaDu cells with HPV16 E6 and E7 oncogenes via the PA317 LXSN 16E6/E7 vector and remains the only available human HPV16-related HPSCC cell line. Another limitation is the use of a single HPV16-related OPSCC cell line.[31] Inclusion of additional models would have strengthened the study and improved our understanding of the heterogeneity among HPV16-positive tumors. Unfortunately, very few HPV16-related cell lines of oropharyngeal origin are commercially available. Next, knockdown of cGAS and STING in tumor models would have been useful to directly assess their functional impact. Furthermore, quantification of cytokines using western blotting and immune cell populations with flow cytometry would provide further support to delineate the effects of DNA sensing pathways in context of immune system activation. However, since the activation of DNA sensors did not lead to cytokine induction or immune response in our models, we decided not to pursue this approach in the current study. Finally, the adaptive immune system plays a significant role in the response to IR. However, immunocompromised mice that we used cannot activate it due to the absence of a thymus, which can lead to reduced radiosensitivity of specific tumor models. On the other hand, this way we were able to investigate how the innate immune system itself contributes to sensitivity to IR.

The key finding of our research was that the involvement of cytosolic DNA sensing pathways and innate immune system do not increase radiosensitivity of HPV16-related OPSCC. In PSCC models, DNA sensors and cytokine expression varied depending on IR dose and fractionation, with the most notable changes observed 72 hours after fractionated 3x8 Gy. The HPV16-related OPSCC tumor model showed upregulation of cGAS and STING, without corresponding cytokine induction, suggesting potential for future studies using STING agonists or antagonists to modulate tumor response. In addition, we detected differences in cytosolic accumulation of dsDNA across cell lines, which may be influenced by TREX1 activity. Furthermore, our results partially refute the notion that the activation of cytosolic DNA sensing pathways depends on HPV16 status, as similar activation patterns were observed in both HPV16-related and unrelated HPSCC tumor models. Additional research exploring the interplay between adaptive immunity and cytosolic DNA sensing pathways could help clarify the mechanisms underlying the enhanced radiotherapy responses observed in patients with HPV16-related OPSCC. The recently developed HPV16-positive murine model MOC-1 could be particularly valuable in this context, as it enables the investigation of adaptive immune responses to IR.[46]

Acknowledgments

The research was supported by the Slovenian Research and Innovation Agency (ARIS) (grant numbers P3-0003 and P3-0307) and bilateral research project funding (grant number BT-AT/23-24-027). We would like to thank Mira Lavric, Teja Valant and Bostjan Markelc (Institute of Oncology Ljubljana, Ljubljana, Slovenia) for all the technical assistance.

References

1. Bray F, Laversanne M, Sung H, Ferlay J, Siegel RL, Soerjomataram I, et al. Global cancer statistics 2022: GLOBOCAN estimates of incidence and mortality worldwide for 36 cancers in 185 countries. *CA Cancer J Clin* 2024; **74:** 229-63. doi: 10.3322/caac.21834

2. Machiels JP, René Leemans C, Golusinski W, Grau C, Licitra L, Gregoire V. Squamous cell carcinoma of the oral cavity, larynx, oropharynx and hypopharynx: EHNS-ESMO-ESTRO Clinical Practice Guidelines for diagnosis, treatment and follow-up. *Ann Oncol* 2020; **31:** 1462-75. doi: 10.1016/j.annonc.2020.07.011

3. Tanaka TI, Alawi F. Human papillomavirus and oropharyngeal cancer. *Dent Clin North Am* 2018; **62:** 111-20. doi: 10.1016/j.cden.2017.08.008

4. Kobayashi K, Hisamatsu K, Suzui N, Hara A, Tomita H, Miyazaki T. A review of HPV-related head and neck cancer. *J Clin Med* 2018; **7:** 241. doi: 10.3390/jcm7090241

5. Tota JE, Best AF, Zumsteg ZS, Gillison ML, Rosenberg PS, Chaturvedi AK. Evolution of the oropharynx cancer epidemic in the United States: moderation of increasing incidence in younger individuals and shift in the burden to older individuals. *J Clin Oncol* 2019; **37:** 1538-46. doi: 10.1200/jco.19.00370

6. Lechner M, Liu J, Masterson L, Fenton TR. HPV-associated oropharyngeal cancer: epidemiology, molecular biology and clinical management. *Nat Rev Clin Oncol* 2022; 19**:** 306-27. doi: 10.1038/s41571-022-00603-7

7. Wang MB, Liu IY, Gornbein JA, Nguyen CT. HPV-positive oropharyngeal carcinoma: a systematic review of treatment and prognosis. *Otolaryngol Head Neck Surg* 2015; **153**: 758-69. doi: 10.1177/0194599815592157

8. Mirghani H, Amen F, Tao Y, Deutsch E, Levy A. Increased radiosensitivity of HPV-positive head and neck cancers: molecular basis and therapeutic perspectives. *Cancer Treat Rev* 2015; **41:** 844-52. doi: 10.1016/j.ctrv.2015.10.001

9. Ang KK, Harris J, Wheeler R, Weber R, Rosenthal DI, Nguyen-Tân PF, et al. Human papillomavirus and survival of patients with oropharyngeal cancer. *N Engl J Med* 2010; **363:** 24-35. doi: 10.1056/NEJMoa0912217

10. Lo Cigno I, Calati F, Albertini S, Gariglio M. Subversion of host innate immunity by human papillomavirus oncoproteins. *Pathogens* 2020; **9:** 292. doi: 10.3390/pathogens9040292

11. Storozynsky Q, Hitt MM. The impact of radiation-induced DNA damage on cGAS-STING-mediated immune responses to cancer. *Int J Mol Sci* 2020; **21:** 8877. doi:10.3390/ijms21228877

12. Deng L, Liang H, Fu S, Weichselbaum RR, Fu YX. From DNA damage to nucleic acid sensing: a strategy to enhance radiation therapy. *Clin Cancer Res* 2016; **22:** 20-5. doi: 10.1158/1078-0432.CCR-14-3110

13. Deng L, Liang H, Xu M, Yang X, Burnette B, Arina A, et al. STING-dependent cytosolic DNA sensing promotes radiation-induced type I interferon-dependent antitumor immunity in immunogenic tumors. *Immunity* 2014; **41:** 843-52. doi: 10.1016/j.immuni.2014.10.019

14. Shaikh MH, Bortnik V, McMillan NA, Idris A. cGAS-STING responses are dampened in high-risk HPV type 16 positive head and neck squamous cell carcinoma cells. *Microb Pathog* 2019; 1**32:** 162-5. doi: 10.1016/j.micpath.2019.05.004

15. Chiang C, Pauli EK, Biryukov J, Feister KF, Meng M, White EA, et al. The human papillomavirus E6 oncoprotein targets USP15 and TRIM25 to suppress RIG-I-mediated innate immune signaling. *J Virol* 2018; **92:** e01737-17. doi: 10.1128/JVI.01737-17

16. Fuertes MB, Woo SR, Burnett B, Fu YX, Gajewski TF. Type I interferon response and innate immune sensing of cancer. *Trends Immunol* 2013; **34:** 67-73. doi: 10.1016/j.it.2012.10.004

17. Livak KJ, Schmittgen TD. Analysis of relative gene expression data using real-time quantitative PCR and the 2(-Delta Delta C(T)) method. *Methods* 2001; **25:** 402-8. doi: 10.1006/meth.2001.1262

18. Hoppe-Seyler K, Bossler F, Braun JA, Herrmann AL, Hoppe-Seyler F. The HPV E6/E7 oncogenes: key factors for viral carcinogenesis and therapeutic targets. *Trends Microbiol* 2018; **26:** 158-68. doi: 10.1016/j.tim.2017.07.007

19. Bortnik V, Wu M, Julcher B, Salinas A, Nikolic I, Simpson KJ, et al. Loss of HPV type 16 E7 restores cGAS-STING responses in human papilloma virus-positive oropharyngeal squamous cell carcinomas cells. *J Microbiol Immunol Infect* 2021; **54:** 733-9. doi: 10.1016/j.jmii.2020.09.003

20. Shaikh MH, Bortnik V, McMillan NA, Idris A. cGAS-STING responses are dampened in high-risk HPV type 16 positive head and neck squamous cell carcinoma cells. *Microb Pathog* 2019; **132:** 162-5. doi: 10.1016/j.micpath.2019.05.001

21. Willemsen J, Neuhoff MT, Hoyler T, Noir E, Tessier C, Sarret S, et al. TNF leads to mtDNA release and cGAS/STING-dependent interferon responses that support inflammatory arthritis. *Cell Rep* 2021; **37:** 109977. doi: 10.1016/j.celrep.2021.109977

22. Almine JF, O'Hare CAJ, Dunphy G, Haga IR, Naik RJ, Atrih A, et al. IFI16 and cGAS cooperate in the activation of STING during DNA sensing in human keratinocytes. *Nat Commun* 2017; **8:** 14392. doi: 10.1038/ncomms14392

23. Sponza S, De Andrea M, Mondini M, Gugliesi F, Gariglio M, Landolfo S. Role of the interferon-inducible IFI16 gene in the induction of ICAM-1 by TNF-alpha. *Cell Immunol* 2009; **257:** 55-60. doi: 10.1016/j.cellimm.2009.02.007

24. Lim GY, Cho SW, Ka NL, Lee KH, Im SA, Kim SS, et al. IFI16/Ifi202 released from breast cancer induces secretion of inflammatory cytokines from macrophages and promotes tumor growth. *J Cell Physiol* 2023; **238:** 1507-19. doi: 10.1002/jcp.31022

25. Liu W, Ding I, Chen K, Olschowka J, Xu J, Hu D, et al. Interleukin 1beta (IL1B) signaling is a critical component of radiation-induced skin fibrosis. *Radiat Res* 2006; **165:** 181-91. doi: 10.1667/rr3478.1

26. Kang AR, Cho JH, Lee NG, Kwon JH, Song JY, Hwang SG, et al. Radiation-induced IL-1β expression and secretion promote cancer cell migration/invasion via activation of the NF-κB–RIP1 pathway. *Biochem Biophys Res Commun* 2021; **534:** 973-9. doi: 10.1016/j.bbrc.2020.10.057

27. Vanpouille-Box C, Alard A, Aryankalayil MJ, Sarfraz Y, Diamond JM, Schneider RJ, et al. DNA exonuclease Trex1 regulates radiotherapy-induced tumour immunogenicity. *Nat Commun* 2017; **8:** 15618. doi: 10.1038/ncomms15618

28. Jesenko T, Bosnjak M, Markelc B, Sersa G, Znidar K, Heller L, et al. Radiation induced upregulation of DNA sensing pathways is cell-type dependent and can mediate the off-target effects. *Cancers* 2020; **12:** 3365. doi: 10.3390/cancers12113365

29. Ge Z, Ding S. Regulation of cGAS/STING signaling and corresponding immune escape strategies of viruses. *Front Cell Infect Microbiol* 2022; **12:** 954581. doi: 10.3389/fcimb.2022.954581

30. Park JW, Nickel KP, Torres AD, Lee D, Lambert PF, Kimple RJ. Human papillomavirus type 16 E7 oncoprotein causes a delay in repair of DNA damage. *Radiother Oncol* 2014; **113:** 337-44. doi: 10.1016/j.radonc.2014.08.026

31. Harris M, Wang XG, Jiang Z, Goldberg GL, Casadevall A, Dadachova E. Radioimmunotherapy of experimental head and neck squamous cell carcinoma (HNSCC) with E6-specific antibody using a novel HPV-16 positive HNSCC cell line. *Head Neck Oncol* 2011; **3:** 9. doi: 10.1186/1758-3284-3-9

32. Ziemann F, Arenz A, Preising S, Wittekindt C, Klussmann JP, Engenhart-Cabillic R, et al. Increased sensitivity of HPV-positive head and neck cancer cell lines to x-irradiation ± Cisplatin due to decreased expression of E6 and E7 oncoproteins and enhanced apoptosis. *Am J Cancer Res* 2015; **5:** 1017-31. PMID: 26045983

33. Santin AD, Hermonat PL, Ravaggi A, Chiriva-Internati M, Pecorelli S, Parham GP. Radiation-enhanced expression of E6/E7 transforming oncogenes of human papillomavirus-16 in human cervical carcinoma. *Cancer* 1998; **83:** 2346-52. doi: 10.1002/(sici)1097-0142(19981201)83:11<2346::aid-cncr14>3.0.co;2-g

34. Zhang C, Liang Z, Ma S, Liu X. Radiotherapy and cytokine storm: risk and mechanism. *Front Oncol.* 2021; **11:** 670464. doi: 10.3389/fonc.2021.670464

35. Ong ZY, Gibson RJ, Bowen JM, Stringer AM, Darby JM, Logan RM, et al. Pro-inflammatory cytokines play a key role in the development of radiotherapy-induced gastrointestinal mucositis. *Radiat Oncol* 2010; **5:** 22. doi: 10.1186/1748-717X-5-22

36. Reinholz M, Kawakami Y, Salzer S, Kreuter A, Dombrowski Y, Koglin S, et al. HPV16 activates the AIM2 inflammasome in keratinocytes. *Arch Dermatol Res* 2013; **305:** 723-32. doi: 10.1007/s00403-013-1375-0

37. Prati B, da Silva Abjaude W, Termini L, Morale M, Herbster S, Longatto-Filho A, et al. Three prime repair exonuclease 1 (TREX1) expression correlates with cervical cancer cells growth *in vitro* and disease progression *in vivo*. *Sci Rep* 2019; **9:** 351. doi: 10.1038/s41598-018-37064-x

38. Demaria S, Vanpouille-Box C. TREX1 is a checkpoint for innate immune sensing of DNA damage that fosters cancer immune resistance. *Emerg Top Life Sci* 2017; **1:** 509-15. doi: 10.1042/ETLS20170107

39. Hu MM, Shu HB. Innate immune response to cytoplasmic DNA: mechanisms and diseases. *Annu Rev Immunol* 2020; **38:** 79-98. doi: 10.1146/annurev-immunol-022619-111801

40. Barber GN. Cytoplasmic DNA innate immune pathways. *Immunol Rev* 2011; **243:** 99-108. doi: 10.1111/j.1600-065X.2011.01051.x

41. Woo SR, Fuertes MB, Corrales L, Spranger S, Furdyna MJ, Leung MY, et al. STING-dependent cytosolic DNA sensing mediates innate immune recognition of immunogenic tumors. *Immunity* 2014; **41:** 830-42. doi: 10.1016/j.immuni.2014.10.017

42. Russell SM, Angell TE, Lechner MG, Liebertz DJ, Correa AJ, Sinha UK, et al. Immune cell infiltration patterns and survival in head and neck squamous cell carcinoma. *Head Neck Oncol* 2013; **5:** 24. doi: 10.1186/1758-3284-5-24

43. Mandal R, Şenbabaoğlu Y, Desrichard A, Havel JJ, Dalin MG, Riaz N, et al. The head and neck cancer immune landscape and its immunotherapeutic implications. *JCI Insight* 2016; **1:** e89829. doi: 10.1172/jci.insight.89829

44. Todorovic V, Prevc A, Zakelj MN, Savarin M, Brozic A, Groselj B, et al. Mechanisms of different response to ionizing irradiation in isogenic head and neck cancer cell lines. *Radiat Oncol* 2019; **14:** 214. doi: 10.1186/s13014-019-1418-6

45. Browman GP, Mohide EA, Willan A, Hodson I, Wong G, Grimard L, et al. Association between smoking during radiotherapy and prognosis in head and neck cancer: a follow-up study. *Head Neck* 2002; **24:** 1031-7. doi: 10.1002/hed.10168

46. Modic Z, Cemazar M, Markelc B, Cör A, Sersa G, Kranjc Brezar S, et al. HPV-positive murine oral squamous cell carcinoma: development and characterization of a new mouse tumor model for immunological studies. *J Transl Med* 2023; **21:** 376. doi: 10.1186/s12967-023-04221-4

research article

Induction chemotherapy and concurrent chemoradiotherapy for larynx preservation in laryngeal and hypopharyngeal cancer

Primoz Strojan[1,2], Gaber Plavc[1,2], Robert Sifrer[2,3], Simona Jereb[1], Bostjan Lanisnik[4], Marko Kokalj[1], Ales Groselj[2,3], Cvetka Grasic Kuhar[1,2]

[1] Institute of Oncology Ljubljana, Ljubljana, Slovenia
[2] University of Ljubljana, Faculty of Medicine, Ljubljana, Slovenia
[3] Department of Otorhinolaryngology and Cervicofacial Surgery, University Medical Centre Ljubljana, Ljubljana, Slovenia
[4] Department of Otolaryngology - Head and Neck Surgery, University Medical Center Maribor, Maribor, Slovenia

Radiol Oncol 2025; 59(4): 579-588.

Received 21 July 2025
Accepted 05 September 2025

Correspondence to: Prof. Primož Strojan, M.D., Ph.D., Department of Radiation Oncology, Institute of Oncology Ljubljana, Zaloška 2, SI-1000 Ljubljana, Slovenia. E-mail: pstrojan@onko-i.si

Disclosure: No potential conflicts of interest were disclosed.

Background. To test the hypothesis that clinical tumor response after a single cycle of induction chemotherapy (ICT) can reliably differentiate between chemo-/radiosensitive and resistant tumors in the larynx preservation setting.

Patients and methods. Treatment consisted of docetaxel/cisplatin/5-fluorouracil (TPF) ICT followed by concurrent chemoradiotherapy (cCRT) with weekly cisplatin. The response of the primary tumor was assessed by transnasal endoscopy after the first ICT cycle.

Results. 37/39 (95%) patients with laryngeal (46%) or hypopharyngeal (54%) carcinoma responded to one cycle of ICT, and two patients were referred for salvage surgery. Laryngectomy-free survival at 2 and 5 years was 87% and 75%, respectively. The corresponding rates for locoregional control (and also for disease-free survival) were 79% and 70% and for overall survival 92% and 82%.

Conclusions. Clinical assessment of tumor response to one cycle of TPF ICT serves as a valid and easy-to-use predictor of tumor sensitivity to platinum-based cCRT.

Key words: induction chemotherapy; response; organ preservation; laryngeal cancer; hypopharyngeal cancer

Introduction

Total laryngectomy with loss of natural voice and permanent tracheostomy is one of the most mutilating surgical procedures in the head and neck region, leaving patients with significant physical impairments and social stigmatization.[1] Therefore, the development of non-surgical treatment strategies that provide comparable survival outcomes and allow preservation of the larynx in almost 60% of cases is an important alternative for patients with locally advanced laryngeal and hypopharyngeal cancer.[2] In this context, it should be emphasized the importance of preserving the larynx functionally and not just anatomically, in order to enable natural speech, swallowing and breathing without the need for permanent tube feeding and/or tracheostomy. According to the RTOG 91-11 trial, patients treated with concurrent chemoradiotherapy (cCRT) with cisplatin have the best chance of laryngeal preservation, albeit with no improvement in survival compared to induction chemotherapy (ICT) followed by radiotherapy (RT) or RT alone.[3,4] However, the impact of the pri-

mary tumor stage, including the mobility status of the vocal cords, and the location of the primary tumor (larynx vs. hypopharynx) must be considered when assessing the prospects for a favorable treatment outcome.

Since not all tumors are equally sensitive to chemotherapeutic agents and radiation, the ability to identify patients with resistant tumors early in the course of non-surgical therapy who should be treated with laryngectomy is crucial. Several studies have confirmed that ICT is a reliable in vivo assay for determining the chemo/bio/radiosensitivity of tumors.[5,6] In routine clinical practice, after a favorable response to ICT, patients are subsequently treated with RT; the use of a sensitizer concurrently with radiation should be considered investigational.[7] The latter is due to the lack of survival benefit observed in phase 3 clinical trials comparing taxane-based ICT followed by aggressive chemoradiation with chemoradiation alone.[8] In addition, the toxicity of three cycles of taxane-based induction chemotherapy is significant and may seriously compromise the administration of subsequent concurrent chemo/bio-RT.[9]

To mitigate the negative effects of aggressive ICT therapies on subsequent cCRT, the response to a single test cycle of ICT has been proposed as a criterion for selecting patients for non-surgical treatment.[10] Excellent survival results were achieved with this approach, with the larynx being preserved in 66% of patients.[11] In the present study, we retrospectively analyzed the results of larynx-preserving treatment in a prospective cohort of patients with laryngeal and hypopharyngeal cancer who received a limited number of ICT cycles as a chemotherapy response selection strategy prior to platinum-based cCRT. The hypothesis tested was whether the clinical response of the tumor after a single cycle of ICT can be used to differentiate between chemo-/radiosensitive and resistant tumors.

Patients and methods

The study was conducted in accordance with the Declaration of Helsinki and approved by the Protocol Review Committee of the Institute of Oncology Ljubljana, Slovenia (ERIDNPVO-0036/2020, 19.11.2020).

Patients

In 2016, a chemoselection program was introduced based on clinical assessment of tumor response after a single cycle of ICT for patients with laryngeal and hypopharyngeal cancer. At the Multidisciplinary Tumor Board, all consecutive patients with newly diagnosed squamous cell carcinoma of the larynx or hypopharynx (cT2–4a, cN0–3resectable, M0) who were suitable for total laryngectomy (with or without partial hypopharyngectomy) as the only possible surgical option were offered this treatment option. Further inclusion criteria were a WHO performance status of 0–1 and adequate laboratory tests. Patients with tracheostomy, feeding tube, recurrent pneumonia (requiring hospitalization within the last 12 months) suggestive of laryngeal dysfunction, or patients with a medical condition that would prevent safe delivery of the planned therapies were considered ineligible.

Treatment protocol and response evaluation

Prior to treatment, the stage of disease was determined by physical, endoscopic and radiologic (CT and/or chest X-ray and/or abdominal US) examination of the upper aero-digestive tract, neck, chest and abdomen. Other tests (PET-CT, bone scan) were performed when clinically indicated.

ICT consisted of two cycles of docetaxel (75 mg/m^2, day 2), cisplatin (75 mg/m^2, day 2) and 5-fluorouracil, 750 mg/m^2/day, days 1–4 in 96-hour infusion). The substitution of cisplatin with carboplatin (AUC 5) and the dosing recommendations in case of toxicity have been as described elsewhere.[12]

Tumor response was assessed clinically and was performed 3 weeks after the start of ICT by transnasal endoscopy (local assessment) and palpation (regional assessment). A complete response (CR) was defined as the disappearance of all evaluable disease within the treatment field, and a partial response (PR) was defined as a decrease of no less than 50% and at least partial recovery of laryngeal mobility (in the case of initial immobility). Patients with CR or PR of the primary tumor received a second cycle of ICT followed by cCRT, and non-responders were referred for surgery (Figure 1). Patients with responding primary tumors who were diagnosed with either T4a or less than PR in the neck after the first ICT cycle were planned for the 3rd cycle of ICT.

RT was scheduled to begin 3-4 weeks after the start of the last cycle of ICT. All patients had CT-based planning and were irradiated with a 6 MV photon beam from a linear accelerator and a concomitant boost intensity modulated radiotherapy/volumetric modulated arc therapy technique. A

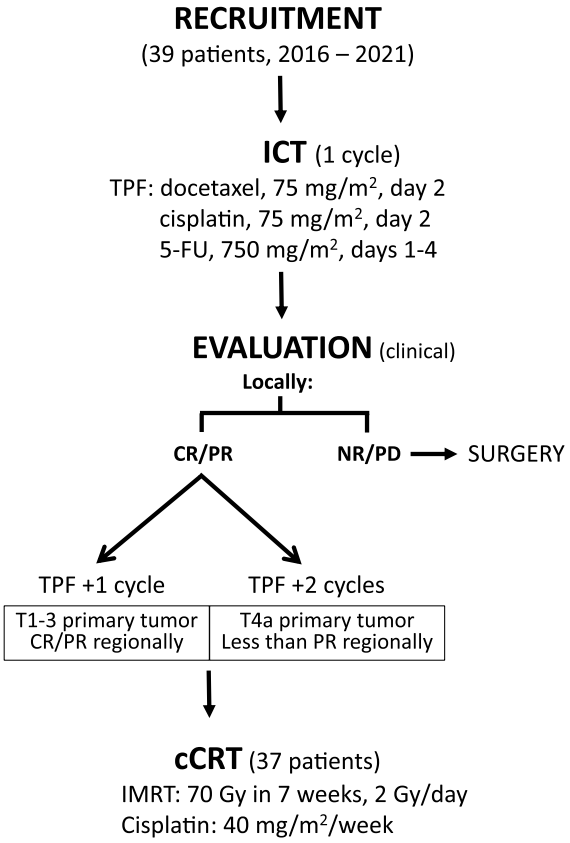

FIGURE 1. Treatment protocol.

CR = complete response; IMRT = intensity-modulated radiotherapy; NR = no response; ICT = induction chemotherapy; PD = disease progression; PR = partial response

dose of 70 Gy was delivered in 35 fractions over 7 weeks (1 fraction/day, 5 days/week) to the original (i.e., pre-ICT) high-risk clinical target volumes (CTV70), taking into account the anatomical barriers to tumor spread. The low-risk CTV56 included areas considered at risk for microscopic disease. The primary tumor and nodal levels were delineated according to the guidelines.[13,14] An isotropic margin of 5 mm was added around the corresponding CTVs to create the planning target volumes (PTVs). During RT, cisplatin was administered intravenously weekly at a dose of 40 mg/m^2 and replaced by carboplatin (1.5 AUC) when creatinine clearance decreased to < 60 mL/min and/or peripheral polyneuropathy or grade >1 hearing impairment was detected. Tumor response was assessed clinically and radiologically 8–14 weeks after cCRT according to RECIST criteria: partial responders and non-responders were referred for surgery if the residual tumor was considered operable.

The acute toxicity of ICT was monitored every 3 weeks and weekly during cCRT. In the first two years, patients were examined at 3-month intervals and later every 4–6 months for toxicity and possible recurrence of the disease or new primary tumors. Toxicities were graded according to the National Cancer Institute's Common Terminology Criteria or Adverse Events v5.0.

Statistics

To ensure a potential minimum follow-up period of 2 years, only patients treated between 2016 and 2021 were analyzed. Descriptive statistics were reported with medians, ranges and IQRs for numeric variables and as percentages for categorical variables. Survival curves were calculated using the Kaplan-Meier method and the log-rank test was used to assess the differences between survival curves. All statistical tests were two-sided and a p-value of < 0.05 was considered statistically significant.

The primary study objective was 2-year laryngectomy-free survival (LFS, event: laryngectomy or death from any cause). Additional endpoints were locoregional control (LRC, event: local and/or regional recurrence or death from any cause except distant metastases); disease-free survival (DFS, event: cancer recurrence or death from any cause); overall survival (OS, event: death from any cause); laryngo-esophageal dysfunction-free survival (leDFS, event: local recurrence, total or partial laryngectomy, tracheostomy or feeding tube at 2 years or death) at 2 and 5 years; acute and late toxicities. Survival times were calculated from the first day of treatment. For patients who did not respond to ICT or did not achieve local and/or regional CR after completion of all therapies, the time to event was set to zero months.

Results

Patients and treatment delivered

Between 2016 and 2021, 39 consecutive patients with a median age of 60 years (range 39–72, interquartile range [IQR] 56–64) were treated according to the protocol. The majority (85%) were male, without comorbidities (64%) and had stage T3 primary tumors (72%), of which a comparable proportion originated from the larynx (18, 46%) or hypopharynx (21, 54%). At diagnosis, 14 patients (36%) had vocal cord fixation and 23 (59%) had metastases in the neck nodes. The clinical characteristics of the patients and tumors are listed in Table 1.

The majority, 27 (69%) patients, received 2 cycles of ICT. Five (13%) patients received only one cycle

TABLE 1. Patient, tumor, and treatment characteristics

Sex (female/male)	6/33 (15%/85%)
Age, in years*	60, 39–72 (IQR 56–64)
Comorbidities	14 (36 %)
Cardiovascular	16 events in 10 patients
Diabetes mellitus, tpe 2	3 patients
Gastrointestinal	2 patients
Hypothireosis	1 patient
Depression	1 patient
WHO performance status	
0	27 (69 %)
1	12 (31 %)
Smoking history	
Non-smoker	1 (3%)
Former smoker†	14 (36%)
pack-years*	23, 5–105 (IQR 15–70)
Active smoker	24 (61%)
pack-years*	43, 20–100 (IQR 30–175)
Primary tumor site	
Larynx	18 (46%)
Hypopharynx	21 (54%
T-stage	
T2	8 (20%)
T3	28 (72%)
T4A	3 (8%)
N-stage	
N0	15 (38%)
N1	12 (31%)
N2	10 (26%)
N3	2 (5%)
Overall UICC-TNM stage	
Stage III	25 (64%)
Stage IVA	12 (31%)
Stage IVB	2 (5%)
Induction chemotherapy	
1 cycle	5[3] (13%)
2 cycles	27 (69%)
3 cycles	7 (18%)
Radiotherapy, 70 Gy	39 (100%)
Concurrent chemotherapy (N = 37) ‡	
Number of cycles*	5, 1–7 (IQR 5–6)
Interval ICT – cCRT, in days*	26, 12–48 (IQR 21–28)
Duration of RT, in days*	51, 47–55 (IQR 50–51)
Total duration of treatment, in weeks*	14, 11–25 (IQR 13–15)

ICT = induction chemotherapy; cCRT = concurrent chemoradiotherapy; IQR = interquartile range; RT = radiotherapy; UICC = the Union for International Cancer Conrol; WHO = World Health organization

*Median, range (interquartile range)

†Stopped smoking > 6 months before diagnosis

‡Two patients were non-responders at primary tumor site

of ICT. The reasons for this were an unresponsive primary tumor (2), febrile neutropenia with sepsis (2) and the patient's refusal to undergo further ICT after complete tumor disappearance (1). Three ICT cycles were administered in 7 (18%) patients, as 3 patients had a cT4a tumor and 4 patients had less than PR of neck metastases (Table 1).

The median interval between the first day of the last ICT cycle and the start of cCRT was 26 days (range 12–48, IQR 21–28) and the median duration of RT course was 51 days (range 47–55, IQR 50–51). Overall, depending on the number of administered ICT cycles, the duration of treatment was between 11 and 25 weeks (median 14, IQR 13–15).

Response to induction chemotherapy

After the first cycle of ICT, transnasal endoscopy revealed CR and PR locally in 5 and 32 patients, respectively (95% of patients in total) and two patients (5%) were identified as local non-responders and sent for salvage surgery (Table 2). There was no statistically significant difference in the proportion of CR and/or PR between patients with tumors of the larynx and hypopharynx. In 14 patients with initial vocal cord fixation, only partial restoration of hemilarynx mobility was observed in two patients and no change was observed in the patient with transglottic (cT3N0) tumor. The latter and the patient with a non-responding hypopharyngeal cT3N2b tumor were directed to surgery. Regionally, 19 of 23 patients (83%) with cN+ disease responded to the first ICT cycle with at least PR.

Response to concurrent chemotherapy

Tumor response after cCRT was assessed in 37 patients with CT (26), PET-CT (8) or both (3). The median time to assessment after completion of cCRT was 13 weeks (range 7–26, IQR 11–17). Local CR was achieved in all (100%) patients and regional in 19 of 22 N+ patients (86%), resulting in a 92% (34/37) CR rate above the clavicles (Table 2).

Salvage therapies and survival

The three patients with residual disease in the neck underwent unilateral neck dissection. Histopathologic report confirmed residual carcinoma in all three cases. Two of them remained tumor-free and the third patient was diagnosed with local recurrence and lung metastases. Of the 34 patients with CR after cCRT, the disease progressed

TABLE 2. Primary tumor response to induction chemotherapy and concurrent chemoradiotherapy

Primary tumor response	Induction chemotherapy			Concurrent chemoradiotherapy
	Cycle 1 (N = 39)	Cycle 2 (N = 34)	Cycle 3 (N = 7)	(N = 37)
Complete response	5	4	2	37
Larynx	1	0	0	17
Hypopharynx	4	4	2	20
Partial response	32	30	5	0
Larynx	16	16	2	
Hypopharynx	16	14	3	
Less than partial response	2	0	0	0
Larynx	1			
Hypopharynx	1			

N = number of patients

in three patients (Table 3). In seven patients (18%), a new primary tumor developed 6 months to 5 years (median 2.2 years) after treatment (6 non-small cell lung carcinomas and uterine cervix carcinoma), which was the cause of death in 5 of them.

On the study close-out date (February 29, 2024), the median follow-up time was 3.8 years (range 1.5–8 years, IQR 3–6.2) and 4.5 years for patients still alive (range 2–8 years, IQR 3.2–6.4). At the last clinical visit, 29 patients were free of treated cancer and one had lung metastases. Two patients died from the treated malignancy (with locoregional recurrence and distant metastases) and seven patients died from intercurrent disease without evidence of index malignancy (second cancer – 5, pulmonary embolism, cardiac arrest). LFS at 2 and 5 years was 87% (95% CI 77–98) and 75% (95% CI 60–89), respectively, and the same rates apply to leDFS. The corresponding 2- and 5-year LRC rates (and also DFS) were 79% (95% CI 67–92) and 70% (95% CI 54–85) and for OS 92% (95% CI 84–100) and 82% (95% CI 69– 95), respectively. There were no statistically significant differences in LFS or other survival outcomes between patients with primary tumors of the larynx and hypopharynx (Figure 2).

Toxicity

In three patients with a history of hearing impairment and impaired renal function, ICT was modified from the outset by replacing cisplatin with carboplatin, and in the second cycle two further patients were switched to carboplatin due to worsening of renal function. In 10 out of 34 patients, the dose of chemotherapeutic agent(s) had to be reduced during the second cycle, and in 2 out of 7 patients during the third cycle. The median change in body weight during ICT was positive (2.5% increase, range -10.2–25.8, IQR 0–5.5). The acute toxicities of the treatment are listed in Table 4.

During cCRT, 5 (14%) patients received less than 5 cycles of chemotherapy due to hematotoxicity (4) or patient refusal (1). Three patients (8%) started concurrent carboplatin treatment (impaired hearing or renal function, chest pain during ICT) and nine (24%) patients were switched to carboplatin

TABLE 3. Disease progression after completion of study therapies

Pt. no.	Sex/ age (yrs)	Primary tumor site	cTNM	No. of ICT cyles	Disease-free interval (mos)	Site of recurrence	Salvage therapy	Outcome, after study therpies
1	M/52	Hypopharynx	T4aN1M0	3	6	Larynx, neck	Tracheostomy, palliative CT	DOD, 1.5 yrs
2	M/70	Supraglottis	T2N2bM0	3	22	Larynx, lungs	Tracheotomy, PEG, CT → ICI	AWD, 6.5 yrs
3	M/59	Hypopharynx	T2N1M0	2	19	Neck, lungs	SURG, RT+CT → ICI	DOD, 6.8 yrs
4	M/53	Glottis	T3N0M0	2	16	Larynx	SURG	NED, 3.4 yrs

AWD = alive with disease; CT = chemotherapy; DOD = death of disease; ICI = immune checkpoint inhibitor; ICT = induction chemotherapy; M = male; NED = no evidence of disease; PEG = percutaneous endoscopic gastrostomy; PT = patient; SURG = surgery; → = followed by

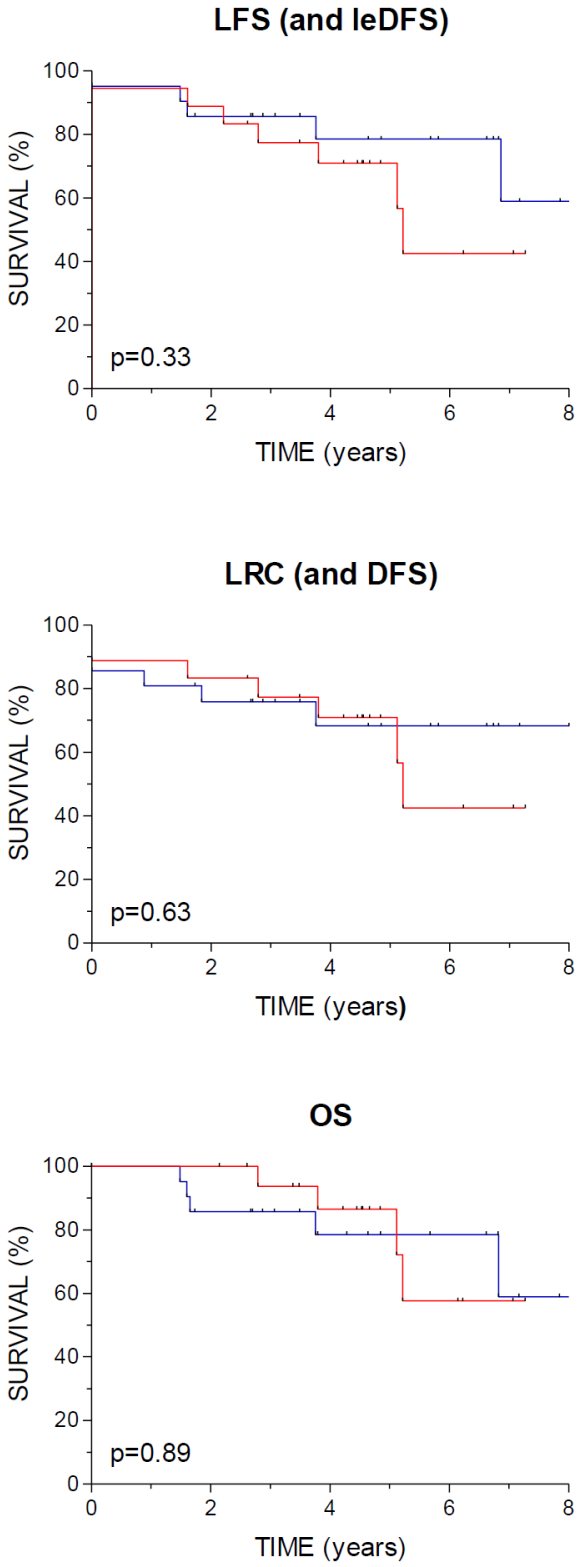

FIGURE 2. Survival outcomes by primary tumor site.

DFS = disease-free survival; leDFS = laryngo-esophageal dysfunction-free survival; LFS = laryngectomy-free survival; LRC = locoregional control; OS = overall survival

— larynx, — hypopharynx

during the course of cCRT due to renal toxicity (6), paresthesia (2) and persistent nausea (1). During the course of RT, eight patients (22%) developed grade 3 radiomucositis and 2 patients (8%; in the 5th and 6th week of RT) had a nasogastric tube placed; one of them remained tube-dependent. The median weight loss during cCRT was 7.3% (range 1.1–16.5, IQR 4.1–11.6) (Table 4).

Late treatment-related toxicities are listed in Table 5. Of 32 patients who survived more than 6 months after therapy and had no active disease, four (13%) experienced no treatment-related adverse events and 16 patients (50%) experienced grade ≥ 2 toxicity. No grade 4 or 5 adverse event was recorded. Twelve of these patients (38%) continued to smoke after stopping therapy.

Discussion

The results of the present study confirmed the hypothesis that treatment selection based on response to chemotherapy with clinical evaluation of tumor response after a single cycle of TPF ICT is a valid discriminator between chemo-/radiosensitive and resistant tumors. The proportion of patients in whom laryngectomy was successfully avoided in the long term (i.e. 5-year LFS) was encouraging and apparently higher than in the most favorable cCRT arm of the pivotal RTOG 91-11 trial, suggesting the superiority of the combination of TPF ICT and platinum-based cCRT over cCRT alone in the larynx preservation setting.[4]

When considering non-surgical treatment options for locally advanced laryngeal and hypopharyngeal tumors, the imperative is to preserve the functional organ without jeopardizing survival. For this reason, the correct selection of candidates is crucial. Any baseline dysfunction of the larynx or major involvement of the laryngeal skeleton by a tumor reduces the possibility of satisfactory restoration of laryngeal function after treatment. Therefore, the selection of patients for non-surgical treatment is usually limited to patients with T2 and T3 tumors who are not suitable for partial surgical procedures, although some patients with T4a tumors can also breathe adequately and swallow solid and liquid food safely and have a usable voice.[7,15] Our patients were only offered larynx preservation after a thorough discussion of all the advantages and disadvantages in the multidisciplinary tumor board. None of them were dependent on a tracheostomy or feeding tube prior to treatment, and 92% of the primary tumors were

TABLE 4. Acute toxicities of induction chemotherapy and concurrent chemoradiotherapy

Toxicity	Toxicity grade							
	Grade 1		Grade 2		Grade 3		Grade 4	
	No.	%	No.	%	No.	%	No.	%
Induction chemotherapy (N = 39, 80 cycles)								
Anemia	28	72	4	10	0	0	0	0
Neutropenia	1	3	1	3	1	3	5	13
Thrombocytopenia	5	13	0	0	0	0	0	0
Febrile neutropenia	-	-	-	-	5	13	1	3
Vomiting	0	0	1	3	0	0	0	0
Diarrhea	0	0	3	8	4	10	0	0
Hearing impairment	0	0	1	3	0	0	0	0
Chest pain	0	0	0	0	1	3	-	-
Weight loss	2	5	1	3	0	0	-	-
Any adverse event (no. of patients)	32	82	10	26	8	21	5	13
Concurrent chemoradiotherapy (N=37)								
Anemia	14	38	23	62	0	0	0	0
Neutropenia	8	22	8	22	6	16	1	3
Thrombocytopenia	23	62	8	22	2	5	0	0
Febrile neutropenia	-	-	-	-	1	3	0	0
Nausea	0	0	0	0	3	8	0	0
Dysphagia	13	35	16	43	5	14	0	0
Weight loss	15	41	11	30	0	0	0	0
Radiomucositis	6	16	23	62	8	22	0	0
Radiodermatitis	22	59	11	30	4	11	0	0
Any adverse event (no. of patients)	36	97	35	95	21	57	1	3

stage T2 or T3. In addition, the relatively low median age and low comorbidity burden assured the best possible adherence to the planned oncological treatment.

Although a meta-analysis has confirmed the association between poor response to ICT and subsequent (cC)RT in larynx preservation trials, the optimal number of ICT cycles to reliably identify tumors suitable for non-surgical treatment scenarios is not known. According to the Larynx Preservation Consensus Panel, assessment should be performed after two cycles of ICT.[16] However, Urba *et al*. showed in their phase II study that after a single cycle of cisplatin/5FU ICT, 75% of laryngeal cancer patients achieved at least a partial response at the primary site; after cCRT in responders or surgery in non-responders, DFS was 80% and 78% after 2 and 3 years, respectively.[10] These results compare favorably to the larynx preservation trials, which used more than one cycle of ICT, and underscore the prognostic importance of tumor shrinkage dynamics during ICT.[5] Several other authors later confirmed the prognostic value of tumor shrinkage after the first cycle of ICT.[17,18] Furthermore, tumor assessment using flexible endoscopy appears to be reliable given the survival results presented and the fact that it correlates well with volumetric CT measurements but has a higher interobserver reliability.[19,20] Moreover, it is easy to perform even in the context of a busy clinical routine. Alternative methods of assessing tumor response to ICT using modern imaging techniques, blood biomarkers or a specific gene signature are either much more complex or less validated, but do not appear to be more reliable.[21-23]

Since we used the TPF ICT regimen, the proportion of responders in our series was, as expected, higher (95%) than in the previously mentioned

TABLE 5. Late toxicities in 32 patients surviving > 6 months after therapy and without active disease (median observation time 4.5 years, range 2–8, interquartile range 3.5–6)

Toxicity	Toxicity grade					
	Grade 1		Grade 2		Grade 3	
	No.	%	No.	%	No.	%
Voice changes	15	47	1	3	0	0
Laryngeal edema	9	28	0	0	0	0
Dysphagia	4	13	2	6	0	0
Alteration of taste	2	6	1	3	0	0
Xerostomia	15	47	5	16	0	0
Skin fibrosis	9	28	2	6	1	3
Altered skin pigmentation	15	47	0	0	0	0
Chronic neuropathy, sensory	2	6	1	3	0	0
Thyroid dysfunction	1	3	15	47	0	0
Any adverse event (no. of patients)	26	81	16	50	1	3

study by Urba *et al.* (75%) or in other studies using a platinum-based/5FU combination.[3,10] However, it was comparable to the reported experience with TPF ICT, although tumor response assessment in these studies occurred later in the course of ICT.[9,24] Another observation in our study is that both primary laryngeal and hypopharyngeal tumors responded to TCF ICT, with no statistically significant differences in the proportion of CRs and PRs between the two groups. The reliability of early assessment of tumor response during the ICT phase of treatment, as applied in our study, was confirmed by the low rate of local and/or regional recurrence (in 4 patients, 10%), half of which were cured after timely salvage surgery. Only two patients died of the disease and the third is still alive with the lung metastases 5.8 years after the treatment. In addition, the 2- and especially the 5-year LFS (and leDFS) of 87% and 75%, respectively, in our patients compares favorably with the results of the RTOG 91-11 study, despite a significant proportion of prognostically less favorable hypopharyngeal primary tumors in our group.[3,4] Exactly the same applies to the comparison with other prospective randomized trials and nonrandomized cohort studies that included patients with both laryngeal and hypopharyngeal cancer.[9,17,24,25] The encouraging results suggest the efficacy of the approach tested and emphasize the importance of treating such patients in an experienced multidisciplinary team that provides a balanced assessment of each case, therapeutic expertise, follow-up and timely surgical salvage.[26] In addition, the number of systemic progressions was low (2/39) and most deaths were due to smoking-related metachronous cancers (5/9 deaths). The latter reflects the high proportion of smokers (97%) among our patients, 62% of whom were active smokers at the time of diagnosis and half of whom did not stop smoking after treatment.

The majority of our patients received only two cycles of ICT and the cumulative doses of chemotherapeutic agents were significantly lower than in the pivotal TAX 323 and TAX 324 trials, in which TPF was compared with the PF ICT regimen.[27,28] Still, toxicity was significant: the median interval between the start of the last ICT cycle and the start of cCRT was 26 days, and grade 3 and 4 adverse events were observed in 21% and 13% of patients, respectively, so that a second cycle could not be performed in two (5%) patients. Furthermore, it is questionable whether the third ICT cycle contributed to the efficacy of the treatment, as the disease recurred in 2 of these 7 patients. On the other hand, all three responders who had received only one ICT cycle were free of malignant disease at the last follow-up. Considering the aggressiveness of subsequent cCRT, it seems reasonable to limit ICT to the smallest number of cycles that is still safe. In fact, the proportion of patients with cCRT-related toxicities of grade ≥ 3 was 57%. Although this is within the expected range, it requires optimization of the induction phase of treatment.[12] The role of immune checkpoint inhibitors in the induction

phase of larynx preservation therapy is currently the subject of intensive clinical research.[29]

Despite the significant proportion (54%) of prognostically unfavorable hypopharyngeal cancers in our group, the calculated DFS and OS rates were high, suggesting that treatment intensification by combining ICT and cCRT is important in larynx preservation setting. This has also been noted by other authors.[10,11] However, the results of randomized trials investigating the role of the addition of TPF ICT to cCRT in head and neck cancers contradict our observation of a positive contribution of ICT to treatment efficacy.[8] The reason for this could be the difference in tumor burden, which is generally lower in the larynx preservation setting than in the reported studies.

Our study has limitations primarily related to the small sample size, the retrospective design, and the inclusion of laryngeal and hypopharyngeal cancers, which differ significantly in terms of prognosis.[30] However, in our group, no difference in survival was found between patients with primary laryngeal and hypopharyngeal tumors, and the same was found in the TREMPLIN trial.[31] Furthermore, the study was not originally designed to answer the question of the optimal number of ICT cycles required for reliable identification of chemo-/radiosensitive tumors, nor to test the contribution of ICT to the efficacy of a particular treatment scenario. However, given the toxicity of TPF ICT and the lack of a clear benefit of a third ICT cycle for prognosis, two applications of ICT appear to be sufficient. Whether a single "chemoselector" cycle of TPF ICT followed by platinum-based cCRT would lead to an equally favorable outcome remains to be determined.

We conclude that clinical assessment of tumor response to one cycle of TPF ICT serves as a valid and easy-to-use predictor of tumor sensitivity to platinum-based cCRT. The tested combination of two cycles of ICT and cCRT resulted in a favorable larynx preservation rate and survival outcomes, with no difference between laryngeal and hypopharyngeal primary tumors. However, due to the toxicity of combination therapy, further de-intensification of the ICT component to a single chemoselector cycle with possible optimization of the drug combination appears to be justified.

Acknowledgments

This research was funded by Slovenian Research and Innovation Agency (ARIS), grant number P3-0307.

AI disclosure

During the preparation of this paper, the author(s) used InstaText in the writing process to improve the readability and language of the manuscript. After using this tool/service, the author(s) have reviewed and edited the content as required and take full responsibility for the content of the publication.

References

1. Singer S, Danker H, Guntinas-Lichius O, Oeken J, Pabst F, Schock J, et al. Quality of life before and after total laryngectomy: results of a multicenter prospective cohort study. *Head Neck* 2014; **36:** 359-68. doi: org/10.1002/hed.23305
2. Argiris A, Lefebvre JL. Laryngeal preservation strategies in locally advanced laryngeal and hypopharyngeal cancers. *Front Oncol* 2019; **9:** 419. doi: org/10.3389/fonc.2019.00419
3. Forastiere AA, Goepfert H, Maor M, Pajak TF, Weber R, Morrison W, et al. Concurrent chemotherapy and radiotherapy for organ preservation in advanced laryngeal cancer. *N Engl J Med* 2003; **349:** 2091-8. doi: 10.1056/NEJMoa031317
4. Forastiere AA, Zhang Q, Weber RS, Maor MH, Goepfert H, Pajak TF, et al. Long-term results of RTOG 91-11: a comparison of three nonsurgical treatment strategies to preserve the larynx in patients with locally advanced larynx cancer. *J Clin Oncol* 2013; **31:** 845-52. doi: org/10.1200/JCO.2012.43.6097
5. Strojan P, Haigentz M Jr, Bradford CR, Wolf GT, Hartl DM, Langendijk JA, et al. Chemoradiotherapy vs. total laryngectomy for primary treatment of advanced laryngeal squamous cell carcinoma. *Oral Oncol* 2013; **49:** 283-6. doi: org/10.1016/j.oraloncology.2012.11.002
6. Kiong KL, de Souza NN, Sultana R, Iyer NG. Meta-analysis of induction chemotherapy as a selection marker for chemoradiation in the head and neck. *Laryngoscope* 2018; **128:** 1594-601. doi: org/10.1002/lary.27011
7. Forastiere AA, Ismaila N, Lewin JS, Nathan CA, Adelstein DJ, Eisbruch A, et al. Use of larynx-preservation strategies in the treatment of laryngeal cancer: American Society of Clinical Oncology Clinical Practice Guideline update. *J Clin Oncol* 2018; **36:** 1143-69. doi: org/10.1200/JCO.2017.75.7385
8. Vidal L, Ben Aharon I, Limon D, Cohen E, Popovtzer A. Role of induction chemotherapy prior to chemoradiation in head and neck squamous cell cancer - systematic review and meta-analysis. *Cancer J* 2017; **23:** 79-83. doi: org/10.1097/PPO.0000000000000253
9. Lefebvre JL, Pointreau Y, Rolland F, Alfonsi M, Baudoux A, Sire C, et al. Induction chemotherapy followed by either chemoradiotherapy or bioradiotherapy for larynx preservation: the TREMPLIN randomized phase II study. *J Clin Oncol* 2013; **31:** 853-9. doi: org/10.1200/JCO.2012.42.3988
10. Urba S, Wolf G, Eisbruch A, Worden F, Lee J, Bradford C, et al. Single-cycle induction chemotherapy selects patients with advanced laryngeal cancer for combined chemoradiation: a new treatment paradigm. *J Clin Oncol* 2006; **24:** 593-8. doi: org/10.1200/JCO.2005.01.2047
11. Wolf GT, Bellile E, Eisbruch A, Urba S, Bradford CR, Peterson L, et al. Survival rates using individualized bioselection treatment methods in patients with advanced laryngeal cancer. *JAMA Otolaryngol Head Neck Surg* 2017; **143:** 355-66. doi: org/10.1001/jamaoto.2016.3669
12. Strojan P, Gražič Kuhar C, Žumer B, Kadivec M, Karner K, Fajdiga I, et al. TPF induction chemotherapy and concomitant irradiation with cisplatin and cetuximab in unresectable squamous cell carcinoma of the head and neck. *Head Neck* 2014; **36:** 1555-61. doi: org/10.1002/hed.23506
13. Grégoire V, Evans M, Le QT, Bourhis J, Budach V, Chen A, et al. Delineation of the primary tumour Clinical Target Volumes (CTV-P) in laryngeal, hypopharyngeal, oropharyngeal and oral cavity squamous cell carcinoma: AIRO, CACA, DAHANCA, EORTC, GEORCC, GORTEC, HKNPCSG, HNCIG, IAG-KHT, LPRHHT, NCIC CTG, NCRI, NRG Oncology, PHNS, SBRT, SOMERA, SRO, SSHNO, TROG consensus guidelines. *Radiother Oncol* 2018; **126:** 3-24. doi: org/10.1016/j.radonc.2017.10.016

14. Grégoire V, Ang K, Budach W, Grau C, Hamoir M, Langendijk JA, et al. Delineation of the neck node levels for head and neck tumors: a 2013 update. DAHANCA, EORTC, HKNPCSG, NCIC CTG, NCRI, RTOG, TROG consensus guidelines. *Radiother Oncol* 2015; **117:** 83-90. doi: org/10.1016/j.radonc.2015.07.041

15. Beitler JJ, Ridge JA, Vermorken JB, Bradford CR, Strojan P, Saba NF, et al. T4 laryngeal cancer with good function: should we be reluctant to treat without surgery? *Int J Radiat Oncol Biol Phys* 2018; **102:** 400-3. doi: org/10.1016/j.ijrobp.2018.03.007

16. Lefebvre JL, Ang KK. Larynx Preservation Consensus Panel. Larynx preservation clinical trial design: key issues and recommendations - a consensus panel summary. *Head Neck* 2009; **31:** 429-41. doi: org/10.1002/hed.21081

17. Wichmann G, Krüger A, Boehm A, Kolb M, Hofer M, Fischer M, et al. Induction chemotherapy followed by radiotherapy for larynx preservation in advanced laryngeal and hypopharyngeal cancer: outcome prediction after one cycle induction chemotherapy by a score based on clinical evaluation, computed tomography-based volumetry and 18F-FDG-PET/CT. *Eur J Cancer* 2017; **72:** 144-55. doi: org/10.1016/j.ejca.2016.11.013

18. Popovtzer A, Burnstein H, Stemmer S, Limon D, Hili O, Bachar G, et al. Phase II organ-preservation trial: concurrent cisplatin and radiotherapy for advanced laryngeal cancer after response to docetaxel, cisplatin, and 5-fluorouracil-based induction chemotherapy. *Head Neck* 2017; **39:** 227-33. doi: org/10.1002/hed.24571

19. Garcia GCTE, Gorphe P, Hartl D, Ammari S, Even C, Tao Y, et al. Computed tomography evaluation after induction chemotherapy for T3 laryngeal cancer: does response correlate with vocal cord mobility? *Oral Oncol* 2019; **90:** 13-6. doi: 10.1016/j.oraloncology.2019.01.009

20. Ferrari M, Mularoni F, Taboni S, Crosetti E, Pessina C, Carobbio ALC, et al. How reliable is assessment of true vocal cord-arytenoid unit mobility in patients affected by laryngeal cancer? A multi-institutional study on 366 patients from the ARYFIX collaborative group. *Oral Oncol* 2024; **152:** 106744. doi: 10.1016/j.oraloncology.2024.106744

21. de Bree R, Wolf GT, de Keizer B, Nixon IJ, Hartl DM, Forastiere AA, et al. Response assessment after induction chemotherapy for head and neck squamous cell carcinoma: from physical examination to modern imaging techniques and beyond. *Head Neck* 2017; **39:** 2329-49. doi: 10.1002/hed.24883

22. Xu J, Yang Y, Zhong Q, Hou L, Ma H, Zhang Y, et al. A study of peripheral blood parameters to predict response to induction chemotherapy and overall survival in advanced laryngeal squamous cell carcinoma. *Curr Oncol* 2022; **29:** 6472-84. doi: 10.3390/curroncol29090509

23. Tan C, Wang L, Yang Y, He S, Chen GG, Chan JY, et al. Construction of a novel six-gene signature to predict tumour response to induction chemotherapy and overall survival in locoregionally advanced laryngeal and hypopharyngeal carcinoma. *Genes Dis* 2023; **11:** 101022. doi: 10.1016/j.gendis.2023.05.018

24. Janoray G, Pointreau Y, Garaud P, Chapet S, Alfonsi M, Sire C, et al. Long-term results of a multicenter randomized phase III trial of induction chemotherapy with cisplatin, 5-fluorouracil, ± docetaxel for larynx preservation. *J Natl Cancer Inst* 2016; **108:** djv368. doi: 10.1093/jnci/djv368

25. Dietz A, Wichmann G, Kuhnt T, Pfreundner L, Hagen R, Scheich M, et al. Induction chemotherapy (IC) followed by radiotherapy (RT) versus cetuximab plus IC and RT in advanced laryngeal/hypopharyngeal cancer resectable only by total laryngectomy: final results of the larynx organ preservation trial DeLOS-II. *Ann Oncol* 2018; **29:** 2105-14. doi: 10.1093/annonc/mdy332

26. Sanabria A, Chaves ALF, Kowalski LP, Wolf GT, Saba NF, Forastiere AA, et al. Organ preservation with chemoradiation in advanced laryngeal cancer: the problem of generalizing results from randomized controlled trials. *Auris Nasus Larynx* 2017; **44:** 18-25. doi: 10.1016/j.anl.2016.06.005

27. Vermorken JB, Remenar E, van Herpen C, Gorlia T, Mesia R, Degardin M, et al; EORTC 24971/TAX 323 Study Group. Cisplatin, fluorouracil, and docetaxel in unresectable head and neck cancer. *N Engl J Med* 2007; **357:** 1695-704. doi: 10.1056/NEJMoa071028

28. Posner MR, Hershock DM, Blajman CR, Mickiewicz E, Winquist E, Gorbounova V, et al; TAX 324 Study Group. Cisplatin and fluorouracil alone or with docetaxel in head and neck cancer. *N Engl J Med* 2007; **357:** 1705-15. doi: org/10.1056/NEJMoa070956

29. Peng J, Luo G, Yu Y, Ning K, Liu X. Retrospective assessment of neoadjuvant camrelizumab combined with induction chemotherapy: efficacy in laryngeal preservation for advanced hypopharyngeal and laryngeal squamous cell carcinoma. *Cancer Immunol Immunother* 2024; **73:** 54. doi: org/10.1007/s00262-023-03579-0

30. Chow LQM. Head and neck cancer. *N Engl J Med* 2020; **382:** 60-72. doi: org/10.1056/NEJMra1715715

31. Janoray G, Pointreau Y, Alfonsi M, Sire C, Geoffrois L, de Raucourt D, et al. Induction chemotherapy followed by cisplatin or cetuximab concomitant to radiotherapy for laryngeal/hypopharyngeal cancer: long-term results of the TREMPLIN randomised GORTEC trial. *Eur J Cancer* 2020; **133:** 86-93. doi: 10.1016/j.ejca.2020.04.009

research article

The influence of periodontal disease and periodontal treatment on colorectal cancer

Ursa Potocnik Rebersak[1,2], Erik Brecelj[3], Rok Schara[1,2]

[1] Center of Oral Diseases and Periodontology, Dental Clinic, University Medical Centre Ljubljana, Slovenia
[2] Faculty of Medicine, University of Ljubljana, Slovenia
[3] Institute of Oncology Ljubljana, Slovenia

Radiol Oncol 2025; 59(4): 589-596.

Received 18 February 2025
Accepted 26 March 2025

Correspondence to: Urša Potočnik Reberšak, D.M.D., Center of Oral Diseases and Periodontology, Dental Clinic, University Medical Centre Ljubljana, Hrvatski trg 6, SI-1000 Ljubljana, Slovenia, E-mail: ursa.potocnik.rebersak@kclj.si

Disclosure: No potential conflicts of interest were disclosed.

Background. Periodontal disease (PD) is associated with more than 50 diseases and conditions, including colorectal cancer. The study aimed to investigate if periodontal treatment influences the blood levels of C-reactive protein (CRP) in colorectal cancer patients. In addition, the aim was to isolate periodontal pathogenic bacteria *Fusobacterium nucleatum* (FN) and *Porphyromonas gingivalis* (PG), which are most linked to colorectal cancer (CRC), from the mucosa of the cancer-affected intestine.

Patients and methods. To assess the effect of periodontal treatment on colorectal cancer, we measured the CRP levels in the blood during cancer therapy on the day of the initial examination by the oncological surgeon, two days following surgery, and at the first follow-up appointment. We compared the CRP levels between two groups: the group of subjects who underwent periodontal treatment and the patients who did not receive periodontal disease treatment. An attempt was made to isolate the periodontal pathogenic bacteria FN and PG from the mucosa of the cancerous tissue in the colon by using quantitative culture.

Results. We found no statistically significant difference between the groups in the initial CRP measurements before starting cancer treatment. There was no statistically significant difference between the groups in the CRP measurements taken 1st and 2nd day after surgery and at the follow-up appointment. We could not isolate periodontal pathogenic bacteria FN and PG from cancer-altered intestine mucosa using the quantitative culture method.

Conclusions. Our study did not find any correlation between periodontal treatment and CRC.

Key words: periodontal disease; colorectal cancer; periodontal treatment; fusobacterium nucleatum; porphyromonas gingivalis; C-reactive protein

Introduction

Periodontal disease (PD) is a chronic multifactorial inflammatory disease triggered by dysbiosis in the dental plaque biofilm and characterized by severe chronic inflammation, which leads to the progressive destruction of the tooth's supporting tissue. PD is a significant public health problem.[1,2]

According to the World Health Organization, approximately 19% of the global population suffers from severe periodontal disease, representing more than 1 billion cases in individuals over the age of 15.[3]

Periodontal disease (PD) is associated with more than 50 diseases and conditions, such as cardiovascular diseases, Alzheimer's disease, diabetes, rheumatoid arthritis, aspiration pneumonia, and cancer, including colorectal cancer (CRC).[4] CRC is the third most common type of cancer worldwide. In 2022, more than 1.9 million cases were diagnosed. CRC

is the second most common cause of cancer-related death, with more than 900,000 deaths annually.[5]

An increasing body of evidence has confirmed that, in addition to smoking, obesity, aging, and other risk factors, chronic inflammation also plays a role in the development of CRC.[6] PD is one of humans' most common chronic inflammatory diseases.[7] In 2010, PD was the 6th most common health condition.[8]

Despite the anatomical distance between the oral cavity and the intestine, studies have shown that bacteria from the mouth can spread to the intestine, especially in the presence of PD. Periodontopathogenic bacteria, such as *Fusobacterium nucleatum (FN) and Porphyromonas gingivalis (PG),* can alter the composition of the local microbiome in the colorectal region, which subsequently leads to the development of gastrointestinal diseases.[9]

In a study by Li *et al*., a systematic review of the literature and meta-analysis investigated the potential link between PD and CRC. They found that there is a 44% increased risk of developing CRC associated with PD. This connection could help raise awareness of the importance of maintaining periodontal health and, consequently, contribute to reducing the burden of CRC.[10]

The study aimed to investigate if periodontal treatment influences the blood levels of C-reactive protein (CRP) in colorectal cancer patients. In addition, the aim was to isolate periodontal pathogenic bacteria *Fusobacterium nucleatum* (FN) and *Porphyromonas gingivalis* (PG), which are most linked to colorectal cancer (CRC), from the mucosa of the cancer-affected intestine.

Patients and methods

The study was conducted at the Center of Oral Diseases and Periodontology at the Dental Clinic, University Medical Centre Ljubljana, Slovenia, in collaboration with the Institute of Oncology Ljubljana, Slovenia, from October 2023 to September 2024. The study was approved by the Medical Ethics Committee of the Republic of Slovenia (No. 0120-486/2021/6). ClinicalTrials.gov Identifier: NCT06799182

Patients

The patients included in the study were divided into two groups: the experimental group and the control group. Due to ethical concerns, patients were not randomly assigned to the control group. All patients newly diagnosed with CRC underwent an oral cavity examination and received periodontal treatment based on the examination results. Samples were taken for microbiological testing using quantitative culture for *FN* and *PG.*

Inclusion criteria for the experimental group

A new diagnosis of CRC, planned for surgical treatment, and consent to participate in the study.

Exclusion criteria for the experimental group

The exclusion criteria were patient refusal to participate in the study, age under 18, periodontal treatment in the last 12 months, antibiotic therapy 3 months before the study, edentulism, advanced cancer for which only palliative treatment was planned, prior radiation of the intestines, and chemotherapy before surgery that could alter the composition of the intestinal microbiome.

Inclusion criteria for the control group

Patients who had started CRC therapy before the beginning of our study in October 2023 were selected. The study included patients who attended a follow-up examination for CRC at the Institute of Oncology Ljubljana surgical clinic between June 2024 and September 2024, met the inclusion criteria, and consented to participate. Patients were recruited through targeted questionnaires. Inclusion criteria for the control group were: CRC primarily treated surgically, consent to participate (completion of the questionnaire), blood tests for CRP as part of cancer treatment at the first examination, after surgery, and at the first follow-up, and age over 18 years.

Exclusion criteria for the control group

The exclusion criteria were edentulism, non-cooperation, periodontal treatment 12 months before surgery, advanced cancer for which only palliative treatment was planned, and smokers (to match the experimental group).

Oral clinical examination

All patients in the experimental group underwent a comprehensive oral cavity examination, including the mucosa, dental, and periodontal tissues. Precise recordings of probing depths, gingival

recession, and bleeding on probing at six sites around each tooth, degree of tooth mobility, and involvement of furcations in multi-rooted teeth were made. Each patient also underwent radiographic imaging (panoramic radiograph, with a local radiograph performed later if needed). The periodontal condition was diagnosed according to the 2017 Classification of Periodontal and Peri-implant Diseases and Conditions.

Periodontal treatment

All patients with diseased periodontal tissues underwent non-surgical treatment for periodontal disease. Treatment included the removal of supragingival and subgingival plaque, root scaling and planing at all sites with increased probing depth (≥ 4 mm), and bleeding on probing. Tooth extractions were performed for teeth with a hopeless prognosis. We also provided oral hygiene instructions and demonstrated the use of tools for maintaining thorough oral hygiene.

CRC diagnosis and CRP blood testing

From the medical records of the participants at the Institute of Oncology Ljubljana, who were included in the study, we obtained data on the CRC diagnosis, histopathological type, disease stage, and CRP values at the first examination after surgery (2 consecutive measurements), and at the first follow-up examination.

Microbiological testing

Samples for microbiological testing were taken from both periodontal pockets and the mucosa of cancer-altered intestines.

Samples from the periodontal pocket were taken from the most inflamed spot. After removing supragingival plaque (if present) and relative drying of the sampling area, we inserted a paper point (0.3 mm diameter, Maillefer, Ballaigues, Switzerland) into the periodontal pocket for 30 seconds. The paper point was placed in a transport medium (RTF 1.5 ml) and delivered to the laboratory within 2 hours.

Samples of cancer-altered colon tissue were taken at the Institute of Oncology Ljubljana during CRC surgery. All tissue samples were obtained in a manner that did not jeopardize further cancer diagnostics. After collection, the tissue samples were placed in the transport medium (RTF 1.5 ml) and delivered to the laboratory within 24 hours.

Microbiological testing - quantitative culture for Fusobacterium nucleatum (FN) and Porphyromonas gingivalis (PG)

Samples from periodontal pockets and the mucosa of cancer-altered intestines were cultured at the Laboratory for Bacteriological Diagnostics of Respiratory Infections, Institute of Microbiology and Immunology, Medical Faculty, Ljubljana, using standard procedures on non-selective anaerobic media. All samples were processed within 24 hours of collection. Before processing, the samples were stored in an RTF transport medium at room temperature.

The samples were first diluted 10-fold with PBS solution (NaCl 8 g/l, KCl 2 g/l, Na3HPO4 *H2O 1.15 g/l, KH2PO4 0.2 g/l). Then, 100 µl of each dilution was inoculated onto non-selective blood agar (Oxoid No. 2; Oxoid, Basingstoke, UK) supplemented with 5% horse blood, hemin (5 mg/l), where the bacteria were cultured in anaerobic conditions (80% N2, 10% H2, 10% CO2) at 37°C. After one week, all grown colonies were counted, and the colonies of *FN* and *PG* were identified and counted.

For the identification of bacterial colonies, standard methods were used: recognition of colony morphology, cell morphology (Gram staining), aerotolerance, catalase production, and mass spectrometry (MALDI, Biotyper, Bruker Daltonics, Germany)[11].

Statistical analysis

Descriptive statistics in tables and graphs were used to analyze patients' data and the results of microbiological tests.

Statistical analysis was performed using IBM SPSS Statistics for Windows, Version 29.0.2.0 (IBM Corp., Armonk, NY: IBM Corp., 2023).

To determine the differences in CRP levels during CRC treatment between the experimental group with additional periodontal disease therapy and the control group, we used the t-test for independent samples. A p-value of <0.05 was considered statistically significant.

Results

Patient data

Experimental group

A total of ten patients were included in the experimental group, all of whom met the inclusion criteria and agreed to participate in the study. The

TABLE 1. Patient data for the experimental group

Patient	Gender	Age (years)	Clinical diagnosis and location of the CRC	Histo-pathological diagnosis	TNM** classification	BMI*	Other systemic diseases	Smoker
1	M	64	Transverse colon cancer	Adenocarcinoma	T3N0	28.3	High cholesterol, high blood pressure	NO
2	F	60	Right colon cancer	Adenocarcinoma	T3N1bM0	25	No systemic diseases	NO
3	F	87	Cecum cancer	Adenocarcinoma	T4N3bM0	27.2	Asthma, hypothyroidism	NO
4	M	60	Sigmoid colon cancer	Adenocarcinoma	T2N0M0	30	Asthma, hypothyroidism	NO
5	M	83	Ascending colon cancer	Adenocarcinoma	T3N1bM0	25.1	Type 2 diabetes, high blood pressure	NO
6	F	70	Colon polyp	Tubular adenoma with low dysplasia	/	25.4	High blood pressure	NO
7	M	64	Ascending colon cancer	Non-Hodgkin lymphoma	T3N1cM0	28	No systemic diseases	NO
8	F	68	Transverse colon cancer	Squamous cell carcinoma	T4aN1M0	21	Rheumatoid arthritis, hypothyroidism	YES 0-5/day
9	F	57	Cecum cancer	Adenocarcinoma	T3bN1bM0	22.5	Hypothyroidism	NO
10	F	53	Sigmoid colon cancer	Adenocarcinoma	pT2N0	21	No systemic diseases	NO

*BMI = mody mass index;

**TNM classification: T0 - tumor not present, T1 - invasion into submucosa, T2 - invasion into muscularis propria, T3 - invasion into subserosa, T4 - invasion through all layers of the colon and into the visceral peritoneum or adjacent structures; N (lymph nodes): N0 - no regional lymph nodes involved, N1 - 1–3 regional lymph nodes involved, N2 - 4–6 regional lymph nodes involved, N3 - 7+ regional lymph nodes involved; M (metastasis): M0 - no distant metastases, M1 - presence of distant metastases;

Ca = cancer; CRC = colorectal cancer; F = female; M = male

average age of the patients was 66.6 years, with six female and four male participants. In the study, nine patients were non-smokers, and 1 was an occasional smoker who smoked 0-5 cigarettes daily. Table 1 presents the patient data.

In the experimental group, a detailed examination of the periodontal tissues was performed, and a diagnosis of periodontal disease was made according to the 2017 classification of periodontal diseases and conditions. Out of the ten patients, four had generalized periodontal disease (stage IV, grade B), five had localized periodontal disease (stage III, grade B), and one had localized periodontal disease (stage III, grade A). None of the patients had healthy periodontal tissues.

Control group

Ten patients completed the questionnaires. One patient was excluded from the study due to having undergone periodontal treatment in the year before starting cancer treatment. The average age of the remaining nine participants was 65.1 years. The group consisted only of non-smokers, including five males and four females. Table 2 presents the patient data.

No dental examination was performed for the control group, and the status of periodontal tissues was obtained through the questionnaires. Of the nine participants, five did not report any issues with their gums during cancer treatment, while 4 reported problems with their gums. Among them, three had been diagnosed with periodontal disease and had lost one or more teeth as a result.

CRP levels

We found no statistically significant difference between the groups in the initial CRP measurements before starting colorectal cancer (CRC) treatment ($p = 0.242$; 95% CI [-3.9897; 14.7385]). There was also no statistically significant difference between the groups in the CRP measurements taken 1 day after surgery for CRC ($p = 0.592$; 95% CI [-34.915; 59.2661]). Similarly, no statistically significant difference was observed between the groups in the second CRP measurement taken 2 days after the surgery ($p = 0.485$; 95% CI [-77.409; 38.3646]). Additionally, no statistically significant difference was found when comparing the control CRP measurements between the groups ($p = 0.533$; 95% CI [-7.2638; 3.9083]).

TABLE 2. Patient data from the control group

Patient	Gender	Age (years)	Clinical diagnosis and location of the CRC	Histo-pathological diagnosis	TNM** classification	B*MI	Other systemic diseases	Smoker
K1	M	72	Cecum carcinoma	Adenocarcinoma	T3N1	21.4	High blood pressure, heart rhythm disorders, prostate cancer survivor, hyper lipoproteinemia	NO
K2	M	58	Sigmoid colon cancer	Adenocarcinoma	T2	26	High blood pressure, high cholesterol	NO
K3	M	52	Sigmoid colon cancer	Adenocarcinoma	T3cN1a	37.2	High cholesterol, hyperglycemia	NO
K4	M	86	Transverse colon cancer	Adenocarcinoma	T3N1	21.9	High blood pressure, enlarged prostate	NO
K5	F	51	Sigmoid colon cancer	Adenocarcinoma	T1N1a	16.67	Herniated disc	NO
K6	M	67	Colorectal cancer (location not specified)	Adenocarcinoma	T3N1a	27	No systemic diseases	NO
K7	F	72	Sigmoid colon cancer	Adenocarcinoma	T3bN0	28.4	High blood pressure, hyper-lipoproteinemia, mild heart failure, ischemic heart disease	NO
K8	F	60	Left colon cancer	Adenocarcinoma	T1N0	21.5	No systemic diseases	NO
K9	F	68	Sigmoid colon cancer	Adenocarcinoma	T2N0	27.2	High blood pressure, high cholesterol, glaucoma	NO

*BMI = mody mass index;

**TNM classification: T0 - tumor not present, T1 - invasion into submucosa, T2 - invasion into muscularis propria, T3 - invasion into subserosa, T4 - invasion through all layers of the colon and into the visceral peritoneum or adjacent structures; N (lymph nodes): N0 - no regional lymph nodes involved, N1 - 1–3 regional lymph nodes involved, N2 - 4–6 regional lymph nodes involved, N3 - 7+ regional lymph nodes involved; M (metastasis): M0 - no distant metastases, M1 - presence of distant metastases;

Ca = cancer; CRC = colorectal cancer; F = female; M = male

Figure 1 schematically shows the movement of CRP levels in the blood during cancer therapy for the control and experimental groups.

Microbiological tests performed in the experimental group

Isolation of Porphyromonas gingivalis (PG)

We successfully isolated the PG bacteria from periodontal pockets in five out of ten patients (50%). However, using the quantitative culture method, we could not isolate the bacteria from any of the colorectal cancer (CRC) tissue samples (0%).

Isolation of Fusobacterium nucleatum (FN)

We successfully isolated the FN bacteria from the periodontal pockets in all the patients (100%). However, using the quantitative culture method, we could not isolate the bacteria from any of the CRC tissue samples (0%).

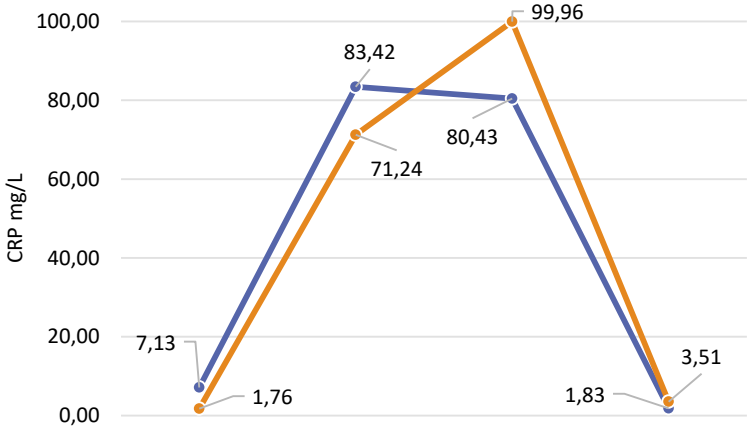

FIGURE 1. Changes in the CRP levels in the serum of the experimental (blue line) and control groups (orange line) during colorectal cancer therapy.

Discussion

In our study, using quantitative culture, we successfully isolated FN from the periodontal pockets

of all patients (ten out of ten). In contrast PG was isolated from the periodontal pockets of half the patients (five out of ten). However, in the cancer-altered mucosa of the colon, none of the tested periodontal pathogenic bacteria were isolated.

Furthermore, we compared the impact of periodontal treatment between the experimental group, which had undergone non-surgical periodontal therapy before the surgical phase of CRC treatment, and the control group. Due to ethical concerns, we did not conduct a randomized clinical trial. The patients in the control group were recruited through directed questionnaires. They were patients who had completed the active phase of CRC therapy and were attending follow-up appointments at the Institute of Oncology in Ljubljana. Data on CRP levels were obtained retrospectively from their medical records. Our study did not find statistically significant differences between the groups regarding CRP measurements before and during CRC therapy.

One potential mechanism linking PD and CRC is the spread of periodontal pathogens, particularly PG and FN, from the oral cavity to the intestinal mucosa. In theory, there are two pathways through which bacteria can spread from the oral cavity to the intestine. The first is the hematogenous route, where bacteria enter the bloodstream through lesions in the oral cavity, like that of the ulcerated epithelium of the periodontal pocket, and reach the intestinal mucosa via the blood. The second is the enteral route, where bacteria travel through the stomach to the intestine. Although the human body has defense mechanisms along this path, such as neutralization by stomach acid and a colonization barrier against foreign microorganisms, there are cases where these defense mechanisms are weakened.[12]

In the study by Abed *et al*., the researchers aimed to confirm the hypothesis that FN originates from the oral cavity and that colonization of the intestine by the bacteria is effective. They collected samples from the oral cavity and adenocarcinoma during resections. As in our study, FN was successfully isolated in all saliva samples. Additionally, FN DNA was confirmed in the adenocarcinoma samples using PCR, but live FN was only successfully cultured from one sample. So, they attempted to isolate FN from adenocarcinoma samples obtained during colonoscopy, where antibiotic prophylaxis is not required. They received numerous colonies of FN from both biopsy samples and saliva samples, and genomic analysis indicated a high degree of similarity between the strains isolated from the oral cavity and the adenocarcinoma of the same patient. This suggested that the strains of FN in the oral cavity might have migrated and proliferated in the colorectal cancer tissue.[13]

In contrast to Abed *et al*., our study did not isolate any live FN from colorectal cancer tissue (zero out of nine) collected during resective surgery. Like in the study of Abed *et al*., all our patients had received preoperative antibiotics (cefazolin and metronidazole), which may have hindered the isolation of live bacteria from the cancerous tissue. We tried to mitigate the effects of antibiotic treatment and collected tissue samples during colonoscopy from one patient who had not received antibiotics preoperatively. However, FN was not isolated from this sample either. We also attempted to isolate PG from the cancerous colorectal mucosa but were unable to detect it in the colon in any of the patients, but we were successful in isolating it from the periodontal pocket in 50% of patients. Other studies have used molecular methods like PCR to detect PG in colorectal cancer tissue. Kerdreux *et al*. used PCR to detect PG in 6.2% of colorectal cancer tissue samples[14], and Wang *et al.* used qPCR to find PG in 10 out of 31 CRC tissue samples, with a statistically significant difference in the presence of PG between cancerous and adjacent normal tissue.[15]

Although culture methods remain the gold standard, they have limitations, including difficulties in culturing certain bacteria, imprecision in counting microorganisms, and the costs involved. This has led to developing more sensitive, accurate, and cost-effective molecular methods for detecting and quantifying bacteria in biofilms. In our study, we could not isolate live PG and FN from colorectal cancer tissue using quantitative cultures, and this failure could be attributed to several factors. These include the perioperative administration of antibiotics, possible errors in sample collection, storage, and transport, or the absence of these bacteria in the colorectal cancer tissue of our patients.

Some studies have focused on the other mechanisms, inflammatory mediators, and molecules that could serve as a link between PD and systemic diseases. Among these mediators is C-reactive protein (CRP). CRP is an acute-phase inflammatory mediator whose primary functions include complement activation, phagocytosis promotion, and immune response enhancement. CRP concentration in plasma directly indicates inflammation, and the liver stimulates its synthesis under the influence of IL-1 and IL-6. The normal serum concentration is below 5 mg/L, but it can increase rapidly in response to inflammation (even up to

1000 times), although it also decreases quickly afterward. Increased CRP levels are commonly associated with infections (including PD), inflammation, injuries, pregnancy, and cancer.[16]

Some studies have suggested that periodontal treatment reduces CRP levels in serum. Kumar *et al*. investigated the impact of periodontal therapy on CRP in gingival crevicular fluid (GCF). They collected samples before treatment (6.345 ± 3.781) as well as on the 15th (2.675 ± 1.528) and 45th (0.587 ± 0.082) days after therapy. The study included patients diagnosed with generalized periodontitis, probing depth ≥5 mm, radiographic bone loss, no systemic disease, and satisfactory oral hygiene. They found that CRP levels decreased by 57% on day 15 and 90% on day 45 compared to baseline measurements. This reduction was attributed to the inflammation being resolved after non-surgical periodontal treatment, which lowered CRP levels.[17] D'Aiuto *et al*. also observed a reduction of 0.5 mg/L in CRP levels 6 months after periodontal therapy, concluding that non-surgical treatment of periodontal disease decreases serum mediators and markers of acute inflammatory response.[18]

It is also important to mention that non-surgical periodontal treatment alone could cause a transient increase in CRP levels. In another study by D'Aiuto *et al*., they measured the transient increase in blood CRP levels following intensive periodontal treatment (full mouth treatment in 6 hours). Measurements were taken before the periodontal therapy and on the 1st, 3rd, 5th, 7th, and 30th days. They found a transient increase in CRP levels in the blood. A significant increase in CRP was observed on the first day after therapy and persisted from the initial measurement on days 3, 5, and 7 post-treatment. The CRP levels returned to pre-therapy concentrations only after 1 month. The conclusion was that the most intense rise in CRP occurs 2-5 hours after performing periodontal therapy. This study demonstrates that even intensive periodontal treatment alone leads to a transient increase in CRP levels in the blood, which takes about one month to return to pre-therapy levels. The cause of this increase is the transient bacteremia and the extent of surgical trauma.[19] Graziani *et al*. demonstrated that this can be avoided using less intensive periodontal treatment approaches, such as quadrant-based therapy.[20] In our study, the average time from non-surgical periodontal treatment to the surgical procedure was 40.3 days, which, according to research, should not impact the increase in CRP levels after the cancer resection surgery.

The results of our study did not show a statistically significant difference between the groups. However, when observing the movement of average CRP levels throughout the therapy, we noticed a considerable increase in CRP levels in the control group on the second day after the surgical procedure (the difference was 19.53 from the test group) despite a lower baseline CRP level. Similarly, the final average CRP level in the test group was lower (1.83) than in the control group (3.51) despite higher initial values.

The key difference between our study and the studies mentioned above is that our patients were not systemically healthy individuals with periodontal disease but already had at least one severe systemic disease that influenced CRP levels. This may explain why the differences observed after periodontal therapy in a systemically healthy population did not manifest in our study. At the time of this writing, no other studies have explored the impact of periodontal therapy on CRP levels in patients undergoing CRC treatment.

A limitation of our study is the small sample size and the lack of randomization in the control group. Future studies with a larger cohort of CRC patients, including a control group with healthy periodontal tissues, would help better understand periodontal therapy's impact on CRP levels during CRC treatment. Additionally, employing molecular methods for microbiological analysis would provide more accurate and sensitive detection of PG and FN in cancerous colorectal tissue.

In our study, with all its limitations, we did not find any correlation between periodontal treatment and CRC.

Acknowledgments

I want to thank Dr. Jurij Bednarik, M.D., who was willing to listen to our ideas and help recruit the patients.

We sincerely thank Curaden Slovenia for their generous donation of supplies, which enabled us to provide our patients with thorough oral hygiene education.

References

1. European Federation of Periodontology. What is periodontitis? [internet]. [cited 2025 Jan 18]. Available at: https://www.efp.org/for-patients/what-is-periodontitis/

2. Papapanou PN, Sanz M, Buduneli N, Dietrich T, Feres M, Fine DH, et al. Periodontitis: consensus report of workgroup 2 of the 2017 World Workshop on the Classification of Periodontal and Peri-Implant Diseases and Conditions. *J Periodontol* 2018; **89(Suppl 1):** S173-82. doi: 10.1002/JPER.17-0721

3. Global oral health status report: towards universal health coverage for oral health by 2030. Executive summary. Geneva: World Health Organization; 2022. [internet]. [cited 2025 Jan 19]. Available at: https://www.who.int/team/noncommunicable-diseases/global-status-report-on-oral-health-2022

4. Hajishengallis G, Chavakis T. Local and systemic mechanisms link-ing periodontal disease and inflammatory comorbidities. *Nat Rev Immunol* 2021; **21:** 426-40. doi: 10.1038/s41577-020-00488-6

5. World Health Organization. Colorectal cancer. [internet]. [cited 2025 Jan 20]. Available at: https://www.iarc.who.int/cancer-type/colorectal-cancer/

6. Wang D, Dubois RN. The role of COX-2 in intestinal inflammation and colorectal cancer. *Oncogene* 2010; **29:** 781-8. doi: 10.1038/onc.2009.421

7. Rajeshwari HR, Dhamecha D, Jagwani S, Rao M, Jadhav K, Shaikh S, et al. Local drug delivery systems in the management of periodontitis: a scientific review. *J Control Release* 2019; **307:** 393-409. doi: 10.1016/j.jconrel.2019.06.038

8. Frencken JE, Sharma P, Stenhouse L, Green D, Laverty D, Dietrich T. Global epidemiology of dental caries and severe periodontitis - a comprehensive review. *J Clin Periodontol* 2017; **44(Suppl 18):** S94-105. doi: 10.1111/jcpe.12677

9. Koliarakis I, Messaritakis I, Nikolouzakis TK, Hamilos G, Soug-lakos J, Tsiaoussis J. Oral bacteria and intestinal dysbiosis in colo-rectal cancer. *Int J Mol Sci* 2019; **20:** 4146. doi: 10.3390/ijms20174146

10. Li W, Xu J, Zhang R, Li Y, Wang J, Zhang X, et al. Is periodontal disease a risk indicator for colorectal cancer? A systematic review and meta-analysis. *J Clin Periodontol* 2021; **48:** 336-47. doi: 10.1111/jcpe.13402

11. Čuk K, Tomšič K. [The influence of the presence of periodontogenic bacteria and their sensitivity to antibiotics on the success of the treatment of chronic periodontitis with azithromycin]. [Slovenian]. [Prešeren's research paper]. Ljubljana: K. Čuk, K. Tomšič; 2019

12. Khor B, Snow M, Herrman E, Ray N, Mansukhani K, Patel KA, et al. Interconnections between the oral and gut microbiomes: reversal of microbial dysbiosis and the balance between systemic health and disease. *Microorganisms* 2021; **9:** 496. doi: 10.3390/microorganisms9030496

13. Abed J, Maalouf N, Manson AL, Earl AM, Parhi L, Emgård JEM, et al. Colon cancer-associated Fusobacterium Nucleatum may originate from the oral cavity and reach colon tumors via the circulatory system. *Front Cell Infect Microbiol* 2020, **10;** 400. doi: 10.3389/fcimb.2020.00400

14. Kerdreux M, Edin S, Löwenmark T, Bronnec V, Löfgren-Burström A, Zingmark C, et al. Porphyromonas gingivalis in colorectal cancer and its association to patient prognosis. *J Cancer* 2023; **14:** 1479-85. doi: 10.7150/jca.83395

15. Wang D, Dubois RN. The role of COX-2 in intestinal inflammation and colorectal cancer. *Oncogene* 2010; **29:** 781-8. doi: 10.1038/onc.2009.421

16. Skalerič E. [The levels of some inflammatory mediators and cytokines in the sera of patients with periodontal disease]. [Slovenian]. *Med Razgl* 2004; **43:** 1-17.

17. Kumar S, Shah S, Budhiraja S, Desai K, Shah C, Mehta D. The effect of periodontal treatment on C-reactive protein: a clinical study. *J Nat Sci Biol Med* 2013; **4:** 379-82. doi: 10.4103/0976-9668.116991

18. D'Aiuto F, Parkar M, Andreaou G, Brett PM, Ready D, Tonetti MS. Periodontitis and atherogenesis: causal association or simple coincidence. *J Clin Periodontol* 2004; **31:** 402-11. doi: 10.1111/j.1600-051X.2004.00580.x

19. D'Aiuto F, Nibali L, Mohamed-Ali V, Vallance P, Tonetti MS. Periodontal therapy: a novel non-drug-induced experimental model to study human inflammation. *J Periodontal Res* 2004; **39:** 294-9. doi: 10.1111/j.1600-0765.2004.00741.x

20. Graziani F, Cei S, Orlandi M, Gennai S, Gabriele M, Filice N, et al. Acute-phase response following full-mouth versus quadrant non-surgical periodontal treatment: a randomized clinical trial. *J Clin Periodontol* 2015; **42:** 843-52. doi: 10.1111/jcpe.12451

research article

Prostate cancer treatment with electrochemotherapy (ECT): safety, efficacy and clinical experience in 144 patients

Mara Stevanovic[1], Mathias Heringer[1], Mohammad Hjouj[2], Alessandro Zanasi[3], Francesca de Terlizzi[3], Michael K Stehling[1,2]

[1] VITUS Privatklinik, Offenbach, Germany
[2] Department of Medical Imaging, Al-Quds University, Jerusalem
[3] IGEA S.p.a. Biophysics Lab. Carpi, Modena, Italy

Radiol Oncol 2025; 59(4): 597-606.

Received 23 September 2025
Accepted 6 November 2025

Correspondence to: Francesca de Terlizzi, IGEA S.p.a. Biophysics Lab. Carpi, Modena, Italy. E-mail: f.deterlizzi@igeamedical.com

Disclosure: No potential conflicts of interest were disclosed. Alessandro Zanasi and Francesca de Terlizzi are IGEA employees.

Background. Prostate cancer (PCa) is a common cancer in men in developed countries. PCa treatment depends on the disease's stage; focal therapy provides an intermediate approach, with lower toxicity compared to radical prostatectomy, and better tumor control than active surveillance. We report the first retrospective analysis of prostate cancer patients treated with ECT at our institution.

Patients and methods. A cohort of 144 men with prostate cancer who were ineligible for or refused standard therapies were included and treated with ECT. Routine follow-up included PSA tests and MRI scans, as well as toxicity and genitourinary function evaluation by means of standard questionnaires. Local response was evaluated with MRI at 3 months after treatment, following the RECIST criteria for solid tumors.

Results. The procedure was technically successful in all patients and was well tolerated, with mild and temporary adverse events. Urinary and erectile functions were mostly preserved. A complete response was observed in 75% of evaluated patients, a partial response in 18%, stable disease in 5%, and disease progression in 2%. Short-term response was associated with TNM stage ($p < 0.05$), Gleason score ($p = 0.0066$), and pre-ECT PSA levels ($p = 0.0070$). During follow-up, 18 patients (13%) experienced disease progression; 1-year PFS was 88% (95% CI: 80%–97%) and was found to be significantly associated with tumor stage and pre-treatment PSA levels.

Conclusions. ECT is a feasible, safe, and effective treatment for prostate cancer, with extremely low toxicity and side effects. Preliminary results suggest that it offers promising outcomes in terms of local disease control in early-stage tumors, but also in locally advanced cases where other treatments may not be viable.

Key words: prostate cancer; focal therapy; electrochemotherapy; local therapy; local progression free survival

Introduction

Prostate cancer (PCa) is the second most common non-skin cancer in men and a major cause of cancer-related mortality in developed countries. In 2022, PCa occurred in an estimated 1.5 million new cases and was responsible for approximately 397,000 deaths worldwide.[1]

Two well-established risk factors for prostate cancer are advanced age (over 65) and family history.[2] While smoking, obesity, and certain dietary factors are speculated to influence prostate cancer risk, genetic susceptibility and Western African ancestry are also significant contributors.[3]

Prostate cancer treatment depends on the stage of the disease, with different approaches used for

localized, locally advanced, and metastatic cases. For localized disease, current treatment options include active surveillance or watchful waiting for low-risk PCa, and radical prostatectomy (RPE) or radiation therapy (RT) for intermediate-risk and high-risk PCa.[4] With a median PSA level of 15 ng/ml for prostate cancer treated with RPE and radiotherapy, there is a slight reduction in mortality, metastases, and local progression. At the same time, the incidence of adverse effects, such as urinary incontinence and erectile dysfunction, remains significant.[5] Locally advanced prostate cancer, defined as PCa spreading outside the prostate but not metastasized, is typically treated with a combination of radiation and androgen deprivation therapy (ADT).[4] In contrast, metastatic disease is treated primarily with ADT, sometimes combined with chemotherapy or androgen receptor-targeted therapies. However, resistance to treatment often results in castration-resistant prostate cancer (CRPC), which remains difficult to treat and has a poor prognosis.[6]

Focal therapy (FT), including high-intensity focused ultrasound (HIFU), cryotherapy, radiofrequency ablation (RFA), irreversible electroporation (IRE), and focal radiation, provide an intermediate and innovative approach to PCa[7], offering lower toxicity compared to radical prostatectomy, while providing better tumor control than active surveillance.[7] FT targets the tumor while sparing healthy tissue, offering a less invasive option with a lower risk of side effects such as incontinence and erectile dysfunction. Until now, FT has been limited to carefully selected patients with localized focal disease.[8,9] Balancing treatment efficacy, extent of intervention, and quality of life remains a major challenge at all stages of the disease.

Electrochemotherapy (ECT) is a localized, non-thermal anticancer technique that combines reversible electroporation of tumor cells with concurrent, low-dose intravenous chemotherapy, usually bleomycin. Reversible electroporation enhances bleomycin efficacy by enabling it to reach its intracellular target.[10] ECT has been established as an effective treatment for superficial tumors, including squamous cell carcinoma, basal cell carcinoma, sarcoma, and cutaneous metastases of various histological origin.[11] Additionally, ECT has been applied to deep-seated tumors such as hepatocellular carcinoma, colorectal liver metastases, and bone metastases.[12-15] ECT strategies for deep-seated tumors include open surgery, percutaneous, and laparoscopic techniques.[13,16,17] The major advantage of ECT is its selective ability to kill dividing cancer cells while sparing non-dividing healthy cells and surrounding anatomical structures.[18]

To date, ECT in prostate cancer patients has been described in one case report only, involving locally advanced prostate cancer with infiltration of the external urethral sphincter, for which radical prostatectomy or radiation therapy would have most likely resulted in incontinence and impotence. ECT was effective with no sign of tumor activity on MRI at 6 months follow-up, whilst fully preserving sphincter function. The patient maintained continence and potency within the prior scoring range, indicating that ECT for prostate cancer is safe, feasible and can even be performed in patients with PCas which are not organ-confined.[19] In this first large cohort study, we report the outcomes and safety profiles of prostate cancer patients treated with ECT to confirm its feasibility, efficacy, and impact on recurrence-free survival.

Patients and methods

Patients

Men with prostate cancer who were ineligible for or refused standard therapies were included. Inclusion criteria were: histological or radiological diagnosis of prostate cancer at any stage, age ≥18 years, Eastern Cooperative Oncology Group (ECOG) performance status ≤ 2, and life expectancy of at least three months. Exclusion criteria were: previous allergic reactions to bleomycin or any components required for anaesthesia, exceeding a cumulative lifetime dose of 250 mg bleomycin/m^2 body surface (400,000 IU bleomycin/m^2) previously exceeded, chronic renal dysfunction (serum creatinine > 150 μmol/L), or acute lung dysfunction.

All patients were informed about the nature of their disease, prognosis, standard treatment options according to the S3 guidelines for PCa issued by the German Urological Society[20], the experimental nature of the ECT treatment, and details of the diagnostic work-up regarding tumor localization. Patients signed informed consent for treatment, which was personalized based on individual medical needs and preferences. Each treatment was personalized according to the patient's individual needs and wishes (individual medical treatment). Data collection was purely retrospective. No treatment was adapted to suit scientific purposes. All procedures performed in present study were in accordance with the ethical standards and with the 1964 Helsinki declaration and its later amendments or comparable ethical standards.

ECT treatment

All patients underwent multi-parametric magnetic resonance imaging (mpMRI) at least once prior to ECT. All but one patient had histopathological confirmation of PCa.

The procedure was performed with the patient in the lithotomy position, followed by disinfection and sterile covering of the pelvic floor area. Urethral gel was instilled, and catheterization (Charr. 16) with continuous bladder irrigation was performed. Transrectal ultrasound was used to visualize the insertion and final position of 5 to 8 electrodes (IGEA Spa, Carpi, Italy) depending on the size and shape of the lesion, guided by preoperative MRI images. The electrodes were manually inserted through the perineum under ultrasound guidance. Electrode positioning was planned based on MRI images ensuring that electrode couples to be activated were optimally placed max. 3 cm apart and a needle geometry covering the target volume was obtained. The catheter was then retracted into the mid-urethra. The body-surface-adjusted bleomycin dose was administered intravenously in a bolus. Eight minutes after intravenous bleomycin administration, reversible electroporation was performed by applying between 8 and 24 electric pulses of 1000 V/cm electric field intensity per electrodes pair, with possible repositioning of electrodes at varying depths within the organ to fully cover the lesion. After electrode retraction, the bladder was re-catheterized with a Charr. 16 transurethral catheter, and continuous bladder irrigation was resumed. Periprostatic local anaesthesia was administered with ropivacaine (20–40 mg), and peri-interventional antibiotic prophylaxis was performed. The whole procedure was performed under general anaesthesia, and patients were expected to stay in the hospital for 2 nights: admitted the day before treatment, they underwent preparation with laxatives and antibiotic prophylaxis; after treatment, they stayed overnight for observation and discharged the next day. All treatments were performed using the Cliniporator® (IGEA Spa, Italy).

Follow-up

Routine follow-up included PSA tests and MRI scans, following protocols suggested for other local treatments.[21] PSA testing was recommended every 3 months during the first 2 years, then every 6 months. MRI was performed 1 day after treatment, and at 3 and 9 months, then annually. Biochemical recurrence was defined as a rise in PSA above baseline 3 months post-treatment, confirmed by mpMRI and, if necessary, additional biopsy or prostate-specific membrane antigen (PSMA)-PET/CT. Patients were also interviewed regarding adverse events and their evolution over time.

Safety and toxicity

Acute toxicity was recorded intra- and post-operatively until the removal of the bladder catheter. All patients had an MRI 24 hours post-ECT to confirm the alignment of the treatment field with the tumor extent and to assess any procedure-related side effects, such as haemorrhage or rectal damage.

Assessment of genitourinary function

All patients were asked to complete the International Prostate Symptom Score (IPSS) questionnaire to evaluate urinary toxicity before and after ECT. The International Consultation on Incontinence Questionnaire-Urinary Incontinence (ICIQ-UI) was also used to assess continence status pre- and post-treatment and during follow-up. Erectile function was evaluated using the standard International Index of Erectile Function (IIEF-5) score before and after ECT.

Response evaluation

Local response was evaluated with MRI at 3 months after treatment, following the RECIST criteria for solid tumors: complete response (CR) was defined as disappearance of the target lesion; partial response (PR) with at least 30% decrease in the size of the target lesion. Progressive disease (PD) was defined as at least 20% increase in the size of the target lesion and stable disease (SD) with neither sufficient shrinkage to qualify for PR or sufficient increase to qualify for PD. MRI and PSA were used to evaluate treatment response over time. PSMA-PET/CT and re-biopsy were performed when either PSA or MRI indicated a new suspicious lesion. Biochemical recurrence was defined by three consecutive PSA increases (ASTRO definition).[22] MRI recurrence was assessed based on PI-RADS v2 criteria.[23] Cases with suspected recurrences were discussed by a multidisciplinary board of urologists, oncologists, and radiologists. Re-biopsy was recommended for confirmed or strongly suspected recurrences, with re-treatment considered based on the patient's preference.

TABLE 1. Descriptive characteristics of patients included

	Mean	St.Dev.	Median	Min	Max
Age (yrs)	68	8	67	50	83
Height (cm)	180	7	180	156	196
Weight (kg)	81	11	82	51	110
PSA (ng/ml)	24.9	28.5	15.1	1.8	177.0
Prostate volume (ml)	44	18	40	6	117

Since most patients declined re-biopsy, PSMA-PET/CT with Gallium 69 was used in addition to MRI for local re-staging and whole-body re-staging.

Statistical analysis

Descriptive statistics, including mean, standard deviation, median, and range, were used for continuous variables. Categorical variables were described by absolute numbers and percentages. Chi-square tests and contingency table analysis were used for comparisons of categorical variables. The Wilcoxon-Mann-Whitney test assessed differences in paired continuous variables (e.g., questionnaire outcomes). Kaplan-Meier curves were calculated for progression-free survival (PFS) for the entire cohort and subgroups, with statistical significance set at $p < 0.05$. NCSS 9 software (NCSS, LLC. Kaysville, Utah, USA) was used for statistical analysis.

TABLE 2. Patient cancer stage and grade

Gleason score	N	%
6 (3+3) + 7a (3+4)	52	36%
7b (4+3)	40	28%
8–10 (4+4/5+3/4+5/5+4/5+5)	51	35%
Not available (no biopsy)	1	1%
D'Amico risk classification		
Low	2	1%
Intermediate	18	13%
High	124	86%
Stage	N	%
T1c	6	4%
T2a	16	11%
T2b	3	2%
T2c	25	18%
T3a	36	25%
T3b	26	18%
T4	32	22%
N0	111	77%
N1	33	23%
M0	112	78%
M1	32	22%

Results

A cohort of 144 patients with prostate cancer was treated with electrochemotherapy (ECT) at the VITUS Clinic Institute between January 2017 and June 2024. The baseline characteristics of the patients are presented in Table 1.

Cancer stage and grade of the cohort are described in Table 2. Patients with Gleason Score of 6 or 7a (3+4) have been specifically analysed as they represent a low-intermediate-risk class of patients: 52 patients with mean age 67±7 yrs, mean PSA 16.8±10.4 ng/ml. Patients that received previous treatments, as reported in Table 3.

Treatment

The procedure was technically successful in all patients. Treatment coverage included the entire prostate, with tumor volume extending beyond the capsule in 133 patients (93%), half of the organ in 6 cases (4%), focal treatment in 3 patients (2%), whilst treatment was palliative without complete tumor volume coverage in 2 patients (1%). The mean duration of the procedure was 106 ± 26 minutes (time in the operating theatre), and the mean intravenous bleomycin dose administered was 29 ± 1 mg. The mean number of variable geometry electrodes used during each treatment was 7 ± 1, ranging from 5 to 8 electrodes.

Toxicity

The treatment was well tolerated, with adverse events being mild and temporary. These were primarily characterized by intraprostatic oedema in 21 patients (14.5%) and anterior rectal wall irritation in 5 patients (3.4%).

Quality of life (QoL)

A total of 86 patients completed QoL questionnaires (ICIQ, IPSS, IIEF-5) before ECT, and 60 completed them after ECT. Data from pre- and post-ECT questionnaires are available for 36 patients.

TABLE 3. Previous treatments

Previous treatments		
No	95	66%
Irreversible electroporation (IRE)	10	7%
Systemic therapy	8	6%
Radiotherapy/Radioligand	5	4%
Radical prostatectomy/TURP	3	2%
High-intensity focused ultrasound (HIFU)	2	1%
Thermoablation	2	1%
Multiple	19	13%

TURP = transurethral resection of the prostate

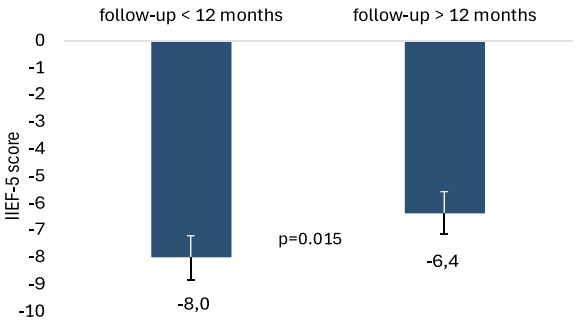

FIGURE 1. Mean International Index of Erectile Function (IIEF-5) reduction at follow-up with respect to pre-ECT values, during the first 12 months of follow-up and after 12 months of follow-up.

Urinary continence

In patients who were fully continent before ECT, no urinary incontinence was observed during the follow-up period. Nine percent of patients reported severe incontinence (ICIQ > 10) prior to ECT; this percentage remained similar (10%) during the first year of follow-up and dropped to zero after 12 months.

In patients Gleason Score 6 or 7a, only 1 patient out of 52 (2%) reported severe incontinence (ICIQ > 10) prior to ECT; this percentage slightly increased (6%) during the first year of follow-up and dropped to zero after 12 months.

Similar results were observed with the IPSS score, where 5% of patients reported severe urinary incontinence (IPSS ≥ 20) before ECT. This increased slightly to 6% during the first 12 months of follow-up but dropped to 0% after one year.

In patients at low-intermediate-risk, only 1 of the 52 patients (2%) reported severe urinary incontinence (IPSS ≥ 20) before ECT. At follow-up no patients in this group reported sever urinary incontinence.

Erectile function

Nine patients (6%) developed severe erectile dysfunction after ECT, as indicated by a decrease in their IIEF-5 score from normal values before treatment, to a score ≤ 7 afterwards, which persisted for longer than one year in only one patient (0.7%).

Overall, 56% of patients had impaired erectile function before ECT (defined as an IIEF-5 score < 22), of which 17% presented a severe erectile dysfunction. After treatment, a decrease of -8.0±9.4 is observed during the first year, which significantly reduces the gap to -6.4±8.0 after the first 12 months ($p = 0.015$) (Figure 1).

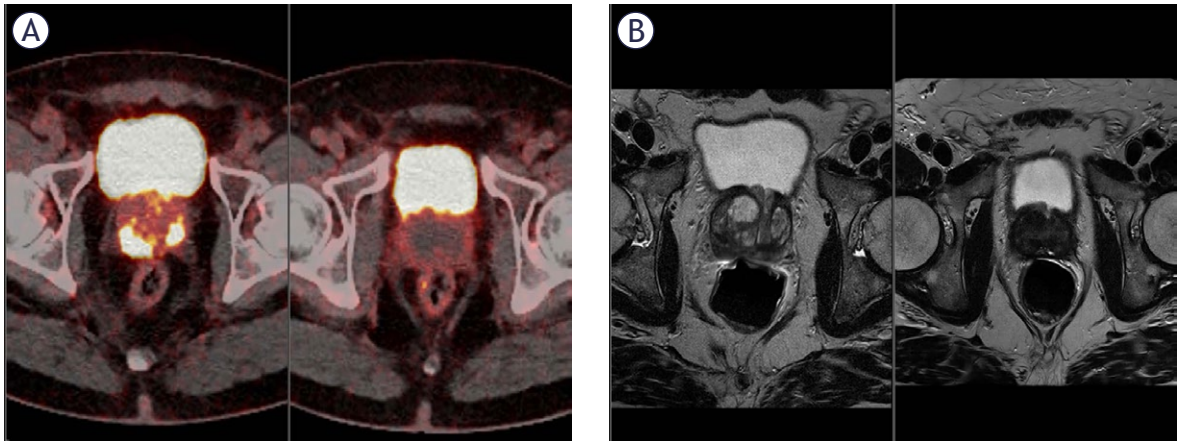

FIGURE 2. 61 years old patient with biopsy-confirmed Gleason 6 multifocal prostate cancer but based on tracer uptake on prostate-specific membrane antigen (PSMA) PET and apparent diffusion coefficients (ADCs) on MRI, a higher-grade cancer. **(A)** Gallium-68 PSMA PET CT scan of the prostate before treatment (left) and 3 months after ECT (right). **(B)** MRI images of the prostate before treatment (left) and approximately 3 months after ECT (right).

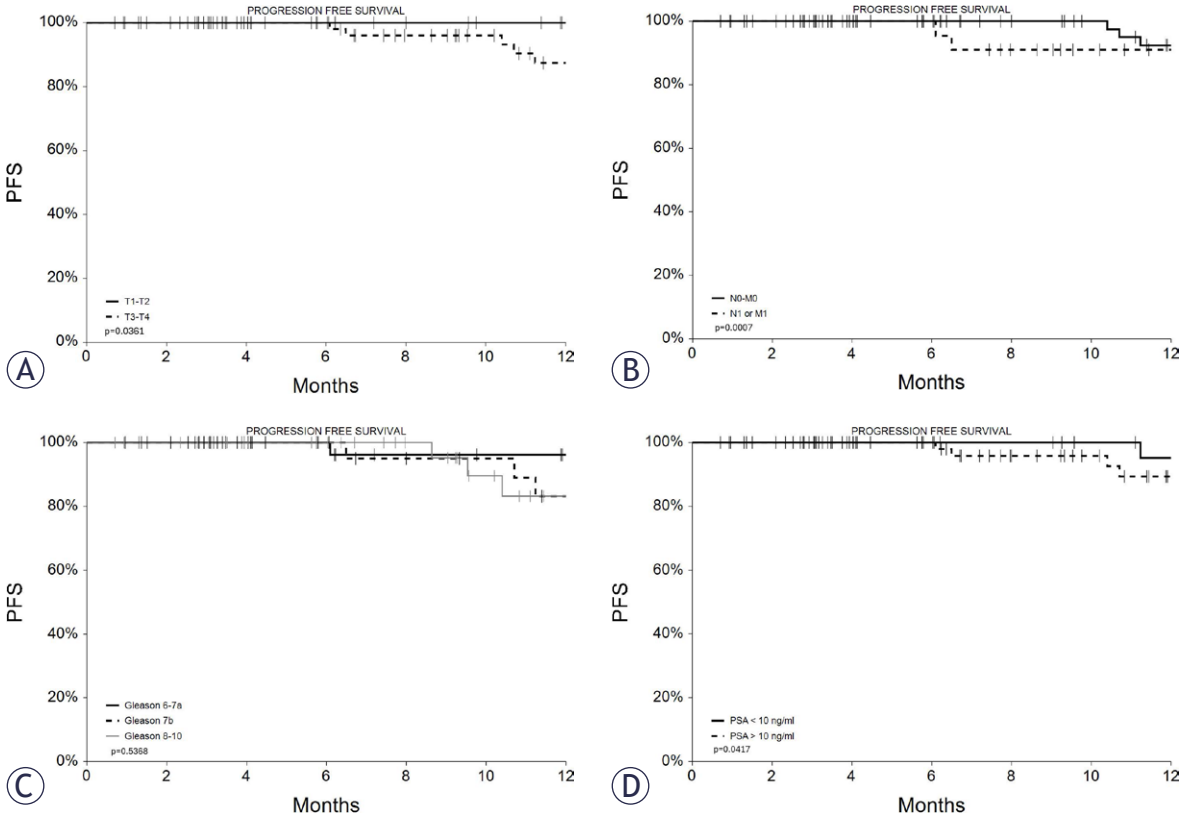

FIGURE 3. Progression free survival (PFS) curves for patients according to stage: **(A)** T1/T2 vs. T3/T4, **(B)** N0 and M0 vs. N1 or M1, **(C)** Gleason score, **(D)** PSA value.

In the group of patients with Gleason Score of 6 or 7a, 10% suffered for severe erectile disfunction before ECT, but only 4% had impaired erectile function after 12 months from ECT.

Short term response to ECT

Short-term response was evaluated at the 3-month follow-up and defined as a reduction in PSA levels, confirmed by a negative MRI performed within 1 month of the PSA evaluation. Short-term response data are available for 117 patients (81%). A complete response was observed in 88 patients (75%) (Figure 2), a partial response in 21 patients (18%), stable disease in 6 patients (5%), and disease progression in 2 patients (2%). Short-term response was associated with the TNM stage of the disease, the Gleason score, and pre-ECT PSA levels, as detailed in Table 4.

Long term response

During the follow-up period, 18 patients (13%) experienced disease progression. Among these, 11 patients (8%) had local progression or recurrence within the prostate, 5 (3%) developed systemic progression (involving lymph nodes, bones, or distant metastases), and further 2 patients (1%) experienced both conditions. The mean time to progression was 15 ± 6 months (median 16, range 3–25 months). Progression-free survival (PFS) was calculated based on both local and systemic disease progression, and the 1-year PFS for the entire cohort was 88% (95% CI: 80%–97%). This figure is similar when considering only local progression (1-year local progression-free survival [LPFS] of 92%, 95% CI: 84%–99%).

PFS was found to be directly and significantly associated with tumor stage and pre-treatment PSA levels, as shown in Figure 3 and Table 5. However, it was not related to the Gleason score.

Patients under concomitant immunotherapy

In this cohort of patients, 10 subjects who received ECT were undergoing immunotherapy (pembrolizumab). No increased toxicity was ob-

served in these patients, as only two experienced mild, temporary oedema after the ECT treatment. Additionally, only one patient had a recurrence 9 months after the ECT session. This patient was a young individual (55 years old) with high-risk disease, a Gleason score of 9, T4N1M1 staging, and a PSA level of 90 ng/ml. No cases of urinary or erectile dysfunction were observed in any of these patients.

Discussion

Focal therapy is an option for treatment of PCa with the aim of reducing known side effects of primary whole-gland treatments such as radical prostatectomy or radiotherapy and simultaneously providing sufficient oncological control. In the earlier days, FT was only considered for low-risk patients. During the past two decades however, there has been a gradual shift in FT towards targeting larger volumes and higher grades of PCa.[24-26]

Electrochemotherapy (ECT) is a minimally invasive, local tumour ablation technique that combines chemotherapy with transient permeabilization of the cell membrane by reversible electroporation. The latter is achieved by applying a series of short non-thermal electric pulses through electrodes that are placed directly at the site of the tumor. Potent chemotherapeutics which are poorly permeant under normal conditions can thus easily pass the membrane barrier and reach their intracellular target. Cytotoxicity is thereby dramatically increased: the effect of bleomycin, the most utilized drug for ECT, is potentiated several hundred times when combined with electroporation in vitro.[27] At a preclinical level, a significant improvement of the anticancer activity of bleomycin via reversible electroporation was also shown in mice bearing human prostate cancer xenograft.[28]

In this study, to our knowledge, the first observational cohort study on the use of ECT in the treatment of prostate cancer, a cohort of 144 patients with prostate cancer at various stages underwent ECT. According to D'Amico Risk classification 86% of the patients had high-risk, 13% intermediate risk and only 1% low risk PCa. 34% of the patients had previously received other treatments, such as IRE, surgery, radiotherapy, or systemic therapies, but experienced recurrence or progression, with no further therapeutic options deemed feasible or indicated; 66% of the patients received ECT as a primary local treatment after having refused standard therapies and aiming to obtain better tu-

TABLE 4. Association between short term response and disease specific characteristics

SHORT TERM RESPONSE				P value
T Stage	**T1/T2**	**T3/T4**		
CR	92%	66%		
PR	5%	25%		
SD	3%	6%		
PD	0%	3%		0.0190
N- M Stage	**N0 and M0**	**N1 or M1**		
CR	89%	43%		
PR	9%	40%		
SD	1%	14%		
PD	1%	3%		< 0.0001
Gleason score	**6–7a**	**7b**	**8–10**	
CR	98%	68%	56%	
PR	0%	26%	32%	
SD	0%	3%	12%	
PD	2%	3%	0%	0.0002
PSA level	**< 10 ng/ml**	**> 10 ng/ml**		
CR	94%	66%		
PR	2%	26%		
SD	2%	7%		
PD	2%	1%		0.0070

CR = complete response; PD = progressive disease; PR = progressive disease; SD = stable disease)

TABLE 5. One-year progression free survival in the analysis by subgroups

GROUPS	1-year PFS	C.I. 95%	N at risk at 12 months	P value
Whole cohort	88%	80%–97%	43	
Stage				
T1/T2	100%	100%	15	
T3/T4	83%	71%–95%	28	0.0361
N0 and M0	92%	84%–100%	33	
N1 or M1	79%	61%–98%	10	0.0007
Gleason score				
6–7a	96%	89%–100%	19	
7b	83%	66%–100%	13	
8–10	83%	66%–100%	10	0.5368
PSA				
< 10 ng/ml	95%	86%–100%	20	
> 10 ng/ml	84%	72%–96%	23	0.0417

mor control than active surveillance while reducing toxicity compared to radical treatments.

Most patients underwent a technically successful treatment, with ECT with coverage of the entire tumor site. Tumor volume extended beyond the prostate capsule in 133 patients (93%), involved half of the organ in 6 cases (4%), and was focal in 3 patients (2%). Only in 2 patients was the tumor so extensive that it could not be fully covered, resulting in palliative treatment.

The treatment was well tolerated, with only mild adverse events observed, such as intraprostatic oedema in 21 patients (14.5%) and anterior rectal wall irritation in 5 patients (3.4%). The major benefit of ECT lies in its selective capacity to destroy dividing cancer cells while preserving non-dividing healthy cells and surrounding anatomical structures[10,18], resulting in reduced toxicity and fewer side effects post-treatment.

Urinary and erectile functions were indeed preserved. Among patients with good urinary functionality prior to treatment, no urinary incontinence was observed post-ECT or during the follow-up period. In those who experienced some urinary incontinence before ECT, ranging from 5% to 9% depending on the evaluation questionnaire (ICIQ or IPSS), dysfunction persisted during the first year of follow-up but resolved completely after 12 months. This finding aligns with our previous study on patients who underwent irreversible electroporation (IRE)[9] and is likely due to treatment-induced reduction of benign cellular hyperplasia in the prostate's transitional zone, whilst non-cellular elements (primarily fibers) remained in place and temporarily obstructed urinary outflow. In contrast, standard treatments for prostate cancer have shown urinary incontinence rates ranging from 36% to 49% after radical prostatectomy[29], and nocturia rates of 42% to 43% after external beam radiotherapy (eBRT) or brachytherapy (BT), with urinary incontinence occurring in 1% to 10% of cases.[29-31]

In this cohort, 9 patients (6%) developed erectile dysfunction post-ECT. Notably, 56% of patients already had impaired erectile function prior to treatment, with 17% experiencing severe erectile dysfunction. After 12 months of follow-up, erectile dysfunction persisted in only 1 of the 9 patients, while the condition resolved in the remaining 8. As anticipated, the rate of erectile dysfunction following ECT is significantly lower compared to other treatments: radical prostatectomy (80%–95%)[29,30], eBRT (69%)[23], high-intensity focused ultrasound (HIFU) (36%)[32], cryosurgery (27%)[33], and radiofrequency ablation (40%)[34], while being comparable to IRE (11%)[9].

Regarding treatment efficacy, a complete response was observed in 88 patients (75%), a partial response in 21 patients (18%), stable disease in 6 patients (5%), and disease progression in 2 patients (2%). 98% of patients with a Gleason score of 6 or 7a achieved a complete response, while those with PSA levels below 10 ng/ml had a 94% complete response rate and an overall response (OR) rate of 96%. Patients with T1 or T2 stage disease showed a complete response rate of 92% and an overall OR rate of 97%. Significantly lower response rates were observed in patients with more advanced or aggressive disease (T3/T4, N1, or M1 stages, Gleason score > 6, PSA > 10 ng/ml), which is expected, given that 65% of patients in the cohort were classified as T3–T4 stage, indicating locally advanced and non-organ-confined disease. Furthermore, 28% had a Gleason score of 7b, and 35% had scores of 8 to 10, i.e. high-risk tumors. Additionally, 34% of patients had previously been treated with standard systemic or focal therapies but experienced recurrence or progression.

The preliminary results suggest that ECT yields better outcomes in smaller, organ-confined, and less aggressive tumors, which is consistent with expectations for a local treatment.

As this is a preliminary study, the follow-up period is limited, with a median duration of 9 months (range: 1 to 64 months), preventing the collection of long-term survival data. The 1-year progression-free survival (PFS) rate for the overall cohort was 88% (95% CI: 80%–97%). For patients with early-stage disease (T1 or T2), the 1-year PFS rate was 100%. Similarly, patients with a Gleason score of 6 or 7a had a 96% 1-year PFS rate, while those with a Gleason score of 7b had an 83% 1-year PFS rate (95% CI: 66%–100%). For patients with Gleason scores of 8 or higher, the 1-year PFS rate dropped to 83% (95% CI: 66%–100%). These results are comparable to those from IRE data at 1 year, where recurrence-free survival (RFS) rates are 100% for Gleason 6, 96% for Gleason 7, and 88% for Gleason > 7.[9]

In a subset of the cohort, 10 subjects received ECT while undergoing immunotherapy. No increased toxicity was observed in these patients, and the results in terms of response and progression-free survival were favourable. Only one patient experienced a recurrence, 8.6 months after ECT. This patient was a young individual (55 years old) with high-risk disease, a Gleason score of 9, T4N1M1 staging, and a PSA of 90 ng/ml.

This study has several limitations, including the high variability and heterogeneity in the patients' disease conditions, the relatively short follow-up duration that precludes comparisons with other studies on recurrence-free survival or overall survival, and the limited data on urinary and erectile function, which should be confirmed in prospective studies with larger, more homogeneous cohorts.

Despite these limitations, the study concludes that ECT is a feasible, safe, and effective treatment for prostate cancer, with extremely low toxicity and side effects. Preliminary results suggest that it offers promising outcomes in terms of local disease control, especially in early-stage tumors, but also in locally advanced cases where other treatments may not be viable. Furthermore, ECT appears to be compatible with immunotherapy without increasing toxicity.

References

1. Bray F, Laversanne M, Sung H, Ferlay J, Siegel RL, Soerjomataram I, et al. Global cancer statistics 2022: GLOBOCAN estimates of incidence and mortality worldwide for 36 cancers in 185 countries. *CA Cancer J Clin* 2024; **74:** 229-63. doi: 10.3322/caac.21834
2. Gandaglia G, Leni R, Bray F, Fleshner N, Freedland SJ, Kibel A, et al. Epidemiology and prevention of prostate cancer. *Eur Urol Oncol* 2021; **4:** 877-92. doi: 10.1016/j.euo.2021.09.006
3. Rebbeck TR, Devesa SS, Chang BL, Bunker CH, Cheng I, Cooney KA, et al. Global patterns of prostate cancer incidence, aggressiveness, and mortality in men of African descent. *Prostate Cancer* 2013; **2013:** 560857. doi: 10.1155/2013/560857
4. Cornford P, van den Bergh RCN, Briers E, Van den Broeck T, Brunckhorst O, Darraugh J, et al. EAU-EANM-ESTRO-ESUR-ISUP-SIOG guidelines on prostate cancer – 2024 update. Part I: Screening, diagnosis, and local treatment with curative intent. *Eur Urol* 2024; **86:** 148-63. doi: 10.1016/j.eururo.2024.03.027
5. Wilt TJ, Brawer MK, Jones KM, Barry MJ, Aronson WJ, Fox S, et al. Radical prostatectomy versus observation for localized prostate cancer. *N Engl J Med* 2012; **367:** 203-13. doi: 10.1056/nejmoa1113162
6. Tilki D, van den Bergh RCN, Briers E, Van den Broeck T, Brunckhorst O, Darraugh J, et al. EAU-EANM-ESTRO-ESUR-ISUP-SIOG guidelines on prostate cancer. Part II – 2024 update: Treatment of relapsing and metastatic prostate cancer. *Eur Urol* 2024; **86:** 164-82. doi: 10.1016/j.eururo.2024.04.010
7. Kovács A, Pinkawa M. Interventional therapy in malignant conditions of the prostate. *Radiologe* 2019; **59:** 28-39. doi: 10.1007/s00117-019-00632-x
8. Nahar B, Ajami T, Williams A, Soodana Prakash N, Khandekar A, Freitas PFS, et al. Survival outcomes and recurrence patterns following focal high-intensity focused ultrasound treatment for localized prostate cancer: Insights on patient selection and lessons learned. *Eur Urol Focus* 2025; **11:** 235-41. doi: 10.1016/j.euf.2024.11.005
9. Guenther E, Klein N, Zapf S, Weil S, Schlosser C, Rubinsky B, et al. Prostate cancer treatment with irreversible electroporation (IRE): safety, efficacy and clinical experience in 471 treatments. *PLoS One* 2019; **14:** e0215093. doi: 10.1371/journal.pone.0215093
10. Sersa G, Cemazar M, Snoj M. Electrochemotherapy of tumours. *Curr Oncol* 2009; **16:** 34-5. doi: 10.3747/co.v16i2.368
11. Clover AJP, de Terlizzi F, Bertino G, Curatolo P, Odili J, Campana LG, et al. Electrochemotherapy in the treatment of cutaneous malignancy: Outcomes and subgroup analysis from the cumulative results from the pan-European International Network for Sharing Practice in Electrochemotherapy database for 2482 lesions in 987 patients (2008–2019). *Eur J Cancer* 2020; **138:** 30-40. doi: 10.1016/j.ejca.2020.06.020
12. Iezzi R, Posa A, Caputo CT, De Leoni D, Sbaraglia F, Rossi M, et al. Safety and feasibility of analgosedation for electrochemotherapy of liver lesions. *Life* 2023; **13:** 631. doi: 10.3390/life13030631
13. Djokic M, Cemazar M, Bosnjak M, Dezman R, Badovinac D, Miklavcic D, et al. A prospective Phase II study evaluating intraoperative electrochemotherapy of hepatocellular carcinoma. *Cancers* 2020; **12:** 3778. doi: 10.3390/cancers12123778
14. Granata V, Fusco R, D'Alessio V, Simonetti I, Grassi F, Silvestro L, et al. Percutanous electrochemotherapy (ECT) in primary and secondary liver malignancies: a systematic review. *Diagnostics* 2023; **13:** 209. doi: 10.3390/diagnostics13020209
15. Deschamps F, Tselikas L, Yevich S, Bonnet B, Roux C, Kobe A, et al. Electrochemotherapy in radiotherapy-resistant epidural spinal cord compression in metastatic cancer patients *Eur J Cancer* 2023; **186:** 62-8. doi: 10.1016/j.ejca.2023.03.012
16. Spallek H, Bischoff P, Zhou W, de Terlizzi F, Jakob F, Kovàcs A. Percutaneous electrochemotherapy in primary and secondary liver malignancies – local tumor control and impact on overall survival. *Radiol Oncol* 2022; **56:** 102-10. doi: 10.2478/raon-2022-0003
17. Trotovsek B, Hadzialjevic B, Cemazar M, Sersa G, Djokic M. Laparoscopic electrochemotherapy for the treatment of hepatocellular carcinoma: technological advancement. *Front Oncol* 2022; **12:** 996269. doi: 10.3389/fonc.2022.996269
18. Mir LM. Bases and rationale of the electrochemotherapy. *Eur J Cancer Suppl* 2006; **4:** 38-44. doi: 10.1016/j.ejcsup.2006.08.005
19. Klein N, Gunther E, Zapf S, El-Idrissi R, Atta J, Stehling M, et al. Prostate cancer infiltrating the bladder sphincter successfully treated with Electrochemotherapy: a case report. *Clin Case Rep* 2017; **5:** 2127-32. doi: 10.1002/ccr3.1270
20. Thomas C, Schrader AJ. [New S3 guideline prostate cancer 2021 (Version 6.2) – What has changed in advanced prostate cancer?] [German]. *Urologie* 2023; **62:** 171-5. doi: 10.1007/s00120-022-01927-z
21. Scheltema MJ, Chang JI, van den Bos W, Böhm M, Delprado W, Gielchinsky I, et al. Preliminary diagnostic accuracy of multiparametric magnetic resonance imaging to detect residual prostate cancer following focal therapy with irreversible electroporation. *Eur Urol Focus* 2019; **5:** 585-91. doi: 10.1016/j.euf.2017.10.007
22. American Society for Therapeutic Radiology and Oncology Consensus Panel. Consensus statement: Guidelines for PSA following radiation therapy. *Int J Radiat Oncol Biol Phys* 1997; **37:** 1035-41. doi: 10.1016/S0360-3016(97)00002-3
23. Barentsz JO, Weinreb JC, Verma S, Thoeny HC, Tempany CM, Shtern F, et al. Synopsis of the PI-RADS v2 guidelines for multiparametric prostate magnetic resonance imaging and recommendations for use. *Eur Urol* 2016; **69:** 41-9. doi: 10.1016/j.eururo.2015.08.038
24. Ghoreifi A, Gomella L, Hu JC, Konety B, Lunelli L, Rastinehad AR, et al. Identifying the best candidate for focal therapy: a comprehen-sive review. *Prostate Cancer Prostatic Dis* 2025; **28:** 684-92. doi: 10.1038/s41391-024-00907-y
25. Guillaumier S, Peters M, Arya M, Afzal N, Charman S, Dudderidge T, et al. A multicentre study of 5-year outcomes following focal therapy in treating clinically significant nonmetastatic prostate cancer. *Eur Urol* 2018; **74:** 422-9. doi: 10.1016/j.eururo.2018.06.006
26. Richardson S, Gonzalez S, Mahajan A, Kwan L, Delfin M, Brisbane W, et al. MP04-16 focal therapy in high-risk prostate cancer: can we expand eligibility criteria? *J Urol* 2025; **213:** e125. doi: 10.1097/01.ju.0001109744.01835.94.16.
27. Gehl J, Skovsgaard T, Mir LM. Enhancement of cytotoxicity by electropermeabilization: an improved method for screening drugs. *Anti-Cancer Drugs* 1998; **9:** 319-26. doi: 10.1097/00001813-199804000-00005

28. Ueki T, Uemura H, Nagashima Y, Ohta S, Ishiguro H, Kubota Y. Antitumour effect of electrochemotherapy with bleomycin on human prostate cancer xenograft. *BJU Int* 2008; **102:** 1467-71. doi: 10.1111/j.1464-410x.2008.07793.x

29. Parker C, Castro E, Fizazi K, Heidenreich A, Ost P, Procopio G, et al. Prostate cancer: ESMO Clinical Practice Guidelines for diagnosis, treatment and follow-up. *Ann Oncol* 2020; **31:** 1119-34. doi: 10.1016/j.annonc.2020.06.011

30. Lane JA, Donovan JL, Young GJ, Davis M, Walsh EI, Avery KNL, et al. Functional and quality of life outcomes of localised prostate cancer treatments (Prostate Testing for Cancer and Treatment [PROTECT] study). *BJU Int* 2022; **130:** 370-80. doi: 10.1111/bju.15739

31. Seymour ZA, Daignault-Newton S, McLaughlin PW, Sandler H, Jackson W, Johnson SB, et al. Patient reported outcomes for quality of life (QOL) by Expanded Prostate Cancer Index (EPIC) on average 15 years post treatment. *Clin Transl Radiat Oncol* 2022; **36:** 56-62. doi: 10.1016/j.ctro.2022.05.007

32. Shoji S, Kuroda S, Uemura K, Oda K, Kano T, Ogawa T, et al. Risk factors for severe erectile dysfunction after focal therapy with high-intensity focused ultrasound for prostate cancer. *Biomedicines* 2022; **10:** 2876. doi: 10.3390/biomedicines10112876

33. Zhou JT, Fang DM, Xia S, Li T, Liu RL. The incidence proportion of erectile dysfunction in patients treated with cryotherapy for prostate cancer: a meta-analysis. *Clin Transl Oncol* 2019; **21:** 1152-8. doi: 10.1007/s12094-019-02036-8

34. Tucker RD, Huidobro C, Larson T. Ablation of stage T1 /T2 prostate cancer with permanent interstitial temperature self-regulating rods. *J Endourol* 2005; **19:** 865-7. doi: 10.1089/end.2005.19.865

research article

Are there clinically relevant prognostic factors in diffuse large B-cell lymphoma beyond International Prognostic Index?

Milica Miljkovic[1,2], Vita Setrajcic Dragos[2,3], Gorana Gasljevic[4,5], Srdjan Novakovic[2,3], Lucka Boltezar[1,2], Barbara Jezersek Novakovic[1,2]

[1] Department of Medical Oncology, Institute of Oncology Ljubljana, Ljubljana, Slovenia
[2] Faculty of Medicine, University of Ljubljana, Ljubljana, Slovenia
[3] Department of Molecular Diagnostics, Institute of Oncology Ljubljana, Ljubljana, Slovenia
[4] Department of Pathology, Institute of Oncology Ljubljana, Ljubljana, Slovenia
[5] Faculty of Medicine, University of Maribor, Maribor, Slovenia

Radiol Oncol 2025; 59(4): 607-616.

Received 3 March 2025
Accepted 28 March 2025

Correspondence to: Prof. Barbara Jezeršek Novaković, M.D., Ph.D., Department of Medical Oncology, Institute of Oncology Ljubljana, Zaloška 2, SI-1000 Ljubljana. E-mail: bjezersek@onko-i.si.

Disclosure: No potential conflicts of interest were disclosed.

Background. Diffuse large B-cell lymphoma (DLBCL) has variable prognosis, with only 50 to 60% of patients cured by standard first line treatment. Identifying patients unlikely to benefit from standard first line therapy is therefore crucial. Schmitz's study identified four molecular subtypes of DLBCL with differing prognoses: MCD, BN2, N1, and EZB, with BN2 and EZB showing more favorable outcomes. This study aimed to evaluate the effectiveness of the Archer FusionPlex Lymphoma Assay in identifying the newly defined genetic subtypes of DLBCL, while also exploring the association between immunohistochemical (IHC) and next-generation sequencing (NGS) methods for classifying the cell of origin (COO) and assessing their predictive value for patient survival.

Materials and methods. We classified 131 DLBCL patients using Hans algorithm into GCB (germinal center B-cell-like) and ABC (activated B-cell-like) subtypes, and with NGS applying Archer FusionPlex lymphoma assay into ABC, GCB, unclassified, and into Schmitz's novel genetic subtypes. A mutational analysis of just 7 genes (*MYD88*^{L265P}, *CD79B*, *EZH2*, *NOTCH1*, *NOTCH2*, *BCL2*, and *BCL6*) was used for genetic classification. Various statistical models were applied to assess survival differences between subtypes. Finally, STRATOS analysis was conducted to validate our preliminary statistical findings.

Results. 35.9% of patients were successfully classified into new genetic subtypes, with acceptable consistency between IHC and NGS method for COO determination. However, the new genetic subtype classification by NGS did not correlate with overall survival, nor did the COO classifications by IHC or NGS. The inclusion of these classifications also did not improve the predictive value of models compared to the basic model based on the International Prognostic Index (IPI) only.

Conclusions. The Archer FusionPlex Lymphoma assay showed a somewhat lower detection rate of novel genetic subtypes compared to reports based on exome sequencing, yet identified novel genetic subtypes in over one-third of patients. However, an in-depth STRATOS statistical analysis did not confirm its predictive value for DLBCL prognosis, likely due to factors like patient selection and sample size limitations.

Key words: diffuse large B-cell lymphoma; next generation sequencing; new genetic types; prognostic factors

Introduction

Diffuse large B-cell lymphoma (DLBCL) is the most common subtype of non-Hodgkin's lymphomas (NHL), accounting for approximately 30% of all NHL.[1] It is a heterogeneous disease in terms of clinical presentation, as well as in terms of its biological and pathological features. Diffuse large

B-cell lymphoma, not otherwise specified (DLBCL, NOS), is the most common subtype, representing 80-85% of all cases.[1-3] Still, even the DLBCL, NOS, is not a homogeneous entity and can be subdivided into several morphological, immunohistochemical and molecular subgroups.[1-3]

The addition of rituximab to standard chemotherapy CHOP (cyclophosphamide, doxorubicin, vincristine and prednisone) has substantially improved the outcomes of patients with the DLBCL, yet to a variable extent among different patients. Only between 50 to 60% of patients will be cured with R-CHOP, while up to 10% will be refractory to this treatment and another 30% will relapse after achieving their first complete remission.[4,5] It is therefore important to identify upfront those patients who will not be cured with R-CHOP in order to tailor their individual first line treatment. One of the widely accepted robust prognostic tools to categorize the DLBCL patients in risk groups is the International Prognostic Index (IPI), introduced in the pre-rituximab era and validated also in the rituximab era.[6,7]

However, treatment outcomes can vary significantly, even within the same IPI risk group, and the IPI alone is not sufficient for the unequivocal identification of patients who may not be cured with R-CHOP. This outcome can be attributed to the important genetic and molecular heterogeneity of DLBCL, NOS, highlighting the need for the identification of additional prognostic markers.

Gene-expression profiling (GEP) studies have identified different molecular subtypes ("germinal center B-cell-like" – GCB, "activated B-cell-like" – ABC (non-GCB), and non-classified types of DLBCL) related to the cell of origin (COO), which are supposed to be of prognostic significance.[8-12] Immunohistochemical (IHC) algorithms, such as the one proposed by Hans *et al*., have also been introduced as rapid and inexpensive alternatives to GEP that are readily available and have demonstrated reasonable concordance to gene expression profiling.[13]

Nonetheless, clinical interest extends to other prognostic markers, including the determinants of molecular heterogeneity in DLBCL, NOS, as indicated by the new molecular subtypes introduced by Schmitz *et al*., Chapuy *et al*., and other authors.[14-17] The study of Schmitz *et al*. identified four molecular subtypes of DLBCL: MCD (based on the co-occurrence of *MYD88* and *CD79B* alterations), BN2 (based on *BCL6* fusions and *NOTCH2* mutation), N1 (based on *NOTCH1* mutation), and EZB (based on *EZH2* mutation and *BCL2* translocations), that were determined to be of prognostic significance.[14] A more favorable prognosis has been predicted for BN2 and EZB in comparison to other two subtypes.[14] Chapuy *et al*., on the other hand, identified five molecular subtypes showing certain overlapping with subtypes identified by Schmitz: C1 (resembling BN2), C2 (*TP53* mutation and *TP53BP1* alteration), C3 (resembling EZB), C4 (*RHOA* mutations, *TET2*, *ZFP36L1* alterations) and C5 (resembling MCD). If the genetic driver could not be identified, the DLBCL was categorized as C0.[15] In the mentioned studies, in addition to genetic changes useful for genetic classification, gene expression signatures related to the tumor microenvironment, rearrangements of *BCL2* and *MYC* and other markers (such as *TP53* mutations, high proliferative activity, CD5, and CD30 expression) appear to play an important role in the prognostication process of high grade lymphomas.

To the best of our knowledge, there are currently no commercial gene panels available on the market specifically designed to define the genetic subtypes of DLBCL as determined in Schmitz's or Chapuy's classification.

Our retrospective study aimed to evaluate the effectiveness of the Archer FusionPlex Lymphoma Kit in identifying the new genetic subtypes of DLBCL as defined by Schmitz *et al*.[14] Additionally, we examined the association between the IHC (Hans algorithm) and next generation sequencing (NGS) methods for classifying the COO and assessed their ability to predict survival.

Patients and methods

Patients

One hundred and thirty-one patients with DLBCL, NOS, were enrolled in this retrospective clinical study. The inclusion criteria were as followed: all patients were older than 18 years, were diagnosed with DLBCL at least 5 years prior to beginning of this study, and were (except of one patient) treated with R-CHOP/RCHOP-like therapy between 2011 and 2017 at the Institute of Oncology Ljubljana (OIL), Slovenia. This study included only patients with DLBCL, NOS, and excluded patients with testicular lymphoma, primary central nervous system lymphoma or plasmablastic lymphoma. Patients with HIV positive lymphomas were also excluded from this study. All clinical data were obtained from medical records available in hospital's information system (patients' age at diagnosis, clinical stage of the disease, data for IPI score, treatment

protocols applied and number of treatment cycles, treatment outcomes - overall response rate [ORR], progression-free survival [PFS], and overall survival [OS]). Survival data were retrieved from the Cancer Registry of the Republic of Slovenia and survival status was censored for all patients on 20th of June, 2023.

The study was approved by the National Medical Ethics Committee of the Republic of Slovenia (Approval Number 0120-103/2020/4) and by Institutional Review Board (Approval number KSOPKR-0012/2020) as well as the Institutional Medical Ethics Committee (Approval number EK-0120-103/2020/4). The requirement for individual informed consent was waived, as this was a retrospective database analysis. Additionally, the institutional informed consent form for treatment included permission to use patients' data, materials, and/or test results for research purposes. The study was conducted according to the Declaration of Helsinki.

Pathological examination

For all patients included in the study, paraffin blocks and corresponding hematoxylin and eosin-stained slides were retrieved from the archive of Department of Pathology of the Institute of Oncology Ljubljana, and diagnoses were reviewed. The tissue microarrays (TMA) were constructed and IHC staining as well as interpretations were performed as already described by Boltezar *et al*.[18] to classify patients according to the Hans algorithm into the GCB and ABC (non-GC) types.[13] At the same time, material for genetic analysis was cut from each paraffine block. The review, TMA evaluations and the classification of patients according to the Hans algorithm, were performed by a skilled hematopathologist who was blinded to all clinical data.

Next generation sequencing (NGS)

The Archer FusionPlex Lymphoma kit was selected for the NGS procedure due to its commercial availability and its targeting of 125 lymphoma-related genes, which we considered potentially advantageous for classifying samples into novel genetic subtypes.

RNA was isolated using the MagMAX™ FFPE DNA/RNA Ultra Kit (ThermoFisher, Waltham, MA, USA). A total of 250 ng of RNA was reverse transcribed into cDNA, and NGS was performed using the Archer FusionPlex Lymphoma Kit, following the manufacturer's protocol (Invitae ArcherDX, San Francisco, CA, USA). The quality of the starting material was evaluated by assessing the quality of the cDNA synthesized from the RNA. For this purpose, the Archer PreSeq RNA QC assay was employed (InvitaeArcherDX, San Francisco, CA, USA). The library was quantified using the qPCR Library Quantification Kit (KAPA Biosystems, Wilmington, MA, USA) and sequenced on the MiSeqDx system (Illumina, San Diego, CA, USA). Data were analyzed using the Archer Analysis version 6.0.3.2. A genetic variant was considered true positive if the allele fraction was at least 10% and the coverage depth was at least 100x. Fusions were considered true positive if covered by five or more unique reads and represented over 10% of reads. Variants listed in the GnomAD database were excluded as germline. Only previously identified pathogenic variants were used for patient subgrouping. Variants were considered pathogenic if listed in Schmitz *et al*.[14] Supplementary Table or the OncoKB database as oncogenic.[19] Variants of uncertain significance and benign variants were excluded. *CD79B* gene amplification was considered true positive when its relative expression exceeded 8 on a 0-9 scale calculated by the Archer analysis software. Cases were classified by gene expression patterns into the ABC, GCB, and unclassified subgroups according to the COO classification. We used a simplified approach of mutational analysis of just 7 genes, as alterations in *MYD88*^{L265P}, *CD79B*, *EZH2*, *NOTCH1*, *NOTCH2*, *BCL2*, and *BCL6* were employed for genetic classification into novel subtypes. This decision was based on literature data indicating that hallmark genetic alterations for each subtype include *MYD88* (66.2% prevalence) and *CD79B* (50.0% prevalence) for the MCD subtype; *EZH2* (44.7% prevalence) and/or *BCL2* (68.4% prevalence) for the EZB subtype; *BCL6* (72.8% prevalence) and/or *NOTCH2* (41.8% prevalence) for the BN2 subtype; and *NOTCH1* (100% prevalence) for the N1 subtype. Other alterations used by Chapuy and Schmitz to define specific genetic subtypes were mostly reported with a lower prevalence.[8,14,15] Cases with *CD79B* and *MYD88* alterations were therefore classified as "MCD," with *EZH*2 and/or *BCL2* as "EZB," with *BCL6* and/or *NOTCH2* as "BN2" and with *NOTCH1* as "N1." Remaining cases were genetically unclassified.[14]

Statistical analysis

The median age, stage at the time of diagnosis, bone marrow infiltration, IPI score, number

TABLE 1. Patients' characteristics

	N	%
Number of patients:	131	
Gender		
Male	59	45.0%
Female	72	55.0%
Age		
Age range	28–89	/
Median age	65	/
Stages (Ann Arbor):		
Stage I	19	14.5%
Stage II	25	19.0%
Stage III	21	16.0%
Stage IV	66	50.4%
Median stage:	4 (range 1–4)	
Other characteristics		
Bone marrow involvement	41	31.3%
Elevated LDH level	77	58.8%
B symptoms	65	49.6%
IPI group:		
Low risk	32	24.4%
Low-intermediate risk	31	23.7%
High-intermediate risk	37	28.2%
High risk	31	23.7%
Median IPI value:	3 (range 0-5)	
Treatment		
R-CHOP/R-CHOP like	128	97.7%
R-COEP	2	1.5%
Palliative care	1	0.8%
Treatment response	130	
CR	65	50.0%
PR	48	36.9%
SD	1	0.8%
PD	16	12.3%

CR = complete response; IPI = International Prognostic Index; PD =progressive disease; PR = partial response; R-CHOP = rituximab, cyclophosphamide, doxorubicin, vincristine and prednisone; R-CHOP like = R-CHOP +/- middle dose methotrexate; R-COEP = rituximab, cyclophosphamide, etoposide, vincristine and prednisone; SD = stable disease

of treatment cycles, subtype by IHC (ABC and GCB), subtype by NGS (ABC and GCB and non-classified) and new genetic subtypes according to Schmitz's classification were determined. PFS was defined as the time from the end of first systemic treatment to disease progression or death from any cause for patients achieving partial (PR) and complete response (CR). OS was defined as the time from the date of diagnosis to the time of death from any cause. The PFS and OS were estimated using the Kaplan-Meier method and differences were compared using the log-rank test. The IPI score was used as a categorical variable: low (score of 0 or 1), low-intermediate (score 2), high-intermediate (score 3) and high-risk group (score of 4 or 5) for the purpose of survival analyses and as a numeric variable for STRATOS initiative analyses. P value ≤0.05 was considered to indicate a statistically significant difference. GraphPad Prism software 9.0.0 (GraphPadSoftware, Boston, MA, USA) was used for analyses. Additional statistical analysis was performed – namely the STRATOS analysis, to check our basic statistic. The analysis was run in R (v4.3.2) in RStudio (v2023.12.1+402) using the packages boot (v1.3.28.1), dplyr (v1.1.4), forcats (v1.0.0.), ggplot2 (v3.4.4), ggpubr (v0.6.0), gridExtra(v2.3), gtsummary(v1.7.2), Hmisc (v5.1.1.), kableExtra (v1.3.4), knitr (v1.45), lubridate (v1.9.3), readxl (1.4.3), pacman (v0.5.1), purr (v1.0.2), readr (v2.1.4), readaxl (v1.4.3), rio (v1.0.1), rms (v6.7.1), rsample (v1.2.0), stringr (v1.5.1), survival (v3.5.7) and survminer (v0.4.9), tibble (v3.2.1), tidyr (v1.3.0), tidyverse (v2.0.0), timeROC (v0.4), webshot (v0.5.5) and their dependencies. According to the guidelines of the STRATOS initiative, we also compared the calibration, discrimination, Brier scores and clinical utility of various tested Cox models in order to test our model more profoundly.[20-22] Lacking an additional dataset for external validation, we validated our models using optimism-corrected internal validation with bootstrapping.

Results

Demographic data

A total of 131 patients with DLBCL were included in the study. The patients' characteristics are summarized in Table 1. There was a slight female predominance, median age was 65 years (range 28-89). More than half of our group had stage IV disease (50.4%) and elevated serum lactate dehydrogenase level (LDH) (58.8%), while nearly half had B symptoms (49.6%). The highest percentage of patients were in the high-intermediate risk group (28.2% of patients), other three risk groups were quite evenly distributed. All patients except one (130 patients - 99.2%) received first line systemic treatment. Treatment regimen was R-CHOP (rituximab, cyclophosphamide, doxorubicin, vincristine and prednisolone) +/- middle dose of methotrexate (500

mg/m²) in 128 patients (97.7%). Two patients (1.5%) received R-COEP (rituximab, cyclophosphamide, vincristine, etoposide and prednisolone) therapy due to their cardiac conditions, while one patient underwent just palliative treatment (and was excluded from cohort analysis). The median follow-up time was 61 months (range 2–152 months).

For each patient, response to first line treatment was defined as CR, PR, stable disease (SD) or progressive disease (PD) based on the revised criteria of Cheson *et al*.[23] The ORR for the entire group was 86.9% (with the CR at 50% and the PR at 36.9%).

Classification of diffuse large B-cell lymphoma (DLBCL) according to the cell of origin (COO)

According to the COO determined by IHC method, 54 patients (41.2%) were classified as ABC subtype and 77 patients (58.8%) as GCB subtype. According to the NGS, 42 patients (32.0%) were classified as ABC subtype and 62 patients (47.3%) as GCB subtype, while 12 patients (9.2%) remained unclassified, and for 15 patients (11.5%) the NGS method could not provide a clear result (QC failed). NGS served as the reference method and concordance between the determined COO subtypes according to the IHC and the NGS method is presented in Table 2. The overall concordance between NGS determined COO and IHC determined COO in the whole study group was 61.8% (81 of total 131 patients).

Genetic classification of diffuse large B-cell lymphoma (DLBCL) by next generation sequencing (NGS) according to the Schmitz's classification

Of the entire group of 131 patients, 47 patients (35.9%) were successfully categorized into one of the new genetic subtypes of DLBCL, 70 patients remained unclassified (53.4%), while 14 patients (10.7%) were categorized as QC failed. Among those 47 patients, 17 patients had MCD (13%), none had N1, 12 had BN2 (9.2%), and 18 patients had EZB (13.7%) subtype. New genetic subtypes in the context of COO groups ABC, GCB and unclassified group are presented in Figures 1 and 2.

When focusing only on the QC failed (as determined by NGS) group of 15 patients of the entire 131 patient cohort, 1 patient was categorized with the EZB subtype (6.7%). The remaining 14 patients remained unclassified to the new genetic subtypes.

TABLE 2. Concordance between the IHC and NGS method in determination of the COO. The reference method was NGS. A pairwise comparison between the results of both methods was performed for each patient. Each patient who was subclassified into the same (ABC or GCB) subtype by both NGS and IHC was considered concordant. Patients who were subclassified differently by IHC and NGS were considered discordant

	COO by NGS	COO by IHC	Concordance (%)
ABC subtype	42	31	73.8
GCB subtype	62	50	80.6

ABC = activated B-cell like; COO = cell of origin; GCB = germinal center B-cell like; IHC = immunohistochemical determination; NGS = next generation sequencing

Overall response rate according to the immunohistochemical (IHC) and next generation sequencing (NGS) determination of cell of origin (COO) and NGS determination of new genetic subtypes

According to the IHC classification of COO into ABC and GCB subtype, the ORR for ABC subtype was 84.9 % and 88.3% for the GCB subtype. Based on the NGS classification of COO, the ORR for the ABC subtype was 82.9%, 88.7% for the GCB subtype and 91.7 % for the unclassified group. The ORR for MCD genetic subtype was 76.5%, for BN2 genetic subtype 91.7%, for EZB genetic subtype 94.4%, for unclassified group 87.1%, and for QC failed group 85.7%. There was no association between the ORR and classification to the abovementioned subgroups regarding COO by IHC, COO by NGS and classification to new genetic subtypes by NGS ($p = 0.59$, $p = 0.76$, and $p = 0.80$, respectively).

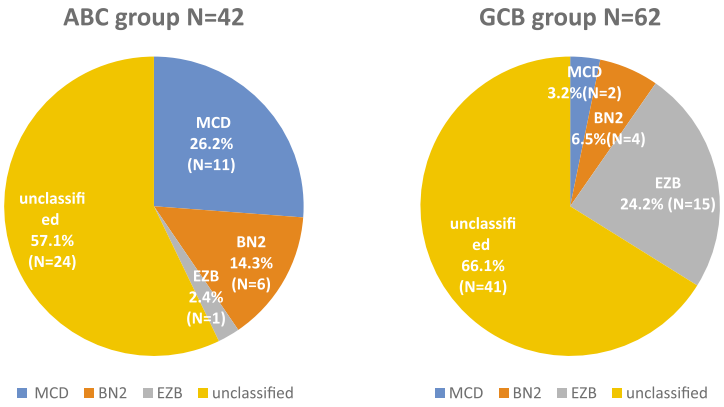

FIGURE 1. New genetic subtypes in the context of COO groups ABC and GCB, as determined by NGS (N1 group is not included in the Figure since there were no patients with this subtype).

ABC = activated B-cell; COO = cell of origin; GCB = germinal center B-cell; NGS = next generation sequencing

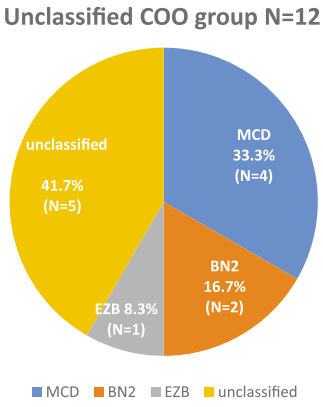

FIGURE 2. New genetic subtypes in the context of COO unclassified group, as determined by NGS (N1 group is not included in the Figure since there were no patients with this subtype).

COO = cell of origin; NGS = next generation sequencing

Overall survival according to the immunohistochemical (IHC) and next generation sequencing (NGS) determination of cell of origin (COO) and NGS determination of new genetic subtypes, and according to the International Prognostic Index (IPI)

Five-year overall survival (OS) of the entire group was 67.8% (Figure 3). According to the IHC classification of COO into ABC and GCB subtype, the 5-year OS for ABC subtype was 62.5% and 71.4% for GCB subtype. Survival was not significantly different between the two groups, (p = 0.27, HR = 1.36 [95% CI 0.76–2.42]) Supplementary Figure 1. Based on the NGS classification, the five-year OS for ABC subtype was 54.8% and 74.2% for GCB subtype, 64.2 % for the unclassified group and 80% for the QC failed group, and, again, there was no statistically significant difference between groups (p = 0.06) – Supplementary Figure 2. The 5-year OS for patients diagnosed with the new genetic subtypes according to the Schmitz's classification was 66.7% for the BN2 subtype, 77.8% for the EZB subtype, 64.7% for the MCD subtype, 78.6% in the QC failed group, and 63.9% for the unclassified group (p = 0.61) - Supplementary Figure 3. The 5-year OS was 87.5% in low risk IPI group, 87.0% in low-intermediate risk IPI group, 70.3% in high-intermediate risk IPI group and 25.8% in high risk IPI group (p < 0.0001, HR = 0.117 [95% CI 0.06–0.245]) (Figure 4).

Cox models

We are not giving the PFS data as we consider them to be only of predictive and not of a prognostic significance. Even though we are aware of the potential influence of subsequent therapies to the OS, we chose to evaluate the prognostic significance of the three classifications that had been applied in the study – namely the COO by IHC classification, COO by NGS classification and the new genetic types by NGS classification. We used the Cox proportional model to investigate the association between the OS and the particular classification (COO by IHC, COO by NGS, and new genetic types by NGS, respectively) as well as the IPI score. The following Tables summarize the four models used - Supplementary Tables 1, 2 and 3. The base model uses only IPI as an independent variable and the three classifications available to IPI as a second independent variable. However, when combining IPI score and any of classifications (COO by IHC, COO by NGS, and new genetic types by NGS) into one model, none of the classifications had a significant prognostic impact on patients' survival and only IPI remained prognostic for OS. So, regardless of the classification used, the survival of patients was not statistically significantly different between the ABC and GCB subtype (and unclassified subtype) or between the new genetic subtypes in our data set.

STRATOS statistical analyses

The STRATOS initiative produced guidelines for comparing Cox models**.** For technical reasons, IPI is included as a numerical variable (i.e. the number of risk factors present). As shown previously, regardless of the model/classification used, only the IPI remains statistically significantly associated with survival.

Given that each individual classification (COO by IHC, COO by NGS, and new genetic types by NGS) was not associated with survival, we expected the subsequent analysis to show that inclusion of any one of the classifications into the model would not improve the quality of the model or its clinical usefulness.

Discrimination and calibration

Corrected internal discriminations of the compared models at a fixed time point 5 years after diagnosis are given in Supplementary Table 4 and calibrations at a fixed time point 5 years after diagnosis are given in Supplementary Table 5. The addition of any classification did not improve the quality of the model, which was expected, given that none of them was significantly associated with overall survival.

Overall quality

The Brier score and the scaled Brier score (Index of Prediction Accuracy, IPA) estimate the overall model quality. Brier score estimates the average difference between predicted and observed values at time t (and a lower value indicates a better model). IPA improves the interpretability of the score and estimates the reduction in Brier score when using a more complex model compared to the base model (a higher value therefore indicates a better model). The Brier score and IPA are given in Supplementary Table 6. We can conclude that the additional information about the classification does not improve the model quality (the addition of IPI compared to the null model improves the Brier score by 20%, while the extended models (with COO by IHC, COO by NGS and new genetic subtypes by NGS) improve it by 17% to 19%).

Calibration, discrimination and overall quality were assessed using bootstrap (B = 1000) and optimism corrected internal validation, since an additional data source for external validation was not available. As expected, we demonstrated that the addition of any one of the available classifications did not improve the performance of the base model that only included the IPI score.

Clinical usefulness

Discrimination and calibration are necessary to assess the model quality or to compare different models, but they are not enough to evaluate their clinical usefulness. When an additional marker is available (in this case the subtype classification, whether histological or genetic), the evaluation of clinical usefulness should tell us whether the use of the additional marker leads to improved clinical decision making. We assessed the clinical usefulness of the extended models (with COO by IHC, COO by NGS and new genetic subtypes by NGS) compared to the base model at various possible risk thresholds. We have shown that the extended models do not improve the net benefit to patients when used in clinical decision making, regardless of the threshold or extended model chosen (Supplementary Figure 4, Supplementary Table 7).

Discussion

DLBCL is highly heterogeneous in its genetic characteristics, making accurate sub-classification of patients based on tumor genetic changes essential for optimal treatment approaches. The classifications proposed by Schmitz and Chapuy are currently the most effective in grouping patients according to disease prognosis and treatment outcomes.[14,15] However, no commercial tool (gene panel) is at present available that could classify patients into the genetic groups proposed by these authors. Therefore, the aim of our study was to evaluate the utility of the Archer FusionPlex Lymphoma Kit in classifying DLBCL into the groups outlined

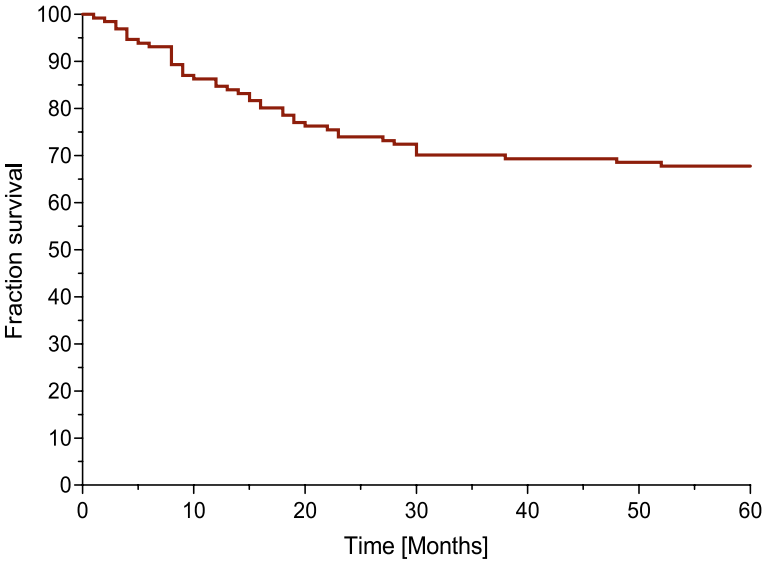

FIGURE 3. Overall survival (Kaplan-Meier) of all patients (N = 131).

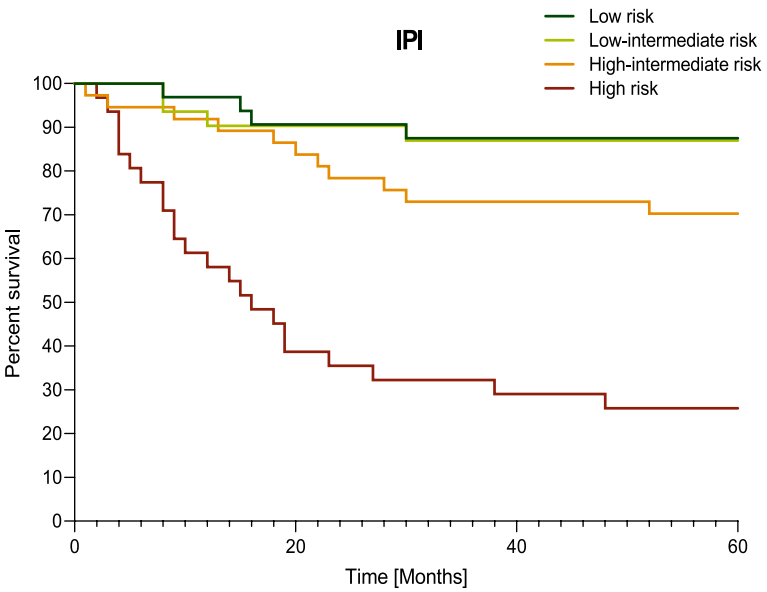

FIGURE 4. Overall survival (Kaplan-Meier) of patients according to International Prognostic Index (IPI) risk groups; (p < 0.0001).

by Schmitz *et al*.[14] Furthermore, we specifically assessed the impact of IHC classification of COO, NGS classification of COO, and NGS classification of new genetic subtypes based on Schmitz's proposal on overall survival in patients with diffuse large B-cell lymphomas.

In fact, similar approaches for the genetic categorization of lymphomas have been used by other authors. Crotty *et al*. conducted a smaller study involving 41 DLBCL patients using the Archer FusionPlex Lymphoma platform to analyze a panel of 125 lymphoma-related genes and evaluate its concordance with the IHC Hans algorithm, observing an 80.5% concordance for COO.[24] Another group, led by Scott, used the Lymph2Cx assay, to test 20 genes and compare it to GEP by NanoString to define the COO. This assay provided concordant COO definitions in 96% of their cases.[25] Multivariate analyses in their report showed that COO defined by Lymph2Cx was independently prognostic of survival, regardless of the IPI score.[25]

However, in the present study, the overall concordance between NGS determined COO and IHC determined COO was lower, at only 61.8%, likely because we did not exclude the QC-failed samples and on account of the NGS determined unclassified group. Specifically, we observed a 73.8% concordance in the ABC group and 80.6% in the GCB group. In contrast, the study by Crotty *et al*. included far fewer patients (41) compared to ours (131), and while the proportions of ABC, GCB, and unclassified subgroups in Crotty's study were evenly distributed, similar to our findings, they did not report any failed results.[24]

Regarding Schmitz's proposed classification of the new genetic subtypes of DLBCL, we were able to subclassify 35.9% of our patients using the Archer FusionPlex Lymphoma kit. This represents a lower proportion of classified cases compared to Schmitz's study, where 46.6% of patients were categorized into the new genetic subtypes.[14] Considering the fact that Schmitz's study performed exome and transcriptome sequencing, while we conducted a limited panel of RNA sequencing, the difference in the proportion of successfully classified cases is relatively small. Our cohort included a larger number of samples with mutations that were not helpful to classify correctly patients into subgroups, suggested by Schmitz. The clinical impact of these mutations is, nevertheless, still unknown. Still, in other studies using a classification similar to Schmitz's, the proportion of successfully classified patients was also less than 100%. Lacey performed a whole-exome sequencing on tumor samples of 928 patients (including primary central nervous system lymphomas and plasmablastic lymphomas), in a panhematological malignancy panel of 293 genes, and found some overlapping groups over Schmitz's and Chapuy's classification**.** They identified 5 genomic clusters and had a 27% rate of "unclassified cases".[16] Wright and his colleagues created the LymphGen algorithm that provided a probabilistic classification of the tumor from an individual patient into a genetic subtype and with a similar methodology as Schmitz they managed to subclassify 63.1% of patients.[17]

A closer comparison of our results with those of other authors indicates that with our simplified approach, we detected a relatively low proportion of the EZB subtype – namely, 21.8% in Schmitz's study, 18.9% in Lacey's study, and only 13.7% in our study.[14,16] The EZB subgroup is primarily included within the GCB cases. Since the GCB subgroup is more prevalent in our study (58.8% of GCB by IHC and 47.3% by NGS) compared to Schmitz's study (28.2% of GCB cases), the relatively low EZB detection rate in our study remains unexplained.[14]

Schmitz *et al*. reported the predicted 5-year overall survival rates for the MCD, BN2 and EZB subtypes of 26%, 65%, and 68%, respectively, while in our study they were numerically superior - 64.7%, 66.7%, and 77.8%.[14] Lacey's genomic cluster MYD88, which overlaps with the MCD subtype, showed a 5-year OS of 62.8% in R-CHOP treated population.[16] Their MYD88 group included testicular and primary CNS lymphomas, while in our study those patients were not included. Lacey's BCL-2 cluster that overlaps with EZB subtype, and whose 5-year OS of 69.5% adjusts with the one reported in Schmitz's study, was, compared to the EZB survival of our group, inferior.[16] But, as stated previously, the EZB group was relatively weakly represented in our study in comparison with other studies.

Furthermore, Schmitz's study investigated the survival data of only 119 patients (treated with R-CHOP/CHOP like chemotherapy) diagnosed with new genetic subtypes out of all 257 patients classified into novel subgroups, so their survival data deficiently cover only half of the new genetic subtypes' population.[14] To the contrary, our study reports survival data of all included patients. In Lacey's study, only two thirds of patients were treated with R-CHOP, however, they reported results of survival for patients treated with R-CHOP separately.[16] In some of the studies, genetic subclassification essentially had a prognostic impact on survival of their patients.[14,16,17] Finally, Zhang

et al. conducted a randomized phase II trial of addition of a targeted therapy to R-CHOP in patients with DLBCL, driven after the first cycle of R-CHOP by newly determined genetic subtypes. Their study was not powered to show survival differences, but it did meet its primary endpoint by achieving higher complete response rates with novel therapeutic approaches. This indicates that the spectrum of possible future decisions in choosing of an optimal first line therapy might have to be based on gene expression analyses.[26]

The classification of the new genetic types by NGS used in our study, however, was not associated with overall survival, as were also not the other two classifications of COO determined by IHC or by NGS. Similarly, the inclusion of any of the three classifications (COO by IHC, COO by NGS and new genetic types by NGS according to Schmitz's proposal) improved neither the calibration and the discrimination nor the clinical utility of the tested models, when compared to the basic model including only IPI values.

One of the strengths of our study is the use of advanced statistical methods,[20,21,22] as well as the thorough histopathological evaluation of all samples by a skilled hematopathologist who was blinded to the clinical data. The STRATOS analysis of Cox regression, a novel and advanced statistical method to analyse the potential differences between classifications, has, to the best of our knowledge, never been done in the setting of the DLBCL. This advanced methodology disclosed no difference in survival regardless of the classification (COO by IHC, COO by NGS, and new genetic types by NGS) used. Based on the data and subanalysis of this study, the only factor with valid prognostic significance for overall survival was IPI, which remained significant regardless of the classification method applied (COO by IHC, COO by NGS, or new genetic subtypes by NGS per Schmitz's proposal). Schmitz *et al*. and Chapuy *et al*. also showed IPI's prognostic significance for overall survival in a multivariate model.[14,15] However, their studies reported also significantly different survival outcomes based on COO subtypes, which was not confirmed in our study. Additionally, the prognostic value of COO subtyping has been questioned in a Hungarian study of 247 DLBCL patients, where the COO subtype failed to predict prognosis.[27] Thus, the prognostic impact of COO subtypes appears more complex than initially suggested by Hans *et al*.[13]

The disadvantages of this study are its retrospective nature, and when compared to the Schmitz's, Chapuy's and Lacey's study, a smaller number of patients included (they included 574, 304 and 928 patients, respectively).[14-16] Yet, the number is still higher than in Crotty's and Scott's study.[24,25] Another limitation of this study is the relatively high number of samples that failed quality control (QC failed category). The sequencing quality control likely failed for several reasons. The most common issue was the contamination of sample with DNA, as indicated by an imbalanced ratio of RNA to DNA reads. In a few cases, the final library concentration was low, leading to insufficient coverage for meaningful analysis. On the other hand, the limited number of just 7 genes analyzed in our study can be either regarded as a limitation of the study on classification capabilities into novel genetic subtypes due to the reduced impact of alterations in other genes (mutated in lymphoma) or as the strength of the study by offering a simplified approach to this classification in clinical practice.

Conclusions

The Archer FusionPlex Lymphoma assay tested in our study showed a somewhat lower detection rate of novel genetic subtypes compared to reports based on exome sequencing. An in-depth statistical analysis of patients' survival across the groups defined by our approach did not confirm its value in predicting outcome of DLBCL patients. However, the difference in proportion of successfully categorized patients within novel genetic subgroups, as proposed by Schmitz *et al*., with Archer's FusionPlex Lymphoma assay compared to exome sequencing was relatively small, making our simplified approach to classifying of DLBCL patients potentially useful in everyday practice.

Acknowledgments

This study was partially supported by the Slovenian Research Agency [grant number P3-0321].

We would also like to extend our gratitude to Mrs. Violet Ruparchic for her generous donation to the Institute of Oncology Ljubljana, which partially funded the next generation sequencing kits used in this study.

Technical assistance with genetic analysis of Mrs. Simona Traven is acknowledged, as well as assistance with STRATOS analysis of Assist. Maša Kušar, MD, PhD.

References

1. Tilly H,da Silva GM, Vitolo U, Jack A, Meignan M, Lopez-Guillermo A, et al. Diffuse large B-cell lymphoma: ESMO Clinical Practice Guidelines. *Ann Oncol* 2015; **26:** 116-25. doi: 10.1093/annonc/mdv304
2. National Comprehensive Cancer Network. Clinical Practice Guidelines in Oncology (2025). B-cell lymphoma (version 1.2025) [Internet]. [cited 2025 Feb 15]. Available at: https://www.nccn.org/professionals/physician_gls/pdf/b-cell.pdf
3. Khoury JD, Solary E, Abla O, Akkari Y, Alaggio R, Apperley JF, et al. The 5th edition of the World Health Organization Classification of Haematolymphoid Tumours: myeloid and histiocytic/dendritic neoplasms. *Leukemia* 2022; **36:** 1703-19. doi: 10.1038/s41375-022-01613-1
4. Sarkozy C, Sehn LH. New drugs for the management of relapsed or refractory diffuse large B-cell lymphoma. *Ann Lymphoma* 2019; **3:** 10. doi: 10.21037/aol.2019.09.01
5. Crump M, Neelapu SS, Farooq U, Van Den Neste E, Kuruvilla J, Westin J, et al. Outcomes in refractory diffuse large B-cell lymphoma: results from the international SCHOLAR-1 study. *Blood* 2017; **130:** 1800-8. doi: 10.1182/blood-2017-03-769620
6. International Non-Hodgkin's Lymphoma Prognostic Factors Project. A predictive model for aggressive non-Hodgkin's lymphoma. *New Engl J Med* 1993; **329:** 987-94. doi: 10.1056/NEJM199309303291402
7. Ziepert M, Hasenclever D, Kuhnt E, Glass B, Schmitz N, Pfreundschuh M, et. al. International prognostic index remains a valid predictor of outcome for patients with aggressive CD20+ B-cell lymphoma in the rituximab era. *J Clin Oncol* 2010; **28:** 2373-80. doi: 10.1200/JCO.2009.26.2493
8. Shimikus G, Nonaka T. Molecular classification and therapeutics in diffuse large B-cell lymphoma. *Front Mol Biosci* 2023; **10:** 1124360. doi: 10.3389/fmolb.2023.1124360
9. Weber T, Schmitz R. Molecular subgroups of diffuse large b cell lymphoma: biology and implications for clinical practice. *Curr Oncol Rep* 2022; **24:** 13-21. doi: 10.1007/s11912-021-01155-2
10. Alizadeh AA, Eisen MB, Davis RE, Ma C, Lossos IS, Rosenwald A, et al. Distinct types of diffuse large B-cell lymphoma identified by gene expression profiling. *Nature 2*000; **403**: 503-11. doi: 10.1038/35000501
11. Rosenwald A, Wright G, Chan WC, Connors JM, Campo E, Fisher RI, et al. The use of molecular profiling to predict survival after chemotherapy for diffuse large-B-cell lymphoma. *N Engl J Med* 2002; **346:** 1937-47. doi: 10.1056/NEJMoa012914
12. López AB, Villambrosía GS, Francisco M, Malatxeberria S, Sáez A, Montalban C, et al. Stratifying diffuse large B-cell lymphoma patients treated with chemoimmunotherapy: GCB/non-GCB by immunohistochemistry is still a robust and feasible marker. *Oncotarget* 2016; **7:** 18036-49. doi: 10.18632/oncotarget.7495
13. Hans CHP, Weisenburger DD, Greiner TC, Gascoyne RD, Delabie J, Ott G, et al. Confirmation of the molecular classification of diffuse large B-cell lymphoma by immunohistochemistry using a tissue microarray. *Blood* 2004; **103:** 275-82. doi: 10.1182/blood-2003-05-1545
14. Schmitz R, Wright GW, Huang DW, Johnson CA, Phelan JD, Wang JQ, et al. Genetics and pathogenesis of diffusse large B-cell lymphoma. *N Engl J Med* 2018; **378:** 1396-1407. doi: 10.1056/NEJMoa1801445
15. Chapuy B, Stewart CH, Dunford AJ, Kim J, Kamburov A, Redd RA, et al. Molecular subtypes of diffuse large B cell lymphoma are associated with distinct pathogenic mechanisms and outcomes. *Nature Med* 2018; **24:** 679-90. doi: 10.1038/s41591-018-0016-8
16. Lacy SE, Barrans SHL, Beer PHA, Painter D, Smith AG, Roman E, et al. Targeted sequencing in DLBCL, molecular subtypes, and outcomes: a Haematological Malignancy Research Network report. *Blood* 2020; **135:** 1759-71. doi: 10.1182/blood.2019003535
17. Wright GW, Huang DW, Phelan JD, Coulibaly ZA, Roulland S, Young RM, et al. A Probabilistic classification tool for genetic subtypes of diffuse large b cell lymphoma with therapeutic implications. *Cancer Cell* 2020; **37:** 551-68.e14. doi: 10.1016/j.ccell.2020.03.015
18. Boltežar L, Kloboves Prevodnik V, Pohar Perme M, Gašljević G, Jezeršek Novaković B. Comparison of the algorithms classifying the ABC and GCB subtypes in diffuse large B-cell lymphoma. *Oncol Lett* 2018; **15:** 6903-12
19. Suehnholz SP, Nissan MH, Zhang H, Kundra R, Nandakumar S, Lu C, et al. Quantifying the expanding landscape of clinical actionability for patients with cancer. *Cancer Discov* 2024; **14:** 49-65. doi: 10.1158/2159-8290.CD-23-0467
20. Crowson CS, Atkinson EJ, Therneau TM. Assessing calibration of prognostic risk scores. *Stat Methods Med Res* 2016; **25:** 1692-706. doi: 10.1177/0962280213497434
21. Austin PC, Harrell Jr FE, Klaveren D. Graphical calibration curves and the integrated calibration index (ICI) for survival models. *Stat Med* 2020; **39:** 2714-42. doi: 10.1002/sim.8570
22. McLernon DJ, Giardiello D, Calster BV, Wynants L, Geloven N, Smeden M, et al. Assessing performance and clinical usefulness in prediction models with survival outcomes: Practical Guidance for Cox Proportional Hazards Models. *Ann Intern Med* 2023; **176:** 105-14. doi: 10.7326/M22-0844
23. Cheson BD, Pfistner B, Juweid ME, Gascoyne RD, Specht L, Horning SJ, et al. Revised response criteria for malignant lymphoma. *J Clin Oncol* 2007; **25:** 579-86. doi: 10.1200/JCO.2006.09.2403
24. Crotty R, Hu K, Stevenson K, Maggie Y, Pontius MY, Sohani AR, et al. Simultaneous identification of cell of origin, translocations, and hotspot mutations in diffuse large B-cell lymphoma using a single RNA-sequencing assay. *Am J Clin Pathol* 2021; **155:** 748-54. doi: 10.1093/ajcp/aqaa185
25. Scott DW, Mottok A, Ennishi D, Wright GW, Farinha P, Ben-Neriah S, et al. Prognostic significance of diffuse large B-cell lymphoma cell of origin determined by digital gene expression in formalin-fixed paraffin-embedded tissue biopsies. *J Clin Oncol* 2015; **33:** 2848-56. doi: 10.1200/JCO.2014.60.2383
26. Zhang MCH, Tian SH, Fu D, Wang L, Cheng SH, MeiYi H, et al. Genetic subtype-guided immunochemotherapy in diffuse large B cell lymphoma: the randomized GUIDANCE-01 trial. *Cancer Cell* 2023; **41:** 1705-16.e5. doi: 10.1016/j.ccell.2023.09.004
27. Baliko A, Szakacs Z, Kajtar B, Ritter Z, Gyenesei A, Farkas N, et al. Clinicopathological analysis of diffuse large B-cell lymphoma using molecular biomarkers: a retrospective analysis from 7 Hungarian centers. *Front Oncol* 2023; **3:** 1224733. doi: 10.3389/fonc.2023.1224733

research article

Anlotinib monotherapy in recurrent or metastatic nasopharyngeal carcinoma: a multicenter case-series analysis

Guan-Jie Qin[1,2], Yi-Xin Su[3], Yong Liang[4], Bin Zhang[5], Yu-Fei Pan[6], Jian-Xun Lu[7], Yue-Yun Xie[8], Jin-Xuan Dai[1,2], Ke-Quan Chen[4], Feng-Fei Qin[4], Hui-Yun Yang[1,2], Xiang-Yun Kong[1,2], Yuan Xie[5], Xiao-Lan Ruan[6], Yun-Yan Mo[1,2], Ru-Yun Zhang[1,2], Jian Zhang[9], Wei Jiang[1,2]

[1] Department of Radiation Oncology, Affiliated Hospital of Guilin Medical University, Guilin, China
[2] Key Laboratory of Functional Genomics and Precision Prevention and Treatment of Oncology, Education Department of Guangxi Zhuang Autonomous Region, Guilin Medical University, Guilin, China
[3] Department of Radiation Oncology, Lingshan People's Hospital, Lingshan, China
[4] Department of Oncology, Guiping People's Hospital, Guiping, China
[5] Department of Radiation Oncology, Wuzhou Red Cross Hospital, Wuzhou, China
[6] Department of Oncology, Nanxishan Hospital of Guangxi Zhuang Autonomous Region, Guilin, China
[7] Department of Oncology, Nanning First People's Hospital, Nanning, China
[8] Department of Oncology, The 924th Hospital of the Chinese people's Liberation Army, Guilin, China
[9] Department of Oncology, Laibin People's Hospital, Laibin, China

Radiol Oncol 2025; 59(4): 617-623.

Received 21 July 2024
Accepted 15 August 2025

Correspondence to: Wei Jiang, Ph.D., Department of Radiation Oncology, Affiliated Hospital of Guilin Medical University, 15 Lequn Road, Guilin 541001, China. E-mail: weijiang@glmc.edu.cn and Jian Zhang, Department of Oncology, Laibin People's Hospital, Laibin 546100, China. E-mail: 565725048@qq.com

Guan-Jie Qin, Yi-Xin Su, Yong Liang, Bin Zhang, Yu-Fei Pan, Jian-Xun Lu, and Yue-Yun Xie contributed equally to this work and share first authorship.

Disclosure: No potential conflicts of interest were disclosed.

Background. Anlotinib has shown encouraging therapeutic effect on various solid tumors. This study assessed the efficacy and safety of anlotinib monotherapy in patients with recurrent or metastatic nasopharyngeal carcinoma (rmNPC).

Patients and methods. This study retrospectively included 30 patients with rmNPC, most following at least one previous line of systemic therapy. Patients underwent anlotinib monotherapy (12 or 10 mg/day). The primary endpoint was objective response rate (ORR). The secondary endpoints included progression-free survival (PFS), overall survival (OS), and toxicity.

Results. Thirteen patients (43.3%) had metastatic NPC, 10 (33.3%) had recurrent NPC, and 7 (23.3%) had both metastatic and recurrent NPC. Twenty-two patients (73.3%) were platinum-refractory, and 23 (76.7%) received at least three cycles of anlotinib therapy. The best overall response was partial response observed in four patients, stable disease in 18, and progressive disease in eight. The ORR was 13.3% (95% CI, 0.4−26.2%) and disease control rate was 73.3% (95% CI, 56.5−90.1%). The median OS and PFS were 11.5 months (95% CI, 7.5−15.5) and 5.7 months (95% CI, 4.7−6.7), respectively. The relatively common grade 3 or higher adverse events were hand-foot syndrome (13.3%) and oral mucositis (13.3%).

Conclusions. Anlotinib monotherapy demonstrated positive efficacy in patients with rmNPC. It was well tolerated by these patients and had acceptable toxicity.

Key words: anlotinib; nasopharyngeal carcinoma; recurrent; metastasis; tyrosine kinase inhibitors (TKI)

Introduction

Nasopharyngeal carcinoma (NPC) has a tremendous heterogeneity in geographical distribution and is highly prevalent in southern China. The age-standardized rates in prevalence areas are 50–100 times higher than in non endemic areas of the world.[1] About 70% of patients present with locoregionally advanced disease at diagnosis, and approximately 30% of these eventually develop locoregional recurrence or distant metastasis, even after radical chemoradiotherapy.[2,3] The combination of gemcitabine and cisplatin chemotherapy with or without PD-1 inhibitor-based immunotherapy is the first-line therapy for recurrent or metastatic nasopharyngeal carcinoma (rmNPC).[4-7] No commonly accepted second-line therapy is available for platinum-refractory patients.[8] Even with a growing number of treatment choices for patients with platinum-refractory rmNPC in recent clinical studies, only modest improvement in survival has been achieved, the median progression-free survival (PFS) being only 1.6–13.8 months.[9-11]

Angiogenesis induction has been considered as one of the ten hallmarks of cancer.[12] Recently, the clinical application of tyrosine kinase inhibitors (TKI) targeting proangiogenic receptors, particularly the vascular endothelial growth factor receptor (VEGFR) family, has significantly improved the survival of several solid tumors, including NPC.[13-17] Our previous study showed that apatinib, a novel small-molecule VEGFR signaling pathway inhibitor, achieved a high objective response rate (ORR) of 36.4% in patients with rmNPC who had experienced first-line treatment failure.[17] However, apatinib tolerance in patients with rmNPC was poor, with 57.6% of the patients required dose adjustment during treatment.[17]

Anlotinib hydrochloride is a novel multi-target TKI used to treat angiogenesis and proliferative signaling of tumors, with high efficacy by inhibiting VEGFR-1-3, platelet-derived growth factor receptor-α and β, fibroblast growth factor receptor-1-4, c-Kit, and Ret.[18] The phase 3 ALTER0303 trial showed that anlotinib monotherapy as third-line treatment of advanced non-small cell lung cancer can significantly prolong the median PFS from 1.4 months to 5.4 months and the median overall survival (OS) from 6.3 months to 9.6 months.[19] Anlotinib showed moderate efficacy and tolerable toxicity in patients with platinum-refractory ovarian cancer.[20] This data analysis was conducted in patients with rmNPC who had failed prior platinum-based chemotherapy or were unwilling to undergo further chemotherapy, aiming to investigate the clinical efficacy and safety of anlotinib in these patients.

Patients and methods

Patients of the study

This study retrospectively included patients with histopathologically diagnosed rmNPC from eight centers in the Guangxi Zhuang Autonomous Region, China, between January 1, 2019, and September 30, 2021. Patients were eligible for anlotinib treatment due to the following reasons: 1) no standard second-line treatment was available for rmNPC; 2) further chemotherapy was contraindicated; 3) refusal of chemotherapy due to toxicity from prior treatment. The inclusion criteria were: 1) histologically and/or radiographically confirmed rmNPC; 2) adequate hematological and biochemical parameters (absolute neutrophil count $\geq 1.5\times10^9$/L; haemoglobin level ≥ 90 g/L; total bilirubin up to 1.5 times the upper limit of normal; alanine aminotransferase, aspartate aminotransferase or alkaline phosphatase up to 2.5 times the upper limit of normal; serum creatinine up to 1.5 times the upper limit of normal); 3) performance status of 0–2 (Eastern Cooperative Oncology Group [ECOG]); 4) measurable lesion according to RECIST Version 1.1 criteria; and 5) disease progression after platinum-based chemotherapy (evaluated by RECIST Version 1.1) or refusal to receive further chemotherapy. Exclusion criteria included: 1) prior treatment with antiangiogenic drugs before anlotinib therapy; 2) involvement or invasion of a major vascular structure by the tumor; 3) serious comorbidities that could potentially affect patient survival; 4) pregnant or breastfeeding women.

This study was approved by the ethics committees of all eight participating centers and adhered to the Declaration of Helsinki and Good Clinical Practice guidelines. All patients provided written informed consent before initiation of anlotinib treatment, and confidentiality of their medical data was maintained.

Treatment

One cycle of oral anlotinib consisted of once-daily administration on days 1–14 followed by a pause of seven days.[19] The initial anlotinib dose was 12 or 10 mg/day, based on the investigators' assessment and the patients' general conditions. Dose modification to 10 or 8 mg/day was permitted based on treatment-related toxicities. When ≥ Grade 2

adverse reactions occurred, anlotinib treatment would be interrupted until the adverse reaction recovered to < Grade 2. If tolerated, the patient continued with the same anlotinib dosage; otherwise, the dose was adjusted. Treatment was permanently discontinued if the patient experienced persistent toxicities despite dose adjustments or if progressive disease (PD) was documented.

Patient evaluation and follow-up

Objective treatment response was assessed according to RECIST Version 1.1, based on imaging examinations performed at baseline and every two cycles of anlotinib treatment until treatment discontinuation or disease progression. Adverse events were recorded and graded according to the Common Terminology Criteria for Adverse Events (CTCAE, Version 5.0) during anlotinib treatment. Physical examination and laboratory parameters were recorded at baseline and at each follow-up examination during treatment. Laboratory tests and safety assessments were conducted within one month after the last dose of anlotinib in patients who discontinued treatment.

Statistical analysis

The ORR was the primary endpoint, and secondary endpoints included disease control rate (DCR), PFS, OS, and adverse events. ORR was calculated as the proportion of patients with complete response (CR) and partial response (PR) in the entire cohort. DCR was calculated as the proportion of patients with CR, PR, and stable disease (SD) in the entire cohort. PFS was calculated from the start of anlotinib treatment to the time of PD or death from any cause. OS was defined as the time from the start of anlotinib treatment to death from any cause. Survival endpoints were censored at the time of the last follow-up for patients who reached the end of the study without progression or death.

The 95% confidence intervals (CI) of the ORR and DCR were calculated using the Clopper-Pearson method. Survival curves were estimated using Kaplan-Meier method. Multivariable analysis was performed using the Cox proportional hazards analysis and backward stepwise selection. Adverse events were summarized by frequency and percentage. Statistical significance was defined as a two-sided P-value < 0.05. All statistical analyses were performed using IBM SPSS Statistics for Windows, Version 24.0 (IBM Corp, Armonk, NY, USA).

Results

Patient characteristics

A total of 30 eligible patients with rmNPC were included. The median age of the participants was 55 years (range, 35–76 years). Table 1 summarizes the baseline characteristics of all included patients. Most patients (n = 28; 93.3%) were disease stage III or IV at diagnosis. Among the included patients, 10 (33.3%) had locoregional recurrence (nasopharynx, cervical lymph nodes, or both), 13 (43.3%) had distant metastatic disease (nine after chemoradiotherapy and four at the time of diagnosis), and 7 (23.3%) had both locoregional recurrence and distant metastasis. The most common organ involved in metastasis was the liver (11 patients; 36.7%). Anlotinib was administered after one line of chemotherapy to 13 (43.3%) patients, while 9 (30.0%) received at least two prior lines of systemic therapy before anlotinib treatment. Sixteen patients (53.3%) had platinum-refractory disease. Of the remaining 14 patients, eight rejected chemotherapy and used anlotinib as first-line treatment (two patients were older than 70 years; one patient had chronic renal insufficiency; five patients refused chemotherapy due to hematological toxicity from previous chemoradiotherapy), three could not continue chemotherapy due to toxicity from first-line platinum based chemotherapy, and three did not receive a platinum-containing regime as first-line treatment for personal reasons.

Treatment administration

The end of follow-up in this study was December 28, 2021, at which time nine patients were still alive, and four continued with the anlotinib treatment. The median follow-up time was 18.3 months (range, 12.5–24.1 months). A total of 173 cycles of anlotinib were administered to the 30 patients (median, 4 cycles; range, 1–21 cycles), with 23 (76.7%) patients receiving more than three cycles and 6 (20.0%) receiving over ten cycles. The anlotinib starting dose was 12 mg/day in 21 patients (70.0%) and 10 mg/day in 9 (30.0%). Dose reductions were uncommon, occurring in only 4 (13.3%) patients (from 12 mg/day to 10 mg/day due to Grade 3 oral mucositis in two patients, and from 10 mg/day to 8 mg/day due to Grade 3 hand-foot syndrome [HFS] in one patient and Grade 2 hypothyroidism in another). Drug interruption occurred in 8 patients (26.7%) to alleviate adverse reactions (four for oral mucositis, two for HFS, and two for nasal bleeding). Overall, 10 (33.3%) patients had dose reduction or discontinuation of treatment due to toxicities (of these, two pa-

TABLE 1. Baseline characteristics of 30 patients with recurrent or metastatic nasopharyngeal carcinoma treated with anlotinib monotherapy

Characteristics	No. of patients (%)
Age (years)	
Median (55) Range (35–76)	
Sex	
Male	25 (83.3)
Female	5 (16.6)
ECOG status	
0-1	24 (80.0)
2	6 (20.0)
Disease stage[a] at diagnosis	
Stage II	2 (6.7)
Stage III	9 (30.0)
Stage IV	19 (63.3)
Disease status when starting anlotinib therapy	
Local recurrence	10 (33.3)
Metastatic disease[b]	13 (43.3)
Both	7 (23.3)
Metastatic sites	
Liver	11 (36.7)
Lung	10 (33.3)
Bone	10 (33.3)
Distant lymph node	8 (26.7)
Number of prior systemic therapy lines	
0	8 (26.7)
1	13 (43.3)
≥ 2	9 (30.0)
Platinum-refractory disease[c]	
Yes	16 (53.3)
No	14 (46.7)
Anlotinib starting dose	
12 mg	21 (70.0)
10 mg	9 (30.0)
RT for recurrent/metastatic lesions	
Yes	3 (10.0)
No	27 (90.0)
Surgical treatment for recurrent lesions	
Yes	2 (6.7)
No	28 (93.3)
Immunotherapy before anlotinib	
Yes	3 (10.0)
No	27 (90.0)

[a] According to the 8th American Joint Committee on Cancer Stage (AJCC) staging system.
[b] Includes patients with metastatic disease at diagnosis and those after radical treatment.
[c] Patients with disease progression within 6 months after first-line chemotherapy with a platinum-containing regimen.
ECOG = Eastern Cooperative Oncology Group; RT = radiotherapy

tients continued treatment with a reduced dose after treatment interruption). By the end of the study, 26 (86.7%) patients had discontinued therapy, 20 (66.7%) due to disease progression, and 6 (20.0%) for other reasons, including unacceptable toxicity related to anlotinib (n = 2), change to other treatment options (n = 2), voluntary termination of antitumor therapy (n = 1), and loss to follow-up for unknown reason (n = 1).

Treatment efficacy

Among the 30 evaluable patients, the best overall response was categorized as follow: PR in 4 patients (13.3%), SD in 18 patients (60.0%), and PD in 8 patients (26.7%). These results translated into an ORR of 13.3% (95% CI, 0.4–26.2%) and a DCR of 73.3% (95% CI, 56.5–90.1%; Figure 1A). Further analysis of the patients who achieved PR revealed that 2 patients maintained remission for more than three months, while the other 2 patients sustained remission for over six months (Figure 1B). By the cutoff date, a total of 22 patients (73.3%) experienced PD, with 20 of them succumbing to the disease (66.7%). In terms of survival outcomes, the median PFS was 5.7 months (95% CI, 4.7–6.7 months; Figure 2A), and the median OS was 11.5 months (95% CI, 7.5–15.5 months; Figure 2B).

Toxicity

Toxicity data were collected and analyzed for the 30 patients who received anlotinib. The most common drug-related adverse events included HFS (n = 15; 50.0%), hypertension (n = 12; 40.0%), oral mucositis (n = 11; 36.7%), hypothyroidism (n = 9; 30.0%), and fatigue (n = 8; 26.7%) (Table 2). Bleeding events were observed in seven patients (23.3%), with four (13.3%) exhibiting Grade 1 urinary occult blood and three (10.0%) experiencing Grade 3 nasal bleeding. Other adverse events of ≥ Grade 3 severity included HFS (n = 4; 13.3%), oral mucositis (n = 4; 13.3%), hypertension (n = 1; 3.3%), and arthralgia (n = 1; 3.3%). All adverse events were deemed tolerable and manageable with appropriate interventions.

Discussion

This study offers valuable insights into the efficacy and safety of anlotinib monotherapy in patients with rmNPC, the majority of whom had received at least one prior systemic treatment. The cohort demonstrated an ORR of 13.3% (95% CI, 0.4–26.2%),

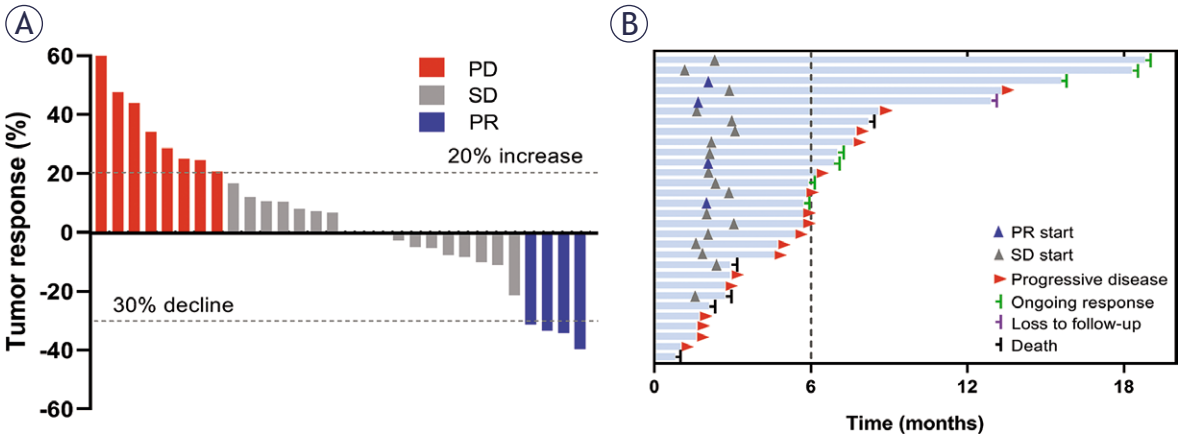

FIGURE 1. Treatment efficacy of anlotinib in patients with recurrent or metastatic nasopharyngeal carcinoma. **(A)** Waterfall plot shows the maximum change in target lesion diameter relative to baseline in each patient, following RECIST criteria, Version 1.1. **(B)** Swimmer's plot shows the duration of response for each patient.

a DCR of 73.3% (95% CI, 56.5–90.1%). The median PFS was 5.7 months (95% CI, 4.7–6.7 months), and median OS was 11.5 months (95% CI, 7.5–15.5 months). Grade 3 and 4 toxicities were relatively infrequent, with 10 patients (33.3%) undergoing dose reductions or discontinuation of treatment due to adverse events. Overall, these findings indicate that anlotinib may offer efficacy and a tolerable safety profile in patients with rmNPC.

Patients with rmNPC typically experience disease progression within 7.0 months following chemotherapy.[4] Recent phase III clinical trials have demonstrated that the combination of cisplatin, gemcitabine, and PD-1 monoclonal antibody can significantly extend the median PFS to 9.7–11.7 months. However, most patients eventually developed disease progression, resulting in a 1-year PFS of 45.8–49.4%.[5,6] There is currently no standard salvage treatment for patients whose platinum-containing regimen. Previous studies have shown that single-drug chemotherapy or PD-1 monoclonal antibody monotherapy yields an ORR of 2.9–48%, a median OS was 7.6–17.1 months and a median PFS was 2.4–9.9 months.[9,13] Our results indicate that anlotinib has comparable efficacy to these treatments, with a median PFS approaching six months.

The lack of a standardized treatment for platinum-refractory patients has prompted several clinical trials evaluating VEGF-VEGFR signaling pathway inhibitors in heavily pretreated patients. These studies have reported variable ORRs of 2.7–36.4% and median PFS of 1.8–5.0 months.[21-25] For instance, sunitinib[21] achieved an ORR of 7.1% and pazopanib[22] achieved an ORR of 6.1%, while sorafenib[23] demonstrated an ORR of 3.7%. Apatinib, which showed an ORR of over 30%, re-

TABLE 2. Most common adverse reactions due to anlotinib treatment (incidence > 5%)

Adverse reaction	All grades	Grade 1	Grade 2	Grade 3	Grade 4
	n (%)				
Hand-foot syndrome	15 (50.0)	6 (20.0)	5 (16.7)	4 (13.3)	0
Hypertension	12 (40.0)	8 (26.7)	3 (10.0)	1 (3.3)	0
Oral mucositis	11 (36.7)	5 (16.7)	2 (6.7)	4 (13.3)	0
Hypothyroidism	9 (30.0)	7 (23.3)	2 (6.7)	0	0
Fatigue	8 (26.7)	5 (16.7)	3 (10.0)	0	0
Proteinuria	5 (16.7)	5 (16.7)	0	0	0
Positive urinary occult blood	4 (13.3)	4 (13.3)	0	0	0
Leukopenia	3 (10.0)	3 (10.0)	0	0	0
Nasal bleeding	3 (10.0)	0	0	3 (10.0)	0
Arthralgia	2 (6.7)	0	1 (3.3)	1 (3.3)	0

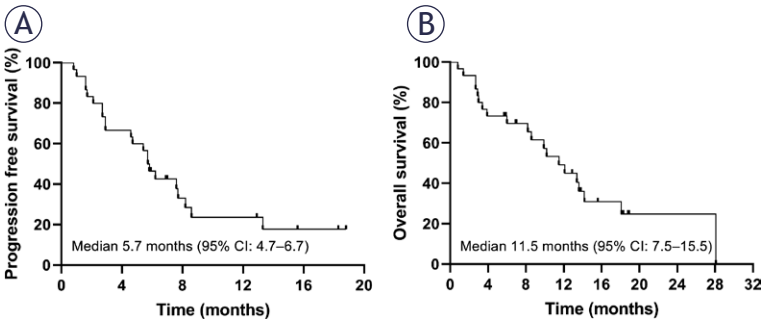

FIGURE 2. Survival curves for the 30 patients under anlotinib monotherapy in this study. **(A)** Progression-free survival and **(B)** overall survival.

quired dose modifications in over 40% of patients due to intolerable toxicities.[24] In comparison, anlotinib exhibited a modest ORR and had relatively acceptable toxicities in this study. This result is consistent with another prospective phase II study, in which anlotinib had an ORR of 20.5% and a median PFS of 5.7 months in 39 patients with rmNPC treated with third line therapy.[25]

The most common adverse reactions in this study were consistent with those reported for targeted therapies in solid tumors. Grade 3 or higher adverse events included HFS (n = 4; 13.3%), oral mucositis (n = 4; 13.3%), nasal bleeding (n = 3; 10.0%), hypertension (n = 1; 3.3%), and arthralgia (n = 1; 3.3%). The relatively low toxicity of anlotinib may be attributed to its low half-maximal inhibitory concentration (IC_{50}).[26] Previous phase III clinical trials have reported that the incidence of Grade 3 oral mucositis associated with anlotinib treatment was as low as 1%.[19] However, in this study, Grade 3 oral mucositis occurred at a higher rate and emerged as the primary reason for dose reduction or discontinuation of anlotinib. Similar findings were observed in a recent prospective phase II study, which demonstrated that the incidence of grade 3 oral mucositis during anlotinib treatment for rmNPC was 21.1% (8 of 38 patients), with 6 patients requiring dose adjustment.[25] These results can be attributed to the widespread late radiation toxicity in patients with NPC who previously received high-dose radiotherapy, predisposing them to oral mucositis when using antiangiogenic drugs.

One of the risks associated with the use of tyrosine kinase inhibitors is bleeding, particularly in patients with recurrent NPC who have undergone radiotherapy and chemotherapy.[16,21] Both sunitinib and pazopanib have been linked to fatal hemorrhagic events in patients with rmNPC.[21,22] Phase II clinical studies reported a high bleeding risk for patients with rmNPC under sunitinib therapy, with 9 (64%) of the patients experiencing such events and 2 patients suffering from fatal bleeding.[21] In a prospective study of 33 patients with rmNPC treated with pazopanib, one patient experienced fatal bleeding.[22] Adverse bleeding reactions were rarely reported in previous studies on the use of anlotinib in solid tumors.[27,28] A recent prospective study did not identify any grade 3 bleeding events caused by anlotinib in patients with rmNPC.[25] In our study, Grade 3 nasal bleeding caused by anlotinib occurred in three patients (10%), two of whom had nasopharynx recurrence and one had liver and lung metastasis. No fatal hemorrhages or bleeding from other organs occurred in our study. Vascular radiation injury and the resulting regression or necrosis of tumor-invading vessels have been suggested as potential main cause of these bleeding events.[21] Given the finding from previous studies and this study, the occurrence of bleeding events should be closely monitored during the clinical application of antiangiogenesis therapy in patients with rmNPC who have previously received radiotherapy, particularly in those with nasopharynx recurrence.

The current study has several limitations that should be acknowledged. First, the relatively small sample size and the short duration of follow-up may have introduced bias into the survival analysis, potentially obscuring the true efficacy of anlotinib. Second, the heterogeneous nature of the patient population, particularly the varying proportions of patients with liver metastasis, could have influenced the observed outcomes. Third, we were unable to investigate potential biomarkers associated with anlotinib efficacy, such as VEGFR-2 expression. Future studies should focus on exploring these biomarkers to better guide individualized treatment strategies.

In conclusion, this study provides evidence supporting the efficacy of anlotinib monotherapy in patients with recurrent or metastatic nasopharyngeal carcinoma (rmNPC). The treatment was generally well-tolerated, with a manageable toxicity profile. However, these findings require further validation through larger-scale, prospective studies.

Acknowledgments

This study was supported by the Natural Science Foundation Key Projects of Guangxi (No. 2018GXNSFDA050021), The "139" Talent Cultivation Plan Program of Guangxi Medical

High-level Backbone, the National Natural Science Foundation of China (No. 82160479), the Key Research and Development Program of Guangxi (No. AB19110016), the CSCO Youth Innovative Oncology Research Fund (No. Y-Young2020-0520), the Scientific Research Program of the Health Commission of Guangxi Zhuang Autonomous Region (Nos. Z20201200, Z20170816, Z20170207).

References

1. Bray F, Ferlay J, Soerjomataram I, Siegel RL, Torre LA, Jemal A. Global cancer statistics 2018: GLOBOCAN estimates of incidence and mortality worldwide for 36 cancers in 185 countries. *CA Cancer J Clin* 2018; **68:** 394-424. doi: 10.3322/caac.21492
2. Ren Y, Qiu H, Yuan Y, Ye J, Tian Y, Wen B, et al. Evaluation of 7th edition of AJCC staging system for nasopharyngeal carcinoma. *J Cancer* 2017; **8:** 1665-72. doi: 10.7150/jca.19197
3. Zhang MX, Li J, Shen GP, Zou X, Xu JJ, Jiang R, et al. Intensity-modulated radiotherapy prolongs the survival of patients with nasopharyngeal carcinoma compared with conventional two-dimensional radiotherapy: a 10-year experience with a large cohort and long follow-up. *Eur J Cancer* 2015; **51:** 2587-95. doi: 10.1016/j.ejca.2015.08.006
4. Zhang L, Huang Y, Hong S, Yang Y, Yu G, Jia J, et al. Gemcitabine plus cisplatin versus fluorouracil plus cisplatin in recurrent or metastatic nasopharyngeal carcinoma: a multicentre, randomised, open-label, phase 3 trial. *Lancet* 2016; **388:** 1883-92. doi: 10.1016/S0140-6736(16)31388-5
5. Yang Y, Qu S, Li J, Hu C, Xu M, Li W, et al. Camrelizumab versus placebo in combination with gemcitabine and cisplatin as first-line treatment for recurrent or metastatic nasopharyngeal carcinoma (CAPTAIN-1st): a multicentre, randomised, double-blind, phase 3 trial. *Lancet Oncol* 2021; **22:** 1162-74. doi: 10.1016/S1470-2045(21)00302-8
6. Mai HQ, Chen QY, Chen D, Hu C, Yang K, Wen J, et al. Toripalimab or placebo plus chemotherapy as first-line treatment in advanced nasopharyngeal carcinoma: a multicenter randomized phase 3 trial. *Nat Med* 2021; **27:** 1536-43. doi: 10.1038/s41591-021-01444-0
7. Yang Y, Pan J, Wang H, Zhao Y, Qu S, Chen N, et al. Tislelizumab plus chemotherapy as first-line treatment for recurrent or metastatic nasopharyngeal cancer: a multicenter phase 3 trial (RATIONALE-309). *Cancer Cell* 2023; **41:** 1061-72.e4. doi: 10.1016/j.ccell.2023.04.014
8. Wong KCW, Hui EP, Lo KW, Lam WKJ, Johnson D, Li L, et al. Nasopharyngeal carcinoma: an evolving paradigm. *Nat Rev Clin Oncol* 2021; **18:** 679-95. doi: 10.1038/s41571-021-00524-x
9. Lv JW, Li JY, Luo LN, Wang ZX, Chen YP. Comparative safety and efficacy of anti-PD-1 monotherapy, chemotherapy alone, and their combination therapy in advanced nasopharyngeal carcinoma: findings from recent advances in landmark trials. *J Immunother Cancer* 2019; **7:** 159. doi: 10.1186/s40425-019-0636-7
10. Chong WQ, Low JL, Tay JK, Le TBU, Goh GS, Sooi K, et al. Pembrolizumab with or without bevacizumab in platinum-resistant recurrent or metastatic nasopharyngeal carcinoma: a randomised, open-label, phase 2 trial. *Lancet Oncol* 2025; **26:** 175-86. doi: 10.1016/S1470-2045(24)00677-6
11. Chan ATC, Lee VHF, Hong RL, Ahn MJ, Chong WQ, Kim SB, et al. Pembrolizumab monotherapy versus chemotherapy in platinum-pretreated, recurrent or metastatic nasopharyngeal cancer (KEYNOTE-122): an open-label, randomized, phase III trial. *Ann Oncol* 2023; **34:** 251-61. doi: 10.1016/j.annonc.2022.12.007
12. Hanahan D, Weinberg RA. Hallmarks of cancer: the next generation. *Cell* 2011; **144:** 646-74. doi: 10.1016/j.cell.2011.02.013
13. Lee V, Kwong D, Leung TW, Lam KO, Tong CC, Lee A. Palliative systemic therapy for recurrent or metastatic nasopharyngeal carcinoma – How far have we achieved? *Crit Rev Oncol Hematol* 2017; **114:** 13-23. doi: 10.1016/j.critrevonc.2017.03.030
14. Qin S, Li A, Yi M, Yu S, Zhang M, Wu K. Recent advances on anti-angiogenesis receptor tyrosine kinase inhibitors in cancer therapy. *J Hematol Oncol* 2019; **12:** 27. doi: 10.1186/s13045-019-0718-5
15. Lee NY, Zhang Q, Pfister DG, Kim J, Garden AS, Mechalakos J, et al. Addition of bevacizumab to standard chemoradiation for locoregionally advanced nasopharyngeal carcinoma (RTOG 0615): a phase 2 multi-institutional trial. *Lancet Oncol* 2012; **13**: 172-80. doi: 10.1016/S1470-2045(11)70303-5
16. Hui EP, Ma BBY, Loong HHF, Mo F, Li L, King AD, et al. Efficacy, safety, and pharmacokinetics of axitinib in nasopharyngeal carcinoma: a preclinical and phase II correlative study. *Clin Cancer Res* 2018; **24**: 1030-7. doi: 10.1158/1078-0432.CCR-17-1667
17. Ruan X, Liang JH, Pan Y, Cai R, Zhang RJ, He Z, et al. Apatinib for the treatment of metastatic or locoregionally recurrent nasopharyngeal carcinoma after failure of chemotherapy: a multicenter, single-arm, prospective phase 2 study. *Cancer* 2021; **127:** 3163-71. doi: 10.1002/cncr.33626
18. Sun Y, Niu W, Du F, Du C, Li S, Wang J, et al. Safety, pharmacokinetics, and antitumor properties of anlotinib, an oral multi-target tyrosine kinase inhibitor, in patients with advanced refractory solid tumors. *J Hematol Oncol* 2016; **9:** 105. doi: 10.1186/s13045-016-0332-8
19. Han B, Li K, Wang Q, Zhang L, Shi J, Wang Z, et al. Effect of anlotinib as a third-line or further treatment on overall survival of patients with advanced non-small cell lung cancer: the ALTER 0303 phase 3 randomized clinical trial. *JAMA Oncol* 2018; **4:** 1569-75. doi: 10.1001/jamaoncol.2018.3039
20. Cui Q, Hu Y, Ma D, Liu H. A retrospective observational study of anlotinib in patients with platinum-resistant or platinum-refractory epithelial ovarian cancer. *Drug Des Devel Ther* 2021; **15:** 339-47. doi: 10.2147/DDDT.S286529
21. Hui EP, Ma BBY, King AD, Mo F, Chan SL, Kam MKM, et al. Hemorrhagic complications in a phase II study of sunitinib in patients of nasopharyngeal carcinoma who has previously received high-dose radiation. *Ann Oncol* 2011; **22:** 1280-7. doi: 10.1093/annonc/mdq629
22. Lim WT, Ng QS, Ivy P, Leong SS, Singh O, Chowbay B, et al. A Phase II study of pazopanib in Asian patients with recurrent/metastatic nasopharyngeal carcinoma. *Clin Cancer Res* 2011; **17:** 5481-9. doi: 10.1158/1078-0432.CCR-10-3409
23. Elser C, Siu LL, Winquist E, Agulnik M, Pond GR, Chin SF, et al. Phase II trial of sorafenib in patients with recurrent or metastatic squamous cell carcinoma of the head and neck or nasopharyngeal carcinoma. *J Clin Oncol* 2007; **25:** 3766-73. doi: 10.1200/JCO.2006.10.2871
24. Huang L, Zhang X, Bai Y, Chua KLM, Xie Y, Shu X, et al. Efficacy and safety of apatinib in recurrent/metastatic nasopharyngeal carcinoma: a pilot study. *Oral Oncol* 2021; **115:** 105222. doi: 10.1016/j.oraloncology.2021.105222
25. Fang Y, Su N, Zou Q, Cao Y, Xia Y, Tang L, et al. Anlotinib as a third-line or further treatment for recurrent or metastatic nasopharyngeal carcinoma: a single-arm, phase 2 clinical trial. *BMC Med* 2023; **21:** 423. doi: 10.1186/s12916-023-03140-x
26. Lin B, Song X, Yang D, Bai D, Yao Y, Lu N. Anlotinib inhibits angiogenesis via suppressing the activation of VEGFR2, PDGFRβ and FGFR1. *Gene* 2018; **654:** 77-86. doi: 10.1016/j.gene.2018.02.026
27. Shen G, Zheng F, Ren D, Du F, Dong Q, Wang Z, et al. Anlotinib: a novel multi-targeting tyrosine kinase inhibitor in clinical development. *J Hematol Oncol* 2018; **11:** 120. doi: 10.1186/s13045-018-0664-7
28. Gao Y, Liu P, Shi R. Anlotinib as a molecular targeted therapy for tumors. *Oncol Lett* 2020; **20:** 1001-14. doi: 10.3892/ol.2020.11685

research article

Baseline and dynamic changes in skeletal muscle mass as predictive biomarkers in patients with metastatic renal cell carcinoma treated with Nivolumab

Erdem Ozkan[1], Murathan Koksal[2], Bunyamin Ece[3], Mustafa Koyun[1], Omer Faruk Kuzu[4], Yusuf Acikgoz[5], Efnan Algin[6]

[1] Radiology Department, Kastamonu Training and Research Hospital, Kastamonu, Türkiye
[2] Radiology Department, Ankara Bilkent City Hospital, Ankara, Türkiye
[3] Radiology Department, Kastamonu University, Faculty of Medicine, Kastamonu, Türkiye
[4] Department of Medical Oncology, Çankırı State Hospital, Çankırı, Türkiye
[5] Department of Medical Oncology, Lokman Hekim University Ankara Hospital, Ankara, Türkiye
[6] Department of Medical Oncology, Ankara Bilkent City Hospital, Ankara, Türkiye

Radiol Oncol 2025; 59(4): 624-634.

Received 25 June 2025
Accepted 20 October 2025

Correspondence to: Erdem Özkan, Radiology Department, Kastamonu Training and Research Hospital, Kastamonu, Türkiye.
E-mail: erdem.ozkan1@saglik.gov.tr

Disclosure: No potential conflicts of interest were disclosed.

Background. Low skeletal muscle mass has been increasingly recognized as a negative prognostic factor in oncology. According to the European Working Group on Sarcopenia in Older People 2 (EWGSOP2), sarcopenia is defined as a progressive and generalized skeletal muscle disorder characterized by the loss of muscle strength and muscle mass, which can lead to impaired physical performance. This study aimed to investigate whether baseline low muscle mass and dynamic changes in muscle mass during immunotherapy could predict treatment response and survival in patients with metastatic renal cell carcinoma (mRCC) treated with Nivolumab.

Patients and methods. This retrospective cohort study included 50 mRCC patients (35 men, 15 women; mean age 59.1 ± 10.2 years) who received Nivolumab between 2019 and 2022 and underwent abdominal computed tomography (CT) before and during treatment. Muscle mass was assessed by calculating the skeletal muscle index (SMI) at the third lumbar vertebra using standard Hounsfield unit thresholds (−29 to +150 HU). Treatment response was evaluated according to immune Response Evaluation Criteria in Solid Tumors (iRECIST). Overall survival (OS) and progression-free survival (PFS) were analyzed using Kaplan–Meier curves and Cox regression models.

Results. Low muscle mass was identified in 60% of patients and was significantly associated with multiple organ metastases ($p = 0.003$). Patients with baseline low muscle mass or a negative change in SMI during treatment demonstrated poorer treatment response ($p = 0.027$ and $p = 0.021$, respectively). Both OS and PFS were significantly shorter in patients with low muscle mass and those with declining muscle mass during treatment.

Conclusions. Pre-treatment low muscle mass and muscle mass decline during immunotherapy were independently associated with inferior survival and treatment response in mRCC patients receiving Nivolumab. CT-based muscle mass assessment may serve as an imaging-based prognostic biomarker in this population.

Keywords: renal cell carcinoma; low muscle mass; computed tomography; nivolumab

Introduction

Kidney cancer accounts for approximately 5% of all new cancer diagnoses in men and 3% in women worldwide.[1] According to Global Cancer Observatory (GLOBOCAN) 2020 estimates, renal cell carcinoma (RCC) ranks as the 14th most commonly diagnosed cancer globally and represents more than 85% of all primary renal malignancies.[1,2] Furthermore, updated GLOBOCAN data reveal that in 2022, approximately 20 million new cancer cases and 9.7 million cancer-related deaths occurred worldwide, reflecting the growing global burden of malignancies.[3] At initial diagnosis, approximately 70% of patients have localized disease in the kidney, while the remaining 30% present with regional or distant organ metastases.[4] The treatment of renal malignancies differs between localized and metastatic disease; standard treatments such as partial or radical nephrectomy are applied for localized disease, whereas in advanced or metastatic cases, in addition to cytoreductive nephrectomy, "targeted" therapies, cytokine treatments, and immunotherapy can be utilized. Significant advancements have been made in the treatment of metastatic renal cell carcinoma (mRCC), particularly in recent years. Tyrosine kinase inhibitors targeting vascular endothelial growth factor, platelet derived growth factor receptor, MET, AXL and immunotherapeutic agents effective at immune checkpoint inhibition have emerged as the most prominent treatment modalities.[5] Nivolumab, an immunotherapeutic agent, is the first immune checkpoint inhibitor approved for the treatment of mRCC, developed against the programmed death-1 (PD-1) antigen.[6] Nivolumab prevents the programmed death ligand-1 molecule on tumor cells from binding to the PD-1 molecule on T cells, thus facilitating the activation of T cells against tumor cells in RCC with single or multiple metastases. However, as with many treatment modalities, there are numerous factors influencing the treatment response to Nivolumab. These factors include tumor burden, tumor subtype, type of mutation, cancer stage, number and location of metastatic organs, patient performance status, and comorbidities.[6]

According to the European Working Group on Sarcopenia in Older People 2 (EWGSOP2), sarcopenia is defined as a progressive and generalized skeletal muscle disorder characterized by the loss of muscle strength and muscle mass, which can lead to impaired physical performance.[7] Low muscle strength is considered the most important and primary indicator of sarcopenia, with 'confirmed sarcopenia' diagnosed when low muscle strength is accompanied by low muscle quantity or quality.[7] However, in oncological research, CT-based assessment of skeletal muscle mass has been widely used as a surrogate marker for overall muscle status due to its availability in routine clinical practice. Low skeletal muscle mass, as measured by CT, represents a key component of cancer cachexia and has been consistently associated with poor clinical outcomes. The rate of sarcopenia in patients with localized RCC is reported to be approximately 47%, while in mRCC patients, this rate has been indicated to vary between 29% and 68%.[8,9,10] The presence or absence of low muscle mass is considered one of the prognostic factors in assessing treatment response and tolerance in mRCC, as well as in overall survival (OS) and progression-free survival (PFS).[10]

In the evaluation of low muscle mass in cancer patients, computed tomography (CT) is considered the gold standard imaging modality, as cross-sectional muscle measurements, particularly at the third lumbar vertebra (L3), provide validated surrogate markers of total body muscle mass.[7] In patients with non-cancerous conditions or in healthy populations, alternative methods such as bioelectrical impedance analysis or dual-energy X-ray absorptiometry are often preferred due to the high radiation exposure associated with CT imaging.[11] The Skeletal Muscle Index (SMI), derived from the ratio of the cross-sectional area of skeletal muscle (SMA) measured from a single CT slice to the square of the height in meters, is the most commonly used parameter in the assessment of muscle mass.[12]

While previous studies have established that low muscle mass is associated with poor outcomes in mRCC patients, several gaps remain in the literature. First, most studies have focused on baseline muscle assessment without evaluating dynamic changes during treatment. Second, the use of immune Response Evaluation Criteria in Solid Tumors (iRECIST) for response evaluation in the context of muscle mass assessment has been underexplored. Third, the predictive value of muscle mass changes specifically during nivolumab therapy, as opposed to other systemic treatments, requires further investigation given the unique mechanisms of immunotherapy.

The aim of this study is to conduct quantitative muscle mass analyses based on CT examinations obtained at baseline and during the 6th to 12th weeks of Nivolumab treatment in patients with

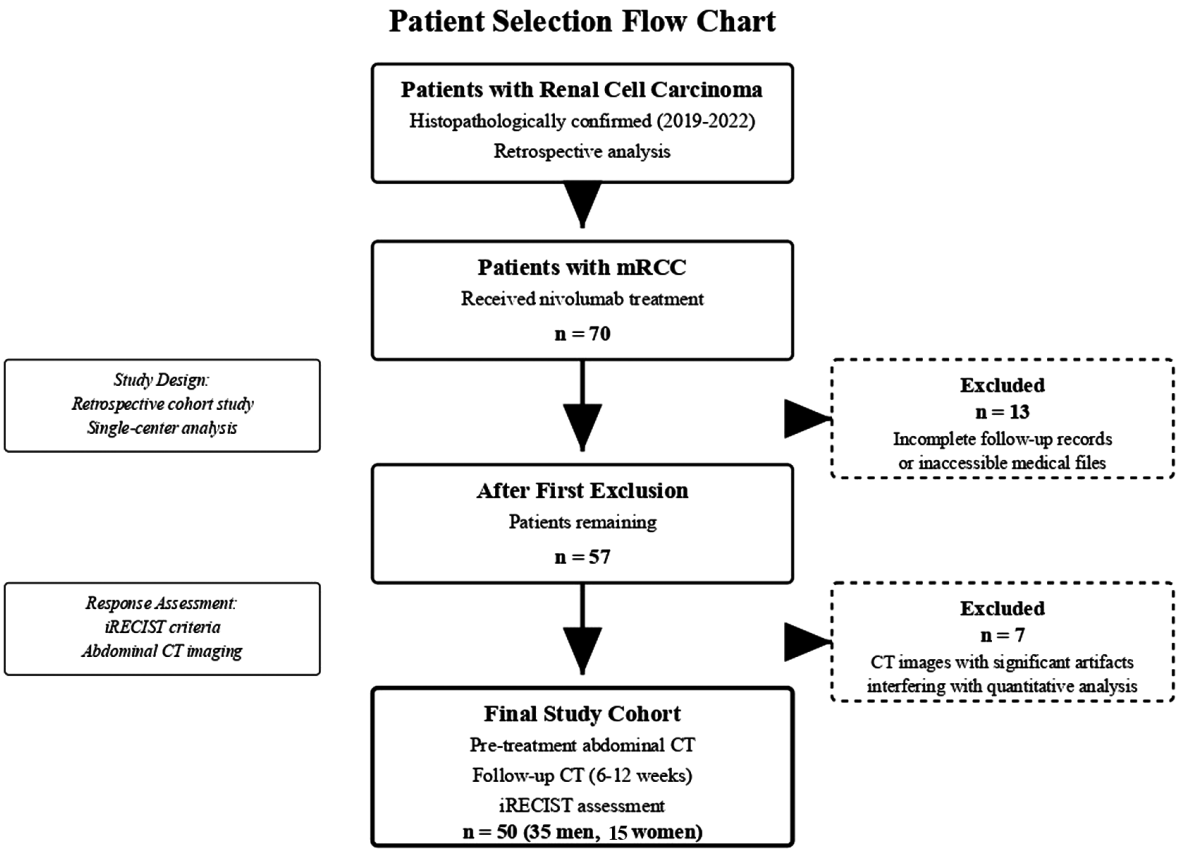

FIGURE 1. Patient selection flow chart for the retrospective analysis of nivolumab treatment in metastatic renal cell carcinoma.

mRCC. We aim to evaluate the effect of pre-treatment low muscle mass on OS, PFS, and treatment response. Additionally, we aimed to determine the impact of dynamic changes in muscle mass during the treatment process on OS, PFS, and treatment response – an aspect that has received limited attention in the immunotherapy literature.

The inclusion of patients treated with Nivolumab, an immunotherapeutic agent, and the use of "immune Response Evaluation Criteria in Solid Tumours" (iRECIST) criteria for response evaluation distinguish our study from similar research in the literature.[13] This methodological choice is particularly important given the potential for pseudoprogression, a transient increase in tumor burden caused by immune cell infiltration, which is frequently observed during immunotherapy. In addition, the evaluation of changes in SMI during treatment and their association with both treatment response and survival represents another key strength of our study.

Patients and methods

Patients

The present retrospective cohort study received approval from the Clinical Research Ethics Committee of our hospital (Decision No: E1-22-2532, April 6, 2022) prior to its initiation. Patients diagnosed with RCC histopathologically at our hospital between 2019 and 2022 were retrospectively analyzed. Of those, 70 patients with mRCC and received Nivolumab for mRCC were identified as eligible for the study. 13 patients with incomplete follow-up records or inaccessible files were excluded from the study group. 7 patients whose CT images exhibited significant artifacts that interfered with accurate interpretation and caused errors in quantitative analysis were excluded from the study (Figure 1). Consequently, 50 patients (35 men, 15 women) who underwent abdominal CT imaging prior to nivolumab treatment and follow-up abdominal CT scans within

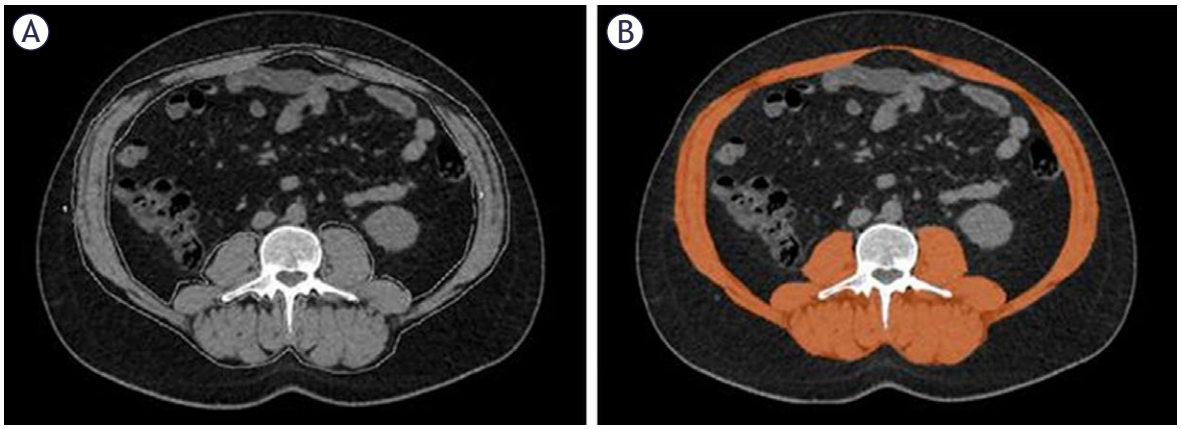

FIGURE 2. Axial computed tomography images at the level of the third lumbar vertebra. **(A)** Unprocessed image used for skeletal muscle area analysis. **(B)** Skeletal muscle areas (highlighted in orange) were manually segmented based on a Hounsfield unit (HU) threshold range of -29 to +150 to quantify muscle tissue area.

6 to 12 weeks for response assessment based on the iRECIST were included in the final cohort. Demographic characteristics including age and sex distribution were recorded for all patients. Age data are reported as mean ± standard deviation, and categorical variables as frequencies and percentages. Immunotherapy agents may elicit unconventional tumour responses, such as pseudoprogression, which challenge standard assessment criteria. The iRECIST guideline provides a standardized framework to capture and classify these atypical patterns, improving the accuracy of response evaluation in immunotherapy trials. Therefore, control CT scans obtained 6 to 12 weeks after treatment were reviewed and patients' responses to immunotherapy were assessed according to iRECIST criteria. The patients' sex, age at the time of RCC initial diagnosis, method of diagnosis (biopsy, nephrectomy), whether they underwent surgery, stage at diagnosis, histopathological type of RCC, Fuhrman grade, 'International Metastatic RCC Database Consortium' (IMDC) score and risk group, metastasis characteristics (lymph node metastasis, distant organ metastasis, combination of lymph node and distant organ metastases, etc.), the date of initiation of Nivolumab treatment, and whether progression occurred under nivolumab were recorded. The OS and PFS outcomes of the patients were calculated.

CT protocol and image analysis

Abdominal CT examinations were obtained using a 128-slice multidetector CT scanner (General Electric Revolution Evo 128, Milwaukee, USA). The technical parameters used in the scan protocol in both CT scans of the patients were as follows: 2 mm collimation, 2 mm slice thickness, rotation time: 0.6 seconds, pitch: 1, FOV: 40 cm, kV: 120, mA: 200–400. Two radiologists (15 and 5 years of experience with abdominal CT) evaluated the cases independently and blinded to clinical notes and laboratory and radiological reports in the picture archiving and communication systems (PACS). A specialized software program (Advantage Workstation 4.7 Revolution, General Electric, Milwaukee, USA) was used for the quantitative assessment of muscle mass. In the abdominal CT scans obtained before the initiation of nivolumab treatment, skeletal muscles at the L3 vertebral level (rectus abdominis, lateral and oblique abdominal muscles, psoas major, quadratus lumborum, erector spinae, and multifidus muscles) were evaluated from a single slice. To identify muscle structures, a density range of (-29)/(150) Hounsfield unit, widely accepted in the literature, was selected.[14] The area of the muscle structures in the determined density range at the L3 vertebral level was measured in square centimeters (cm^2) and the SMA value was found (Figure 2). To normalize the measurements, the SMA was divided by the square of the patient's height, resulting in the SMI expressed in cm^2/m^2. SMI was considered a continuous variable and was used as an indicator of total body muscle mass based on studies indicating that the total cross-sectional area of skeletal muscle at the L3 vertebral level is linearly associated with total body muscle mass.[15,16] The cutoff values for SMI used to determine the presence or absence of low muscle mass were derived from previous studies conducted in

similar populations, with values below 52.4 cm²/m² in men and 38.5 cm²/m² in women being considered as low muscle mass.[17,18] In the follow-up abdominal CT scans performed for treatment response assessment, SMI values were re-measured from the same anatomical slices, and changes in muscle mass-related parameters were recorded throughout the treatment period. Additionally, the difference between pre-treatment SMI and post-treatment SMI was evaluated to investigate its relationship with patients' PFS, OS, and objective response. Furthermore, patients' treatment responses were assessed according to iRECIST criteria, and the statistical relationship with muscle mass was analyzed. Changes in SMI, denoted as ΔSMI, were calculated by subtracting the SMI value measured on CT scans obtained before the initiation of Nivolumab treatment from the value measured on control CT scans performed for treatment response evaluation. A positive ΔSMI indicated an increase in muscle mass during treatment, whereas a negative ΔSMI indicated a decrease.

Statistical analysis and statistical power analysis

Statistical analysis was performed using SPSS 22 (Statistical Package for the Social Sciences Version 22.0 for Windows) (SPSS Inc., Chicago, IL, USA). Sex distribution within muscle mass groups was analyzed using Chi-square test. Age differences between groups were compared using independent t-test for normally distributed data or Mann-Whitney U test for non-normally distributed data, with results reported as mean ± standard deviation or median (range) as appropriate. The Chi-square test or Fisher's exact test was used for the comparison of categorical variables, as appropriate. Univariate and multivariate analyses for OS were conducted using the Cox regression model. Survival analyses were performed using the Kaplan-Meier method, and the results were analyzed with the Log-rank test. OS was defined as the time from the start of nivolumab treatment to death or the last follow-up date for living patients. PFS was defined as the time from the start of nivolumab treatment to progression.

To assess interobserver agreement for SMA measurements, the intraclass correlation coefficient (ICC) was calculated with 95% confidence intervals. ICC values were interpreted as follows: < 0.50 indicated poor agreement, 0.50–0.75 moderate agreement, 0.75–0.90 good agreement, and 0.90–1.00 excellent agreement. Test-retest reliability was evaluated by calculating ICC between measurements obtained from CT scans performed at different time points, using the same interpretation criteria as interobserver agreement. Statistical significance was set at $p < 0.05$ with 95% confidence intervals.

Post hoc power analysis was conducted to evaluate the study's ability to detect clinically meaningful differences between groups. Power calculations were performed using G*Power 3.1.9.7 and R software (version 4.3.0), based on observed effect sizes, event rates, and sample sizes. For survival endpoints, power was estimated using the log-rank test and Cox proportional hazards models; for categorical outcomes, Chi-square tests and logistic regression models were used. All calculations assumed a two-sided alpha level of 0.05.

The study achieved adequate power (> 75%) for the primary survival comparisons between low muscle mass and normal muscle mass groups (85.2% for overall survival; 78.6% for progression-free survival). Multivariate Cox regression modeling also demonstrated high power (89.6%) for detecting combined effects of low muscle mass, ΔSMI, and metastatic burden on overall survival. Power for secondary endpoints, particularly treatment response analyses, ranged between 68.9% and 74.3%, which is considered acceptable for exploratory purposes. Considering the retrospective design, no prior sample size calculation was performed.

Results

Interobserver agreement for SMA measurements was assessed using a two-way mixed-effects model with absolute agreement for single measurements ICC(2,1). The analysis demonstrated excellent agreement between the two radiologists (ICC = 0.947, $p < 0.001$).

Characteristics of patients

The study included 50 patients (35 men [70%], 15 women [30%]) with a mean age of 59.1 ± 10.2 years. The mean age was 59.9 ± 9.5 years in males and 57.1 ± 11.8 years in females. Histopathologically, only 4 patients (8%) had papillary type RCC, while 46 (92%) had clear cell type RCC. IMDC score of 5 patients could not be calculated due to missing parameters. In 45 patients for whom IMDC data were available, 36 patients (80%) were classified as good risk, 5 patients (11%) as moderate risk and 4 patients (9%) as poor risk according to risk catego-

TABLE 1. Comparison of clinical characteristics and survival outcomes by baseline muscle mass status

Feature	Low buscle mass present (n = 30)	Low muscle mass absent (n = 20)	p-value
Patients, n (%)	30 (60)	20 (40)	-
Age, mean ± SD	60 ± 10.5	57.7 ± 9.9	0.382
Sex (men / women)	25 / 5	10 / 10	0.013*
IMDC score (favorable / intermediate / poor)	23 / 2 / 2	13 / 3 / 2	0.541
Objective treatment response (Yes / No)	2 / 28	6 / 14	0.027*
Overall Survival, Months (95% CI)	20 (8.1–31.9)	NR	< 0.001*
Progression-Free Survival, Months (95% CI)	8.8 (5.7–11.9)	30.2 (13.1–47.4)	0.004*

Statistically significant p-values are marked with an asterisk (*). Mann–Whitney U, Chi-square, and log-rank tests were used where appropriate.

CI = confidence ınterval; HR = hazard ratio; IMDC = International Metastatic Renal Cell Carcinoma Database Consortium; ΔSMI = change in skeletal muscle ındex

TABLE 2. Association of change in skeletal muscle index with clinical and survival outcomes

Variable	ΔSMI Negative (n = 25)	ΔSMI Positive (n = 25)	p-value
Age, mean ± SD	61.0 ± 10.1	57.1 ± 10.1	0.180
Sex (men/ women)	18 / 7	17 / 8	0.758
IMDC score (favorable / intermediate / poor)	18 / 1 / 3	18 / 4 / 1	0.249
Presence of multiple metastases, n (%)	19 (76)	11 (44)	0.021*
Baseline low muscle mass, n (%)	19 (76)	11 (44)	0.021*
Objective treatment response (Yes / No)	1 / 24	7 / 18	0.021*
Overall survival, months (95% CI)	15.8 (0–37.0)	NR	0.027*
Progression-free survival, months (95% CI)	8.1 (1.6–14.6)	30.2 (11.5–49.0)	0.005*

Low muscle mass defined as SMI < 52.4 cm2 / m2 in men and < 38.5 cm2/m2 in women . Statistically significant p-values are marked with an asterisk (*). Mann–Whitney U, chi-square, and log-rank tests were used where appropriate.

CI = confidence ınterval; IMDC = International Metastatic Renal Cell Carcinoma Database Consortium; NR = not reached; ΔSMI = change in skeletal muscle ındex

ries. At initial diagnosis, 20 patients (40%) had no metastasis, while metastasis was present in 30 patients (60%). All patients received at least one line of systemic therapy, including interferon, pazopanib, sunitinib or everolimus, prior to nivolumab, and received nivolumab after failure of these therapies. First-line treatments included interferon in 27 patients (54%), sunitinib in 12 patients (24%), and pazopanib in 11 patients (22%). Nivolumab was administered as second-line therapy in 18 patients (36%), third-line therapy in 17 patients (34%), fourth-line therapy in 12 patients (24%), and fifth-line therapy in 3 patients (6%).

In the quantitative analyses obtained from pre-treatment CT scans, low muscle mass was present in 30 patients (60%) of the entire patient group, whereas 20 patients (40%) had normal muscle mass. Sex distribution showed a difference between muscle mass groups: in the low muscle mass group, 25 patients (83.3%) were male and 5 (16.7%) were female, while in the normal muscle mass group, 10 patients (50%) were male and 10 (50%) were female (p = 0.013). The mean age in the low muscle mass group was 60.0 ± 10.5 years, while the mean age in the normal muscle mass group was 57.7 ± 9.9 years, which was not a statistically significant difference (p = 0.382).

When evaluated with respect to the organs involved in metastasis, no statistically significant association was found between low muscle mass and specific metastasis locations. However, the presence of low muscle mass was found to be statisti-

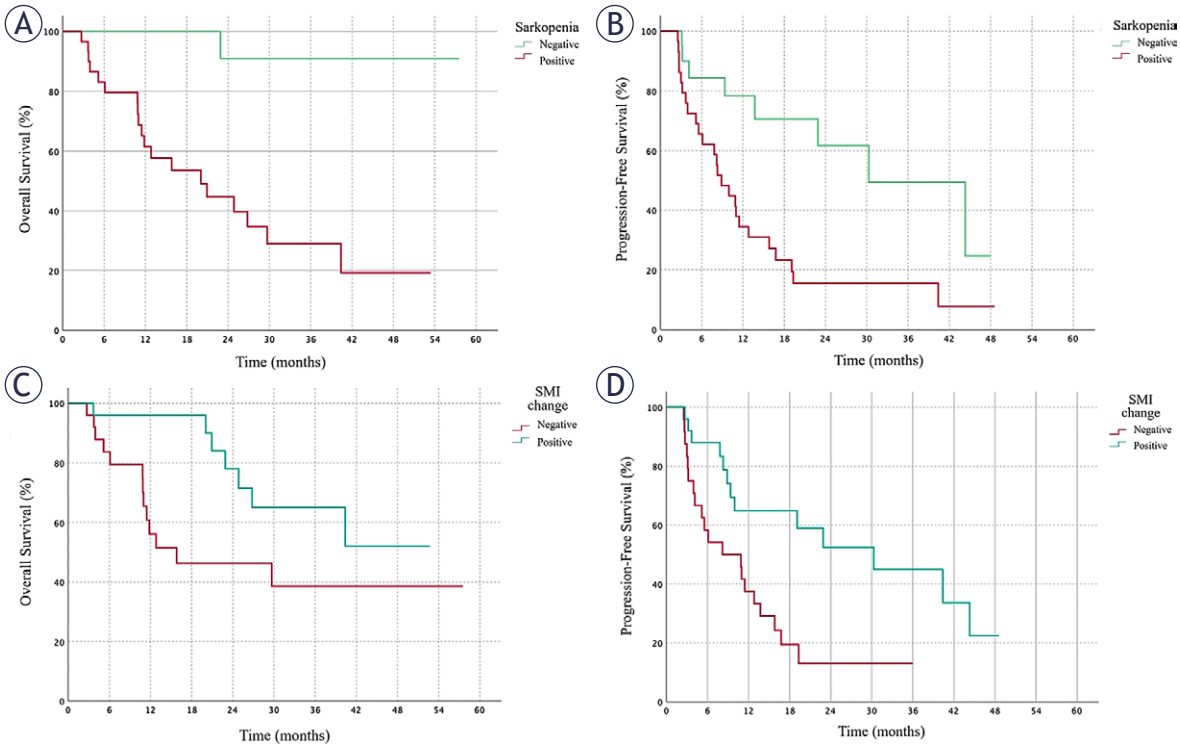

FIGURE 3. Kaplan-Meier survival curves illustrating overall survival (OS) and progression-free survival (PFS) in patients with metastatic renal cell carcinoma stratified by muscle mass status and skeletal muscle index (SMI) change. **(A)** OS was significantly shorter in patients with low muscle mass compared to those normal muscle mass group (HR: 35.00; 95% CI: 3.22-381.69; p = 0.003). **(B)** PFS was significantly shorter in patients with low muscle mass than in normal muscle mass group (HR: 12.50; 95% CI: 2.10-73.91; p = 0.004). **(C)** Patients with a negative ΔSMI had significantly reduced OS compared to those with a positive ΔSMI (HR: 6.10; 95% CI: 1.46-25.47; p = 0.013). **(D)** A negative ΔSMI was associated with significantly shorter PFS compared to a positive ΔSMI (HR: 4.50; 95% CI: 1.15-17.65; p = 0.031)

CI = confidence interval; HR = hazard ratio; HU = Hounsfield unit; OS = overall survival; PFS = progression-free survival; ΔSMI = change in skeletal muscle index

cally significantly higher in patients with multiple organ metastases (p = 0.003).

In the group with a negative change in SMI (ΔSMI-negative), the mean age was 61.0 ± 10.1 years, while in the group with a positive change (ΔSMI-positive), it was 57.1 ± 10.1 years. The mean age was higher in the ΔSMI-negative group, though this difference was not statistically significant (p = 0.180). No significant association was observed between sex and ΔSMI groups (p = 0.758). Additionally, no significant statistical relationships were identified with respect to IMDC categories, the type of organs involved in metastasis, and histological subtypes. When evaluating the number of metastatic organs, the presence of multiple metastases was significantly associated with a negative change in ΔSMI, similar to the association observed with low muscle mass (p = 0.021).

Evaluation of response to treatment

In the sarcopenic group, only 2 patients (7%) had an objective response to treatment, while 28 patients (93%) had no response. In the normal muscle masss group, 6 patients (30%) had an objective response to treatment, while 14 patients (70%) had no objective response. The objective response rate in the normal muscle mass group was found to be statistically significant (p = 0.027). When evaluated in terms of objective response, 24 patients (96%) in the ΔSMI-negative group did not achieve an objective response to treatment, whereas 18 patients (72%) in the ΔSMI-positive group also did not achieve an objective response (p = 0.021). The association of the presence or absence of low muscle mass and change in SMI with response to treatment is summarized in Table 1 and Table 2.

TABLE 3. Cox regression analysis for overall survival

Variable	Univariate HR (95% CI)	p-value	Multivariate HR (95% CI)	p-value
Age	1.01 (0.96–1.05)	0.594	0.98 (0.92–1.05)	0.713
Sex (female vs. male)	0.89 (0.34–2.33)	0.818	0.86 (0.22–3.25)	0.825
Low muscle masss (present vs. absent)	17.50 (2.33–131.10)	0.005*	35.00 (3.22–381.69)	0.003*
ΔSMI (negative vs. positive)	2.72 (1.07–6.87)	0.034*	6.10 (1.46–25.47)	0.013*
IMDC score (intermediate/poor vs. favorable)	0.67 (0.15–2.94)	0.600	1.57 (0.26–9.38)	0.621
Multiple metastases (present vs. absent)	3.11 (1.12–8.64)	0.029*	5.21 (1.00–27.10)	0.050*
Histologic subtype (non-clear cell vs. clear cell)	0.85 (0.11–6.40)	0.877	0.68 (0.04–9.56)	0.779
Lymph node metastasis (present vs. absent)	0.82 (0.34–1.98)	0.665	0.31 (0.07–1.22)	0.094
Lung metastasis (present vs. absent)	1.26 (0.51–3.09)	0.614	0.27 (0.05–1.39)	0.118
Liver metastasis (present vs. absent)	1.78 (0.71–4.49)	0.216	0.94 (0.24–3.67)	0.940

Statistically significant p-values are marked with an asterisk (*).

CI = confidence ınterval; HR = hazard ratio; IMDC = International Metastatic Renal Cell Carcinoma Database Consortium; ΔSMI = change in skeletal muscle ındex

TABLE 4. Cox regression analysis for progression-free survival

Variable	Univariate HR (95% CI)	p-value	Multivariate HR (95% CI)	p-value
Age	0.99 (0.96–1.03)	0.647	0.98 (0.93–1.03)	0.437
Sex (female vs. male)	0.87 (0.38–2.00)	0.739	1.00 (0.33–3.05)	0.994
Low muscle mass (present vs. absent)	4.17 (1.91–9.10)	< 0.001*	4.98 (1.99–12.42)	< 0.001*
ΔSMI (Negative vs. Positive)	3.52 (1.50–8.26)	0.004*	6.42 (2.18–18.91)	0.001*
IMDC score (intermediate/poor vs. favorable)	1.13 (0.33–3.84)	0.849	2.12 (0.48–9.30)	0.321
Multiple metastases (present vs. absent)	2.53 (1.07–5.97)	0.035*	1.97 (0.59–6.63)	0.267
Histologic subtype (non-clear cell vs. clear cell)	0.95 (0.18–5.01)	0.950	1.39 (0.15–12.92)	0.771
Lymph node metastasis (present vs. absent)	0.76 (0.34–1.70)	0.510	0.52 (0.17–1.63)	0.264
Lung metastasis (present vs. absent)	1.18 (0.52–2.67)	0.692	0.59 (0.18–1.89)	0.374
Liver metastasis (present vs. absent)	1.33 (0.62–2.88)	0.466	0.89 (0.30–2.66)	0.839

Statistically significant p-values are marked with an asterisk (*).

CI = confidence ınterval; HR = hazard ratio; IMDC = International Metastatic Renal Cell Carcinoma Database Consortium; ΔSMI = change in skeletal muscle ındex

Survival analysis

The median OS for the entire group was 40.3 months (95% CI, 16.9–63.8), and the median PFS was 12.8 months (95% CI, 6.9–18.6). While the median survival could not be reached in the normal muscle mass group, the median OS in the low muscle mass group was 20 months ($p < 0.001$) (Figure 3A). The PFS for the low muscle mass group was 8.8 months , while it was 30.2 months in the normal muscle mass group, which was statistically significantly higher ($p = 0.004$) (Figure 3B). The association of low muscle mass with clinical features and survival is summarized in Table 1. Furthermore, OS and PFS were significantly higher in the ΔSMI-positive group compared to the ΔSMI-negative group ($p = 0.027$ and $p = 0.05$, respectively) (Figure 3C–D). The association of changes in muscle mass with survival is summarized in Table 2.

Univariate and multivariate analysis

Univariate and multivariate analyses were performed to assess the associations of OS and PFS

with age, sex, histologic type, presence or absence of low muscle mass, ΔSMI, IMDC risk group, number of metastases and metastasis site.

In the univariate Cox regression analysis, low muscle mass prior to nivolumab treatment (hazard ratio [HR]: 17.50; 95% CI: 2.53–121.03; p = 0.005), a negative change in ΔSMI (HR: 2.72; 95% CI: 1.08–6.88; p = 0.034), and the presence of multiple organ metastases (HR: 3.11; 95% CI: 1.12–8.64; p = 0.029) were found to be significant prognostic factors for OS.

In the multivariate analysis, low muscle mass remained an independent predictor of mortality, with affected patients exhibiting significantly shorter OS compared to normal muscle mass individuals (HR: 35.00; 95% CI: 3.22–381.69; p = 0.003). Likewise, a negative ΔSMI was associated with increased mortality (HR: 6.10; 95% CI: 1.46–25.47; p = 0.013), and multiorgan metastases showed a borderline association with poorer OS (HR: 5.21; 95% CI: 1.00–27.10; p = 0.050) (Table 3).

In the univariate analysis, low muscle mass (HR: 5.80; 95% CI: 1.80–18.60; p = 0.003), negative ΔSMI (HR: 3.40; 95% CI: 1.20–9.70; p = 0.027), and multiple organ metastases (HR: 2.88; 95% CI: 1.05–7.92; p = 0.038) were identified as significant predictors of shorter PFS.

Multivariate analysis revealed that low muscle mass remained an independent predictor of disease progression (HR: 12.50; 95% CI: 2.10–73.91; p = 0.004), as did negative ΔSMI (HR: 4.50; 95% CI: 1.15–17.65; p = 0.031). The association between multiorgan metastases and PFS remained borderline significant (HR: 3.80; 95% CI: 0.98–14.80; p = 0.053) (Table 4).

Discussion

This study demonstrated that both baseline low muscle mass and negative change in SMI during nivolumab therapy were strongly associated with reduced treatment efficacy, shorter PFS and lower OS in patients with mRCC. Additionally, both low muscle mass and a negative ΔSMI were significantly correlated with a higher incidence of multiorgan metastases. These findings underscore the prognostic importance of skeletal muscle status in the context of immunotherapy.

While the association between low muscle mass and poor outcomes in mRCC has been previously established, our study provides several novel insights. First, we demonstrate that dynamic changes in muscle mass during nivolumab treatment (ΔSMI) serve as independent predictors of both survival outcomes and treatment response, with patients experiencing muscle mass decline showing significantly worse outcomes even when baseline muscle status is considered. This dynamic assessment approach has been underexplored in the immunotherapy literature. Second, our use of iRECIST criteria for response evaluation in the context of muscle mass assessment addresses the unique challenges of immunotherapy response patterns, including pseudoprogression, which may confound traditional response assessments. Third, our findings specifically validate the prognostic utility of muscle mass assessment in nivolumab-treated patients, contributing to the growing evidence base for precision medicine approaches in immunotherapy selection and monitoring.

Our results are in line with a recent meta-analysis, which reported significantly worse OS in sarcopenic patients compared to non-sarcopenic individuals across both localized and mRCC populations.[19] While Herrmann *et al*. did not find a statistically significant OS difference, other studies such as those by Fukushima *et al*. and Sharma *et al*. demonstrated that sarcopenia is an independent predictor of poor survival.[10,20,21] Our cohort further supports these findings, with significantly shorter median OS in sarcopenic patients. Furthermore, patients who developed a positive ΔSMI during the course of treatment were found to have longer OS compared to patients who experienced a decrease in muscle mass.

The PFS findings in our study are also consistent with the existing literature. Ueki *et al*. reported a median PFS of 8.3 months in sarcopenic patients and 48.4 months in non-sarcopenic patients in their study in mRCC patients using nivolumab.[22] In our cohort, median PFS was similarly reduced in sarcopenic patients and those with negative ΔSMI, emphasizing the potential value of dynamic muscle assessment during immunotherapy.

Another clinically important observation was the significantly lower objective response rate in sarcopenic patients and those with reduced SMI. These findings echo those of Ishihara *et al.* who reported reduced treatment response in patients with progressive muscle wasting during targeted therapy.[23] While their study is relevant to sunitinib, the consistency in our nivolumab-treated cohort suggests a broader association between low muscle mass and therapeutic resistance.

Importantly, we observed that patients with baseline low muscle mass were more likely to experience additional muscle loss during treatment.

This observation, consistent with previous findings in sunitinib-treated patients, may reflect a compounding effect of pre-existing low muscle mass and treatment-related catabolism. Additionally, patients with negative ΔSMI were significantly older, suggesting that age-related sarcopenia and tumor-related cachexia may exert synergistic effects in promoting muscle degradation.[23]

Skeletal muscle acts as a dynamic endocrine and immunomodulatory organ by releasing myokines that influence immune responses, including the activation and regulation of cytotoxic T lymphocytes.[24] Sarcopenia, compromises immune surveillance and reduces therapeutic response to immune checkpoint inhibitors.[25,26] Furthermore, chronic systemic inflammation, commonly observed in sarcopenic individuals, contributes to the development of an immunosuppressive tumor microenvironment, further compromising treatment efficacy.[27]

Generally, sarcopenia has emerged as a promising imaging-derived biomarker reflecting host physiology, immune competence and systemic inflammation.[28] Unlike molecular biomarkers such as PD-L1 expression and tumor mutation burden, which have shown limited predictive utility in immunotherapy, muscle status provides a comprehensive, patient-level insight into biological reserve and treatment tolerance. Several systemic inflammatory markers such as C-reactive protein and neutrophil/lymphocyte ratio have been investigated as prognostic indicators.[22,23] However, these are non-specific and are vulnerable to confounding by infections or treatment-related toxicities.

Muscle mass can be objectively and reproducibly assessed by imaging modalities such as CT, making it a practical tool for the assessment of low muscle mass in oncology. However, although CT-based quantitative muscle mass measurement is a validated and reproducible method to assess amount of muscle mass, it does not capture muscle strength or physical performance. Accordingly, integrating imaging assessments with functional assessments such as grip strength or walking speed would improve the clinical relevance of measuring sarcopenia.

Recent studies have emphasized the importance of muscle quality, particularly skeletal muscle radiodensity, as an additional determinant of treatment outcomes. Low muscle attenuation values, indicative of increased fat infiltration (myosteatosis), have been associated with worse clinical outcomes in patients receiving immunotherapy.[29,30] However, variability in CT protocols, including the use of intravenous contrast agents, may limit the consistency of radiodensity measurements between centers.

This study has several limitations. First, its retrospective and single-center design may affect the generalizability of our findings. Second, while our sample size (n = 50) is comparable to other nivolumab studies, it limits the statistical power for subgroup analyses. Additionally, it is important to acknowledge that our study assessed only muscle quantity (mass) through CT-based SMI measurements, which represents only one component of the comprehensive sarcopenia assessment as defined by EWGSOP2. True sarcopenia diagnosis requires assessment of muscle strength and potentially physical performance in addition to muscle mass. Therefore, our findings specifically relate to low muscle mass rather than confirmed sarcopenia. While muscle mass serves as a practical and widely available imaging biomarker, future studies incorporating functional assessments would provide a more comprehensive evaluation of muscle status and its relationship to treatment outcomes.

Despite these limitations, the primary outcomes in our study were robust, and both low muscle mass and ΔSMI remained independent predictors of OS and PFS in multivariate analyses. Our findings support the integration of skeletal muscle evaluation into routine oncologic assessment for patients receiving immunotherapy. Future prospective studies incorporating nutritional and rehabilitative interventions are warranted to validate and expand these observations.

Conclusions

This study demonstrates that both baseline low muscle mass and treatment-related muscle mass decline are associated with poorer treatment response, shorter PFS, and lower OS in mRCC patients receiving nivolumab. The dynamic assessment of muscle mass changes during treatment provides additional prognostic information beyond baseline measurements. Routine CT-based assessment of muscle mass can serve as a practical imaging biomarker to complement existing prognostic tools, though integration with functional assessments would enhance its clinical utility. Larger-scale prospective studies incorporating both structural and functional muscle parameters are needed to validate these findings and explore interventional strategies.

Acknowledgments

This article is derived from the medical specialty thesis of Dr. Erdem Özkan, conducted at Ankara Bilkent City Hospital, Türkiye. No funding was received for this study. The authors acknowledge the radiologists who performed the quantitative image analyses and the clinical team involved in patient care. All listed authors meet the ICMJE criteria for authorship.

References

1. Capitanio U, Bensalah K, Bex A, Boorjian SA, Bray F, Coleman J, et al. Epidemiology of renal cell carcinoma. *Eur Urol* 2019; **75:** 74-8. doi: 10.1016/j.eururo.2018.08.036
2. Ferlay J, Ervik M, Lam, F, Colombet M, Mery L, Piñeros M, et al. *Global cancer observatory: cancer today*. Lyon, France: International Agency for Research on Cancer; 2020.
3. Bray F, Laversanne M, Sung H, Ferlay J, Siegel RL, Soerjomataram I, et al. Global cancer statistics 2022: GLOBOCAN estimates of incidence and mortality worldwide for 36 cancers in 185 countries. *CA Cancer J Clin* 2024; **74:** 229-63. doi: 10.3322/caac.21834
4. Mathers CD. History of global burden of disease assessment at the World Health Organization. *Arch Public Health* 2020: **24;** 78-87. doi: 10.1186/s13690-020-00458-3
5. Sherafat NS, Keshavarz A, Mardi A, Mohammadiara A, Aghaei M, Aghebati-Maleki L, et al. Rationale of using immune checkpoint inhibitors (ICIs) and anti-angiogenic agents in cancer treatment from a molecular perspective. *Clin Exp Med* 2025; **25:** 238. doi: 10.1007/s10238-025-01751-7
6. Venur VA, Joshi M, Nepple KG, Zakharia Y. Spotlight on nivolumab in the treatment of renal cell carcinoma: design, development, and place in therapy. *Drug Des Devel Ther* 2017: **11:** 1175-82. doi: 10.2147/DDDT.S110209
7. Cruz-Jentoft AJ, Bahat G, Bauer J, Boirie Y, Bruyère O, Cederholm T, et al. Writing group for the European Working Group on Sarcopenia in Older People 2 (EWGSOP2), and the Extended Group for EWGSOP2. Sarcopenia: revised European consensus on definition and diagnosis. *Age Ageing* 2019; **48:** 16-31. doi: 10.1093/ageing/afy169
8. Psutka SP, Boorjian SA, Moynagh MR, Schmit GD, Costello BA, Thompson RH, et al. Decreased skeletal muscle mass is associated with an ıncreased risk of mortality after radical nephrectomy for localized renal cell cancer. *J Urol* 2016; **195:** 270-6. doi: 10.1016/j.juro.2015.08.072
9. Sharma P, Zargar-Shoshtari K, Caracciolo JT, Fishman M, Poch MA, Pow-Sang J, et al. Sarcopenia as a predictor of overall survival after cytoreductive nephrectomy for metastatic renal cell carcinoma. *Urol Oncol* 2015; **33:** 339. e17-23. doi: 10.1016/j.urolonc.2015.01.011
10. Fukushima H, Nakanishi Y, Kataoka M, Tobisu K, Koga F. Prognostic significance of sarcopenia in patients with metastatic renal cell carcinoma. *J Urol* 2016; **195:** 26-32. doi: 10.1016/j.juro.2015.08.071
11. Nikodinovska V, Ivanoski S. Sarcopenia, more than just muscle atrophy: ımaging methods for the assessment of muscle quantity and quality. *Rofo* 2023; **195:** 777-89. doi: 10.1055/a-2057-0205.
12. Ryan AM, Prado CM, Sullivan ES, Power DG, Daly LE. Effects of weight loss and sarcopenia on response to chemotherapy, quality of life, and survival. *Nutrition* 2019; **67-68:** 110539. doi: 10.1016/j.nut.2019.06.020
13. Seymour L, Bogaerts J, Perrone A, Ford R, Schwartz LH, Mandrekar S, et al. RECIST working group. iRECIST: guidelines for response criteria for use in trials testing immunotherapeutics. *Lancet Oncol* 2017; **18:** e143-52. doi: 10.1016/S1470-2045(17)30074
14. Aubrey J, Esfandiari N, Baracos VE, Buteau FA, Frenette J, Putman CT, et al. Measurement of skeletal muscle radiation attenuation and basis of its biological variation. *Acta Physiol* 2014; **210:** 489-97. doi: 10.1111/apha.12224
15. Ryan AM, Power DG, Daly L, Cushen SJ, Ní Bhuachalla Ē, Prado CM. Cancer-associated malnutrition, cachexia and sarcopenia: the skeleton in the hospital closet 40 years later. *Proc Nutr Soc* 2016; **75:** 199-211. doi: 10.1017/S002966511500419X
16. Mourtzakis M, Prado CM, Lieffers JR, Reiman T, McCargar LJ, Baracos VE. A practical and precise approach to quantification of body composition in cancer patients using computed tomography images acquired during routine care. *Appl Physiol Nutr Metab* 2008; **33:** 997-1006. doi: 10.1139/H08-075
17. Lee J, Suh J, Song C, You D, Jeong IG, Hong B; et al. Association between sarcopenia and survival of patients with organ-confined renal cell carcinoma after radical nephrectomy. *Ann Surg Oncol* 2022; **29:** 2473-9. doi: 10.1245/s10434-021-10881-7
18. Prado CM, Birdsell LA, Baracos VE. The emerging role of computerized tomography in assessing cancer cachexia. *Curr Opin Support Palliat Care* 2009; **3:** 269-75. doi: 10.1097/SPC.0b013e328331124a.
19. Hu X, Liao DW, Yang ZQ, Yang WX, Xiong SC, Li X. Sarcopenia predicts prognosis of patients with renal cell carcinoma: a systematic review and meta-analysis. *Int J Brauz Urol* 2020; **46:** 705-15. doi. 10.1590/S1677-5538.IBJU.2019.0636
20. Herrmann T, Mione C, Montoriol PF, Molnar I, Ginzac A, Durando X, et al. Body mass ındex, sarcopenia, and their variations in predicting outcomes for patients treated with nivolumab for metastatic renal cell carcinoma. *Oncology* 2022; **100:** 114-23. doi: 10.1159/000520833
21. Sharma P, Zargar-Shoshtari K, Caracciolo JT, Fishman M, Poch MA, Pow-Sang J, et al. Sarcopenia as a predictor of overall survival after cytoreductive nephrectomy for metastatic renal cell carcinoma. *Urol Oncol* 2015; **33:** 339. e17-23. doi: 10.1016/j.urolonc.2015.01.011
22. Ueki H, Hara T, Okamura Y, Bando Y, Terakawa T, Furukawa J, et al. Association between sarcopenia based on psoas muscle index and the response to nivolumab in metastatic renal cell carcinoma: a retrospective study. *Investig Clin Urol* 2022; **63:** 415-24. doi: 10.4111/icu.20220028
23. Ishihara H, Takagi T, Kondo T, Fukuda H, Yoshida K, Iizuka J et al. Effect of changes in skeletal muscle mass on oncological outcomes during first-line sunitinib therapy for metastatic renal cell carcinoma. *Target Oncol* 2018; **13:** 745-55. doi: 10.1007/s11523-018-0600-3
24. Severinsen MCK, Pedersen BK. Muscle-organ crosstalk: the emerging roles of myokines. *Endocr Rev* 2020; **41:** 594-609. doi: 10.1210/endrev/bnaa016
25. Deng Y, Zhao L, Huang X, Zeng Y, Xiong Z, Zuo M. Contribution of skeletal muscle to cancer immunotherapy: a focus on muscle function, inflammation, and microbiota. *Nutrition* 2023; **105:** 111829. doi: 10.1016/j.nut.2022.111829
26. Li S, Wang T, Tong G, Li X, You D, Cong M. Prognostic ımpact of sarcopenia on clinical outcomes in malignancies treated with ımmune checkpoint ınhibitors: a systematic review and meta-analysis. *Front Oncol* 2021; **11:** 726257. doi: 10.3389/fonc.2021.726257
27. Bilen MA, Martini DJ, Liu Y, Shabto JM, Brown JT, Williams M, et al. Combined effect of sarcopenia and systemic ınflammation on survival in patients with advanced stage cancer treated with ımmunotherapy. *Oncologist* 2020; **25:** e528-35. doi: 10.1634/theoncologist.2019-0751
28. McKinnon MB, Rini BI, Haake SM. Biomarker-informed care for patients with renal cell carcinoma. *Nat Cancer* 2025; **6:** 573-83. doi: 10.1038/s43018-025-00942-1
29. Sahin TK, Guven DC. Prognostic impact of myosteatosis on survival with immune checkpoint inhibitors: a systematic review and meta-analysis. *Clin Nutr ESPEN* 2024; **63:** 829-36. doi: 10.1016/j.clnesp.2024.08.015
30. Ahn H, Kim DW, Ko Y, Ha J, Shin YB, Lee J, et al. Updated systematic review and meta-analysis on diagnostic issues and the prognostic impact of myosteatosis: a new paradigm beyond sarcopenia. *Ageing Res Rev* 2021; **70:** 101398. doi: 10.1016/j.arr.2021.101398

Radiol Oncol 2025; 59(4): 467-476.
doi: 10.2478/raon-2025-0063

Med obrambo in dostavo. Odziv zaznavanja DNA po genskemu elektroprenosu

Jesenko T, Omerzel M, Heller LC, Čemažar M

Izhodišča. Genska terapija se je uveljavila kot prelomni biomedicinski pristop, ki omogoča nove terapevtske možnosti za številne doslej neozdravljive bolezni z vnosom rekombinantnih nukleinskih kislin v tarčne celice. Med nevirusnimi tehnikami vnosa genov je genski elektroprenos *(angl. gene electrotransfer*, GET) postal ena najpogosteje uporabljenih metod v kliničnih raziskavah. Temelji na uporabi kratkih, visoko intenzivnih električnih impulzov, ki začasno povečajo prepustnost celičnih membran in omogočijo učinkovit prenos plazmidne DNA ali drugih vrst rekombinantnih nukleinskih kislin v različne tipe celic. Poleg vloge pri dostavi genov lahko GET sproži kompleksne celične odzive, saj vnesena DNA interagira z znotrajceličnimi signalnimi potmi za zaznavanje DNA, ki sodelujejo v prirojeni imunosti in vnetju. Ti odzivi lahko vplivajo na terapevtski izid – bodisi z okrepitvijo protitumorske učinkovitosti in imunske aktivacije po cepljenju ali z zmanjšanjem učinkovitosti transfekcije, kadar pride do pretiranega vnetja ali celične smrti. Naši eksperimentalni izsledki v tumorskih, mišičnih in kožnih modelih so pokazali, da lahko tudi nekodirajoča plazmidna DNA, dostavljena z GET, sproži lokalno imunsko stimulacijo in tkivno specifično vnetno signalizacijo, kar nakazuje, da vnesena DNA sama prispeva k terapevtski učinkovitosti.

Zaključki. Dvojna narava celičnih odzivov po GET plazmidne DNA predstavlja hkrati priložnost in izziv. Nadzorovano aktivacijo prirojene imunosti lahko izkoristimo za okrepitev protitumorskega učinka ali imunske stimulacije po cepljenju, medtem ko lahko pretirani odzivi ovirajo delovanje tistih učinkovin, kjer sta ključni preživetje celic in dolgotrajna izražanja gena. Razumevanje teh mehanizmov omogoča racionalno optimizacijo parametrov GET in zasnove plazmidnih vektorjev, da bi se v celoti izkoristil adjuvantni učinek ali zmanjšal nezaželeni učinek zaznavanja DNA po GET, glede na želeno uporabo.

Radiol Oncol 2025; 59(4): 477-487.
doi: 10.2478/raon-2025-0060

Premagovanje bolečine. Zdravljenje z implantibilno intratekalno črpalko je prelomnica za obvladovanje bolečine pri bolnikih z rakom

Potočnik I, Stražišar B, Lenasi H, Zupanc T

Izhodišča. Kronična bolečina pri raku, zlasti v napredovalih stadijih, ostaja pomemben klinični izziv, ki pogosto zahteva kombinirane postopke. Čeprav so sistemski opioidi standardno zdravljenje, mnogi bolniki ne čutijo zadostnega olajšanja ali imajo zdravila hude stranske učinke. Implantibilni intratekalni sistemi za dajanje zdravil (angl. implantable intrathecal drug delivery systems, IDDS) so se pojavili kot obetavna možna ozbira, ki omogoča ciljno analgezijo z zmanjšanim bremenom opioidov in izboljšano kakovostjo življenja.

Bolniki in metode. V narativni pregled literature smo vključili slovensko poročilo o primeru, ki podrobno opisuje prve nacionalne izkušnje z implantacijo IDDS za refraktorno bolečino pri raku. Klinične raziskave ocenjujejo učinkovitost in varnost takšnega zdravljenja z vizualno analogno lestvico (VAS), vprašalnikom Evropske organizacije za raziskave in zdravljenje raka o kakovosti življenja (EORTC QLQ-C30) in z revidiranim sistemom za ocenjevanje simptomov po Edmontonu (r-ESAS).

Rezultati. Ugotovitve iz literature potrjujejo, da intratekalne črpalke zagotavljajo znatno in dolgotrajno lajšanje bolečin, pogosto z znatnim zmanjšanjem sistemskih odmerkov opioidov in povezanih stranskih učinkov. V primerjavi s konvencionalno farmakoterapijo je intratekalna aplikacija zdravil povezana z izboljšanimi izidi, o katerih poročajo bolniki, manjšim številom hospitalizacij in nižjimi dolgoročnimi stroški zdravstvene oskrbe. V prikazanem primeru so se vrednosti v VAS kmalu po implantaciji zmanjšale z > 8 na 3, hkrati pa so se izboljšali indeksi kakovosti življenja.

Zaključki. DDS predstavljajo klinično učinkovito in ekonomsko vzdržno možnost za izbrane bolnike s kompleksno bolečino zaradi raka, zlasti kadar se sistemsko zdravljenje izkaže za nezadostno. Njihova vključitev v multidisciplinarne poti paliativne oskrbe podpira bolniku prilagojene, varne in sočutne pristope zdravljenja. Združevanjem pregleda literature s pridobljenimi nacionalnimi izkušnjami pokaže dodatno vrednost intratekalnega zdravljenja in spodbuja k širši klinični ozaveščenosti in prihodnjim raziskavam.

Radiol Oncol 2025; 59(4): 488-497.
doi: 10.2478/raon-2026-0002

Uporabnost ^{18}F-FDG PET/CT pri ocenjevanju prizadetosti kostnega mozga in napoved poteka bolezni pri novo diagnosticiranem difuznem velikoceličnem limfomu B

Yang C, Hong L, Duan F, Wang X, Li P, Wang D

Izhodišče. Prizadetost kostnega mozga pri bolnikih z difuznim velikoceličnim limfomom B pomembno vpliva na načrte zdravljenja in napoved poteka bolezni, čeprav je klinična diagnoza težavna. Namen raziskave je bil oceniti uporabnost PET/CT pri ocenjevanju prizadetosti kostnega mozga in napovedi poteka bolezni pri na novo diagnosticiranih bolnikih s to boleznijo.

Bolniki in metode. V retrospektivno raziskavo smo vključili 57 bolnikov z difuznim velikoceličnim limfomom B, ki smo jim pred začetkom zdravljenja naredili biopsijo kostnega mozga in PET/CT. Povečan privzem FDG v kostnem mozgu na PET/CT posnetkih je kazal na prizadetost kostnega mozga, kar ni bilo moči pripisati benignim spremembam. Če je bila biopsija kostnega mozga pozitivna ali če se je privzem v kostnem mozgu med PET/CT spremljanjem zmanjšal sočasno kot v drugih limfomskih lezijah, smo potrdili diagnozo prizadetost kostnega mozga. Pri oceni stanja kostnega mozga s PET/CT smo upoštevali tako vizualno analizo kot kvantitativni indeks, natančneje, razmerje med največjimi standardiziranimi vrednostmi privzema v kostnem mozgu in jetrih. Dejavnike, povezane z 2-letnim preživetjem brez napredovanja bolezni, smo analizirali z uporabo Coxovega regresijskega modela proporcionalnih tveganj.

Rezultati. Prizadetost kostnega mozga smo diagnosticirali pri 34 bolnikih. PET/CT je pokazal večjo natančnost (93,0 % v primerjavi s 75,4 %) in občutljivost (94,1 % v primerjavi z 58,8 %) kot biopsija kostnega mozga. Med obdobjem spremljanja je bolezen napredovala pri 15 bolnikih. Edini neodvisni napovedovalci preživetja brez napredovanja bolezni so se pokazali stanje zmogljivosti po lestvici Vzhodne kooperativne onkološke skupine (*angl. Eastern Cooperative Oncology Group*, ECOG), razmerje med največjimi standardiziranimi vrednostmi privzema v kostnem mozgu in jetrih ter ocena kostnega mozga s PET/CT (p = 0,010; 0,002 ter 0,015).

Zaključki. V raziskavi je imel PET/CT pomembno vlogo pri ocenjevanju prizadetosti kostnega mozga in napovedovanju preživetja brez napredovanja bolezni pri novo ugotovljenih bolnikih z difuznim velikoceličnim limfomom B.

Radiol Oncol 2025; 59(4): 498-509.
doi: 10.2478/raon-2025-0046

Primerjava perkutanih aortnih zaklopk Myval, Sapien in Evolut pri simptomatskih bolnikih z aortno stenozo in nizkim do zmernim kirurškim tveganjem

Bunc M, Steblovnik K, Terseglav S, Ambrožič J, Bervar M, Dimitrovska L, Čerček M, Kovač A, Pleskovič P, Kogoj P, Fras Z, Šusteršič M, Vrtovec B

Izhodišča. V članku na podatkih iz vsakdanje klinične prakse primerjamo učinkovitost in varnost treh vrst perkutanih bioloških aortnih zaklopk: Myval, Sapien in Evolut pri bolnikih s hudo simptomatsko aortno stenozo in nizkim do zmernim kirurškim tveganjem.

Bolniki in metode. Med septembrom 2019 in septembrom 2023 smo v Univerzitetnem kliničnem centru Ljubljana opravili 1053 perkutanih vstavitev aortnih zaklopk (*angl. transcatheter aortic valve implantation*, TAVI). Z analizo ujemanja rezultatov nagnjenosti smo primerjali tri vrste zaklopk: Myval, Sapien in Evolute. V raziskavo smo vključili 180 bolnikov, 60 z vsako od različnih zaklopk. Opazovali smo hemodinamske parametre, hospitalne zaplete zdravljenja ter mortaliteto po 30 dneh in 1 letu od posega.

Rezultati. Med vrstami zaklopk nismo ugotovili razlik v najvišji hitrosti pretoka preko aortne zaklopke, srednjem gradientu preko aortne zaklopke, površini aortnega ustja in v iztisnem deležu levega prekata. Po analizi ujemanja rezultatov nagnjenosti prav tako nismo ugotavljali razlik med vrstami zaklopk Myval, Sapien in Evolut v pojavnosti neželenih učinkov, kot so možganska kap (3,4 % *vs.* 3,4 % *vs.* 0,0 %; p = 0,548), življenjsko ogrožujoča krvavitev **(**1.7% *vs.* 1.7% *vs.* 1.7 %), periproceduralni miokardni infarkt (3,3 % *vs.* 0,0 % *vs.* 0,0 %; p = 0,330), potreba po vstavitvi stalnega srčnega spodbujevalnika (11,9 % *vs.* 10,2 % *vs.* 15,0 %, p = 0,719), smrtnost po 30 dneh (3,3 % *vs.* 5,0 % *vs.* 3,3%; p = 1.000) in po enem letu (8,3 % *vs.* 8,3 % *vs.* 10,0 %; p = 0,934). Zabeležili smo dva primera zmerne paravlvularne regurgitacije, enega pri uporabi zaklopke Myval in enega pri zaklopki vrste Sapien. V ostalih primerih ni bilo paravalvularne regurgitacije ali pa je bila največ blaga.

Zaključki. Analiza rezultatov iz vsakdanje klinične prakse pri simptomatskih bolnikih z aortno stenozo in nizkim do zmernim kirurškim tveganjem je pokazala, da je uporaba bioloških aortnih zaklopk vrst Myval, Sapien ali Evolut podobno učinkovita ter varna in s primerljivo smrtnostjo.

Radiol Oncol 2025; 59(4): 510-521.
doi: 10.2478/raon-2025-0043

Kardiotoksičnost pri bolnicah z nizkim do zmernim kardiovaskularnim tveganjem, ki so prejemale zdravila proti HER2. Prospektivna raziskava s kardialno magnetno resonanco

Cheng S, Deng M, Qi L, Li F, Chen J, Cui S, Wang Y, Liu J, Fan Y, Xie L, Wang J

Izhodišča. Namen raziskave je bil ovrednotiti kardiotoksičnost pri bolnicah, ki smo jih zdravili z zdravili proti HER2 in so imele nizko do zmerno tveganje za kardiovaskularne zaplete. Uporabili smo slikanje z magnetno resonanco srca (CMR).

Bolniki in metode. Med januarjem 2021 in decembrom 2022 smo v prospektivno raziskavo vključili bolnice s pozitivnim HER2 rakom dojke, pri katerih smo pred zdravljenjem in med njim naredili preiskavo CMR. Sledili smo jih 3−5 mesecev ter 6−12 mesecev po pričetku zdravljenja in pri vsaki bolnici na začetku zdravljenja ocenili tveganje za kardiovaskularno toksičnost.

Rezultati. Obravnavali smo 35 bolnic s pozitivnim HER2 rakom dojke (stare 48,86 ± 10,34 let). Nizko tveganje za kardiovaskularno toksičnost je imelo 89 %, zmerno pa 11 % bolnic. S kontrolno CMR smo pri 9 (25,71 %) bolnicah ugotovili, da se je pojavila motnja srčnega delovanja. Ob prvem sledenju so se v primerjavi z izhodiščnim stanjem opazno zmanjšali iztisni delež levega prekata, indeks utripnega volumna srca, indeks minutnega volumna srca in absolutne vrednosti deformacije, ki so jih spremljale višje vrednosti T1 in T2 ter indeks končnega sistoličnega volumna ($p \leq 0,002$). Ob drugem sledenju so se vrednosti T1 in T2 vrnile skoraj na izhodiščno vrednost. Pri indeksu minutnega volumna srca je bilo opaziti kontinuirano upadanje ($p = 0,022$), medtem ko so bile druge spremenljivke podobne ($p > 0,05$). Poleg tega je vrednost T1 ob prvem sledenju pokazala izrazito povečanje pri bolnikih s stopnjo 1 do 3 dejavnikov tveganja za srčno-žilno toksičnost v primerjavi z bolnicah brez dejavnikov tveganja ($p \leq 0,043$).

Zaključki. Zgodnja kardiotoksičnost med zdravljenjem z anti-HER2 se je pogosto pojavila pri bolnicah z majhnim do zmernim kardiovaskularnim tveganjem. Upoštevanje spremembe vrednosti T1 lahko pomaga pri vrednotenju specifičnega obsega manjših tkivnih poškodb.

Radiol Oncol 2025; 59(4): 522-525.
doi: 10.2478/raon-2025-0037

Vpliv vrste katetra, števila šivov in starosti bolnika na izpad perkutane nefrostome

Kuhelj D, Šušteršič A, Zdešar U

Izhodišča. Izpad katetra perkutane nefrostome onemogoča uspešno drenažo urina ter tako poslabša kakovost življenja bolnikov. Namen pričujoče analize bolnikov je bil prispevati h razjasnitvi dejavnikov, ki vplivajo na izpad katetra, saj je takih podatkov v literature sorazmerno malo.

Bolniki in metode. V prospektvno raziskavo smo vključili bolnike, ki so bili med 3. marcem in 3. oktobrom 2023 napoteni na Klinični radiološki inštitut Univerzitetnega kliničnega centra Ljubljana zaradi zamenjave perkutane nefrostome. Kot možne dejavnike, ki bi lahko vplivali na izpad katetra, smo pregledali vrsto katetra, število šivov in starost bolnikov. Za analizo podatkov smo uporabili deskriptivno statistiko ter Pearsonov hi^2 test; statistična pomembnost je bila določena pri vrednosti pod 0,05.

Rezultati. V izbranem času smo nadomestili katetre pri 57 bolnikih (35 moških, povprečna starost vseh bolnikov 71,4 let); uporabili smo 58 katetrov z zanko (*angl. loop catheters*), ki so imeli nitko in 17 katetrov z zanko brez nitke; 55 katetrov je bilo pritrjenih z enim šivom, 20 pa z dvema šivoma. V opazovanem času je 17 perkutanih nefrostomskih katetrov (22,7%) izpadlo; srednji čas od postavitve do menjave katetra je bil 4,16 mesecev. Statistično pomembnih razlik med vrsto katetra, številom šivov in starostjo bolnikov, ki bi prispevale h izpadu katetra, nismo zabeležili (hi^2 0,57; 0,34 in 0,61).

Zaključki. Raziskava ni pokazala vpliva vrste katetra, števila šivov ali starosti bolnikov na pogostost izpadanja katetrov. Najpogostejši vzroki za izpadanje katetrov so najverjetneje bili večja aktivnost bolnikov ter pomanjkljiva nege katetrov v mesecih po vstavitvi. Ustrezna razlaga bolniku o skrbi za kateter ter ustrezna nega katetra bi lahko povečala dolgoročno uspešno drenažo.

Radiol Oncol 2025; 59(4): 526-534.
doi: 10.2478/raon-2025-0064

Učinkovitost in varnost perkutane mikrovalovne ablacije jetrnih tumorjev ob uporabi antene s protifazno tehnologijo, ki omogoča ultrasferično ablacijo

Arik E, Taydas O, Dertli T, Sevinc OF, Kara AB, Topaloglu OF, Ozdemir M, Senturk A, Canturk AO, Hacibekiroglu I, Ozturk MH

Izhodišča. Protifazna tehnologija, ki je novost na področju mikrovalovnih anten za perkutano ablacijo jeter, omogoča oblikovanje bolj sferičnih ablacijskih področij. Namen raziskave je bil oceniti učinkovitost in varnost mikrovalovne ablacije pri zdravljenju jetrnih tumorjev z mikrovalovno anteno, ob uporabi protifazne tehnologije.

Bolniki in metode. V raziskavo smo vključili 92 bolnikov (skupaj 133 lezij), ki smo jih zdravili z mikrovalovno ablacijo zaradi hepatocelularnega karcinoma ali zasevkov v jetrih. Med njimi je imelo 9 bolnikov hepatocelularni karcinoma, 83 pa zasevke (46 kolorektalne in 37 nekolorektalne). Pri retrospektivni analizi smo upoštevali starost bolnikov, spol, laboratorijske vrednosti pred in po posegu (število belih krvnih celic, razmerje nevtrofilcev in limfocitov), dimenzijo tumorja in ablacijskega področja (1. dan pred posegom ter 1., 3. in 6. mesec po posegu), podrobnosti izvedbe mikrovalovne ablacije z enim posegom (trajanje, izhodna moč), zaplete, povezane s posegom, in lokalno napredovanje bolezni/ponovitev med spremljanjem bolnikov.

Rezultati. Tehnično smo uspešno izvedli mikrovalovno ablacijo100-odstotno. Uporabili smo srednjo izhodno moč 80 vatov (razpon: 50–100), povprečna trajanje ablacije je bilo 5,2 ± 2,1 minute. Nadaljnje slikanje je pokazalo razmerje med premerom ablacijskega področja in premerom tumorja 1,63 ± 0,3. Večji zapleti so se pojavili pri 3 bolnikih (3,2 %) in so vključevali jetrni abces (n = 1/92), krvavitev (n = 1/92) in plevralni izliv (n = 1/92). Manjše zaplete smo zaznali pri 29 bolnikih (31,5 %). Srednji čas spremljanja bolnikov je bil 33 mesecev (razpon 10–36). Srednji čas preživetja brez ponovitve bolezni je bil 25 mesecev (95 % IZ: 21–27 mesecev). Med 24-mesečnim spremljanjem smo pri 39 bolnikih (42,4 %) ugotovili lokalno napredovanje tumorja. Velikost tumorja je bila neodvisni dejavnik tveganja za lokalno napredovanje bolezni (p = 0,012).

Zaključki. Pričujoča raziskava predstavlja najdaljše obdobje spremljanja in največjo skupino bolnikov z jetrnimi tumorji, ki so bili zdravljeni z mikrovalovno ablacijo ob uporabi protifazne tehnologije. Rezultati so pokazali visoko tehnično uspešnost in sprejemljivo lokalno kontrolo ter sprejemljivo stopnjo zapletov.

Radiol Oncol 2025; 59(4): 535-550.
doi: 10.2478/raon-2025-0058

Spremembe invazivnih lastnosti primarnih glioblastomskih celic po izpostavitvi reverzibilni elektroporaciji

Blažič A, Majc B, Novak M, Breznik B, Rems L

Izhodišča. Pri zdravljenju glioblastoma s pomočjo elektroporacije raziskujemo učinek zdravljenja na dva načina: kot postopek za izboljšanje vnosa zdravil v celice in/ali kot metodo za netermično ablacijo tumorskega tkiva. Kljub obetavnim predkliničnim rezultatom ostaja slabo raziskan vpliv reverzibilne elektroporacije na invazivne lastnosti glioblastomskih celic.

Materiali in metode. Pri petih glioblastomskih celičnih linijah, ki smo jih pridobili z odvzemom vzorcev bolnikov, smo najprej ovrednotili njihovo osnovno invazivno zmožnost. Za nadaljnje poskuse z elektroporacijo smo izbrali dve najbolj invazivni celični liniji (*NIB140 CORE* in *NIB216 CORE*). Celice v suspenziji smo izpostavili visokofrekvenčnim bifaznim električnim pulzom, ki so ustvarili električno polje jakosti 1 kV/cm in povzročili reverzibilno elektroporacijo. Spremembe v invazivnosti in izražanju genov smo analizirali 24 ur po izpostavitvi celic električnim pulzom z uporabo testa *transwell* in sekvenciranja RNK.

Rezultati. Reverzibilna elektroporacija pri 1 kV/cm je povečala invazivno sposobnost pri obeh testiranih celičnih linijah, vendar ne v enaki meri. Srednja vrednost števila invazivnih celic se je po izpostavitvi električnemu polju povečala za 3,74-krat (274 %) v celični liniji *NIB140 CORE* in za 1,30-krat (30 %) v celični liniji *NIB216 CORE*. Nadaljnja transkripcijska analiza je v celični liniji *NIB140 CORE* pokazala spremembe v izražanju genov, povezanih z organizacijo zunajceličnega matriksa in aktivnostjo ionskih kanalov, v *NIB216 CORE* pa spremembe genov povezanih s citoskeletom, kar nakazuje na aktivacijo celičnih poti, povezanih s procesom invazije.

Zaključki. Rezultati pričujoče raziskave nakazujejo, da lahko glioblastomske celice, ki preživijo izpostavitev elektroporaciji, pridobijo povečano invazivno sposobnost, spremembe pa so odvisne od tipa celic. Pri ablaciji tumorjev z ireverzibilno elektroporacijo lahko takšne celice ležijo na obrobju izpostavljenega območja. Pri elektrokemoterapiji pa se celice, ki preživijo elektroporacijo, lahko pojavijo v primeru nezadostne lokalne koncentracije kemoterapevtika. Raziskava tudi kaže potrebo po nadaljnji validaciji v fiziološko ustreznejših modelih.

Radiol Oncol 2025; 59(4): 551-565.
doi: 10.2478/raon-2025-0056

Heterogena ultrastruktura mitohondrijev in metabolizem človeških glioblastomskih celic. Razlike med matičnimi in diferenciranimi rakavimi celicami v odzivu na kemoterapijo

Bogataj U, Novak M, Galun SK, Fon Tacer K, Vittori M, Van Noorden CJF, Breznik B

Izhodišča. Glioblastomske matične celice prispevajo k odpornosti glioblastoma na standardno zdravljenje. Odpornost glioblastomskih matičnih celic na kemoterapevtik temozolomid še ni povsem pojasnjena v povezavi celičnega metabolizma in vloge mitohondrijev. Cilj raziskave je bil podrobno opredeliti mitohondrijsko ultrastrukturo glioblastomskih matičnih celic pred in po izpostavitvi temozolomidu ter jo primerjati z diferenciranimi celicami glioblastoma.

Materiali in metode. Uporabili smo celične linije glioblastoma, pridobljene iz biopsij bolnikov, in trajne celične linije. Mitohondrijsko ultrastrukturo celičnih linij smo analizirali s presevno elektronsko mikroskopijo. Mikroskopsko analizo smo dopolnili in primerjali z analizo celičnega metabolizma in pri tem uporabili analizo metabolne aktivnosti živih celic v realnem času *Seahorse*.

Rezultati. Ugotovili smo, da je metabolni vzorec glioblastomskih matičnih celic mirujoč in aeroben. Njihovi podolgovati mitohondriji z visoko organiziranimi kristami kažejo na povečano biogenezo in mitohondrijsko fuzijo ter ustrezajo metabolizmu odvisnemu od oksidativne fosforilacije. Metabolizem glioblastomskih matičnih celic je odvisen od te oksidativne fosforilacije in po zdravljenju s temozolomidom ni sprememb v deležu poškodovanih mitohondrijev teh celic. Nasprotno pa so diferencirane celice glioblastoma z fragmentiranimi mitohondriji, ki imajo manj organiziranih krist, metabolno bolj aktivne in glikolitične. Zdravljenje z temozolomidom je povzročilo ultrastrukturne poškodbe v mitohondrijih v diferenciranih celicah glioblastoma.

Zaključki. Pokazali smo razlike v mitohondrijski ultrastrukturi in celičnem metabolizmu med glioblastomskimi matičnimi celicami in diferenciranimi celicami glioblastoma ob odzivu na temozolomid. To kaže, da mitohondriji igrajo pomembno vlogo pri odpornosti glioblastomaskih matičnih celic na temozolomid. Raziskava postavlja temelje za nadaljnje raziskave odpornosti glioblastomaskih matičnih celic na kemoterapijo v povezavi z mitohondrijsko strukturo in funkcijo.

Radiol Oncol 2025; 59(4): 566-578.
doi: 10.2478/raon-2025-0057

S humanim papilomavirusom povezan ploščatocelični karcinom orofarinksa je bolj radiosenzitiven kljub zavrti aktivaciji molekularnih poti zaznavanja citosolne DNK in prirojenega imunskega odgovora

Levpušček K, Jesenko T, Komel T, Kranjc Brezar S, Serša G, Čemažar M, Strojan P

Izhodišča. Ploščatocelični karcinom žrela predstavlja pomemben zdravstveni problem, humani papilomavirus tipa 16 (HPV16) pa ima ključno vlogo pri nastanku ploščatoceličnega karcinoma orofarinksa. Če je povezan s HPV16, je bolj radiosenzitiven v primerjavi s tistim, kjer povezave nismo odkrili. Mehanizmi, ki to omogočajo, še niso razjasnjeni. Znano je, da onkoproteina E6 in E7 HPV16 vplivata na signalne poti zaznavanja citosolne DNK in s tem na prirojen imunski odziv. Namen raziskave je bil preučiti, kako obsevanje vpliva na aktivacijo citosolnih poti zaznavanja DNK in prirojenega imunskega odziva ter ali to prispeva k povečani radiosenzitivnosti ploščatoceličnega karcinoma orofarinksa, ki je povezan s HPV16.

Materiali in metode. V raziskavi smo uporabili modele s HPV16 povezanimi in nepovezanimi ploščatoceličnimi karcinomi žrela. Določili smo izražanje posameznih senzorjev DNK in citokinov ter ovrednotili učinek obsevanja na prisotnost dvoverižne DNK v citosolu, aktivacijo citosolnih senzorjev DNK, izražanje citokinov in infiltracijo imunskih celic tako *in vitro* kot *in vivo*. Analize smo izvedli z metodo kvantitativne polimerazne rekcije v realnem čas (*angl. real-time quantitative* polymerase chain reaction, RT-qPCR) in z imunofluorescentnim barvanjem.

Rezultati. S HPV16 povezani ploščatocelični karcinom orofarinksa se od preostalih ploščatoceličnih karcinomov žrela razlikuje v izražanju senzorjev DNK in citokinov, kar je posledica zaviranja poti genskega stimulatorja interferona (*angl. stimulator of interferon genes,* STING). V drugih modelih smo po obsevanju zaznali aktivacijo senzorjev DNK, ki je bila časovno in dozno odvisna. Medtem ko je bila z obsevanjem povezana aktivacija senzorjev DNK v vseh modelih odvisna od doze in časa, smo pri s HPV16 povezanim ploščatoceličnim karcinomom orofarinksa opazili selektivno aktivacijo ciklične GMP-AMP sintaze (*angl. cyclic GMP-AMP synthase*, cGAS) in STING-a brez pomembnega povečanja izražanja citokinov ali aktivacije imunskega sistema. Nasprotno pa smo pri tako s HPV16 povezani kot nepovezani modeli ploščatoceličnega karcinoma žrela opazili aktivacijo senzorjev DNK, povečano izražanje citokinov in večjo infiltracijo imunskih celic po obsevanju.

Zaključki. Ključna ugotovitev raziskave je bila, da na povečano radiosenzitivnost s HPV16 povezanega ploščatoceličnega karcinoma orofarinksa ne vpliva aktivacija molekularnih poti zaznavanja citosolne DNK in prirojenega imunskega odziva. Med modeli ploščatoceličnega karcinoma žrela so bile razlike v izražanju senzorjev DNK in citokinov glede na dozo in frakcioniranje obsevanja.

Radiol Oncol 2025; 59(4): 579-588.
doi: 10.2478/raon-2025-0055

Indukcijska kemoterapija in sočasna kemoradioterapija za ohranitev grla pri raku grla in hipofaringealnem raku

Strojan P, Plavc G, Šifrer R, Jereb S, Lanišnik B, Kokalj M, Grošelj A, Grašič Kuhar C

Izhodišča. Namen raziskave je bil preveriti hipotezo, da lahko klinični odziv tumorja pri zdravljenju z ohranitvijo grla zanesljivo razlikujemo med kemo-/radioterapevtsko občutljivimi in rezistentnimi tumorji že po enem krogu indukcijske kemoterapije.

Bolniki in metode. Bolnike smo zdravili z indukcijsko kemoterapijo, ki je obsegala docetaksel/cisplatin/5-fluorouracil, sledila je sočasna kemoradioterapija s tedenskimi aplikacijami cisplatina. Odgovor primarnega tumorja na zdravljenje smo ocenjevali s transnazalno endoskopijo po prvem krogu indukcijske kemoterapije.

Rezultati. Po enem krogu indukcijske kemoterapije smo odgovor ugotovili pri 37/39 (95 %) bolnikih z laringealnim (46 %) oziroma hipofaringealnim (54 %) karcinomom, dva bolnika pa sta bila napotena na rešilno operacijo. Preživetje brez laringektomije po 2 in 5 letih je bilo 87 % in 75 %. Stopnji lokoregionalnega nadzora bolezni (in tudi preživetji brez bolezni) sta bili pri obeh vrstah tumorja 79 % oziroma 70 %, celokupni preživetji pa 92 % oziroma 82 %.

Zaključki. Klinična ocena odziva tumorja na zdravljenje po enem krogu indukcijske kemoterapije s docetakselom/cisplatinom/5-fluorouracilom lahko služi kot veljaven in enostaven napovedovalec občutljivosti tumorja na sočasno kemoradioterapijo na osnovi platine.

Radiol Oncol 2025; 59(4): 589-596.
doi: 10.2478/raon-2025-0025

Vpliv parodontalne bolezni in parodontalnega zdravljenja na raka debelega črevesa in danke

Potočnik Reberšak U, Brecelj E, Schara R

Izhodišča. S parodontalno boleznijo povezujejo več kot 50 bolezni in stanj, med njimi tudi z rakom debelega črevesa in danke. Namen raziskave je bil ugotoviti, ali zdravljenje parodontalne bolezni pred terapijo raka vpliva na raven C-reaktivnega proteina (CRP) v krvi bolnikov. Iz sluznice rakavo spremenjenega črevesja smo želeli izolirati bakteriji *Fusobacterium nucleatum* (FN) in *Porphyromonas gingivalis (*PG*)*, ki ju pogosto povezujejo z rakom debelega črevesa in danke.

Bolniki in metode. Da bi ocenili učinek parodontalnega zdravljenja na rak debelega črevesa in danke, smo merili nivo CRP-ja v krvi bolnikov ob prvem obisku pri onkološkem kirurgu, pred začetkom terapije raka, dva zaporedna dneva po operativnem posegu in ob prvem kontrolnem pregledu po operaciji. Nivo CRP-ja smo primerjali med skupino, kateri smo opravili parodontalno zdravljenje in skupino, ki parodontalnega zdravljenja ni prejela. Z metodo kvantitativne kulture smo poskusili izolirati parodonto patogeni bakteriji FN in PG iz obzobnega žepa in sluznice rakavo spremenjenega črevesja.

Rezultati. Med skupinama ni bilo statistično značilne razlike v vrednosti CRP-ja pred začetkom zdravljenja raka. Prav tako ni bilo statistično pomembnih razlik med skupinama v meritvah CRP, opravljenih prvi in drugi dan po operativnem posegu ter ob prvem kontrolnem pregledu. Z metodo kvantitativne kulture nismo uspeli izolirati parodonto patogeni bakteriji FN in PG iz sluznice rakavo spremenjenega črevesja.

Zaključki. Naša študija ni pokazala nobene korelacije med parodontalnim zdravljenjem in rakom debelega črevesja in danke.

Radiol Oncol 2025; 59(4): 597-606.
doi: 10.2478/raon-2025-0061

Zdravljenje raka prostate z elektrokemoterapijo. Varnost, učinkovitost in klinične izkušnje pri 144 bolnikih

Stevanovic M, Heringer M, Hjouj M, Zanasi A, de Terlizzi F, Stehling MK

Izhodišča. Rak prostate je pogost rak pri moških v razvitih državah. Zdravljenje je odvisno od stadija bolezni; fokalna terapija pa predstavlja vmesni obliko zdravljenja, ki ima manjšo toksičnost v primerjavi z radikalno prostatektomijo in boljši nadzor bolezni kot aktivno spremljanje bolnika. Poročamo o prvi retrospektivni analizi bolnikov z rakom prostate, ki smo jih zdravili z elektrokemoterapijo v centru *Vitus Prostate Centre* v Offenbachu.

Bolniki in metode. V raziskavo smo vključili 144 moških z rakom prostate, ki niso bili primerni za standardna zdravljenja ali so jih zavrnili, in smo jih zdravili z elektrokemoterapijo. Bolnike smo spremljali s testi prostatičnega specifičnega antigena (PSA) in preiskavami MR ter ocenjevali toksičnost in genitourinarne funkcije s pomočjo standardnih vprašalnikov. Lokalni odgovor na zdravljenje smo ocenjevali z MR 3 mesece po zdravljenju, v skladu s kriteriji RECIST za solidne tumorje.

Rezultati. Postopek zdravljenja je bil tehnično uspešen pri vseh bolnikih. Zdravljenje so dobro prenašali. Pojavili so se zgolj blagi in začasni neželeni učinki. Uriniranje brez izrazitih motenj in erektilna funkcija sta bila večinoma ohranjena. Popoln odgovor na zdravljenje smo ugotovili pri 75 % ocenjevanih bolnikov, delni odgovor pri 18 %, stabilno bolezen pri 5 % in napredovanje bolezni pri 2 %. Kratkoročni odziv je bil povezan s stadijem bolezni TNM ($p < 0,05$), oceno stopnje bolezni po Gleasonu ($p = 0,0066$) in ravnijo PSA pred elektrokemoterapijo ($p = 0,0070$). Med spremljanjem smo pri 18 bolnikih (13 %) ugotovili napredovanje bolezni; 1-letno preživetje brez napredovanja bolezni je bilo 88 % (95 % IZ 80–97 %) in je bil pomembno povezano s stadijem bolezni in ravnijo PSA pred zdravljenjem.

Zaključki. Elektrokemoterapija je izvedljivo, varno in učinkovito zdravljenje raka prostate z izredno nizko toksičnostjo in blagimi stranskimi učinki. Predhodni izsledki nakazujejo, da ponuja obetavne rezultate v smislu lokalnega nadzora bolezni v zgodnjih stadijih tumorjev, pa tudi v lokalno napredovalih primerih, kjer se druga zdravljenja ne kažejo izvedljiva.

Radiol Oncol 2025; 59(4): 607-616.
doi: 10.2478/raon-2025-0028

Ali obstajajo klinično pomembni napovedni dejavniki pri difuznem velikoceličnem limfomu B poleg mednarodnega prognostičnega indeksa?

Milica Miljković M, Šetrajčič Dragoš V, Gašljević G, Novaković S, Boltežar L, Jezeršek Novaković B

Izhodišča. Difuzni velikocelični limfom B (DVCLB) ima zelo raznoliko napoved poteka bolezni, saj s standardnim prvim zdravljenjem ozdravi le 50 do 60 % bolnikov. Zato je pomembno vnaprej opredeliti tiste bolnike, ki se ne bodo dobro odzvali na prvo zdravljenje in bi morda potrebovali drugačno začetno zdravljenje. Raziskava Schmitza je opredelila štiri nove molekularne podtipe DVCLB z različnimi napovedmi poteka bolezni: MCD, BN2, N1 in EZB. Podtipa BN2 in EZB imata boljšo napoved. Namen pričujoče raziskave je bil oceniti učinkovitost testa *Archer FusionPlex Lymphoma* pri prepoznavanju novo opredeljenih genetskih podtipov DVCLB ter raziskati povezavo med imunohistokemičnimi (IHK) metodami in metodami sekvenciranja naslednje generacije (*angl. next-generation sequencing*, NGS) za določanje celice izvora (*angl. cell of origin*, COO) ter njihovo napovedno vrednost za preživetje bolnikov.

Bolniki in metode. V retrospektivno klinično raziskavo smo vključili 131 bolnikov z DVCLB, ki smo jih razvrstili po Hansovem algoritmu v podtip B-celični profil germinalnega centra (*angl. germinal center B-cell-like*, GCB) in podtip aktivirani B-celični profil (*angl. activated B-cell-like,* ABC) ter z metodo NGS ob uporabi panela *Archer FusionPlex Lymphoma* v podtipe GCB, ABC in neklasificiran podtip. V skladu s predlogom Schmitzove raziskave pa smo jih razvrstili v nove genetske podtipe. Za njihovo opredelitev smo analizirali mutacije samo sedmih genov - *MYD88*^{L265P}*, CD79B, EZH2, NOTCH1, NOTCH2, BCL2* in *BCL6*. Za primerjavo preživetij med podtipoma ABC in GCB ter med novimi genetskimi podtipi smo uporabili napredne statistične modele in na koncu naše ugotovitve potrdili s analizo STRATOS.

Rezultati. Uspešno smo klasificirali 35,9 % bolnikov v nove genetske podtipe, hkrati smo dosegli tudi zadovoljivo skladnost pri določitvi podtipa celice izvora z metodama IHK in NGS. Kljub temu pa klasifikacija novih genetskih podtipov z NGS ni pokazala statistično značilne povezave s preživetjem, prav tako pa tudi ne ostali dve klasifikaciji glede na celico izvora ob uporabi IHK ali NGS. Kot edini napovedni dejavnik smo opredelili le mednarodni prognostični indeks (*angl. International Prognostic Index*, IPI).

Zaključki. Panel *Archer FusionPlex Lymphoma* je bil nekoliko manj učinkovit pri opredelitvi novih genetskih podtipov v primerjavi z eksomskim sekvenciranjem v Schmitzovi raziskavi, vendar smo kljub temu uspeli razvrstiti več kot tretjino vzorcev z uporabo poenostavljenega modela oziroma analize le sedmih genov. Poglobljena statistična analiza preživetja bolnikov med skupinami, opredeljenimi z našim poenostavljenim modelom, pa ni potrdila njegove uporabnosti pri napovedovanju izida bolnikov z DVCLB, verjetno zaradi dejavnikov, kot sta bila izbira bolnikov in omejena velikost vzorca.

Radiol Oncol 2025; 59(4): 617-623.
doi: 10.2478/raon-2025-0059

Monoterapija z anlotinibom pri ponavljajočem se ali metastatskem karcinomu nazofarinksa. Multicentrična analiza skupine primerov

Qin GJ, Su YX, Liang Y, Zhang B, Pan YF, Lu JX, Xie YY, Dai JX, Chen KQ, Qin FF, Yang HY, Kong XY, Xie Y, Ruan XL, Mo YY, Zhang RY, Zhang J, Jiang W

Izhodišča. Anlotinib je pokazal spodbuden terapevtski učinek pri različnih solidnih tumorjih. Namen pričujoče raziskave je bil oceniti učinkovitost in varnost monoterapije z anlotinibom pri bolnikih s ponavljajočim ali metastatskim nazofaringealnim karcinomom.

Bolniki in metode. Retrospektivno smo v raziskavo vključili 30 bolnikov s ponavljajočim ali metastatskim nazofaringealnim karcinomom. Večina bolnikov je predhodno prejela vsaj en red sistemskega zdravljenja, vsi bolniki pa monoterapijo z anlotinibom (12 ali 10 mg/dan). Primarni opazovani dogodek je bil delež objektivnih odgovorov na zdravljenje, sekundarni opazovani dogodki pa so vključevali preživetje brez napredovanja bolezni, celokupno preživetje in toksičnost.

Rezultati. Metastatskim nazofaringealnim karcinomom je imelo 13 bolnikov (43,3 %), ponavlajoči nazofaringealnim karcinomom 10 (33,3 %), obojega pa 7 (23,3 %) bolnikov. Neodzivnih na platino je bilo 22 (73,3 %) bolnikov, vsaj tri kroge zdravljenja z anlotinibom pa je prejelo 23 (76,7 %) bolnikov. Najboljši odgovor je bil delni odgovor pri 4 bolnikih, stabilna bolezni pri 18 in napredovanje bolezni pri 8 bolnikih. Objektivni odgovorov na zdravljenje smo zabeležili pri 13,3 % (95 % IZ, 0,4–26,2 %) in nadzor pri 73,3 % (95 % IZ, 56,5–90,1 %) bolnikih. Srednja vrednost celokupnega preživetja in preživetja brez napredovanja bolezni sta bila 11,5 mesecev (95 % IZ, 7,5–15,5) ter 5,7 meseca (95 % IZ, 4,7–6,7). Relativno pogosta neželena učinka stopnje 3 ali več sta bila sindrom roka-noga (13,3 %) in oralni mukozitis (13,3 %).

Zaključki. Monoterapija z anlotinibom je bila v raziskavi učinkovita pri bolnikih s ponavljajočim ali metastatskim nazofaringealnim karcinomom. Anlotinib so bolniki dobro prenašali in imel je sprejemljivo toksičnost.

Radiol Oncol 2025; 59(4): 624-634.
doi: 10.2478/raon-2025-0065

Izhodiščne vrednosti in dinamične spremembe skeletne mišične mase kot napovedni biološki označevalci pri bolnikih z metastatskim ledvičnim rakom, zdravljenim z nivolumabom

Özkan E, Köksal M, Ece B, Koyun M, Kuzu ÖF, Açıkgöz Y, Algın E

Izhodišča. Nizko skeletno mišično maso vse pogosteje prepoznavamo kot negativen napovedni dejavnik v onkologiji. Po definiciji Evropske delovne skupine za sarkopenijo pri starejših (*angl. European Working Group on Sarcopenia in Older People 2*, EWGSOP2) je sarkopenija progresivna in splošna motnja skeletnih mišic, za katero sta značilna izguba mišične moči in mišične mase, kar lahko vodi v zmanjšano telesno zmogljivost. Namen raziskave je bil ugotoviti, ali lahko izhodiščno nizka mišična masa in dinamične spremembe mišične mase med imunoterapijo napovedujejo odziv na zdravljenje in preživetje pri bolnikih z metastatskim ledvičnim rakom, zdravljenih z nivolumabom.

Bolniki in metode. V retrospektivno kohortno raziskavo smo vključili 50 bolnikov z metastatskim ledvičnim rakom (35 moških, 15 žensk; povprečna starost 59,1 ± 10,2 let), ki so med letoma 2019 in 2022 prejemali Nivolumab ter so pred in med zdravljenjem opravili računalniško tomografijo (CT) trebuha. Mišično maso smo ocenili z izračunom indeksa skeletnih mišic (*angl. skeletal muscle index*, SMI) na ravni tretjega ledvenega vretenca z uporabo standardnih mejnih vrednosti Hounsfieldovih enot (−29 do +150 HU). Odgovor na zdravljenje smo ocenili v skladu z imunološkimi merili za oceno odgovora pri solidnih tumorjih (*angl. immune Response Evaluation Criteria in Solid Tumors*, iRECIST). Celokupno preživetje in preživetje brez napredovanja bolezni smo analizirali z uporabo Kaplan-Meierjevih krivulj in Coxovih regresijskih modelov.

Rezultati. Nizko mišično maso smo ugotovili pri 60 % bolnikov in je bila statistično značilno povezana z metastazami v več organih ($p = 0,003$). Bolniki z izhodiščno nizko mišično maso ali z negativno spremembo SMI med zdravljenjem so kazali slabši odziv na zdravljenje ($p = 0,027$ in $p = 0,021$). Tako celokupno preživetje kot preživetje brez napredovanja bolezni sta bila statistično značilno krajša pri bolnikih z nizko mišično maso in pri tistih z upadom mišične mase med zdravljenjem.

Zaključki. Nizka mišična masa pred začetkom zdravljenja in upad mišične mase med imunoterapijo sta bila neodvisno povezana s slabšim preživetjem in odzivom na zdravljenje pri bolnikih z metastatskim ledvičnim rakom, ki so prejemali nivolumab. Ocena mišične mase s pomočjo slik CT-ja bi lahko služila kot slikovno podprt napovedni biološki označevalec pri tej skupini bolnikov.

Fundacija ''Docent dr. J. Cholewa''
je neprofitno, neinstitucionalno in nestrankarsko
združenje posameznikov, ustanov in organizacij, ki želijo
materialno spodbujati in poglabljati raziskovalno
dejavnost v onkologiji.

Dunajska 106
1000 Ljubljana
IBAN: SI56 0203 3001 7879 431

ZDRAVILO VERZENIOS PRINAŠA
NOVE PREBOJNE PODATKE O CELOKUPNEM PREŽIVETJU

Verzenios® abemaciklib
A Lilly Medicine

ONA SE PRIPRAVLJA NA ODPRTJE SVOJE GALERIJE – NE NA POSLABŠANJE BOLEZNI

Pri bolnikih s HR+ HER2- zgodnjim rakom dojk s pozitivnimi bezgavkami in z velikim tveganjem za ponovitev bolezni
Samo zdravilo Verzenios dokazano podaljšuje preživetje in zagotavlja dolgotrajno zaščito pred ponovitvijo bolezni z 2 leti zdravljenja.[†,1-4]

SKRAJŠAN POVZETEK GLAVNIH ZNAČILNOSTI ZDRAVILA

IME ZDRAVILA Verzenios 50 mg/100 mg/150 mg filmsko obložene tablete **KAKOVOSTNA IN KOLIČINSKA SESTAVA** Ena filmsko obložena tableta vsebuje 50 mg/100 mg/150 mg abemacikliba. Ena filmsko obložena tableta vsebuje 14 mg/28 mg/42 mg laktoze (v obliki monohidrata). **Terapevtske indikacije** Zgodnji rak dojk Zdravilo Verzenios je v kombinaciji z endokrinim zdravljenjem indicirano za adjuvantno zdravljenje odraslih bolnikov z na hormonske receptorje (HR) pozitivnim, na receptorje humanega epidermalnega rastnega faktorja 2 (HER2) negativnim zgodnjim rakom dojk s pozitivnimi bezgavkami, pri katerih obstaja veliko tveganje za ponovitev. Pri ženskah v pred- ali perimenopavzi je treba endokrino zdravljenje z zaviralcem aromataze kombinirati z agonistom gonadoliberina LHRH – luteinizing hormone-releasing hormone). Napredovali ali metastatski rak dojk Zdravilo Verzenios je indicirano za zdravljenje žensk z lokalno napredovalim ali metastatskim, na hormonske receptorje (HR) pozitivnim in na receptorje humanega epidermalnega rastnega faktorja 2 (HER2) negativnim rakom dojk v kombinaciji z zaviralcem aromataze ali s fulvestrantom kot začetnim endokrinim zdravljenjem ali pri ženskah, ki so prejele predhodno endokrino zdravljenje. Pri ženskah v pred- ali perimenopavzi je treba endokrino zdravljenje kombinirati z agonistom LHRH. **Odmerjanje in način uporabe** Zdravljenje z zdravilom Verzenios mora uvesti in nadzorovati zdravnik, ki ima izkušnje z uporabo zdravil za zdravljenje rakavih bolezni. Priporočeni odmerek abemacikliba je 150 mg dvakrat na dan, kadar se uporablja v kombinaciji z endokrinim zdravljenjem. *Zgodnji rak dojk* Zdravilo Verzenios je treba jemati neprekinjeno dve leti, ali do ponovitve bolezni ali pojava nesprejemljive toksičnosti. *Napredovali ali metastatski rak dojk* Zdravilo Verzenios je treba jemati, dokler ima bolnica od zdravljenja klinično korist ali do pojava nesprejemljive toksičnosti. Če bolnica bruha ali izpusti odmerek zdravila Verzenios, ji je treba naročiti, da naj naslednji odmerek vzame ob predvidenem času; dodatnega odmerka ne sme vzeti. Obvladovanje nekaterih neželenih učinkov lahko zahteva prekinitev in/ali zmanjšanje odmerka. Zdravljenje z abemaciklibom prekinite v primeru povišanja vrednosti AST in/ali ALT >3 x ZMN SKUPAJ s celokupnim bilirubinom > 2,0 x ZMN v odsotnosti holestaze ter pri bolnicah z intersticijsko pljučno boleznijo (ILD)/pnevmonitis stopnje 3 ali 4. Sočasni uporabi močnih zaviralcev CYP3A4 se je treba izogibati. Če se uporabi močnih zaviralcev CYP3A4 ni mogoče izogniti, je treba odmerek abemacikliba znižati na 100 mg dvakrat na dan. Pri bolnicah, pri katerih je bil odmerek znižan na 100 mg abemacikliba dvakrat na dan in pri katerih se sočasnemu dajanju močnega zaviralca CYP3A4 ni mogoče izogniti, je treba odmerek abemacikliba dodatno znižati na 50 mg dvakrat na dan. Pri bolnicah, pri katerih je bil odmerek znižan na 50 mg abemacikliba dvakrat na dan in pri katerih se sočasnemu dajanju močnega zaviralca CYP3A4 ni mogoče izogniti, je mogoče z odmerkom abemacikliba nadaljevati ob natančnem spremljanju znakov toksičnosti. Alternativno je mogoče odmerek abemacikliba znižati na 50 mg enkrat na dan ali prekiniti dajanje abemacikliba. Če je uporaba zaviralca CYP3A4 prekinjena, je treba odmerek abemacikliba povečati na odmerek, kakršen je bil pred uvedbo zaviralca CYP3A4 (po 3–5 razpolovnih časih zaviralca CYP3A4). Prilagajanje odmerka glede na starost in pri bolnicah z blago ali zmerno ledvično okvaro ter z blago (Child Pugh A) ali zmerno (Child Pugh B) jetrno okvaro ni potrebno. Pri dajanju abemacikliba bolnicam s hudo ledvično okvaro sta potrebna previdnost in skrbno spremljanje glede znakov toksičnosti. Način uporabe Zdravilo Verzenios je namenjeno za peroralno uporabo. Odmerek se lahko vzame s hrano ali brez nje. Zdravila se ne sme jemati z grenivko ali grenivkinim sokom. Bolnice naj odmerke vzamejo vsak dan ob približno istem času. Tableto je treba pogoltniti celo (bolnice tablet pred zaužitjem ne smejo gristi, drobiti ali deliti). **Kontraindikacije** Preobčutljivost na učinkovino ali katero koli pomožno snov. **Posebna opozorila in previdnostni ukrepi** Pri bolnicah, ki so prejemale abemaciklib, so poročali o nevtropeniji, o večji pogostnosti okužb kot pri bolnicah, zdravljenih s placebom in endokrinim zdravljenjem, o povečanih vrednostih ALT in AST. Pri bolnicah, pri katerih se pojavi nevtropenija stopnje 3 ali 4, je priporočljivo prilagoditi odmerek. Do primerov nevtropenične sepse s smrtnim izidom je prišlo pri < 1 % bolnic z metastatskim rakom dojk. Bolnicam je treba naročiti, naj o vsaki epizodi povišane telesne temperature poročajo zdravstvenemu delavcu. Bolnice je treba spremljati za znake in simptome globoke venske tromboze (VTE) in pljučne embolije ter jih zdraviti, kot je medicinsko utemeljeno. Glede na stopnjo VTE bo morda treba spremeniti odmerek abemacikliba. Pri bolnikih, pri katerih se pojavi resni arterijski trombembolični dogodek (ATE), je treba oceniti koristi in tveganja nadaljnjega zdravljenja z abemaciklibom. Glede na povečanje vrednosti ALT ali AST je mogoče potrebna prilagoditev odmerka. Driska je najpogostejši neželeni učinek. Bolnice je treba ob prvem znaku tekočega blata začeti zdraviti z antidiaroiki, kot je loperamid, povečati vnos peroralnih tekočin in obvestiti zdravnika. Sočasni uporabi induktorjev CYP3A4 se je treba izogibati zaradi tveganja za zmanjšano učinkovitost abemacikliba. Bolnice z redkimi dednimi motnjami, kot so intoleranca za galaktozo, popolno pomanjkanje laktaze ali malapsorpcija glukoze/galaktoze, tega zdravila ne smejo jemati. Bolnice je treba spremljati glede pljučnih simptomov, ki kažejo na ILD/pnevmonitis, in jih ustrezno zdraviti. Glede na stopnjo ILD/pnevmonitisa je morda potrebno prilagajanje odmerka abemacikliba. **Medsebojno delovanje z drugimi zdravili in druge oblike interakcij** Abemaciklib se primarno presnavlja s CYP3A4. Sočasna uporaba abemacikliba in zaviralcev CYP3A4 lahko poveča plazemsko koncentracijo abemacikliba. Uporabi močnih zaviralcev CYP3A4 sočasno z abemaciklibom se je treba izogibati. Če je močne zaviralce CYP3A4 treba dajati sočasno, je treba odmerek abemacikliba zmanjšati, nato pa bolnico skrbno spremljati glede toksičnosti. Pri bolnicah, zdravljenih z zmernimi ali šibkimi zaviralci CYP3A4, ni potrebno prilagajanje odmerka, vendar jih je treba skrbno spremljati za znake toksičnosti. Sočasni uporabi močnih induktorjev CYP3A4 (vključno, vendar ne omejeno na: karbamazepin, fenitoin, rifampicin in šentjanževko) se je treba izogibati zaradi tveganja za zmanjšano učinkovitost abemacikliba. Abemaciklib in njegovi glavni aktivni presnovki zavirajo prenašalce v ledvicah, in sicer kationski organski prenašalec 2 (OCT2) ter prenašalca MATE1. *In vivo* lahko pride do medsebojnega delovanja abemacikliba in klinično pomembnih substratov teh prenašalcev, kot je dofelitid ali kreatinin. Trenutno ni znano, ali lahko abemaciklib zmanjša učinkovitost sistemskih hormonskih kontraceptivov, zato se ženskam, ki uporabljajo sistemske hormonske kontraceptive, svetuje, da hkrati uporabljajo tudi mehansko metodo. **Neželeni učinki** Najpogostejši neželeni učinki so driska, okužbe, nevtropenija, levkopenija, anemija, utrujenost, navzea, bruhanje in zmanjšanje apetita. *Zelo pogosti:* okužbe, nevtropenija, levkopenija, anemija, trombocitopenija, limfopenija, zmanjšanje apetita, glavobol, disgevzija, omotica, driska, bruhanje, navzea, stomatitis, alopecija, pruritus, izpuščaj, pireksija, utrujenost, povečana vrednost alanin-aminotransferaze, povečana vrednost aspartat-aminotransferaze *Pogosti:* povečano solzenje, venska trombembolija, ILD/pnevmonitis, dispepsija, spremembe na nohtih, suha koža, mišična šibkost *Občasni:* febrilna nevtropenija, fotopsija, keratitis **Rok uporabnosti** 3 leta **Posebna navodila za shranjevanje** Za shranjevanje zdravila niso potrebna posebna navodila. **Imetnik dovoljenja za promet z zdravilom**: Eli Lilly Nederland B.V., Papendorpseweg 83, 3528BJ, Utrecht, Nizozemska. Datum prve odobritve dovoljenja za promet: 27. september 2018 **Datum zadnje revizije besedila**: 18. 9. 2025 **Režim izdaje:** Rp/Spec - Predpisovanje in izdaja zdravila je le na recept zdravnika specialista ustreznega področja medicine ali od njega pooblaščenega zdravnika.

Okrajšave: AI: zaviralec aromataze; CDK 4/6: od ciklina odvisne kinaze 4 in 6; IZ: interval zaupanja; DRFS: preživetje brez oddaljene ponovitve bolezni; HER2-: receptorjI humanega epidermalnega rastnega faktorja 2-negativni; HR: razmerje ogroženosti; HR+: hormonski receptorji-pozitivni; HT: hormonska terapija; IDFS: preživetje brez invazivne bolezni; ITT: populacija, ki so jo nameravali zdraviti; OS: celokupno preživetje; ZRD: zgodnji rak dojk

Opombe:

[†] Statistično značilna korist celokupnega preživetja je opažena pri populaciji ITT. Po regulativnem posvetovanju pri primarni analizi IDFS je bil načrt analize celokupnega preživetja spremenjen, da bi se končni dogodki povečali s 390 na 650, da bi zagotovili ≥ 5-letno spremljanje. Zdravilo Verzenios je odobreno za kohorto 1 (91 % populacije ITT); analiza celokupnega preživetja v tej podpopulaciji ni bila statistično močna ali alfa-kontrolirana.[1,2]

Reference: 1. Johnston S, Martin M, O'Shaughnessy J, et al. Overall survival with abemaciclib in early breast cancer. *Ann Oncol.* 2025. DOI:10.1016/j.annonc.2025.10.005. **2.** Rastogi P et al. *J Clin Oncol.* 2024;42(9):987-93. **3.** Hortobagyi GN et al. *Ann Oncol.* 2025;36(2):149-57. **4.** Zadnji odobreni Povzetek glavnih značilnosti zdravila Verzenios.

Pomembno: Predpisovanje in izdaja zdravila je le na recept zdravnika specialista ustreznega področja medicine ali od njega pooblaščenega zdravnika. Pred predpisovanjem zdravila Verzenios si preberite zadnji veljavni Povzetek glavnih značilnosti zdravil. Podrobne informacije o zdravilu so objavljene na spletni strani Evropske agencije za zdravila http://www.ema.europa.eu

Eli Lilly farmacevtska družba, d.o.o., Dunajska cesta 167, 1000 Ljubljana, telefon 01 / 580 00 10
PP-AL-SI-0371, 5.11.2025, Samo za strokovno javnost.

Lilly
A MEDICINE COMPANY

Jaypirca je prvi in edini odobreni reverzibilni BTK inhibitor,
ki lahko ponovno vzpostavi odgovor pri odraslih bolnikih z MCL in KLL potem ko kovalentni BTK inhibitor ni več opcija[1,2]

Indikaciji

Zdravilo Jaypirca je kot monoterapija indicirano za zdravljenje odraslih bolnikov s ponovitvijo limfoma plaščnih celic (MCL – mantle cell lymphoma), ali za na zdravljenje neodzivne oblike te bolezni, po predhodnem zdravljenju z zaviralcem Brutonove tirozin kinaze (BTK).

Zdravilo Jaypirca je kot monoterapija indicirano za zdravljenje odraslih bolnikov s ponovitvijo kronične limfocitne levkemije (KLL), ali za na zdravljenje neodzivne oblike te bolezni, po predhodnem zdravljenju z zaviralcem BTK.

Skrajšan povzetek glavnih značilnosti zdravila

▽ Za to zdravilo se izvaja dodatno spremljanje varnosti. Tako bodo hitreje na voljo nove informacije o njegovi varnosti. Zdravstvene delavce naprošamo, da poročajo o katerem koli domnevnem neželenem učinku zdravila.
Ime zdravila Jaypirca 50 mg filmsko obložene tablete, Jaypirca 100 mg filmsko obložene tablete. **Kakovostna in količinska sestava** Ena filmsko obložena tableta vsebuje 50 mg/100 mg pirtobrutiniba. **Terapevtske indikacije** Zdravilo Jaypirca je kot monoterapija indicirano za zdravljenje odraslih bolnikov s ponovitvijo limfoma plaščnih celic (MCL – mantle cell lymphoma), ali za na zdravljenje neodzivne oblike te bolezni, po predhodnem zdravljenju z zaviralcem Brutonove tirozin kinaze (BTK). Zdravilo Jaypirca je kot monoterapija indicirano za zdravljenje odraslih bolnikov s ponovitvijo kronične limfocitne levkemije (KLL), ali za na zdravljenje neodzivne oblike te bolezni, po predhodnem zdravljenju z zaviralcem BTK. **Odmerjanje in način uporabe** Zdravljenje z zdravilom Jaypirca mora uvesti in spremljati zdravnik, ki ima izkušnje z uporabo zdravil za zdravljenje rakavih bolezni. Odmerjanje Priporočeni odmerek je 200 mg pirtobrutiniba enkrat dnevno. Zdravljenje se mora nadaljevati do napredovanja bolezni ali nesprejemljive toksičnosti. Prilagajanje odmerka glede na starost, pri bolnikih z blago, zmerno ali hudo okvaro ledvic ali pri bolnikih z blago, zmerno ali hudo okvaro jeter ni potrebno. Način uporabe Zdravilo Jaypirca je namenjeno za peroralno uporabo. **Kontraindikacije** Preobčutljivost na učinkovino ali katero koli pomožno snov. **Posebna opozorila in previdnostni ukrepi** Pri bolnikih, zdravljenih z zdravilom Jaypirca, je prišlo do resnih okužb, vključno s smrtnimi primeri. Okužbe stopnje 3 ali višje, o katerih so najpogosteje poročali, so bile pljučnica, covidna pljučnica, covid-19 in sepsa. Pri bolnikih s povečanim tveganjem za oportunistične okužbe je treba razmisliti o profilaktičnem protimikrobnem zdravljenju. Na podlagi stopnje okužbe in morebitne pridružene nevtropenije bo morda potrebna prekinitev zdravljenja. Pri bolnikih, zdravljenih z zdravilom Jaypirca, je prišlo do krvavitev, vključno s smrtnimi primeri, s trombocitopenijo ali brez nje. Opazili so večje krvavitve stopnje 3 in višje, vključno z gastrointestinalno in intrakranialno krvavitvijo. Bolnike je treba spremljati glede znakov in simptomov krvavitve. Pri krvavitvah stopnje 3 ali 4 bo morda potrebna prekinitev zdravljenja. Pri bolnikih, zdravljenih z zdravilom Jaypirca, je prišlo do citopenij stopnje 3 ali 4, vključno z nevtropenijo, anemijo in trombocitopenijo. Med zdravljenjem je treba spremljati celotno krvno sliko, kot je medicinsko indicirano. Na podlagi stopnje citopenije bo morda potrebna prekinitev zdravljenja. Pri bolnikih, zdravljenih z zdravilom Jaypirca, so opazili atrijsko fibrilacijo in atrijsko undulacijo, zlasti pri bolnikih z atrijsko fibrilacijo v anamnezi in/ali več pridruženimi srčno-žilnimi boleznimi. Bolnike je treba spremljati glede znakov in simptomov atrijske fibrilacije in atrijske undulacije, potrebno je posneti elektrokardiogram, kot je medicinsko indicirano. Na podlagi stopnje atrijske fibrilacije/atrijske undulacije bo morda potrebna prekinitev zdravljenja. Pri bolnikih, zdravljenih z zdravilom Jaypirca, je pogosto prišlo do drugih primarnih malignih bolezni, najpogosteje nemelanomskih kožnih rakov. Med zdravljenjem z zdravilom Jaypirca so redko poročali o sindromu tumorske lize (TLS – *tumour lysis syndrome*). Bolniki z velikim tveganjem za TLS so tisti, ki imajo pred zdravljenjem veliko tumorsko breme. Bolnike je treba oceniti glede morebitnega tveganja za TLS in jih skrbno spremljati, kot je klinično indicirano. Bolniki z redko dedno intoleranco za galaktozo, odsotnostjo encima laktaze ali malabsorpcijo glukoze/galaktoze ne smejo jemati tega zdravila. **Medsebojno delovanje z drugimi zdravili in druge oblike interakcij** Pirtobrutinib se presnavlja predvsem prek CYP3A4, UGT1A8 in UGT1A9. V klinični študiji je itrakonazol, močan zaviralec CYP3A4, povečal vrednost AUC pirtobrutiniba za 48 %, vrednosti C_{max} pirtobrutiniba pa ni spremenil. V klinični študiji je rifampin, močan induktor CYP3A, zmanjšal vrednost AUC in C_{max} pirtobrutiniba za 71 % oziroma 42 %. Pirtobrutinib je zmeren zaviralec CYP2C8 in BCRP. Pirtobrutinib je šibek zaviralec P-gp,CYP2C19 in CYP3A. **Neželeni učinki** Najpogostejši neželeni učinki katere koli stopnje so: utrujenost, nevtropenija, driska in kontuzije. *Zelo pogosti:* pljučnica, okužba zgornjih dihal, nevtropenija, trombocitopenija, anemija, glavobol, krvavitev, podplutbe, kontuzije, driska, bolečine v trebuhu, navzea, izpuščaj, artralgija, utrujenost, periferni edem *Pogosti:* okužba sečil, limfocitoza, atrijska fibrilacija/atrijska undulacija, hematurija, epistaksa, hematom, vezнична krvavitev, petehije. **Imetnik dovoljenja za promet z zdravilom** Eli Lilly Nederland B.V., Papendorpseweg 83, 3528 BJ Utrecht, Nizozemska. **Datum zadnje revizije besedila** 28.03.2025. **Režim izdaje** Rp/Spec - Predpisovanje in izdaja zdravila je le na recept zdravnika specialista ustreznega področja medicine ali od njega pooblaščenega zdravnika. **Samo za strokovno javnost.**

BTK=Brutonova tirozin kinaza; MCL=mantle cell lymphoma; KLL=kronična limfocitna levkemija.

Referenci: 1. Povzetek glavnih značilnosti zdravila Jaypirca, zadnja odobrena verzija. **2.** Mato AR, Shah NN, Jurczak W, *et al.* Pirtobrutinib in relapsed or refractory B-cell malignancies (BRUIN): a phase 1/2 study. *Lancet.* 021;397(10277):892-901.

Pomembno: Predpisovanje in izdaja zdravila je le na recept zdravnika specialista ustreznega področja medicine ali od njega pooblaščenega zdravnika. Pred predpisovanjem zdravila Jaypirca si preberite zadnji veljavni Povzetek glavnih značilnosti zdravil. Podrobne informacije o zdravilu so objavljene na spletni strani Evropske agencije za zdravila http://www.ema.europa.eu

Eli Lilly farmacevtska družba, d.o.o., Dunajska cesta 167, 1000 Ljubljana, telefon 01 / 580 00 10, faks 01 / 569 17 05

Lilly
A MEDICINE COMPANY

PP-PT-SI-0089, 9.5.2025, Samo za strokovno javnost.

Jaypirca®▼
pirtobrutinib
A Lilly Medicine

PR/BSI/BEN/2024/008

TANTUM VERDE®

benzidaminijev klorid

Za lajšanje bolečine in oteklin v ustni in žrelu, ki so posledica radiomukozitisa

Bistvene informacije iz Povzetka glavnih značilnosti zdravila

Tantum Verde 1,5 mg/ml oralno pršilo, raztopina
Tantum Verde 3 mg/ml oralno pršilo, raztopina

Sestava: 1,5 mg/ml: 1 ml raztopine vsebuje 1,5 mg benzidaminijevega klorida, kar ustreza 1,34 mg benzidamina. V enem razpršku je 0,17 ml raztopine. En razpršek vsebuje 0,255 mg benzidaminijevega klorida, kar ustreza 0,2278 mg benzidamina. **Sestava 3 mg/ml:** 1 ml raztopine vsebuje 3 mg benzidaminijevega klorida, kar ustreza 2,68 mg benzidamina. V enem razpršku je 0,17 ml raztopine. En razpršek vsebuje 0,51 mg benzidaminijevega klorida, kar ustreza 0,4556 mg benzidamina. **Terapevtske indikacije:** Samozdravljenje: Lajšanje bolečine in oteklin pri vnetju v ustni votlini in žrelu, ki so lahko posledica okužb in stanj po operaciji. Po nasvetu in navodilu zdravnika: Lajšanje bolečine in oteklin v ustni votlini in žrelu, ki so posledica radiomukozitisa. **Odmerjanje in način uporabe:** Uporaba: 2- do 6-krat na dan (vsake 1,5 do 3 ure). Odmerjanje 1,5 mg/ml: Odrasli: 4 do 8 razprškov 2- do 6-krat na dan. Pediatrična populacija: Mladostniki, stari od 12 do 18 let: 4-8 razprškov 2- do 6-krat na dan. Otroci od 6 do 12 let: 4 razprški 2- do 6-krat na dan. Otroci, mlajši od 6 let: 1 razpršek na 4 kg telesne mase; do največ 4 razprške 2- do 6-krat na dan. Odmerjanje 3 mg/ml: Odrasli: 2 do 4 razprški 2- do 6-krat na dan. Pediatrična populacija: Mladostniki, stari od 12 do 18 let: 2 do 4 razprški 2- do 6-krat na dan. Otroci od 6 do 12 let: 2 razprška 2- do 6-krat na dan. Otroci, mlajši od 6 let: 1 razpršek na 8 kg telesne mase; do največ 2 razprška 2- do 6-krat na dan. Starejši bolniki, bolniki z jetrno okvaro in bolniki z ledvično okvaro: niso potrebni posebni previdnostni ukrepi. Trajanje zdravljenja ne sme biti daljše od 7 dni. Način uporabe: Za orofaringealno uporabo. Zdravilo se razprši v usta in žrelo. **Kontraindikacije:** Preobčutljivost na učinkovino ali katero koli pomožno snov. **Posebna opozorila in previdnostni ukrepi:** Pri nekaterih bolnikih lahko resne bolezni povzročijo ustne/žrelne ulceracije. Če se simptomi v treh dneh ne izboljšajo, se mora bolnik posvetovati z zdravnikom ali zobozdravnikom, kot je primerno. Uporaba benzidamina ni priporočljiva za bolnike s preobčutljivostjo na salicilno kislino ali druga nesteroidna protivnetna zdravila. Pri bolnikih, ki imajo ali so imeli bronhialno astmo, lahko pride do bronhospazma. Pri takih bolnikih je potrebna previdnost. To zdravilo vsebuje 13,6 mg alkohola (etanola) v enem razpršku (0,17 ml), kar ustreza manj kot 0,34 ml piva oziroma 0,14 ml vina. Majhna količina alkohola v zdravilu ne bo imela nobenih opaznih učinkov. To zdravilo vsebuje metilparahidroksibenzoat (E218). Lahko povzroči alergijske reakcije (lahko zapoznele). To zdravilo vsebuje manj kot 1 mmol (23 mg) natrija v enem razpršku (0,17 ml), kar v bistvu pomeni 'brez natrija'. Zdravilo vsebuje aromo poprove mete z benzilalkoholom, cinamilalkoholom, citralom, citronelolom, geraniolom, izoevgenolom, linalolom, evgenolom in D-limonen, ki lahko povzročijo alergijske reakcije. Zdravilo z jakostjo 3 mg/ml vsebuje makrogolglicerol hidroksistearat 40. Lahko povzroči želodčne težave in drisko. **Medsebojno delovanje z drugimi zdravili in druge oblike interakcij:** Študij medsebojnega delovanja niso izvedli. **Nosečnost in dojenje:** O uporabi benzidamina pri nosečnicah in doječih ženskah ni zadostnih podatkov. Uporaba zdravila med nosečnostjo in dojenjem ni priporočljiva. **Vpliv na sposobnost vožnje in upravljanja strojev:** Zdravilo v priporočenem odmerku nima vpliva na sposobnost vožnje in upravljanja strojev. **Neželeni učinki:** Neznana pogostnost (ni mogoče oceniti iz razpoložljivih podatkov): anafilaktične reakcije, preobčutljivostne reakcije, odrevenelost, laringospazem, suha usta, navzea in bruhanje, oralna hipestezija, angioedem, fotosenzitivnost, pekoč občutek v ustih. Neposredno po uporabi se lahko pojavi občutek odrevenelosti v ustih in v žrelu. Ta učinek se pojavi zaradi načina delovanja zdravila in po kratkem času izgine. **Način in režim izdaje zdravila:** BRp-Izdaja zdravila je brez recepta v lekarnah in specializiranih prodajalnah. **Imetnik dovoljenja za promet:** Aziende Chimiche Riunite Angelini Francesco – A.C.R.A.F. S.p.A., Viale Amelia 70, 00181 Rim, Italija **Datum zadnje revizije besedila:** 05. 04. 2022

Pred svetovanjem ali izdajo preberite celoten Povzetek glavnih značilnosti zdravila.

Samo za strokovno javnost.

Datum priprave informacije: julij 2024

ANGELINI

Odgovoren za trženje: Bonifar d.o.o.

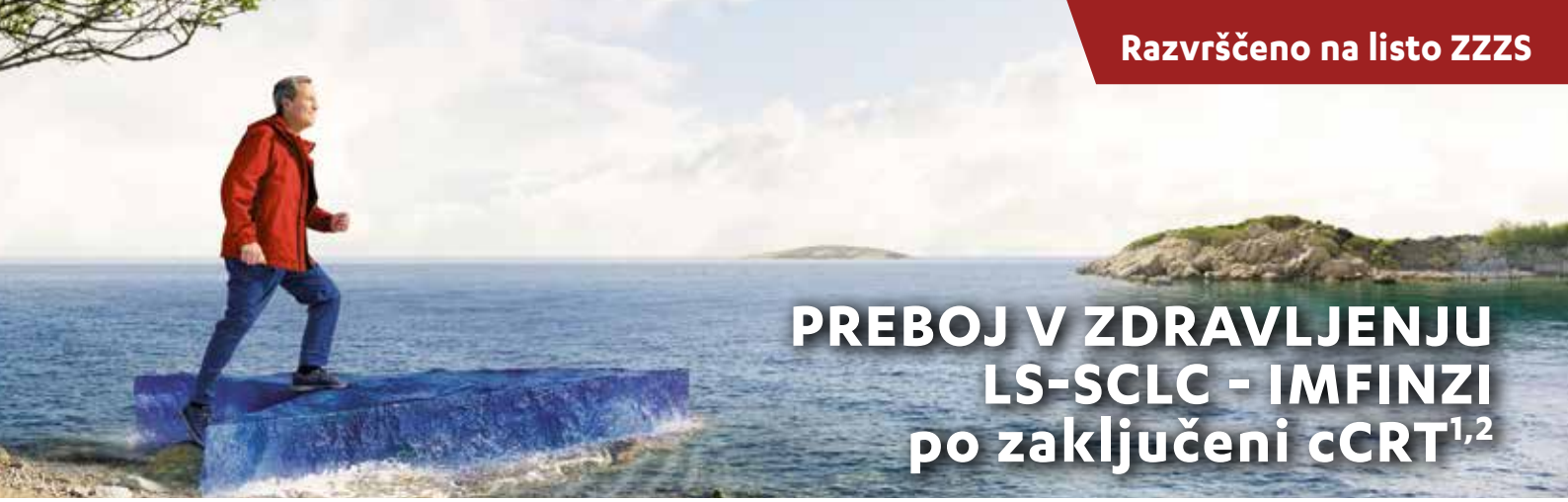

Zdravilo IMFINZI je **PRVA** in **EDINA** imunoterapija, ki je pri LS-SCLC pokazala značilno podaljšanje OS and PFS po zaključeni cCRT v primerjavi s placebom[1,2]

CELOKUPNO PREŽIVETJE [1,2]

VEČ KOT 22 MESECEV DALJŠE mOS

(**ROg=0,73**; 95% CI, 0,57-0,93; *P*=0,0104)

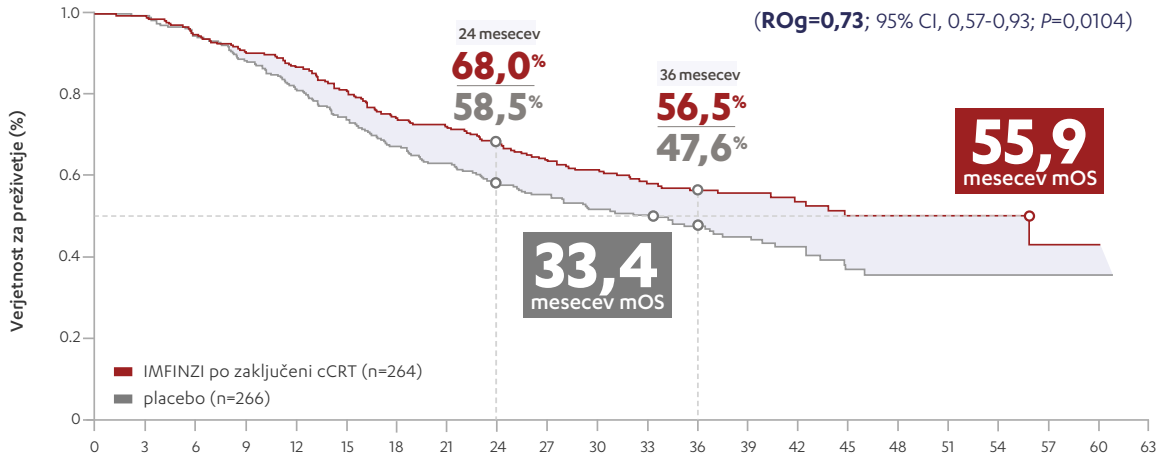

Število ogroženih bolnikov

IMFINZI po zaključeni cCRT	264	261	248	236	223	207	189	183	172	162	141	110	90	68	51	39	27	19	11	5	1	0
placebo	266	260	247	231	214	195	175	164	151	143	123	97	80	62	44	31	23	19	8	5	1	0

Zdravilo IMFINZI je prva imunoterapija odobrena za zdravljenje obeh stadijev SCLC[1]

cCRT=sočasna kemoradioterapija; IZ=interval zaupanja; ROg=razmerje ogroženosti; mOS=mediano celokupno preživetje; OS=celokupno preživetje; PFS=preživetje brez napredovanja bolezni; SCLC=drobnocelični pljučni rak.

Skrajšan povzetek glavnih značilnosti zdravila

Imfinzi 50 mg/ml koncentrat za raztopino za infundiranje

SESTAVA: 1 ml koncentrata za raztopino za infundiranje vsebuje 50 mg durvalumaba. Ena viala z 2,4 ml koncentrata vsebuje 120 mg durvalumaba. Ena viala z 10 ml koncentrata vsebuje 500 mg durvalumaba. **INDIKACIJE:** Nedrobnocelični pljučni rak (NSCLC) Zdravilo IMFINZI je v kombinaciji s kemoterapijo na osnovi platine indicirano kot neoadjuvantno zdravljenje in nato kot samostojno adjuvantno zdravljenje pri odraslih z operabilnim nedrobnoceličnim pljučnim rakom (NSCLC – non-small cell lung cancer), ki imajo veliko tveganje za ponovitev in nimajo mutacij EGFR ali prerearditev ALK. Zdravilo IMFINZI je kot samostojno zdravljenje indicirano za zdravljenje lokalno napredovalega, neoperabilnega nedrobnoceličnega pljučnega raka (NSCLC – non small cell lung cancer) pri odraslih, ki imajo tumorje z ≥ 1 % izraženostjo PD-L1 na tumorskih celicah in pri katerih bolezen ni napredovala po kemoradioterapiji na osnovi platine. Zdravilo IMFINZI je v kombinaciji s tremelimumabom in kemoterapijo na osnovi platine indicirano za prvo linijo zdravljenja odraslih z metastatskim NSCLC brez senzibilizirajočih mutacij EGFR ali pozitivnih mutacij ALK. Drobnocelični pljučni rak (SCLC) Zdravilo IMFINZI je kot samostojno zdravljenje indicirano za zdravljenje odraslih bolnikov z drobnoceličnim pljučnim rakom v omejenem stadiju (LS-SCLC - limited-stage small cell lung cancer), pri katerih bolezen ni napredovala po kemoradioterapiji na osnovi platine. Zdravilo IMFINZI je v kombinaciji z etopozidom in bodisi karboplatinom bodisi cisplatinom indicirano za prvo linijo zdravljenja odraslih z razsejanim drobnoceličnim pljučnim rakom (ES- SCLC – extensive stage small cell lung cancer). Rak bilarnega trakta (RBT) Zdravilo IMFINZI je v kombinaciji z gemcitabinom in cisplatinom indicirano za prvo linijo zdravljenja odraslih z neoperabilnim ali metastatskim rakom bilarnega trakta (RBT). Hepatocelularni karcinom (HCK) Zdravilo IMFINZI je kot samostojno zdravljenje indicirano za prvo linijo zdravljenja odraslih z napredovalim ali neoperabilnim hepatocelularnim karcinomom (HCK). Zdravilo IMFINZI je v kombinaciji s tremelimumabom indicirano za prvo linijo zdravljenja odraslih z napredovalim ali neoperabilnim hepatocelularnim karcinomom (HCK). Rak endometrija Zdravilo IMFINZI je v kombinaciji s karboplatinom in paklitakselom indicirano za prvo linijo zdravljenja odraslih s primarno napredovalim ali ponovljenim rakom endometrija, ki so kandidati za sistemsko zdravljenje, kateremu sledi vzdrževalno zdravljenje z: • zdravilom IMFINZI kot monoterapijo pri raku endometrija z okvaro MMR v tumorju (dMMR - Mismatch Repair Deficient) • zdravilom IMFINZI v kombinaciji z olaparibom pri raku endometrija brez okvare MMR v tumorju (pMMR - Mismatch Repair Proficient). Mišično invazivni rak sečnega mehurja Zdravilo IMFINZI v kombinaciji z gemcitabinom in cisplatinom kot neoadjuvantno zdravljenje, ki mu po radikalni cistektomiji sledi zdravilo IMFINZI kot adjuvantno zdravljenje v monoterapiji, je indicirano za zdravljenje odraslih z operabilnim mišično invazivnim rakom sečnega mehurja (MIBC). **ODMERJANJE IN NAČIN UPORABE:** Zdravljenje mora uvesti in nadzorovati zdravnik, ki ima izkušnje na področju zdravljenja raka. Odmerjanje: Priporočeni odmerek zdravila Imfinzi pri samostojnem zdravljenju pri lokalno napredovalem NSCLC je 10 mg/kg na 2 tedna ali 1500 mg na 4 tedne do napredovanja bolezni, nesprejemljivih toksičnih učinkov ali največ 12 mesecev, pri LS-SCLC 1500 mg na 4 tedne do napredovanja bolezni, nesprejemljivih toksičnih učinkov ali največ 24 mesecev, pri HCK 1500 mg na 4 tedne do napredovanja bolezni ali do nesprejemljivih toksičnih učinkov. Priporočeni odmerek zdravila Imfinzi pri kombiniranem zdravljenju za operabilni NSCLC je 1500 mg v kombinaciji s kemoterapijo na osnovi platine na 3 tedne do 4 cikle pred operacijo, nato samostojno zdravljenje s 1500 mg na 4 tedne do 12 ciklov po operaciji. Trajanje zdravljenja v neoadjuvantni fazi je do napredovanja bolezni, ki onemogoča definitivno operacijo ali do nesprejemljivih toksičnih učinkov, v adjuvantni fazi pa do ponovitve bolezni, nesprejemljivih toksičnih učinkov ali največ 12 ciklov po operaciji, za metastatski NSCLC je med kemoterapijo s platino: 1500 mg v kombinaciji s 75 mg tremelimumaba in kemoterapijo na osnovi platine na 3 tedne (21 dni) 4 cikle (12 tednov), po kemoterapiji s platino: 1500 mg na 4 tedne kot monoterapija in vzdrževalno zdravljenje s pemetreksedom (na podlagi histologije) na 4 tedne, peti odmerek 75 mg tremelimumaba je treba dati 16. teden skupaj z zdravilom Imfinzi. Trajanje zdravljenja je do napredovanja bolezni ali nesprejemljivih toksičnih učinkov. Pri ES-SCLC je priporočeni odmerek zdravila Imfinzi 1500 mg v kombinaciji s kemoterapijo na 3 tedne (21 dni) 4 cikle in nato 1500 mg na 4 tedne kot samostojno zdravljenje do napredovanja bolezni ali nesprejemljivih toksičnih učinkov. Pri RBT je priporočeni odmerek zdravila Imfinzi 1500 mg v kombinaciji s kemoterapijo na 3 tedne (21 dni) do 8 ciklov, nato po 1500 mg na 4 tedne kot samostojno zdravljenje do napredovanja bolezni ali nesprejemljivih toksičnih učinkov. Pri HCK je priporočeni odmerek 1500 mg zdravila Imfinzi v kombinaciji s 300 mg tremelimumaba v enem odmerku 1. dan 1. cikla, nato zdravilo Imfinzi kot monoterapija na 4 tedne do napredovanja bolezni ali nesprejemljivih toksičnih učinkov. Pri raku endometrija je priporočeni odmerek 1120 mg zdravila Imfinzi v kombinaciji s karboplatinom in paklitakselom na 3 tedne (21 dni) minimalno 4 cikle in največ 6 ciklov, nato pa 1500 mg zdravila Imfinzi na 4 tedne kot monoterapija (bolnice z dMMR) ali v kombinaciji s 300 mg olapariba dvakrat na dan (bolnice s pMMR) do napredovanja bolezni ali nesprejemljivih toksičnih učinkov. Pri MIBC je priporočeni odmerek zdravila Imfinzi 1500 mg v kombinaciji s kemoterapijo na 3 tedne v 4 ciklih pred operacijo, nato pa 1500 mg na 4 tedne kot monoterapija do 8 ciklov po operaciji. Trajanje zdravljenja je v neoadjuvantni fazi do napredovanja bolezni, ki onemogoča definitivno operacijo ali do nesprejemljivih toksičnih učinkov, v adjuvantni fazi pa do ponovitve bolezni, nesprejemljivih toksičnih učinkov ali največ 8 ciklov po operaciji; Način uporabe: Zdravilo Imfinzi je namenjeno za intravensko uporabo. Dati ga je treba kot raztopino za intravensko infundiranje v obdobju 1 ure. Če je zdravilo Imfinzi uporabljeno v kombinaciji s kemoterapijo, je treba dati zdravilo Imfinzi pred kemoterapijo na isti dan. Če je zdravilo Imfinzi uporabljeno v kombinaciji s tremelimumabom in kemoterapijo na osnovi platine, je treba najprej dati tremelimumab, ki mu v istem dnevu sledita zdravilo Imfinzi in nato kemoterapija na osnovi platine. Če je zdravilo Imfinzi uporabljeno v kombinaciji s petim odmerkom tremelimumaba in vzdrževalnim zdravljenjem s pemetreksedom 16. teden, je treba najprej dati tremelimumab, ki mu v istem dnevu sledita zdravilo Imfinzi in potem vzdrževalno zdravljenje s pemetreksedom. Zdravilo Imfinzi, tremelimumab in kemoterapijo na osnovi platine je treba dati v ločenih intravenskih infuzijah. Če je zdravilo Imfinzi uporabljeno v kombinaciji s tremelimumabom, je treba za neoperabilni HCK dati tremelimumab pred zdravilom Imfinzi na isti dan. Zdravilo Imfinzi in tremelimumab je treba dati v ločenih intravenskih infuzijah. **KONTRAINDIKACIJE:** Preobčutljivost na učinkovino (učinkovine) ali katero koli pomožno snov. **POSEBNA OPOZORILA IN PREVIDNOSTNI UKREPI:** Za domnevne imunsko pogojene neželene učinke je treba opraviti ustrezno ovrednotenje za potrditev etiologije ali izključitev drugih etiologij. Glede na resnost neželenega učinka je treba uporabo zdravila Imfinzi ali zdravilo Imfinzi v kombinaciji s tremelimumabom prekiniti ali trajno ukiniti. Začeti je treba zdravljenje s kortikosteroidi ali endokrino terapijo. Pri dogodkih, ki zahtevajo zdravljenje s kortikosteroidi, in po izboljšanju na ≤ 1. stopnjo, je treba začeti z zmanjševanjem kortikosteroida in ga zmanjševati v obdobju vsaj 1 meseca. Če pride do poslabšanja ali pa če ni izboljšanja, je treba razmisliti o povečanju odmerka kortikosteroidov in/ali o dodatni uporabi sistemskih imunosupresivov. Pri bolnikih, ki so prejemali zdravilo Imfinzi, zdravilo Imfinzi v kombinaciji s tremelimumabom ali zdravilo Imfinzi v kombinaciji s kemoterapijo na osnovi platine, ki mu sledi zdravilo Imfinzi v kombinaciji z olaparibom ali v kombinaciji s kemoterapijo, sta se pojavila imunsko pogojeni pnevmonitis ali intersticijska bolezen pljuč. Pri bolnikih, zdravljenih z radioterapijo pljuč, je pogost radiacijski pnevmonitis in klinična slika pnevmonitisa in radiacijskega pnevmonitisa je zelo podobna. Bolnike je treba spremljati glede znakov in simptomov pnevmonitisa ali radiacijskega pnevmonitisa. Pri bolnikih, ki so prejemali zdravilo Imfinzi ali zdravilo Imfinzi v kombinaciji s tremelimumabom ali v kombinaciji s kemoterapijo, se je pojavil imunsko pogojeni hepatitis, imunsko pogojeni kolitis, imunsko pogojene hipotiroidizem, hipertiroidizem in tiroiditis, imunsko pogojena adrenalna insuficienca, imunsko pogojena sladkorna bolezen tipa 1, imunsko pogojeni hipofizitis/hipopituitarizem, imunsko pogojeni nefritis, imunsko pogojeni izpuščaj, imunsko pogojeni miokarditis, drugi imunsko pogojeni neželeni učinki (miastenija gravis, transverzni mielitis, miozitis, polimiozitis, rabdomioliza, meningitis, encefalitis, Guillain Barréjev sindrom, imunska trombocitopenija, imunsko pogojeni artritis, uveitis in neinfektivni cistitis), z infundiranjem povezane reakcije. Pri bolnikih, ki so prejemali zdravilo Imfinzi v kombinaciji s tremelimumabom in kemoterapijo ali v kombinaciji s kemoterapijo, se je pojavil imunsko pogojeni pankreatitis. Pri bolnikih z že obstoječo avtoimunsko boleznijo podatki iz opazovalnih študij kažejo na povečano tveganje za imunsko pogojene neželene učinke po terapiji z zaviralci imunske kontrolne točke v primerjavi z bolniki brez obstoječe avtoimunske bolezni. Poleg tega so bili pogosti izbruhi osnovne obstoječe avtoimunske bolezni, vendar je bila večina blagih in obvladljivih. Za bolezen specifični previdnostni ukrepi (RBT): Bolnike z RBT (zlasti tiste z biliarno opornico) je treba natančno nadzorovati glede holangitisa ali okužb biliarnega trakta tako pred uvedbo zdravljenja kot redno med zdravljenjem. Za zdravljenje specifičen previdnostni ukrep (zdravilo Imfinzi v kombinaciji z olaparibom pri raku endometrija): Hematotoksičnost: Med vzdrževalnim zdravljenjem z olaparibom v kombinaciji z zdravilom Imfinzi, po zdravljenju z zdravilom Imfinzi v kombinaciji s kemoterapijo na osnovi platine so poročali o čisti aplaziji rdečih krvnih celic (PRCA – Pure Red Cell Aplasia) in avtoimunski hemolitični anemiji (AIHA - Autoimmune Haemolytic Anemia). Če je PRCA ali AIHA potrjena, je treba zdravljenje z zdravilom Imfinzi in olaparibom prenehati. Metastatski NSCLC: Podatkov o starejših bolnikih (≥ 75 let), zdravljenih z zdravilom Imfinzi v kombinaciji s tremelimumabom in kemoterapijo na osnovi platine, je malo. Morebitno korist/tveganje te sheme je priporočljivo skrbno pretehtati za vsakega bolnika posebej. **MEDSEBOJNO DELOVANJE Z DRUGIMI ZDRAVILI:** Razen fiziološkim odmerkov sistemskih kortikosteroidov (≤ 10 mg na dan prednizona ali ekvivalenta) pred uvedbo durvalumaba ni priporočljivo uporabljati sistemskih kortikosteroidov ali imunosupresivov, ker lahko vplivajo na farmakodinamično aktivnost in učinkovitost durvalumaba. Vendar pa je mogoče kortikosteroide ali druge imunosupresivne uporabiti po začetku zdravljenja z durvalumabom za zdravljenje imunsko pogojenih neželenih učinkov. Z durvalumabom niso izvedli formalnih farmakokinetičnih (PK) študij medsebojnega delovanja zdravil. Primarni poti odstranjevanja durvalumaba sta katabolizem beljakovin preko retikuloendotelijskega sistema oziroma tarčno posredovano odstranjevanje, zato ni pričakovati presnovnih medsebojnih delovanj med zdravili. **PLODNOST, NOSEČNOST IN DOJENJE:** Ženske v rodni dobi morajo med zdravljenjem z durvalumabom in vsaj še 3 mesece po zadnjem odmerku durvalumaba uporabljati učinkovito kontracepcijo. Podatkov o uporabi durvalumaba pri nosečnicah ni. Glede na mehanizem delovanja durvalumab lahko vpliva na vzdrževanje nosečnosti; v alogenskem modelu nosečnosti pri miših je bilo ugotovljeno, da moteno signaliziranje PD-L1 poveča izgubo plodov. Pri nosečnici uporabljeni durvalumab lahko škoduje plodu in ga ni priporočljivo uporabljati med nosečnostjo in pri ženskah v rodni dobi, ki ne uporabljajo učinkovite kontracepcije med zdravljenjem in vsaj še 3 mesece po zadnjem odmerku. Ni znano, ali se durvalumab pri človeku izloča v materinem mleku. Pri človeku protitelesa lahko prehajajo v materino mleko, a možnost absorpcije in škode za novorojenčka ni znana. Toda možnega tveganja za dojenega otroka ni mogoče izključiti. Odločiti se je treba, ali naj ženska prekine z dojenjem ali naj prekine zdravljenje z durvalumabom oziroma sploh ne začne zdravljenja z njim, pri čemer je treba upoštevati koristi dojenja za otroka in koristi zdravljenja za žensko. Podatkov o možnih vplivih durvalumaba na plodnost pri človeku ali živalih ni. **NEŽELENI UČINKI:** Ugotovitve o varnosti zdravila Imfinzi pri samostojnem zdravljenju temeljijo na kumulativnih podatkih 4642 bolnikov z več vrstami tumorjev. Zdravilo Imfinzi so uporabljali v odmerku 10 mg/kg na 2 tedna, 20 mg/kg na 4 tedne ali 1500 mg/kg na 4 tedne. Najpogostejši neželeni učinki (> 10 %) so bili kašelj/produktiven kašelj (18,1 %), driska (15,1 %), izpuščaj (15,0 %), artralgija (12,4 %), zvišana telesna temperatura (12,5 %), bolečine v trebuhu (11,8 %), okužbe zgornjih dihal (11,8 %), srbenje (11,1 %) in hipotiroidizem (11,6 %). Podatki o varnosti zdravila Imfinzi v kombinaciji s kemoterapijo temeljijo na kumulativnih podatkih 1769 bolnikov iz 5 študij (TOPAZ-1, CASPIAN, DUO-E, AEGEAN in NIAGARA). Najpogostejši (> 10 %) neželeni učinki so bili nevtropenija (41,7 %), anemija (40,8 %), navzea (40,1 %), utrujenost (39,6 %), zaprtje (29,7 %), zmanjšanje apetita (22,2 %), trombocitopenija (21,5 %), alopecija (19,7 %), izpuščaj (19,7 %), driska (18,2 %), bruhanje (16,8 %), bolečine v trebuhu (16,7 %), periferna nevropatija (16,3 %), levkopenija (14,8 %), zvišana telesna temperatura (14,0 %), pruritus (13,0 %), hipotiroidizem (11,9 %), artralgija (11,5 %), kašelj/produktiven kašelj (11,0 %) in zvišana aspartat-aminotransferaza/alanin-aminotransferaza (10,7 %). Izsledki o varnosti zdravila Imfinzi v kombinaciji s 75 mg tremelimumaba in kemoterapijo temeljijo na podatkih 338 bolnikov z metastatskim NSCLC. Najpogostejši (> 20 %) neželeni učinki so bili anemija (49,7 %), navzea (41,5 %), nevtropenija (41,2 %), utrujenost (36,1 %), izpuščaj (25,8 %), trombocitopenija (24,5 %) in driska (21,5 %). Izsledki o varnosti zdravila Imfinzi v kombinaciji z enkratnim odmerkom 300 mg tremelimumaba temeljijo na združenih podatkih 462 bolnikov s HCK iz študije HIMALAYA in še ene študije pri bolnikih s HCK, študija 22. Najpogostejši neželeni učinki (> 10 %) so bili izpuščaj (32,5 %), srbenje (25,5 %), driska (25,3 %), bolečine v trebuhu (19,7 %), zvišana aspartat aminotransferaza/zvišana alanin aminotransferaza (18,0 %), zvišana telesna temperatura (13,9 %), hipotiroidizem (13,0 %), kašelj/produktiven kašelj (10,8 %), periferni edemi (10,4 %) in zvišana lipaza (10,0 %). Varnost zdravila Imfinzi v kombinaciji s kemoterapijo na osnovi platine, ki ji sledi zdravilo Imfinzi v kombinaciji s 300 mg olapariba dvakrat na dan, temelji na podatkih 238 bolnic z rakom endometrija. Najpogostejši (> 20 %) neželeni učinki so bili anemija (61,8 %), navzea (54,6 %), utrujenost (54,2 %), periferna nevropatija (51,7 %), alopecija (50,8 %), nevtropenija (39,5 %), zaprtje (32,8 %), trombocitopenija (29,8 %), driska (28,2 %), bruhanje (25,6 %), artralgija (24,4 %), izpuščaj (23,5 %), bolečine v trebuhu (23,5 %), zmanjšan apetit (23,1 %) in levkopenija (20,2 %). **VRSTA IN VSEBINA OVOJNINE:** 2,4 ml (skupno 120 mg durvalumaba) koncentrata v stekleni viali iz stekla tipa 1 z elastomernim zamaškom in sivo snemno aluminijsko zaporo. Pakiranje vsebuje 1 vialo. 10 ml (skupno 500 mg durvalumaba) koncentrata v stekleni viali iz stekla tipa 1 z elastomernim zamaškom in belo snemno aluminijsko zaporo. Pakiranje vsebuje 1 vialo. **NAČIN IZDAJANJA ZDRAVILA:** H - Predpisovanje in izdaja zdravila je le na recept.

DATUM REVIZIJA BESEDILA: 2.7.2025 (SI-3708) **IMETNIK DOVOLJENJA ZA PROMET:** AstraZeneca AB, S-151 85, Sodertalje, Švedska

Pred predpisovanjem, prosimo, preberite celoten povzetek glavnih značilnosti zdravila. Dodatne informacije so na voljo pri družbi AstraZeneca UK Limited, Podružnica v Sloveniji, Verovškova 55, Ljubljana, telefon +386 1 51 35 600.

Samo za strokovno javnost. Informacija pripravljena avgust 2025.

Reference: 1. Povzetek glavnih značilnosti zdravila Imfinzi, julij 2025 2. Cheng Y, Spigel DR, Cho BC, et al. Durvalumab after chemoradiotherapy inlimited-stage small-cell lung cancer. N Engl J Med. 2024;391(14):1313-1327 (Including Protocol).

AstraZeneca

IMFINZI™ durvalumab
50 mg/ml koncentrat za raztopino za infundiranje

SI-5214

ENHERTU®
trastuzumab derukstekan

PREMIKAMO MEJE ZDRAVLJENJA

Z UČINKOVITOSTJO, KI PRESEGA PRIČAKOVANJA

- Terapija izbora v smernicah za 2L HER2+ raka dojk[1-5]
- Prvo in edino zdravljenje proti HER2, ki je učinkovito tudi pri bolnikih z rakom dojk z (zelo) nizkim izražanjem HER2*.[1,3-7]

Učinkovitost pri bolnikih s HER2+ razsejanim rakom dojk in možganskimi metastazami ob izhodišču zdravljenja[8, 9]

Čas do napredovanja bolezni

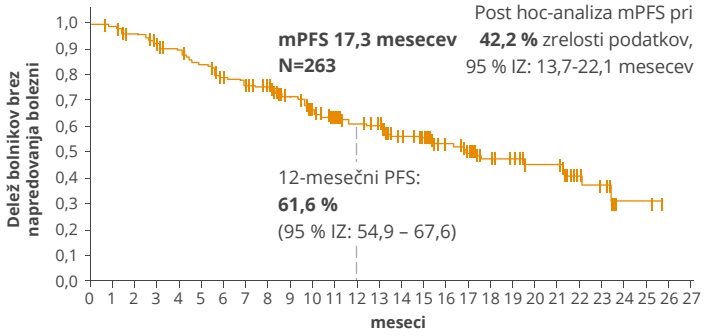

Celotna populacija bolnikov z možganskimi metastazami ob izhodišču zdravljenja (analiza Kaplan-Meier)

Delež objektivnega odgovora v CŽS

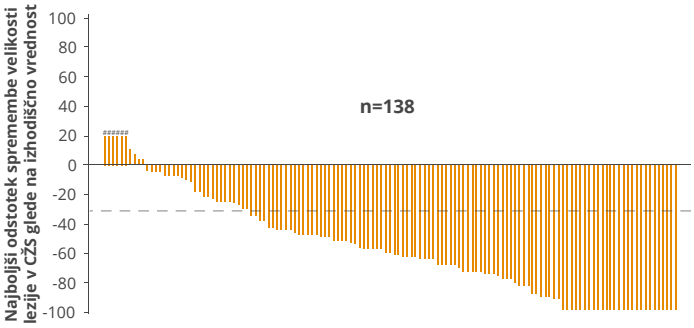

Bolniki z merljivo boleznijo v CŽS ob izhodišču zdravljenja (post-hoc analiza)

Ob zdravljenju s trastuzumab derukstekanom je potrebno bolnike spremljati za pojav intersticijskega pnevmonitisa in ukrepati ob prvih simptomih.

SKRAJŠAN POVZETEK GLAVNIH ZNAČILNOSTI ZDRAVILA

▼Za to zdravilo se izvaja dodatno spremljanje varnosti. Tako bodo hitreje na voljo nove informacije o njegovi varnosti. Zdravstvene delavce naprošamo, da poročajo o katerem koli domnevnem neželenem učinku zdravila.

ENHERTU 100 mg prašek za koncentrat za raztopino za infundiranje

SESTAVA: Ena viala praška za koncentrat za raztopino za infundiranje vsebuje 100 mg trastuzumab derukstekana. Po rekonstituciji ena viala s 5 ml raztopine vsebuje 20 mg/ml trastuzumab derukstekana. Trastuzumab derukstekan je konjugat protitelesa in zdravila, ki vsebuje humanizirano monoklonsko protitelo IgG1 proti HER2 z istim zaporedjem aminokislin, kot ga ima trastuzumab. Proizvajajo ga sesalske celice (ovarij kitajskega hrčka) in je prek razcepljivega veznika na tetrapeptidni bazi kovalentno vezan na DXd, ki je derivat eksatekana in zaviralec topoizomeraze I. Na vsako molekulo protitelesa je vezanih približno 8 molekul derukstekana. *Pomožne snovi:* L-histidin, L-histidinijev klorid monohidrat, saharoza, polisorbat 80 (E433). **TERAPEVTSKE INDIKACIJE:** ***Rak dojk:*** *HER2-pozitiven rak dojk:* Zdravilo Enhertu kot monoterapija je indicirano za zdravljenje odraslih bolnikov z neresektabilnim ali metastatskim HER2-pozitivnim rakom dojk, ki so pred tem že prejeli eno ali več shem zdravljenja na podlagi anti-HER2. *Rak dojk z nizkim statusom HER2 in zelo nizkim statusom HER2:* Zdravilo Enhertu kot monoterapija je indicirano za zdravljenje odraslih bolnikov z neresektabilnim ali metastatskim rakom dojk, pozitivnim na hormonske receptorje, z nizkim statusom HER2 ali zelo nizkim statusom HER2, ki so pred tem prejeli vsaj eno endokrino terapijo v prisotnosti metastaz in ki ne veljajo za primerne za endokrino terapijo kot naslednjo linijo zdravljenja ter rakom dojk z nizkim statusom HER2, ki so pred tem že prejeli kemoterapijo v prisotnosti metastaz ali pa se je pri njih bolezen ponovila med adjuvantno kemoterapijo ali znotraj 6 mesecev po njenem zaključku. ***Nedrobnocelični rak pljuč*** (NSCLC - non-small cell lung cancer): Zdravilo Enhertu kot monoterapija je indicirano za zdravljenje odraslih bolnikov z napredovalim NSCLC, ki imajo tumorje z aktivirajočo mutacijo HER2 (ERBB2) in potrebujejo sistemsko terapijo po kemoterapiji na podlagi platine z imunoterapijo ali brez nje. ***Rak želodca:*** Zdravilo Enhertu v obliki monoterapije je indicirano za zdravljenje odraslih bolnikov z napredovalim HER2-pozitivnim adenokarcinomom želodca ali gastroezofagealnega prehoda, ki so pred tem že prejeli shemo na podlagi trastuzumaba. **ODMERJANJE IN NAČIN UPORABE:** Zdravilo Enhertu mora predpisati zdravnik in njegovo dajanje nadzorovati zdravstveni delavec, ki sta izkušena v uporabi zdravil proti raku. Za preprečitev napak, povezanih z zdravili, je pomembno, da preverite nalepke na vialah in se prepričate, da je zdravilo, ki se pripravlja in daje, res zdravilo Enhertu (trastuzumab derukstekan), in ne trastuzumab ali trastuzumab emtanzin. Zdravilo Enhertu se ne sme zamenjati s trastuzumabom ali trastuzumab emtanzinom. Bolniki, ki se zdravijo s trastuzumab derukstekanom zaradi *HER2-pozitivnega raka dojk, raka želodca ali gastroezofagealnega prehoda*, morajo imeti dokumentiran HER2pozitiven status tumorja, ki je opredeljen kot ocena 3 + na podlagi imunohistokemije (IHC) ali razmerje ≥ 2,0 na podlagi *in situ* hibridizacije (ISH) ali fluorescenčne *in situ* hibridizacije (FISH), ocenjeno z *in vitro* diagnostičnim (IVD) medicinskim pripomočkom z oznako CE. Bolniki, ki se zdravijo s trastuzumab derukstekanom zaradi *raka dojk z nizkim in zelo nizkim statusom HER2*, morajo imeti dokumentiran nizek status HER2 tumorja, ki je opredeljen kot ocena IHC 1+ ali IHC 2+/ISH-, ali zelo nizek status HER2, opisan kot IHC 0 z obarvanjem membrane (IHC >0<1+) ocenjen z IVD z oznako CE. Bolniki, ki se zdravijo s trastuzumab derukstekanom zaradi napredovalega NSCLC, morajo imeti aktivirajočo mutacijo HER2 (ERBB2), odkrito z *in vitro* diagnostičnim (IVD) medicinskim pripomočkom, označenim s CE. Če IVD z oznako CE ni na voljo, je treba status HER2 in status mutacije HER2 oceniti z drugim potrjenim testom. Odmerjanje: *Rak dojk in NSCLC:* Priporočeni odmerek zdravila Enhertu je 5,4 mg/kg, ki se daje z intravensko infuzijo enkrat vsake 3 tedne (21-dnevni cikel) do napredovanja bolezni ali nesprejemljive toksičnosti. *Rak želodca:* Priporočeni odmerek zdravila Enhertu je 6,4 mg/kg, ki se daje z intravensko infuzijo enkrat vsake 3 tedne (21-dnevni cikel) do napredovanja bolezni ali nesprejemljive toksičnosti. Začetni odmerek je treba dati z 90-minutno intravensko infuzijo. Če bolnik prejšnjo infuzijo dobro prenaša, se lahko naslednji odmerki zdravila Enhertu dajejo kot 30-minutne infuzije. Hitrost infundiranja zdravila Enhertu je treba zmanjšati ali infundiranje prekiniti, če se pri bolniku razvijejo simptomi, povezani z infuzijo. V primeru hudih reakcij na infuzijo je treba zdravilo Enhertu trajno ukiniti. Premedikacija: Zdravilo Enhertu je emetogeno, kar vključuje zapoznelo navzeo in/ali bruhanje. Pred vsakim odmerkom zdravila Enhertu je treba bolnike premedicirati s kombiniranim režimom dveh ali treh zdravil (npr. deksametazon z antagonistom receptorjev 5-HT3 in/ali antagonistom receptorjev NK1 ter drugimi zdravili, kot je indicirano) za preprečevanje navzee in bruhanja zaradi kemoterapije. Prilagajanje odmerka: Obvladovanje neželenih učinkov lahko zajema začasno prekinitev uporabe, zmanjšanje odmerka ali ukinitev zdravljenja z zdravilom Enhertu, skladno s smernicami, podanimi v povzetku glavnih značilnosti zdravila (preglednici 1 in 2). Po zmanjšanju odmerka zdravila Enhertu se odmerek ne sme več ponovno povečati. Načrt zmanjševanja odmerka: Priporočeni začetni odmerek je 5,4 mg/kg pri raku dojk in NSCLC oz. 6,4 mg/kg pri raku želodca; prvo zmanjšanje odmerka (4,4 mg/kg oz. 5,4 mg/kg), drugo zmanjšanje odmerka (3,2 mg/kg oz. 4,4 mg/kg), pri potrebi po nadaljnjem zmanjšanju odmerka ukinite zdravljenje. *Prosimo, glejte celoten povzetek glavnih značilnosti zdravila Enhertu za prilagajanje odmerka zaradi neželenih učinkov: intersticijska pljučna bolezen (IPB)/pnevmonitis* (asimptomatska IPB/asimptomatski pnevmonitis (stopnja 1), simptomatska IPB/simptomatski pnevmonitis (stopnja 2 ali višja)), *nevtropenija* (stopnja 3 (manj kot 1,0-0,5 × 10^9/l), stopnja 4 (manj kot 0,5 × 10^9/l)), *febrilna nevtropenija* (absolutno število nevtrofilcev manj kot 1,0 × 10^9/l in telesna temperatura višja od 38,3 °C, ali telesna temperatura 38 °C ali višja, ki vztraja več kot eno uro), *zmanjšan iztisni delež levega prekata* (LVEF) (LVEF več kot 45 % in absolutno zmanjšanje glede na izhodiščno vrednost za 10 % do 20 %; LVEF 40 % do 45 %; LVEF manj kot 40 % ali absolutno zmanjšanje glede na izhodiščno vrednost za več kot 20 %; simptomatično kongestivno srčno popuščanje). Zakasnjen ali izpuščen odmerek: Če se načrtovani odmerek zakasni ali izpusti, ga je treba dati takoj, ko je mogoče, brez čakanja na naslednji načrtovani cikel. Časovni načrt dajanja je treba prilagoditi, da se ohrani 3-tedenski razmik med odmerki. Infuzijo je treba dati s hitrostjo in odmerkom, ki ga je bolnik prenašal pri zadnji infuziji. Posebne populacije: *Starejši:* Pri bolnikih, starih 65 let ali starejših, prilagajanje odmerka zdravila Enhertu ni potrebno. Podatki pri bolnikih, starih ≥ 75 let, so omejeni. *Okvara ledvic:* Prilagajanje odmerka pri bolnikih z blago (očistek kreatinina [CLcr] ≥ 60 in < 90 ml/min) ali zmerno (CLcr ≥ 30 in < 60 ml/min) okvaro ledvic ni potrebno. Morebitne potrebe po prilagajanju odmerka pri bolnikih s hudo okvaro ledvic ali končno ledvično odpovedjo ni mogoče opredeliti, ker je bila huda okvara ledvic v kliničnih študijah izključitveni kriterij. Pri bolnikih z zmerno okvaro ledvic so opazili višjo pogostnost IPB stopnje 1 in 2/pnevmonitisa, ki sta vodila do zvečanja števila prekinitev zdravljenja. Pri bolnikih z zmerno okvaro ledvic v izhodišču, ki so prejemali zdravilo Enhertu 6,4 mg/kg, so ugotovili večjo pogostnost resnih neželenih učinkov kot pri tistih z normalnim delovanjem ledvic. Bolnike z zmerno ali hudo okvaro ledvic je treba natančno spremljati glede neželenih učinkov, vključno z IPB/pnevmonitisom. *Okvara jeter:* Pri bolnikih, ki imajo celokupni bilirubin ≤ 1,5-kratnik zgornje meje normalnih vrednosti (ZMN), ne glede na vrednost aspartat transaminaze (AST), odmerka ni treba prilagajati. Morebitne potrebe po prilagajanju odmerka pri bolnikih, ki imajo celokupni bilirubin > 1,5-kratnik ZMN, ne glede na vrednost AST, ni mogoče opredeliti zaradi omejenih podatkov. Zato je treba te bolnike natančno spremljati. Način uporabe: Zdravilo Enhertu je za intravensko uporabo. Zdravstveni delavec ga mora rekonstituirati in razredčiti. Treba ga je dati z intravenskim infundiranjem. Zdravilo Enhertu se ne sme dati kot hitro intravensko injekcijo ali bolus. **KONTRAINDIKACIJE:** Preobčutljivost na učinkovino ali katero koli pomožno snov. **POSEBNA OPOZORILA IN PREVIDNOSTNI UKREPI:** Intersticijska pljučna bolezen/pnevmonitis: Pri zdravilu Enhertu so poročali o primerih intersticijske pljučne bolezni (IPB) in/ali pnevmonitisa. Nekateri primeri so bili smrtni. Bolnikom je treba naročiti, naj takoj poročajo o kašlju, dispneji, zvišani telesni temperaturi in/ali katerih koli novih dihalnih simptomih ali poslabšanju obstoječih. Bolnike je treba spremljati glede znakov in simptomov IPB/pnevmonitisa. Dokaze za IPB/pnevmonitis je treba takoj proučiti. Bolnike s sumom na IPB/pnevmonitis je treba oceniti z radiografskimi posnetki, najbolje z računalniško tomografijo (CT). Treba je razmisliti o posvetu s pulmologom. Nevtropenija: V kliničnih študijah z zdravilom Enhertu so poročali o primerih nevtropenije, vključno s primeri febrilne nevtropenije s smrtnim izidom. Pred uvedbo zdravila Enhertu in pred vsakim odmerkom ter vsakič, ko je klinično indicirano, je treba preveriti celotno krvno sliko. Morda bo treba začasno prekiniti dajanje zdravila Enhertu ali zmanjšati odmerek, odvisno od tega, kako huda je nevtropenija. Okvara levega prekata: Pri zdravljenjih anti-HER2 so poročali o zmanjšanem iztisnem deležu levega prekata (LVEF). Pred uvedbo zdravljenja z zdravilom Enhertu in v rednih intervalih med njim (v skladu s kliničnimi indikacijami) je treba izvesti standardne preiskave delovanja srca (ehokardiografija ali slikanje MUGA) za oceno LVEF. Zmanjšanje LVEF je treba obvladovati s prekinitvami zdravljenja. Zdravljenje z zdravilom Enhertu je treba trajno ukiniti, če se potrdi LVEF manj kot 40 % ali absolutno zmanjšanje glede na izhodiščno vrednost za več kot 20 %. Zdravilo Enhertu je treba trajno ukiniti pri bolnikih s simptomatskim kongestivnim srčnim popuščanjem. Embrio-fetalna toksičnost: Zdravilo Enhertu lahko ima škodljiv vpliv na plod, če se da nosečnici. Pri ženskah v rodni dobi je treba pred uvedbo zdravljenja z zdravilom Enhertu preveriti status nosečnosti. Bolnice je treba seznaniti z možnimi tveganji za plod. Ženskam v rodni dobi je treba svetovati, da uporabljajo učinkovito kontracepcijo med zdravljenjem in še vsaj 7 mesecev po zadnjem odmerku zdravila Enhertu. Moškim bolnikom s partnerkami v rodni dobi je treba svetovati, da uporabljajo učinkovito kontracepcijo med zdravljenjem z zdravilom Enhertu in še vsaj 4 mesece po zadnjem odmerku zdravila Enhertu. Bolniki z zmerno ali hudo okvaro jeter: Zdravilo Enhertu je treba pri bolnikih z zmerno in hudo okvaro jeter dajati previdno. **MEDSEBOJNO DELOVANJE Z DRUGIMI ZDRAVILI IN DRUGE OBLIKE INTERAKCIJ:** Pri sočasnem dajanju trastuzumab derukstekana z zdravili, ki so zaviralci CYP3A ali OATP1B ali prenašalcev P-gp, odmerka ni treba prilagajati. **PLODNOST, NOSEČNOST IN DOJENJE:** Nosečnost: Dajanje zdravila Enhertu nosečnicam se ne priporoča. Bolnice je treba seznaniti z možnimi tveganji za plod, preden zanosijo. Ženske, ki zanosijo, se morajo takoj obrniti na zdravnika. Če ženska zanosi med zdravljenjem z zdravilom Enhertu ali v obdobju 7 mesecev po zadnjem odmerku zdravila Enhertu, se priporoča natančno spremljanje. Dojenje: Ni znano, ali se trastuzumab derukstekan izloča v materino mleko. Humani IgG se izloča v materino mleko in potencial za absorpcijo in resne neželene učinke na dojenčka ni znan. Zato ženske ne smejo dojiti med zdravljenjem z zdravilom Enhertu in še 7 mesecev po zadnjem odmerku. Odločiti se je treba med prenehanjem dojenja in prenehanjem zdravljenja z zdravilom Enhertu, pri čemer je treba pretehtati prednosti dojenja za otroka in prednosti zdravljenja za mater. Plodnost: Namenskih študij plodnosti s trastuzumab derukstekanom niso izvedli. Ni znano, ali so trastuzumab derukstekan ali njegovi presnovki prisotni v semenski tekočini. Pred začetkom zdravljenja je treba moškim bolnikom svetovati, da se posvetujejo o možnosti shranjevanja semena. Moški bolniki v celotnem obdobju zdravljenja in še najmanj 4 mesece po zadnjem odmerku zdravila Enhertu ne smejo zamrzniti ali darovati semena. **NEŽELENI UČINKI:** *Zdravilo Enhertu 5,4 mg/kg:* Združeno varnostno populacijo so ocenili pri bolnikih, ki so v kliničnih študijah dobili vsaj en odmerek 5,4 mg/kg zdravila Enhertu (N = 2335) zaradi različnih vrst tumorjev. Mediani čas trajanja zdravljenja v tej združeni populaciji je bil 9,0 meseca (razpon: 0,7-45,1 meseca). *Zelo pogosti:* okužba zgornjih dihal, anemija, nevtropenija, trombocitopenija, levkopenija, hipokaliemija, zmanjšan apetit, glavobol, intersticijska pljučna bolezen, kašelj, navzea, bruhanje, zaprtje, driska, bolečina v trebuhu, stomatitis, dispepsija, zvišane transaminaze, alopecija, mišično-skeletna bolečina, utrujenost, pireksija, hipokaliemija, zmanjšan apetit, glavobol, intersticijska pljučna bolezen, kašelj, navzea, bruhanje, zaprtje, driska, bolečina v trebuhu, stomatitis, dispepsija, zvišane transaminaze, alopecija, mišično-skeletna bolečina, utrujenost, pireksija, zmanjšan iztisni delež, zmanjšanje telesne mase. *Pogosti:* pljučnica, limfopenija, febrilna nevtropenija, pancitopenija, dehidracija, omotica, disgevzija, suhe oči, zamegljen vid, dispneja, epistaksa, abdominalna distenzija, gastritis, flatulenca, izpuščaj, pruritus, hiperpigmentacija kože, perifermni edem, zvišana alkalna fosfataza v krvi, zvišan kreatinin v krvi, reakcije, povezane z infuzijo. *Zdravilo Enhertu 6,4 mg/kg:* Združeno varnostno populacijo so ocenili za bolnike, ki so v kliničnih študijah dobili vsaj en odmerek 6,4 mg/kg zdravila Enhertu (N = 669) zaradi različnih vrst tumorjev. Mediani čas trajanja zdravljenja v tej združeni populaciji je bil 5,7 meseca (razpon: 0,7-41,0 meseca). *Zelo pogosti:* pljučnica, okužba zgornjih dihal, anemija, nevtropenija, trombocitopenija, levkopenija, limfopenija, hipokaliemija, zmanjšan apetit, glavobol, disgevzija, intersticijska pljučna bolezen, dispneja, kašelj, navzea, bruhanje, driska, zaprtje, bolečina v trebuhu, stomatitis, zvišane transaminaze, alopecija, mišično-skeletna bolečina, utrujenost, pireksija, perifermni edem, zmanjšan iztisni delež, zmanjšanje telesne mase. *Pogosti:* febrilna nevtropenija, pancitopenija, dehidracija, omotica, suhe oči, zamegljen vid, epistaksa, dispepsija, abdominalna distenzija, gastritis, flatulenca, izpuščaj, pruritus, hiperpigmentacija kože, zvišana alkalna fosfataza v krvi, zvišan bilirubin v krvi, zvišan kreatinin v krvi, reakcije, povezane z infuzijo. **IMETNIK DOVOLJENJA ZA PROMET Z ZDRAVILOM:** Daiichi Sankyo Europe GmbH, Zielstattstrasse 48, 81379 München, Nemčija **DATUM ZADNJE REVIZIJE BESEDILA:** 31. marec 2025 (SI-5034) **REŽIM PREDPISOVANJA IN IZDAJE:** H **Prosimo, da pred predpisovanjem preberete celoten povzetek glavnih značilnosti zdravila.** Dodatne informacije so na voljo pri podjetju AstraZeneca UK Limited, Podružnica v Sloveniji, Verovškova 55, 1000 Ljubljana, telefon: 01/51 35 600.

Literatura: 1. Povzetek glavnih značilnosti zdravila ENHERTU, 31. 3. 2025, **2.** Cortes J et al; Trastuzumab Deruxtecan versus Trastuzumab Emtansine for Breast Cancer; NEJM 2022;386(12):1143-1154, **3.** Gennari A et al: Ann Oncol 2021;32(12): 1475-1495 **4.** Gennari A et al. ESMO Metastatic Breast Cancer Living Guidelines, v1.2 April 2025, https://www.esmo.org/living-guidelines/esmo-metastatic-breast-cancer-living-guideline, dostopano 11. 9. 2025 **5.** NCCN guidelines Breast Cancer, v4.2025, https://www.nccn.org/professionals/physician_gls/pdf/breast.pdf, dostopano 11. 9. 2025. **6.** Modi S et al. Trastuzumab deruxtecan in previously treated HER2-low advanced breast cancer. N Engl J Med. 2022;387:9-20. in dodati referenco **7.** Bardia A et al. Trastuzumab deruxtecan after endocrine therapy in metastatic breast cancer. NEJM 2024; 391:2110-2122. **8.** Harbeck et al. Nat Med. 2024. doi: 10.1038/s41591-024-03261-7. **9.** Lin NU, et al. Presented at: European Society of Medical Oncology (ESMO) Meeting 2024. Sep 13-17, 2024.

* rak dojk z nizkim izražanjem HER2 je definiran kor IHK1+ ali IHK2+/ISH-, # Pripisane vrednosti: pripisana je bila vrednost +20 %, če deleža najboljše spremembe ni bilo mogoče izračunati zaradi manjkajočih podatkov v primerih, da je imel bolnik novo lezijo ali napredovanje neciljnih ali ciljnih lezij ali se je umaknil zaradi napredovnja bolezni in pred tem ali ob napredovanju bolezni ni bilo podatkov za oceno odziva v ciljni leziji.
2L - drugi red, **CŽS** - centralni živčni sistem, **mPFS** - srednji čas do napredovanja bolezni, **IZ** - interval zaupanja

Datum priprave materiala: september 2025. Samo za strokovno javnost. SI-5361

Daiichi-Sankyo | AstraZeneca

KEYTRUDA® je odobrena za zdravljenje več kot 30 indikacij rakavih obolenj[1]

Referenca: 1. Povzetek glavnih značilnosti zdravila KEYTRUDA

SKRAJŠAN POVZETEK GLAVNIH ZNAČILNOSTI ZDRAVILA • Pred predpisovanjem, prosimo, preberite celoten Povzetek glavnih značilnosti zdravila! • Ime zdravila: KEYTRUDA 25 mg/ml koncentrat za raztopino za infundiranje vsebuje pembrolizumab. • **Terapevtske indikacije:** Zdravilo KEYTRUDA je kot samostojno zdravljenje indicirano za zdravljenje: odraslih in mladostnikov, starih 12 let ali več, z napredovalim (neoperabilnim ali metastatskim) melanomom; za adjuvantno zdravljenje odraslih in mladostnikov, starih 12 let ali več, z melanomom v stadiju IIB, IIC ali III, in sicer po popolni kirurški odstranitvi; za adjuvantno zdravljenje odraslih z nedrobnoceličnim pljučnim rakom, ki imajo visoko tveganje za ponovitev bolezni po popolni kirurški odstranitvi in kemoterapiji na osnovi platine; metastatskega nedrobnoceličnega pljučnega raka (NSCLC) v prvi liniji zdravljenja pri odraslih, ki imajo tumorje z ≥ 50 % izraženostjo PD-L1 (TPS) in brez pozitivnih tumorskih mutacij EGFR ali ALK; lokalno napredovalega ali metastatskega NSCLC pri odraslih, ki imajo tumorje z ≥ 1 % izraženostjo PD-L1 (TPS) in so bili predhodno zdravljeni z vsaj eno shemo kemoterapije, bolniki s pozitivnimi tumorskimi mutacijami EGFR ali ALK so pred prejemom zdravila KEYTRUDA morali prejeti tudi tarčno zdravljenje; odraslih in pediatričnih bolnikov, starih 3 leta ali več, s ponovljenim ali neodzivnim klasičnim Hodgkinovim limfomom (cHL), pri katerih avtologna presaditev matičnih celic (ASCT) ni bila uspešna, ali po najmanj dveh predhodnih zdravljenjih kadar ASCT ne pride v poštev kot možnost zdravljenja; lokalno napredovalega ali metastatskega urotelijskega raka pri odraslih, predhodno zdravljenih s kemoterapijo, ki je vključevala platino; lokalno napredovalega ali metastatskega urotelijskega raka pri odraslih, ki niso primerni za zdravljenje s kemoterapijo, ki vsebuje cisplatin in imajo tumorje z izraženostjo PD-L1 ≥ 10, ocenjeno s kombinirano pozitivno oceno (CPS); ponovljenega ali metastatskega ploščatoceličnega raka glave in vratu (HNSCC) pri odraslih, ki imajo tumorje z ≥ 50 % izraženostjo PD-L1 (TPS), in pri katerih je bolezen napredovala med zdravljenjem ali po zdravljenju s kemoterapijo, ki je vključevala platino; za adjuvantno zdravljenje odraslih z rakom ledvičnih celic s povišanim tveganjem za ponovitev bolezni po nefrektomiji, ali po nefrektomiji in kirurški odstranitvi metastatskih lezij, za zdravljenje odraslih z MSI-H (microsatellite instability-high) ali dMMR (mismatch repair deficient) kolorektalnim rakom v naslednjih terapevtskih okoliščinah: prva linija zdravljenja metastatskega kolorektalnega raka; zdravljenje neoperabilnega ali metastatskega kolorektalnega raka po predhodnem kombiniranem zdravljenju, ki je temeljilo na fluoropirimidinu; in za zdravljenje MSI-H ali dMMR tumorjev pri odraslih z: napredovalim ali ponovljenim rakom endometrija, pri katerih je bolezen napredovala med ali po predhodnem zdravljenju, ki je vključevalo platino, v katerih koli terapevtskih okoliščinah, in ki niso kandidati za kurativno operacijo ali obsevanje; neoperabilnim ali metastatskim rakom želodca, tankega črevesa ali biliarnega trakta, pri katerih je bolezen napredovala med ali po vsaj enem predhodnem zdravljenju. Zdravilo KEYTRUDA je kot samostojno zdravljenje ali v kombinaciji s kemoterapijo s platino in 5-fluorouracilom (5-FU) indicirano za prvo linijo zdravljenja metastatskega ali neoperabilnega ponovljenega ploščatoceličnega raka glave in vratu pri odraslih, ki imajo tumorje z izraženostjo PD-L1 s CPS ≥ 1. Zdravilo KEYTRUDA je v kombinaciji s kemoterapijo, ki vključuje platino, indicirano za neoadjuvantno zdravljenje, in v nadaljevanju kot samostojno zdravljenje za adjuvantno zdravljenje odraslih z operabilnim nedrobnoceličnim pljučnim rakom, ki imajo visoko tveganje za ponovitev bolezni; v kombinaciji s pemetreksedom in kemoterapijo na osnovi platine je indicirano za prvo linijo zdravljenja metastatskega neploščatoceličnega NSCLC pri odraslih, pri katerih tumorji nimajo pozitivnih mutacij EGFR ali ALK; v kombinaciji s karboplatinom in bodisi paklitakselom bodisi nab-paklitakselom je indicirano za prvo linijo zdravljenja metastatskega ploščatoceličnega NSCLC pri odraslih; v kombinaciji s pemetreksedom in kemoterapijo na osnovi platine je indicirano za prvo linijo zdravljenja pri odraslih z neoperabilnim neepiteloidnim malignim mezoteliomom plevre; v kombinaciji z enfortumab vedotinom je indicirano za prvo linijo zdravljenja neoperabilnega ali metastatskega urotelijskega raka pri odraslih; v kombinaciji z aksitinibom ali v kombinaciji z lenvatinibom je indicirano za prvo linijo zdravljenja napredovalega raka ledvičnih celic (RCC) pri odraslih; v kombinaciji s kemoterapijo s platino in fluoropirimidinom je indicirano za prvo linijo zdravljenja lokalno napredovalega neoperabilnega ali metastatskega raka požiralnika pri odraslih, ki imajo tumorje z izraženostjo PD-L1 s CPS ≥ 10; v kombinaciji s kemoterapijo za neoadjuvantno zdravljenje, in v nadaljevanju kot samostojno adjuvantno zdravljenje po kirurškem posegu, je indicirano za zdravljenje odraslih z lokalno napredovalim trojno negativnim rakom dojk ali trojno negativnim rakom dojk v zgodnjem stadiju z visokim tveganjem za ponovitev bolezni; v kombinaciji s kemoterapijo je indicirano za zdravljenje lokalno ponovljenega neoperabilnega ali metastatskega trojno negativnega raka dojk pri odraslih, ki imajo tumorje z izraženostjo PD-L1 s CPS ≥ 10 in predhodno niso prejeli kemoterapije za metastatsko bolezen; v kombinaciji s karboplatinom in paklitakselom je indicirano za prvo linijo zdravljenja primarno napredovalega ali ponovljenega raka endometrija (EC) pri odraslih, ki so kandidati za sistemsko zdravljenje; v kombinaciji z lenvatinibom je indicirano za zdravljenje napredovalega ali ponovljenega raka endometrija pri odraslih z napredovalo boleznijo med ali po predhodnem zdravljenju s kemoterapijo, ki je vključevala platino, v katerih koli terapevtskih okoliščinah, in ki niso kandidati za kurativno operacijo ali obsevanje; v kombinaciji s kemoradioterapijo (zdravljenje z zunanjim obsevanjem, ki mu sledi brahiterapija) je indicirano za zdravljenje lokalno napredovalega raka materničnega vratu v stadiju III - IVA po FIGO 2014 pri odraslih, ki niso prejeli predhodne definitivne terapije; v kombinaciji s kemoterapijo, z bevacizumabom ali brez njega, je indicirano za zdravljenje persistentnega, ponovljenega ali metastatskega raka materničnega vratu pri odraslih bolnicah, ki imajo tumorje z izraženostjo PD-L1 s CPS ≥ 1; v kombinaciji s trastuzumabom, fluoropirimidinom in kemoterapijo, ki vključuje platino, je indicirano za prvo linijo zdravljenja lokalno napredovalega neoperabilnega ali metastatskega HER2-pozitivnega adenokarcinoma želodca ali gastroezofagealnega prehoda pri odraslih, ki imajo tumorje z izraženostjo PD-L1 s CPS ≥ 1; v kombinaciji s fluoropirimidinom in kemoterapijo, ki vključuje platino, je indicirano za prvo linijo zdravljenja lokalno napredovalega neoperabilnega ali metastatskega HER2-negativnega adenokarcinoma želodca ali gastroezofagealnega prehoda pri odraslih, ki imajo tumorje z izraženostjo PD-L1 s CPS ≥ 1; v kombinaciji z gemcitabinom in cisplatinom je indicirano za prvo linijo zdravljenja lokalno napredovalega neoperabilnega ali metastatskega raka biliarnega trakta pri odraslih. • **Odmerjanje in način uporabe:** Testiranje PD-L1: Če je navedeno v indikaciji, je treba izbiro bolnika za zdravljenje z zdravilom KEYTRUDA na podlagi izraženosti PD-L1 tumorja potrditi z validirano preiskavo. Testiranje MSI/MMR: Če je navedeno v indikaciji, je treba izbiro bolnika za zdravljenje z zdravilom KEYTRUDA na podlagi MSI-H/dMMR statusa tumorja potrditi z validirano preiskavo. Odmerjanje: Priporočeni odmerek zdravila KEYTRUDA pri odraslih je bodisi 200 mg na 3 tedne ali 400 mg na 6 tednov, apliciran z intravensko infuzijo v 30 minutah. Priporočeni odmerek zdravila KEYTRUDA za samostojno zdravljenje pri pediatričnih bolnikih s cHL, starih 3 leta ali več, ali bolnikih z melanomom, starih 12 let ali več, je 2 mg/kg telesne mase (do največ 200 mg) na 3 tedne, apliciran z intravensko infuzijo v 30 minutah. Za uporabo v kombinaciji glejte povzetke glavnih značilnosti zdravil sočasno uporabljenih zdravil. Če se zdravilo KEYTRUDA uporablja kot del kombiniranega zdravljenja skupaj z intravensko kemoterapijo, je treba zdravilo KEYTRUDA aplicirati prvo. Če se zdravilo KEYTRUDA uporablja kot del kombiniranega zdravljenja skupaj z enfortumab vedotinom, je treba zdravilo KEYTRUDA aplicirati po enfortumab vedotinu, kadar sta uporabljena na isti dan. Bolnike je treba zdraviti do napredovanja bolezni ali nesprejemljivih toksičnih učinkov (in do maksimalnega trajanja zdravljenja, če je le to določeno za indikacijo). Pri adjuvantnem zdravljenju melanoma, NSCLC ali RCC je treba zdravilo uporabljati do ponovitve bolezni, pojava nesprejemljivih toksičnih učinkov oziroma mora zdravljenje trajati do enega leta. Za neoadjuvantno in adjuvantno zdravljenje operabilnega NSCLC morajo bolniki neoadjuvantno prejeti zdravilo KEYTRUDA v kombinaciji s kemoterapijo, in sicer 4 odmerke po 200 mg na 3 tedne ali 2 odmerka po 400 mg na 6 tednov ali do napredovanja bolezni, ki izključuje definitivni kirurški poseg, ali do pojava nesprejemljivih toksičnih učinkov, čemur sledi adjuvantno zdravljenje z zdravilom KEYTRUDA kot samostojnim zdravljenjem, in sicer 13 odmerkov po 200 mg na 3 tedne ali 7 odmerkov po 400 mg na 6 tednov ali do ponovitve bolezni ali do pojava nesprejemljivih toksičnih učinkov. Bolniki, pri katerih pride do napredovanja bolezni, ki izključuje definitivni kirurški poseg, ali do nesprejemljivih toksičnih učinkov, povezanih z zdravilom KEYTRUDA kot neoadjuvantnim zdravljenjem v kombinaciji s kemoterapijo, ne smejo prejeti zdravila KEYTRUDA kot samostojnega zdravljenja za adjuvantno zdravljenje. Za neoadjuvantno in adjuvantno zdravljenje TNBC morajo bolniki neoadjuvantno prejeti zdravilo KEYTRUDA v kombinaciji s kemoterapijo, in sicer 8 odmerkov po 200 mg na 3 tedne ali 4 odmerke po 400 mg na 6 tednov, ali do napredovanja bolezni, ki izključuje definitivni kirurški poseg, ali do pojava nesprejemljivih toksičnih učinkov, čemur sledi adjuvantno zdravljenje z zdravilom KEYTRUDA kot samostojnim zdravljenjem, in sicer 9 odmerkov po 200 mg na 3 tedne ali 5 odmerkov po 400 mg na 6 tednov ali do ponovitve bolezni ali pojava nesprejemljivih toksičnih učinkov. Bolniki, pri katerih pride do napredovanja bolezni, ki izključuje definitivni kirurški poseg, ali do nesprejemljivih toksičnih učinkov povezanih z zdravilom KEYTRUDA kot neoadjuvantnim zdravljenjem v kombinaciji s kemoterapijo, ne smejo prejeti zdravila KEYTRUDA kot samostojnega zdravljenja za adjuvantno zdravljenje. Za lokalno napredovalega raka materničnega vratu morajo bolnice prejeti zdravilo KEYTRUDA sočasno s kemoradioterapijo, čemur sledi samostojno zdravljenje z zdravilom KEYTRUDA. Zdravilo KEYTRUDA se lahko daje v odmerku 200 mg na 3 tedne ali 400 mg na 6 tednov do napredovanja bolezni, pojava nesprejemljivih toksičnih učinkov ali do 24 mesecev. Če je aksitinib uporabljen v kombinaciji s pembrolizumabom, se lahko razmisli o povečanju odmerka aksitiniba nad začetnih 5 mg v presledkih šest tednov ali več. V primeru uporabe v kombinaciji z lenvatinibom je treba zdravljenje z enim ali obema zdraviloma prekiniti, kot je primerno. Uporabo lenvatiniba je treba zadržati, odmerek zmanjšati ali prenehati z uporabo, v skladu z navodili v povzetku glavnih značilnosti zdravila za lenvatinib, in sicer za kombinacijo s pembrolizumabom. Pri bolnikih starih ≥ 65 let, bolnikih z blago do zmerno okvaro ledvic, bolnikih z blago ali zmerno okvaro jeter prilagoditev odmerka ni potrebna. Odložitev odmerka ali ukinitev zdravljenja: Zmanjšanje odmerka zdravila KEYTRUDA ni priporočljivo. Za obvladovanje neželenih učinkov je treba uporabo zdravila KEYTRUDA zadržati ali ukiniti, prosimo, glejte celoten Povzetek glavnih značilnosti zdravila. • **Kontraindikacije:** Preobčutljivost na učinkovino ali katero koli pomožno snov. • **Povzetek posebnih opozoril, previdnostnih ukrepov, interakcij in neželenih učinkov:** Imunsko pogojeni neželeni učinki (pnevmonitis, kolitis, hepatitis, nefritis, endokrinopatije, neželeni učinki na kožo in drugi): Pri bolnikih, ki so prejemali pembrolizumab, so se pojavili imunsko pogojeni neželeni učinki, vključno s hudimi in smrtnimi primeri. Večina imunsko pogojenih neželenih učinkov, ki so se pojavili med zdravljenjem s pembrolizumabom, je bila reverzibilnih in so jih obvladali s prekinitvami uporabe pembrolizumaba, uporabo kortikosteroidov in/ali podporno oskrbo. Pojavijo se lahko tudi po zadnjem odmerku pembrolizumaba in hkrati prizadanejo več organskih sistemov. V primeru suma na imunsko pogojene neželene učinke je treba poskrbeti za ustrezno oceno za potrditev etiologije oziroma izključitev drugih vzrokov. Glede na izrazitost neželenega učinka je treba zadržati uporabo pembrolizumaba in uporabiti kortikosteroide – za natančna navodila, prosimo, glejte Povzetek glavnih značilnosti zdravila Keytruda. Zdravljenje s pembrolizumabom lahko poveča tveganje za zavrnitev pri prejemnikih presadkov čvrstih organov. Pri bolnikih, ki so prejemali pembrolizumab, so poročali o hudih z infuzijo povezanih reakcijah, vključno s preobčutljivostjo in anafilaksijo. Pembrolizumab se iz obtoka odstrani s katabolizmom, zato presnovnih medsebojnih delovanj zdravil ni pričakovati. Uporabi sistemskih kortikosteroidov ali imunosupresivov pred uvedbo pembrolizumaba se je treba izogibati, ker lahko vplivajo na farmakodinamično aktivnost in učinkovitost pembrolizumaba. Vendar pa je kortikosteroide ali druge imunosupresive mogoče uporabiti za zdravljenje imunsko pogojenih neželenih učinkov. Kortikosteroide je mogoče uporabiti tudi kot premedikacijo, če je pembrolizumab uporabljen v kombinaciji s kemoterapijo, kot antiemetično profilakso in/ali za ublažitev neželenih učinkov, povezanih s kemoterapijo. Ženske v rodni dobi morajo med zdravljenjem s pembrolizumabom in vsaj še 4 mesece po zadnjem odmerku pembrolizumaba uporabljati učinkovito kontracepcijo, med nosečnostjo in dojenjem se ga ne sme uporabljati. Varnost pembrolizumaba pri samostojnem zdravljenju so v kliničnih študijah ocenili pri 7631 bolnikih, ki so imeli različne vrste raka, s štirimi odmerki (2 mg/kg telesne mase na 3 tedne, 200 mg na 3 tedne in 10 mg/kg telesne mase na 2 ali 3 tedne). V tej populaciji bolnikov je mediani čas opazovanja znašal 8,5 meseca (v razponu od 1 dneva do 39 mesecev), najpogostejši neželeni učinki zdravljenja s pembrolizumabom pa so bili utrujenost (31 %), diareja (22 %) in navzea (20 %). Večina poročanih neželenih učinkov pri samostojnem zdravljenju je bila po izrazitosti 1. ali 2. stopnje. Najresnejši neželeni učinki so bili imunsko pogojeni neželeni učinki in hude z infuzijo povezane reakcije. Pojavnost imunsko pogojenih neželenih učinkov pri uporabi pembrolizumaba samega za adjuvantno zdravljenje je znašala 37 % za vse stopnje in 9 % od 3. do 5. stopnje, pri metastatski bolezni pa 25 % za vse stopnje in 6 % od 3. do 5. stopnje. Pri adjuvantnem zdravljenju niso zaznali nobenih novih imunsko pogojenih neželenih učinkov. Varnost pembrolizumaba pri kombiniranem zdravljenju s kemoterapijo ali CRT so ocenili pri 6334 bolnikih z različnimi vrstami raka, ki so v kliničnih študijah prejemali pembrolizumab v odmerkih 200 mg, 2 mg/kg telesne mase ali 10 mg/kg telesne mase na vsake 3 tedne. V tej populaciji bolnikov so bili najpogostejši neželeni učinki naslednji: navzea (52 %), anemija (51 %), utrujenost (36 %), diareja (35 %), zaprtost (32 %), bruhanje (28 %), zmanjšano število nevtrofilcev (27 %) in zmanjšanje apetita (27 %). Pojavnost neželenih učinkov 3. do 5. stopnje je pri bolnikih z NSCLC pri kombiniranem zdravljenju s pembrolizumabom znašala 69 % in pri zdravljenju samo s kemoterapijo 61 %, pri bolnikih s HNSCC pri kombiniranem zdravljenju s pembrolizumabom 85 % in pri zdravljenju s kemoterapijo v kombinaciji s cetuksimabom 84 %, pri bolnikih z rakom požiralnika pri kombiniranem zdravljenju s pembrolizumabom 86 % in pri zdravljenju samo s kemoterapijo 83 %, pri bolnikih s TNBC pri kombiniranem zdravljenju s pembrolizumabom 80 % in pri zdravljenju samo s kemoterapijo 77 %, pri bolnicah z rakom materničnega vratu pri kombiniranem zdravljenju s pembrolizumabom (kemoterapija z ali brez bevacizumaba ali v kombinaciji s CRT) 77 % in pri zdravljenju s kemoterapijo z ali brez bevacizumaba ali samostojno s CRT 71 %, pri bolnikih z rakom želodca pri kombiniranem zdravljenju s pembrolizumabom (kemoterapija z ali brez trastuzumaba) 74 % in pri kemoterapiji v kombinaciji z ali brez trastuzumaba 68 %, pri bolnikih z rakom biliarnega trakta pri kombiniranem zdravljenju s pembrolizumabom 85 % in pri samostojni kemoterapiji 84 %, pri bolnicah z EC pri kombiniranem zdravljenju s pembrolizumabom 59 % in pri samostojni kemoterapiji 46 %, in pri bolnikih z malignim mezoteliomom plevre pri kombiniranem zdravljenju s pembrolizumabom 44 % in pri samostojni kemoterapiji 30 %. Varnost pembrolizumaba v kombinaciji z aksitinibom ali lenvatinibom pri napredovalem RCC in v kombinaciji z lenvatinibom pri napredovalem EC so ocenili pri skupno 1456 bolnikih z napredovalim RCC ali napredovalim EC, ki so v kliničnih študijah prejemali 200 mg pembrolizumaba na 3 tedne skupaj s 5 mg aksitiniba dvakrat na dan ali z 20 mg lenvatiniba enkrat na dan, kot je bilo ustrezno. V teh populacijah bolnikov so bili najpogostejši neželeni učinki diareja (58 %), hipertenzija (54 %), hipotiroidizem (46 %), utrujenost (41 %), zmanjšan apetit (40 %), navzea (40 %), artralgija (30 %), bruhanje (28 %), zmanjšanje telesne mase (28 %), disfonija (28 %), bolečine v trebuhu (28 %), proteinurija (27 %), sindrom palmarno-plantarne eritrodizestezije (26 %), izpuščaj (26 %), stomatitis (25 %), zaprtost (25 %), mišično-skeletna bolečina (23 %), glavobol (23 %) in kašelj (21 %). Neželenih učinkov od 3. do 5. stopnje je bilo pri bolnikih z RCC med uporabo pembrolizumaba v kombinaciji z aksitinibom ali lenvatinibom 80 % in med uporabo sunitiniba samega 71 %. Pri bolnicah z EC je bilo neželenih učinkov od 3. do 5. stopnje med uporabo pembrolizumaba v kombinaciji z lenvatinibom 89 % in med uporabo kemoterapije same 73 %. Varnost pembrolizumaba v kombinaciji z enfortumab vedotinom so ocenili pri 564 bolnikih z neoperabilnim ali metastatskim urotelijskim rakom, ki so prejemali 200 mg pembrolizumaba 1. dan in 1,25 mg/kg enfortumab vedotina 1. in 8. dan vsakega 21-dnevnega ciklusa. Na splošno so opazili, da je bila pojavnost neželenih učinkov za pembrolizumab v kombinaciji z enfortumab vedotinom višja kot pri samostojnem zdravljenju s pembrolizumabom, kar odraža prispevek enfortumab vedotina in daljšega trajanja kombiniranega zdravljenja. Neželeni učinki so bili na splošno podobni neželenim učinkom, ki so jih opazili pri bolnikih, ki so prejemali pembrolizumab ali enfortumab vedotin kot samostojno zdravljenje. Pojavnost makulopapuloznega izpuščaja vseh stopenj je bila 36 % (10 % od 3. do 4. stopnje), kar je višje, kot je bilo opaženo pri samostojnem zdravljenju s pembrolizumabom. Na splošno so bile pogostnosti neželenih učinkov višje pri bolnikih, starih ≥ 65 let, v primerjavi z bolniki, starimi < 65 let, predvsem za resne neželene učinke (56,3 % pri bolnikih, starih ≥ 65 let, in 35,3 % pri bolnikih, starih < 65 let) in učinke ≥ 3. stopnje (80,3 % pri bolnikih, starih ≥ 65 let, in 64,2 % pri bolnikih, starih < 65 let), podobno kot opažanja pri primerjalni kemoterapiji. Za celoten seznam neželenih učinkov, prosimo, glejte celoten Povzetek glavnih značilnosti zdravila. Za dodatne informacije o varnosti v primeru uporabe pembrolizumaba v kombinaciji glejte povzetke glavnih značilnosti zdravila za posamezne komponente kombiniranega zdravljenja. • **Način in režim izdaje zdravila:** H – Predpisovanje in izdaja zdravila je le na recept, zdravilo se uporablja samo v bolnišnicah. • **Imetnik dovoljenja za promet z zdravilom:** Merck Sharp & Dohme B.V. , Waarderweg 39, 2031 BN Haarlem, Nizozemska.

MSD
Merck Sharp & Dohme inovativna zdravila d.o.o.
Ameriška ulica 2, 1000 Ljubljana; tel: +386 1/ 520 42 01, fax: +386 1/ 520 43 50

Samo za strokovno javnost | H - Predpisovanje in izdaja zdravila je le na recept, zdravilo pa se uporablja samo v bolnišnicah. Pred predpisovanjem, prosimo, preberite celoten Povzetek glavnih značilnosti zdravila Keytruda, ki je na voljo pri naših strokovnih sodelavcih ali na lokalnem sedežu družbe.

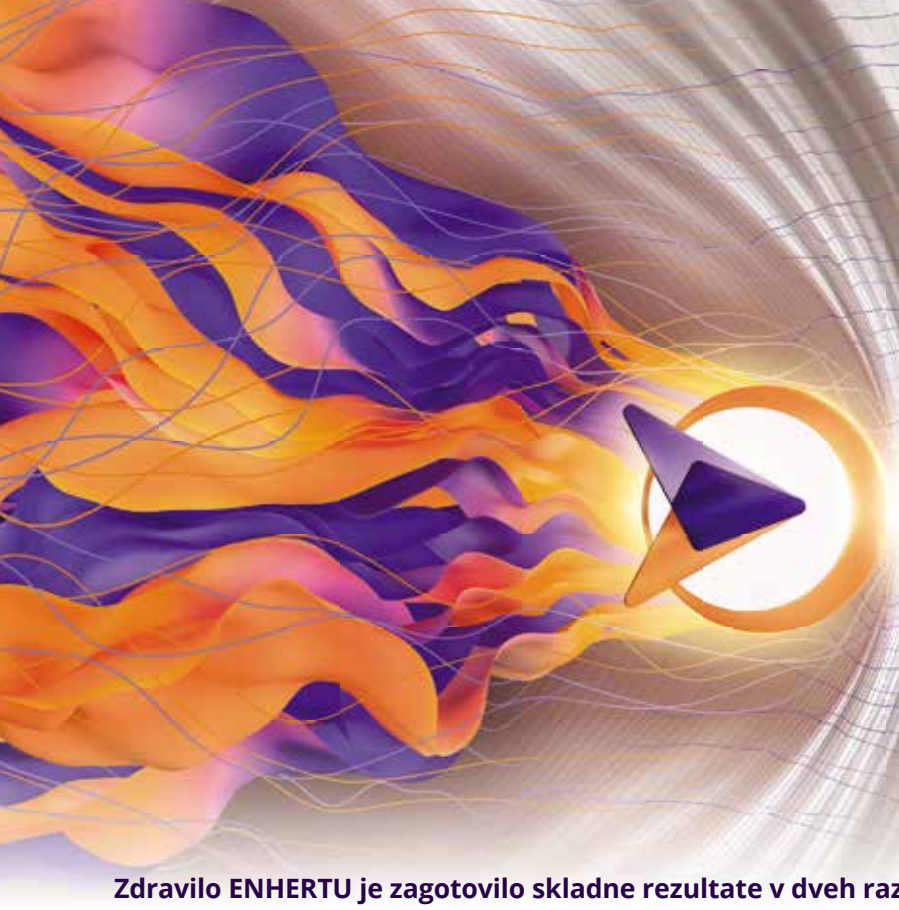

ENHERTU®
trastuzumab derukstekan

PRVO IN EDINO ZDRAVLJENJE, USMERJENO V HER2 Z DOKAZANIM IZBOLJŠANJEM CELOKUPNEGA PREŽIVETJA PRI BOLNIKIH V 2L+ ZDRAVLJENJA, V PRIMERJAVI S KEMOTERAPIJO.[1-3]

PREMIKAMO MEJE ZDRAVLJENJA

Smernice vključujejo zdravilo ENHERTU kot terapevtsko možnost za 2L HER2+ napredovalega adenokarcinoma želodca in gastroezofagealnega prehoda.[4]

Zdravilo ENHERTU je zagotovilo skladne rezultate v dveh različnih kliničnih preskušanjih pri predhodno zdravljenih bolnikih z napredovalim adenokarcinomom želodca ali gastroezofagealnega prehoda[1, 5, 6]

DESTINY-Gastric01

42,9-% **potrjena ORR z zdravilom ENHERTU**
(n = 51/119; 95-% IZ: 33,8; 52,3)

v primerjavi z
P < 0,0001

12,5-% **potrjena ORR** z irinotekanom ali paklitakselom
(n = 7/56; 95-% IZ: 5,2; 24,1)

12,5 **meseca mOS z zdravilom ENHERTU**
(n = 125; 95-% IZ: 9,6; 14,3)

v primerjavi z
P < 0,01
HR = 0,59 (95-% IZ: 0,39; 0,88)

8,4 **meseca** z irinotekanom ali paklitakselom
(n = 62; 95-% IZ: 6,9; 10,7)

DESTINY-Gastric02

41,8-% **potrjena ORR z zdravilom ENHERTU**
(n = 33/79; 95-% IZ: 30,8; 53,4)

12,1 **meseca mOS z zdravilom ENHERTU**
(n = 79; 95-% IZ: 9,4; 15,4)

DESTINY-Gastric01: multicentrično, odprto, randomizirano preskušanje 2. faze na Japonskem/v Južni Koreji pri 188 odraslih bolnikih s HER2+ lokalno napredovalim ali metastatskim adenokarcinomom želodca ali GEJ, pri katerih je bolezen napredovala pri ≥ 2 predhodnih shemah, vključno s trastuzumabom ter kemoterapevtsko shemo s fluoropirimidinom in platino. Bolniki v skupini z zdravilom ENHERTU so prejemali 6,4 mg/kg i.v. enkrat vsake 3 tedne do napredovanja bolezni, smrti, umika privolitve ali nesprejemljive toksičnosti. Merilo primarnega izida učinkovitosti je bila ORR po oceni ICR na podlagi meril RECIST v1.1. Ključni sekundarni opazovani dogodek je bilo OS. Dodatna merila sekundarnega izida so bili PFS, DOR, potrjena ORR in varnost.[1]

DESTINY-Gastric02: multicentrično, odprto preskušanje 2. faze z eno skupino v Evropi/ZDA pri 79 odraslih bolnikih s HER2+ lokalno napredovalim ali metastatskim adenokarcinomom želodca ali GEJ, pri katerih je bolezen napredovala pri predhodni shemi na osnovi HER2 ali po njej. Bolniki so prejemali zdravilo ENHERTU 6,4 mg/kg i.v. enkrat vsake 3 tedne do nesprejemljive toksičnosti ali napredovanja bolezni. Merilo primarnega izida učinkovitosti je bila potrjena ORR po oceni ICR na podlagi meril RECIST v1.1. Sekundarni opazovani dogodki so bili DOR, PFS, OS, varnost in izidi po navedbah bolnikov.[5-7]

Primerjav med preskušanji ni mogoče opraviti. Pomembno je upoštevati, da sta se študiji razlikovali po zasnovi preskušanja, populaciji bolnikov in trajanju spremljanja.

ORR, objektivna stopnja odziva; **OS**, celokupno preživetje; **mOS**, mediana celokupnega preživetja; **PFS**, preživetje brez napredovanja bolezni; **DOR**, trajanje odziva; **RECIST**, merila za vrednotenje odziva pri solidnih tumorjih; **ICR**, neodvisni centralni pregled; **GEJ**, gastroezofagealni prehod; **HR**, razmerje ogroženosti; **IZ**, interval zaupanja

Indikacija
Zdravilo ENHERTU je indicirano za zdravljenje odraslih bolnikov z lokalno napredovalim ali metastatskim HER2-pozitivnim adenokarcinomom želodca ali gastroezofagealnega prehoda (GEJ), ki so pred tem že prejeli shemo na podlagi trastuzumaba.

Literatura: 1. Shitara K, Bang YJ, Iwasa S, et al. Trastuzumab deruxtecan in previously treated HER2-positive gastric cancer. N Engl J Med. 2020;382(25):2419-2430. doi:10.1056/NEJMoa2004413 **2.** Curea FG, Hebbar M, Ilie SM, et al. Current targeted therapies in HER2-positive gastric adenocarcinoma. Cancer Biother Radiopharm. 2017;32(10):351-363. doi:10.1089/cbr.2017.2249 **3.** Zhao D, Klempner SJ, Chao J. Progress and challenges in HER2-positive gastroesophageal adenocarcinoma. J Hematol Oncol. 2019;12(1):50. doi:10.1186/s13045-019-0737-2 **4.** Lordick F, Carneiro F, Cascinu S, et al; on behalf of the ESMO Guidelines Committee. Gastric cancer: ESMO Clinical Practice Guideline for diagnosis, treatment and follow-up. Ann Oncol. 2022;33(10):1005-1020. **5.** Ku G, di Bartolomeo M, Smyth E, et al. Updated analysis of DESTINY-Gastric02: a Phase 2 single-arm trial of trastuzumab deruxtecan (T-DXd) in western patients with HER2-positive unresectable/metastatic gastric/gastroesophageal junction (GEJ) cancer who progressed on or after trastuzumab-containing regimen. Predstavljeno na: letnem srečanju ESMO 2022; 9.–13. september 2022; Pariz, Francija. **6.** Povzetek glavnih značilnosti zdravila Enhertu, marec 2025. **7.** DS-8201a in HER2-positive gastric cancer that cannot be surgically removed or has spread (DESTINY-Gastric02). Identifikator na ClinicalTrials.gov: NCT04014075. Dostopno na: https://clinicaltrials.gov/ct2/show/record/NCT04014075.

SKRAJŠAN POVZETEK GLAVNIH ZNAČILNOSTI ZDRAVILA

▼Za to zdravilo se izvaja dodatno spremljanje varnosti. Tako bodo hitreje na voljo nove informacije o njegovi varnosti. Zdravstvene delavce naprošamo, da poročajo o katerem koli domnevnem neželenem učinku zdravila.

ENHERTU 100 mg prašek za koncentrat za raztopino za infundiranje

SESTAVA: Ena viala praška za koncentrat za raztopino za infundiranje vsebuje 100 mg trastuzumab derukstekana. Po rekonstituciji ena viala s 5 ml raztopine vsebuje 20 mg/ml trastuzumab derukstekana. Trastuzumab derukstekan je konjugat protitelesa in zdravila, ki vsebuje humanizirano monoklonsko protitelo IgG1 proti HER2 z istim zaporedjem aminokislin, kot ga ima trastuzumab. Proizvajajo ga sesalske celice (ovarij kitajskega hrčka) in je prek razcepljivega veznika na tetrapeptidni bazi kovalentno vezan na DXd, ki je derivat eksatekana in zaviralec topoizomeraze I. Na vsako molekulo protitelesa je vezanih približno 8 molekul derukstekana. *Pomožne snovi*: L-histidin, L-histidinijev klorid monohidrat, saharoza, polisorbat 80 (E433). **TERAPEVTSKE INDIKACIJE:** ***Rak dojk:*** *HER2-pozitiven rak dojk:* Zdravilo Enhertu kot monoterapija je indicirano za zdravljenje odraslih bolnikov z neresektabilnim ali metastatskim HER2-pozitivnim rakom dojk, ki so pred tem že prejeli eno ali več shem zdravljenja na podlagi anti-HER2. *Rak dojk z nizkim statusom HER2 in zelo nizkim statusom HER2:* Zdravilo Enhertu kot monoterapija je indicirano za zdravljenje odraslih bolnikov z neresektabilnim ali metastatskim rakom dojk, pozitivnim na hormonske receptorje, z nizkim statusom HER2 ali zelo nizkim statusom HER2, ki so pred tem prejeli vsaj eno endokrino terapijo v prisotnosti metastaz in ki ne veljajo za primerne za endokrino terapijo kot naslednjo linijo zdravljenja ter rakom dojk z nizkim statusom HER2, ki so pred tem že prejeli kemoterapijo v prisotnosti metastaz ali pa se je pri njih bolezen ponovila med adjuvantno kemoterapijo ali znotraj 6 mesecev po njenem zaključku. ***Nedrobnocelični rak pljuč*** (NSCLC - non-small cell lung cancer): Zdravilo Enhertu kot monoterapija je indicirano za zdravljenje odraslih bolnikov z napredovalim NSCLC, ki imajo tumorje z aktivirajočo mutacijo HER2 (ERBB2) in potrebujejo sistemsko terapijo po kemoterapiji na podlagi platine z imunoterapijo ali brez nje. ***Rak želodca:*** Zdravilo Enhertu v obliki monoterapije je indicirano za zdravljenje odraslih bolnikov z napredovalim HER2-pozitivnim adenokarcinomom želodca ali gastroezofagealnega prehoda, ki so pred tem že prejeli shemo na podlagi trastuzumaba. **ODMERJANJE IN NAČIN UPORABE:** Zdravilo Enhertu mora predpisati zdravnik in njegovo dajanje nadzorovati zdravstveni delavec, ki sta izkušena v uporabi zdravil proti raku. Za preprečitev napak, povezanih z zdravili, je pomembno, da preverite nalepke na vialah in se prepričate, da je zdravilo, ki se pripravlja in daje, res zdravilo Enhertu (trastuzumab derukstekan), in ne trastuzumab ali trastuzumab emtanzin. Zdravilo Enhertu se ne sme zamenjati s trastuzumabom ali trastuzumab emtanzinom. Bolniki, ki se zdravijo s trastuzumab derukstekanom zaradi *HER2-pozitivnega raka dojk, raka želodca ali gastroezofagealnega prehoda*, morajo imeti dokumentiran HER2pozitiven status tumorja, ki je opredeljen kot ocena 3 + na podlagi imunohistokemije (IHC) ali razmerje ≥ 2,0 na podlagi *in situ* hibridizacije (ISH) ali fluorescenčne *in situ* hibridizacije (FISH), ocenjeno z *in vitro* diagnostičnim (IVD) medicinskim pripomočkom z oznako CE. Bolniki, ki se zdravijo s trastuzumab derukstekanom zaradi *raka dojk z nizkim in zelo nizkim statusom HER2*, morajo imeti dokumentiran nizek status HER2 tumorja, ki je opredeljen kot ocena IHC 1+ ali IHC 2+/ISH-, ali zelo nizek status HER2, opisan kot IHC 0 z obarvanjem membrane (IHC >0<1+) ocenjen z IVD z oznako CE. Bolniki, ki se zdravijo s trastuzumab derukstekanom zaradi napredovalega NSCLC, morajo imeti aktivirajočo mutacijo HER2 (ERBB2), odkrito z *in vitro* diagnostičnim (IVD) medicinskim pripomočkom, označenim s CE. Če IVD z oznako CE ni na voljo, je treba status HER2 in status mutacije HER2 oceniti z drugim potrjenim testom. Odmerjanje: *Rak dojk in NSCLC:* Priporočeni odmerek zdravila Enhertu je 5,4 mg/kg, ki se daje z intravensko infuzijo enkrat vsake 3 tedne (21-dnevni cikel) do napredovanja bolezni ali nesprejemljive toksičnosti. *Rak želodca:* Priporočeni odmerek zdravila Enhertu je 6,4 mg/kg, ki se daje z intravensko infuzijo enkrat vsake 3 tedne (21-dnevni cikel) do napredovanja bolezni ali nesprejemljive toksičnosti. Začetni odmerek je treba dati z 90-minutno intravensko infuzijo. Če bolnik prejšnjo infuzijo dobro prenaša, se lahko naslednji odmerki zdravila Enhertu dajejo kot 30-minutne infuzije. Hitrost infundiranja zdravila Enhertu je treba zmanjšati ali infundiranje prekiniti, če se pri bolniku razvijejo simptomi, povezani z infuzijo. V primeru hudih reakcij na infuzijo je treba zdravilo Enhertu trajno ukiniti. Premedikacija: Zdravilo Enhertu je emetogeno, kar vključuje zapoznelo navzeo in/ali bruhanje. Pred vsakim odmerkom zdravila Enhertu je treba bolnike premedicirati s kombiniranim režimom dveh ali treh zdravil (npr. deksametazon z antagonistom receptorjev 5-HT3 in/ali antagonistom receptorjev NK1 ter drugimi zdravili, kot je indicirano) za preprečevanje navzee in bruhanja zaradi kemoterapije. Prilagajanje odmerka: Obvladovanje neželenih učinkov lahko zajema začasno prekinitev uporabe, zmanjšanje odmerka ali ukinitev zdravljenja z zdravilom Enhertu, skladno s smernicami, podanimi v povzetku glavnih značilnosti zdravila (preglednici 1 in 2). Po zmanjšanju odmerka zdravila Enhertu se odmerek ne sme več ponovno povečati. Načrt zmanjševanja odmerka: Priporočeni začetni odmerek je 5,4 mg/kg pri raku dojk in NSCLC oz. 6,4 mg/kg pri raku želodca; prvo zmanjšanje odmerka (4,4 mg/kg oz. 5,4 mg/kg), drugo zmanjšanje odmerka (3,2 mg/kg oz. 4,4 mg/kg), pri potrebi po nadaljnjem zmanjšanju odmerka ukinite zdravljenje. *Prosimo, glejte celoten povzetek glavnih značilnosti zdravila Enhertu za prilagajanje odmerka zaradi neželenih učinkov: intersticijska pljučna bolezen (IPB)/pnevmonitis* (asimptomatska IPB/asimptomatski pnevmonitis (stopnja 1), simptomatska IPB/simptomatski pnevmonitis (stopnja 2 ali višja)), *nevtropenija* (stopnja 3 (manj kot 1,0-0,5 × 10^9/l), stopnja 4 (manj kot 0,5 × 10^9/l)), *febrilna nevtropenija* (absolutno število nevtrofilcev manj kot 1,0 × 10^9/l in telesna temperatura, višja od 38,3 °C, ali telesna temperatura 38 °C ali višja, ki vztraja več kot eno uro), *zmanjšan iztisni delež levega prekata* (LVEF) (LVEF več kot 45 % in absolutno zmanjšanje glede na izhodiščno vrednost za 10 % do 20 %; LVEF 40 % do 45 %; LVEF manj kot 40 % ali absolutno zmanjšanje glede na izhodiščno vrednost za več kot 20 %; simptomatično kongestivno srčno popuščanje). Zakasnjen ali izpuščen odmerek: Če se načrtovani odmerek zakasni ali izpusti, ga je treba dati takoj, ko je mogoče, brez čakanja na naslednji načrtovani cikel. Časovni načrt dajanja je treba prilagoditi, da se ohrani 3-tedenski razmik med odmerki. Infuzijo je treba dati s hitrostjo in odmerkom, ki ga je bolnik prenašal pri zadnji infuziji. Posebne populacije: *Starejši:* Pri bolnikih, starih 65 let ali starejših, prilagajanje odmerka zdravila Enhertu ni potrebno. Podatki pri bolnikih, starih ≥ 75 let, so omejeni. *Okvara ledvic:* Prilagajanje odmerka pri bolnikih z blago (očistek kreatinina [CLcr] ≥ 60 in < 90 ml/min) ali zmerno (CLcr ≥ 30 in < 60 ml/min) okvaro ledvic ni potrebno. Morebitne potrebe po prilagajanju odmerka pri bolnikih s hudo okvaro ledvic ali končno ledvično odpovedjo ni mogoče opredeliti, ker je bila huda okvara ledvic v kliničnih študijah izključitveni kriterij. Pri bolnikih z zmerno okvaro ledvic so opazili višjo pogostnost IPB stopnje 1 in 2/pnevmonitisa, ki sta vodila do zvečanja števila prekinitev zdravljenja. Pri bolnikih z zmerno okvaro ledvic v izhodišču, ki so prejemali zdravilo Enhertu 6,4 mg/kg, so ugotovili večjo pogostnost resnih neželenih učinkov kot pri tistih z normalnim delovanjem ledvic. Bolnike z zmerno ali hudo okvaro ledvic je treba natančno spremljati glede neželenih učinkov, vključno z IPB/pnevmonitisom. *Okvara jeter:* Pri bolnikih, ki imajo celokupni bilirubin ≤ 1,5-kratnik zgornje meje normalnih vrednosti (ZMN), ne glede na vrednost aspartat transaminaze (AST), odmerka ni treba prilagajati. Morebitne potrebe po prilagajanju odmerka pri bolnikih, ki imajo celokupni bilirubin > 1,5-kratnik ZMN, ne glede na vrednost AST, ni mogoče opredeliti zaradi omejenih podatkov. Zato je treba te bolnike natančno spremljati. Način uporabe: Zdravilo Enhertu je za intravensko uporabo. Zdravstveni delavec ga mora rekonstituirati in razredčiti. Treba ga je dati z intravenskim infundiranjem. Zdravilo Enhertu se ne sme dati kot hitro intravensko injekcijo ali bolus. **KONTRAINDIKACIJE:** Preobčutljivost na učinkovino ali katero koli pomožno snov. **POSEBNA OPOZORILA IN PREVIDNOSTNI UKREPI:** Intersticijska pljučna bolezen/pnevmonitis: Pri zdravilu Enhertu so poročali o primerih intersticijske pljučne bolezni (IPB) in/ali pnevmonitisa. Nekateri primeri so bili smrtni. Bolnikom je treba naročiti, naj takoj poročajo o kašlju, dispneji, zvišani telesni temperaturi in/ali katerih koli novih dihalnih simptomih ali poslabšanju obstoječih. Bolnike je treba spremljati glede znakov in simptomov IPB/pnevmonitisa. Dokaze za IPB/pnevmonitis je treba takoj proučiti. Bolnike s sumom na IPB/pnevmonitis je treba oceniti z radiografskimi posnetki, najbolje z računalniško tomografijo (CT). Treba je razmisliti o posvetu s pulmologom. Nevtropenija: V kliničnih študijah z zdravilom Enhertu so poročali o primerih nevtropenije, vključno s primeri febrilne nevtropenije s smrtnim izidom. Pred uvedbo zdravila Enhertu in pred vsakim odmerkom ter vsakič, ko je klinično indicirano, je treba preveriti celotno krvno sliko. Morda bo treba začasno prekiniti dajanje zdravila Enhertu ali zmanjšati odmerek, odvisno od tega, kako huda je nevtropenija. Okvara levega prekata: Pri zdravljenjih anti-HER2 so poročali o zmanjšanem iztisnem deležu levega prekata (LVEF). Pred uvedbo zdravljenja z zdravilom Enhertu in v rednih intervalih med njim (v skladu s kliničnimi indikacijami) je treba izvesti standardne preiskave delovanja srca (ehokardiografija ali slikanje MUGA) za oceno LVEF. Zmanjšanje LVEF je treba obvladovati s prekinitvami zdravljenja. Zdravljenje z zdravilom Enhertu je treba trajno ukiniti, če se potrdi LVEF manj kot 40 % ali absolutno zmanjšanje glede na izhodiščno vrednost za več kot 20 %. Zdravilo Enhertu je treba trajno ukiniti pri bolnikih s simptomatskim kongestivnim srčnim popuščanjem. Embrio-fetalna toksičnost: Zdravilo Enhertu lahko ima škodljiv vpliv na plod, če se da nosečnici. Pri ženskah v rodni dobi je treba pred uvedbo zdravljenja z zdravilom Enhertu preveriti status nosečnosti. Bolnice je treba seznaniti z možnimi tveganji za plod. Ženskam v rodni dobi je treba svetovati, da uporabljajo učinkovito kontracepcijo med zdravljenjem in še vsaj 7 mesecev po zadnjem odmerku zdravila Enhertu. Moškim bolnikom s partnerkami v rodni dobi je treba svetovati, da uporabljajo učinkovito kontracepcijo med zdravljenjem z zdravilom Enhertu in še vsaj 4 mesece po zadnjem odmerku zdravila Enhertu. Bolniki z zmerno ali hudo okvaro jeter: Zdravilo Enhertu je treba pri bolnikih z zmerno in hudo okvaro jeter dajati previdno. **MEDSEBOJNO DELOVANJE Z DRUGIMI ZDRAVILI IN DRUGE OBLIKE INTERAKCIJ:** Pri sočasnem dajanju trastuzumab derukstekana z zdravili, ki so zaviralci CYP3A ali OATP1B ali prenašalcev P-gp, odmerka ni treba prilagajati. **PLODNOST, NOSEČNOST IN DOJENJE:** Nosečnost: Dajanje zdravila Enhertu nosečnicam se ne priporoča. Bolnice je treba seznaniti z možnimi tveganji za plod, preden zanosijo. Ženske, ki zanosijo, se morajo takoj obrniti na zdravnika. Če ženska zanosi med zdravljenjem z zdravilom Enhertu ali v obdobju 7 mesecev po zadnjem odmerku zdravila Enhertu, se priporoča natančno spremljanje. Dojenje: Ni znano, ali se trastuzumab derukstekan izloča v materino mleko. Humani IgG se izloča v materino mleko in potencial za absorpcijo in resne neželene učinke na dojenčka ni znan. Zato ženske ne smejo dojiti med zdravljenjem z zdravilom Enhertu in še 7 mesecev po zadnjem odmerku. Odločiti se je treba med prenehanjem dojenja in prenehanjem zdravljenja z zdravilom Enhertu, pri čemer je treba pretehtati prednosti dojenja za otroka in prednosti zdravljenja za mater. Plodnost: Namenskih študij plodnosti s trastuzumab derukstekanom niso izvedli. Ni znano, ali so trastuzumab derukstekan ali njegovi presnovki prisotni v semenski tekočini. Pred začetkom zdravljenja je treba moškim bolnikom svetovati, da se posvetujejo o možnosti shranjevanja semena. Moški bolniki v celotnem obdobju zdravljenja in še najmanj 4 mesece po zadnjem odmerku zdravila Enhertu ne smejo zamrzniti ali darovati semena. **NEŽELENI UČINKI:** *Zdravilo Enhertu 5,4 mg/kg:* Združeno varnostno populacijo so ocenili pri bolnikih, ki so v kliničnih študijah dobili vsaj en odmerek 5,4 mg/kg zdravila Enhertu (N = 2335) zaradi različnih vrst tumorjev. Mediani čas trajanja zdravljenja v tej združeni populaciji je bil 9,0 meseca (razpon: 0,7-45,1 meseca). *Zelo pogosti:* okužba zgornjih dihal, anemija, nevtropenija, trombocitopenija, levkopenija, hipokaliemija, zmanjšan apetit, glavobol, intersticijska pljučna bolezen, kašelj, navzea, bruhanje, zaprtje, driska, bolečina v trebuhu, stomatitis, dispepsija, zvišane transaminaze, alopecija, mišično-skeletna bolečina, utrujenost, pireksija, zmanjšan iztisni delež, zmanjšanje telesne mase. *Pogosti:* pljučnica, limfopenija, febrilna nevtropenija, pancitopenija, dehidracija, omotica, disgevzija, suhe oči, zamegljen vid, dispneja, epistaksa, abdominalna distenzija, gastritis, flatulenca, izpuščaj, pruritus, hiperpigmentacija kože, perifermni edem, zvišana alkalna fosfataza v krvi, zvišan bilirubin v krvi, zvišan kreatinin v krvi, reakcije, povezane z infuzijo. *Zdravilo Enhertu 6,4 mg/kg:* Združeno varnostno populacijo so ocenili za bolnike, ki so v kliničnih študijah dobili vsaj en odmerek 6,4 mg/kg zdravila Enhertu (N = 669) zaradi različnih vrst tumorjev. Mediani čas trajanja zdravljenja v tej združeni populaciji je bil 5,7 meseca (razpon: 0,7-41,0 meseca). *Zelo pogosti:* pljučnica, okužba zgornjih dihal, anemija, nevtropenija, trombocitopenija, levkopenija, limfopenija, hipokaliemija, zmanjšan apetit, glavobol, disgevzija, intersticijska pljučna bolezen, dispneja, kašelj, navzea, bruhanje, driska, zaprtje, bolečina v trebuhu, stomatitis, zvišane transaminaze, alopecija, mišično-skeletna bolečina, utrujenost, pireksija, perifermni edem, zmanjšan iztisni delež, zmanjšanje telesne mase. *Pogosti:* febrilna nevtropenija, pancitopenija, dehidracija, omotica, suhe oči, zamegljen vid, epistaksa, dispepsija, abdominalna distenzija, gastritis, flatulenca, izpuščaj, pruritus, hiperpigmentacija kože, zvišana alkalna fosfataza v krvi, zvišan bilirubin v krvi, zvišan kreatinin v krvi, reakcije, povezane z infuzijo. **IMETNIK DOVOLJENJA ZA PROMET Z ZDRAVILOM:** Daiichi Sankyo Europe GmbH, Zielstattstrasse 48, 81379 München, Nemčija **DATUM ZADNJE REVIZIJE BESEDILA:** 31. marec 2025 (SI-5034) **REŽIM PREDPISOVANJA IN IZDAJE:** H **Prosimo, da pred predpisovanjem preberete celoten povzetek glavnih značilnosti zdravila.** Dodatne informacije so na voljo pri podjetju AstraZeneca UK Limited, Podružnica v Sloveniji, Verovškova 55, 1000 Ljubljana, telefon: 01/51 35 600.

Informacija pripravljena oktobra 2025. Samo za strokovno javnost. Koda: SI-5406

Daiichi-Sankyo | AstraZeneca

TECENTRIQ®
atezolizumab

Roche

DVE OBLIKI zdravila Tecentriq (atezolizumab):[1]

PODKOŽNA INJEKCIJA:

Tecentriq 1875 mg raztopina za injiciranje

INTRAVENSKA INFUZIJA:

Tecentriq 840 mg koncentrat za raztopino za infundiranje,
Tecentriq 1200 mg koncentrat za raztopino za infundiranje.

Bolniki, ki prejemajo intravensko obliko atezolizumaba, lahko preidejo na zdravilo Tecentriq v obliki raztopine za injiciranje in obratno.[1]

ZDRAVILO TECENTRIQ JE INDICIRANO ZA ZDRAVLJENJE RAZLIČNIH VRST RAKA:[1]

- NEDROBNOCELIČNI RAK PLJUČ
- DROBNOCELIČNI RAK PLJUČ
- TROJNO NEGATIVNI RAK DOJK
- UROTELIJSKI KARCINOM
- HEPATOCELULARNI KARCINOM

Vir: 1. Povzetek glavnih značilnosti zdravila Tecentriq: https://www.ema.europa.eu/sl/documents/product-information/tecentriq-epar-product-information_sl.pdf

Skrajšan povzetek glavnih značilnosti zdravila Tecentriq

Ime zdravila: Tecentriq 840 mg koncentrat za raztopino za infundiranje, Tecentriq 1200 mg koncentrat za raztopino za infundiranje in Tecentriq 1875 mg raztopina za injiciranje. **Kakovostna in količinska sestava:** 840 mg i.v.: ena 14-ml viala s koncentratom vsebuje 840 mg atezolizumaba. 1200 mg i.v.: ena 20-ml viala s koncentratom vsebuje 1200 mg atezolizumaba. Po redčenju je končna koncentracija razredčene raztopine med 3,2 mg/ml in 16,8 mg/ml. 1875 mg s.c.: ena viala s 15 ml raztopine za injiciranje vsebuje 1875 mg atezolizumaba. 1 ml raztopine vsebuje 125 mg atezolizumaba. **Terapevtske indikacije:** Urotelijski karcinom (UC): Zdravilo Tecentriq je kot monoterapija indicirano za zdravljenje odraslih bolnikov z lokalno napredovalim ali razsejanim UC, ki: so bili predhodno zdravljeni s kemoterapijo na osnovi platine ali niso primerni za zdravljenje s cisplatinom in katerih tumorji izražajo PD-L1 v ≥ 5 %. Zgodnji stadij nedrobnoceličnega raka pljuč (NDRP): Zdravilo Tecentriq je kot monoterapija indicirano za adjuvantno zdravljenje po popolni resekciji in kemoterapiji na osnovi platine za odrasle bolnike z NDRP in velikim tveganjem za ponovitev, katerih tumorji izražajo PD-L1 na ≥ 50 % tumorskih celic (TC) in nimajo EGFR mutiranega ali ALK pozitivnega NDRP. Napredovali NDRP: Zdravilo Tecentriq je v kombinaciji z bevacizumabom, paklitakselom in karboplatinom indicirano v prvi liniji zdravljenja odraslih bolnikov z razsejanim neploščatoceličnim NDRP. Pri bolnikih z EGFR mutiranim ali ALK pozitivnim NDRP je zdravilo Tecentriq v kombinaciji z bevacizumabom, paklitakselom in karboplatinom indicirano le, ko so izčrpana ustrezna tarčna zdravljenja. Zdravilo Tecentriq je v kombinaciji z nab-paklitakselom in karboplatinom indicirano v prvi liniji zdravljenja odraslih bolnikov z razsejanim neploščatoceličnim NDRP, ki ni EGFR mutiran ali ALK pozitiven. Zdravilo Tecentriq je kot monoterapija indicirano v prvi liniji zdravljenja odraslih bolnikov z razsejanim NDRP, pri katerih je PD-L1 izražen na ≥ 50 % TC ali ≥ 10 % imunskih celic (IC), ki infiltrirajo tumor, ter nimajo EGFR mutiranega ali ALK pozitivnega NDRP. Zdravilo Tecentriq je kot monoterapija indicirano v prvi liniji zdravljenja odraslih bolnikov z napredovalim NDRP, ki niso primerni za zdravljenje s kemoterapijo na osnovi platine. Zdravilo Tecentriq je kot monoterapija indicirano za zdravljenje odraslih bolnikov z lokalno napredovalim ali razsejanim NDRP, ki so bili predhodno zdravljeni s kemoterapijo. Bolniki z EGFR mutiranim ali ALK pozitivnim NDRP morajo pred uvedbo zdravila Tecentriq prejeti tudi tarčna zdravljenja. Drobnocelični rak pljuč (DRP): Zdravilo Tecentriq je v kombinaciji s karboplatinom in etopozidom indicirano v prvi liniji zdravljenja odraslih bolnikov z razsejanim DRP. Trojno negativni rak dojk (TNRD): Zdravilo Tecentriq je v kombinaciji z nab-paklitakselom indicirano za zdravljenje odraslih bolnikov z inoperabilnim lokalno napredovalim ali razsejanim TNRD, katerih tumorji izražajo PD-L1 v ≥ 1 % in predhodno še niso prejemali kemoterapije zaradi razsejane bolezni. Hepatocelularni karcinom (HCC): Zdravilo Tecentriq je v kombinaciji z bevacizumabom indicirano za zdravljenje odraslih bolnikov z napredovalim ali neresektabilnim HCC, ki predhodno še niso prejemali sistemskega zdravljenja. **Odmerjanje in način uporabe:** Zdravilo Tecentriq morajo uvesti in nadzorovati zdravniki z izkušnjami pri zdravljenju raka. Odmerjanje: 840 mg in 1200 mg i.v.: priporočeni odmerek zdravila Tecentriq je 840 mg, danega intravensko na dva tedna, ali 1200 mg, danega intravensko na tri tedne, ali 1680 mg, danega intravensko na štiri tedne. 1875 mg s.c.: priporočeni odmerek je 1875 mg, dan na tri tedne. Kadar zdravilo Tecentriq dajete v kombinaciji, glejte tudi celotne informacije za predpisovanje zdravil, ki se uporabljajo v kombinaciji. *Prilagoditev odmerka med zdravljenjem:* odmerkov zdravila Tecentriq ni priporočljivo zmanjševati. *Zapoznitev odmerka ali prenehanje uporabe* glede na neželeni učinek je opisano v SmPC. Način uporabe: Pomembno je preveriti nalepke zdravila in se tako prepričati, da bo bolnik dobil pravo obliko zdravila (intravensko ali subkutano), kot je predpisano. Intravenska oblika zdravila Tecentriq ni namenjena za subkutano uporabo in se jo sme injicirati le intravensko. Infuzij se ne sme dajati kot hiter intravenski odmerek ali bolus. Bolniki, ki trenutno prejemajo intravensko obliko zdravila Tecentriq, lahko preidejo na prejemanje atezolizumaba v obliki raztopine za injiciranje ali obratno. Začetni odmerek intravenske oblike zdravila Tecentriq je treba dati v 60 minutah. Če bolnik prvo infuzijo dobro prenese, je mogoče vse nadaljnje infuzije dati v 30 minutah.Zdravilo Tecentriq 1875 mg raztopina za injiciranje ni namenjeno za intravensko uporabo in se ga sme injicirati le subkutano (v približno 7 minutah v stegno). **Kontraindikacije:** Preobčutljivost na atezolizumab ali katero koli pomožno snov. **Posebna opozorila in previdnostni ukrepi:** Sledljivost: Z namenom izboljšanja sledljivosti bioloških zdravil je treba jasno zabeležiti ime in številko serije uporabljenega zdravila. Imunsko pogojeni neželeni učinki: Večina imunsko pogojenih neželenih učinkov, ki so se pojavili med zdravljenjem, je bila po prekinitvi atezolizumaba in uvedbi kortikosteroidov in/ali podpornega zdravljenja reverzibilna. Imunsko pogojeni neželeni učinki, povezani z atezolizumabom, se lahko pojavijo po zadnjem odmerku atezolizumaba. Pri sumu na imunsko pogojene neželene učinke je treba opraviti temeljito oceno za potrditev etiologije oziroma izključitev drugih vzrokov. Glede na izrazitost neželenega učinka je treba uporabo atezolizumaba odložiti in uvesti kortikosteroide. Atezolizumab je treba trajno prenehati uporabljati pri vseh imunsko pogojenih neželenih učinkih 3. stopnje, ki se ponovijo, in pri vseh imunsko pogojenih neželenih učinkih 4. stopnje, z izjemo endokrinopatij, ki jih je mogoče nadzorovati z nadomestnimi hormoni. Podatki iz opazovalnih študij kažejo, da imajo bolniki z obstoječo avtoimunsko boleznijo po zdravljenju z zaviralci imunskih kontrolnih točk lahko povečano tveganje imunsko pogojenih neželenih učinkov v primerjavi z bolniki brez obstoječe avtoimunske bolezni. Bolnike je treba spremljati glede znakov in simptomov pnevmonitisa ter izključiti druge možne vzroke. Bolnike je treba spremljati glede znakov in simptomov hepatitisa. Vrednosti AST, ALT in bilirubina je treba spremljati pred začetkom zdravljenja z atezolizumabom, redno med zdravljenjem in kot je potrebno glede na klinično oceno. Bolnike je treba spremljati glede znakov in simptomov kolitisa in endokrinopatij, meningitisa ali encefalitisa, motorične in senzorične nevropatije. Bolnike je treba nadzorovati glede znakov in simptomov, ki kažejo na mielitis, akutni pankreatitis, miokarditis, miozitis. Imunsko pogojeni nefritis: bolnike je treba nadzorovati glede sprememb v delovanju ledvic. Bolnike je treba spremljati glede sumov na hude kožne neželene učinke in izključiti druge vzroke. V primeru suma na hude kožne neželene učinke je treba bolnike napotiti k specialistu po nadaljnjo diagnozo in zdravljenje. Pri zdravljenju z atezolizumabom so opažali perikardialne motnje. Pri bolnikih, ki so prejemali atezolizumab, so poročali o hemofagocitni limfohistiocitozi. Pri sumu na HLH je treba trajno prenehati zdravljenje z atezolizumabom in bolnike napotiti k specialistu po nadaljnjo diagnozo in zdravljenje. Z infundiranjem povezane reakcije: pri zdravljenju z atezolizumabom so opažali z infundiranjem povezane reakcije, vključno z anafilaksijo. Pri bolnikih, ki imajo z infundiranjem povezane reakcije 1. ali 2. stopnje, je treba hitrost infundiranja/injiciranja zmanjšati ali zdravljenje/injiciranje prekiniti. Pri bolnikih, ki imajo z infundiranjem povezane reakcije 3. ali 4. stopnje, je treba zdravljenje z atezolizumabom trajno ukiniti. Kartica za bolnika: Zdravnik, ki predpiše zdravilo, se mora z bolnikom pogovoriti o tveganjih zdravljenja z zdravilom Tecentriq. Bolniku je treba dati kartico za bolnika in mu naročiti, naj jo ima vedno pri sebi. **Medsebojno delovanje z drugimi zdravili in druge oblike interakcij:** Formalnih farmakokinetičnih študij medsebojnega delovanja z atezolizumabom niso izvedli. Ker se atezolizumab odstrani iz obtoka s katabolizmom, ni pričakovati presnovnih medsebojnih delovanj med zdravili. Uporabi sistemskih kortikosteroidov ali imunosupresivov se je pred uvedbo atezolizumaba treba izogibati, ker lahko vplivajo na farmakodinamično aktivnost in učinkovitost atezolizumaba. Vendar pa se sistemske kortikosteroide ali druge imunosupresive lahko uporabi po začetku zdravljenja z atezolizumabom za zdravljenje imunsko pogojenih neželenih učinkov. **Neželeni učinki:** *Informacije o varnosti atezolizumaba v monoterapiji:* najpogostejši neželeni učinki (> 10 %) so bili utrujenost, zmanjšan apetit, izpuščaj, navzea, kašelj, diareja, zvišana telesna temperatura, dispneja, artralgija, srbenje, astenija, bolečina v hrbtu, bruhanje, okužba sečil in glavobol. *Varnost intravenske oblike atezolizumaba v kombinaciji z drugimi učinkovinami:* najpogostejši neželeni učinki (≥ 20 %) so bili anemija, nevtropenija, navzea, utrujenost, alopecija, izpuščaj, diareja, trombocitopenija, zaprtost, zmanjšan apetit in periferna nevropatija. Varnostni profil zdravila Tecentriq raztopina za injiciranje je bil na splošno podoben znanemu varnostnemu profilu intravenske oblike; dodaten neželeni učinek so bile reakcije na mestu injiciranja. Poročanje o domnevnih neželenih učinkih: Poročanje o domnevnih neželenih učinkih zdravila po izdaji dovoljenja za promet je pomembno. Omogoča namreč stalno spremljanje razmerja med koristmi in tveganji zdravila. Od zdravstvenih delavcev se zahteva, da poročajo o katerem koli domnevnem neželenem učinku zdravila na: Javna agencija Republike Slovenije za zdravila in medicinske pripomočke, Sektor za farmakovigilanco, Nacionalni center za farmakovigilanco, Slovenčeva ulica 22, SI-1000 Ljubljana, Tel: +386 (0)8 2000 500, Faks: +386 (0)8 2000 510, e-pošta: h-farmakovigilanca@jazmp.si, spletna stran: www.jazmp.si. Za zagotavljanje sledljivosti zdravila je pomembno, da pri izpolnjevanju obrazca o domnevnih neželenih učinkih zdravila navedete številko serije biološkega zdravila. **Režim izdaje zdravila:** H. **Imetnik dovoljenja za promet:** Roche Registration GmbH, Emil-Barell-Strasse 1, 79639 Grenzach-Wyhlen, Nemčija. Za podrobnejše informacije glejte celoten Povzetek glavnih značilnosti zdravila. **Verzija: 2.0/25**

DODATNE INFORMACIJE SO NA VOLJO PRI: Roche farmacevtska družba d.o.o., Stegne 13G, 1000 Ljubljana

Samo za strokovno javnost.

Roche

Datum priprave informacije: september 2025 M-SI-00000349(v5.0)

Širimo obzorja v 3. liniji zdravljenja metastatskega kolorektalnega raka (mCRC)

VEČ KOT 10-MESEČNO CELOKUPNO PREŽIVETJE

Lonsurf® v kombinaciji z bevacizumabom je pokazal edinstvene rezultate pri zdravljenju mCRC v 3. liniji, saj je bila prvič dosežena mediana celokupnega preživetja (mOS) 10,8 meseca, s skoraj polovico živih bolnikov po enem letu in v dobri kondiciji za nadaljnje zdravljenje.[1]

Lonsurf®
trifluridin/tipiracil

Usmerjen v prihodnost

Literatura: 1. Prager GW et al. N Engl J Med 2023;388:1657-67.
Družba Servier ima licenco družbe Taiho za zdravilo Lonsurf®. Pri globalnem razvoju zdravila sodelujeta obe družbi in ga tržita na svojih določenih področjih.

Skrajšan povzetek glavnih značilnosti zdravila: Lonsurf 15 mg/6,14 mg filmsko obložene tablete in Lonsurf 20 mg/8,19 mg filmsko obložene tablete

SESTAVA*: Lonsurf 15 mg/6,14 mg: Ena filmsko obložena tableta vsebuje 15 mg trifluridina in 6,14 mg tipiracila (v obliki klorida). **Lonsurf 20 mg/8,19 mg**: Ena filmsko obložena tableta vsebuje 20 mg trifluridina in 8,19 mg tipiracila (v obliki klorida). **TERAPEVTSKE INDIKACIJE*:** V kombinaciji z bevacizumabom za zdravljenje odraslih bolnikov z metastatskim kolorektalnim rakom (KRR), ki so prejeli dva predhodna režima zdravljenja raka, vključno s kemoterapijo na osnovi fluoropirimidina, oksaliplatina in irinotekana, zdravljenje z zaviralci žilnega endotelijskega rastnega dejavnika (VEGF – Vascular Endothelial Growth Factor) in/ali zaviralci receptorjev za epidermalni rastni dejavnik (EGFR – Epidermal Growth Factor Receptor). V monoterapiji za zdravljenje odraslih bolnikov z metastatskim kolorektalnim rakom, ki so bili predhodno že zdravljeni ali niso primerni za zdravljenja, ki so na voljo. Ta vključujejo kemoterapijo na osnovi fluoropirimidina, oksaliplatina in irinotekana, zdravljenje z zaviralci VEGF in zaviralci EGFR. V monoterapiji za zdravljenje odraslih bolnikov z metastatskim rakom želodca, vključno z adenokarcinomom gastro-ezofagealnega prehoda, ki so bili predhodno že zdravljeni z najmanj dvema sistemskima režimoma zdravljenja za napredovalo bolezen. **ODMERJANJE IN NAČIN UPORABE*:** Priporočeni začetni odmerek zdravila Lonsurf pri odraslih je 35 mg/m^2/odmerek peroralno dvakrat dnevno na 1. do 5. dan in 8. do 12. dan vsakega 28dnevnega cikla zdravljenja, najpozneje 1 uro po zaključku jutranjega in večernega obroka (20 mg/m^2/odmerek dvakrat dnevno pri bolnikih s hudo ledvično okvaro). Odmerek, izračunan glede na telesno površino, ne sme preseči 80 mg/odmerek. Možne prilagoditve odmerka glede na varnost in prenašanje zdravila pri posameznem bolniku: dovoljena so zmanjšanja odmerka na najmanjši odmerek 20 mg/m^2 dvakrat dnevno (oz. 15 mg/m^2/odmerek dvakrat dnevno pri bolnikih s hudo ledvično okvaro). Potem ko je bil odmerek zmanjšan, povečanje ni dovoljeno. Kadar se zdravilo Lonsurf uporablja v kombinaciji z bevacizumabom za zdravljenje metastatskega KRR, je odmerek bevacizumaba 5 mg/kg telesne mase enkrat na 2 tedna. **KONTRAINDIKACIJE*:** Preobčutljivost na učinkovini ali katero koli pomožno snov. **OPOZORILA IN PREVIDNOSTNI UKREPI*:** Supresija kostnega mozga: Pred uvedbo zdravljenja in po potrebi za spremljanje toksičnosti zdravila, najmanj pred vsakim ciklom zdravljenja, je treba pregledati celotno krvno sliko. Zdravljenja ne smete začeti, če je absolutno število nevtrofilcev < 1,5 x 10^9/l, če je število trombocitov < 75 x 10^9/l ali če se je pri bolniku zaradi predhodnih zdravljenj pojavila klinično pomembna nehematološka toksičnost 3. ali 4. stopnje, ki še traja. Bolnike je treba skrbno spremljati zaradi morebitnih okužb, uvesti je treba ustrezne ukrepe, kot je klinično indicirano. Toksičnost za prebavila: Potrebna je uporaba antiemetikov, antidiaroikov ter drugih ukrepov, kot je klinično indicirano. Če je potrebno, prilagodite odmerke. Ledvična okvara: Uporaba zdravila ni priporočljiva pri bolnikih s končno stopnjo ledvične bolezni. Bolnike z ledvično okvaro je potrebno med zdravljenjem skrbno spremljati; bolnike z zmerno ali hudo ledvično okvaro je treba zaradi hematološke toksičnosti bolj pogosto spremljati. Jetrna okvara: Uporaba zdravila Lonsurf pri bolnikih z obstoječo zmerno ali hudo jetrno okvaro ni priporočljiva. Proteinurija: Pred začetkom zdravljenja in med njim je priporočljivo spremljanje proteinurije z urinskimi testnimi lističi. Pomožne snovi: Zdravilo vsebuje laktozo. **INTERAKCIJE*:** Previdnost: Zdravila, ki medsebojno delujejo z nukleozidnimi prenašalci CNT1, ENT1 in ENT2, zaviralci OCT2 ali MATE1, substrati humane timidin-kinaze (npr. zidovudin), hormonski kontraceptivi. **PLODNOST*.** Bolnikom, ki želijo spočeti otroka, je treba svetovati, da se odločijo za svetovanje o reprodukciji ter shranjevanje jajčnih celic oz. sperme z zamrzovanjem pred začetkom zdravljenja z zdravilom Lonsurf. **NOSEČNOST IN DOJENJE*:** Ni priporočljivo. **KONTRACEPCIJA*:** Ženske in moški morajo uporabljati zelo učinkovite metode kontracepcije med zdravljenjem in do 6 mesecev po zaključku zdravljenja. **VPLIV NA SPOSOBNOST VOŽNJE IN UPRAVLJANJA STROJEV*:** Med zdravljenjem se lahko pojavijo utrujenost, omotica ali splošno slabo počutje. **NEŽELENI UČINKI*:** *Zelo pogosti:* nevtropenija, levkopenija, anemija, trombocitopenija, zmanjšan apetit, diareja, navzea, bruhanje, utrujenost, stomatitis. *Pogosti:* okužba spodnjih dihal, okužba, febrilna nevtropenija, limfopenija, hipoalbuminemija, disgevzija, omotica, glavobol, hipertenzija, dispneja, bolečina v trebuhu, zaprtje, razjede v ustih, bolezni ustne votline, hiperbilirubinemija, izpuščaj, artralgija, mialgija, alopecija, pruritus, suha koža, proteinurija, pireksija, edem, vnetje sluznice, splošno slabo počutje, zvišanje jetrnih encimov, zvišanje alkalne fosfataze v krvi, zmanjšanje telesne mase. *Občasni:* okužba žolčevoda, gripa, okužba sečil, gingivitis, herpes zoster, okužba s kandido, bakterijska okužba, nevtropenična sepsa, okužba zgornjih dihal, konjunktivitis, bolečina zaradi raka, pancitopenija, monocitopenija, eritropenija, levkocitoza, monocitoza, dehidracija, hiperglikemija, hiperkaliemija, hipokaliemija, hipofosfatemija, hiponatriemija, hipokalciemija, anksioznost, nespečnost, periferna nevropatija, nevrotoksičnost, parestezija, letargija, vrtoglavica, angina pektoris, aritmija, palpitacije, hipotenzija, vročinski oblivi, pljučna embolija, disfonija, epistaksa, izcedek iz nosu, kašelj, krvavitev v prebavilih, ileus, kolitis, gastritis, moteno praznjenje želodca, abdominalna distenzija, analno vnetje, dispepsija, gastroezofagealna refluksna bolezen, glositis, bolezen zob, siljenje na bruhanje, flatulenca, hepatotoksičnost, sindrom palmarne-plantarne eritrodisestezije, urtikarija, akne, hiperhidroza, bolezni nohtov, bolečina v kosteh, mišična oslabelost, mišični krči, bolečina v okončinah, ledvična odpoved, motnje mikcije, hematurija, motnje menstruacije, poslabšanje splošnega zdravstvenega stanja, bolečina, občutek spremembe telesne temperature, neugodje v okončinah, zvišanje kreatinina v krvi, povečanje mednarodnega umerjenega razmerja (INR), zvišanje sečnine v krvi, zvišanje laktatne dehidrogenaze v krvi, zvišanje C-reaktivnega proteina, zmanjšan hematokrit. *Redki:* infekcijski enteritis, tinea pedis, septični šok, granulocitopenija, putika, hipernatriemija, pekoč občutek, disestezija, hiperestezija, hipoestezija, sinkopa, katarakta, suho oko, zamegljen vid, diplopija, zmanjšana ostrina vida, neugodje v ušesu, embolija, orofaringealna bolečina, plevralni izliv, ascites, akutni pankreatitis, subileus, slab zadah, bukalni polip, hemoragični enterokolitis, krvavitev dlesni, ezofagitis, parodontalna bolezen, proktalgija, refluksni gastritis, razširitev žolčnih vodov, mehur, eritem, preobčutljivostne reakcije na svetlobo, luščenje kože, otekanje sklepov, neinfektivni cistitis, levkociturija, kseroza, podaljšanje aktiviranega parcialnega tromboplastinskega časa, podaljšanje intervala QT na elektrokardiogramu, znižanje celokupnih proteinov. *Post-marketinške izkušnje:* intersticijska bolezen pljuč. **PREVELIKO ODMERJANJE***: Neželeni učinki, o katerih so poročali v povezavi s prevelikim odmerjanjem, so bili v skladu z uveljavljenim varnostnim profilom. Glavni pričakovani zaplet prevelikega odmerjanja je supresija kostnega mozga. **FARMAKODINAMIČNE LASTNOSTI*:** *Farmakoterapevtska skupina:* zdravila z delovanjem na novotvorbe, antimetaboliti, oznaka ATC: L01BC59. Zdravilo Lonsurf sestavljata antineoplastični timidinski nukleozidni analog, trifluridin, in zaviralec timidin-fosforilaze (TPaze), tipiracilijev klorid. Po privzemu v rakave celice timidin-kinaza fosforilira trifluridin. Ta se v celicah nato presnovi v substrat deoksiribonukleinske kisline (DNA), ki se vgradi neposredno v DNA ter tako preprečuje celično proliferacijo. TPaza hitro razgradi trifluridin in njegova presnova po peroralni uporabi je hitra zaradi učinka prvega prehoda, zato je v zdravilo vključen zaviralec TPaze, tipiracilijev klorid. **PAKIRANJE*:** 20 filmsko obloženih tablet. **NAČIN PREDPISOVANJA IN IZDAJE ZDRAVILA:** Rp/Spec - Predpisovanje in izdaja zdravila je le na recept zdravnika specialista ustreznega področja medicine ali od njega pooblaščenega zdravnika. **Imetnik dovoljenja za promet:** Les Laboratoires Servier, 50, rue Carnot, 92284 Suresnes cedex, Francija. Številka dovoljenja za promet z zdravilom: EU/1/16/1096/001 (Lonsurf 15 mg/6,14 mg), EU/1/16/1096/004 (Lonsurf 20 mg/8,19 mg). **Datum zadnje revizije besedila: julij 2023. *Pred predpisovanjem preberite celoten povzetek glavnih značilnosti zdravila. Celoten povzetek glavnih značilnosti zdravila in podrobnejše informacije so na voljo pri: Servier Pharma d.o.o., Podmilščakova ulica 24, 1000 Ljubljana, www.servier.si.**

SERVIER
moved by you

LON AD1 C1 2025-26. Samo za strokovno javnost. Datum priprave informacije: september 2025.

Instructions for authors

The editorial policy

Radiology and Oncology is a multidisciplinary journal devoted to the publishing original and high-quality scientific papers and review articles, pertinent to oncologic imaging, interventional radiology, nuclear medicine, radiotherapy, clinical and experimental oncology, radiobiology, medical physics, and radiation protection. Papers on more general aspects of interest to the radiologists and oncologists are also published (no case reports).

The Editorial Board requires that the paper has not been published or submitted for publication elsewhere; the authors are responsible for all statements in their papers. Accepted cannot be published elsewhere without the written permission of the editors.

Submission of the manuscript

The manuscript written in English should be submitted to the journal via online submission system Editorial Manager available for this journal at: www.radioloncol.com.

In case of problems, please contact Sašo Trupej at saso.trupej@computing.si or the Editor of this journal at gsersa@onko-i.si

All articles are subjected to the editorial review and when the articles are appropriated they are reviewed by independent referees. In the cover letter, which must accompany the article, the authors are requested to suggest 3-4 researchers, competent to review their manuscript. However, please note that this will be treated only as a suggestion; the final selection of reviewers is exclusively the Editor's decision. The authors' names are revealed to the referees, but not vice versa.

Manuscripts which do not comply with the technical requirements stated herein will be returned to the authors for the correction before peer-review. The editorial board reserves the right to ask authors to make appropriate changes of the contents as well as grammatical and stylistic corrections when necessary. Page charges will be charged for manuscripts exceeding the recommended length, as well as additional editorial work and requests for printed reprints.

Articles are published printed and on-line as the open access:

(https://content.sciendo.com/raon).

All articles are subject to 1500 EUR + VAT publication fee. Exceptionally, waiver of payment may be negotiated with editorial office, at the time of article submission.

Manuscripts submitted under multiple authorship are reviewed on the assumption that all listed authors concur in the submission and are responsible for its content; they must have agreed to its publication and have given the corresponding author the authority to act on their behalf in all matters pertaining to publication. The corresponding author is responsible for informing the co-authors of the manuscript status throughout the submission, review, and production process.

Preparation of manuscripts

Radiology and Oncology will consider manuscripts prepared according to the Uniform Requirements for Manuscripts Submitted to Biomedical Journals by International Committee of Medical Journal Editors (www.icmje.org). The manuscript should be written in grammatically and stylistically correct language. Abbreviations should be avoided. If their use is necessary, they should be explained at the first time mentioned. The technical data should conform to the SI system. The manuscript, excluding the references, tables, figures and figure legends, must not exceed 5000 words, and the number of figures and tables is limited to 8. Organize the text so that it includes: Introduction, Materials and methods, Results and Discussion. Exceptionally, the results and discussion can be combined in a single section. Start each section on a new page, and number each page consecutively with Arabic numerals. For ease of review, manuscripts should be submitted as a single column, double-spaced text. The template for preparation of the manuscript is available in the editorial manager.

The Title page should include a concise and informative title, followed by the full name(s) of the author(s); the institutional affiliation of each author; the name and address of the corresponding author (including telephone, fax and E-mail), and an abbreviated title (not exceeding 60 characters). This should be followed by the abstract page, summarizing in less than 250 words the reasons for the study, experimental approach, the major findings (with specific data if possible), and the principal conclusions, and providing 3-6 key words for indexing purposes. Structured abstracts are required. Slovene authors are requested to provide title and the abstract in Slovene language in a separate file. The text of the research article should then proceed as follows:

Introduction should summarize the rationale for the study or observation, citing only the essential references and stating the aim of the study.

Materials and methods should provide enough information to enable experiments to be repeated. New methods should be described in details.

Results should be presented clearly and concisely without repeating the data in the figures and tables. Emphasis should be on clear and precise presentation of results and their significance in relation to the aim of the investigation.

Discussion should explain the results rather than simply repeating them and interpret their significance and draw conclusions. It should discuss the results of the study in the light of previously published work.

Charts, Illustrations, Images and Tables

Charts, Illustrations, Images and Tables must be numbered and referred to in the text, with the appropriate location indicated. Charts, Illustrations and Images, provided electronically, should be of appropriate quality for good reproduction. Illustrations and charts must be vector image, created in CMYK color space, preferred font "Century Gothic", and saved as .AI, .EPS or .PDF format. Color charts, illustrations and Images are encouraged, and are published without additional charge. Image size must be 2.000 pixels on the longer side and saved as .JPG (maximum quality) format. In Images, mask the identities of the patients. Tables should be typed double-spaced, with a descriptive title and, if appropriate, units of numerical measurements included in the column heading. The files with the figures and tables can be uploaded as separate files.

References

References must be numbered in the order in which they appear in the text and their corresponding numbers quoted in the text. Authors are responsible for the accuracy of their references. References to the Abstracts and Letters to the Editor must be identified as such. Citation of papers in preparation or submitted for publication, unpublished observations, and personal communications should not be included in the reference list. If essential, such material may be incorporated in the appropriate place in the text. References follow the style of Index Medicus, DOI number (if exists) should be included.

All authors should be listed when their number does not exceed six; when there are seven or more authors, the first six listed are followed by "et al.". The following are some examples of references from articles, books and book chapters:

Dent RAG, Cole P. In vitro maturation of monocytes in squamous carcinoma of the lung. *Br J Cancer* 1981; **43:** 486-95. doi: 10.1038/bjc.1981.71

Chapman S, Nakielny R. *A guide to radiological procedures*. London: Bailliere Tindall; 1986.

Evans R, Alexander P. Mechanisms of extracellular killing of nucleated mammalian cells by macrophages. In: Nelson DS, editor. *Immunobiology of macrophage.* New York: Academic Press; 1976. p. 45-74.

Authorization for the use of human subjects or experimental animals

When reporting experiments on human subjects, authors should state whether the procedures followed the Helsinki Declaration. Patients have the right to privacy; therefore, the identifying information (patient's names, hospital unit numbers) should not be published unless it is essential. In such cases the patient's informed consent for publication is needed, and should appear as an appropriate statement in the article. Institutional approval and Clinical Trial registration number is required. Retrospective clinical studies must be approved by the accredited Institutional Review Board/Committee for Medical Ethics or other equivalent body. These statements should appear in the Materials and methods section.

The research using animal subjects should be conducted according to the EU Directive 2010/63/EU and following the Guidelines for the welfare and use of animals in cancer research (Br J Cancer 2010; 102: 1555 – 77). Authors must state the committee approving the experiments, and must confirm that all experiments were performed in accordance with relevant regulations.

These statements should appear in the Materials and methods section (or for contributions without this section, within the main text or in the captions of relevant figures or tables).

Transfer of copyright agreement

For the publication of accepted articles, authors are required to send the License to Publish to the publisher on the address of the editorial office. A properly completed License to Publish, signed by the Corresponding Author on behalf of all the authors, must be provided for each submitted manuscript.

Conflict of interest

When the manuscript is submitted for publication, the authors are expected to disclose any relationship that might pose real, apparent or potential conflict of interest with respect to the results reported in that manuscript. Potential conflicts of interest include not only financial relationships but also other, non-financial relationships. In the Acknowledgement section the source of funding support should be mentioned. The Editors will make effort to ensure that conflicts of interest will not compromise the evaluation process of the submitted manuscripts; potential editors and reviewers will exempt themselves from review process when such conflict of interest exists. The statement of disclosure must be in the Cover letter accompanying the manuscript or submitted on the form available on www.icmje.org/coi_disclosure.pdf

The use and explanation of AI and AI-assisted technologies in scientific writing

When authors use artificial intelligence (AI) and AI-assisted technologies in the writing process, they should consider that:

- These technologies should only be used to improve readability and language and to assist in the investigation of data. They should not replace researchers' primary tasks of explaining, the interpretation of data and drawing valid scientific conclusions.
- Apply the technology under human supervision and control, and carefully review and edit the result, because AI can produce authoritative-sounding results that may be incorrect, incomplete, or biased.
- Do not list AI or AI-assisted technologies as authors or co-authors, and do not cite AI as an author. Authorship carries with it responsibilities and tasks that only humans can perform.
- Disclose in your manuscript the use of AI and AI-enabled technologies in the writing process by following the instructions below. An appropriate statement should appear in the published paper. Please note that authors are ultimately responsible and accountable for the content of the paper.

Disclosure notes

Authors must disclose the use of AI and AI-assisted technologies in the writing process by adding a statement at the end of their manuscript in the main manuscript file before the bibliography, at the time of manuscript submission. The statement should be included in a new section titled 'Statement on the Use of AI and AI-Assisted Technologies in the Writing Process'.

Statement: during the preparation of this paper, the author(s) used [NAME TOOL / SERVICE] to create [REASON]. After using this tool/service, the author(s) have reviewed and edited the content as required and take full responsibility for the content of the publication.

This statement does not apply to the use of basic tools to check grammar, spelling, references, etc. If there is nothing to disclose, it is not necessary to add a statement.

Page proofs

Page proofs will be sent by E-mail to the corresponding author. It is their responsibility to check the proofs carefully and return a list of essential corrections to the editorial office within three days of receipt. Only grammatical corrections are acceptable at that time.

Open access

Papers are published electronically as open access on https://content.sciendo.com/raon, also papers accepted for publication as E-ahead of print.

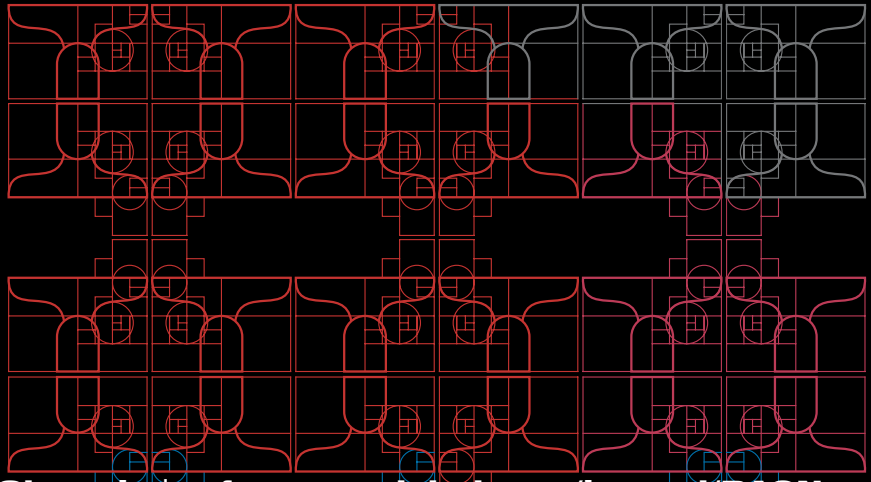

Radiology and Oncology | Ljubljana | Slovenia | reference-global.com/journal/RAON

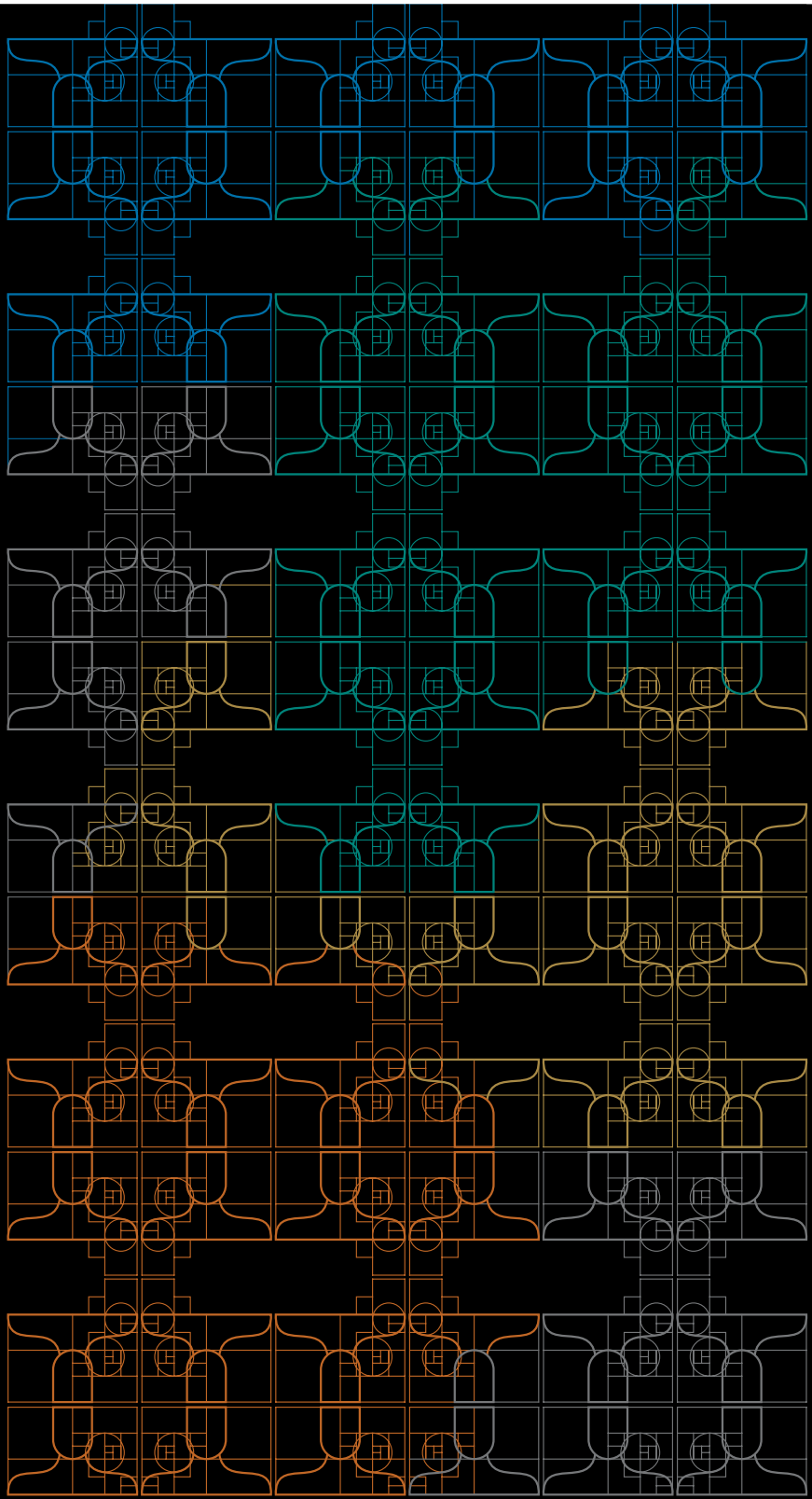

ISSN 1318 - 2099